

Principles of Reinforced Concrete

Zhenhai Guo



Principles of Reinforced Concrete

This page intentionally left blank

Principles of Reinforced Concrete

Zhenhai Guo



AMSTERDAM • BOSTON • HEIDELBERG • LONDON
NEW YORK • OXFORD • PARIS • SAN DIEGO
SAN FRANCISCO • SINGAPORE • SYDNEY • TOKYO

Butterworth-Heinemann is an imprint of Elsevier



Butterworth-Heinemann is an imprint of Elsevier
The Boulevard, Langford Lane, Kidlington, Oxford OX5 1GB, UK
225 Wyman Street, Waltham, MA 02451, USA

First edition 2014

Copyright © 2014 Tsinghua University Press. Published by Elsevier Inc. All rights reserved.

No part of this publication may be reproduced, stored in a retrieval system or transmitted in any form or by any means electronic, mechanical, photocopying, recording or otherwise without the prior written permission of the publisher

Permissions may be sought directly from Elsevier's Science & Technology Rights Department in Oxford, UK: phone (+44) (0) 1865 843830; fax (+44) (0) 1865 853333; email: permissions@elsevier.com. Alternatively you can submit your request online by visiting the Elsevier web site at <http://elsevier.com/locate/permissions>, and selecting *Obtaining permission to use Elsevier material*

Notice

No responsibility is assumed by the publisher for any injury and/or damage to persons or property as a matter of products liability, negligence or otherwise, or from any use or operation of any methods, products, instructions or ideas contained in the material herein. Because of rapid advances in the medical sciences, in particular, independent verification of diagnoses and drug dosages should be made

British Library Cataloguing in Publication Data

A catalogue record for this book is available from the British Library

Library of Congress Cataloging-in-Publication Data

A catalog record for this book is available from the Library of Congress

ISBN-13: 978-0-12-800859-1

For information on all Butterworth-Heinemann publications
visit our web site at store.elsevier.com

Printed and bound in the US

14 15 16 17 18 10 9 8 7 6 5 4 3 2 1



Working together
to grow libraries in
developing countries

www.elsevier.com • www.bookaid.org

Contents

Preface	XV
CHAPTER 1 Introduction.....	1
1.1 Development and features of reinforced concrete structure	1
1.2 Characteristics of this course.....	4
PART 1 MECHANICAL BEHAVIOR OF CONCRETE	
CHAPTER 2 Basic Mechanical Behavior	9
2.1 Material composition and characteristic.....	10
2.1.1 Composition and internal structure	10
2.1.2 Basic characteristics	13
2.1.3 General mechanism of failure process	17
2.2 Compressive strength.....	19
2.2.1 Cubic compressive strength.....	19
2.2.2 Failure process of prism specimen.....	21
2.2.3 Main indices of mechanical behavior	24
2.3 Complete compressive stress—strain curve	28
2.3.1 Testing method.....	28
2.3.2 Equation for complete curve	29
2.4 Tensile strength and deformation	33
2.4.1 Testing method and index of tensile behavior	33
2.4.2 Tensile failure process and characteristic	39
2.4.3 Equation of complete stress—strain curve.....	42
2.5 Shear strength and deformation.....	44
2.5.1 Rational testing method.....	44
2.5.2 Failure characteristic and shear strength.....	48
2.5.3 Shear strain and modulus	49
CHAPTER 3 Behavior Under Influence of Main Factors	53
3.1 Load acted repeatedly	54
3.2 Eccentric compression	59
3.2.1 Testing method.....	59
3.2.2 Main experimental results	60
3.2.3 Stress—strain relation.....	64
3.3 Eccentric and flexural tensions	66
3.3.1 Failure process	66
3.3.2 Ultimate tensile strength and plasticity-dependent coefficient.....	67

3.3.3	The maximum tensile strain at ultimate load	69
3.3.4	Variations of strain and neutral axis of section.....	69
3.3.5	Equations for complete stress—strain curve.....	70
3.4	Age	71
3.4.1	Compressive strength.....	72
3.4.2	Modulus of elasticity	74
3.5	Shrinkage.....	75
3.5.1	Kind and quantity of cement.....	76
3.5.2	Property, size, and quantity of aggregate	76
3.5.3	Curing condition	76
3.5.4	Environmental condition of service stage.....	76
3.5.5	Shape and size of structural member	76
3.5.6	Other factors	76
3.6	Creep	78
3.6.1	Basic concept.....	78
3.6.2	Main influence factors	82
3.6.3	Calculation formulas.....	85
CHAPTER 4	Various Structural Concrete.....	89
4.1	High-strength concrete.....	90
4.1.1	Application and preparation	90
4.1.2	Basic mechanical behavior	92
4.2	Light-weight concrete	99
4.2.1	Classification.....	99
4.2.2	Basic mechanical behavior	101
4.3	Fiber concrete.....	106
4.3.1	Classification.....	106
4.3.2	Basic mechanical behavior	108
CHAPTER 5	Multiaxial Strength and Constitutive Relation	113
5.1	Experimental equipment and method.....	115
5.2	General regularities of multiaxial strength and deformation	118
5.2.1	Biaxial stress states.....	119
5.2.2	Triaxial stress states.....	122
5.2.3	Different materials and loading paths	129
5.3	Typical failure patterns and their boundaries.....	132
5.3.1	Breaking in tension.....	132
5.3.2	Columnar crushing.....	133
5.3.3	Splitting into pieces	134

5.3.4 Inclined shearing.....	134
5.3.5 Extruding and shifting.....	135
5.4 Failure criterion.....	137
5.4.1 Shape of failure envelope and its expression.....	137
5.4.2 Failure criterion	141
5.4.3 Calculation charts for multiaxial strength.....	146
5.5 Constitutive relation.....	147
5.5.1 Models of linear elasticity	149
5.5.2 Models of non-linear elasticity.....	150
5.5.3 Models of other categories	151

PART 2 COMBINATION FUNCTION OF REINFORCEMENT AND CONCRETE

CHAPTER 6 Mechanical Behavior of Reinforcement..... 159

6.1 Reinforcement used in concrete structure	159
6.1.1 Reinforcement (diameter 6—40 mm)	160
6.1.2 High-strength wire (diameter 4—9 mm)	161
6.1.3 Shape steel	161
6.1.4 Ferrocement	162
6.1.5 Other substitutive materials.....	162
6.2 Stress—strain relation.....	163
6.2.1 Mild steel	163
6.2.2 Hard steel (wire).....	166
6.3 Deformation under action of cyclic loads.....	167
6.4 Behavior after cold-worked	172
6.4.1 Cold-stretching and age-hardening	173
6.4.2 Cold-drawn	175
6.5 Creep and relaxation.....	176
6.5.1 Kind of steel	178
6.5.2 Sustaining time of control stress	178
6.5.3 Stress level	178
6.5.4 Temperature	179

CHAPTER 7 Bond Between Reinforcement and Concrete..... 181

7.1 Function and composition of bond.....	182
7.1.1 Function and classification	182
7.1.2 Composition.....	184
7.2 Test method and bond mechanism	186
7.2.1 Test method.....	186

7.2.2 Plain reinforcement.....	189
7.2.3 Deformed reinforcement.....	190
7.3 Influence factors.....	193
7.3.1 Strength of concrete (f_{cu} or f_t)	194
7.3.2 Thickness of concrete cover (c)	195
7.3.3 Bond length of reinforcement (l)	195
7.3.4 Diameter and shape of reinforcement	196
7.3.5 Transverse stirrup (ρ_{sv})	197
7.3.6 Transverse compressive stress (q)	198
7.3.7 Other factors	198
7.4 Constitutive model for bond stress—slip	199
7.4.1 Calculation of characteristic values	200
7.4.2 Equation for τ — s curve.....	201
CHAPTER 8 Mechanical Behavior Under Axial Force.....	205
8.1 Compressive member.....	206
8.1.1 Basic equations	206
8.1.2 Analysis of stress and strain ($\epsilon_y < \epsilon_p$).....	209
8.1.3 Analysis of stress and strain ($\epsilon_y > \epsilon_p$).....	210
8.2 Tensile member.....	212
8.2.1 Basic equations for analysis.....	212
8.2.2 Analyses of stress and deformation within every stage	213
8.2.3 Minimum reinforcement rate.....	215
8.2.4 Tension stiffening	216
8.3 General regularity	218
CHAPTER 9 Confined Concrete	221
9.1 Column with spiral bar	222
9.1.1 Mechanical mechanism and failure process	222
9.1.2 Ultimate strength	224
9.2 Rectangular tied column	226
9.2.1 Failure process	226
9.2.2 Working mechanism of rectangular tie.....	229
9.2.3 Equation for complete stress—strain curve	234
9.3 Steel-tube-confined concrete.....	238
9.3.1 Mechanical characteristic and mechanism.....	238
9.3.2 Calculation of ultimate strength.....	241
9.4 Local compression	244
9.4.1 Mechanical characteristic and mechanism.....	244
9.4.2 Calculation of strength	249

CHAPTER 10	Mechanical Response of Deformation Difference.....	253
10.1	Shrinkage of concrete	254
10.1.1	General analysis method	254
10.1.2	Practical calculation method	256
10.2	Difference of thermal deformation.....	259
10.3	Creep of concrete.....	263
10.3.1	Stress redistribution on section under sustained load	263
10.3.2	Stress state after unloaded.....	265

PART 3 STRENGTH AND DEFORMATION OF STRUCTURAL MEMBER

CHAPTER 11	Strength of Member Under Compression and Bending	269
11.1	Mechanical process and failure pattern.....	269
11.1.1	Rectangular beam with tensile reinforcement only	269
11.1.2	Suitably, less-, and over-reinforced beams	272
11.1.3	Eccentrically compressed column (and tensed member).....	275
11.2	Additional flexure of long column	280
11.3	General method for sectional analysis	283
11.4	Ultimate strength	289
11.4.1	Calculation formulas	289
11.4.2	Member under biaxial bending	295
11.5	Members of various materials and structural details	298
11.5.1	High-strength concrete	298
11.5.2	Light-weight concrete.....	299
11.5.3	Reinforcements with different strengths	300
11.5.4	Reinforcement without yielding plateau	301
11.5.5	Reinforcements distributed along sectional depth	301
11.5.6	Non-rectangular sections	303
CHAPTER 12	Tensile Crack.....	305
12.1	Cause and limitation of crack.....	305
12.1.1	Action of load.....	305
12.1.2	Non-loading factors	306
12.2	Internal force at cracking.....	309
12.3	Mechanism of cracking	311
12.3.1	Bond-and-slip method	312

12.3.2 Non-slip method	314
12.3.3 Comprehensive analysis	318
12.4 Calculation of crack width	322
CHAPTER 13 Flexural Stiffness and Deformation	329
13.1 Deformation of member and its limitation	329
13.1.1 Influences of structural deformation	329
13.1.2 Stiffness of section and deformation of member.....	331
13.2 Calculation of sectional stiffness.....	334
13.2.1 Effective moment of inertia.....	334
13.2.2 Analytical method for stiffness	337
13.2.3 Modification of tension stiffening	340
13.3 Calculation of deformation.....	342
13.3.1 General method.....	342
13.3.2 Practical methods.....	344
CHAPTER 14 Strength of Member Under Shear Force	349
14.1 Failure pattern and strength of beam without web reinforcement	350
14.1.1 Typical failure pattern (shear-compression).....	350
14.1.2 Failure patterns of inclined compression and tension.....	354
14.1.3 Ultimate shear strength.....	356
14.2 Effect of web reinforcement and components of shear resistance.....	360
14.2.1 Effect of web reinforcement.....	360
14.2.2 Composition of ultimate shear strength	363
14.3 Calculation of ultimate shear strength	364
14.3.1 About finite element method.....	364
14.3.2 Empirical regression	365
14.3.3 Simplified mechanical models	369
14.4 Various members and mechanical conditions	373
14.4.1 Load acted on beam web.....	373
14.4.2 Beam of T section	374
14.4.3 Beam with variable section (depth)	376
14.4.4 Influence of axial force.....	377
14.4.5 Both positive and negative bending moments exist within shear span	378
14.4.6 Bracket.....	380
14.4.7 Punching of slab	382

CHAPTER 15	Strength of Member Under Torsion	385
15.1	Elasticity and plasticity solutions.....	386
15.2	Ultimate strength of member under torsion alone.....	390
15.2.1	Member without web reinforcement.....	390
15.2.2	Member with web reinforcement.....	392
15.2.3	Influence of contents of reinforcement and stirrup.....	393
15.3	Members with composite internal forces.....	395
15.3.1	Member with axial force and torsion.....	395
15.3.2	Member with shear force and torsion	395
15.3.3	Member with bending moment and torsion.....	397
15.3.4	Member with bending moment, shear force and torsion together.....	400
15.4	Calculation of ultimate strength.....	401
15.4.1	Empirical formulas	401
15.4.2	Truss model	403
15.4.3	Ultimate equilibrium of inclined twisted surface	405

PART 4 SPECIAL BEHAVIORS OF STRUCTURAL MEMBERS

CHAPTER 16	Seismic Resistance	411
16.1	Characteristics of structural behavior under earthquake	411
16.2	Ductility under monotonic load.....	413
16.2.1	Concept and expression of ductility.....	413
16.2.2	Calculation method.....	416
16.2.3	Angular rotation of plastic region.....	418
16.3	Hysteretic characteristic under reversed load of low cycles.....	421
16.3.1	General characteristics of hysteretic curves.....	421
16.3.2	Hysteretic curves under various conditions	426
16.3.3	Calculation model.....	434
CHAPTER 17	Fatigue Resistance	437
17.1	Fatigue of concrete	438
17.1.1	Experimental results and expression	438
17.1.2	Influence factors and calculation formula.....	441
17.2	Fatigue of reinforcement	443
17.3	Fatigue of bond between reinforcement and concrete.....	446
17.4	Fatigue of structural member and its checking calculation.....	449
17.4.1	Fatigue under bending moment.....	450
17.4.2	Fatigue under shear force	454

CHAPTER 18	Explosion Resistance.....	457
18.1	Characteristics of explosion resistance of structures	457
18.2	Behaviors of materials under high-speed loading.....	461
18.2.1	Testing equipment and method	461
18.2.2	Reinforcement.....	463
18.2.3	Concrete	465
18.3	Behaviors of structural members.....	468
18.3.1	Flexural member.....	468
18.3.2	Compressive member	472
CHAPTER 19	Fire Resistance	475
19.1	Characteristics of fire resistance of structures	475
19.2	Temperature field on section	479
19.2.1	Temperature—time curve	479
19.2.2	Thermal behaviors of materials.....	481
19.2.3	Basic equation for heat conduction and determination of temperature field.....	485
19.3	Mechanical behaviors of materials at elevated temperature	487
19.3.1	Behavior of reinforcement.....	487
19.3.2	Basic behavior of concrete	491
19.4	Coupling constitutive relation of concrete	499
19.4.1	Upper and lower bounds of compressive strength.....	500
19.4.2	Thermal strain under stress and transient thermal strain.....	501
19.4.3	Short-term creep at elevated temperature	504
19.4.4	Coupling constitutive relation	505
19.5	Behavior and calculation of structural members at elevated temperature	505
19.5.1	Flexural and compressive members	505
19.5.2	Statically indeterminate structure.....	513
19.5.3	Analysis and approximate calculation	516
CHAPTER 20	Durability.....	521
20.1	Characteristics of durability of concrete structure.....	521
20.1.1	Relevant problems raised in engineering practice	521
20.1.2	Characteristics of durability failure.....	523
20.1.3	Porosity texture of concrete	524
20.2	Several durability problems.....	527
20.2.1	Permeation	527
20.2.2	Freeze—thaw	530

20.2.3 Alkali—aggregate reaction.....	531
20.2.4 Carbonation.....	533
20.2.5 Chemical corrosion.....	536
20.2.6 Rust of reinforcement.....	538
20.3 Design and evaluation of structure durability.....	542
20.3.1 Design of durability.....	542
20.3.2 Examination and evaluation of durability for existing concrete structures	543
Appendix.....	547
References.....	559
Index	581

This page intentionally left blank

Preface

The courses “Theory of Reinforced Concrete Structures” [1-1] and “Strength and Constitutive Relation of Concrete” [1-2] were started in early 1980’s for the post-graduate students in structural engineering and related fields in Tsinghua University. The lectures, and the syllabus and contents of both courses are varied during the teaching practice. Two courses are composed and named “Principles of Reinforced Concrete” in 1990’s. The author gave a lecture on this course for several years and wrote the textbook of same name [1-3], based on the teaching draft.

After the book was published in 1999, it is also adopted as the textbook or main reference for similar courses of both post- and under- graduates of many universities in China. And, it is helpful as well for the university lecturers. In addition, sometimes the book is used by the structural engineers during their scientific or technical work.

In 2001, Education Committee of Beijing decided to establish “the elite textbooks for university education of Beijing”, and the textbook was selected after appraisal. The new textbook is renamed as “Principle and Analysis of Reinforced Concrete” [1-4] and published in 2003. The new textbook or the second edition contains most contents of the original one, but some chapters and sections are reformed and two new chapters, i.e. general analysis method of structural member and durability, are added. In addition, the exercises are attached to its text.

This book is the English version of textbook “Principle and Analysis of Reinforced Concrete” (in Chinese), but some contents are modified and slightly abridged to reduce its length. There are four parts including twenty chapters in this book.

In Part One, the strength and deformation behavior and its variation regularity of concrete are introduced in detail, based on its basic characteristic and failure mechanism. The main mechanical behaviors of various structural concrete, i.e. high-strength, light-weight, and fiber concrete, are presented as well. And, the multi-axial strength and constitutive relation of concrete are briefly contained.

The combination function of reinforcement and concrete is a special problem with importance, when reinforced concrete is considered as a composed structural material and is distinguished from a single structural material. So, bond and deformation difference between reinforcement and concrete, and confined concrete are discussed in Part Two.

In Part Three, the strength, crack, and deformation of flexural and compressive members, and shear- and torsion-resistances of structural members of reinforced concrete are introduced in detail based on the corresponding experiments. And, the general regularities, working mechanisms, and analysis methods of them are concluded.

A reinforced concrete structure may experience some extreme circumstances during its long life, e.g. earthquake, explosion, fatigue, high temperature (fire), or long-term damage (durability). So, the special behaviors of reinforcement and

concrete materials, and the mechanical responses and analysis methods of the structural members under these conditions are introduced briefly in Part Four.

“Reinforced Concrete Structures” or the similar [1-5] is a course for the undergraduate students of Structural Engineering in Chinese university. The main objective of it is to help them to conduct the structural design. Therefore, the main contents of the course include: the mechanical behaviors of reinforcement and concrete are briefly introduced, the behavior, calculation method, and requirement of design and construction of the basic structural members under various internal forces are presented in detail, and the concept and method of structural design and relevant design codes are introduced and explained.

This book is used for the post-graduate students in structural engineering. The main contents are research and analysis of the mechanical behavior and its regularity of reinforced concrete structural members, and the main objective is to solve various questions occurred in engineering practice. Therefore, the general regularities of strength and deformation of concrete under uni- and multi-axial stresses, even under several extreme circumstances, are introduced systematically, as this is the basis for understanding and analyzing the structural members. When the mechanical behavior of the structural members under various conditions are discussed, the results of corresponding experimental investigations are emphasized, the stress and deformation states, cracking and failure process, and influences of important factors are analyzed in detail, and the working mechanism, the principle and method of calculation, and the determinations of the technical indices are concluded. It is hoped that the reader not only knows the general regularities of the materials and members of reinforced concrete, but also understands the general way and reasonable method for analyzing and solving the practical problems in reinforced concrete structural engineering, after reading this book.

When this book is sent to press, the author sincerely thanks the professors of elder generation, who worked in the Department of Civil Engineering, Tsinghua University. They worked and studied seriously and their teaching experiences [1-5][1-6] and research achievements in reinforced concrete structure field enrich my knowledge, which partly composes the basis of this book. My colleagues, including technicians and workers, and post- and under-graduate students, who worked together within the processes of experimental and theoretical researches within many years, are appreciated as well. Their cooperation with effort helps to bring about the research achievement, which substantiate and improve the contents of this book. In addition my special thanks is due to my wife, retired professor Suying Qian, who not only patiently typed and input the entire manuscript of this book to form the original computer text, but also takes care thoughtfully of my life. Of course, the print and publication of this book is relied on the efforts of Tsinghua University Press, it is also appreciated.

Zhenhai Guo
September 2013

Introduction

1

CHAPTER OUTLINE

1.1 Development and features of reinforced concrete structure.....	1
1.2 Characteristics of this course	4

1.1 Development and features of reinforced concrete structure

Since the first product of reinforced concrete was manufactured and used in structural engineering, only about one hundred years have passed. Compared with soil and timber structure, which is the earliest on earth, used by the original mankind, the masonry structure of stone or brick appeared in the early society of ancient civilizations, and steel and other metal structures developed after the Industrial Revolution, reinforced concrete structure is the youngest one among the structure family. However, the performance and manufacture technique of reinforced concrete structure are continuously improving and being enhanced, structural configuration and construction get more variety, and the application scope is widely expanded. Now, reinforced concrete structure is the most prosperous one in structural engineering in many countries, especially in China.

Now, the engineering fields using widely reinforced concrete structure are as follows.

Building engineering — various civil and public buildings, single- and multi-storey industrial buildings, high-rise and long-span buildings ...

Bridge and communication engineering — slab, beam, arch, and truss upper structures, abutments, piers, and foundations, slope protection, retaining walls, highway pavements, railway sleepers ...

Hydraulic and harbor engineering — dams, hydropower stations, coasts and docks, offshore platforms, ponds and pipelines, aqueducts ...

Underground engineering — tunnels, railways, mines, caissons, piles, foundations of heavy equipment, military defense works ...

Special engineering — television towers, transmission poles, viaducts, silos, chimneys, pavements and parking aprons of airports Even reinforced concrete structures enter into the machine building field, e.g. reactor vessels and

containment of nuclear power plants, hydraulic presses, shipbuilding, lathes, etc., which are occupied traditionally only by steel structures.

The inherent certainty of a combination of reinforcement and concrete is due to the mutual compensation of the behavior of both materials and the advantage of each material is fully utilized. Concrete is the main body of the structural material and has some advantages, e.g. easy manufacturing, utilizing local materials, low investment. However, concrete has lower tensile strength and is fragile and cracks easily. Therefore, only when the reinforcement of a proper type and quantity is put into the concrete, the strength and ductility of the reinforced concrete structure is improved and enhanced to satisfy the necessary safety and service conditions. In the meantime, the disadvantages of reinforcement, e.g. poor environmental stability, and corrosion and fire resistance, will be overcome when it is buried into concrete. So, reinforcement and concrete can effectively be composed of a structural material with high strength, good integrity, corrosion and fire resistances, and flexible uses.

In addition, concrete is a shapeless substance and can be made into any structure of complicated shape and different sizes, when a proper mold is manufactured and installed. There are so many different reinforced concrete structures which include not only the one-dimensional members, e.g. beam, slab, column, of solid and hollow sections of different shapes, but also the two-dimensional members, e.g. flat plate, slab, wall panel, shear-wall, folded plates, and the three-dimensional, e.g. thin and thick shells and irregular solid, structures.

Reinforced concrete itself is composed of two materials and can also be used as a kind of structural material and combined with other structural materials to compose various composite structures, such as reinforced concrete-steel and reinforced concrete-masonry structures. Then, more varieties of structure scheme are developed and the adaptability and application scope of it are expanded.

As reinforced concrete structure is widely used in engineering practice, the requirement of production accelerates the research work in all aspects. The plentiful research results on structural scheme and configuration, kind and quality of material, construction technique, mechanical behavior of structural members, design concept and calculation method, construction measures, etc., are achieved and great progress is made as below.

Some disadvantages of concrete material, such as higher dead weight, lower cracking resistance, strength increasing slowly, and seasonal limitation of construction, have been improved or overcome, when the technical measures, which include selection of raw materials, mix and cure technique, construction management, reinforcement construction, prestressing, and improvement of calculation method, are utilized.

In order to enhance the performance of concrete and to reduce its self weight, high-strength ($>C50$), light-weight ($\gamma = 500\text{--}1900 \text{ kg/m}^3$), fiber, and high-performance concretes of various categories are developed successively and applied in engineering practice.

When various chemical additives are mixed into concrete during its mixing, the higher workability, freezing resistance, high strength, and earlier coagulating of

concrete are achieved, even heat-resisting and acid-resisting concrete can be obtained. And, pumping, spraying, and self-compacting concrete may be used to improve the manufacturing technique. All kinds of these concretes are suited to different construction and application conditions of reinforced concrete structures.

The strength of the steel reinforcement used for reinforced concrete structure is gradually increased from low value into medium and high values. The steel reinforcements of low relaxation and with anticorrosion coating are used frequently. Various resins and carbonic fiber bars (or sheets) of high strength and anticorrosion are also used successfully now to replace the steel reinforcement.

The behavior of concrete under uni- and multi-axial stress states and its failure criterion and constitutive relation have been investigated experimentally and theoretically, and great progress has been made. The strength and deformation of concrete under various conditions, e.g. repeated load, high-speed loading, sustained load, at elevated temperature, are also tested and many results are reported.

The bond behavior between reinforcement and concrete, including working mechanism, characteristic values of bond strength and slip, shape and calculation model of τ - s curve, have been investigated for many years. The anchorage of reinforcement is important in engineering practice and an effective measure is available now.

The mechanical behaviors of various structural members under static and dynamic loads are always the key topics of research on reinforced concrete. Most of them already have definite conclusions and ripe calculation methods. The mechanical responses of them under extreme circumstances, e.g. earthquake, explosion, fire accident, also have plenty experimental and theoretical results.

In the initial stage of application, the design concept and calculation method of a reinforced concrete structure are based on the allowable stress and elastic analysis, which follow that of the steel structure. Then, they were changed into single safety coefficient and ultimate strength analysis respectively. Now, the limit state design method, based on the probability statistics and reliability analysis, is used worldwide. In the meantime, the calculation method of the structural internal forces is also developed from the classical elastic analysis into the ultimate equilibrium method considering plastic deformation, and again into the non-linear analysis along loading history. The combination of the finite-element analysis method and the computer technique is a very powerful means for accurate and quick analysis of a complicated reinforced concrete structure and is widely used now in engineering practice.

The progress of experimental method and high technicalities of experimental equipment and measuring instrument raise the capability and accuracy of structural testing. Various environmental and loading conditions of the structures can be simulated better and more and meticulous information and data can be obtained in the testing. These are helpful for understanding correctly the responses of the testing structure and discovering its new physical phenomena and regularity.

All of these research achievements promote deeper understanding of the behavior regularities of reinforced concrete materials and structures and raise the

technical levels of structural design and construction. So, reinforced concrete structure is developed continuously and will have wider prospects.

1.2 Characteristics of this course

Principle of Reinforced Concrete is a special textbook of the course for post-graduate students in structural engineering and similar. They have learned the undergraduate courses of Basic Structural Members of Reinforced Concrete [0-5] and Design Reinforced Concrete Structure and known the basic characteristics of reinforced concrete and its design method. This course contains the main theoretical basis and experimental evidence for research and design of reinforced concrete structure, and its contents and role are just like the course ‘Strength of Materials’ for the structure of homogeneous linear-elastic materials. However, reinforced concrete is mainly composed of two materials of different properties, i.e. reinforcement and concrete, and concrete is an inhomogeneous and non-linear material and has different values of compressive and tensile strengths. So, the mechanical behavior of reinforced concrete is more varied and complicated, and the contents of this course are more plentiful.

Reinforced concrete structure is a science branch of structural engineering and certainly follows the general regularity of structural engineering. Various technical requirements and questions are often raised from engineering practice, and corresponding solutions and measurement are obtained by different ways such as survey and statistics, experimental investigation, theoretical analysis, calculation and comparison. After concluding the general variation regularity, revealing the working mechanism, establishing the physical and mathematic models, and determining the calculation method and construction measures, they go back to engineering practice and are demonstrated, improved, and complemented. Generally, after experiencing several cycles of practice—research—practice, they will gradually approach a satisfactory answer and finally serve well the engineering.

Since reinforced concrete is composed of two materials with considerably different properties, it certainly has some particularities which distinguish from the single material, e.g. steel or timber, used for the structure. Therefore, the behavior of reinforced concrete depends upon not only the properties of the two materials on their own, but also, to a greater extent, on the combination and relative comparison of them, for example:

Different forms of reinforcement — longitudinal or transverse, concentrated or spread, over or under-reinforced, natural or prestressed ...

Relative value of behavior indices of both materials — strength ratio, area or volume ratio, ratio of elastic moduli, ratio of characteristic strains, differences of thermal strain, shrinkage, and creep

Therefore, the load-bearing capacity and deformation behavior of reinforced concrete vary considerably. Sometimes, a special reinforced concrete can be

designed and manufactured, using reasonably raw materials and proper reinforcement form, to satisfy the technical indices which fit the requirement of a particular engineering project.

It is known that concrete is an inhomogeneous and non-linear composite material, and its mechanical behavior is complicated and varied with time and its technical indices are scattered considerably. In addition, the combination of reinforcement and concrete is of variform, this makes the mechanical behavior of reinforced concrete vary significantly. Up to now, many experimental and theoretical results of reinforced concrete structural members under various loading and environmental conditions are obtained and corresponding calculation method and structural detailing are established and satisfied for engineering practice. However, there is still no unified and accurate theoretical theory and method for reinforced concrete under all situations.

Considering these characteristics of concrete material and reinforced concrete structural members, the following principles are insisted upon in this book.

Basing on experimental evidence — Generally, the mechanical indices of concrete material and behavior responses of reinforced concrete structural members can only be determined accurately from reasonable and careful tests. Therefore, a certain amount of experimental data are presented, the variation regularities are concluded, the mechanism is analyzed, the rational knowledge is summarized, the physical and mathematical models are established, and finally, the experimental and engineering demonstrations are performed.

Macroscopic mechanical response — The microscopic analyses of the stress, strain, and crack of structural concrete are hardly reached the accurate results, because of non-uniform micro-structure, local defects, and scattered behavior of concrete material itself. The behaviors of concrete material and reinforced concrete structure discussed in this book represent the average values of them within a certain scale (e.g. about ≥ 70 mm, or 3 or 4 times the coarse aggregate size). It is accurate enough when they are used in engineering practice.

Regularity and mechanism analysis of mechanical behavior — The behavior responses of concrete material and reinforced concrete structure vary considerably under different loading and environmental conditions, because of the influences of various factors. However, the stress and deformation processes, failure pattern, and ultimate strength of them still present certain regularities. It is hoped to analyze their working mechanisms and to find the inherent essence of the mechanical characteristics of the structure, which is relatively stable and more important. In contrast, the particular calculation method and formula will be changed both in form and parameters, as the experimental data are accumulated, varied, or deleted.

Actual mechanical behavior and index — The experimental values and the theoretical calculation values, listed in this book, for concrete material and reinforced concrete structural member are generally the measured or average values. These values can be used for calculating the actual strength and

deformation of the structure. However, there are systematic differences between these values and the corresponding nominal values or design values, which are used in the structural design after considering the necessary safety of the structure. So, these values have to be converted properly and then be used if necessary.

Reflecting the new research at home and abroad — Reinforced concrete structure and its materials develop continuously, new experiences are accumulated and new questions are raised in engineering practice, and relevant experimental and theoretical achievements appear year after year. The basic concept and analysis method are relatively stable and retained in this book, and the new research results, and different academic points of view and method, are contained.

In addition, this book mainly serves the research and analysis of reinforced concrete structure, the reinforcement and other structural detailing are, generally, not stipulated and the requirements of design code are also not included. When a practical question in the structural engineering is dealt with, the relevant literatures and references, including the design code, have to be consulted.

Mechanical Behavior of Concrete

1

Concrete is a kind of manmade composite material, of which the main adhesive substance is the cement of hydro-coagulation and most parts are coarse and fine aggregates of different mineral compositions. Concrete is the main body of reinforced concrete and contains and surrounds the reinforcements of different forms, and both compose the composite structural material. Therefore, the mechanical behaviors of reinforced concrete structure and its members depend upon, to a great extent, the behavior of concrete material and the supporting and confining actions of concrete to the reinforcement.

The strength and deformation behaviors of concrete are obviously different from those of the single material of structure, e.g. steel from metallurgical industry or natural timber. The tensile and compressive strengths (and deformations) of concrete make a great difference, and they vary considerably with time (age) and environmental factors. Also, concrete is quite fragile and cracks easily. In addition, the stabilities of its quality and behavior depend upon the technical and management levels of the contractor, and various indices of concrete behavior may deviate greatly.

The main contents introduced in this part are the general characteristics and failure mechanism of concrete material, its strength and deformation

under fundamental stress states, i.e. compressive, tensile and shearing stresses, and their variation regularities influenced by the main factors, and its strength and constitutive relation under the actions of multi-axial stress states. These are the basis for understanding and analyzing the various mechanical behaviors of reinforced concrete, which are presented in the succeeding parts and chapters.

The concrete discussed in this book is normally ordinate concrete mixed with Portland cement and natural coarse and fine aggregates. And its density and strength grade are 2200–2400 kg/m³ and C20–C50 respectively. Some other structural concretes and their main characteristics and mechanical behaviors will be introduced in Chapter 4.

Basic Mechanical Behavior

2

CHAPTER OUTLINE

2.1 Material composition and characteristic.....	10
2.1.1 Composition and internal structure	10
2.1.2 Basic characteristics	13
2.1.2.1 <i>Complicated internal micro stress and strain states and crack</i>	13
2.1.2.2 <i>Plural compositions of deformation</i>	14
2.1.2.3 <i>Influences of stress state and path</i>	16
2.1.2.4 <i>Influences of time factors and environmental conditions</i>	16
2.1.3 General mechanism of failure process	17
2.1.3.1 <i>Stage of relative stability ($\sigma/\sigma_{max} < 0.3-0.5$)</i>	18
2.1.3.2 <i>Developing stage of stable crack ($\sigma/\sigma_{max} < 0.75-0.9$)</i>	18
2.1.3.3 <i>Developing stage of unstable crack ($\sigma/\sigma_{max} > 0.75-0.9$)</i>	19
2.2 Compressive strength	19
2.2.1 Cubic compressive strength.....	19
2.2.2 Failure process of prism specimen	21
2.2.3 Main indices of mechanical behavior.....	24
2.3 Complete compressive stress–strain curve.....	28
2.3.1 Testing method	28
2.3.2 Equation for complete curve.....	29
2.4 Tensile strength and deformation	33
2.4.1 Testing method and index of tensile behavior.....	33
2.4.2 Tensile failure process and characteristic	39
2.4.3 Equation of complete stress–strain curve	42
2.5 Shear strength and deformation	44
2.5.1 Rational testing method	44
2.5.1.1 <i>Direct shear of short rectangular beam</i>	44
2.5.1.2 <i>Z shape specimen with single shear section</i>	45
2.5.1.3 <i>Four forces acted on the beam with notches</i>	46
2.5.1.4 <i>Torsional circular tube</i>	46
2.5.1.5 <i>Biaxial tension–compression</i>	46
2.5.2 Failure characteristic and shear strength	48
2.5.3 Shear strain and modulus	49

The actual stress state of concrete in a reinforced concrete structure varies significantly, hence its strength and deformation values are different. Obviously, the simplest and basic stress states are uniform uniaxial compression and tension. Although, the stress states in the concrete of simple structural members, i.e. beam, slab, and column, which are used most extensively in engineering practice, are not an ideal uniaxial compression or tension, the results of calculation using these values still satisfy the requirement of accuracy for structural engineering.

The strength and deformation behaviors of concrete under uniaxial compression and tension show clearly the mechanical characteristics, which are distinguished from other structural materials, e.g. steel, timber, and brick. These are the most important indices of mechanical behavior of concrete, and are not only used as the unique basis to define the strength grade of concrete, but also used as the main factor to determine other important behaviors and indices of concrete, e.g. elastic modulus, strain at peak stress, failure feature, ductility index, and multiaxial strength and strain [2-1].

2.1 Material composition and characteristic

The composite materials of concrete are cement, sand, gravel, and water, sometimes mixed with a small amount of various additives. These raw materials are successively mixed, cast, compacted, and cured, and gradually coagulated and hardened and, then, concrete is made. The compositions, properties, and relative ratio of these composite materials and the various conditions and environmental factors during manufacturing and hardening have considerable influences on the mechanical behavior of concrete. Therefore, concrete has more complicated and variable mechanical behavior, compared with other single structural materials, e.g. steel and timber.

2.1.1 Composition and internal structure

The main reason for concrete having complicated behavior is that concrete is a multiphase material of inhomogeneous and anisotropic and is varied with time and environmental conditions, as shown by the existing experimental investigation.

When a piece of concrete is sawn from a concrete structure, the internal non-uniform construction of concrete (Fig. 2-1(a)) can be seen by the naked eye and the main compositions contained are as below.

Solid granule — coarse aggregates of different colors, sizes, shapes, and mineral compositions, unhydrated cement lump, and various foreign substances, e.g. brick and wood pieces. They occupy most parts of the concrete volume and distribute randomly.

Hardened cement mortar — most fine aggregates (sand), cement and water are uniformly mixed and compose the cement mortar, which fills the gap between solid granules or surrounds the solid granules. The hardened cement in concrete forms an irregular and non-uniform strip or net structure.

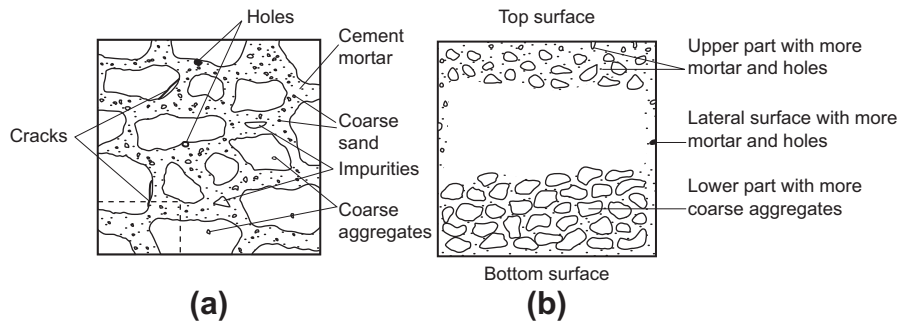


FIG. 2-1 Non-uniform distribution of composite materials in concrete

Holes and cracks — A small amount of air is blended into concrete during mixing and casting, and a part of it still remains in the cement mortar after the concrete is compacted and gets approximately into the shape of a circular hole. Most holes are placed in the surface layer of the concrete (Fig. 2-1(b)) and under the larger coarse aggregates and the reinforcement. In addition, the irregular fine cracks occur on the boundary between coarse aggregate and cement mortar and in the interior of cement mortar, because of evaporation of water and shrinkage of cement mortar during concrete coagulating. The structures of the hole will be introduced in detail in Section 20.1.3.

The two basic components of concrete, i.e. coarse aggregate and cement mortar, distribute randomly in its interior and they have considerable differences in their physical and mechanical behaviors (Table 2-1). These are the basic reasons for the inhomogeneous and anisotropic properties of concrete.

In addition, there are many other structural and environmental factors causing inhomogeneity and anisotropy of concrete. For example: the coarse aggregates of higher density and larger size sink to the bottom of concrete during casting and compacting, while the aggregates of lower density, blowing cement mortar, and air bubbles float up; more cement mortar and air holes exit near the side and top surface layers of structural member; water loss and moisture content are different in the outer and internal parts of a structure of large size, and the microcracks caused by the temperature difference there are also different; horizontal or other construction joint is, sometimes, necessary for the massive structure.

When a concrete is stressed in different directions, i.e. parallel, perpendicular, and inclined to its casting direction, its strength and deformation values are also different. For example, the cubic concrete specimen is loaded along the direction perpendicular to the casting direction according to the testing standard [2-3], the compressive strength measured is slightly lower than that measured when the load parallels the casting direction. In addition, when a concrete column is vertically cast, the property is symmetrical, theoretically, on any cross-section, but is different for the upper and lower sections; when the column is horizontally cast, the situations

Table 2-1 Typical Values of Physical and Mechanical Indices of Coarse Aggregates and Hardened Cement Mortar [2-2]

Behavior Indices	Compressive Strength N/mm^2	Tensile Strength N/mm^2	Modulus of Elasticity 10^4 N/mm^2	Poisson's Ratio	Density kg/m^3	Ultimate Shrinkage 10^{-6}	Specific Creep $10^{-6}/\text{Nmm}^{-2}$	Expansion Coefficient $10^{-6}/^\circ\text{C}$
Hardened Cement mortar	15–150	1.4–7	0.7–2.8	0.25	1700–2200	2000–3000	150–450	12–20
Coarse aggregate	70–350	1.4–14	3.5–7.0	0.1–0.25	2500–2700	Negligible	Negligible	6–12

are just opposite. Therefore, these two columns will have different strength and deformation when a load is acted.

The levels of inhomogeneity and anisotropy of concrete material mainly depend upon the homogeneous and steady state of raw materials, and the rigorous levels of production and management during construction. It directly influences the quality, i.e. technical index and scatter, of concrete.

2.1.2 Basic characteristics

The composition and internal structure of concrete material decide the four basic mechanical characteristics of it.

2.1.2.1 Complicated internal micro stress and strain states and crack

When a piece of concrete is magnified proportionally, it can be considered as an irregular three-dimensional solid structure composed of two main materials, i.e. coarse aggregate and hardened cement mortar, and is inhomogeneous, nonlinear, and uncontinuous. Complicated micro stress and strain states and cracks exist in the interior of concrete before it is loaded, and vary significantly after loading.

When the cement particles are hydrated during the coagulating process of concrete, the gelation is formed on its surface, and the cement mortar gradually gets thicker and hardened and coheres with the coarse aggregate into an integral solid. The cement mortar loses water in this process and its shrinkage is far greater than that of the coarse aggregate (Table 2-1). The difference of shrinkage strains causes the coarse aggregate compressed, cement mortar tensioned, and other stress distribution (Fig. 2-2(a)). The resultant of the stress field on the section should be zero, but the local stress may be considerable and causes microcracks on the boundary of aggregate [2-4].

The thermal behaviors, e.g. linear expansion coefficient, of coarse aggregate and hardened cement mortar are different as well (see Table 2-1). When the environmental temperature changes and the hydration heat generates in the concrete, the

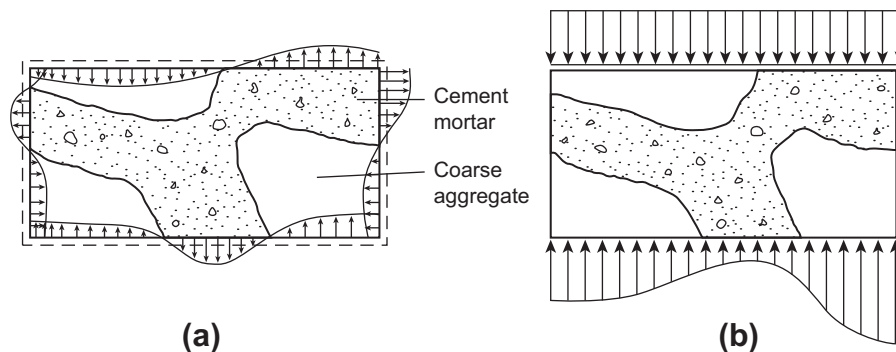


FIG. 2-2 Micro-stress distribution in the interior (a) caused by shrinkage and temperature differences (b) under action of uniform stress

difference of thermal strains of both components causes the thermal stress field due to the mutual confinement between them. And, because concrete is a thermo-inertial material (see Chapter 19), a larger temperature gradient occurs and the thermal stress is increased in the concrete structure.

When concrete is loaded from outside and even if the stress applied distributes uniformly, a spatial micro-stress field results non-uniformly in its interior (Fig. 2-2(b)) and mainly depends upon the area (volume) ratio, shape, arrangement, and moduli of elasticity of the coarse aggregate and cement mortar and the contact condition on their boundary. If the stress is sustained for a long period, the difference of the creeps of both components (Table 2-1) causes the stress redistribution in the interior of the concrete, and the coarse aggregate will support larger stress.

The internal air holes and microcracks are unavoidable in the interior of concrete, and the stress concentration areas are formed locally near their tips due to shrinkage, temperature variation, and stress acted. And, the stress on these areas distributes even more complicatedly with very high value.

All of these indicate that concrete has a very complicated and randomly distributed three-dimensional stress (strain) state from the microscopic point of view. This has important influence on the macroscopic behaviors of concrete, e.g. cracking, expansion of crack, deformation, ultimate strength and failure pattern.

2.1.2.2 Plural compositions of deformation

Concrete has to deform correspondingly when a stress is acted on it or the environmental condition changes. The deformation value of concrete is composed of three components shown below, according to its composition and structure characteristics.

Elastic deformation of aggregate The coarse and fine aggregates occupy most parts of concrete, and the values of their strength and moduli of elasticity are much greater than that of concrete (Table 2-1). Even when concrete reaches its ultimate strength, the aggregate in the concrete is not broken and its strain is kept in the elastic region, which means that the strain is directly proportional to the stress, the strain will reduce to zero and no residual strain exists after unloading (Fig. 2-3(a)).

Viscous flow of cement gelation The gelation is generated after hydration of the cement in concrete. It deforms instantaneously under the action of stress, and also its viscous flow (move) occurs slowly as the stress is sustained. So, the deformation of concrete continuously increases and the plastic deformation is formed (Fig. 2-3(b)). This part of concrete deformation will not reduce after unloading and the residual deformation appears.

Formation and expansion of crack The crack in concrete is formed perpendicular to the direction of tensile stress acted, and it exists only on the boundary of the coarse aggregate and in the interior of cement mortar. New cracks are formed and expanded gradually as the stress increases, so the tensile deformation of concrete increases quickly. When compressive stress is applied on the concrete, the longitudinal splitting crack occurs approximately in parallel with the stress and passes through the boundary of coarse aggregates and the interior of cement mortar. These cracks

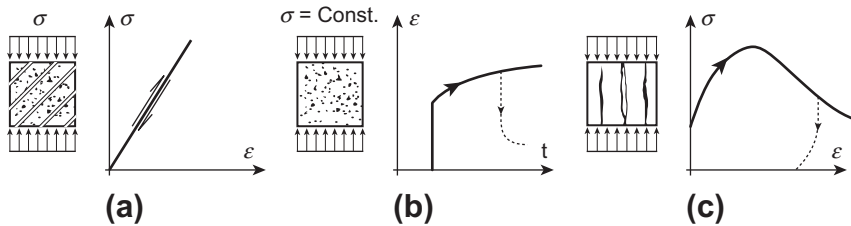


FIG. 2-3 Deformation components of concrete: (a) elastic deformation of aggregate, (b) viscous flow of cement gelation (c) formation and expansion of crack

increase, expand, and extend continuously as the stress increases, and finally the concrete is split into several small columns (Fig. 2-4) and its longitudinal deformation increases greatly. When the stress is decreased, still the deformation continuously increases, and most parts of the deformation can not recover after unloading (Fig. 2-3(c)).

The last two components of concrete deformation do not vary proportionally with the stress acted and most parts of them can not recover after being unloaded. They are generally considered as the plastic deformation of concrete.

The ratios among the three deformation components vary greatly for concretes of different raw materials, compositions, and stress levels acted. When the stress level acted on the concrete is lower, the total deformation of concrete is limited and the elastic deformation of the aggregate constitutes its majority. The deformation of concrete caused by the viscous flow of cement gelation accelerates gradually with the stress. The deformation caused by the crack appears obviously only when the concrete is approaching its ultimate strength, but it increases very quickly and soon exceeds two other components. After the stress passes its peak value and enters into the descending branch of the stress—strain curve, the elastic deformation of the aggregate starts to recover, the viscous flow of the cement gelation increases slowly, while the deformation caused by the crack increases considerably when the stress is decreased.

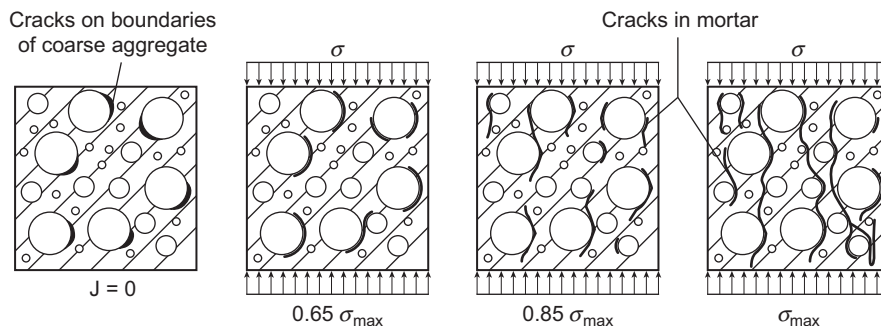


FIG. 2-4 Cracking process of concrete under uniaxial compression observed by X-ray camera [2-7]

2.1.2.3 Influences of stress state and path

The ratio between the strengths of concrete under uniaxial tensile and compressive stress states is about 1:10, while the ratio between the corresponding peak strains is about 1:20. In addition, the failure patterns of both stress states are essentially distinct (Section 2.4.2). These are obviously different from that of other structural materials, e.g. steel and timber, of which the tensile and compressive strengths and deformations are close.

Because of the significant difference of the mechanical behaviors of concrete under the two basic stress states, different stress states have great influences on the mechanical responses of concrete. The strength, deformation, and failure pattern of concrete under multiaxial stress state of different stress ratio vary considerably (Chapter 5). The transverse and longitudinal stress (strain) gradients have influence on the strength and deformation of concrete (Sections 3.2 and 3.3). When the load is acted repeatedly, the phenomena of strain retarded, stiffness degradation, and residual deformation of concrete yield at different levels (Section 3.1). When the stress paths (or histories) of multiaxial stress state are different, the development of internal microcracks and the confinement condition between the stresses acted on different directions are changed, different mechanical responses of concrete are present (Section 5.2.3).

The great influence of mechanical behavior of concrete caused by the different stress states is certainly decided by the characteristics and internal microstructure of concrete material. The difference of material property is sufficient to cause great influence on mechanical behaviors of concrete structure and its member. This should be paid attention to in engineering practice.

2.1.2.4 Influences of time factors and environmental conditions

Concrete comes to maturity as the hydration of the cement develops. It is demonstrated experimentally that the hydration of cement particles develops gradually from its surface layer into the interior and does not stop even after 20 years. As the maturity of concrete increases, the adhesive strength between the cement and aggregate increases as well, and the cement gelation gets thicker and its viscous flow is slower, so the values of the ultimate strength and modulus of elasticity of concrete gradually increase with time. However, on the other hand, the creep of concrete under stress caused by the viscous flow of cement gelation and the expansion of internal microcracks also increases with time, when the stress is sustained for a long period. Therefore, the deformations of concrete material and structure gradually develop and their long-term strengths have to be reduced.

The environmental condition surrounding the concrete has influences not only on its maturity, but also on the physical and chemical reactions with the concrete material, which may cause advantageous or disadvantageous results. The variations of environmental temperature and humidity cause variable and non-uniform temperature and humidity fields in the interior of concrete, and have influences on the speeds of cement hydration and water evaporation. Then, the stress and strain fields are formed correspondingly, and the development of internal microcracks

accelerates, macro-cracks even appear on the surface of concrete. The carbon dioxide in the environmental medium acts with the chemical composition of the cement, and a carbonization is formed near the surface of concrete and gradually gets thicker. Also, the chlorine ion in the environmental medium is corrosive to cement and reinforcement in concrete. Both force the durability deterioration of concrete structure (see Chapter 20).

Because these characteristics of concrete cause the complication, variation, and scatter of its mechanical behavior and the composition and property of its raw materials make a great difference, it is very difficult to find an accurate and applicable solution for the mechanical behavior of concrete structure, using totally microscopic and quantitative analysis.

On the other hand, from the structural engineering point of view, when a certain scale of concrete, e.g. about ≥ 70 mm and 3 or 4 times the coarse aggregate size, is considered as a basic element and to be a continuous, uniform, and isotropic material, and when the average values of strength and deformation and the macroscopic failure pattern are used, the relatively stable indices of the mechanical behavior of concrete can be obtained. In the meantime, the standard specimens of the same scale are used to measure the various mechanical behaviors, and the failure criteria and constitutive relations are established correspondingly. When they are used for calculation or design in the engineering practice, sufficient accuracy will be achieved.

Nevertheless, it is quite important to learn these basic characteristics of concrete for deeply understanding and applying various mechanical responses of concrete structure, and also it is helpful for studying the contents of the chapters later on.

2.1.3 General mechanism of failure process

Concrete shows obvious differences on the failure process and patterns under different stress states (Section 5.3). As concrete is mainly used as a compressive material in the structure and the uniaxial compression is the simplest state, the corresponding failure process and working mechanism of concrete are typical and have to be understood in detail. This is quite important and helpful for learning the essence of concrete property, explaining the various damage and failure phenomena of the structure and its members, and finding the measures to improve the quality of concrete and the behavior of concrete structure.

Usually, concrete is known as a fragile material, because it fails quickly under both compression and tension states and the failure process in its interior can not be observed by the naked eye. Now, modern science and technology are highly developed and have provided many progressive loading and measuring equipment for material and structure experiments. For example, the complete stress-strain curves of concrete under compression and tension can be easily recorded by the testing machine controlled by electro-hydraulic servo valve; the microstructure and its variation of concrete under stress can be observed and measured in detail by the ultrasonoscope, X-ray camera, and electron microscope [2-5].

Some experimental observations [2-6, 2-7] demonstrate that a small amount of microcracks exist separately in the interior of structural concrete even before loading, and the width and the maximum length of them are, generally, $(2-5) \times 10^{-3}$ mm and (1–2) mm, respectively. The main reason for this, as described above, is that a microstress field is caused in concrete due to the non-uniform temperature and humidity fields and the shrinkage difference between coarse aggregate and cement mortar during its coagulation. Because the adhesive strength on the boundary between coarse aggregate and cement mortar is only about 35–65% of the tensile strength of cement mortar itself [2-8,2-9] and the tensile strength of coarse aggregate is far higher than that of cement mortar, the microcrack has to appear first on the boundary of coarse aggregate and is called boundary adhesive crack, when the internal microtensile stress is large enough.

The development of the microcrack in the interior of concrete can be observed clearly during its loading process. The experimental results of a series of specimens, which are loaded to different stages, are shown in Fig. 2-4. The specimen used is of square plate (127 mm×127 mm×12.7 mm), it approaches the ideal planar stress state and is convenient to directly obtain the X-ray information of the crack during loading process. There are two kinds of specimens. The ideal specimen is made of circular aggregates of three sizes of diameter but same thickness (12.7 mm), which are randomly buried into the cement mortar (Fig. 2-4). Another kind of the specimen is made of practical concrete. The loading process and the observed results of both specimens are the same, but the former one is more typical.

It is experimentally demonstrated that the initial cracks exist in concrete before loading and occur on the boundaries of larger coarse aggregates. The microcracks gradually increase and expand from the start of loading until the ultimate load (σ_{\max}), and there are three stages as below.

2.1.3.1 Stage of relative stability ($\sigma/\sigma_{\max} < 0.3-0.5$)

As the compressive stress is still lower, the microcrack extends slightly along the boundary of the coarse aggregate because of the stress concentration at its tip, but some other microcracks and gaps in concrete partly close up because of the compressive stress. Both actions appearing together have no obvious influence on the macroscopic deformation of concrete. Even when the load is repeated several times or sustained, the microcrack will not develop much and the residual deformation of concrete is limited after unloading.

2.1.3.2 Developing stage of stable crack [2-10] ($\sigma/\sigma_{\max} < 0.75-0.9$)

When the stress is increased, the cracks existing on the boundaries of coarse aggregates gradually extend and expand and new cracks successively appear on other aggregate boundaries. Some cracks on the boundaries gradually develop into the cement mortar, and some microcracks occur near the holes and gaps in the cement mortar because of stress concentration. So, the microcrack and deformation of concrete accelerate within this stage. However, if the load is not increased again, the development of the microcrack will stagnate and the crack pattern is basically

kept. When the load is sustained for a long period, the deformation of concrete will increase, but no failure will happen.

2.1.3.3 Developing stage of unstable crack [2-10] ($\sigma/\sigma_{max} > 0.75-0.9$)

As the stress acted is somewhat higher, the cracks on the boundaries of coarse aggregates suddenly and considerably expand and extend into the cement mortar, and the cracks in the cement mortar develop rapidly and link with the adjacent cracks on aggregate boundaries. These cracks link up and compose several continuous cracks paralleling approximately to the direction of compressive stress, which is called the longitudinal splitting crack. If some of the coarse aggregates are of low strength or have certain joints or faults in it, they may also split under high stress. The stress increment is small at this stage, but the crack develops very quickly and the deformation of concrete increases considerably. Even if the stress is kept constantly, the crack is not stable any more and develops continuously. Finally, the longitudinal cracks connect and divide the specimen into several small columns, the load-carrying capacity of concrete reduces and its failure is caused.

According to the analysis of the microscopic phenomenon of concrete under compression, the failure mechanism of concrete can be summarized as below. Firstly, the microcracks are formed on the boundary between the coarse aggregate and cement mortar and also in the interior of the latter; these microcracks gradually expand and extend, and link up into macrocracks as the stress increases; the damage of the cement mortar continuously accumulates and breaks the linkage with the aggregate, the integrity of concrete is deteriorated and the strength of concrete gradually losses. When the concrete is acted with other stress states, the failure process is similar and will be introduced later.

The strength of concrete is far lower than that of the coarse aggregate in it (Table 2-1), generally, the crack and breakage in concrete occur only in the interior of the cement mortar, but no damage sign is shown on the aggregate. Therefore, the strength and deformation behavior of concrete depend upon, to a large extent, the quality and compactness of the cement mortar. Any measures for improving the quality of cement mortar can effectively increase the strength of concrete and enhance the behavior of the structure.

2.2 Compressive strength

2.2.1 Cubic compressive strength

According to the Chinese National Standard ‘Standard for test method of mechanical properties on ordinary concrete GB/T 50081-2002’ [2-3], the compressive strength of concrete is tested and measured successively as below. The standard specimen used is a cube of edge length 150 mm; the fresh concrete is cast into the steel mold and compacted, then the specimen is demolded one day later and kept in the standard curing room with temperature $(20 \pm 3)^{\circ}\text{C}$ and relation humidity $>90\%$. The specimen is taken out at the age of 28 days and the water on its

surface is wiped away, then the specimen is put on the working table of a testing machine and the compressive force is acted continuously until its failure, with a loading speed of $(0.3\text{--}0.5)\text{N/mm}^2$ per second, along the direction perpendicular to that of casting. The value of the maximum load measured is divided by the compressive area of the specimen, and the standard cubic compressive strength of concrete (f_{cu} , N/mm^2) is then obtained.

The compressive force is acted on the specimen via a steel plate during testing. Because the stiffness of the plate is limited and the stress states and material behaviors in the interior and near surface of the specimen are different, the vertical compressive stress distributes non-uniformly on the compressed surface of the specimen (Fig. 2-5(a)). In the meantime, the moduli of elasticity (E_s , E_c) and Poisson's ratios (ν_s , ν_c) of the steel plate and the concrete of the specimen are unequal, the transverse strains of them should be different under the same stress ($\nu_s\sigma/E_s < \nu_c\sigma/E_c$). Therefore, the steel plate restrains the transverse strain of the specimen, and the horizontal friction has to act on the compressed surface of the specimen (Fig. 2-5(b)).

These vertical and horizontal forces act simultaneously on the compressed surface of the specimen, a three-dimensional stress field has to form in it. Every point on the vertical central axis is obviously of tri-axial compressions, the point on the four vertical edges is nearly uniaxial compressions, the horizontal periphery on the compressed surface is of bi-axial compressions, the point on the vertical surface is of bi-axial compressions or compression-tension, and most points in the interior are of tri-axial compressions or compression-tension states (Fig. 2-5(c)). It should be noticed that these results are obtained when the specimen is considered as a homogeneous material. If the random composition and property of concrete are taken into account, the actual stress state of the specimen is even more complicated or asymmetrical.

When the specimen is loaded, the contractive and elongated deformations occur respectively in vertical and horizontal directions. The transverse deformations at the

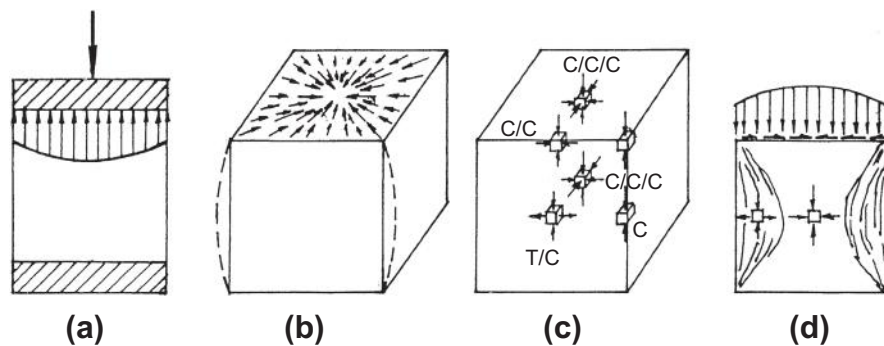


FIG. 2-5 Stress and deformation of cubic specimen under compression. (a) Stress distribution on compressed surface, (b) transverse deformation and restraint on end surface, (c) stress states at several points, (d) failure pattern

top and bottom surfaces of the specimen are quite small because of the restraint of the steel plate, while the transverse expansive deformation at the mid-height reaches the maximum (Fig. 2-5(b)). The deformation of the specimen gradually accelerates when the load or stress increases. The vertical crack appears first near the lateral surface at the mid-height of the specimen, and both ends of it extend up and down respectively and then turn towards the corners (Fig. 2-5(d)). New cracks appear successively and these cracks gradually develop from the surface layer into the interior, as the load increases. Finally, the concrete at the mid-height expands horizontally and starts to spall off, the specimen fails with the pattern of the regular and reverse pyramids.

When the specimens of different shapes and sizes, e.g. the cube of edge length 100 mm or 200 mm, and cylinder of $H/D=2$,¹ are used, the values of the compressive strength of concrete obtained from the testing are unequal because of different mechanical situation and size effect, although their failure process and pattern are the same. The compressive strengths of different specimens can be converted one another by Table 2-2, which are obtained from the comparative tests.

According to the stress and strain conditions of a cubic concrete specimen and its failure process and pattern, it is clear that uniform uniaxial compressive stress state is not established in the specimen tested following the standard method, so the measured result is also not the ideal uniaxial compressive strength of concrete. Of course, again, it can not represent the real compressive strength of the concrete in a practical structure, of which the stress state and the environmental condition vary considerably.

Nevertheless, the cubic compressive strength of concrete obtained from the standard test method is still a relative index of most importance. It can be used to qualify the strength grade of concrete, to evaluate and compare the manufactured quality of concrete, and to estimate and calculate other indices of mechanical behaviors of concrete. This is the technical significance.

In China, the concrete used in structural engineering is divided into different strength grades [2-1], i.e. from C15 to C80, and the difference between the adjacent grades is C5, which can be used for various structures or the different parts of a structure. The strength grade of a structural concrete is defined as the value of compressive strength of the cubic specimens measured under the standard test method [2-3] and with 95% probability.

2.2.2 Failure process of prism specimen

In order to eliminate the influences of the local stress and confined deformation near both ends of the cubic concrete specimen, the simplest way is to use the prism (or

¹The cylinder of height $H = 300$ mm (or 12 inches) and diameter $D = 150$ mm (or 6 inches) is used as the standard specimen for some countries, e.g. USA [2-11] and Japan, and the international academic organizations, e.g. CEB-FIP [2-12]. The measured strength from the testing is called cylinder compressive strength (f_c , N/mm²).

Table 2-2 Relative Values of Compressive Strengths of Concrete Specimens of Different Shapes and Sizes

Specimens	Cube [2-3]			Cylinder (H = 300 mm, D = 150 mm) [2-12]				
	Length (mm)			Strength grade				
	200	150	100	C20–C40	C50	C60	C70	C80
Relative values	0.95	1	1.05	0.80	0.83	0.86	0.875	0.89

cylinder) specimen for a compression test. According to the San Vincent principle, the vertical stress distributed non-uniformly and the horizontal stress, of which the resultant is zero, on the compressed surface have influence only on the local part, of which the height approximates to the width of the section, near the end of the specimen. Therefore, the middle part of the prism is approaching the uniform uniaxial compressive stress state (Fig. 2-6(a)). It is also demonstrated experimentally that the failure occurs only in the mid-height of the prism specimen. When the ultimate load is divided by the section area of the specimen, the prism compressive strength or central compressive strength of concrete (f_c) is obtained [2-1,2-3].

The experimental results show that the prism compressive strength of concrete reduces monotonically as the height–width ratio of the specimen increases, but it varies limitedly when $h/b \geq 2$ (Fig. 2-6 (b)). Therefore, the size of the standard prism specimen is taken as 150 mm×150 mm×300 mm, and the manufacture, cure, age at loading, and test method of it are the same as that of the standard cubic specimen of concrete.

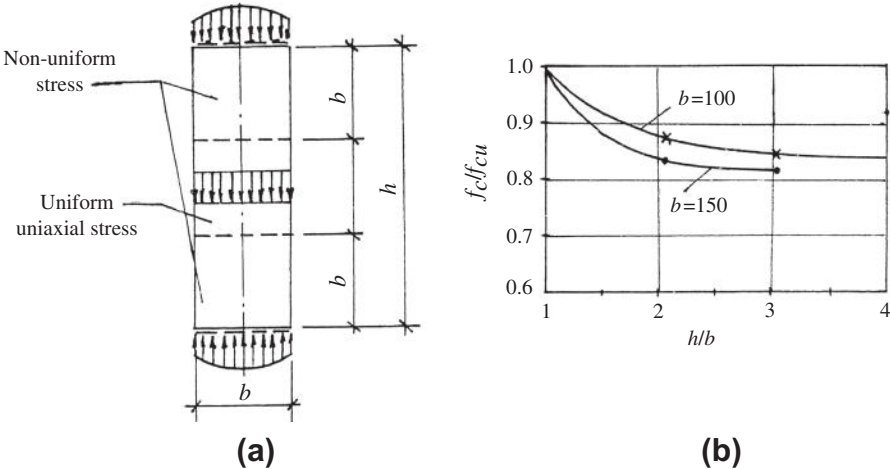


FIG. 2-6 Compression test of prism specimen: (a) stress distributions, (b) influence of height–width ratio

After the longitudinal and transverse strains (ϵ , ϵ') of the prism specimen are measured during the compression test, the complete compressive stress–strain (σ – ϵ) curve and the curves of the secant or tangent Poisson's ratio ($\nu_s = \epsilon'/\epsilon$, $\nu_t = d\epsilon'/d\epsilon$) and the volume strain ($\epsilon_v \approx \epsilon - 2\epsilon'$) can be plotted down. The typical variations of these curves are shown in Fig. 2-7. In addition, the appearance and development process of the macrocracks occur on the surface and the failure process of the specimen can be observed carefully during testing.

When the stress is still lower ($\sigma < 0.4 f_c$, point A in Fig. 2-7) after loading, the strain of the specimen increases almost proportionally. As the stress increases further, the plastic deformation and microcrack of concrete slightly develop and the strain gradually accelerates, so the slope of the stress–strain curve gradually decreases. The Poisson's ratio of the concrete is $\nu_s = 0.16$ – $0.23 < 0.5$ at this time, the volume strain of the concrete (ϵ_v) is contractive, but the variation rate of it decreases as the stress increases.

When the stress of the specimen reaches $\sigma \approx (0.8$ – $0.9) f_c$, the strain is $(0.65$ – $0.86) \epsilon_p$ (point B), the tangent Poisson's ratio is $\nu_t = 0.5$, and the contractive volume strain reaches the maximum and the volume will not reduce again. It shows that the internal microcrack in concrete expands, but no visible crack appears on its surface. Afterwards, the unstable crack (Section 2.1.3) forms in concrete, the strain and Poisson's ratio accelerate, and the contractive volume strain starts to recover. When the stress increases slightly, the peak point (C) of the curve arrives soon. When the deformation (strain) of the specimen increases further, the stress has to reduce and a descending branch of the curve is formed. The stress value at the peak point is the prism compressive strength of concrete (f_c), and the corresponding strain is called as peak strain (ϵ_p).

Soon after the stress–strain curve enters into the descending branch and the stress and strain reach $\epsilon = (1 \sim 1.35) \epsilon_p$ and $\sigma = (1 \sim 0.9) f_c$ respectively (point D), the first crack is visible on the surface at mid-height of the specimen. This crack is fine and short and parallels to the direction of the compressive stress. At this moment, the secant Poisson's ratio and volume strain of the concrete are $\nu_s \approx 0.5$

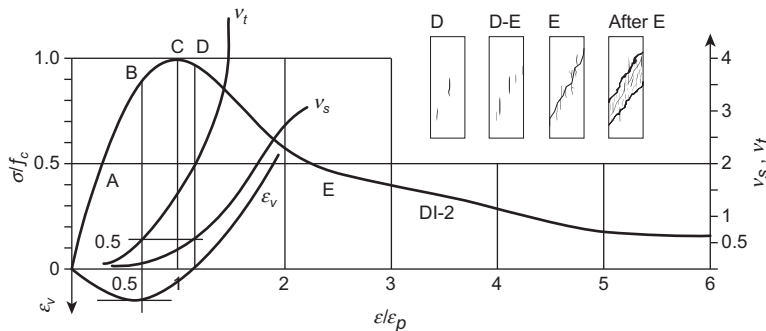


FIG. 2-7 Compressive deformation and failure process of prism concrete specimen [2-13]

and $\varepsilon_v \approx 0$ respectively. It means that the volume caused by the expansions of the crack and microcracks inside has compensated the contractive deformation of concrete that previously occurred.

As the strain of the specimen increases continuously, several short cracks occur successively and separately in the longitudinal direction, the transverse strain (ε'), Poisson's ratio ($\nu_s \approx 0.5$), and volume strain (ε_v) increase much quicker, but the stress of concrete reduces quickly. The adhesive cracks on the aggregate boundary and the cracks in the interior of cement mortar in concrete gradually expand, extend, and are connected together. Eventually, a macroscopic inclined crack is formed along the weakest plane and runs through the whole section (point E). At this situation, the strain of the specimen is about $\varepsilon = (2-3) \varepsilon_p$ and the residual strength of the concrete is $(0.4-0.6) f_c$.

When the strain of the specimen increases further, the inclined crack is gradually widened under the actions of normal compressive and shear stresses and becomes a damaged belt, but the cracks on other parts of the specimen, generally, do not develop again. The load on the specimen is resisted by the friction and residual adhesive strength on the inclined plan, so the residual strength of concrete decreases slowly. It is about $(0.2-0.3) f$ when the strain reaches $\varepsilon = 6 \varepsilon_p$, and will not totally lose under even larger strain.

The angle between the macroscopic, inclined failure plan of the specimen and the line perpendicular to the load is about $\theta = 58^\circ - 64^\circ$ [2-13]. When the failed specimen is separated into two pieces, it is found that the failure plan passes through the aggregate boundary and the interior of the cement mortar, and only very few coarse aggregates of rock are broken.

It should be noticed that the failure phenomenon of the macroscopic inclined crack of the compressive prism concrete specimen occurs only when the strain exceeds twice the peak strain ($\varepsilon > 2 \varepsilon_p$), i.e. on the descending branch of the complete stress-strain curve. Therefore, it is a post-failure pattern, and it has influence only on the residual strength and deformation of the concrete but is not related to the prism compressive strength (f_c) and the ascending branch of the curve. When the concrete reaches its prism strength, the longitudinal, or splitting, cracks dominate in the specimen and divide it into small separate columns (Fig. 2-4) which control the strength of concrete.

2.2.3 Main indices of mechanical behavior

The compressive test of prism concrete is widely conducted and numerous results are reported at home and abroad. However, the experimental results are scattered to some extent because of the differences of the raw materials and compositions of the concretes and the testing and measuring methods and equipment used.

The prism compressive strength of concrete increases monotonically with the cubic compressive strength (Fig. 2-8), and the ratio between them varies in the range of

$$\frac{f_c}{f_{cn}} = 0.70 \sim 0.92 \quad (2-1)$$

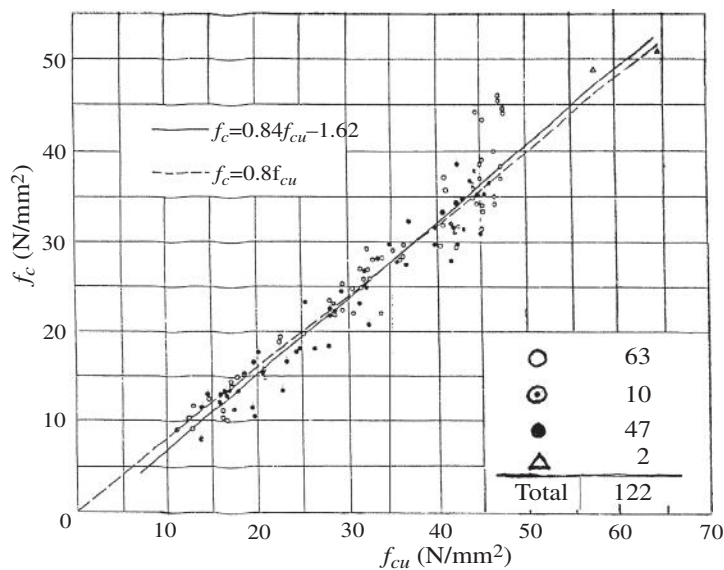


FIG. 2-8 Prism and cubic compressive strengths of concrete [2-14]

The higher the strength grade of concrete (or f_c), the greater the ratio. Several formulas, e.g. Table 2-3, or certain values, generally between 0.78 and 0.88, are given by different researchers. And, the slightly lower values of it are used in the design codes of different countries, considering the safety of the structure. For example, the design value of the compressive strength is taken as $f_c = 0.76 f_{cu}$ for the concrete of strength grade $\leq \text{C50}$, in the Chinese design code [2-1].

Although the peak strain ϵ_p , corresponding to the ultimate compressive strength of prism concrete (f_c), varies to some extent [2-15], it is also obvious that it increases monotonically with the strength (f_c or f_{cu}) of concrete (Fig. 2-9). Various empirical formulas are suggested, e.g. listed in Table 2-4, by the researchers. Analyzing the

Table 2-3 Calculation Formulas for Prism Compressive Strength of Concrete		
From	Calculation Formula	Reference
Germany (Graf)	$f_c = \left(0.85 - \frac{f_{cu}}{172}\right) f_{cu}$	[1-1]
Russia (Gvozdev)	$f_c = \frac{130 + f_{cu}}{145 + 3f_{cu}} f_{cu}$	[1-1]
China	$f_c = 0.84f_{cu} - 1.62$ $f_c = 0.8f_{cu}$	[2-14], Fig. 2-8

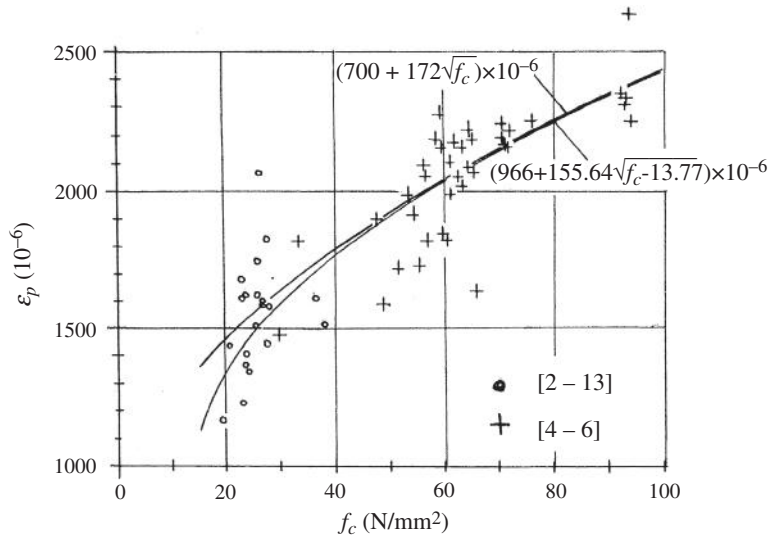


FIG. 2-9 Peak strain and prism compressive strength of concrete [1-2]

experimental data of the concrete strength $f_c = 20 \sim 100 \text{ N/mm}^2$, the formula provided in the reference [1-2] is:

$$\varepsilon_p = (700 + 172\sqrt{f_c}) \times 10^{-6}, \quad (2-2)$$

where f_c -prism compressive strength of concrete in N/mm^2 .

The peak strain of the concrete of strength grade C20 to C50, usually, is taken as a constant, e.g. $\varepsilon_p = 2000 \times 10^{-6}$ [2-11, 2-12], in the design codes of some countries. This value is slightly higher than the experimental datum, but it is compensated for by the advantage factors, such as strain gradient (Section 3.2) and confinement of

Table 2-4 Calculation Formulas for Compressive Peak Strain of Concrete [2-15]

Suggested by	Calculation Formula $\varepsilon_p (10^{-3})$
Ros	$\varepsilon_p = 0.546 + 0.0291f_{uc}$
Emperger	$\varepsilon_p = 0.232\sqrt{f_{cu}}$
Brandtzaeg	$\varepsilon_p = \frac{f_{cu}}{5.97 + 0.26f_{cu}}$
Hungry	$\varepsilon_p = \frac{f_{cu}}{7.9 + 0.395f_{cu}}$
Saenz	$\varepsilon_p = (1.028 - 0.108\sqrt[4]{f_{cu}})\sqrt[4]{f_{cu}}$
Lin-Wang	$\varepsilon_p = 0.833 + 0.121\sqrt{f_{cu}}$

stirrups (Section 9-2), when it is used in the design or analysis of a concrete structure and its members.

The modulus of elasticity is a main index for the deformation behavior of a material. The compressive stress—strain curve of concrete is certainly non-linear, so the modulus of elasticity, or modulus of deformation, of concrete varies continuously with the stress or strain. When the equation of the stress—strain curve is determined (Section 2.3), the secant or tangent modulus ($E_{c,s} = \sigma/\epsilon$, $E_{c,t} = d\sigma/d\epsilon$) of concrete can be calculated easily.

Sometimes, a calibrated value of the modulus of elasticity of concrete (E_c) is needed for comparing the deformation behaviors of different concretes, calculating elastically the deformation of a structure, or determining the relevant ratio between the reinforcement and concrete. Generally, the value is defined as the secant modulus of elasticity of concrete at stress $\sigma = (0.4-0.5)f_c$ on the stress—strain curve, which is about the working stress of the concrete in a structure under service load.

Many experimental results show that the modulus of elasticity of concrete increases monotonically with its strength (f_{cu} or f_c), but with certain scatter (Fig. 2-10). There are several empirical formulas listed in Table 2-5, which may be used for reference.

The transverse strain (ϵ') and Poisson's ratio (ν_s , ν_t) of concrete are also measured during the testing, but it is considerably influenced by the appearance and development of the longitudinal crack and the measuring position. It significantly deviates especially when the stress—strain curve enters the descending branch ($\epsilon > \epsilon_p$). At the beginning of loading, the value of Poisson's ratio of concrete is about

$$\nu_s = \nu_t = 0.16 \sim 0.23, \quad (2-3)$$

and usually it is taken as 0.20. After the unstable crack is formed in the interior of concrete ($\sigma > 0.8f_c$), the Poisson's ratio accelerates quickly and $\nu_t \gg \nu_s$.

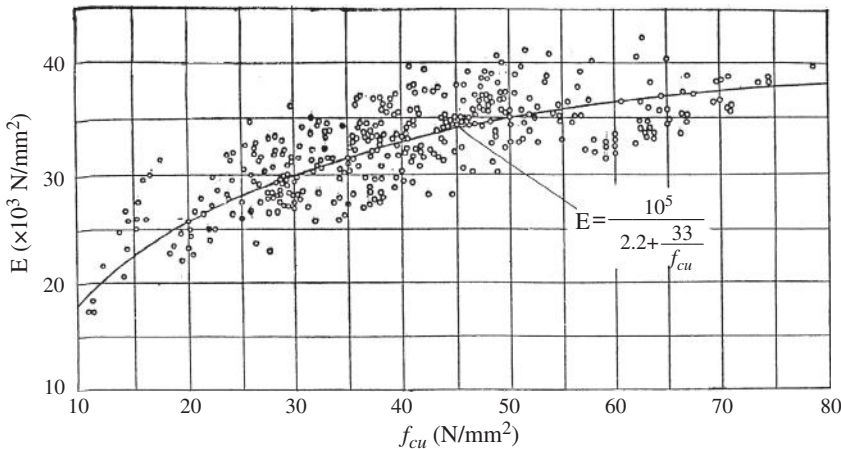


FIG. 2-10 Modulus of elasticity and cubic compressive strength of concrete [2-14]

Table 2-5 Calculation Formulas for Modulus of Elasticity of Concrete

Suggested by	Formula E_c (N/mm ²)
CEB-FIP MC90	$E_c = \sqrt[3]{0.1f_{cu} + 0.8} \times 2.15 \times 10^4$
ACI 318-95	$E_c = 4234\sqrt{f_{cu}}^*$
Russia	$E_c = \frac{10^5}{1.7 + (36/f_{cu})}$
China [2-1]	$E_c = \frac{10^5}{2.2 + (34.7/f_{cu})}$
* Original formula is $E = 57000\sqrt{f_c}$ in lb/in ² .	

2.3 Complete compressive stress—strain curve

The complete compressive stress—strain curve of concrete includes the ascending and descending branches, and it comprehensively reflects the macroscopic mechanical behavior of concrete. The maximum stress at the peak point on the curve is the prism compressive strength, the corresponding strain is the peak strain, the secant and tangent slope of the curve is the modulus of elasticity (or deformation) and the initial slope is the initial modulus of elasticity, the descending branch shows the residual strength after peak stress, the shape and the area under the curve represent the ability of plastic deformation of concrete, and etc.

The equation of compressive stress—strain curve of concrete is the basic constitutive relation and also the basis for multiaxial constitutive relation of concrete. It is a physical relation which is necessary for non-linear analyses of reinforced concrete structure, including the sectional stiffness of a structural member, ultimate stress distribution on the section, ultimate strength and ductility, redistribution of internal forces of statically indeterminate structure. It dominates the accuracy of the calculated result.

2.3.1 Testing method

When the prism concrete specimen is tested compressively on an ordinary hydraulic testing machine, the ascending branch of the stress—strain curve can be measured without difficulty. However, when the ultimate strength (f_c) is reached, the specimen suddenly fails and the effective descending branch of the curve can not be obtained.

Whitney [2-16] pointed out earlier that the reason why the compressive specimen fails suddenly is that the machine is not stiff enough. The machine deforms itself and the elastic strain energy gradually accumulates in it when it exerts a compression on the specimen. The deformation of the machine will recover soon as the ultimate strength of the specimen, and also the compression of the machine, suddenly decreases, and the energy instantaneously released causes the sudden failure of the specimen.

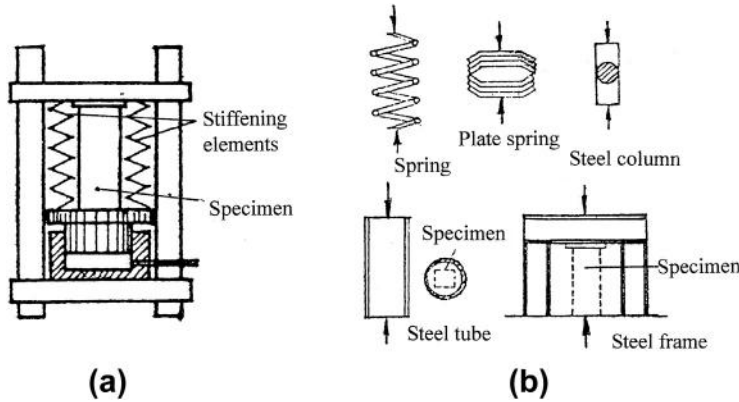


FIG. 2-11 Testing method of adding stiffening element [2-18,2-19]: (a) scheme, (b) various stiffening elements

In order to obtain a stable complete stress—strain curve, especially its descending branch, the deformation of the specimen should be controlled and its sudden failure should be prevented. There are two kinds of the testing method now:

1. A stiff testing machine controlled by the electro-hydraulic servo valve can be directly used for the loading test with constant strain rate of the specimen [2-17].
2. A stiffening element is added on the ordinary hydraulic testing machine (Fig. 2-11(a)) and let the total stiffness of the testing equipment be higher than the maximum linear stiffness of the specimen on the descending branch. Then, the sudden failure of the concrete specimen is prevented during testing. The relevant theoretical analysis can be found in reference [1-2].

The latter one is simple and less expensive. Various kinds of stiffening elements (Fig. 2-11(b)) are used by the different researchers, and the complete compressive stress—strain of concrete is successfully measured within different scopes. The hydraulic jack is designed as the stiffening element in Tsinghua University (Fig. 2-12) [2-20], and it has the advantages of the higher total stiffness of the equipment and the larger deformation measured.

2.3.2 Equation for complete curve

The complete compressive stress—strain of concrete is converted into the dimensionless coordinates:

$$x = \frac{\varepsilon}{\varepsilon_p} \quad \text{and} \quad y = \frac{\sigma}{f_c}, \quad (2-4)$$

and all the geometrical characteristics of the typical curve shown in Fig. 2-13 are described mathematically as below.

1. $x = 0, y = 0$;
2. $d^2y/dx^2 < 0$ when $0 \leq x < 1$, i.e. the slope of the curve (dy/dx) decreases monotonically and no point of inflection appears;
3. $y = 1$ and $dy/dx = 0$ when $x = 1$, i.e. single peak point only;
4. $x_D > 1$ when $d^2y/dx^2 = 0$, i.e. one point of inflection (point D) appears on the descending branch;
5. $x_E > 1$ when $d^3y/dx^3 = 0$, i.e. the point with the maximum slope (point E) appears on the descending branch;
6. $y \rightarrow 0$ and $dy/dx = 0$ when $x \rightarrow \infty$;
7. Every point on the complete curve $x \geq 0$ and $1 \geq y \geq 0$ (2-5).

These mathematical characteristics have definite physical meanings and correspond to the different phenomena during the deformation and failure processes of the prism concrete specimen.

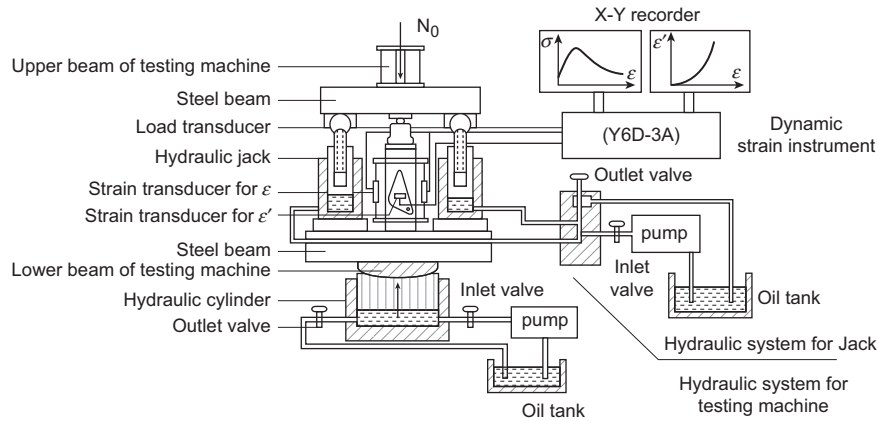


FIG. 2-12 Testing method using hydraulic jack as stiffening element

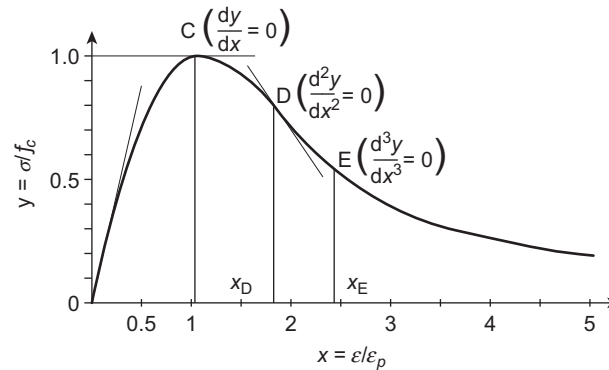


FIG. 2-13 Complete compressive stress-strain curve of concrete

The empirical equations of various mathematic functions, such as polynomial, exponential, trigonometric, and rational fraction functions (Table 2-6), have been suggested to accurately simulate the experimental curve by many researchers [2-21–2-24]. The ascending and descending branches of the curve are simulated by a single function or the separate functions. The simple and practical equations among them are shown in Fig. 2-14, and their mathematic functions can be found in Table 2-6 (the equations of Kent-Park are shown in Eq. (9-15)).

The separate equations of the stress–strain curve:

$$\left. \begin{array}{l} x \leq 1 \quad y = \alpha_a x + (3 - 2\alpha_a)x^2 + (\alpha_a - 2)x^3 \\ x \geq 1 \quad y = \frac{x}{\alpha_d(x-1)^2 + x} \end{array} \right\} \quad (2-6)$$

are suggested in references [2-13, 2-20] and adopted in the design code [2-1]. The ascending and descending branches are continued at the peak point and satisfy all the requirements of the geometrical characteristics of the curve (Eq. (2-5)). There

Table 2-6 Equations for Complete Compressive Stress–Strain Curve of Concrete		
Kind of Function	Mathematic Expression	Suggested by
Polynomial	$\sigma = c_1 \varepsilon^n$	Bach
	$y = 2x - x^2$	Hognestad
	$\sigma_1 = c_1 \varepsilon + c_2 \varepsilon^n$	Sturman
	$\varepsilon = \frac{\sigma}{E_0} + c_1 \sigma^n$	Terzaghi
	$\varepsilon = \frac{\sigma}{E_0} + c_1 \frac{\sigma}{c_2 - \sigma}$	Ros
	$\sigma^2 + c_1 \varepsilon^2 + c_2 \sigma \varepsilon + c_3 \sigma + c_4 \varepsilon = 0$	Kriz-Lee
Exponential	$y = x e^{1-x}$	Sahlin et al
	$y = 6.75(e^{-0.812x} - e^{-1.218x})$	Umemura
Trigonometric	$y = \sin(\frac{\pi}{2}x)$	Young
	$y = \sin[\frac{\pi}{2}(-0.27 x-1 + 0.73x + 0.27)]$	Okayama
Rational fraction	$y = \frac{2x}{1+x^2}$	Desayi et al
	$y = \frac{(c_1+1)x}{c_1+x^n}$	Tulin-Gerstle
	$\sigma = \frac{c_1 \varepsilon}{[(\varepsilon + c_2)^2 + c_3]} - c_4 \varepsilon$	Alexander
	$y = \frac{x}{c_1 + c_2 x + c_3 x^2 + c_4 x^3}$	Saenz
	$y = \frac{c_1 x + (c_2 - 1)x^2}{1 + (c_1 - 2)x + c_2 x^2}$	Sargin
Separate functions	Ascending ($0 \leq x \leq 1$)	Descending ($x \geq 1$)
	$y = 2x - x^2$	$y = 1 - 0.15(x-1)/(x_u-1)$
	$y = 2x - x^2$	$y = 1$

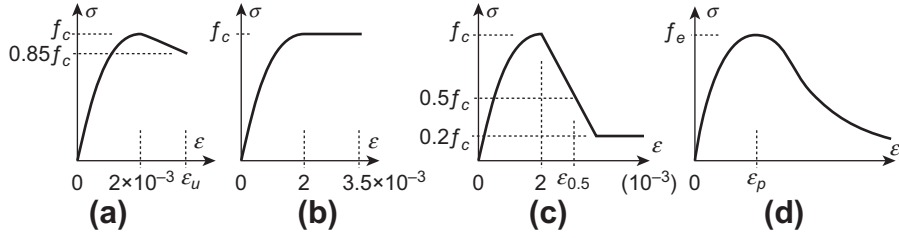


FIG. 2-14 Several theoretical curves: (a) Hognested (b) Rüs ch (c) Kent-Part (d) Sargin, Saenz

is only one parameter, having certain physical meaning, for each function of both branches.

The parameter for the ascending branch is:

$$\left. \begin{aligned} \alpha_a &= \frac{dy}{dx} \Big|_{x=0} \\ 1.5 &\leq \alpha_a \leq 3.0 \end{aligned} \right\}. \quad (2-7)$$

Its value represents the ratio between the initial modulus of elasticity (E_0) and the secant modulus at the peak point ($E_p = f_c / \epsilon_p$), i.e. $\alpha_a = E_0 / E_p = E_0 \epsilon_p / f_c$. When $\alpha_a = 2$, Eq.(2-6) degenerates into the polynomial of second order $y = 2x - x^2$ and is the same as that suggested by Hognestad.

The parameter for the descending branch is:

$$0 \leq \alpha_d \leq \infty. \quad (2-8)$$

when $\alpha_d = 0$, $y \equiv 1$, i.e. a horizontal line after the peak point (total plasticity), and when $\alpha_d = \infty$, $y \equiv 0$, i.e. a vertical line under the peak point (total fragility).

When the parameters α_a and α_d are given different values, the theoretical curves vary correspondingly (Fig. 2-15). When the appropriate values are selected, the theoretical curve fits well with the experimental result for the structural concretes of different raw materials and strength grades, even for the confined concrete. The

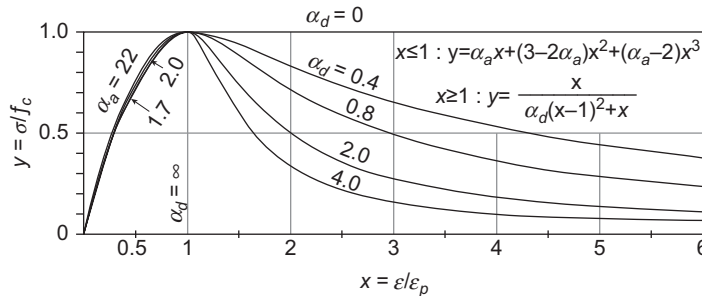


FIG. 2-15 Theoretical stress—strain curve [2-13]

Table 2-7 Parameter Values for the Equations of Complete Stress–Strain Curve

Strength Grade	Grade of Cement Used	α_a	α_d	ϵ_p (10^{-3})
C20, C30	32.5	2.2	0.4	1.40
	42.5	1.7	0.8	1.60
C40	42.5	1.7	2.0	1.80

parameter values suggested by reference [2-13] are listed in [Table 2-7](#) and can be used for the structural analysis and design.

2.4 Tensile strength and deformation

The tensile strength and deformation are also the important basic behavior of concrete. It is the main basis for studying its failure mechanism and strength theory (failure criterion), and has direct influences on the cracking, deformation, and durability of reinforced concrete structures.

Usually, concrete is considered as a fragile material of lower tensile strength, few deformation, and sudden failure. Before the 1960s, the research and knowledge of tensile behavior of concrete was not complete, and was limited only on the ultimate strength and the ascending branch of the stress–strain curve. As the experimental technique was improved afterwards, the measurement of the complete tensile stress–strain curve of concrete was achieved [2-25–2-29]. Then, the characteristics of tensile strength and failure process of concrete are realized deeply, and this helps to analyze accurately and comprehensively reinforced concrete structure.

2.4.1 Testing method and index of tensile behavior

There are three testing methods ([Fig. 2-16](#)) for measuring the tensile strength of concrete, and different values of tensile strength are given respectively.

The central tensile strength of concrete is obtained from the central tensile test of the prism specimen:

$$f_t = P/A. \quad (2-9)$$

The splitting tensile strength is obtained from the splitting test of the cubic specimen:

$$f_{t,s} = \frac{2P}{\pi A} \quad (2-10)$$

where P is the ultimate load of the corresponding specimen, and A is the area of the broken section of the specimen.

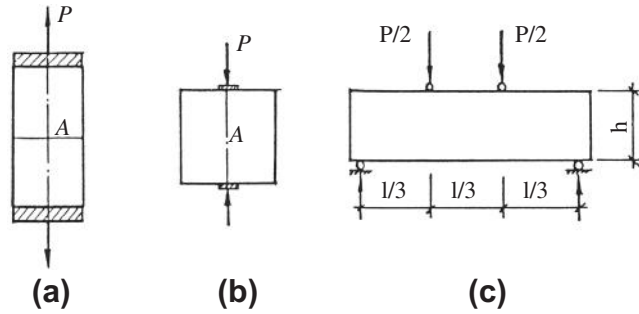


FIG. 2-16 Testing methods for tensile strength: (a) central tension, (b) splitting, (c) bending

And, the modulus of rupture (or flexural tensile strength) of concrete is obtained from the bending test of the prism beam:

$$f_{t,f} = \frac{6M}{bh^2} = \frac{Pl}{bh^2}. \quad (2-11)$$

In order to measure the tensile stress—strain curve of concrete, the central tensile test should be conducted, as the tensile stress distributes clearly and uniformly on the cross-section of the specimen, and the strain gauges and displacement transducers are easily placed. In addition, the descending branch of the complete tensile stress—strain curve can be measured only using the stiff testing machine controlled by electro-hydraulic servo valve or installing the stiffening element to increase the total stiffness of the testing equipment (similar to Section 2.3.1). A simple and practical method introduced in reference [2-29] has successfully measured the complete tensile stress—strain curve of concrete. An ordinary hydraulic testing machine is only used for this method, but a stiff frame composed of steel beams and bars (Fig. 2-17) is installed and paralleled to the prism specimen of concrete.

A large amount of tensile tests of concrete have been conducted in China [2-14] and the indices of the main mechanical behaviors of concrete are given as below.

Central tensile strength The central tensile strength of concrete increases monotonically with the cubic compressive strength but with reducing rate (Fig. 2-18). The empirical formula [1-5] obtained from the regression analysis is

$$f_t = 0.26 f_{cu}^{2/3}. \quad (2-12)$$

It is approaching the formula given in CEB-FIP Model Code [2-12]:

$$f_t = 1.4(f'_c/10)^{2/3}, \quad (2-13)$$

where f_{cu} and f'_c are the cubic and cylinder compressive strength respectively of concrete in N/mm^2 .

The experimental results also show that the measured tensile strength of the specimen of smaller size is higher than that of larger size [2-14]. Generally, it is induced

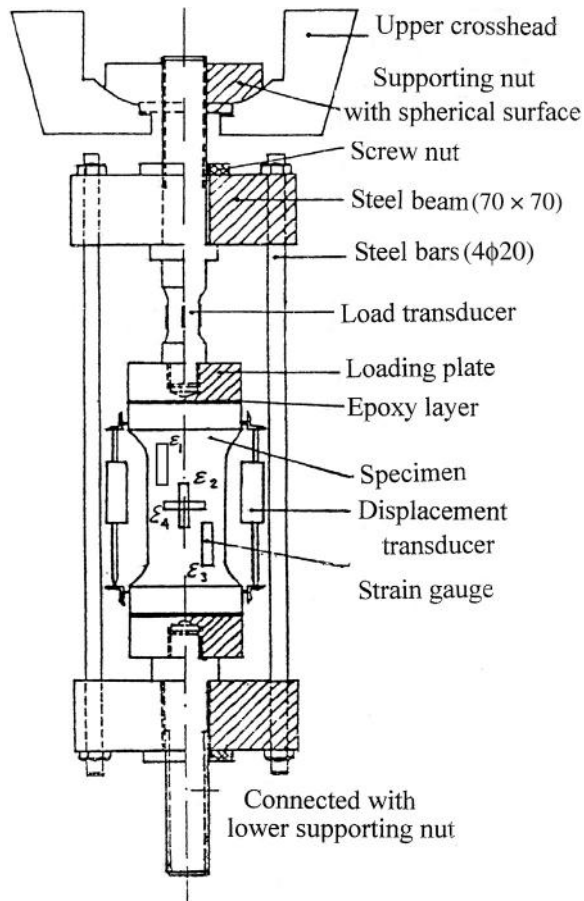


FIG. 2-17 Scheme of complete tensile stress—strain curve test [2-29]

as the size effect. For example, the dam concrete of a hydraulic engineering is tested using the prism specimens of different sizes:

1. 450 mm×450 mm×1400 mm and the maximum size of the aggregate being (80–120) mm;
2. 100 mm×100 mm×550 mm and the maximum size of the aggregate being (20–40) mm.

It is concluded after testing that the central tensile strength of the larger specimen is only (50–64)%, or 57% on the average, of that of the smaller specimen.² It is

²Jinyu Li et al. Investigation of influence of specimen size on strength and deformation characteristics of dam concrete. Beijing: Research Institute of Hydraulic and Electric Power of China, 1996.

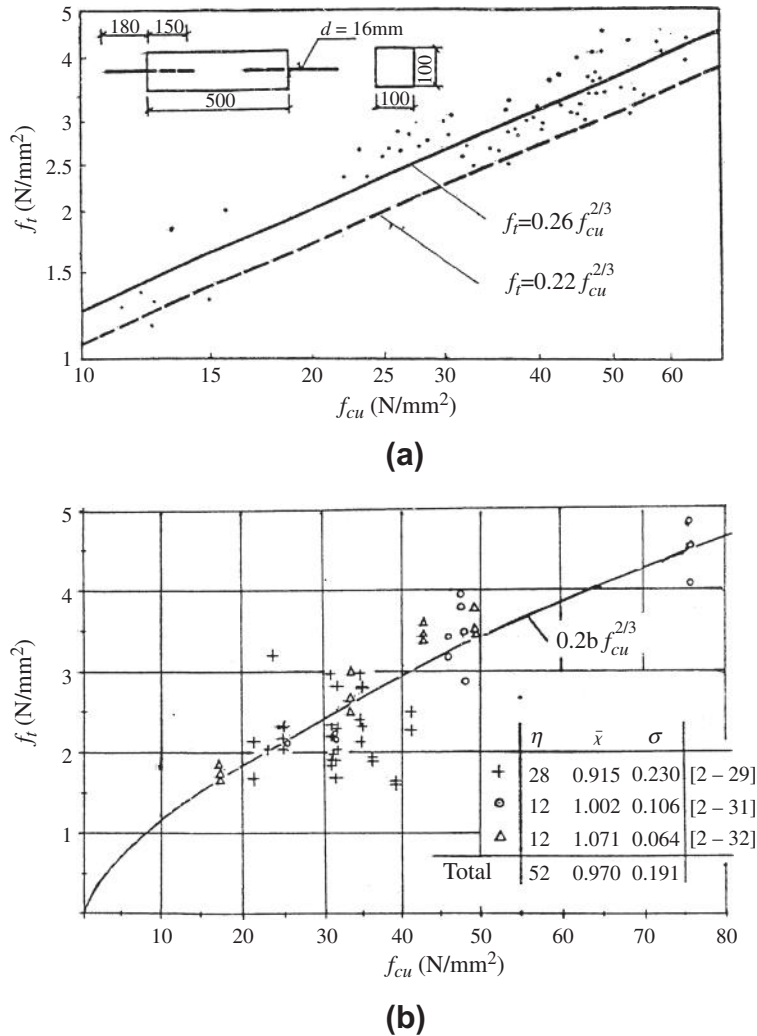


FIG. 2-18 Central tensile strength and cubic compressive strength of concrete: (a) Reference [2-14] (b) Reference [1-2]

caused mainly because of larger probabilities of the crack and defect in interior, severe initial stress condition, and worse adhesion on the boundary of the aggregate for the former. These factors sensitively influence the tensile strength and deformation of concrete.

Splitting tensile strength The splitting test is easily performed and only the standard cubic specimen is used, so it is used most widely. The splitting tensile

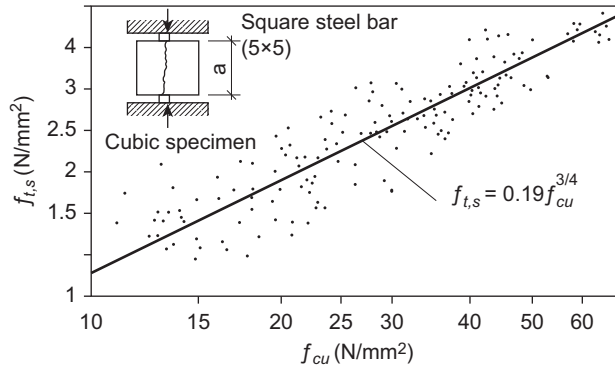


FIG. 2-19 Splitting tensile strength and cubic compressive strength of concrete [2-14]

strength of concrete measured is related to the cubic compressive strength (Fig. 2-19) and the empirical formula [2-14] is:

$$f_{t,s} = 0.19f_{cu}^{3/4} \quad (2-14)$$

It should be noticed that the central tensile strength of concrete is slightly higher than the splitting tensile strength of same concrete:

$$f_t/f_{t,s} = 1.368f_{cu}^{-0.083} = 1.09 \sim 1.0 \text{ when } f_{cu} = 15 \sim 43 \text{ N/mm}^2,$$

according to the experimental results and calculation formulas provided above. However, the opposite conclusion is given by a similar test conducted in some other countries: $f_t = 0.9f_{t,s}$ [2-12]. The contradictory conclusions occur possibly because of the differences between both testing methods: the cubic specimen and square steel loading bars are used for the test in China, while the cylinder specimen and loading bars of softer material (e.g. bakelite) are used in other countries.

Tensile peak strain The strain corresponding to the central tensile strength (f_t) of concrete specimen is the tensile peak strain ($\epsilon_{t,p}$) on the complete stress-strain curve. It increases with the tensile strength (Fig. 2-20) and the calculation formula suggested in reference [1-2] is:

$$\epsilon_{t,p} = 65 \times 10^{-6} f_t^{0.54}. \quad (2-15a)$$

When Eq. (2-12) is substituted into the formula, the relation between the tensile peak strain and the cubic compressive strength of concrete (f_{cu} in N/mm^2) is obtained:

$$\epsilon_{t,p} = 3.14 \times 10^{-6} f_{cu}^{0.36} \quad (2-15b)$$

Modulus of elasticity The nominal value of tensile modulus of elasticity of concrete is taken as the secant slope at the stress $\sigma = 0.5f_t$ on the ascending branch of the stress-strain curve. It is approximately equal to the value of the compressive

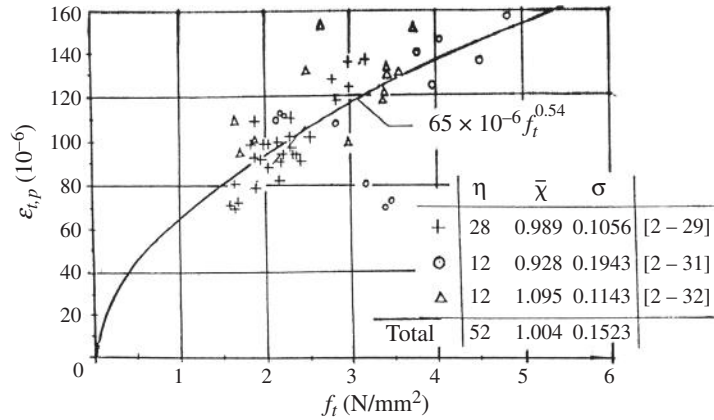


FIG. 2-20 Relation between tensile peak strain and central tensile strength of concrete [1-2]

modulus of elasticity of the same concrete. The experimental data are collected and shown in Fig. 2-21 by reference [2-30], and the calculation formula suggested is:

$$E_t = (1.45 + 0.628f_t) \times 10^4 \text{ N/mm}^2 \quad (2-16)$$

According to the experimental data [2-29], the ratio between the tensile modulus of elasticity and the secant modulus at peak point ($E_{t,p} = f_t/\varepsilon_{t,p}$) of concrete ranges from 1.04 to 1.38, and the average value of the ratio is:

$$E_t/E_{t,p} = 1.20. \quad (2-17)$$

Poisson's ratio The Poisson's ratio of concrete under tension is calculated using the transverse and longitudinal strains of the specimen measured during the testing, and the secant and tangent values of it on the ascending branch of the stress-strain curve are approximately equal:

$$\nu_{t,s} \approx \nu_{t,t} = 0.17 \sim 0.23. \quad (2-18)$$

When the value 0.2 is taken, it is nearly the same for the concrete under compression with low stress (Eq. (2-3)). However, when the tensile stress is approaching the ultimate strength, the longitudinal tensile strain of the specimen accelerates, while the transverse contractive strain increases slowly, because the concrete is tightened in this direction. So, the tensile Poisson's ratio gradually reduces as the stress increases. This is opposite to the compressive Poisson's ratio of concrete, which increases with the compressive stress (see Fig. 2-7).

The longitudinal and transverse strains of the specimen on the descending branch of the stress-strain curve vary irregularly and depend upon the length of the displacement transducer or the strain gauge and the relative position of the transverse crack (Fig. 2-22(b)). Therefore, the reasonable value of Poisson's ratio is very difficult to obtain directly from the testing.

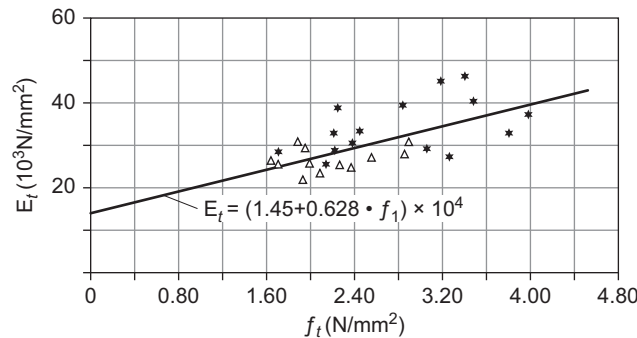


FIG. 2-21 Relation between tensile modulus of elasticity and central tensile strength of concrete [2-30]

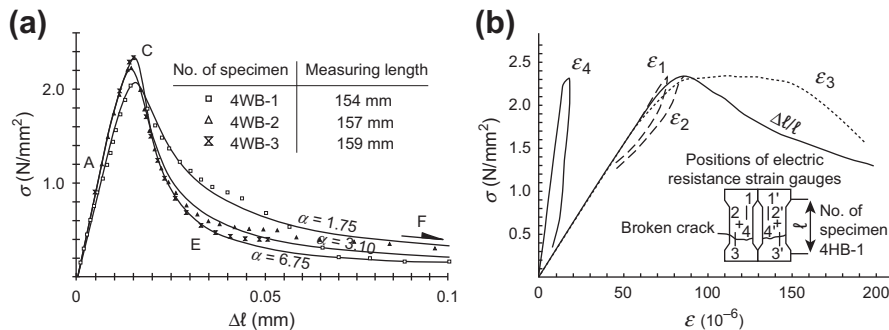


FIG. 2-22 Complete tensile stress–strain (deformation) curve [2-29]: (a) stress–deformation (average strain), (b) stress–strain (measured by strain gauge)

2.4.2 Tensile failure process and characteristic

The complete curve of the average stress (σ) and deformation (Δl , or average strain $\Delta l/l$) of the specimen is measured during testing and shown in Fig. 2-22(a). When the strain value measured by each strain gauge on the specimen is used as the abscissa, Fig. 2-22(b) is plotted. On the ascending branch of the curve, the measured value of every strain gauge is consistent with the average strain measured by the displacement transducer. When the curve approaches the peak point and then enters the descending branch, the strain measured by every strain gauge is considerably different. As the strain gauge intersects a crack appeared and then it quickly breaks. On the other hand, the strains of other strain gauges decrease, i.e. recover, because the specimen is unloaded.

There are four characteristic points A, C, E, and F on the complete tensile stress–strain curve (comparing with the compressive curve shown in Fig. 2-7), and they represent different stages of the tensile behavior of concrete.

After the specimen is loaded and when its stress $\sigma < (0.4 \sim 0.6) f_t$ (point A in Fig. 2-22(a)), the deformation of concrete approximately increases proportionally. As few plastic deformation of concrete appears afterwards, the deformation slightly accelerates and the stress–deformation curve is convex slightly. When the average strain reaches $\varepsilon_{t,p} = (70 - 140) \times 10^{-6}$, the tangent of the curve is horizontal and the tensile strength (f_t) is obtained. The bearing capacity of the specimen reduces quickly later on, and a sharp peak (point C) is formed.

When a crack on the surface of the specimen is observed by the naked eye, the curve has entered into the descending branch (point E). At this time, the crack is transverse, short and fine, and its width is about 0.04–0.08 mm and the corresponding residual stress of the specimen is about 0.2–0.3 f_t . Afterwards, the crack quickly develops and extends, the load slowly reduces, and the curve gradually flattens.

When the surface crack runs through the periphery of the specimen section, its width is about 0.1–0.2 mm. At this time, the central part of the section is still uncracked and the interaction of the aggregate exists on the cracked area, so a small amount of strength, about 0.1–0.15 f_t , remains. Finally, the crack passes through the whole section and the specimen is broken into two pieces (point F), after the total deformation of the specimen or the crack width on the surface reaches about 0.4 mm.

Some of the specimens are unloaded and reloaded several times on the descending branch and the corresponding stress–strain curves are also obtained stably during testing (Fig. 2-23). Also, the envelope (EV) of them is consistent with the complete stress–strain curve of the specimen loaded monotonically.

The broken section of the tensile specimen is uneven, but its outline is clear. Most parts on the broken section are the boundaries of the coarse aggregates pulled off from the cement mortar, others are broken cement mortar. Only very few coarse aggregates are broken off.

Because the composition of concrete is not homogeneous, the initial microcracks and holes exit randomly, and the adhesive strength between coarse aggregate and cement mortar is not equal to the tensile strength of the cement mortar, so the actual

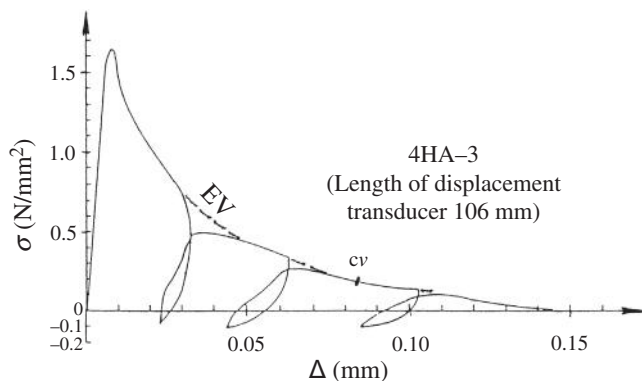


FIG. 2-23 Stress–strain curve of concrete under unloading and reloading test [2-29]

strength and stress distribution are different from section to section of the specimen and the crack always appears first on the weakest part of the weaker section. After a crack appeared on the surface of the specimen, a piece of area on the section is certainly out of work (Fig. 2-24). Both ends of the surface crack extend along the section periphery and the cracked area on the section gradually expands, as the tensile deformation of the specimen increases. Sometimes, a new crack appears on the other side surface, and two cracked areas are separately formed on the section and expand together.

The effective working area on the middle of the cracked section gradually reduces and varies in shape after the specimen is cracked. Therefore, the center of the working area will not coincide again with the position of the load and an eccentric tensile condition is caused. This makes the crack developing faster, and finally the specimen is broken. It can be concluded that the load (nominal stress) decreases within the descending branch of the curve and the main reason is the reduction of the effective working area on the cracked section, when the tensile load is acted continuously on the specimen. However, the actual stress on the working area is not necessarily reduced.

The complete stress—strain curves of concrete under both uniaxial tensile and compressive conditions are alike and are the asymmetrical ones of a single peak. In addition, the internal microcracks appear first in the interiors of both specimens of these conditions, and gradually develop into the macrocracks on their surface, and the failure is finally caused. However, the transverse broken crack of concrete caused under tension is significantly different from the longitudinal splitting crack caused under compression in their surface appearances (Table 2-8). This shows their different working mechanisms.

When a crack appears on the surface of a reinforced concrete structure and even if the conditions of the load and internal forces are unknown, it can be judged whether the crack is a compressive or tensile one, according to the macro appearance

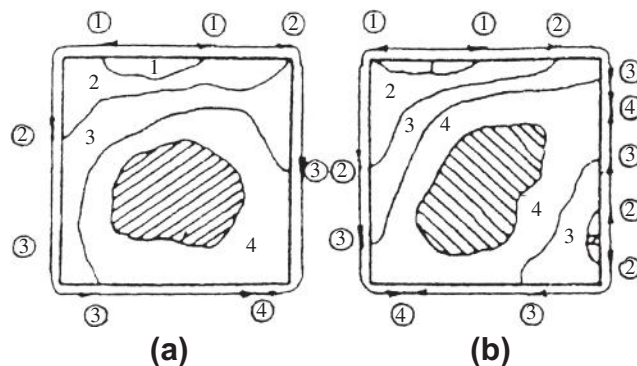




FIG. 2-24 Scheme of crack development on section [2-29]: (a) development of one crack, (b) development of two cracks. Note: The figure in the circle shows the appearance order of surface crack. And \rightarrow shows the extended direction of surface crack

Table 2-8 Comparison of Macro Appearances Between Compressive and Tensile Failure Cracks of Concrete

Crack Appearance	Compression	Tension
	 (a)	 (b)
Basic characteristic	Longitudinal compression-splitting	Transverse tensile broken
Direction	Paralleling with compressive stress, but Inclined crack appearing in later stage	Perpendicular to tensile stress
Number	Several parallel cracks at small distance	Only one, generally
Shape	Wider in middle, but narrower at both ends	Irregular
Developing process	Increases, extends, and widens gradually and slowly	Extends and expands quickly and suddenly
Cracked surface	More cracks and crushed pieces	Clear boundary
Concrete nearby	Loosing and easily peeling off	Solid and stable
Length of failure area	Similar size of cross-section	Limited on one surface (section)

of the crack (Table 2-8). Then, the safety or strengthening measure of the structure can be tentatively analyzed.

2.4.3 Equation of complete stress—strain curve

The complete tensile stress—strain curve of concrete is a smooth one of single peak like the compressive curve, but it is more abrupt and its descending branch ends at the intersection on the abscissa. Therefore, the geometrical characteristics of the complete compressive stress—strain curve (Eq. 2-5) should be also satisfied for the tensile one, except (6) among them.

The separate functions are suggested in reference [2-29] and adopted in the design code [2-1] for the ascending and descending branches respectively of the complete tensile stress—strain curve of concrete. The two functions are continuous

at the peak point and satisfy all the conditions of Eq. (2-5), so the theoretical curve obtained is accurate. The relative values of the strain (or deformation) and stress for the descending branch, are represented as

$$x = \frac{\varepsilon}{\varepsilon_{t,p}} = \frac{\Delta}{\Delta_p} \quad \text{and} \quad y = \frac{\sigma}{f_c}, \quad (2-19)$$

where Δ is the elongation deformation of the specimen, and Δ_p is the deformation corresponding to the peak stress f_t .

The equations of the ascending and descending branches of the curve are respectively:

$$x \leq 1 \quad y = 1.2x - 0.2x^6, \quad (2-20a)$$

$$x \geq 1 \quad y = \frac{x}{\alpha_t(x-1)^{1.7} + x}. \quad (2-20b)$$

The coefficient value 1.2 shows the ratio between the initial modulus of elasticity and the secant modulus of deformation at the peak point, and is consistent with the experimental data (Eq. 2-17). The parameter α_t for the descending branch increases

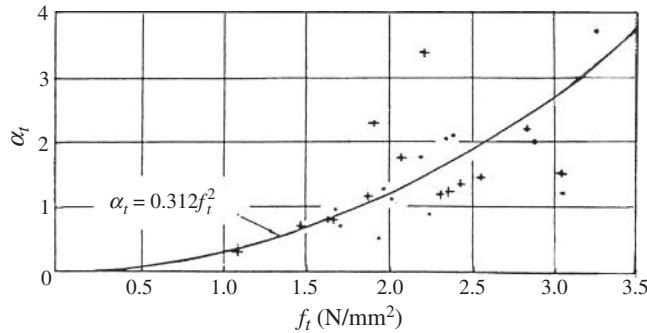


FIG. 2-25 Parameter α_t for descending branch [2-29]

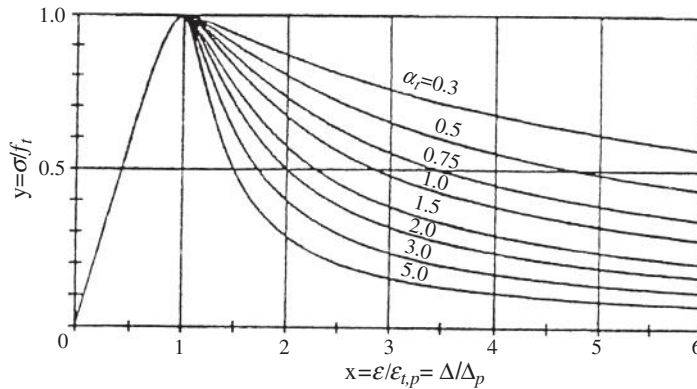


FIG. 2-26 Theoretical tensile stress-strain curve [2-29]

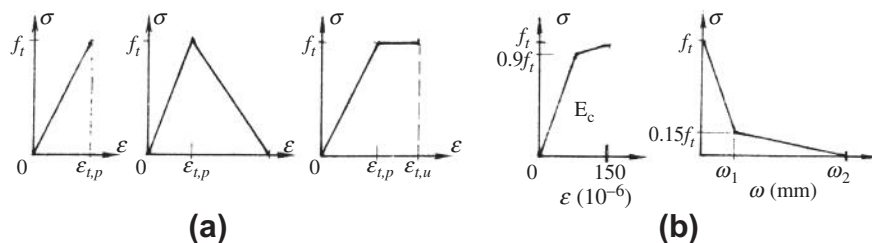


FIG. 2-27 Constitutive model for tensile concrete: (a) simplified models (b) reference [2-12]

with the tensile strength (Fig. 2-25) and can be calculated by the empirical regression formula:

$$\alpha_t = 0.312f_t^2, \quad (2-21)$$

where f_t is tensile strength of concrete in N/mm^2 . The theoretical curves calculated by these formulas are shown in Fig. 2-26.

When the non-linear analysis of reinforced concrete structure is conducted, various simplified stress—strain relations (e.g. Fig. 2-27(a)) can be used considering the influence of tensile action of the concrete. The CEB-FIP Model Code [2-12] suggests that the broken lines of stress—strain and stress—crack width (w , in mm) are used respectively for the concrete before and after cracking, and these lines are shown in Fig. 2-27(b).

2.5 Shear strength and deformation

The strength and deformation of concrete under pure shear stress are also the basic behavior of it and are quite important for the failure process and finite element analysis of the structure. However, there are several testing methods for it, and the shear strengths measured from them are considerably different. In addition, only few experimental data of shear deformation and shear modulus are reported, and different points of view exist.

2.5.1 Rational testing method

Various methods for testing the shear strength of concrete are shown in Fig. 2-28, and the specimen shapes and loading methods used for them are significantly different.

2.5.1.1 Direct shear of short rectangular beam

This is the earliest testing method among them, and is simple and direct. Mörsch et al [1-1] pointed out earlier that the failed shear surface of the specimen is composed of the sawtooth cracks, of which the two directions are controlled separately by the

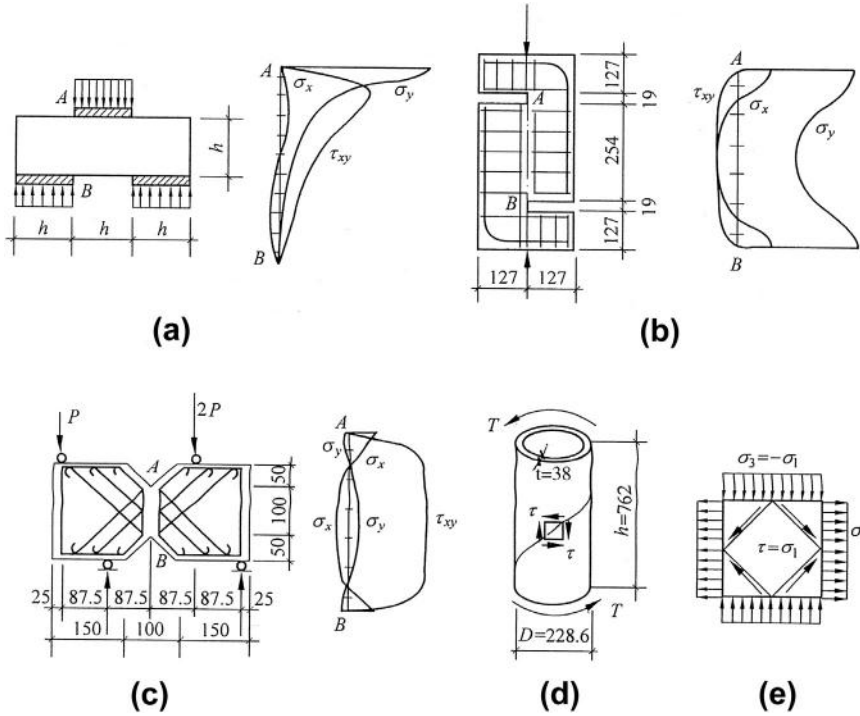


FIG. 2-28 Testing methods for shear resistance of concrete and distributions of shear stress on critical sections [2-31]: (a) short rectangular beam, (b) specimen in Z shape, (c) beam with notches, (d) circular tube, (e) biaxial compression-tension

compressive (f_c) and tensile (f_t) strengths of concrete. The average shear strength can be calculated by the formula:

$$\tau_p = k \sqrt{f_c f_t}, \quad (2-22a)$$

where k is the correctness factor taken as 0.75.

The value of the shear strength of concrete obtained from this kind of the testing method is rather higher:

$$\tau_{p1} = (0.17 \sim 0.25) f_c = (1.5 \sim 2.5) f_t \quad (2-22b)$$

2.5.1.2 Z shape specimen with single shear section [2-32]

The specimen fails under shear force along the critical section between the two notches, and the experimental value of the shear strength of concrete is about:

$$\tau_{p2} = 0.12 f'_c, \quad (2-23)$$

where f'_c is the cylinder compressive strength of concrete in N/mm^2 .

2.5.1.3 Four forces acted on the beam with notches [2-33]

The bending moment at the central section of the beam is zero, and the shear force on the section between the two middle forces equals a constant. Because the notches at the center of the beam are relatively large and the stress concentrations exist at the concave corner of it after loading, the crack starts at the concave corner and then passes through the section between the two notches, and the failure of the specimen is caused. However, it should be noticed that the crack does not occur first at the position of the maximum shear stress, which is located at the center of the section. The experimental value of the shear strength of concrete obtained from this kind of testing (τ_{p3}) approximately equals the tensile strength (f_t) of concrete.

2.5.1.4 Torsional circular tube [2-34]

When the wall thickness of a circular tube specimen is thin enough, an ideal and uniform pure shear state is formed in it under the action of a torque (T). The specimen fails along the helical curve of 45° and the shear strength of concrete can be calculated by the formula:

$$\tau_{p4} = \frac{2T_p}{\pi t(D - t)^2} \approx 0.08f_c \approx f_t, \quad (2-24)$$

where T_p is failure torque of the specimen, D and t are outer diameter and wall thickness of the tube specimen, respectively.

2.5.1.5 Biaxial tension—compression

When a cubic or a square plate specimen is loaded on two directions (see Chapter 5) and the stresses acted are $\sigma_3 = -\sigma_1$ and $\sigma_2 = 0$, it is equivalent to the stress state of pure shear. The relevant experimental results (Fig. 5-3) gives the value of the shear strength of concrete as:

$$\tau_{p5} = \sigma_1 \approx f_t \quad (2-25)$$

The last two among these five testing methods provide the ideal pure shear stress state, but the special testing equipment of complicated technique is needed and is hardly conducted by an ordinary laboratory. So, only the first two methods are used widely now.

The maximum difference among the shear strengths of concrete ($\tau_{p1} \sim \tau_{p5}$) measured from these tests is doubled, or even more. The internal stresses distributed on the critical sections of the first three methods are shown in Fig. 2-28 and some conclusions can be drawn from it. For the first two testing methods, the shear stress distributes non-uniformly on the critical section of the specimen and the normal stresses (σ_x and σ_y) existing there are several times the average shear stress, so these stress states are quite different from pure shear stress state and the values of the shear strength measured from the tests are obviously higher. For the third testing method, the shear stress distributes uniformly on the middle part of the critical section and the normal stresses (σ_x and σ_y) are only 12–15% of the average shear stress, so the stress state is close to pure shear stress state. Therefore, the stress states of

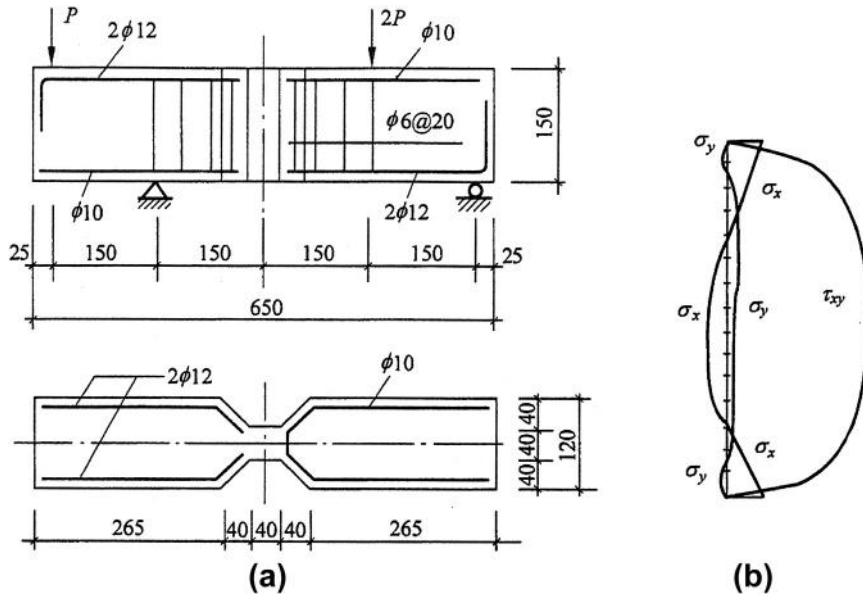


FIG. 2-29 Shear strength test of beam specimen loaded at four points [2-31]: (a) specimen and loading, (b) stress distribution on section

the last three testing methods are reasonable and the values of the shear strength of concrete measured from them approach one another.

A beam specimen of the same depth loaded at four points is specially designed for shear testing of concrete [2-31] (Fig. 2-29), which is an improvement on the third method above. There is no notch in the middle of the specimen to avoid the stress concentration, but the middle part of the specimen is thinned for controlling the position of failure and setting up easily the strain gauges (Fig. 2-30) to measure the principal strains (ϵ_1 and ϵ_3). According to the finite element analysis, the shear stress distributes uniformly on the middle height of the section and the ratio between the shear stress there and the average shear stress over whole section ($\bar{\tau}$) is 1.22–1.28, and the normal stresses there are $\sigma_y \leq 0.1\bar{\tau}$ and $\sigma_x \leq 0.2\bar{\tau}$. Therefore, the stress state on this part of the specimen is nearly a pure shear stress state. The design and manufacture of the specimen and the testing method are presented in detail in reference [2-23]. In addition, the special measure is used to slow down the process of shear failure of concrete specimen during testing for carefully observing.

The shear stress and strain of the specimen are calculated from the experimental data. When the shear force acted on the central section is V and reaches its ultimate value V_p at failure, the corresponding shear stress (τ) and strength (τ_p) of concrete are taken as:

$$\tau = 1.2 \frac{V}{A} \quad \text{and} \quad \tau_p = 1.2 \frac{V_p}{A}, \quad (2-26)$$

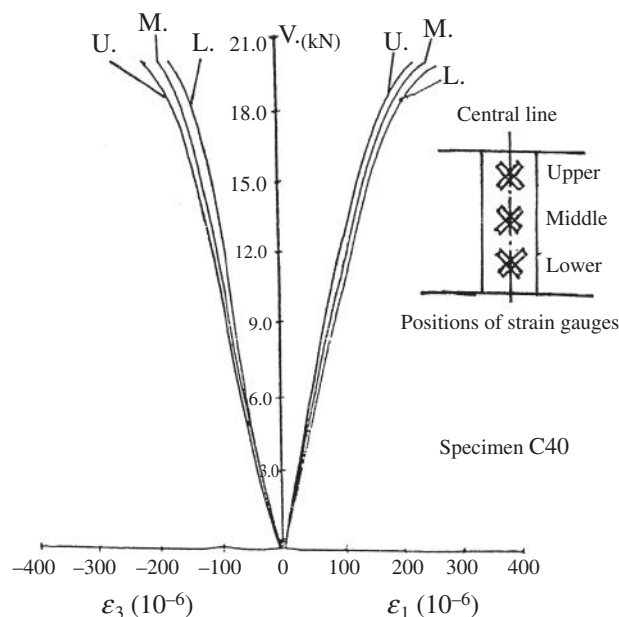


FIG. 2-30 Curves of shear force-principal strains [2-31]

considering the non-uniform distribution of the shear stress. The shear strain (γ) is calculated by the principal tensile and compressive strains measured (ϵ_1 and ϵ_3):

$$\gamma = \epsilon_1 - \epsilon_3, \quad (2-27)$$

where A is the area of the central section of the specimen, ϵ_1 and ϵ_3 are principal strains with positive and negative signs respectively for tensile and compressive one.

2.5.2 Failure characteristic and shear strength

The specimens made of the concretes of different strength grades are tested following the testing method, the typical principal tensile and compressive strains measured during testing are shown in Fig. 2-30. When the load acted on the specimen increases from zero to about 60% of the ultimate load (or V_p), the principal tensile and compressive strains, also the shear strain, increase almost proportionally with the shear stress. When the load reaches $V = (0.6 - 0.8)V_p$, the strains of the specimen accelerate and the curves are convex slightly. When the load increases further, the cracking sound of concrete is sent out from the interior of the specimen. When the ultimate load (V_p) is approaching, an inclined crack at an angle of about 45° with the beam axis appears in the middle part with pure shear stress. Afterwards, both ends of the crack extend simultaneously and quickly, the inclined angle of the crack increases when it passes through the thinned part of the specimen, and the crack is nearly vertical when its ends reach both the top and bottom of the specimen. Finally, the crack runs through the whole section and the specimen is sheared into two pieces.

The specimens of concretes of different strength grades ($\leq C70$) present the same failure pattern, i.e. only one inclined crack in the middle of it. The failed surface shows a clear boundary and the concrete nearby is solid and has no damage sign. The failure characteristic of the specimen is similar to that of inclined tension (principal tensile stress) (Table 2-8).

The shear strength of concrete (τ_p) monotonically increases with the cubic compressive strength (f_{cu}) (Fig. 2-31), and its calculation formula is obtained from the regression analysis [2-31]:

$$\tau_p = 0.39f_{cu}^{0.57}. \quad (2-28)$$

The calculated value is approaching the central tensile strength of concrete (f_t), and is also consistent with the experimental results of the circular tube under torque and the biaxial tension–compression specimens. In addition, same failure pattern and crack characteristic is shown on the specimens of these tests.

2.5.3 Shear strain and modulus

The shear strain (γ_p) and the principal tensile and compressive strains (ε_{1p} , ε_{3p}) at the peak point, i.e. failure of concrete, monotonically increase with the shear strength (τ_p) or the cubic compressive strength (f_{cu}) of concrete (Fig. 2-32). The regression formulas of the peak strains are [2-31]:

$$\left. \begin{aligned} \varepsilon_{1p} &= (156.90 + 33.28\tau_p) \times 10^{-6} \\ \varepsilon_{3p} &= -(19.90 + 50.28\tau_p) \times 10^{-6} \\ \gamma_p &= (176.80 + 83.56\tau_p) \times 10^{-6} \end{aligned} \right\}, \quad (2-29)$$

where τ_p is the shear strength of concrete in N/mm^2 .

The principal tensile and compressive strains at shear failure of concrete are respectively greater than the uniaxial tensile strain (ε_{tp} , Fig. 2-20) and uniaxial

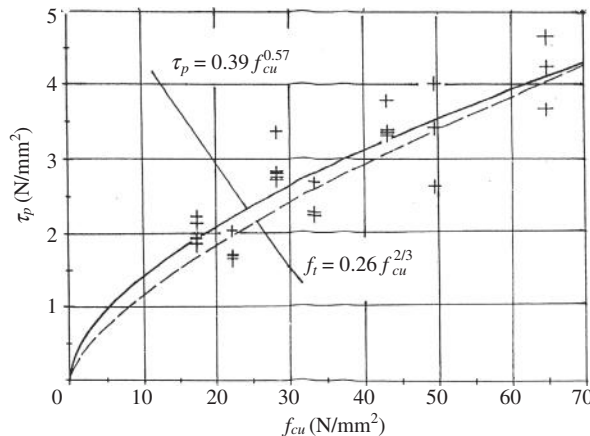


FIG. 2-31 Relation between shear strength and cubic compressive strength of concrete [2-31]

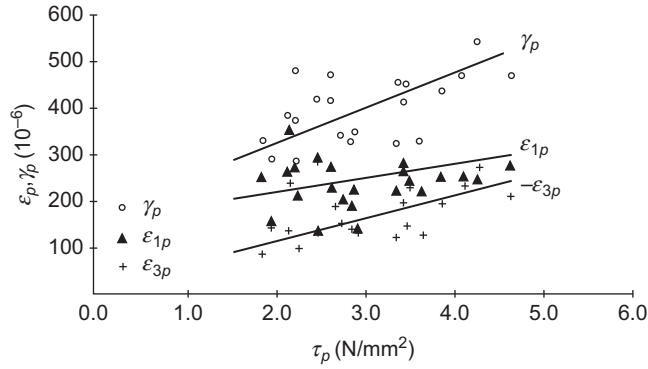


FIG. 2-32 Shear strain and principal strains at failure of concrete [2-31]

compressive strain under same stress ($\sigma = \tau_p$). The main reason is that the pure shear stress state is equivalent to the two-dimensional stress state of tension-compression, and the lateral deformation effect (Poisson's effect) of the stresses on both directions mutually cause larger strain values. In addition, the stresses on both directions act together and cause the internal microcrack appearing earlier and developing quickly in the direction perpendicular to the principal tensile stress. When the peak shear stress is approached, the plastic deformations in both directions increase greatly. Therefore, the shear strain of concrete, especially at peak point, is far greater than the tensile strain under uniaxial stress state, and also greater than the sum of uniaxial tensile and compressive strains, although the shear strength of concrete approximates to its tensile strength.

As the shape of shear stress-strain ($\tau - \gamma$) curve of concrete is between that of the uniaxial compression (Fig. 2-7) and tension (Fig. 2-22) curves, a polynomial of fourth order is suggested in reference [2-31] to simulate the ascending branch of it:

$$y = 1.9x - 1.7x^3 + 0.8x^4, \quad (2-30a)$$

$$\text{Where } x = \gamma/\gamma_p, \quad y = \tau/\tau_p. \quad (2-30b)$$

The theoretical curve and experimental data are compared in Fig. 2-33.

The shear modulus of concrete can be directly drawn from the equation of shear stress-strain curve, and the secant shear modulus (G_s) or tangent shear modulus (G_t) used in the analysis of finite element are separately:

$$G_s = \frac{\tau}{\gamma} = G_{sp} \left[1.9 - 1.7 \left(\frac{\gamma}{\gamma_p} \right)^2 + 0.8 \left(\frac{\gamma}{\gamma_p} \right)^3 \right] \quad (2-31)$$

$$G_t = \frac{d\tau}{d\gamma} = G_{sp} \left[1.9 - 5.1 \left(\frac{\gamma}{\gamma_p} \right)^2 + 3.2 \left(\frac{\gamma}{\gamma_p} \right)^3 \right]. \quad (2-32)$$

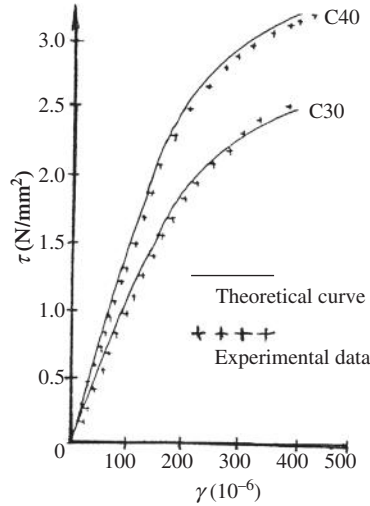


FIG. 2-33 Theoretical curve of shear stress—strain [2-31]

The secant shear modulus at peak point is drawn from Eq. (2-29):

$$G_{sp} = \frac{\tau_p}{\gamma_p} = \frac{10^6}{83.56 + (176.8/\tau_p)}, \quad (2-33)$$

while the initial tangent shear modulus is

$$G_{t0} = 1.9G_{sp}. \quad (2-34)$$

The initial shear modulus and the secant shear modulus at peak point of concrete monotonically increase with its compressive strength (f_{cu}), and the theoretical curves are compared with the experimental data and shown in Fig. 2-34.

If a structural material has different values for its tensile and compressive moduli of elasticity, the calculation formula of its shear modulus can also be drawn according to the principle and method of the elasticity:

$$G' = \frac{E_t E_c}{E_t + E_c + \nu_t E_t + \nu_c E_c} \quad (2-35)$$

where E_t and E_c tensile and compressive moduli of elasticity of the material; ν_t (ν_c) factor (Poisson's ratio) of the principal tensile (compressive) stress influencing on the strains of other principal directions.

When the values of the initial tensile and compressive moduli of elasticity of concrete are substituted into Eq. (2-35), the initial shear modulus G'_{t0} obtained approximates to the value G_{t0} calculated by Eq. (2-34) (Fig. 2-34). However, when the secant moduli of elasticity of concrete under uniaxial tension and compression

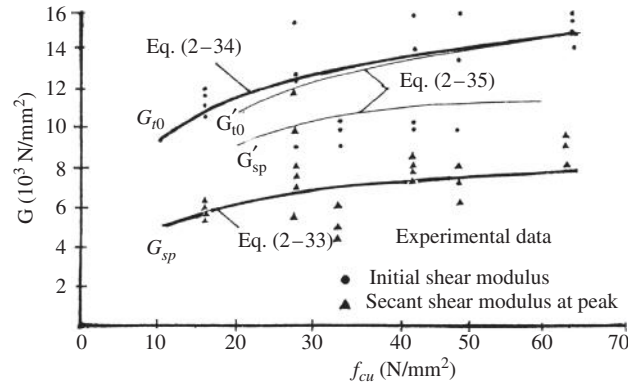


FIG. 2-34 Relation between shear modulus and cubic compressive strength of concrete [2-31]

at the stress $\sigma = \tau_p$ are also substituted into Eq. (2-35), the secant shear modulus G'_{sp} obtained is far greater than the value G_{sp} obtained both experimentally and theoretically. It is demonstrated that Eq. (2-35) can be used only when the shear stress of concrete is lower, but the shear strain obtained from it is less with considerable error when $\tau > 0.5\tau_p$. The reason for this has been introduced above. Therefore, the shear modulus of concrete should not be taken as the value calculated by the formula drawn from the uniaxial tensile and compressive stress states, when non-linear analysis of finite element is conducted for concrete structure.

Behavior Under Influence of Main Factors

3

CHAPTER OUTLINE

3.1 Load acted repeatedly	54
3.2 Eccentric compression	59
3.2.1 Testing method	59
3.2.1.1 Loaded with constant eccentricity ($e_0 = \text{const}$)	59
3.2.1.2 Loaded with zero strain at one side ($\epsilon_2 \equiv 0$)	60
3.2.1.3 Loaded with constant gradient ($\epsilon_1 - \epsilon_2 = \text{const}$)	60
3.2.2 Main experimental results	60
3.2.2.1 Ultimate bearing capacity (N_p) and corresponding maximum strain (ϵ_{1p})	60
3.2.2.2 Failure pattern.....	61
3.2.2.3 Sectional strain.....	63
3.2.2.4 Variation of neutral axis	64
3.2.3 Stress—strain relation	64
3.3 Eccentric and flexural tensions	66
3.3.1 Failure process.....	66
3.3.2 Ultimate tensile strength and plasticity-dependent coefficient	67
3.3.3 The maximum tensile strain at ultimate load	69
3.3.4 Variations of strain and neutral axis of section	69
3.3.5 Equations for complete stress—strain curve	70
3.4 Age	71
3.4.1 Compressive strength.....	72
3.4.2 Modulus of elasticity	74
3.5 Shrinkage	75
3.5.1 Kind and quantity of cement	76
3.5.2 Property, size, and quantity of aggregate	76
3.5.3 Curing condition.....	76
3.5.4 Environmental condition of service stage	76
3.5.5 Shape and size of structural member	76
3.5.6 Other factors.....	76

3.6 Creep	78
3.6.1 Basic concept	78
3.6.2 Main influence factors	82
3.6.2.1 Level of stress	82
3.6.2.2 Age at loading	83
3.6.2.3 Raw materials and mixture	83
3.6.2.4 Manufacturing and curing conditions	83
3.6.2.5 Environmental condition during service stage	83
3.6.2.6 Size of structural member	84
3.6.3 Calculation formulas	85

The basic mechanical behaviors of concrete introduced in the previous chapter are based on the measured results from the assigned specimens under the ideal stress state and loaded monotonically, following the standard testing method. Actually, the concrete in a reinforced concrete structure experiences a variable and complicated loading condition. For example, the load (or stress) is acted repeatedly, the stress distributes non-uniformly, i.e. the stress and strain gradients exist on the section, the specimen is loaded rather than at the age of 28 days, the load acted sustains a long period. Obviously, all of these conditions are different from the standard testing conditions.

These factors exert influences, to different extents, on the mechanical behaviors of concrete. The relevant results of experimental investigation are presented and the variation regularities of them are discussed in this chapter. In addition, some structures may sustain the special or extreme conditions, e.g. high speed or impact action of load, fatigue load, high temperature and load acted simultaneously. The mechanical behavior of concrete under these conditions will be introduced in detail in Part 4.

3.1 Load acted repeatedly

All the structural engineering carries various loads acted repeatedly and randomly or regularly within its service life, the corresponding stress, of course, is acted repeatedly on the concrete in it. The stress state of the concrete is obviously different from that of the standard specimen loaded monotonically until its failure.

The strength and deformation behaviors of concrete loaded repeatedly have been investigated in various paths [3-1—3-3]. Although these experiments can not simulate all the repeated processes occurring in the practical structure, the general regularity and important conclusions are obtained from typical experimental results.

The six paths of compressive stress acted repeatedly are introduced in reference [3-1] and the complete compressive stress—strain curves of concrete are measured respectively and shown in Fig. 3-1:

- A monotonically loading ((a) in the figure) used as a comparative test;
- B completely loading and unloading¹ at the predetermined strains with constant increment (b);
- C similar to B, but the reloading starts when only one half of the load is reduced (c);
- D loading and unloading cyclically at certain stresses (d);
- E loading and unloading cyclically at certain stresses (e);
- F loading and unloading cyclically along the first unloading curve (f).

Some important regularities are concluded for the concrete under repeated load, according to the phenomena observed during testing and the analyses of experimental results.

Envelope A smooth curve is drawn along the outer boundary of the complete stress—strain curve of concrete under repeated load. It is called the envelope (EV) as shown in Fig. 3-1. The envelopes of various repeated loads (B—F) are close to the complete stress—strain curve (A) under monotonic load. The peak point of the envelope corresponds to the prism compressive strength and the peak strain, and it makes no obvious difference to the values (f , ϵ_p) of concrete under monotonic load.

Cracking and failure process The first crack is visible when the total strain of the specimen reaches $1.5\text{--}3.0 \times 10^{-3}$, after the peak point on the curve is passed. The crack is fine, short, and parallel to the direction of compressive stress. More separate cracks appear when the specimen is loaded continuously or the total strain increases. If the total strain is not increased, the cracks do not develop obviously even unloading and reloading cyclically several times. When the total strain of the specimen reaches $3\text{--}5 \times 10^{-3}$, the adjacent cracks extend and connect together, and an inclined crack is formed and runs through its width. When the total strain increases further, the inclined crack gradually widens and forms a damage belt, but still a small amount of residual strength of concrete remains. The process is also consistent with that of the specimen loaded monotonically.

Unloading curve When the specimen is unloaded completely until zero stress from any point (ϵ_u and σ_u) on the envelope or the compressive stress—strain curve of concrete, a complete unloading curve is obtained (Fig. 3-2). The stress of the specimen reduces quickly at the beginning of unloading, while the strain of it recovers less. However, the recovered strain gradually accelerates as the stress decreases, and runs quickly when the stress is less than 20—30% of the stress before

¹The loading and unloading are defined respectively as increasing and decreasing of the strain. The loading means that the compressive strain of concrete increases regardless of whether the corresponding stress is increased (on the ascending branch) or decreased (on the descending branch). On the contrary, when the compressive strain decreases and the stress has to reduce, this is unloading.

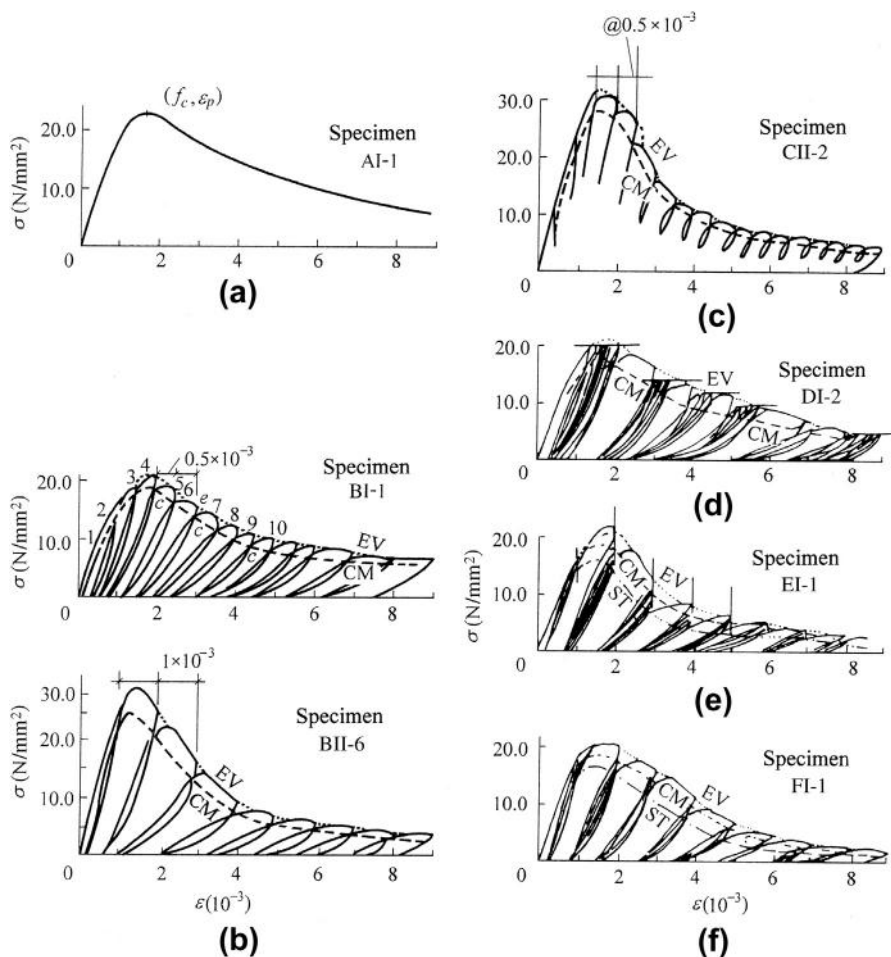


FIG. 3-1 Complete stress—strain curves of concrete under various repeated loadings [3-1]

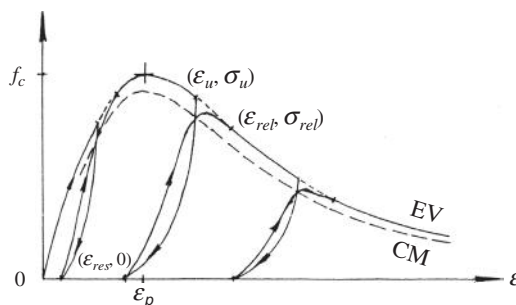


FIG. 3-2 General shapes of unloading and reloading curves

unloading. This is the hysteresis phenomenon of recovered strain of concrete, and the main reason is that the longitudinal crack is not recoverable under high compressive stress (Section 2.1.2). Therefore, the larger the strain (ϵ_u) at unloading, the more severe the cracking, and the more the hysteresis of recovered strain.

A residual strain (ϵ_{res}) appears when the stress of concrete is reduced to zero. It increases with the strain (ϵ_u) at unloading, and also increases slightly when unloading and reloading repeat several times.

Reloading curve The specimen is reloaded from any strain with zero stress ($\epsilon_{res}, 0$) until tangent to and coincidence with the envelope ($\epsilon_{rel}, \sigma_{rel}$), a reloading curve is obtained (Fig. 3-2). There are two kinds of reloading curve. When the strain at the start of reloading is small ($\epsilon_{res}/\epsilon_p < 0.2$), the strain at the upper end of the reloading curve is $\epsilon_{rel}/\epsilon_p \leq 1.0$, i.e. the curve is tangential to the ascending branch of the envelope, so the slope of the curve monotonically decreases and the slope at the upper end is greater than zero, i.e. no point of inflection occurs on it. When the strain at the start of reloading is large enough, the strain at the upper end of the reloading curve is $\epsilon_{rel}/\epsilon_p > 1.0$, i.e. the curve is tangential to the descending branch of the envelope. Because the slope at the upper end or the tangent point is of negative sign, one point of inflection should appear at lower stress on the ascending branch of the reloading curve, and a maximum value (peak point) and a small segment of descending branch appear successively on its top. In addition, the variation amplitude of the reloading curve increases with the strain (ϵ_{res}) at its start.

Transverse strain The transverse strain (ϵ') of the specimen tested under the repeated load (B) is shown in Fig. 3-3(b). The transverse strain is very small at the initially loading stage, but obviously accelerates when the stress is approaching the prism compressive strength of concrete (f_c). When the specimen is unloaded, its longitudinal strain partially recovers, while its transverse strain nearly keeps constant without recovery. When the specimen is reloaded, the longitudinal strain increases instantaneously, while the transverse strain still keeps constant. Only when the reloading curve passes through the common point (CM, see below), the longitudinal strain quickly accelerates and the transverse strain starts to increase. Obviously, this phenomenon is also caused due to the development and hysteresis recovery of the longitudinal crack in the specimen.

When the total strain of the specimen is larger ($\epsilon > 4 \times 10^{-3}$), the transverse strain slightly recovers during unloading. Each cycle of unloading and reloading composes a narrow closed diamond on the $\epsilon' - \epsilon$ curve. Comparing the specimens under repeated load (B) and monotonic load (A), the transverse strains of both specimens, corresponding to same longitudinal strain ϵ , are approaching, and the variation regularities of them are similar (Fig. 3-3(b)).

Locus of common point When the specimen is unloaded from any point on the envelope until zero stress, and then reloaded during the repeated loading test, the intersection point of the unloading and reloading curves is called the common point. Every common point obtained from each unloading and reloading process is successively connected smoothly, the locus of the common point is presented and shown as curve CM in Fig. 3-1. It is found that the slope of the reloading curve considerably

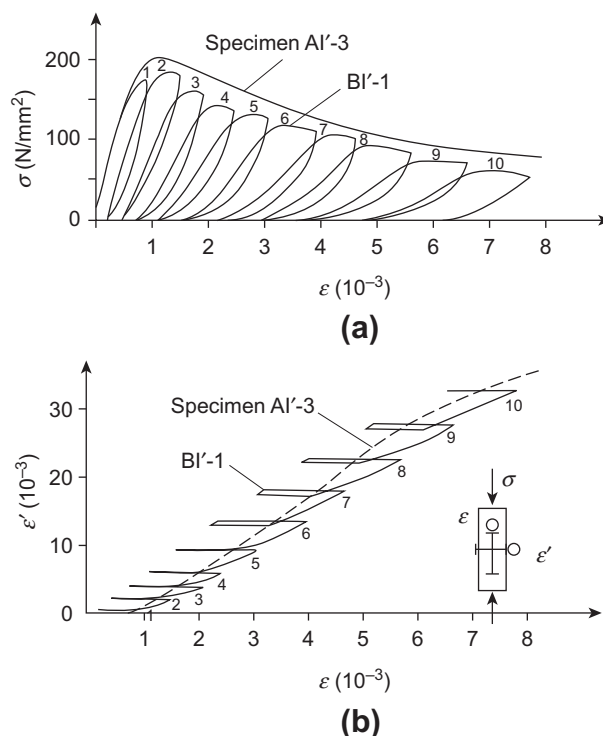


FIG. 3-3 Transverse strain: (a) $\sigma-\varepsilon$, (b) $\varepsilon'-\varepsilon$

decreases after the common point, i.e. the longitudinal strain of the specimen exceeds the strain (ε_u) before unloading and accelerates quickly, and the transverse strain (ε') increases suddenly. This indicates that the longitudinal crack expands or a new crack occurs in the specimen, and the damage to the concrete accumulates.

The locus of common point of various repeated loading is obviously similar to the corresponding envelope of the same test and to the complete stress-strain curve under monotonically loading. The ratio of similarity between both curves is determined after comparison and calculation [3-1]:

$$K_C = 0.86 \sim 0.93, \quad (3-1)$$

and 0.89 on the average. The ratio is 0.91 for the repeated loading test C.

Locus of stability point The specimen is unloaded and reloaded several times at certain predetermined strain values during the repeated loading tests E and F (Fig. 3-1). When the stress does not decrease and the residual strain does not increase further, the unloading and reloading curves compose a stable closed ring and the top of the ring is called the stability point. The stability points obtained from these cycles are connected smoothly, and the curve presented is the locus of stability point and shown as ST in Fig. 3-1. This is also the envelope of the ultimate strength (fatigue) of concrete under lower cycles.

The number of unloading and reloading cycles needed to reach the stability point depends upon the strain value before first unloading. According to the statistics, generally, three or four times are needed for the stability point under the ascending branch, with six to nine times for that under the descending branch.

It is concluded after observation and comparison that the shape of the locus of the stability point is also similar to the corresponding envelope of same test and to the complete stress—strain curve under monotonic loading. The ratio of similarity between them is:

$$K_S = 0.7 \sim 0.8, \quad (3-2)$$

and 0.75 on the average [3-1].

When the non-linear analysis of seismic resistance or other mechanical situation is conducted for a reinforced concrete structure, the stress—strain relations of concrete under the actions of loading and unloading or repeatedly loading are necessarily used. The calculation formulas, including the equations of the envelope, unloading and reloading curves, suggested in reference [3-1] or [3-3] may be adopted, and the former one fits better with the experimental results.

However, it should be noticed that the experimental results given above are obtained from the short time (a few hours) tests of the concrete specimen, the data of them, of course, are different to some extent from the long loading and unloading in engineering practice.

3.2 Eccentric compression

The ideal central compressive member is very seldom in practical structural engineering. Even if a structural member is designed as a central compressive one, the bending moment certainly occurs on its section, because of any occasional transverse load, non-ideal supporting condition, deviation of manufacturing, etc. Therefore, a general compressive member is loaded eccentrically, and the compressive strain (stress) distributes non-uniformly or the strain (stress) gradient exists on its section. Obviously, the larger the bending moment or the eccentricity and the smaller the section depth, the larger the strain gradient on the section.

3.2.1 Testing method

The influence of the strain gradient on the strength and deformation of concrete are experimentally investigated by various testing methods at home and abroad. They are divided into three categories according to the controlling method of the sectional strain (Fig. 3-4), when the prism specimen is used.

3.2.1.1 Loaded with constant eccentricity ($e_0 = \text{const}$) [2-17,3-4,3-5]

The axial load is monotonically acted with the predetermined eccentricity on the specimen until its failure. The strain on its section varies as the load increases, the

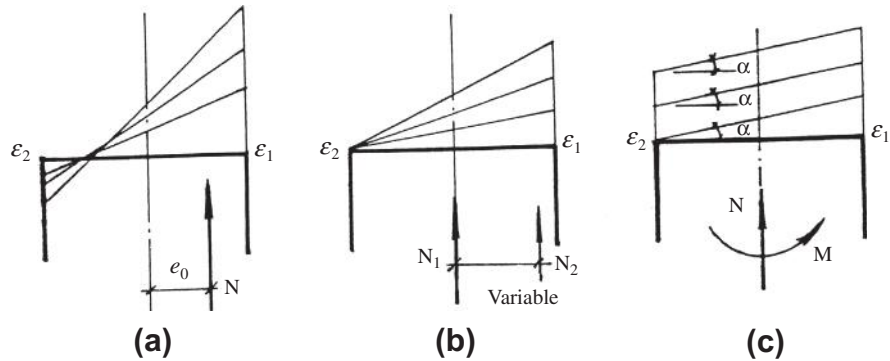


FIG. 3-4 Various testing methods for eccentric compression: (a) $e_0 = \text{const}$, (b) $\epsilon_2 \equiv 0$, (c) $\epsilon_1 - \epsilon_2 = \text{const}$

strain gradient gradually increases, and the neutral axis on the section slightly moves towards the load side, because the plastic compressive deformation of concrete appears and develops.

3.2.1.2 Loaded with zero strain at one side ($\epsilon_2 \equiv 0$) [2-21]

The specimen is loaded by the two compressions and all the strain on its section are compressive. The main one (N_1) is exerted on its center by a testing machine, while the eccentric one (N_2) is exerted by a hydraulic jack. The latter one is controlled during testing to satisfy zero strain at one side of the specimen. Therefore, a triangular distribution of the strain is insisted from beginning to end during testing, but with variable gradient.

3.2.1.3 Loaded with constant gradient ($\epsilon_1 - \epsilon_2 = \text{const}$) [3-6]

The axial force (N) and bending moment (M) of the specimen are exerted respectively by a testing machine and a hydraulic jack on the transverse direction. The values of N and M are controlled simultaneously during testing to satisfy the predetermined strain gradient on the section. Therefore, the strain distribution increases parallel and the strain gradient keeps constant.

3.2.2 Main experimental results

The experimental results from these methods are basically consistent. The test of constant eccentricity is conducted mostly and used here to explain the main behavior and general regularity of concrete compressed eccentrically.

3.2.2.1 Ultimate bearing capacity (N_p) and corresponding maximum strain (ϵ_{1p})

The ultimate bearing capacity of the specimen at failure decreases as the load eccentricity (e_0) increases (Fig. 3-5(a)). Obviously, it is always higher than the bearing

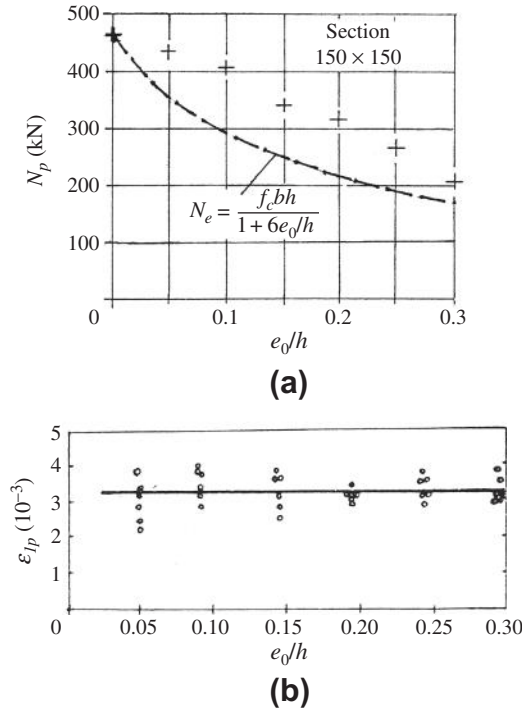


FIG. 3-5 Experimental results of prism specimen compressed eccentrically [3-4]: (a) ultimate bearing capacity, (b) maximum strain on section

capacity of the specimen calculated elastically, i.e. stress distributed linearly on the section:

$$N_e = \frac{f_c b h}{1 + (6e_0/h)} \quad (3-3)$$

It indicates that the stress distributed non-linearly on the section which is caused due to the plastic deformation of concrete is favorable to increase the bearing capacity of the specimen.

The maximum compressive strain (ϵ_{Ip}) of concrete on section of the specimen at ultimate load reaches $3.0\text{--}3.5 \times 10^{-3}$ and does not vary apparently with the load eccentricity. The value of the maximum strain is considerably greater than the peak strain (ϵ_p , Fig. 2-9) of concrete compressed centrally. It shows that the stress-strain curve of the concrete at the extreme side of the section has entered into the descending branch when the ultimate load reaches.

3.2.2.2 Failure pattern

The failure process and pattern of the prism concrete specimen compressed centrally are described above (Fig. 2-7). When the specimen is loaded with smaller eccentricity

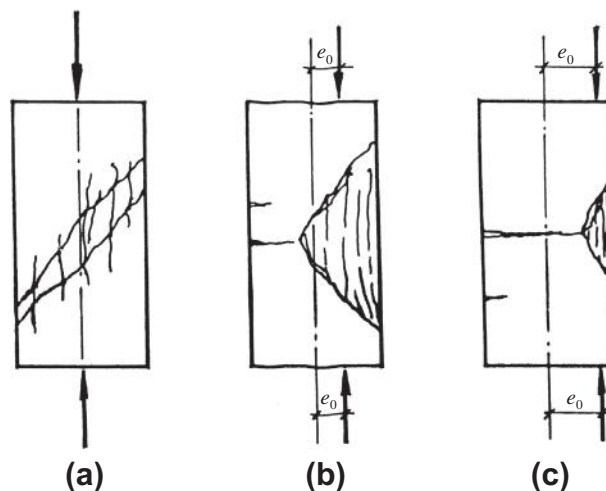


FIG. 3-6 Failure patterns of eccentrically compressive specimen: (a) central compression, (b) $e_0 < 0.15 h$, (c) $e_0 > 0.2 h$

($e_0 < 0.15h$) and the load reaches $0.9\text{--}1.0 N_p$, the longitudinal crack appears first in the area of larger compressive strain. When the load exceeds the peak value (N_p) and then enters into the descending branch, the longitudinal crack continuously extends and expands and the new cracks appear successively, and then a triangular cracking area is formed on one side of the specimen. If another side of the specimen is tensile, the transverse tensile crack appears there. When the specimen is loaded further, two inclined cracks appear on the upper and lower boundaries of the cracking area. As the transverse tensile crack extends, the compressive area on the section reduces gradually. When the tensile crack intersects with the compressive crack, relative rotation and slip occurs between the upper and lower parts of the specimen, and the specimen fails with the final pattern shown in Fig. 3-6(b).

When the specimen is loaded with larger eccentricity ($e_0 > 0.2h$), a tensile zone exists on its section from the beginning. As the maximum tensile strain of the specimen reaches and, then, is greater than the ultimate value of the concrete, a transverse tensile crack appears first and gradually extends and expands. When the ultimate load is approaching, the longitudinal crack occurs near the extreme surface of the compressive zone. When the load enters the descending branch, the transverse tensile crack continuously extends and expands, and the longitudinal compressive cracks increase and develop. Finally, the compressive zone on the section reduces greatly and the crack and damage in it accumulate severely, the relative rotation and slip between the upper and lower parts of the specimen are caused. The failure pattern of the specimen is shown in Fig. 3-6(c).

The compressive failure zones of all the specimens are triangular on the side surface, and the length is about double its width. The length and area (or volume)

of the crushed zone decrease with the compressive depth on the section, as the load eccentricity increases.

3.2.2.3 Sectional strain

The complete load—strain curves at both extreme surfaces (ϵ_1 , ϵ_2) of the specimen are measured during testing and shown in Fig. 3-7. The complete curve of the compressive strain (ϵ_1) near the load side is consistent with the complete stress—strain curve of concrete under central compression. The variation of the compressive strain (ϵ_2) on the other side varies with the load eccentricity. When the eccentricity is $e_0 < 0.15h$, the strain (ϵ_2) is a compressive one at the beginning and turns into a tensile one after being loaded to a certain level. But when the eccentricity is $e_0 > 0.2h$, the strain (ϵ_2) is always a tensile one during loading, and the complete curve is also similar to the complete stress—strain curve of concrete under central compression.

The displacement transducers, of which the measuring length is greater than double the section width, are set up to measure the average strain of concrete along the section depth of the specimen during testing. Then, the strain distribution on the section can be plotted [3-4]. Almost all the experimental results demonstrate that the average strain on the section satisfies the condition of planar deformation from the beginning of loading until the failure of the specimen, regardless of size of the load eccentricity and whether or not a tensile zone exists on the section.

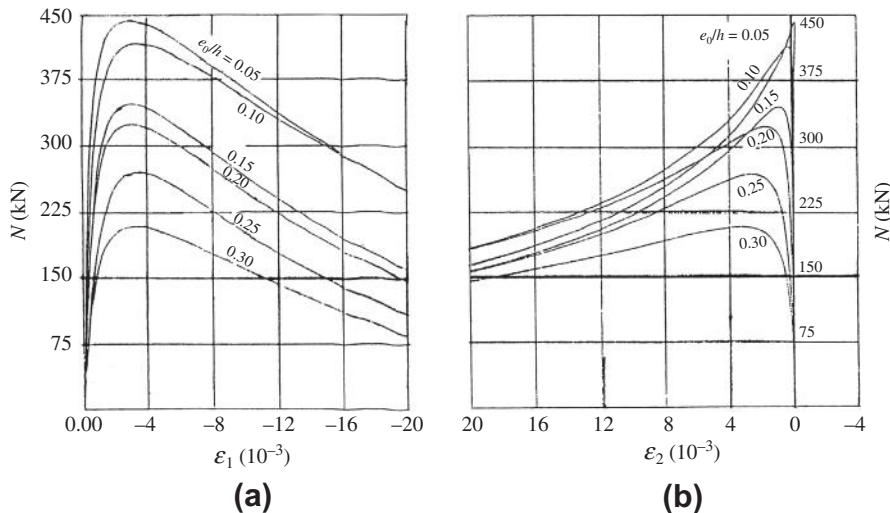


FIG. 3-7 Complete load—strain curve of specimen under eccentric compression [3-4]: (a) load—strain at extreme fiber near the load side, (b) load—strain at extreme fiber on other side

3.2.2.4 Variation of neutral axis

The position of the neutral axis on the section of an eccentrically compressive specimen is easily determined from the known strain distribution on it. When the strain of concrete is lower at the beginning of loading, the position of the neutral axis approximates the result calculated elastically:

$$\frac{x_0}{h} = 0.5 + \frac{h}{12e_0}. \quad (3-4)$$

The plastic deformation and internal microcrack of concrete gradually develop as the load increases (but $e_0 = \text{const.}$), so the stress on the section redistributes non-linearly, although the strain continuously keeps linear distribution. Therefore, the neutral axis on the section moves towards the load side, and the compressive zone on it reduces gradually. The moved distance of the neutral axis may range over $0.25\text{--}0.4 h$, when the ultimate load is reached (Fig. 3-8).

3.2.3 Stress–strain relation

Although the value and position of the load can be accurately determined and the value and distribution of the strain on the section can be easily measured during the eccentric compression testing of the prism concrete specimen, the value and distribution of the stress on the section are still unknown, because of the non-linear relation between stress and strain of the concrete. Therefore, the complete stress–strain curve of concrete under eccentric compression can not be obtained directly from the experimental data.

In order to find the complete stress–strain curve of concrete under eccentric compression, some assumptions have to be made to derive the basic formulas,

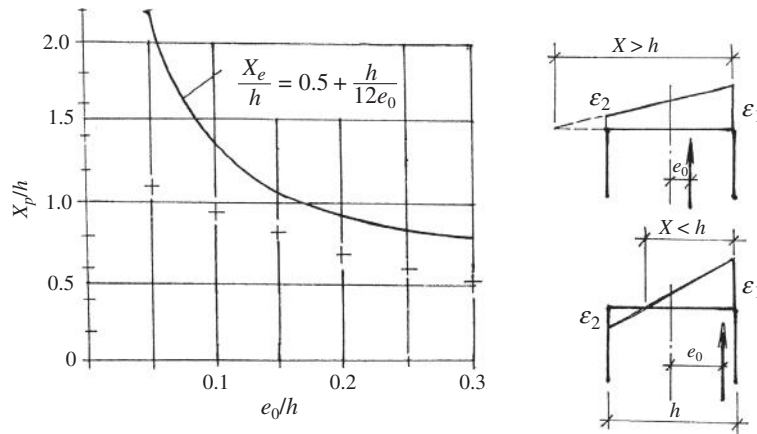


FIG. 3-8 Position of neutral axis of eccentrically compressive specimen [1-2]

and then a large amount of calculations are performed after introducing the experimental data. There are two methods for it.

1. Calculation of incremental equation [2-21,3-4]. The loading process of the specimen is divided into many increments. The incremental data of each load increment are substituted into the basic formulas, and the coupled values of the stress and strain are calculated. The coupled values of all load increments are plotted and connected to form the complete stress–strain curve.
2. Simulating the parameter values for the predetermined equation of the complete curve [3-4]. A rational mathematical equation is selected first for the complete stress–strain curve, and the parameters in it are simulated by the least square regression, using all the experimental data of the specimen.

These two methods have different advantages and disadvantages. The increment method needs not assume any equation for the curve, but the initial curve obtained is not smooth and even has some turns, so smoothing treatment is needed afterwards. On the other hand, the simulate method has to decide in advance a definite shape for the curve and can not be modified, so obviously, the initial selection determined the accuracy of the final result. It is better that both methods are calculated separately, and both results are compared and modified to draw the final one.

Basing on the experimental data and calculation methods of their own, various researchers have derived the common conclusion, i.e. the shape of the complete stress–strain curve of concrete is not related to the load eccentricity or the strain gradient on the section of specimen. Therefore, same equations of the complete stress–strain curve can be used for concrete under both central and eccentric compression. However, the values of the strength ($f_{c,e}$) and corresponding strain ($\varepsilon_{p,e}$) of concrete under eccentric compression, given by various researchers (Table 3-1), are slightly different.

Based on these experimental results and analysis, a simplified formula is suggested in reference [1-2] for calculating the eccentric compressive strength and corresponding peak strain, which vary with the load eccentricity (e_0):

$$\frac{f_{c,e}}{f_c} = \frac{\varepsilon_{p,e}}{\varepsilon_p} = 1.2 - \frac{0.2}{1 + (6e_0/h)} \quad (3-5)$$

The theoretical curve is compared with experimental results in Fig. 3-9.

The ratio calculated by Eq. (3-5) are 1.0 and 1.2 respectively for the structural members under central compression ($e_0=0$) and bending ($e_0=\infty$).

Table 3-1 Ratios Between Central and Eccentric Compressive Strengths and Peak Strains of Concrete

Reference	[2-21]	[3-5]	[3-6]	[3-4]
$f_{c,e}/f_c$	≈ 1.0	≈ 1.2	≈ 1.1	≈ 1.15
$\varepsilon_{p,e}/\varepsilon_p$	≈ 1.0	≈ 1.5	1–1.1	1–1.14

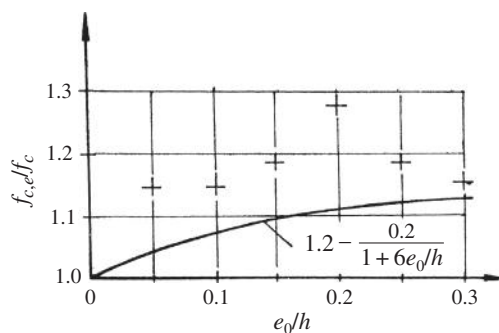


FIG. 3-9 Eccentric compressive strength of concrete

The influence of transverse strain gradient on the behavior of concrete is discussed above. An experiment [3-7] shows that the longitudinal strain gradient, which is caused by the variation of the internal force or section of the structural member, also has certain influence on the strength and deformation of concrete.

3.3 Eccentric and flexural tensions

The ideal central tensile member is also very rare in practical structural engineering. A tensile member usually carries some bending moment because of the mechanical and constructional conditions, and the tensile stress (strain) distributes non-uniformly on its section. The stress that occurs on the tensile zone of a flexural member distributes even more non-uniformly. So, the influences of stress (strain) gradient on the tensile strength and deformation of concrete need to be investigated.

The experimental research on the tensile behavior of concrete under eccentric tension is limited, and the conclusions given are not consistent. The conclusion in reference [3-8], obtained from the experiments, is that the stress—strain relation of concrete under eccentric tension coincides with that under central tension; reference [3-9] holds that the tensile peak strain increases and the stress—strain curve varies with the strain gradient, and the equation of the ascending branch is given and is composed of a straight line and a curve; references [3-10] and [3-11] discuss the improvement of the calculation method for flexural tensile strength of concrete ($f_{t,f}$). And, a series of eccentric tensile and flexural tests are performed and the corresponding complete stress—strain curves are measured in reference [2-30], then the general regularity and calculation formula are presented for the tensile behavior of concrete under eccentric tension.

3.3.1 Failure process

When the tensile specimen is loaded eccentrically, a non-uniform stress distribution occurs on its section. When the ultimate load is reached, one tensile crack appears first at the side of the maximum strain and extends towards another side of the

section along the direction being perpendicular to the tensile stress. Then, the tensile load reduces gradually, and the crack runs through the whole section and the specimen is broken into two pieces. Generally, there is only one crack in the specimen, i.e. the initial crack develops into the broken crack (surface). The failure pattern and the characteristic broken surface of the specimen is the same as that of the central tensile specimen (Table 2-8), they make no difference to the specimens loaded with different eccentricities.

3.3.2 Ultimate tensile strength and plasticity-dependent coefficient

The ultimate tension (N_p) of the specimen at failure decreases as the load eccentricity (e_0) increases, the relevant experimental data are shown in Fig. 3-10. It is clear that the measured value of the ultimate tension is certainly higher than the theoretical values calculated elastically:

$$\frac{N_e}{f_t b h} = \frac{1}{1 + (6e_0/h)}. \quad (3-6)$$

It is the same as Eq. (3-3) used for eccentric compression. However, the amplitude increase of the specimen with eccentric tension is obviously smaller than that with eccentric compression (Fig. 3-5(a)). It shows that the plastic deformation of concrete under tension develops limitedly, and the stress redistribution on the section is less.

The maximum tensile stress of the eccentric tensile and flexural specimens of rectangular section can be calculated elastically basing on the assumption of straight stress distribution on the section, its value at ultimate load is called flexural tensile strength of concrete ($f_{t,f}$, Eq.(2-11)). The ratio (γ) between it and the central tensile strength is called the plasticity-dependent coefficient of sectional resistant moment [2-1]:

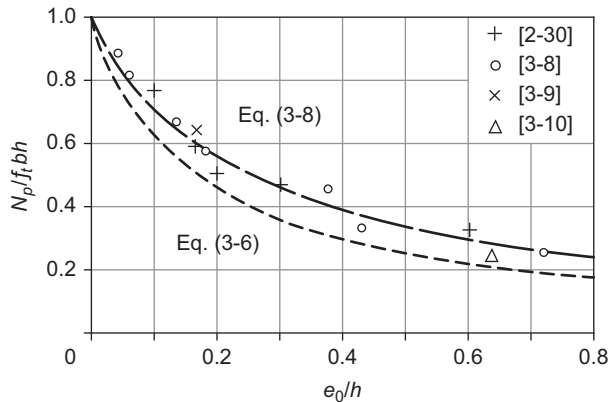


FIG. 3-10 Ultimate strength of concrete under eccentric tension [2-30]

$$\text{for eccentric tension } \gamma = \frac{f_{t,f}}{f_t} = \frac{N_p}{f_t b h} \left(1 + 6 \frac{e_0}{h} \right), \quad (3-7 \text{ (a)})$$

$$\text{for flexure } \gamma = \frac{6M_p}{f_t b h^2}. \quad (3-7 \text{ (b)})$$

When an elastic material is discussed, i.e. $\gamma \equiv 1$, the relation between the ultimate strength and eccentricity is a diagonal in Fig. 3-11, of which the coordinates are $N_p/f_t b h$ and $1/(1+(6e_0/h))$ respectively. Now, all the data from the eccentric tensile and flexural tests are located over the diagonal, it demonstrates $\gamma > 1$ for concrete of non-elastic. The regression formula is obtained:

$$\gamma = 1.51 - \frac{0.77}{1.51 + (6e_0/h)}, \quad (3-8)$$

$$\text{or } \frac{N_p}{f_t b h} = \left(1.51 - \frac{0.77}{1.51 + (6e_0/h)} \right) \frac{1}{1 + (6e_0/h)} \quad (3-9)$$

The value of the coefficient is $\gamma = 1$ for central tensile ($e_0 = 0$) and $\gamma = 1.51$ for flexural ($e_0 = \infty$) members respectively. Actually, the plasticity-dependent coefficient γ of a structural member is also related to the strength grade of concrete (f_{cu}), depth of its section (h), and others [2-1,2-12]. For example, the experimental average value of the coefficient of the flexural specimens reduces from $\gamma = 1.76$

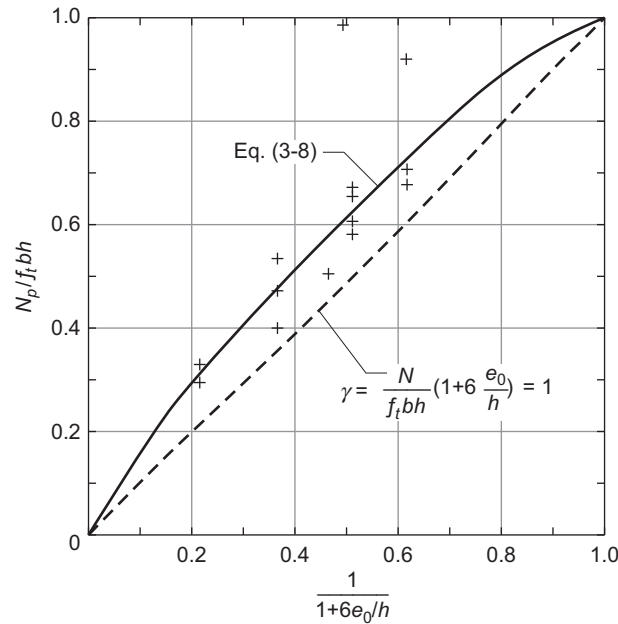


FIG. 3-11 Relation between ultimate strength and eccentricity [2-30]

down to 1.35 [2-30] when the compressive strength of the concrete is increased from $f_{cu} = 25.36\text{N/mm}^2$ up to 74.05N/mm^2 , because the plastic deformation develops less for the concrete of higher strength (see Section 4.1).

The depth of the specimen section determines the strain gradient on it at ultimate state. The larger the depth, the smaller the strain gradient and the plasticity-dependent coefficient. Different corrections are suggested for the coefficient by various researchers or related design codes. In Chinese code [2-1], the basic value of the plasticity-dependent coefficient of resistant moment of rectangular section is taken as $\gamma_m = 1.55$ (see Section 12.2), and it should be modified by Eq.(12-7), considering the sectional depth.

3.3.3 The maximum tensile strain at ultimate load

The maximum tensile strain (ε_{lp}) of the specimen at ultimate load (N_p) increases with the load eccentricity (e_0) (Fig. 3-12), and the corresponding regression formula is:

$$\frac{\varepsilon_{lp}}{\varepsilon_{t,p}} = 2.0 - \frac{1}{1 + (6e_0/h)}, \quad (3-10)$$

where $\varepsilon_{t,p}$ -peak strain of concrete under central tension ($e_0 = 0$).

The maximum strain is $\varepsilon_{lp} = 2\varepsilon_{t,p}$ for the flexural member ($e_0 = \infty$).

3.3.4 Variations of strain and neutral axis of section

The complete load—strain curves of the specimens with different eccentricities are measured during testing and shown in Fig. 3-13, and all of them are similar, to a certain extent, to the curve of concrete under central tension. Then, the strain distribution on the section is plotted and the position of the neutral axis can be determined. It is found that the strain distribution approximates the straight line from the beginning of loading until the failure of the specimen, so the assumption of planar section is basically satisfied.

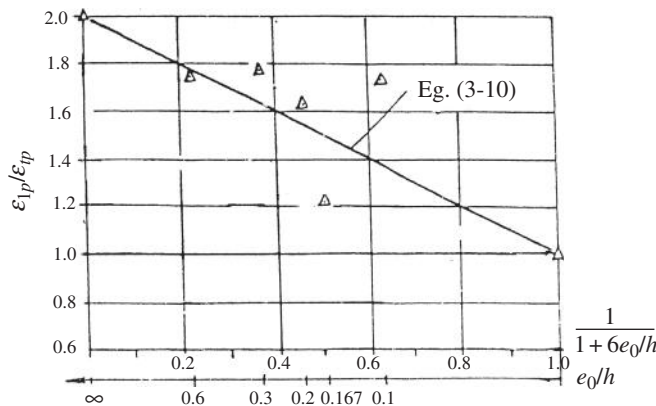


FIG. 3-12 The maximum tensile strain of concrete at ultimate load [2-30]

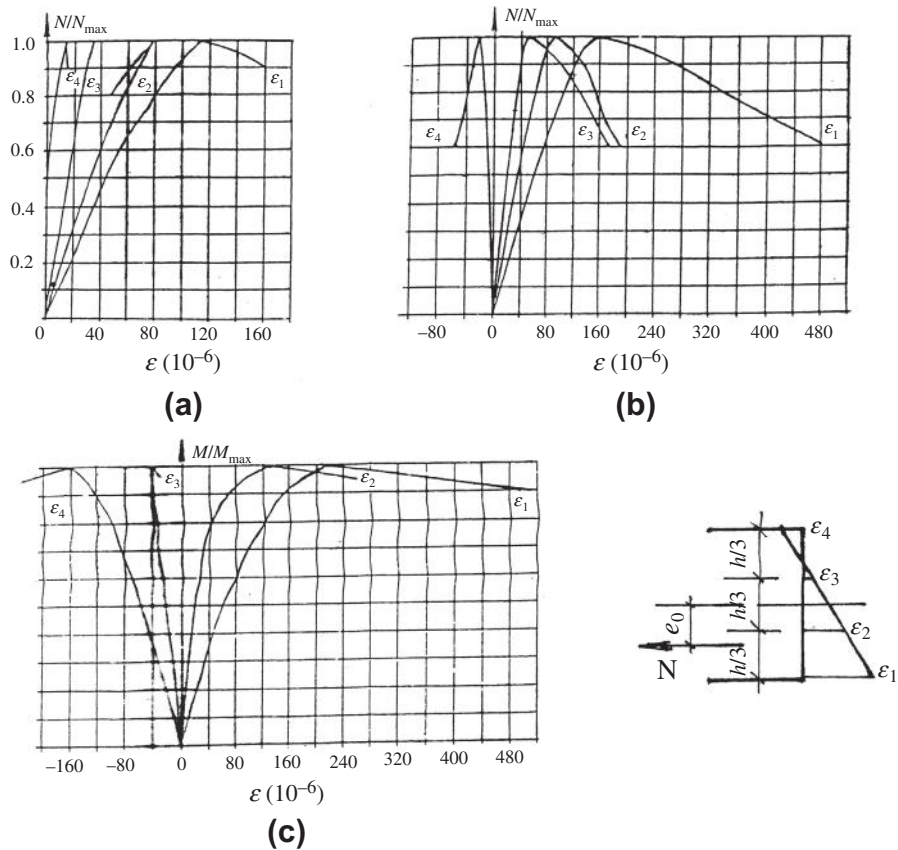


FIG. 3-13 Load—strain curves of specimen under eccentric tension [2-30]: (a) $e_0 = 0.167h$, (b) $e_0 = 0.3h$, (c) $e_0 = \infty$

The position of the neutral axis on the section mainly depends upon the load eccentricity. The position measured is consistent with that calculated elastically (x_e , see Eq. (3-4)) when the load is lower. When the ultimate load is approaching and the plastic deformation of concrete occurs on the tensile zone of the section, the neutral axis slightly moves and the area of the tensile zone increases. The position of the neutral axis (x_p) at ultimate load is shown in Fig. 3-14, and the moving amplitude of it is obviously smaller than that under eccentric compression (Fig. 3-8).

3.3.5 Equations for complete stress—strain curve

The equation of complete stress—strain curve for concrete under eccentric tension can also be determined following the two methods used for that under eccentric compression (Section 3.2.3). The suggestions in references [2-30] and [1-2] are as

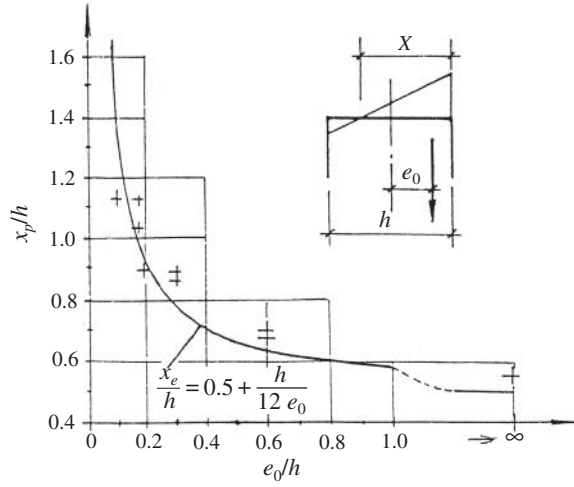


FIG. 3-14 Position of neutral axis of eccentrically tensile specimen at ultimate load [2-30]

below. The tensile strength ($f_{t,e}$) and peak strain ($\varepsilon_{t,e}$) of concrete under eccentric tension and bending moment are calculated by:

$$\frac{f_{t,e}}{f_t} = 1.1 - \frac{0.1}{1 + (6e_0/h)} \quad (3-11)$$

$$\frac{\varepsilon_{t,e}}{\varepsilon_{t,p}} = 1.3 - \frac{0.3}{1 + (6e_0/h)}, \quad (3-12)$$

where f_t and $\varepsilon_{t,p}$ —central tensile strength and corresponding peak strain of concrete, i.e. Eqs. (2-12) and (2-15).

The equation of complete stress—strain curve of concrete under eccentric tension can be taken the same as that under central tension (Eq. 2-20), but the equations suggested for the flexural member are

$$\left. \begin{aligned} x \leq 1 \quad y &= 2x - x^2 \\ x \geq 1 \quad y &= \frac{x}{0.5(x-1)^{1.7} + x} \end{aligned} \right\}, \quad (3-13)$$

where $x = \varepsilon/\varepsilon_{t,e}$ and $y = \sigma/f_{t,e}$.

3.4 Age

The main adhesive material in concrete is cement. The hydration of cement particle progresses gradually from its surface layer into its interior and is a slow process of several decade years. Therefore, it is demonstrated by many experiments and

engineering practice that the maturity, and the strength and modulus of elasticity, of concrete increases gradually with its age, as the hydration of cement develops continuously.

The design codes for reinforced concrete structure generally takes 28 days as the standard age of concrete to determine its indices of strength and other behaviors. If a structure is loaded, including the reinforcement in it is prestressed, at earlier age, it should be calculated or checked using the mechanical indices of concrete actually reached at the age. Most structures carry all the service loads only after the age of 28 days, the strength of the concrete reached later increases and is used for additional safety, but it is not utilized during design. Some structures are exerted all the service loads at the age far later than 28 days, because of, for example, very long construction period or sustained special (explosion) load, the strength of concrete at later age (e.g. 90 days) may be used for calculation and design of the structure.

The strength and modulus of elasticity of concrete varies with its age, and the variation regularity and increasing amplitude of them are influenced by many factors. The important factors include: kind (ordinary or early hardening) and composition (silicate, volcanic ash, or slag) of cement, quality (sintering and grinding) of cement, additives in concrete (hardening accelerated or delayed), curing condition (natural, moist, or water vapor), environmental temperature and humidity and their variations, etc. In addition, when the surface of a concrete structure is exposed to the air and the carbon dioxide in the air acts chemically with the concrete, a carbonate layer is formed near the surface of the concrete and it harms the durability of concrete (see Section 20.2.4).

3.4.1 Compressive strength

Normally, the compressive strength of concrete monotonically increases with its age, but with reducing rate and tending to convergence. The strengths of the concrete specimens made of the two kinds of cement vary with their age as shown in Table 3-2.

The compressive strength of concrete varied with its age can be simulated by various mathematic formulas [1-1], for example:

$$\left. \begin{aligned} f_c(t) &= \frac{\lg t}{\lg n} f_c(n) \\ f_c(t) &= \frac{t}{a + bt} f_c(28) \end{aligned} \right\} \quad (3-14)$$

Table 3-2 Relative Compressive Strength of Concrete Varying with its Age [1-1]

Age (days)	3	7	28	90	360
Ordinary siliceous cement	0.40	0.65	1	1.20	1.35
Early hardening siliceous cement	0.55	0.75	1	1.15	1.20

where $f_c(t)$, $f_c(n)$, and $f_c(28)$ are the compressive strengths of concrete at age of t , n , and 28 days respectively, and a and b are parameters depending upon the kind of cement and curing condition.

The calculation formula suggested in the CEB-FIP Mode Code [2-12] is:

$$f_c(t) = \beta_t f_c \quad (3-15a)$$

$$\beta_t = e^{s(1-\sqrt{28/t})} \quad (3-15b)$$

where s is a parameter depending upon the kind of cement and taking as 0.25 for the ordinary and early hardening cements and 0.20 for the early hardening cement of high strength.

The theoretical curve of the formula is shown in Fig. 3-15, and it gives a slightly lower value for the concrete at later age and fits for use in the engineering practice.

When the compressive stress is sustained, the strain of concrete, called creep (see Section 3.6), increases correspondingly with the time lasted. When the level of the compressive stress is lower ($\sigma < 0.8f_c$), the strain of concrete gradually converges to a limit after a long period. However, if the stress level is rather high ($\sigma \geq 0.8f_c$), the concrete enters the developing stage of unstable crack (Section 2.1.3) and its strain increases continuously even divergence, and it fails finally after a certain period of load is sustained. It is clear that the higher the stress level, the shorter the sustained time. Therefore a strength limit line of concrete can be found (Fig. 3-16), and the maximum stress, at which the concrete may sustain a long period without failure, is called the long-term compressive strength of concrete, normally taken as $0.8f_c$.

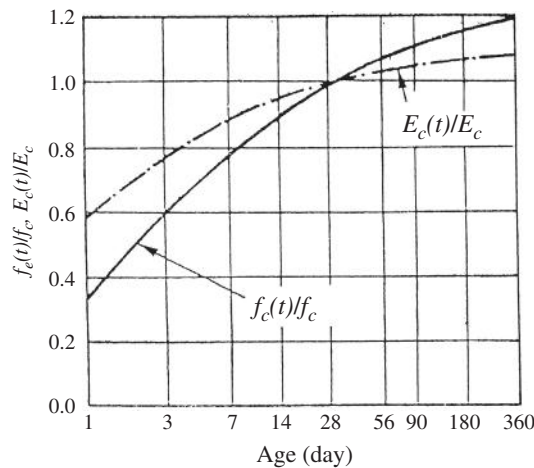


FIG. 3-15 Variations of compressive strength and modulus of elasticity of concrete with its age [3-12]

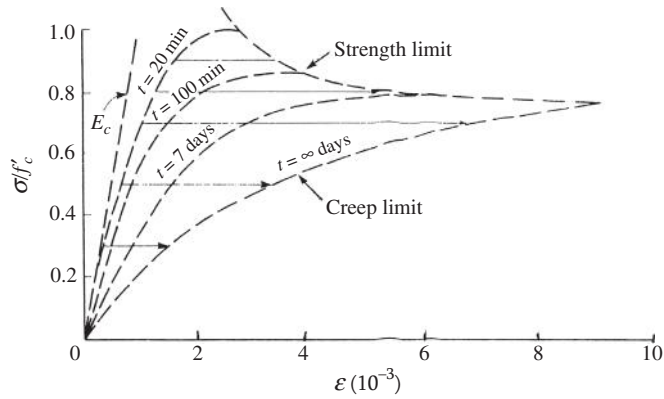


FIG. 3-16 Influences of stress level and sustaining time on strength and deformation of concrete [2-17]

3.4.2 Modulus of elasticity

The modulus of elasticity of concrete also increases with its age (t , days) as shown in Fig. 3-17. The CEB-FIP Model Code suggests a simple calculation formula for it:

$$E_c(t) = \sqrt{\beta_t} E_c \quad (3-16)$$

where E_c the modulus of elasticity of concrete at age of $t = 28$ days, β_t is the coefficient taken as in Eq. (3-15b).

The modulus of elasticity and compressive strength of concrete increase with its age but with reducing rate, and the increasing rate of the former is smaller than that of the latter.

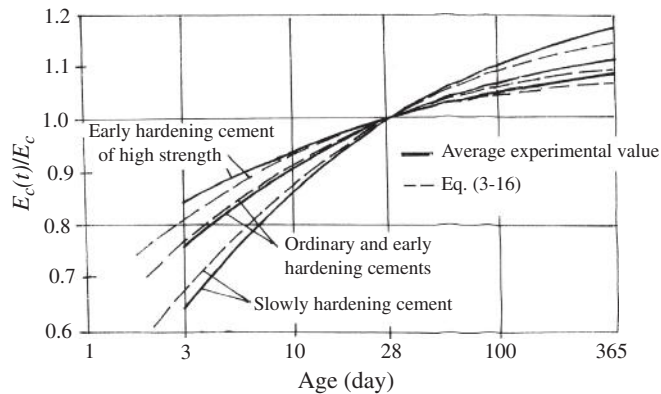


FIG. 3-17 Development of modulus of elasticity of concrete [3-12]

3.5 Shrinkage

The flowing concrete after mixed and the solid concrete during humidly curing basically keeps the same volume because of being full of water. Afterwards, the concrete is gradually hardened in the air, the water in its interior evaporates and its volume reduces. The shrinkage strain of concrete generally ranges from $300\text{--}600 \times 10^{-6}$ after decades, and even reaches $800\text{--}1000 \times 10^{-3}$ under unfavorable condition [2-12,1-1]. However, if the concrete is immersed in water, its volume is increased and the maximum elongation strain may reach 150×10^{-6} .

The final shrinkage strain of concrete exceeds 3–5 times the peak strain of it under central tension. This is one of the main reasons for the appearance and development of internal microcracks and external macrocracks in concrete. Some concrete structures show cracks on the outer surface after use for several years, even before loading. In addition, the shrinkage deformation of concrete causes it to increase the loss of prestress of the reinforcement in a prestressed structure, to reduce the cracking resistance and to increase the deformation of structural members, and to redistribute the stress on sections and the internal forces in a statically indeterminate structure. These may induce unfavorable influence on the structure, and should be paid attention to during its design and analysis.

When concrete is coagulating and hardening in the air, its shrinkage is unavoidable, because the volume of the product of cement hydrated is smaller than that of the original material (chemical shrinkage) and the aggregate particle is compressed due to capillary action after the water has evaporated (physical shrinkage). In addition, the carbonation between carbon dioxide in the air and the surface layer of concrete causes a certain amount of local shrinkage.

Therefore, the shrinkage of concrete should certainly be a long process. It is demonstrated that the shrinkage deformation of concrete develops quickly during the early drying stage and most parts of it appear already within three months, and it develops slowly afterwards but will not stop even twenty years later. The shrinkage deformation of concrete develops with time as shown in Table 3-3.

According to the experimental results, the shrinkage strain of pure cement mortar, composed of cement and water only, reaches $2000\text{--}3000 \times 10^{-6}$ after hardening (Table 2-1). The shrinkage of the rock aggregate mixed in concrete is, generally, very little and negligible. Therefore, the aggregate in concrete obstructs the shrinkage of the cement mortar, and the shrinkage of concrete is surely far less than that of cement mortar. In the meantime, the initial internal stress field is formed in the concrete (Fig. 2-2).

Table 3-3 Development of Shrinkage Deformation of Concrete [1-1]

Age	2 weeks	3 months	1 year	20 years
Relative ratio	0.14–0.30	0.40–0.80	0.60–0.85	1

The main factors having influence on the shrinkage deformation of concrete are as below.

3.5.1 Kind and quantity of cement

The cements of different kind and quality result in corresponding values of shrinkage deformation of concrete. For example, the shrinkage of early hardening cement is about 10% greater than that of ordinary cement; the more cement (kg/m^3) contained in concrete and the larger the water–cement ratio (W/C) used, the greater the shrinkage of the concrete.

3.5.2 Property, size, and quantity of aggregate [3-13]

The more aggregate mixed in concrete and the higher the modulus of elasticity of aggregate, the less the shrinkage of the concrete. The aggregate of larger size in concrete obstructs more the shrinkage of the cement mortar, and needs less water to satisfy the same flowability of fresh concrete, so less shrinkage is caused.

3.5.3 Curing condition

When concrete is cured through time, or under higher temperature and humidity or under steam, the hydration of cement is accelerated and the shrinkage of concrete is reduced. If the concrete is not cured completely and is stocked in a dry environment, its shrinkage increases considerably.

3.5.4 Environmental condition of service stage

If the surrounding of a structure is of high temperature and low humidity, the water contained in the concrete evaporates greatly and its shrinkage increases.

3.5.5 Shape and size of structural member

When the water in the interior of concrete evaporates out, it has to pass through the surface of the structure. Therefore, if the ratio between the volume and surface area of the structure, or the ratio between the section area and periphery length of the section (A_c/u) of a linear member, increases, the quantity of water evaporated decreases and the area carbonated on the surface reduces, so the shrinkage of concrete reduces as well.

3.5.6 Other factors

Various additives mixed in concrete, and the reinforcement rate and the mechanical state of the structure have influences, to different extents, on the shrinkage deformation of concrete.

Generally, the shrinkage deformation of concrete varies significantly and its value is difficult to determine accurately, because many factors have influences on it. The shrinkage deformation of concrete causes cracking on the surface of an ordinary structural member, but will not obviously reduce the safety of it. Therefore, the

shrinkage of concrete and its influences need not be calculated during design of an ordinary member, only some additional structural measures, e.g. setting up reinforcement or wire mesh, are used for compensation.

When some important structural engineering is designed and the shrinkage deformation of concrete needs to be determined accurately, the concrete specimen is specially manufactured from same material and tested within a short period to measure the shrinkage that has occurred, and then the ultimate value of the shrinkage is calculated. Or, the shrinkage of concrete can be calculated directly, following the formulas and parameter values provided in the relevant design code [2-12,3-14].

The calculation of the shrinkage of concrete, provided in the CEB-FIP Model Code [2-12], is used for the conditions: ordinary concrete under normal temperature, humidly curing no more than 14 days, exposed to the environment of average temperature (5–30°C) and relative humidity ($RH = 40\text{--}50\%$). The calculation formula for the average shrinkage (or expansion) strain of plain concrete without loading is:

$$\varepsilon_{cs}(t, t_s) = \varepsilon_{cso} \beta_s(t - t_s), \quad (3-17)$$

where the nominal shrinkage coefficient, i.e. ultimate shrinkage deformation, is calculated by:

$$\varepsilon_{cso} = \beta_{RH} [160 + \beta_{sc}(90 - f_c)] \times 10^{-6}, \quad (3-18)$$

where β_{RH} depending upon the relative humidity ($RH\%$) of the environment:

$$\left. \begin{aligned} 40\% \leq RH \leq 99\% \quad \beta_{RH} &= -1.55 \left[1 - \left(\frac{RH}{100} \right)^3 \right] \\ RH > 99\% \quad \beta_{RH} &= +0.25 \end{aligned} \right\}, \quad (3-19)$$

β_{sc} depending upon the kind of cement, e.g. 5 for the ordinary and early hardening cement and 8 for the early hardening cement of high strength.

And, the coefficient of shrinkage deformation varying with time is:

$$\beta_s(t - t_s) = \sqrt{\frac{t - t_s}{0.035 \left(\frac{2A_c}{u} \right)^2 + (t - t_s)}}. \quad (3-20)$$

Other parameters in these formulas are: t is the age of concrete, at which the shrinkage is calculated, in days; t_s is age of concrete when the shrinkage (or expansion) starts to occur, in days; f_c is compressive strength of concrete, in N/mm^2 ; A_c is area of transverse section of structural member, in mm^2 ; u is periphery length exposed to the air of the section, in mm.

The five main factors, which have influences on the shrinkage deformation of concrete, are included in the calculation model. They are the kind of cement (β_{sc}), relative environmental humidity ($RH\%$), size of structural member (A_c , u), and age (t , t_s), besides the compressive strength (f_c) of concrete. But, it is demonstrated experimentally that the strength value of concrete itself does not have a direct

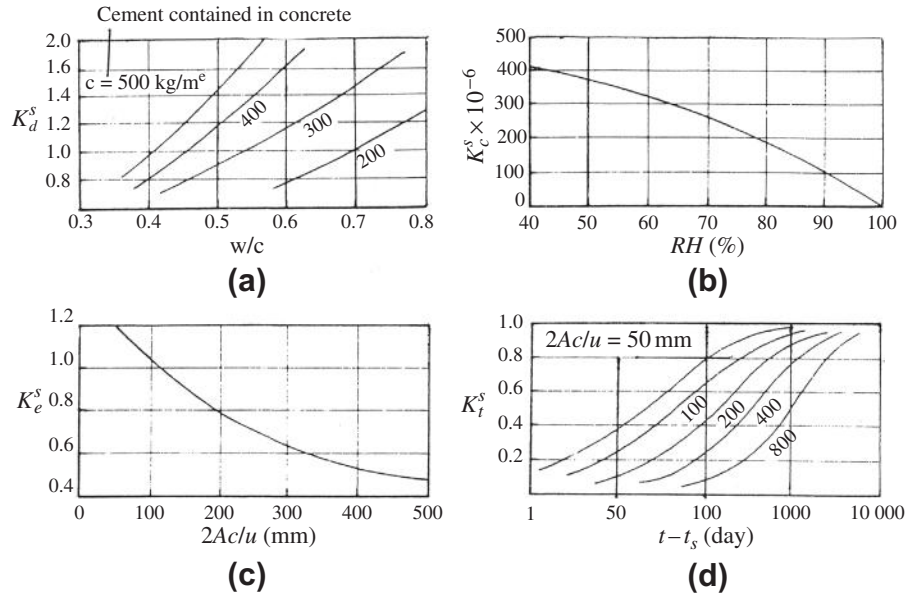


FIG. 3-18 Influences of main factors on shrinkage of concrete [3-15]: (a) cement contained and water—cement ratio, (b) relative environmental humidity, (c) sectional shape and size, (d) period of shrinkage occurred

influence on its shrinkage deformation. However, some other factors, such as the quantity of cement contained, the water—cement ratio, and the aggregate and curing conditions of concrete, also have influences on its shrinkage deformation, and they are not known in advance when the analysis and design of the structure are conducted. So, the compressive strength of concrete is introduced in the calculation to consider indirectly these factors, which are related to different extents, with it.

The shrinkage deformation of concrete calculated by these formulas and its regularities and amplitudes varied with the main factors are shown in Fig. 3-18.

3.6 Creep

3.6.1 Basic concept

Concrete is deformed under the action of stress (σ_c). The initial strain $\epsilon_{ci}(t_0)$ of it occurs instantaneously after stressed at its age (t_0), and, afterwards the strain $\epsilon_{cc}(t, t_0)$ occurs and increases as the stress sustained to the age (t), which is called creep of concrete (Fig. 3-19). The creep of concrete increases with time but with a reducing rate, and varies slightly after two or three years. The final value of creep is called the creep limit of concrete ($\epsilon_{cc}(\infty, t_0)$).

When the specimen is unloaded to zero stress ($\sigma_c = 0$) after a period of stress is sustained, a recovered strain (ϵ_{ce}), or elastic recovery [3-15], appears

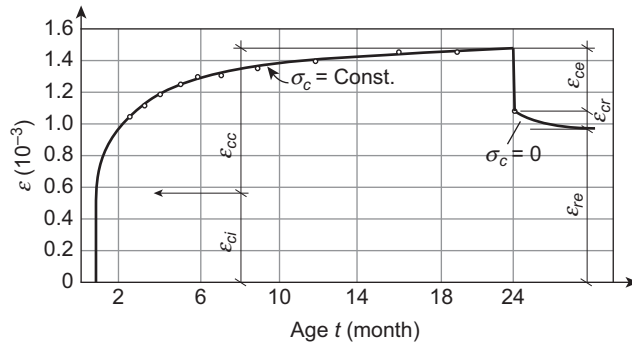


FIG. 3-19 Creep of concrete varied with time [1-1]

instantaneously. Afterwards, a hysteretic recovered strain (ϵ_{cr}), or post elastic effect or creep recovery [3-15], occurs slightly as time permits. However, a certain amount of residual strain (ϵ_{re}) still remains.

The mechanism of concrete creep may be explained from various theoretical points of view [3-16,3-17], but none of them is perfect. It is generally considered that the initial strain of concrete soon after being stressed is composed of the elastic deformations of the aggregate and cement mortar and the microcrack developed slightly, and the creep of concrete results due to the viscid flow (move) of the cement gelation and the development of internal cracks on the boundary of aggregate and in the interior of cement mortar. And, the evaporation of water contained in concrete also causes additional (drying) creep. Similarly, the instantaneous and hysteretic recovered strains of concrete after unload are of corresponding, but opposite, effect.

Relaxation is a phenomenon paralleling creep. When the concrete is loaded to stress $\sigma(t_0)$ at age (t_0), the instantaneous strain $\epsilon_c(t_0)$ is caused. If the value of the strain keeps constantly, the stress $\sigma(t)$ of the concrete has to reduce gradually as the time (age) lasts (Fig. 3-20). This is called stress relaxation or relaxation of concrete.

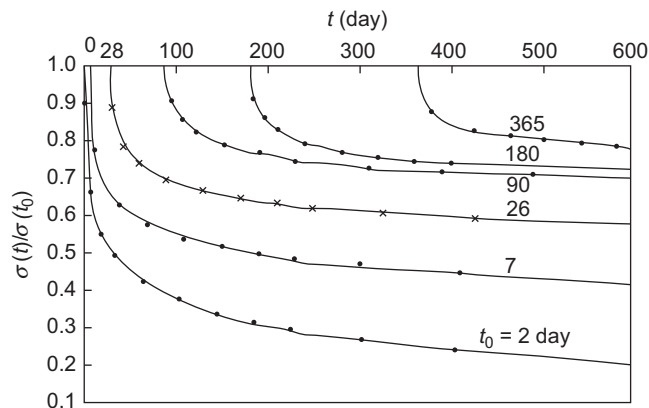


FIG. 3-20 Stress relaxation curve of some dam concrete [3-18]

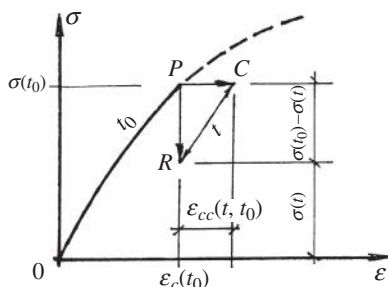


FIG. 3-21 Scheme of relation between creep and relaxation

Actually, creep and relaxation of a material represent the same deformation property varied with time, but show different reflections. The variation regularity and influence factors of both are the same and both can be converted into one another [3-16,3-17]. The stress—strain curve of a concrete at the age t_0 is shown in Fig. 3-21. When the concrete is loaded to the stress $\sigma(t_0)$ and the corresponding strain is $\varepsilon_c(t_0)$ (Point P), the stress will reduce to $\sigma(t)$ (Point R) if the strain is kept constantly for a period $(t-t_0)$, and the stress relaxation is $PR = \sigma(t_0) - \sigma(t)$. On the other hand, when the concrete is loaded to the stress $\sigma(t_0)$ and the stress is kept constant for a period $(t-t_0)$, its creep (Point C) will be $PC = \varepsilon_{cc}(t, t_0)$. If the strain of the concrete is then reduced, its stress has to reduce as well. As the strain reaches $\varepsilon_c(t_0)$, the corresponding stress $\sigma(t)$ coincides with Point R . Conversely, the creep point (C) can also be found from the relaxation point (R).

The creep and relaxation of concrete may cause an unfavorable or favorable influence on the concrete structure. For example, the long-term creep of concrete in a structure may cause: the compressive strength of concrete to be reduced by about 20%; the deflection of beam or slab doubled approximately; the loss of prestress caused being about 50% of the total loss; cracking resistance reduced; the stress on section and the internal forces of the structure redistributed; etc. In addition, the appearance of creep in the hydraulic massive structure reduces the thermal stress (relaxation) and the shrinkage crack in it; the creep of concrete relaxes the stress concentration at the local zone of a structure. These influences caused, to different extents, by creep of concrete have to be treated properly in engineering practice.

When a structural concrete is stressed to $\sigma(t_0)$ at age t_0 , its total strain at age t is composed of the initial strain $\varepsilon_{ci}(t_0)$ and creep $\varepsilon_{cc}(t, t_0)$:

$$\varepsilon_{c\sigma}(t, t_0) = \varepsilon_{ci}(t_0) + \varepsilon_{cc}(t, t_0), \quad (3-21)$$

$$\text{where } \varepsilon_{ci}(t_0) = \frac{\sigma(t_0)}{E_c(t_0)}, \quad (3-22)$$

and $E_c(t_0)$ modulus of elasticity of the concrete at age t_0 .

The creep value of concrete under one unit stress (1 N/mm^2) is called specific creep:

$$C(t, t_0) = \frac{\varepsilon_{cc}(t, t_0)}{\sigma(t_0)} \quad (3-23)$$

The creep limit of concrete under one unit stress varies considerably, as many factors have influences on it:

$$C(\infty, t_0) = \frac{\varepsilon_{cc}(\infty, t_0)}{\sigma(t_0)} = (10 \sim 140) \times 10^{-6} \text{ per N/mm}^2, \quad (3-24)$$

and its average value may be 70×10^{-6} per N/mm^2 .

The ratio between the creep and initial strain of concrete is called coefficient of creep:²

$$\phi(t, t_0) = \frac{\varepsilon_{cc}(t, t_0)}{\varepsilon_{ci}(t_0)}. \quad (3-25)$$

The value of the ratio after creep converged (at $t = \infty$) is called nominal coefficient of creep, or limit value of coefficient of creep:

$$\phi(\infty, t_0) = \frac{\varepsilon_{cc}(\infty, t_0)}{\varepsilon_{ci}(t_0)}, \quad (3-26)$$

and it ranges from 2–4 [2-12] when $t_0 = 28$ days.

Substituting Equations (3-22) and (3-23) into Eq. (3-25), the relation between the coefficient of creep and specific creep of concrete is:

$$\phi(t, t_0) = C(t, t_0)E_c(t_0), \quad (3-27)$$

$$\text{and similarly } \phi(\infty, t_0) = C(\infty, t_0)E_c(t_0). \quad (3-28)$$

When the concrete is unloaded after the load sustained a long period, the instantaneously recovered strain is smaller than the initial strain during loading ($\varepsilon_{ce} < \varepsilon_{ci}$), and the hysteretic recovered strain (ε_{cr}) is about 5–30% of the creep strain. The summation of both recovered strains, i.e. total recovered strain, of concrete is approximately equal to the initial strain:

$$\varepsilon_{ce} + \varepsilon_{cr} \approx \varepsilon_{ci}(t_0) \quad (3-29)$$

The creep of concrete increases continuously even within several decades, but most of it appear within the first one or two years and it develops more quickly within the first few months (typical data are listed in Table 3-4).

²The coefficient of concrete creep, in the CEB-FIP Model Code [2-12], is defined as the ratio between the creep and the elastic strain ($\varepsilon_{ci}(28)$) of concrete at age $t_0 = 28$ days.

Table 3-4 Creep of Concrete Varying with Time [3-18]

Sustaining time of stress ($t-t_0$)	1 month	3 months	6 months	1 year	2 years	5 years	10 years	20 years	30 years
Ratio	0.45	0.74	0.87	1	1.14	1.25	1.26	1.30	1.36

3.6.2 Main influence factors

The main factors having influences on the value and variation of concrete creep are as below.

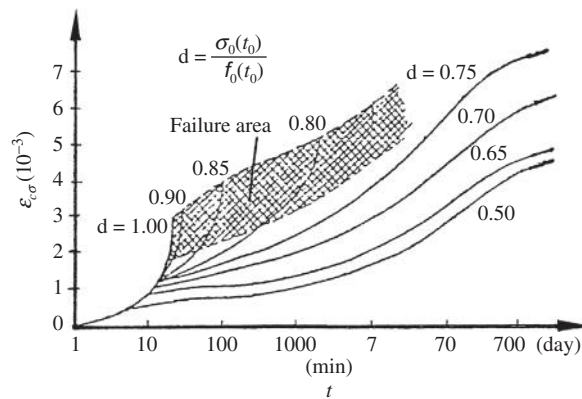
3.6.2.1 Level of stress

When the stress level $\sigma(t_0)/f_c(t_0)$ of loaded concrete is higher, both the initial strain and creep varying with time increase (Fig. 3-22):

$\sigma(t_0)/f_c(t_0) \leq 0.4-0.6$ when the stress acted on concrete is sustained, its creep value at any time is proportional to the stress acted and the specific creep does not relate to the stress, and finally the creep has a limit value and this is called linear creep;

$0.4-0.6 \leq \sigma(t_0)/f_c(t_0) < 0.8$. The creep of concrete still converges with a limited value under the sustained stress, but the specific creep of it increases with the stress level, which is called non-linear creep;

$\sigma(t_0)/f_c(t_0) \geq 0.8$. The creep of concrete under higher stress develops quickly at the early period and diverges later, this causes the failure of concrete. Therefore, the long-term compressive strength of concrete is about $0.8f_c$ (Fig. 3-16).

**FIG. 3-22** Creep of concrete under different stress levels [3-18]

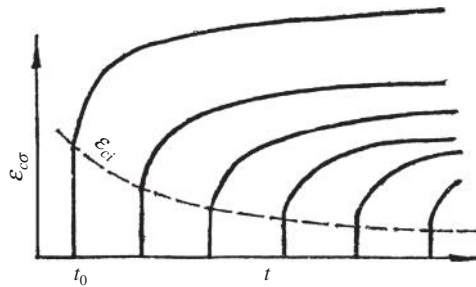


FIG. 3-23 Creep of concrete loaded at different age

Table 3-5 Comparison of Specific Creep of Concrete Loaded at Different Age [3-16]

Age t_0 (days)	3	7	28	90	365
Relative value	1.6–2.3	1.5	1	0.70	0.35–0.50

The stress level of concrete under the action of load in practical structural engineering is, generally, lower and the creep caused is linear.

3.6.2.2 Age at loading

When the concrete is loaded at an earlier age, its maturity is poorer and both initial strain and creep afterwards increase, and the creep limit increases even more (Fig. 3-23). The specific creeps of concrete loaded at different ages are compared in Table 3-5.

3.6.2.3 Raw materials and mixture

The creep of concrete increases with the cement content (kg/m^3), water–cement ratio (W/C), and the quantity of cement mortar (or less quantity of aggregate) contained in concrete. The creep of concrete mixed with ordinary Portland cement is greater than that mixed with early hardening cement.

3.6.2.4 Manufacturing and curing conditions

When the concrete is compacted and cured satisfactorily, especially when it is cured with steam, creep is reduced.

3.6.2.5 Environmental condition during service stage

The drying creep of concrete, caused by evaporation of water contained in it, increases as the relative humidity ($RH\%$) of the environmental medium surrounding the structure decreases (Fig. 3-24(a)). The creep of concrete increases with the

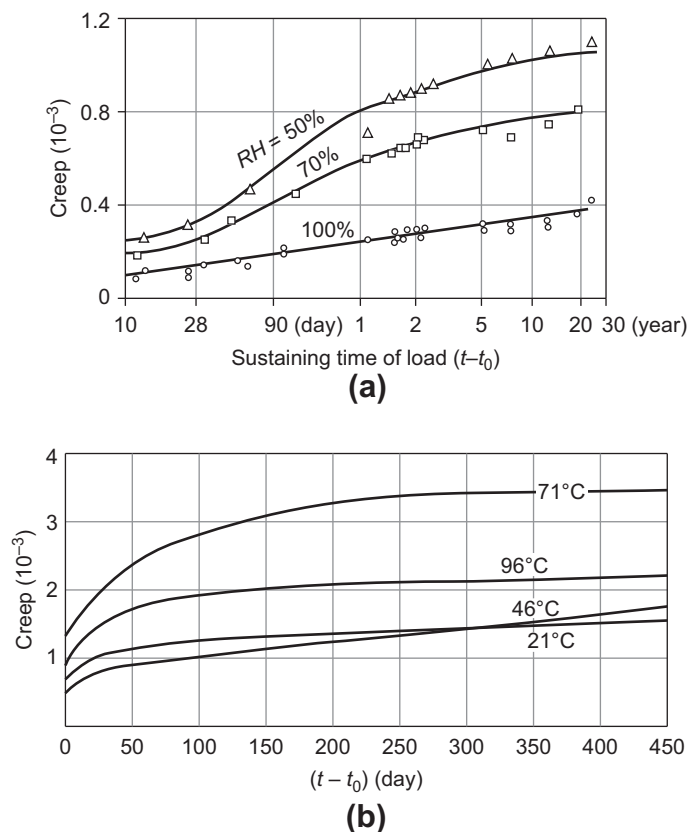


FIG. 3-24 Influences of environmental temperature and humidity on creep [2-8]: (a) relation environmental humidity, (b) environmental temperature

temperature within the range between 20°C and 71°C, however it decreases as the temperature increases from 71°C to 96°C (Fig. 3-24(b)).

3.6.2.6 Size of structural member

The drying creep of concrete increases as the size and section of the structural member reduces, or the ratio between the section area and periphery length (A_c/u) reduces, due to the water in it evaporating quickly (Fig. 3-25). If the concrete is sealed up and no evaporation of water occurs, the size of the structural member has no influence on creep of cement.

In addition, there are many other factors such as the kind, property, and size of aggregate, various additives mixed in, mechanical condition and history of concrete, and random variation of environmental condition.

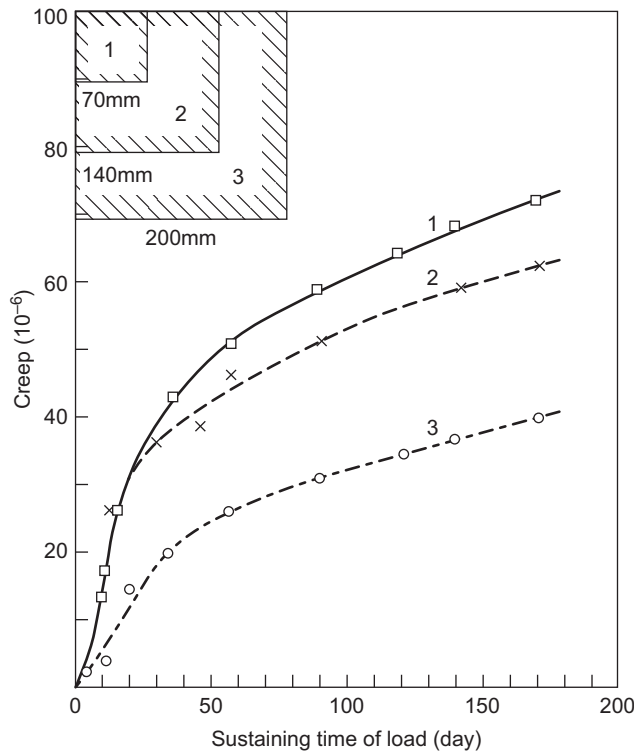


FIG. 3-25 Influence of size of structural member on creep [3-18]

3.6.3 Calculation formulas

The value of concrete creep is difficult to calculate accurately, because of so many influencing factors, wide variation amplitude, and scatter of experimental data. In the design code [2-1] of China, a composite empirical value or coefficient is given for the calculations of the deflection of a structural member under long-term load and the loss of prestress of a prestressed concrete structure. In the Design Code for Hydraulic Concrete Structure of China [3-19], the coefficient of stress relaxation of concrete is directly given for the calculation of thermal action of a massive structure.

When the creep analysis is needed for an important and complicated structure, the accurate value of concrete creep and its regularity varying with time have to be known in advance. It is reliable that the special specimen is made of the same concrete and then tested, and its creep is measured within a long period. Alternatively, the value of long-term creep is calculated from the experimental data measured within a shorter period. If the experimental equipment and environment are not available, the empirical formula based on the existing experimental data is generally used.

There are various mathematic formulas for calculation of the specific creep of concrete [3-16,3-18], for example:

$$\left. \begin{aligned} C(t, t_0) &= A(t - t_0)^B \\ C(t, t_0) &= F(t_0) \ln[(t - t_0) + 1] \\ C(t, t_0) &= \frac{(t - t_0)}{A + B(t - t_0)} \\ C(t, t_0) &= C(\infty, t_0) [1 - e^{-A(t-t_0)}] \\ C(t, t_0) &= C_e(t - t_0) + C_{re}(t, t_0) \end{aligned} \right\} \quad (3-30)$$

The last formula above is composed of two parts: recovered and un-recovered creeps. The parameters A , B , C and F in these formulas are calibrated from the experimental data and depend upon the material used and the environmental condition of the concrete. Some other formulas of complicated functions and containing more parameters are suggested in different literatures, e.g. reference [3-20].

The formulas presented below are suggested in the CEB-FIP Model Code [2-12] for calculation of the coefficient of creep of concrete, and they are suited for the conditions of: stress level $\sigma_c/f_c(t_0) < 0.4$, average temperature (5–30°C) and humidity $RH = 40\text{--}100\%$ of the environment.

The coefficient of creep of concrete is calculated by

$$\phi(t, t_0) = \phi(\infty, t_0) \beta_c(t - t_0) \quad (3-31)$$

The nominal coefficient of creep in the formula is:

$$\phi(\infty, t_0) = \beta(f_c) \beta(t_0) \phi_{RH}, \quad (3-32)$$

$$\text{in where } \beta(f_c) = \frac{16.76}{\sqrt{f_c}} \quad (3-32a)$$

$$\beta(t_0) = \frac{1}{0.1 + t_0^{0.2}} \quad (3-32b)$$

$$\phi_{RH} = 1 + \frac{1 - (RH/100)}{0.1(2A/u)^{1/3}}, \quad (3-32c)$$

and $\beta(f_c)$ parameter is calculated by the average compressive strength of concrete (f_c , in N/mm^2) at age 28 days; $\beta(t_0)$ is the parameter depending upon the age (t_0 , in days) when the concrete is loaded; ϕ_{RH} is the parameter mainly depending upon the relative humidity of the environment (RH , in %). The second part of it is zero when $RH=100\%$, and the size of concrete also has no influence on the creep.

The coefficient of creep varying with the sustaining time of stress is taken as:

$$\beta_c(t - t_0) = \left[\frac{(t - t_0)}{\beta_H + (t - t_0)} \right]^{0.3} \quad (3-33a)$$

$$\text{and } \beta_H = 1.5 \left[1 + \left(1.2 \frac{RH}{100} \right)^{18} \right] \frac{2A_c}{u} + 250 \leq 1500, \quad (3-33b)$$

where β_H depends upon the relative humidity and the size of structural member.

The main factors, including the age (t_0) of concrete at loading, the sustained time ($t-t_0$) of the stress, the relative humidity (RH %) of environment, and the size of structural member (A_c/u), are introduced in this calculation model. In addition, the compressive strength of concrete is also introduced to indirectly consider the influence of the water—cement ratio (W/C) and the quantity of cement contained in concrete.

The creep of concrete under other conditions, e.g. different kind of cement used, environmental temperature ($\leq 80^\circ\text{C}$), higher stress level ($0.4-0.6f_c$), has to be corrected and this is provided in the code. It is said that the theoretical value of the creep fits well with the experimental observation, and the coefficient of deviation of it is about 20%.

Most existent experimental data of concrete creep are obtained from the test under constant stress. However, it is impossible that the actual long-term stress of concrete in a structure keeps constant. The creep of concrete under varying stress, and, correspondingly the creep analysis of the structure, can not directly use the results from the test of constant stress. Therefore, it is necessary to develop the calculation theory, which uses the results of constant stress into the analysis of the structure with varying stress.

Up to now, several theories are available for creep of concrete, e.g. method of effective modulus, aging theory, elastic creep theory, elastic aging theory [3-16,3-18]. Each of them is based on a different concept and simplification or assumption, and then the corresponding formula is established for calculation of concrete creep with varying stress. Therefore, these theories are different in simplex or complex and in calculation accuracy, and may be selected accordingly for the analysis of structure.

This page intentionally left blank

Various Structural Concrete

CHAPTER OUTLINE

4.1 High-strength concrete	90
4.1.1 Application and preparation	90
4.1.1.1 <i>Increasing cement strength, accelerating hydration, and compacting properly</i>	90
4.1.1.2 <i>Reducing water–cement ratio</i>	91
4.1.1.3 <i>Various polymers used as adhesive material replacing cement</i>	91
4.1.2 Basic mechanical behavior	92
4.2 Light-weight concrete	99
4.2.1 Classification	99
4.2.1.1 <i>‘Homogeneous’ porous concrete ($\rho = 500\text{--}800\text{ kg/m}^3$)</i>	99
4.2.1.2 <i>Concrete of light-weight aggregate ($\rho = 900\text{--}1900\text{ kg/m}^3$)</i>	101
4.2.2 Basic mechanical behavior	101
4.3 Fiber concrete	106
4.3.1 Classification	106
4.3.2 Basic mechanical behavior	108

The ordinary concrete used most widely in structural engineering is of density $\rho = 2200\text{--}2400\text{ kg/m}^3$ and cubic compressive strength $f_{cu} = 30\text{--}50\text{ N/mm}^2$, and the strength and deformation behavior of it is introduced in detail in the earlier chapters.

The ratio between the strength and density (f_c/ρ) of this kind of concrete is far smaller than that of other structural materials, e.g. steel and timber, therefore the structure and its members made of concrete is certainly heavier than that of steel or timber with the same load-bearing capacity. Heavy dead load is the main disadvantage of concrete used for reinforced concrete structure, because the load of the supporting structure and foundation underneath is increased, the effective space and net height of the structure is reduced, the application of larger span and higher structure is limited, and the inertia force and response under earthquakes of the structure in a seismic area are increased. Moreover, this kind of concrete also has other weaknesses, including fragility, lower tensile strength, and easily cracking, and they cause reductions in the serviceability and durability of the structure.

As concrete structure is used more widely in various engineering fields, the structures of more height, larger span, and carrying heavier load need to be

developed. However, the disadvantages of concrete material display obviously, and the application of concrete structure is obstructed. Therefore, structural concrete has to be improved to increase the index of mechanical behavior and to reduce its weight.

After the accumulations of the investigation, development, and engineering experience in many years, various structural concretes, including high-strength ($f_c > 50 \text{ N/mm}^2$), light-weight ($\rho \leq 1900 \text{ kg/m}^3$), and fiber concretes, have been developed successfully. They have been used in engineering practice, the technical and economical benefits have been achieved and the development of reinforced concrete structure has been promoted.

4.1 High-strength concrete

4.1.1 Application and preparation

Since the first reinforced concrete structure was built in the late 19th century, the strength grade of concrete used in structural engineering in many countries has been gradually increased, as the technologies of cement manufacturing and concrete mixing are promoted continuously. The structural concrete used widely in practice was of strength C10–C15 only before the 1930s, C20–C30 in the 1950s, and the concrete of C50–C60 was started after the 1970s. Now, concrete of C30–C50 is widely used, and high-strength concrete of C80–C100, even C120, is used frequently in some important engineering. The strength of concrete prepared carefully in the laboratory may reach 300 N/mm^2 , and it is quite close to the absolute maximum compressive strength, i.e. the strength of the coarse aggregate (Table 2-1) in concrete.

In China, the strength grade of concrete used most widely in engineering practice is currently C20–C40, and concrete of C50–C60 is used frequently in many places and that of C60–C80, or even higher, is also used [4-1]. A related guide [4-2] or code for design and construction of high-strength concrete is available already. It is expected that the high-strength concrete will be used more widely and the strength grade of it will be increased continuously, as construction technology is improved and spread gradually.

However, a unified standard for defining high-strength concrete is not available at home and abroad so far. According to the technical levels of structural design and construction in China, high-strength concrete is generally defined as that of strength grade $\geq \text{C50}$. This threshold is approximately consistent with that of the design codes of CEB-FIP, ACI-318, and Japan.

There are different ways to manufacture high-strength concrete.

4.1.1.1 Increasing cement strength, accelerating hydration, and compacting properly

Cement of higher strength and cement grinded further are used effectively to increase the strength of concrete. The strength of concrete can also be increased,

Table 4-1 Influence of Water–Cement Ratio on Strength of Concrete

W/C	0.5	0.4	0.3	0.2
F_{cu}/AR_c	1.43	1.93	2.76	4.43
Relative value	1	1.35	1.93	3.10

Note: It is calculated by the famous formula $f_{cu} = AR_c(\frac{C}{W} - B)$, in which R_c is the strength of cement, A and B are the experimental parameters and B is taken as 0.57.

but with limited amplitude, when it is compacted properly and cured under high-temperature steam conditions.

4.1.1.2 Reducing water–cement ratio

It is concluded from the experimental investigation that the water needed for full hydration of cement is equivalent to a water–cement ratio $W/C = 0.2$. However, the greater water–cement ratio is normally used to satisfy the requirement of the workability of the fresh concrete during construction. Then, the unnecessary water will evaporate gradually during hardening of concrete, and cracks appear in its interior and its strength is deduced. When some additive (e.g. water deducing agent) and mineral admixture are added during mixing of concrete, the water–cement ratio needed for necessary workability can be reduced. The strength of concrete increases obviously with the reduction of the water–cement ratio (Table 4-1), when the same other raw materials are used.

4.1.1.3 Various polymers used as adhesive material replacing cement [4-3]

The compressive strength of polymer soaking concrete easily exceeds 150 N/mm^2 , but it has to experience successively several procedures, i.e. heating, vacuum treatment, soaking, and polymerizing. Therefore, it can not be used widely and is difficult to use in the construction site of structural engineering. In addition, its cost is rather high.

It is concluded that the most realistic and economic way to prepare high-strength concrete is to reduce its water–cement ratio. Various water-reducing agents of high efficiency, or superplasticizers, have been developed and applied since the 1970s. They are surface activators, and they are added in during mixing of concrete and absorbed on the surface of cement particles. This causes the particles to repel and separate from one another, and the workability of cement mortar is significantly increased. Then, the fresh concrete of high workability can be prepared, using a lower water–cement ratio. In addition, the superplasticizer accelerates the hydration of cement and increases the early strength of concrete [4-1].

In addition, some active materials of fine particles, e.g. fly ash, siliceous powder, F mineral powder, are admixed during mixing of fresh concrete in order to improve its workability, and they replace the cement and reduce its cost. Generally, these admixtures are used properly together with the superplasticizer. Therefore,

high-strength concrete can be prepared using this simple technology, which is normally used for ordinary concrete, and various structures and their members can be easily manufactured and applied widely in engineering practice.

Up to now, high-strength concrete has been widely applied to various structural engineering fields: high-rise building, bridge, underground structure and tunnel, defensive work, harbor and seashore engineering, prestressed structure. It is concluded from the engineering experiences that the main advantages of high-strength concrete are: higher compressive strength, smaller section of structural member, higher headroom, and smaller weight; higher early strength and shorter construction period; better compactness, durability, impermeability, freeze proof, and anti-scour abilities, and lower total cost. However, the structure of high-strength concrete should be carefully designed and manufactured: the plastic deformation and ductility of high-strength concrete is worse than that of ordinary concrete, so more structural measures are needed; if the calculation formula fitting well with the structural member of ordinary concrete is used for that of high-strength concrete, the safety of the latter is reduced; the mixing technology and construction management should be strictly controlled to ensure the quality and safety of the structure of high-strength concrete.

High-performance concrete [4-4], of which the characteristics are higher strength, workability, and durability, was developed in the 1990s. However, a unified quantitative definition of it is not available now. The majority emphasizes that high strength and durability are the main objectives of high-performance concrete, but some others pay more attention to the workability, even self-flowing and compact free, of it during construction, as its compactness is still guaranteed.

The main measures for preparing high-performance concrete are: adding sufficient quantity of superplasticizer to reduce water—cement ratio and admixing active admixture of super-fine powder, e.g. silicon, slag, natural zeolite, and fly ash powder. The other measures are: selecting cement of better quality and increasing quantities of cement and sand; using coarse and fine aggregates of better quality and selecting proper size and mixture of them; improving the manufacture technology including mixing, casting, compacting, and curing. All of these measures are of benefit to increase the workability during construction, improving compactness, and reducing permeability, so that concrete of high strength and durability is achieved.

4.1.2 Basic mechanical behavior

The mechanical behavior of high-strength concrete has been experimentally investigated for many years at home and abroad [4-5–4-9]. High-strength concrete is essentially one of concrete, so its basic characteristic and general behavior are consistent with that of ordinary concrete. However, some indices of its mechanical behavior vary gradually, as its strength increases considerably.

The test standard for cubic compressive strength of high-strength concrete is the same as that for ordinary concrete [2-3]. When the cubic specimen is tested, it fails

Table 4-2 Relative Compressive Strength of Different Specimens of High-Strength Concrete [4-1]

Shape	Cube			Prism	Cylinder
Size (mm)	200	150	100	150 × 150 × 450	Φ150 × 300
Relative ratio	0.92	1	1.08	0.82–0.90	0.87–0.94

suddenly and is accompanied by cracking and spalling sounds. The specimen is split and spalled off, but no pyramid is formed as occurred for the specimen of ordinary concrete (Fig. 2-5), because of weakened friction confinement of loading steel plate on the surface of the specimen. When the specimens have different shapes and sizes, the relative compressive strengths of high-strength concrete (Table 4-2) are also different from those of ordinary concrete (Table 2-2).

The complete compressive stress—strain curves measured from the prism specimens of high-strength concrete are shown in Fig. 4-1. Although the general shape of the curve is consistent with that of ordinary concrete (Fig. 2-7), the positions of the geometric characteristic points on the curve, which show respectively cracking in interior, development of surface cracks, and failure process, make obvious

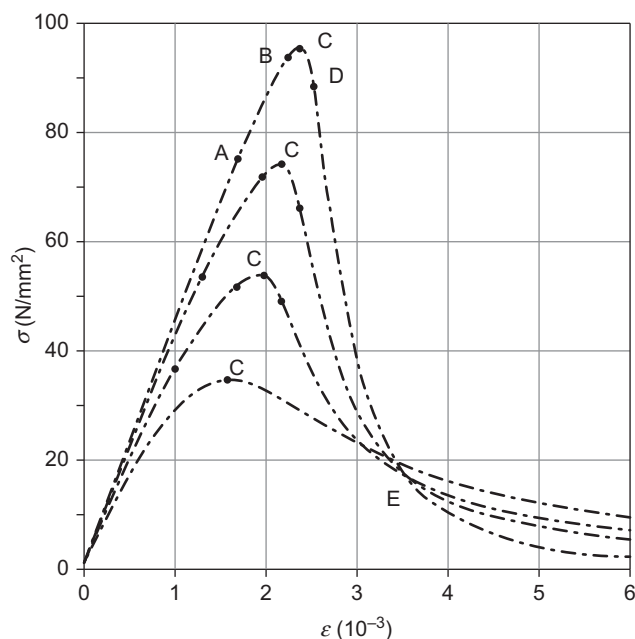
**FIG. 4-1** Complete compressive stress—strain curve of high-strength concrete

Table 4-3 Comparisons of Positions of Characteristic Points and Parameter Value of Equation for Complete Stress–Strain Curve [1-2]

Kinds of Concrete	Point A σ/f_c	B		C ϵ_p (10^{-6})	D		E		σ/f_c at $\epsilon = 3\epsilon_p$	Slope Angle of Failure Plane $\theta(^{\circ}\text{C})$	Parameters of Curve Equation	
		σ/f_c	ϵ/ϵ_p		σ/f_c	ϵ/ϵ_p	σ/f_c	ϵ/ϵ_p			α_a	α_d
Ordinary concrete C20–C40	0.4	0.86	0.65	1400–1800	0.91	1–1.35	0.4–0.6	2–3	0.4–0.7	59–64	2.0	1.0
High-strength concrete C60–C100	0.6–0.8	0.96	0.84	1600–2500	0.97–0.98	1.09–1.10	0.2–0.3	1.26–1.36	0.14–0.22	70–72	1.3–1.5	2.8–4.0
Ceramsite concrete	0.3–0.6	0.90–0.96	0.80–0.87	1800–3000	0.92	1.14	0.40–0.50	1.8	0.15–0.24	66–69	1.7	4.0

differences to that of ordinary concrete. Also the parameter values of the equation for the curve are different (Table 4-3).

Elastic limit (point A). The stress and strain of the specimen increase almost proportionally at the early stage of loading. As the stress is higher than Point A, the plastic deformation of the concrete starts to appear, and its strain accelerates and the stress-strain curve tends convex towards the ordinate (stress axis). The stress value at Point A increases with the strength of concrete, because of better compactness, higher adhesive strength on the boundary of aggregate, and less internal crack and defect of high-strength concrete, and the extension and expansion of microcracks only occurs under higher stress.

Developing of internal crack (Point B, $\nu_t \geq 0.5$). When the specimen is loaded further and the curve reaches Point B, the cracking sound is heard from inside the specimen and its strain accelerates, but no crack is found on its surface. Then, the prism compressive strength of concrete (Point C) is reached soon and the stress reduces quickly afterwards, a sharp peak is formed on the curve.

Appearance of crack and spalling off (Point D). As the stress passed the peak point, the crack develops quickly and is visible on the surface of the specimen, and the cracking sound is heard continuously. Afterwards, small pieces of the surface layer start to spall off and the spalled surface of the specimen is approximately parallel to the direction of the compressive stress. In the meantime, the stress drops quickly while the strain increases slightly, so a sharp descending branch is formed on the curve. When the surface crack develops and runs through the whole section, Point E of the maximum curvature of curve is reached. Afterwards, the specimen is divided into small columns and supported by the interaction and friction between these columns, so the residual stress is limited and the curve descends gradually.

The failed specimen shows less crack on its surface, besides the main inclined crack with a narrow damaged belt. Frequently, the specimen is split into several big blocks and many small pieces, even some coarse aggregates are split too. The angle between the main inclined crack and the normal line of the compressive stress of high-strength concrete is greater than that of ordinary concrete (Table 4-3).

The ratio between the prism and cubic compressive strengths of high-strength concrete (Fig. 4-2) is generally:

$$\frac{f_c}{f_{cu}} = 0.82 \sim 0.90, \quad (4-1)$$

and it increases slightly with its strength. Because, high-strength concrete is more brittle, the friction confinement on the loading surface is of less benefit to the bearing capacity of cubic specimen, and the difference between the prism and cubic compressive strengths of high-strength concrete is reduced. The ratio between them is taken as a lower value in the China design code [2-1], i.e. 0.76 (see Section 2.2.3) and 0.82 respectively for the concrete grades C50 and C80, and linear interpolation is used for that between them.

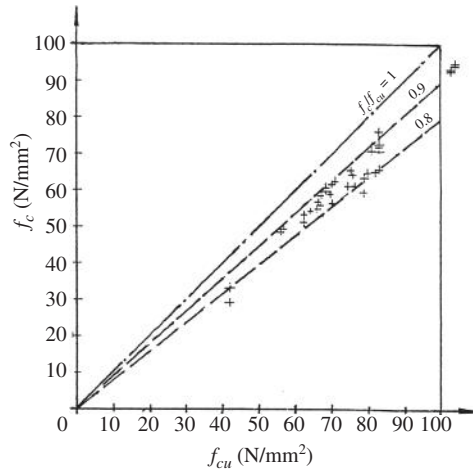


FIG. 4-2 Relation between prism and cubic compressive strengths of high-strength concrete [2-1]

The compressive peak strain (ϵ_p) of high-strength concrete increases with its strength (f_{cu} or f_c) (Fig. 2-9), and its calculation formula is the same as Eq. (2-2):

$$\epsilon_p = (700 + 172\sqrt{f_c}) \times 10^{-6}. \quad (4-2)$$

The modulus of elasticity of high-strength concrete also increases with its compressive strength (Fig. 4-3), but varies with the kind, quality, and quantity of the coarse aggregate used. If the modulus of elasticity of high-strength concrete is calculated following the formula used for ordinary concrete (Table 2-5), the value obtained is obviously lower than the experimental one. According to the

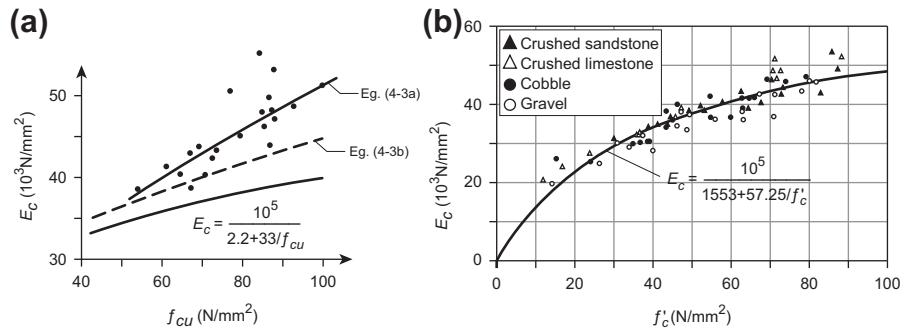


FIG. 4-3 Modulus of elasticity of high-strength concrete [4-1]: (a) Chinese tests, (b) Japanese tests

experimental results of China, the modulus of elasticity of high-strength concrete is about:

$$\text{average value } E_c = 4500\sqrt{f_{cu}} + 5000 \text{ N/mm}^2 \quad (4-3a)$$

$$\text{lower boundary } E_c = 2600\sqrt{f_{cu}} + 1800 \text{ N/mm}^2. \quad (4-3b)$$

It is similar to that suggested by ACI^[4-9] but with different values of the parameters in it:

$$E_c = 3320\sqrt{f_{cu}} + 6900 \text{ N/mm}^2. \quad (4-4)$$

The formula based on the Japanese tests fits the concrete of all strength grades:

$$E_c = \frac{10^5}{1.553 + (57.25/f'_c)} \text{ N/mm}^2. \quad (4-5)$$

The various compressive strengths (f_{cu} , f_c , f'_c) of concrete in the above equations are all in N/mm², and it is also the same for the equations below in this section.

The measured value of Poisson's ratio of high-strength concrete within its elastic stage [4-1,4-8] ranges between 0.20 and 0.28, and is not obviously different from that of ordinary concrete.

The complete compressive stress-strain curve of high-strength concrete also satisfies the geometrical characteristics (Eq. 2-5) for that of ordinary concrete, so same separate equations (Eq.2-6) can be used for it:

$$\left. \begin{aligned} x \leq 1 \quad y &= \alpha_a x + (3 - 2\alpha_a)x^2 + (\alpha_a - 2)x^2 \\ x \geq 1 \quad y &= \frac{x}{\alpha_d(x-1)^2 + x}, \\ x &= \frac{\epsilon}{\epsilon_p}, \quad y = \frac{\sigma}{f_c}. \end{aligned} \right\} \quad (4-6)$$

The parameters α_a and α_d are obtained after regression analysis [1-2] of the experimental data:

$$\left. \begin{aligned} \alpha_a &= 2.4 - 0.1f_{cu} \\ \alpha_d &= 0.132f_{cu}^{0.785} - 0.905 \end{aligned} \right\} \quad (4-7)$$

The empirical formulas for the central and splitting tensile strength (f_t and $f_{t,s}$) of high-strength concrete (Fig. 4-4) are separately:

$$f_t = 0.21f_{cu}^{2/3} \quad (4-8)$$

$$f_{t,s} = 0.30f_{cu}^{2/3} \quad (4-9)$$

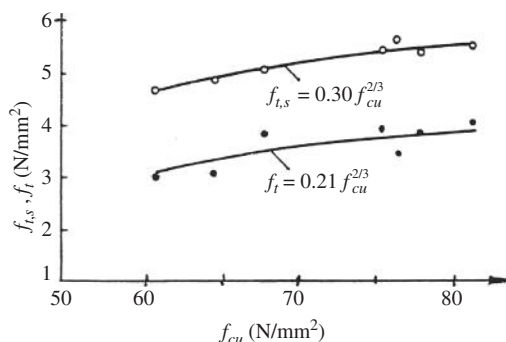


FIG. 4-4 Tensile strength of high-strength concrete [4-1]

The central tensile strength is about 20% lower than that calculated by Eq. (2-12) for ordinary concrete, and this shows that the tensile strength of concrete increases with the compressive strength, but with reducing amplitude.

The flexural tensile strength of high-strength concrete ($f_{t,f}$) is about 1.4–1.6 times the central tensile strength of it, it is consistent with the experimental results introduced above (Eq. (3-8)).

It is concluded from the main mechanical behavior of high-strength concrete ($\geq C50$) introduced above that its main characteristic is: the brittleness of concrete increases with its compressive strength. It means that the internal crack appears suddenly under higher stress level and develops quickly, failure occurs rapidly and residual strength drops sharply, the peak part of the complete stress–strain curve is rather sharp and the relative area under the curve is smaller, i.e. energy absorbability is poorer, and the tensile strength increases slowly with the compressive strength.

High-strength ($\geq C50$) and ordinary ($< C50$) concretes are made from the same kinds of raw materials, their characteristics are basically the same and the indices of their mechanical behavior are continuous. When the various strengths and other indices of concrete are investigated, analyzed, and regressed within its wider range (e.g. from C15 to C100), a unified regularity and empirical formula can be concluded, for example, Fig. 2-9 and Fig. 4-3(b). On the other hand, if the experimental results and empirical formula are obtained from the concrete within a narrow range (e.g. from C15 to C40) but used for the concrete other than that (e.g. $\geq C50$), the calculation error, to a different extent, should be brought.

The most knowledge and analyses of the behaviors of concrete material and structure, and the corresponding calculation formulas established, are mainly based on the experimental results of concrete of strength grade $\leq C40$. They include: the boundary between under- and over-reinforcement or the balance reinforcement rate of flexural member, the boundary between larger and smaller eccentric compressive members, the parameters for the equivalent rectangular stress block on the structural section at ultimate state, the calculation formulas for ultimate strength of eccentric compressive member and shear strength of flexural member, etc.

If these calculation formulas and parameters are directly used to analyze and design the structure of high-strength concrete, the results obtained and error contained will induce unsafe consequences. Some design code, e.g. [2-12], advises clearly that it should be careful when the listed calculation formulas are used for the concrete of strength $\geq C50$.

Therefore, the mechanical behaviors of the structure and its member of high-strength concrete have to be investigated specially. Alternatively, the generalized method of theoretical analysis for ordinary concrete is used but the constitutive relation of high-strength concrete is introduced, and then the calculation results are demonstrated properly to guarantee the necessary safety of the structure and its member.

4.2 Light-weight concrete

4.2.1 Classification

When light-weight concrete (density $\rho = 500 \sim 1900 \text{ kg/m}^3$) is used for the structure to replace ordinary concrete, the weight of the structure with the same load-carrying capacity is reduced by 20–40%. This is an effective and easy way to deduce dead load of the structure. In addition, light-weight concrete is mainly composed of porous material, and its coefficients of heat conduction and linear expansion is smaller than that of ordinary concrete. Therefore, the thermal conservation, high-temperature resistance, and fire endurance of the structure made of light-weight concrete are obviously better than that of ordinary concrete. This is another important advantage of it.

Light-weight concrete has been applied in engineering practice for many years and now is widely used in various structures at home and abroad. Especially, great advantage is shown when it is used for high-rise buildings.

There are two catalogues of structural light-weight concrete used in the engineering practice.

4.2.1.1 'Homogeneous' porous concrete ($\rho = 500\text{--}800 \text{ kg/m}^3$)

Autoclaved aerated concrete is a porous concrete used widely in several countries. The adhesive material of it is cement or lime powder, fly ash, mixed with fine sand or slag and water. In the meantime, the foaming agent is put into the liquid and numerous stable bubbles of diameter 1–2 mm are produced, and the uniform porosity is formed. After the liquid is left for several hours and then, autoclaved under water vapor of high temperature and pressure, a kind of macro homogeneous material of porosity is made [4-10]. The indices of the main mechanical and thermal behaviors of autoclaved aerated concrete are shown and compared with the ordinary concrete in Table 4-4. Various products of different indices and sizes of it are manufactured massively in the factory. The reinforced members are used as roof and floor slabs and wall panels for building [4-11], and small blocks of it are used for masonry wall, which has the advantages of light weight, heat insulation, and an easy process, besides carrying load.

Table 4-4 Comparison of Indices of Main Mechanical and Thermal Behaviors Between Light-Weight and Ordinary Concretes

Kind of Concrete	Density (kg/m ³)	Compressive Strength (N/mm ²)	Strength Ratio f_t/f_c	Modulus of Elasticity $\times 10^3$ (N/mm ²)	Poisson's Ratio	Coefficient of Heat Conduction W/(m.K)	Coefficient of Linear Expansion $\times 10^{-6}/K$
Ordinary	2200–2300	20–50	0.08–0.12	25–35	0.2	1.63–0.58	6–30
Light-weight*	1400–1900	15–30	0.10–0.12	10–18	0.2	1.16–0.29	7–10
Aerated	500–800	3–8	0.08–0.10	1.5–2.2	0.2	0.14–0.31	8

**The indices of light-weight concrete vary with its density.*

4.2.1.2 Concrete of light-weight aggregate ($\rho = 900\text{--}1900 \text{ kg/m}^3$)

When porous coarse aggregate of light-weight is used to replace the ordinary one (natural and crushed gravel) and is mixed with cement, sand, and water, light-weight concrete is composed. Sometimes, light-weight sand is also used and replaces ordinary sand, the concrete composed is called entire light-weight concrete.

The light-weight (coarse) aggregate used for structural concrete are classified as three categories, according to its source and composition:

Natural product crushed and sieved porous rocks, e.g. volcanic pumice stone and lapillus;

Industrial waste product, e.g. natural coal gangue, coal cinder, and sintered ceramsite of fly ash;

Artificial material sintered ceramsites of shale and clay, and expanded perlite.

The different shapes of the coarse aggregate, i.e. ball or ellipsoid, irregular pieces, depend upon its source. The compressive strength of the light-weight coarse aggregate itself is not high, so the maximum size of its particles should not be greater than 20 mm, when it is used in structural engineering. The particle density itself ranges from 600 kg/m^3 to 2000 kg/m^3 , and the piled density of it ranges from 300 kg/m^3 to 1000 kg/m^3 . The light-weight fine aggregate (sand) can also be made from the same raw materials and manufacturing technique, its particle size is $\leq 5 \text{ mm}$ and its piled density ranges from 500 kg/m^3 to 1000 kg/m^3 .

According to the requirement of the structural engineering and provided material, light-weight coarse aggregate (or/and fine aggregate) of various categories and density may be selected to compose and manufacture light-weight concrete of different density and strength grade (Fig. 4-5). The requirements for the raw material, mixing design, construction technique, test method, and classification of strength grade of light-weight concrete can be found in detail in references [4-12–4-14].

The strength grade of light-weight concrete, like that of ordinary concrete, is classified by its compressive strength, which is measured from the cubic specimen of length 150 mm under the standard test method. The strength grades of light-weight concrete used in structural engineering range from CL15 to CL50 and the difference between two adjacent grades is 5 N/mm^2 , and the strength grade of it used in prestressed concrete structure should be $\geq \text{CL25}$, according to the Chinese codes [4-12,4-13]. The density of the light-weight concrete ranges from 1300 kg/m^3 to 1900 kg/m^3 , and the relation between the strength grade (compressive strength) and density of it varies with the aggregate of different category (Fig. 4-5).

4.2.2 Basic mechanical behavior

The main mechanical behavior of light-weight concrete under compression is also represented by the complete stress–strain curve. The complete curve of ceramsite concrete, used as an example here, is shown in Fig. 4-6, its shape is generally consistent with that of ordinary concrete (Fig. 2-7) and it also satisfies all the geometrical

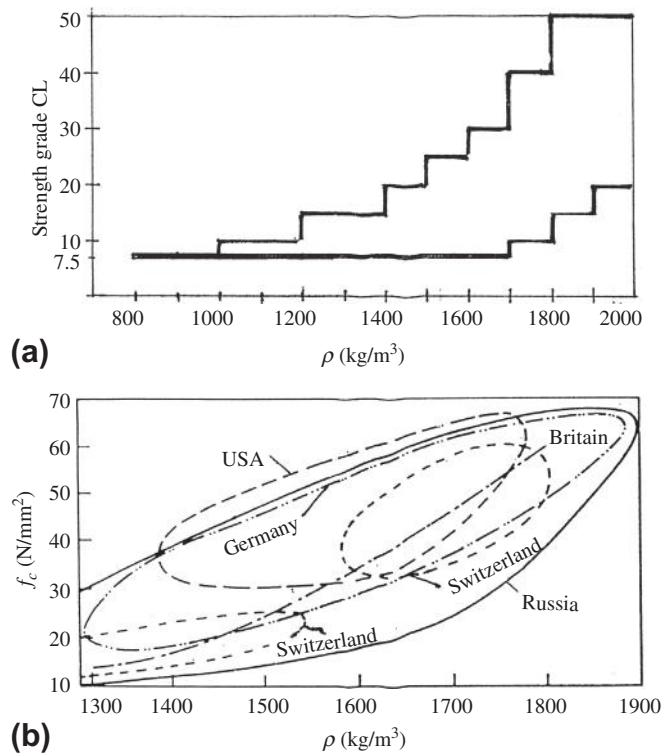


FIG. 4-5 Relation between compressive strength and density of light-weight concrete: (a) reference [4-13], (b) reference [4-14]

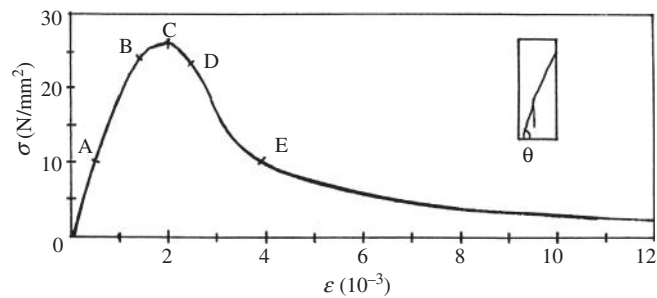


FIG. 4-6 Complete compressive stress-strain curve of ceramsite concrete [2-13]. × The density of the concrete is 1800 kg/m³, and the shale ceramsite used is of particle size 5–20 mm and particle density 1470 kg/m³

characteristics of the latter (Eq. (2-5)). But, the values of the stress and strain at the characteristic points on the curve are different from that of ordinary concrete (Table 4-3).

After the specimen is loaded, its strain approximately increases proportionally with the stress until the elastic limit (Point A), which ranges from $0.3f_{c,L}$ to $0.6f_{c,L}$ depending upon the category of the aggregate and the strength grade of concrete. Afterwards, plastic deformation of the concrete appears and accelerates, the curve turns convex towards the ordinate axis. When the stress and strain reach respectively $(0.90-0.96)f_{c,L}$ and $(0.80-0.87)\epsilon_{p,L}$ (Point B), the tangent Poisson's ratio of the concrete is $\nu_t \approx 0.5$ and internal crack develops, but no visible crack appears on the surface of the specimen. Then, the maximum stress (Point C) is reached soon, which corresponds to the prism compressive strength $f_{c,L}$ of the concrete, and corresponding peak strain is $\epsilon_{p,L}$.

After the curve enters the descending branch, the first crack appears on the surface of the specimen (Point D, $\nu_s \approx 0.5$) and is long with a sharp slop. As the test continues, the crack develops obliquely and cracking sound sends out, the stress drops quickly but no new crack is found. When the inclined crack runs through the whole section of the specimen (Point E), its residual strength is less than $0.5f_{c,L}$ and corresponding strain is about $1.8\epsilon_{p,L}$. Then, the specimen is supported by the residual strength of concrete and the friction on the inclined crack, the stress reduces stably. Sometimes, several longitudinal or slightly deviated cracks appear and start from the main inclined crack. When the strain reaches $3\epsilon_{p,L}$, the residual strength is about $0.15-0.24f_{c,L}$ and reduces slowly as the strain of the specimen increases further.

The angle between the main inclined crack and the normal line of the stress of the ceramsite concrete specimen is $66-69^\circ$, which is obviously greater than that of ordinary concrete. The failed surface of the specimen is clear, and several split pieces of mortar and coarse aggregates of ceramsite can be found there.

The basic difference between the light-weight and ordinary concretes is different aggregate used. As far as ordinary concrete is concerned, the coarse aggregate is solid, stronger, and harder and is surrounded and adhered by the cement mortar of net shape, which forms the weaker part in the concrete. On the contrary, the coarse aggregate is porous, weaker, and softer and is surrounded and adhered by the cement mortar for the light-weight concrete, so its weaker part turns into the coarse aggregate. This causes the difference of behavior between the concretes.

The strength of the coarse aggregate used for ordinary concrete is far greater than that of concrete itself. When the concrete is loaded continuously, the crack occurs and develops on the boundary between the aggregate and cement mortar and in the interior of the cement mortar, but it is obstructed and delayed by the coarse aggregate. Finally, the failure of ordinary concrete occurs also on the boundary of aggregate and in the cement mortar, but the aggregate itself is not damaged.

However, the situation of the light-weight aggregate concrete is quite different. Normally, the light-weight aggregate is a kind of porous and brittle material and its compressive and tensile strengths and modulus of elasticity are rather low, even

lower than that of cement mortar surrounding it. When the light-weight concrete is loaded, the stresses of coarse aggregate and cement mortar distribute differently from that of ordinary concrete (Fig. 2-2), i.e. the stress on coarse aggregate is lower and the cement mortar carries more load. The mechanical model of the light-weight concrete can be approximately simulated as a skeleton of cement mortar filled with light-weight aggregate. In addition, the rough surface of light-weight aggregate is adhered better with the cement mortar, so the crack on its boundary appears later and develops slowly. However, the modulus of elasticity of the aggregate is rather low, and this causes larger deformation, including peak strain ($\varepsilon_{p,L}$), of the light-weight concrete under loading; after the crack appears in cement mortar, it extends quickly and passes through the coarse aggregate which is not strong enough to obstruct it; so, many split coarse aggregates can be found on the failure surface, but the number of cracks on the specimen surface is less; the descending branch of stress–strain curve is sharp and the residual stress drops sharply. Therefore, the strength and deformation behavior of the light-weight concrete depend upon, to a great extent, the strength and property of the coarse aggregate of light-weight.

The measured ratio between the prism and cubic compressive strengths of the light-weight concrete is:

$$\frac{f_{c,L}}{f_{cu,L}} = 0.9 \sim 1.0. \quad (4-10)$$

It is much greater than that of ordinary concrete and also greater than that of high-strength concrete. The main reason for this is that the light-weight concrete is brittle and loose, the confinement action of the compressed plate on the cubic specimen tested is limited and the failure pattern of it is similar to that of prism specimen, so the strengths of both specimens are approached.

The compressive peak strain of the light-weight concrete varies widely in the range of $1.8\text{--}3.0 \times 10^{-3}$ and depends upon not only its strength (or strength grade) but also the category and property of the aggregate. Its empirical formula suggested in reference [4-15] is:

$$\varepsilon_{p,L} = (1.637 + 0.0204f_{c,L}) \times 10^{-3}. \quad (4-11)$$

The modulus of elasticity of the light-weight concrete also depends upon its strength and the property of aggregate (Fig. 4-7), and the latter is represented by the density of the concrete. The empirical formulas suggested in Chinese and USA codes are respectively:

$$\left. \begin{aligned} E_{c,L} &= 1.929\rho\sqrt{f_{cu,L}} \quad [4-13] \\ E_{c,L} &= 0.043\rho^{1.5}\sqrt{f'_c} \quad [2-11] \end{aligned} \right\} \quad (4-12)$$

where ρ —density of light-weight concrete, in kg/m^3 , $f_{cu,L}$ or f'_c cubic or cylinder compressive strength of light-weight concrete, in N/mm^2 .

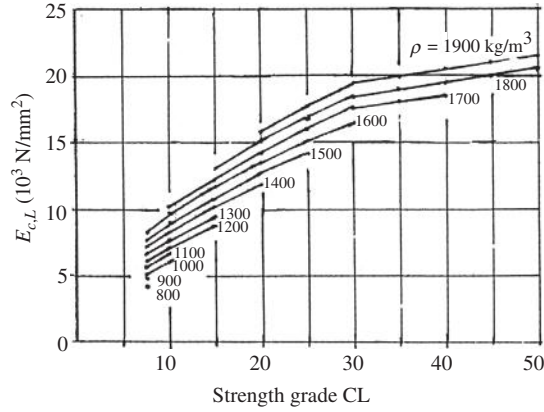


FIG. 4-7 Modulus of elasticity of light-weight concrete [4-13]

The measured Poisson's ratio of the light-weight concrete varies in the range of 0.15–0.26 and is normally taken as 0.2, which is the same for ordinary concrete (Section 2.2.3).

The complete compressive stress–strain curve of light-weight concrete is a sharp one with a raised peak, but the separate equations fitted for ordinary concrete (Eq. (2-6) or Eq. (4-6)) can also be used for it, when the parameters are taken as:

$$\left. \begin{array}{ll} x \leq 1.0 & \alpha_{a,L} = 1.7 \\ x \geq 1.0 & \alpha_{d,L} = 4.0 \end{array} \right\} \quad (4-13)$$

The tensile strength of the light-weight concrete ($f_{t,L}$) and the bond strength between it and reinforcement ($\tau_{p,L}$) vary widely with the factors, including category and quality of coarse aggregate, water content, age, etc. The values of both strengths of the light-weight concrete are approaching or slightly lower than that of ordinary concrete of same compressive strength [4-14]:

$$\frac{f_{t,L}}{f_t} \approx \frac{\tau_{p,L}}{\tau_p} = 0.75 \sim 1.0 \quad (4-14)$$

The shrinkage and creep of the light-weight concrete are also influenced by the above factors, and their values are about equal or slightly greater than the corresponding values of ordinary concrete of same compressive strength.

In summary, the mechanical behavior of the light-weight concrete is similar to but more 'brittle' than that of ordinary concrete, so the differences exist between the mechanical indices of both concretes. Consequently, the behaviors of the light-weight concrete structure and its members are also similar to but more 'brittle' than that of ordinary concrete. If the empirical calculation formula, parameter value, and design and construction methods fitted for ordinary concrete, e.g. equivalent rectangular stress block on section at ultimate state, the boundary between larger

and smaller eccentricities of compressed member, ultimate shear strength, anchorage length of reinforcement, ductility of structural member, are directly used for that of the light-weight concrete, an unsafe consequence will be the result. Therefore, the mechanical behaviors of the light-weight concrete structure and its members have to be investigated specially, or the theoretical method for analyzing the structure of ordinary concrete and the constitutive relation of light-weight concrete are used together, and then the result obtained is experimentally demonstrated. Now, the relevant design code is the summarization of existing experimental investigation and engineering experience and has to be followed.

4.3 Fiber concrete

4.3.1 Classification

A certain amount of dispersed short fiber is mixed in concrete or cement mortar during mixing, the composed material of macro homogeneous and isotropic is obtained after compacted and coagulated and is called fiber concrete.¹ The main function of the fiber in concrete is to strengthen the cracking resistance of the brittle matrix, to prevent sudden failure, and to increase toughness and ductility of it. It likes wheat straw-soil and hemp-fibered plaster, which have existed in China since ancient times.

Now, various kinds of fiber are used for fiber concrete or fiber mortar, and they are classified as three categories, according to their source and manufacture method:

Natural fiber plant, e.g. cotton, sisal hemp;

Mineral, e.g. asbestos, mineral wool;

Artificial fiber, e.g. glass yarn, nylon yarn, artificial silk, polypropylene yarn, ... Steel fibre cut from wire (circle section of diameter $d = 0.25 \sim 0.76$ mm) or thin plate (rectangular section with thickness 0.15–0.41 mm and width 0.25–0.90 mm), or stretched from melted steel under high temperature and speed (of new moon section). The steel fiber is pressed into waves along the longitudinal direction or into bends near its both ends, in order to increase the bond strength between it and concrete.

The fibers used frequently and their main mechanical behaviors are listed in Table 4-5.

The fiber used in structural engineering has to satisfy the geometrical requirement besides the mechanical behavior, i.e. its length–diameter ratio ranges:

$$\frac{l}{d_{eq}} = 30 \sim 150, \quad (4-15)$$

¹Alternatively, when the fiber is weaved into the form of bundle, net, or cloth, and put into concrete, it can be used as the tensile material to replace the steel reinforcement (see Section 6.1). But, this is not so-called fiber concrete.

Table 4-5 Main Mechanical Behavior of the Fibers used in Fiber Concrete [4-16-4-19]

Classification	Kinds	Diameter (10^{-3} mm)	Length (mm)	Density (kg/m ³)	Tensile Strength (N/mm ²)	Modulus of Elasticity (N/mm ²)	Ultimate Elongation (%)	Quantity Contained (%)
Natural	Cotton			1500	400-700	5000	3-10	
	Asbestos	0.1-20	5-10	2500-3300	600-1000	196 000	2-3	8-16
Artificial	Glass	5-15	20-50	2600	2000-4000	80 000	2-3.5	4-6
	Nylon	> 4		1140	800-1000	4000	~ 15	
	Polypropylene	20-200	2-25	900	500-800	3500-5000	~ 20	4-8
Metal	Steel	5-500	12-25	7850	300-3000	210 000	3-4	1-2

where its length is usually $l = 6-76$ mm and d_{eq} is the equivalent diameter for the fiber of non-circle section, of which the area is equal to that of the equivalent circle. The fiber of too short length causes low pull-out strength, while the fiber of too long length is difficult to be mixed uniformly. Both reduce the quality and behavior index of fiber concrete.

The various fibers have been used in structural engineering for many years, and the general conclusions are drawn from the engineering experiences as below. Generally, the natural fiber is of irregular shape, non-uniform quality, low strength, and poor durability, and can be used only for the secondary members, e.g. corrugated plate and small tube. Furthermore, asbestos is harmful to people's health and had been forbidden from being used in many countries. The artificial fiber is industrially manufactured and its quality is easily controlled, and various kinds of it with different properties are available now. However, glass yarn is brittle and broken easily, the synthetic fiber has low strength and modulus of elasticity, and most of them are poor to resist the acid corrosion from cement, so their strength reduces with time and durability is also damaged. The steel-fiber-reinforced concrete is of better, stable, and durable behavior, the technical and economical benefits are achieved when it is properly applied in structural engineering. Some difficulties in its construction technique have been solved, the manufacture technology is improved and special equipment is provided, even spray-concrete of steel fiber succeeded in practice. But, the cost of steel fiber concrete is high, so it should be reasonably used in the key-part of the structure and the technical advantages of it are shown fully.

4.3.2 Basic mechanical behavior

Fiber concrete contains a large amount of fine fibers of high tensile strength distributed randomly in it, and its mechanical behavior is improved considerably, compared with that of plain concrete: tensile and flexural strengths increase 1.4–2.5 times and cracking resistance increases significantly; ductility increases greatly although compressive strength increases limitedly; fatigue strength increases obviously and dynamic strength increases 5–10 times; wear and scour resistances increase as well.

Fiber concrete, especially steel fiber concrete, can be used singly in structural engineering, or it works together with the reinforcement and the reinforced fiber concrete is formed. They are used successfully in the engineering fields including: runway and parking aprons of airports, pavements of highways and bridges, dams, water pools, underground tunnels and mine liners, plate and shell structures, defense works, bridge strengthening, beam-column joint of frame structures in earthquake zone, shear resistance near beam ends, and key parts of building structures.

The mechanical behavior of fiber concrete depends mainly upon the kind, shape, quantity contained (represented by V_f in % to show the ratio between fiber and total volumes), and distributive situation of the fiber, besides the behavior of its matrix,

i.e. plain concrete or cement mortar. The difference between the behaviors of fiber and plain concretes is explained below, as the steel fiber concrete is used as an example.

The complete stress—strain curve of steel fiber concrete under central tension is measured and shown in Fig. 4-8(a). Before cracking of the specimen, the stress of the steel fiber in its interior is low, so the stress—strain curve approaches that of plain concrete. After the matrix of the fiber concrete is cracked, the stress of the steel fiber intersected with the crack increases significantly with the deformation, and gradually replaces the tensile action of the matrix. When the crack runs through the whole section of the specimen, the fiber carries all the tensile force. Because the tensile strength of the steel fiber is rather high but its length is limited (necessary anchorage length is not guaranteed), and it distributes randomly and has no definite direction, the steel fibers slip under high stress and, then, are gradually pulled out one after the other. So, the descending branch of the curve is formed. Finally, the specimen fails

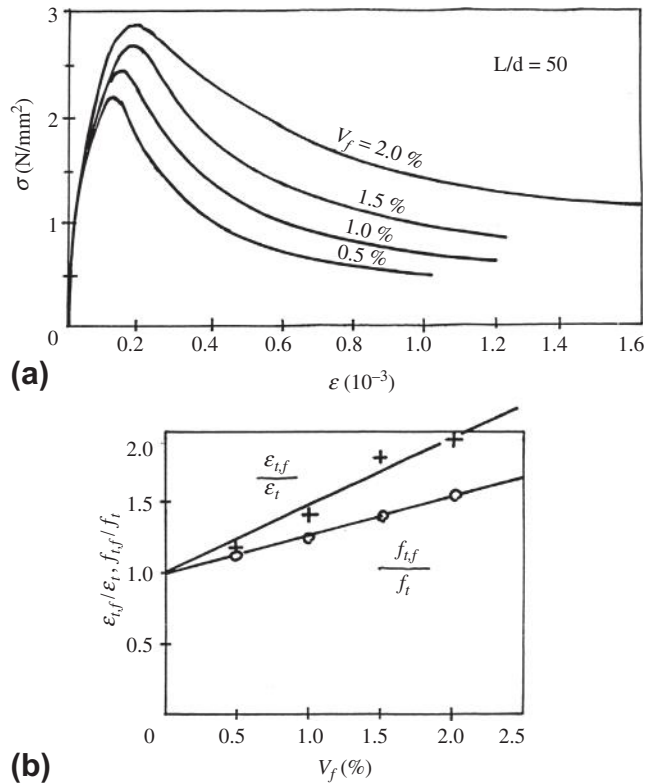


FIG. 4-8 Steel fiber concrete under central tension [4-20,4-21]. (a) Complete stress—strain curve, (b) influence of fiber content on its strength and peak strain

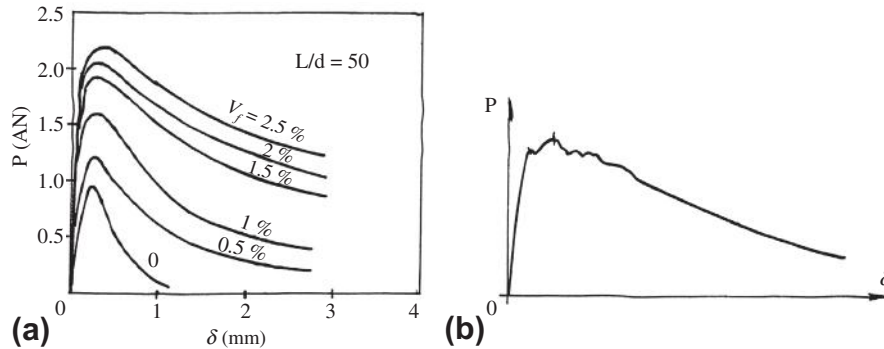


FIG. 4-9 Flexural behavior of steel fiber concrete: (a) load–deflection curve, (b) reference [4-16]

and all the steel fibers on the failure surface are pulled out because of bond failure, only a few of them are broken.

The tensile strength ($f_{t,f}$) of the steel fiber concrete increases by 20–50% and the corresponding peak strain ($\epsilon_{t,f}$) increases by 20–100%, as the volume of the steel fiber content increases from $V_f = 0.5\%$ to 2.0% (Fig. 4-8(b)). In the meantime, the peak point on the complete stress–strain curve moves up and to the right side, and the descending branch of the curve raises and flattens.

The curve of load–deflection at midspan of the flexural specimen of steel fiber concrete is measured during testing and shown in Fig. 4-9(a). Before the crack appears in the tensile zone of the specimen, the load (or stress) and deflection (or strain) vary almost linearly. After the matrix of the fiber concrete is cracked, the stress of the fiber intersected with the crack increases suddenly, the load carried by the specimen increases continuously. As the crack develops further and the neutral axis on the section moves, the matrix in tensile zone is gradually out of work and the fiber has to bear more internal force. When the steel fibers in the tensile zone on the section are pulled out one by one because of bond failure, a flatter descending branch of the curve is formed.

On the load–deflection curves of some specimens, several small turns occur near their peak points (Fig. 4-9(b)). When the matrix of the fiber concrete is cracked, the stress of the fiber intersected with the crack and the deflection of the specimen increase suddenly, and correspondingly the load drops slightly; then more fibers participate and carry more internal force, so the bearing capacity of the specimen increases again and a small turn is formed. As the matrix of the fiber concrete experiences several times sudden cracking, corresponding turns are appeared. After the curve passes its peak part, no load drops suddenly any more and the curve descends smoothly.

The flexural tensile strength ($f_{f,f}$) and the corresponding peak strain ($\epsilon_{f,f}$) of steel fiber concrete increase with the fiber content (V_f , %), and the flexural strength may

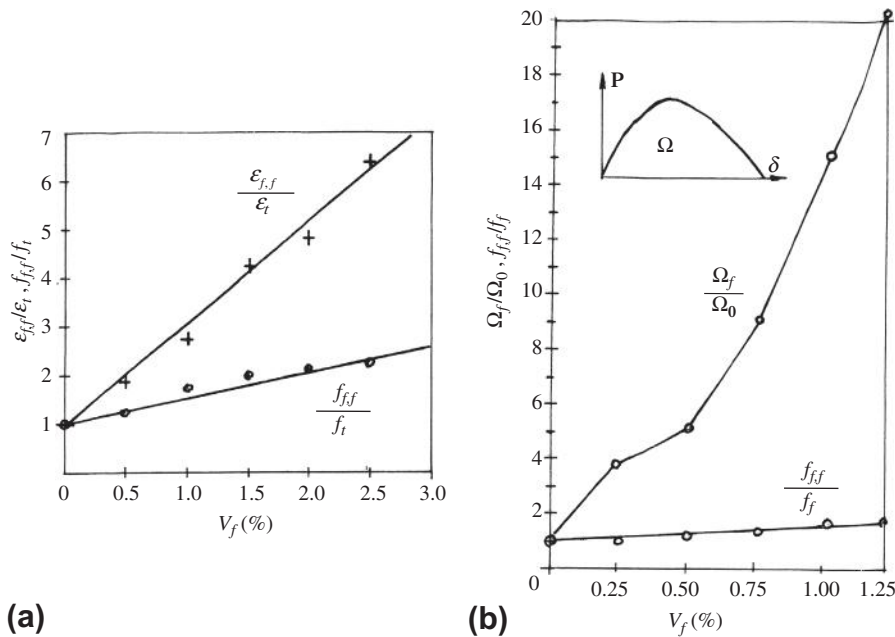


FIG. 4-10 Flexural tensile strength and toughness of steel fiber concrete. (a) Flexural tensile strength and peak strain [4-20], (b) toughness [4-19]

be doubled (Fig. 4-10(a)). When the area under the load–deflection curve (Ω) is defined as the toughness of a material, the toughness of steel fiber concrete (Ω_f) is increased 10 times, and even more, compared with that of plain concrete (Ω_0) (Fig. 4-10(b)).

The complete stress–strain curve of steel fiber concrete under central compression is shown in Fig. 4-11(a), and the geometrical shape and characteristic of it are

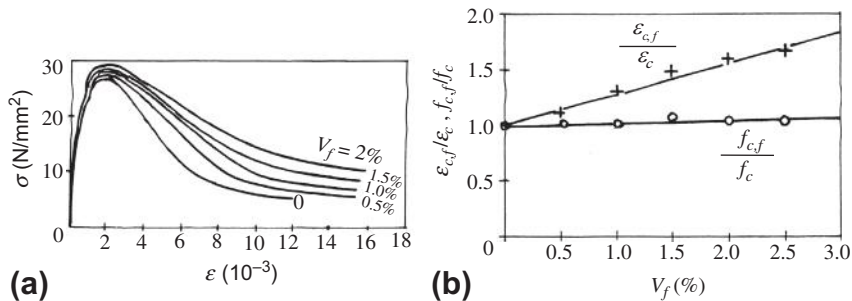


FIG. 4-11 Steel fiber concrete under central compression [4-20]. (a) Complete stress–strain curve, (b) influence of fiber content

the same as that of plain concrete (Fig. 2-7). As far as the ascending branch of the curve is concerned, the fiber mixed in has hardly any influence on the behavior of the matrix, i.e. plain concrete. Only when the curve enters its descending branch and the longitudinal crack appears on the specimen, do the fibers intersected with the crack work effectively and obstruct the development of the crack, so the residual strength post-peak is increased. Afterwards, the fibers slip and, then, are pulled out one after the other as their stress increases considerably, so the curve descends gently. The final failure pattern of steel fiber concrete is similar to that of plain concrete, i.e. a macro inclined cracked belt but with smaller slope angle passes through the whole section.

The compressive strength ($f_{c,f}$) and the corresponding peak strain ($\epsilon_{c,f}$) of steel fiber concrete vary with its fiber content (V_f) (Fig. 4-11(b)). Obviously, the peak strain increases greatly and the ductility and toughness of it increase even more, while the compressive strength increases limitedly.

The other mechanical behaviors, such as bond strength with reinforcement, shear and torsion resistances, fatigue strength, and the behavior under repeated load, of steel fiber concrete can be found in references [4-17–4-21].

The steel fiber concrete can be made of various fibers of different material, section and longitudinal shapes, and length—diameter ratio, and manufactured by different construction methods. Therefore, the mechanical behavior of it varies correspondingly, and also the experimental results provided by the researchers scatter to a certain extent.

According to the basic mechanical behavior of steel fiber concrete introduced above, the general regularity of fiber concrete is concluded as below. Before cracking of the matrix (concrete or cement mortar), the fiber mixed in affects it less; the main effect of the fiber starts only after its matrix cracked and it obstructs and confines the development of the crack, so the strength and especially the deformation ability (ductility and toughness) of fiber concrete increase considerably. And, when the fibers on the critical section slip and are pulled out successively, the failure of fiber concrete is reached.

When steel fiber is mixed in concrete, less benefit is obtained for compressive conditions, but more benefit for tensile condition and the maximum benefit for flexural condition are obtained for the fiber concrete, and its advantages of confining crack and increasing toughness are more important than the increment of strength. Therefore, (steel) fiber concrete should be used reasonably in structural engineering, and let its advantage be utilized fully. On the other hand, the main measure to improve the quality and behavior of fiber concrete is to enhance the bond strength of the fiber, e.g. increasing properly the length—diameter ratio, bent at both ends, irregular section.

When a structure of fiber concrete is designed, the design code or suggestions are available in some countries and can be consulted.

Multiaxial Strength and Constitutive Relation

CHAPTER OUTLINE

5.1 Experimental equipment and method	115
5.2 General regularities of multiaxial strength and deformation	118
5.2.1 Biaxial stress states	119
5.2.1.1 Biaxial compressions (C/C, $\sigma_1 = 0$)	119
5.2.1.2 Biaxial tension–compression (T/C, $\sigma_2 = 0$)	121
5.2.1.3 Biaxial tensions (T/T, $\sigma_3 = 0$)	121
5.2.2 Triaxial stress states	122
5.2.2.1 Conventional triaxial compressions ($0 > \sigma_1 = \sigma_2 > \sigma_3$ or $0 > \sigma_1 > \sigma_2 = \sigma_3$)	122
5.2.2.2 Real triaxial compressions ($0 > \sigma_1 > \sigma_2 > \sigma_3$)	124
5.2.2.3 Triaxial tension–compressions (T/T/C, T/C/C)	126
5.2.2.4 Triaxial tensions (T/T/T)	128
5.2.3 Different materials and loading paths	129
5.3 Typical failure patterns and their boundaries	132
5.3.1 Breaking in tension	132
5.3.2 Columnar crushing	133
5.3.3 Splitting into pieces	134
5.3.4 Inclined shearing	134
5.3.5 Extruding and shifting	135
5.4 Failure criterion	137
5.4.1 Shape of failure envelope and its expression	137
5.4.2 Failure criterion	141
5.4.3 Calculation charts for multiaxial strength	146
5.5 Constitutive relation	147
5.5.1 Models of linear elasticity	149
5.5.1.1 Anisotropic constitutive model	150
5.5.1.2 Orthogonal anisotropic constitutive model	150
5.5.1.3 Isotropic constitutive model	150
5.5.2 Models of non-linear elasticity	150
5.5.3 Models of other categories	151

The concrete in the reinforced concrete structure seldom carries single uniaxial compressive or tensile stress only. Even, the concrete in a simple structural member, e.g. beam, slab, or column, is in fact of a two- or three-dimensional stress state, because bending moment and shear force acted together on its section cause simultaneously normal and shear stresses, the local part near its support or under the concentrated load exists transverse stress besides the longitudinal stress, and the anchorage zone of prestressed reinforcement are obviously of a three-dimensional stress state. The typical two- and three-dimensional structures are widely used in the engineering practice, e.g. two-way slab, wall panel, shear wall, folded plate structure, spatial shell structure, and some special structures of great importance, for example: pressure vessel and containment of nuclear reactor, dam, heavy hydraulic press. The concrete in these structures is undoubtedly of multiaxial stress state.

If the uniaxial compressive and tensile strengths of concrete are taken when the structures and their members are under designing or their strengths are checked, the unreasonable result is certainly induced: either underestimating bi- and tri-axial compressive strength of concrete and causing more materials used, or overestimating multiaxial compressive-tensile strength of concrete and causing unsafe consequence.

In the early 20th century, Föppl (Germany) completed the biaxial compression test of cement mortar and Richart (USA) completed the conventional triaxial compression test of cylinder specimen [1-6]. Afterwards, research on the concrete behavior under multiaxial stress state has almost stagnated because its application in structural engineering is not urgently needed and the level of experimental technique is limited. In the 1960s, nuclear power plants were developed in some countries and the pressure vessel and containment of nuclear reactor of prestressed concrete are needed to be built, the research on multiaxial behavior of concrete was pushed forward and many researches were conducted in the 1970s.

During that time, electronic digital computers have developed very quickly and are used widely and the finite element method came gradually to maturity, both composing a powerful theoretical and calculation measure for accurately analyzing the complicated concrete structures. However, the reasonable and accurate failure criterion and constitutive relation of concrete have to be provided in advance. In the meantime, the electronic measurement and control technique made great progress and provided the possibility for building the experimental equipment for concrete under multiaxial stress state and improving the measuring technique.

Afterwards, a series of experimental and theoretical researches on the multiaxial behavior of concrete had been conducted in several countries, and the results of them have been accepted in the relevant design codes, e.g. the design codes for prestressed concrete pressure vessel of nuclear reactors in the USA, Britain, Germany, and France, the design codes for hydraulic engineering in Russia and Japan, and the CEB-FIP model code. Various calculation formulas or charts for multiaxial strength and constitutive relation of concrete are presented in these codes and have been used

in engineering practice for many years, and great technical and economical benefits have been achieved.

In China, the experimental and theoretical researches on multiaxial behavior of concrete have been conducted successfully in several universities and research institutes since the late 1970s. The relevant results obtained from these researches [5-1–5-6] provide the basis for establishing the provision for multiaxial strength of concrete in the code for design of concrete structures [2-1].

The principal stresses and strains at one point in a structure or the triaxial stresses and strains of a specimen are presented in this chapter as:

$$\sigma_1 \geq \sigma_2 \geq \sigma_3$$

$$\varepsilon_1 \geq \varepsilon_2 \geq \varepsilon_3,$$

and the signs of tensile and compressive ones are respectively positive and negative.

5.1 Experimental equipment and method

There is no unified standard for a triaxial test of concrete and the relevant test machine can not be found on the market. Generally, the experimental equipment for a triaxial test of concrete is designed and manufactured by the researchers themselves [5-7–5-12], and only a few decades of the equipment are used successfully currently. However, the principle and construction of them, including loading method, shape and size of specimen, measuring method for stress and strain of specimen, antifriction measure, are different from one another. So, the experimental data obtained from different equipments are scattered to an extent, this shows the influences of the experimental equipment and method.

There are two categories for the triaxial testing of concrete, according to the stress state of the specimen.

Conventional triaxial test equipment [5-9]. Usually, an independent hydraulic system, including a cylinder with a piston and an oil pump and pipe (Fig. 5-1(a)), is used together with an ordinary hydraulic test machine. After the specimen is put into the cylinder and under the piston, it is loaded laterally by the pressed oil via the pump and pipe, and loaded longitudinally by the test machine via the piston. The specimen is wrapped in advance in the rubber membrane to prevent the pressed oil entering the crack of the specimen after loading, which causes a reduction of its strength.

The specimen used is of a cylinder or square prism. When the specimen is compressed in all directions (C/C/C), two of the three principal stresses of it should be equal, i.e. $\sigma_1 = \sigma_2 > \sigma_3$ or $\sigma_1 > \sigma_2 = \sigma_3$ (Fig. 5-1(b)). This is called conventional triaxial compression, which is distinguished from real triaxial compression. If the specimen of hollow cylinder is used for testing, the stress states of biaxial compression (C/C) and tension-compression (T/C) are achieved separately, when the pressed oil acts respectively on the outside and inside of the specimen (Fig. 5-1(c)).

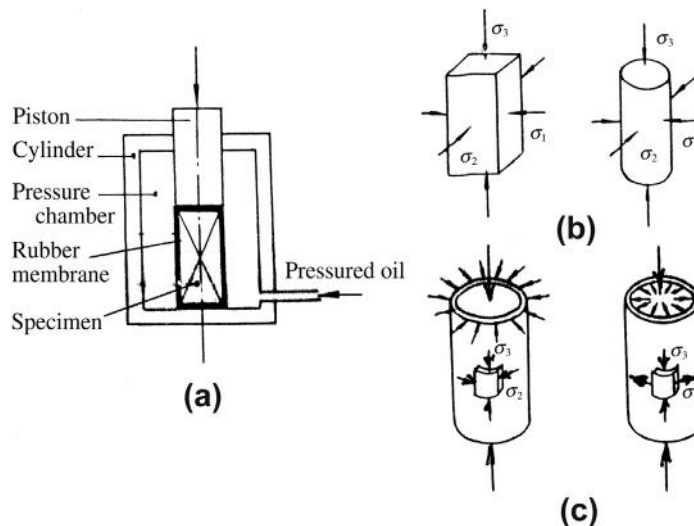


FIG. 5-1 Conventional triaxial test equipment. (a) Scheme of test equipment, (b) triaxial compression, (c) biaxial stress states

The main advantages of the conventional triaxial equipment are that: the typical product of the equipment is available, the lateral oil pressure is uniform and frictionless, loading ability is higher, i.e. the lateral compressive stress reaches 120 N/mm^2 and the longitudinal stress depends upon the maximum compression of the test machine (normally 5000 or 10,000 kN) and the size of the specimen. However, the tests of real triaxial compression ($\sigma_1 \neq \sigma_2 \neq \sigma_3$), biaxial tension (*T/T*), and triaxial tension-compression can not be conducted on this kind of equipment, this is the mortal disadvantage of it.

Real triaxial test equipment [5-3,5-5,5-10–5-12]. The typical constructions of the equipment are shown in Fig. 5-2 and the main characteristic of them is that the hydraulic pipeline and control systems, including cylinder and piston, are separately set up in three directions perpendicular to one another. However, various equipments have different mechanical constructions. The equipment shown in Fig. 5-2(a) is composed of three loading frames, including beams and screws, in three directions. Alternatively, an ordinary hydraulic test machine is used for exerting vertical stress on the specimen, and a stiff loading frame (Fig. 5-2(b)), containing two pairs of cylinders and pistons, is used for exerting horizontal stresses in perpendicular directions. It costs less and occupies less room, and is convenient for testing.

The three principal stresses of concrete in a complicated structure are not equal to one another and may be compressive or tensile. Obviously, the test equipment should be capable of exerting compressive or tensile stress on any direction and with any stress ratios ($\sigma_1:\sigma_2:\sigma_3$). Most of the test equipment developed after the 1970s is of this category.

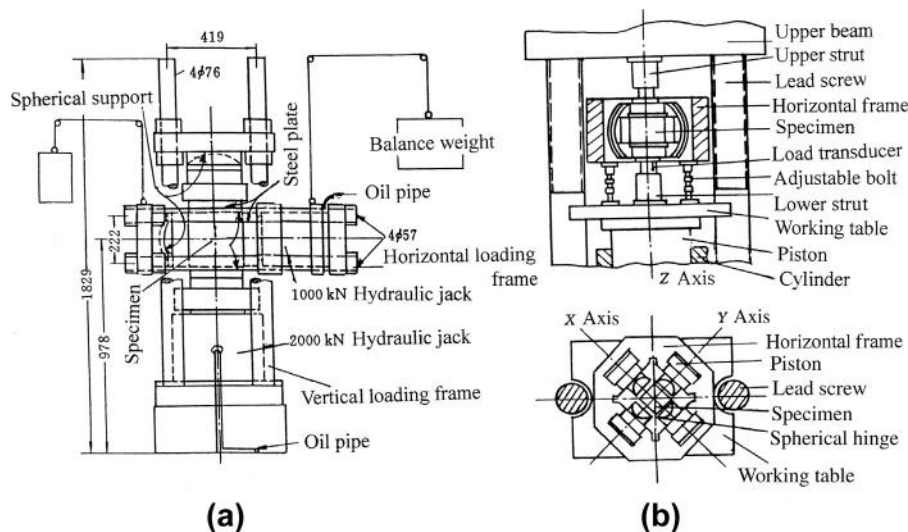


FIG. 5-2 Scheme of real triaxial test equipments: (a) Robinson [5-12], (b) Tsinghua University [1-2]

The maximum loading capacity of the real triaxial test equipment is compressions 3000 kN/2000 kN/2000 kN in three directions and tensions 200 kN/200 kN in two directions. The cubic specimen used generally ranges from 50 mm to 150 mm in edge length, and the plate specimen, of which the maximum size is 200 mm × 200 mm × 50 mm, is also used in biaxial test.

The real triaxial test equipment is normally developed by the researcher himself and no unified test standard can be followed. In addition, several technical difficulties have to be solved during its designing, otherwise the reality and accuracy of the experimental result obtained from it are doubtful. The main difficulties and corresponding measures are as below.

Reducing friction on surface of specimen. When the specimen is compressed simultaneously in three directions, the frictions on the six compressed surfaces confine strongly the deformation of it, and the measured strength of concrete is increased by a few times that under frictionless condition [1-2]. Therefore, the effective measure is necessary for eliminating or reducing the friction during multiaxial test of concrete. Various kinds of the measures are available now: (1) friction reducing pad [1-2], (2) loading brush-plate [5-10], (3) flexible loading plate [5-7], and (4) hydraulic pad [5-8]. The first one among them is used widely and the pad may be composed of different materials and constructions, e.g. two pieces of Teflon (thickness 2 mm) and grease between them, three pieces of aluminum foil (thickness 0.2 mm) and grease between them, separated small stainless pads.

Exerting tension. The tensile force can be exerted on the cubic or plate specimen only when it is firmly adhered with the loading plate via the high-strength

glue. In addition, the surface layer (thickness 2–4 mm) of the cast specimen contains more holes and cement mortar (Fig. 2-1) and has lower tensile strength, so the specimen used for a multiaxial tensile test has to be sawn from the larger concrete block or specimen and the surface layer sawn off should be ≥ 5 mm.

Measuring stress and strain. There are two methods for measuring the stress and strength of the specimen. A pressure transducer is installed in the hydraulic system and the measured oil pressure is used to calculate the load or stress of the specimen. Alternatively, a load transducer is installed between the loading piston and plate and directly measures the value of load. The former is simpler, while the latter is more accurate.

There are also two methods for measuring the strain of the specimen. (1) Directly measuring: the electrical resistance strain gauge is adhered on the shallow groove (depth of 2–3 mm) on the specimen surface and then the groove is filled up with cement mortar. (2) Indirectly measuring: the displacement transducer of electrical resistance or inductance is installed to measure the relative displacement between the two loading plates in the same direction, and the strain of the specimen can be calculated after deducting the deformation of the friction reducing pad, which is calibrated in advance. The former is accurate but its measurement scope is limited, so it fits for the biaxial test and triaxial tension-compression test. While the latter is complicated but its measure scope is large enough, so it fits for the triaxial compression test.

Controlling stress (or strain) path. The values of the three principal stresses at a point in a structure may be reached via different paths. The most triaxial tests completed at home and abroad so far are of monotonically loading with constant stress ratio ($\sigma_1:\sigma_2:\sigma_3 = \text{const.}$) until failure of the specimen. Generally, the test equipment is controlled by the electrical-hydraulic system and can be used for conducting various triaxial tests of other stress paths, e.g. loading in three directions with variable stress ratio, loading with constant lateral pressure, repeated loading and unloading, loading with constant strain rate.

It should be pointed out that the triaxial test equipment can also be used for uniaxial compression or tension test, and the corresponding strength and stress–strain curve of concrete are obtained as well. However, these experimental results are not always consistent with that obtained from the standard tests (Chapter 2). Sometimes, both results are different to a certain extent [5-13], because the loading equipment, shape and size of the specimen, measuring accuracy, friction on compressed surface are different for both conditions. Therefore, the former is generally used for comparison, when the multiaxial behavior of concrete is discussed.

5.2 General regularities of multiaxial strength and deformation

The multiaxial strength of concrete is taken as the measured maximum values of three principal stresses of the specimen at failure and is represented by f_1 , f_2 , and

f_3 . The corresponding peak principal strains are ε_{1p} , ε_{2p} , and ε_{3p} . The rules of these indices are

$$\begin{aligned} f_1 &\geq f_2 \geq f_3 \\ \varepsilon_{1p} &\geq \varepsilon_{2p} \geq \varepsilon_{3p} \end{aligned}$$

and the signs of tensile and compressive ones are respectively positive and negative.

Many experimental data of multiaxial behavior of concrete were reported [5-13–5-22,1-2], but they scatter to a great extent [5-8] because the test equipment and method, and the shape, size, and material of the specimen used in various investigations are considerably different. Nevertheless, the general regularity of multiaxial strength and deformation of concrete varying with the stress state can be found and concluded as below.

5.2.1 Biaxial stress states

5.2.1.1 Biaxial compressions (C/C, $\sigma_1 = 0$)

The experimental results of concrete strength under biaxial stress states are shown in Fig. 5-3(a), and the biaxial compressive strengths of concrete given in various references are compared in Fig. 5-3(b).

The biaxial compressive strength (f_3) of concrete is certainly higher than the uniaxial one (f_c):

$$|f_3| \geq f_c, \quad (5-1)$$

and it varies with the stress ratio as below:

$$\sigma_2/\sigma_3 = 0 \sim 0.2 \quad f_3 \text{ increases quickly with the ratio;}$$

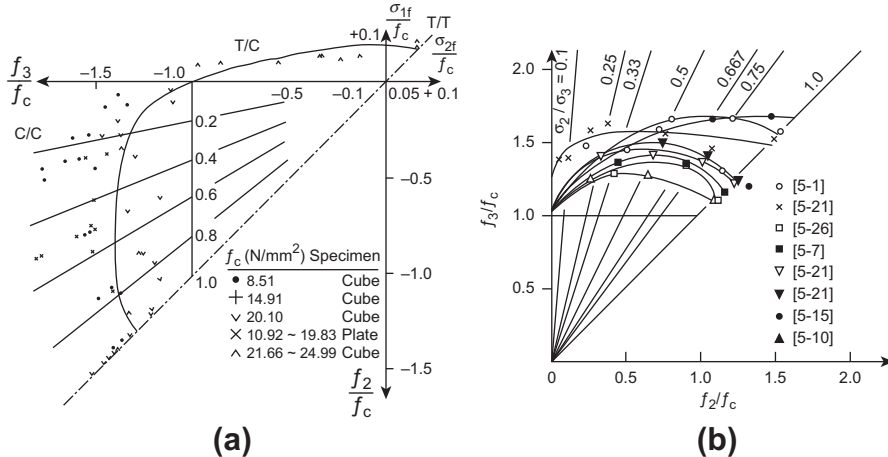


FIG. 5-3 Biaxial strength of concrete: (a) experimental results [1-2], (b) comparison of biaxial compressive strength

$\sigma_2/\sigma_3 = 0.2 \sim 0.7$ f_3 varies gently, and the maximum compressive strength is $(1.25 \sim 1.60)f_c$ occurring in the range of $\sigma_2/\sigma_3 = 0.3$ to 0.6 ;

$\sigma_2/\sigma_3 = 0.7 \sim 1.0$ f_3 decreases as the ratio increases.

And, the biaxial compressive strength of concrete when $\sigma_2/\sigma_3 = 1$ is

$$f_{cc} = (1.15 \sim 1.35)f_c. \quad (5-1a)$$

The stress-strain curve of concrete under biaxial compression is of parabolic including a peak point and a descending branch (Fig. 5-4(a)), and is similar to that under uniaxial compression (Fig. 2-7). The strength (f_3) and peak strain (ϵ_{3p}) of concrete in the direction of the maximum compressive stress (σ_3) are greater than the corresponding values of concrete under uniaxial compression (f_c , ϵ_p).

The peak strains (ϵ_{3p} , ϵ_{2p}) in the directions of the stresses (σ_3 , σ_2) vary with the stress ratio σ_2/σ_3 (Fig. 5-4(b)). The curve of ϵ_{3p} is similar to that of biaxial compressive strength of concrete (Fig. 5-3) and its maximum value occurs at $\sigma_2/\sigma_3 \approx 0.25$. However, the curve of ϵ_{2p} varies almost linearly, and it is tensile at $\sigma_2/\sigma_3 = 0$

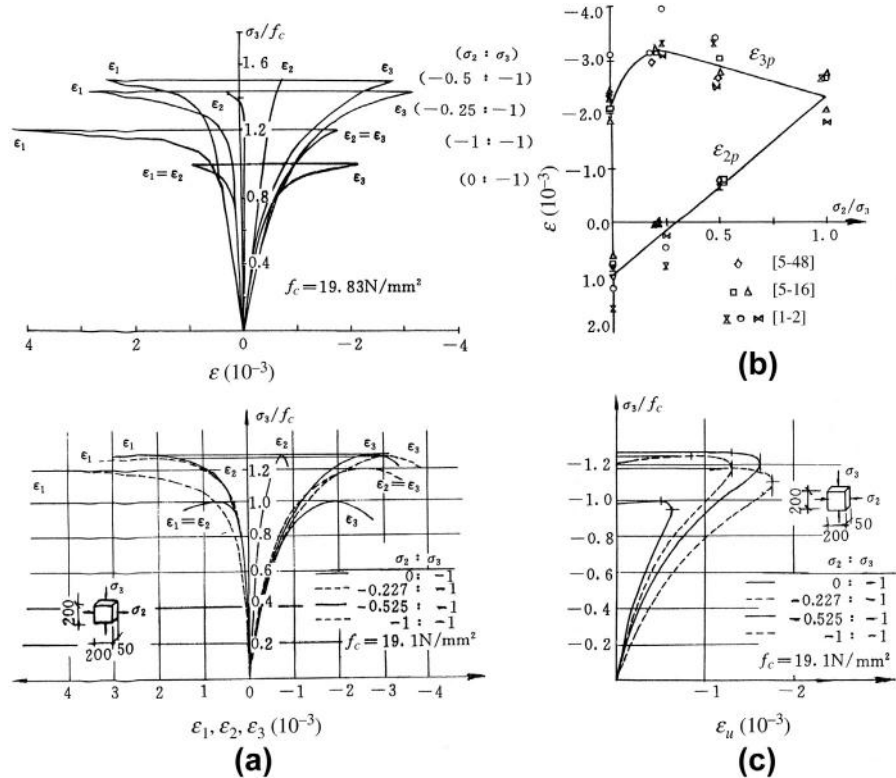


FIG. 5-4 Deformation of concrete under biaxial compression [1-2]: (a) stress-strain curve, (b) peak strain, (c) Volumetric strain

(uniaxial compression) and turns gradually into compressive strain as the ratio increases, and it reaches the maximum compressive strain $\varepsilon_{2p} = \varepsilon_{3p}$ at the ratio $\sigma_2/\sigma_3 = 1$.

The curve of volumetric strain ($\varepsilon_v \approx \varepsilon_1 + \varepsilon_2 + \varepsilon_3$) of concrete under biaxial compression is similar to that under uniaxial compression (Fig. 5-4(c)). The volumetric strain of concrete is compressive ($\varepsilon_v < 0$) when the stress is lower and its Poisson's ratio is $\nu_v < 0.5$. When the stress reaches and exceeds 85–90% of the biaxial strength of concrete, the volumetric strain of the specimen turns into expansion because the crack develops in its interior.

5.2.1.2 Biaxial tension–compression (T/C , $\sigma_2 = 0$)

The compressive strength (f_3) of concrete under a biaxial tension–compression state decreases as the tensile stress in another direction increases. Similarly, the tensile strength (f_1) of it decreases as the compressive stress increases (Fig. 5-3(a)). Therefore, the biaxial tensile/compressive strength of concrete under any stress ratio (σ_1/σ_3) is lower than its corresponding uniaxial strength:

$$T/C \quad |f_3| \leq f_c \quad \text{and} \quad f_1 \leq f_t. \quad (5-2)$$

The stress–strain curve of concrete under a biaxial tension–compression state is shown in Fig. 5-5(a), and the value of the strain and the curvature of the curve are respectively similar to that under uniaxial tension. Most of the specimens are broken with less plastic deformation at failure.

The peak strains (ε_{1p} , ε_{3p}) at failure of the concrete under biaxial tension–compression state decreases quickly as the tensile stress (f_1) or the stress ratio ($|\sigma_1/\sigma_3|$) increases (Fig. 5-5(b)). The ultimate values of them are $\varepsilon_{1p} = \varepsilon_{t,p}$ and $\varepsilon_{3p} = -\nu \varepsilon_{t,p}$ when the stress ratio $|\sigma_1/\sigma_3| \rightarrow \infty$ (i.e. uniaxial tension). The volumetric strain (ε_v) of the specimen is compressive at the beginning of loading, and turns into expansion when the ultimate strength is approaching, because of the appearance of cracking.

5.2.1.3 Biaxial tensions (T/T , $\sigma_3 = 0$)

The biaxial tensile strength (f_1) of concrete under any stress ratio ($\sigma_2/\sigma_1 = 0 \rightarrow 1$) is approaching the uniaxial tensile strength (Fig. 5-3):

$$T/T \quad f_1 \approx f_t \quad (5-3)$$

The stress–strain curve of concrete under biaxial tension state is shown in Fig. 5-6(a) and is consistent with that under uniaxial tension (Fig. 2-22). The value of the strain and the curvature of the curve of concrete under biaxial tension is less, and all the specimens are broken at failure.

As the stress ratio (σ_2/σ_1) increases, both the principal strain ε_1 under same stress and the peak strain ε_{1p} corresponding to the biaxial tensile strength of concrete decrease, because of the influence of the transverse deformation caused by the stress σ_2 (Poisson's effect). However in the meantime, the principal peak strain ε_{2p} turns from contraction (negative value) into elongation (positive value). The peak strain is

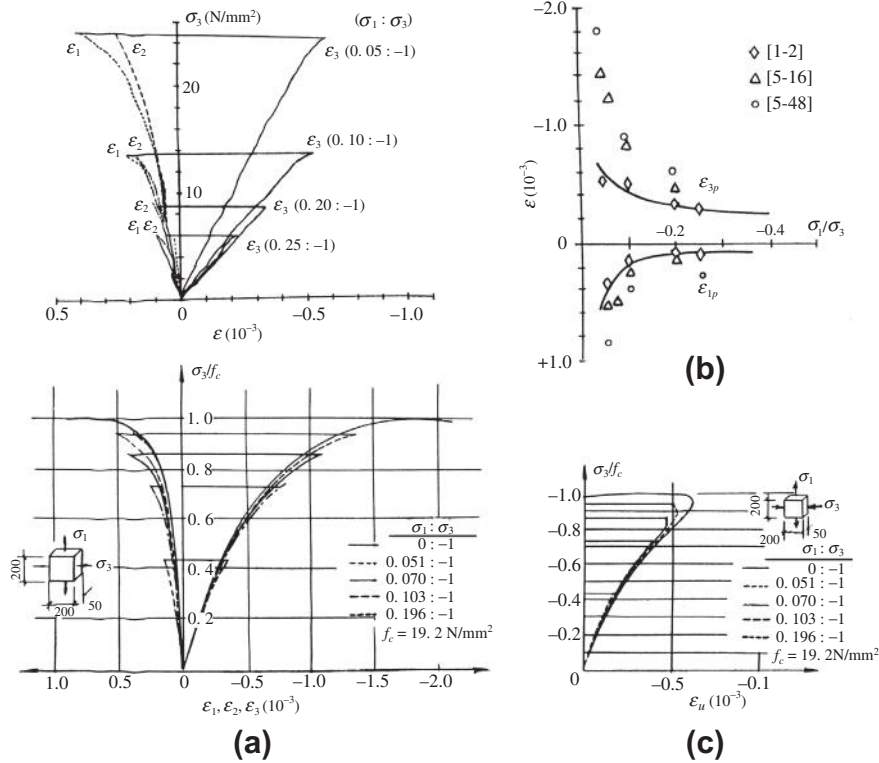


FIG. 5-5 Deformation of concrete under biaxial tension/compression [1-2]: (a) stress–strain curve, (b) peak strain, (c) volumetric strain

$\epsilon_{2p} = 0$ when the stress ratio reaches $\sigma_2/\sigma_1 = 0.2–0.25$, which is consistent with the value of Poisson’s ratio of concrete.

The volumetric strain (ϵ_v) of concrete under a biaxial tension state is expansive from the beginning of loading until the failure of the specimen (Fig. 5-6(c)).

5.2.2 Triaxial stress states

5.2.2.1 Conventional triaxial compressions ($0 > \sigma_1 = \sigma_2 > \sigma_3$ or $0 > \sigma_1 > \sigma_2 = \sigma_3$)

The strength (f_3) of concrete under conventional triaxial compression state increases very quickly with the lateral compressive stress ($\sigma_1 = \sigma_2$), and the corresponding peak strain (ϵ_{3p}) increases even more quickly. For example, the strength is $|f_3| \approx 5f_c$ and the peak strain is $\epsilon_{3p} \approx 50 \times 10^{-3} \approx 30\epsilon_p$, when the lateral stresses (strengths) are $f_1/f_3 = f_2/f_3 = 0.2$ (Fig. 5-7).

The principal strain ϵ_3 is rather small and the stress–strain curve is straight and sharp at the beginning of loading of the specimen, as the lateral compressive stresses

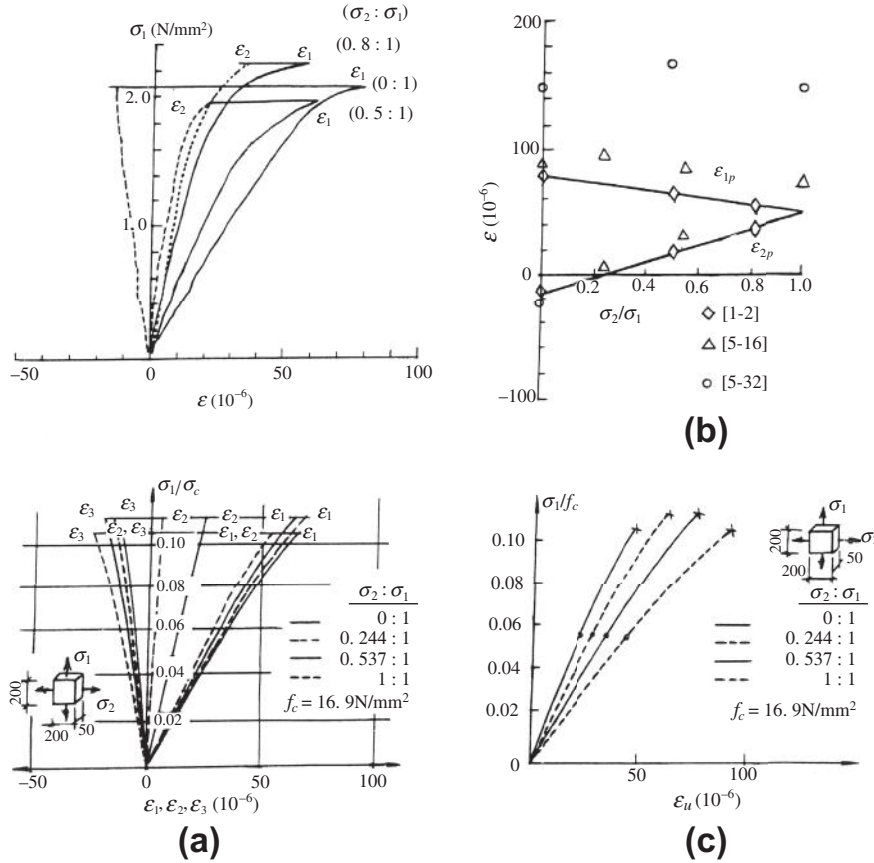


FIG. 5-6 Deformation of concrete under biaxial tensions [1-2]: (a) stress-strain curve, (b) peak strain, (c) volumetric strain

($\sigma_1 = \sigma_2$) act on it. Afterwards, the lateral stresses confine the transverse expansion of concrete and obstruct the appearance and development of the longitudinal crack in it, so the stress-strain curve raises gradually and the plastic deformation of concrete develops considerably. Therefore, the ultimate strength (f_3) of concrete is increased greatly. After the peak point, the residual strength of the specimen decreases gradually under the support of the lateral compressive stresses, and the descending branch of the curve varies gently.

While a sharp peak is obviously shown on the complete stress-strain curve of concrete under uniaxial compression, the peak part on the similar curve of concrete under triaxial compression rises and flattens gradually, as the lateral compressive stresses ($\sigma_1 = \sigma_2$) is increased. When the lateral stresses are $\sigma_1/\sigma_3 = \sigma_2/\sigma_3 \geq 0.15$, the strain before failure of the specimen reaches $\geq 30 \times 10^{-3}$, and the peak part of the curve is approaching a plateau and the peak point is not apparent again.

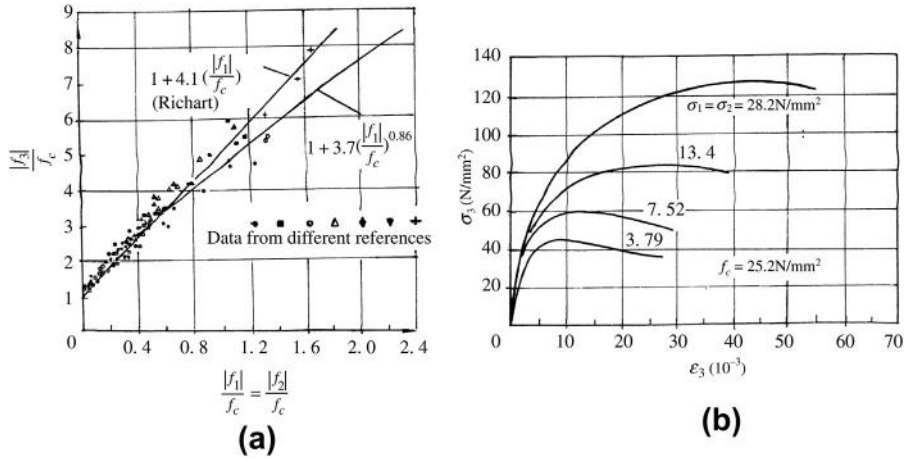


FIG. 5-7 Strength and deformation of concrete under conventional triaxial compression state [1-2]: (a) ultimate strength [5-3], (b) stress–strain curve

Therefore, the shape of the stress–strain curve is not similar to that under uniaxial compression, and also the failure patterns of concrete under both stress states are different.

5.2.2.2 Real triaxial compressions ($0 > \sigma_1 > \sigma_2 > \sigma_3$)

The strength (f_3) of concrete under real triaxial compression state varies with the stress ratios σ_1/σ_3 and σ_2/σ_3 and is shown in Fig. 5-8.

The general regularity for the triaxial compressive strength of concrete is concluded as below.

1. The triaxial compressive strength (f_3) increases very quickly with the stress ratio σ_1/σ_3 and is shown in Table 5-1.
2. The second principal stress (σ_2 or σ_2/σ_3) has an obvious influence on the triaxial compressive strength of concrete. The maximum compressive strength (f_3) occurs in the range of $\sigma_2/\sigma_3 = 0.3$ to 0.6 , and the difference between the maximum and minimum strengths is about 20–25%, when another stress ratio $\sigma_1/\sigma_3 = \text{const.}$
3. When $\sigma_1/\sigma_3 = \text{const.}$, the compressive strength of concrete under $\sigma_2 = \sigma_1$ is lower than that under $\sigma_2 = \sigma_3$, if $\sigma_1/\sigma_3 < 0.15$, i.e. the left end is lower than the right end on the σ_1/σ_3 contour line (Fig. 5-8). To the contrary, the left end is higher than the right end on the contour line, if $\sigma_1/\sigma_3 > 0.15$.

When the concrete is loaded under a real triaxial compression state, the principal strains in three directions should be $\epsilon_1 \neq \epsilon_2 \neq \epsilon_3$ and the shape of the stress–strain curve (Fig. 5-9(a)) is the same as that under a conventional triaxial compression state. The curve approximates an inclined line when the stress is lower and turns gradually with reducing slope as the stress increases, the ultimate strain (ϵ_{3p}) of

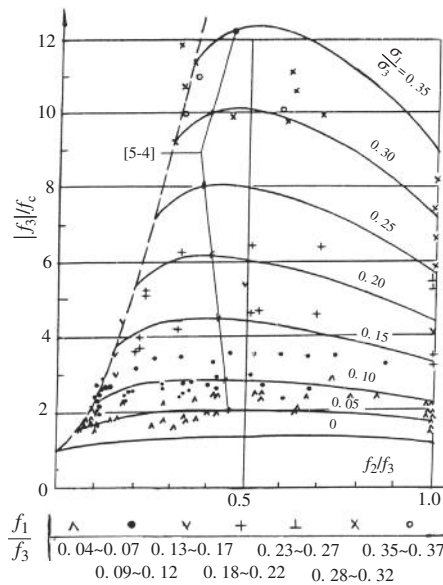


FIG. 5-8 Triaxial compressive strength of concrete [5-4]

Table 5-1 Triaxial Compressive Strength of Concrete Under Different Ratio (σ_1/σ_3)

σ_1/σ_3	0	0.1	0.2	0.3
$ f_3 /f_c$	1.2–1.5	2–3	5–6	8–10

concrete is considerable (Fig. 5-9(b) and Table 5-2) but the peak point is not apparent on the curve.

The peak strain ϵ_{3p} of concrete under a triaxial compression state increases very quickly with the stress ratio (σ_1/σ_3), and varies similarly to the strength under triaxial compression (Fig. 5-8) as another stress ratio (σ_2/σ_3) increases. The maximum value of the peak strain (ϵ_{3p}) occurs in the range of $\sigma_2/\sigma_3 = 0.3$ to 0.6.

The peak strain ϵ_{2p} of concrete, corresponding to the second principal stress (σ_2), varies almost linearly with the stress ratio (σ_2/σ_3). It is elongated at $\sigma_1 = \sigma_2$ ($= 0.15 \sigma_3$), and turns gradually into contraction and reaches the maximum compressive strain $\epsilon_{2p} = \epsilon_{3p}$ at $\sigma_2 = \sigma_3$. The value of the stress ratio (σ_2/σ_3) when $\epsilon_{2p} = 0$ is consistent with that at which the peak strain ϵ_{3p} reaches the maximum. This phenomenon is similar to that under the biaxial compression state (Fig. 5-4(b)).

The peak strain ϵ_{1p} of concrete, corresponding to the minimum principal compressive stress (σ_1), also varies with the stress ratios, and it is elongated at any stress ratio σ_2/σ_3 when $\sigma_1/\sigma_3 = 0.15$.

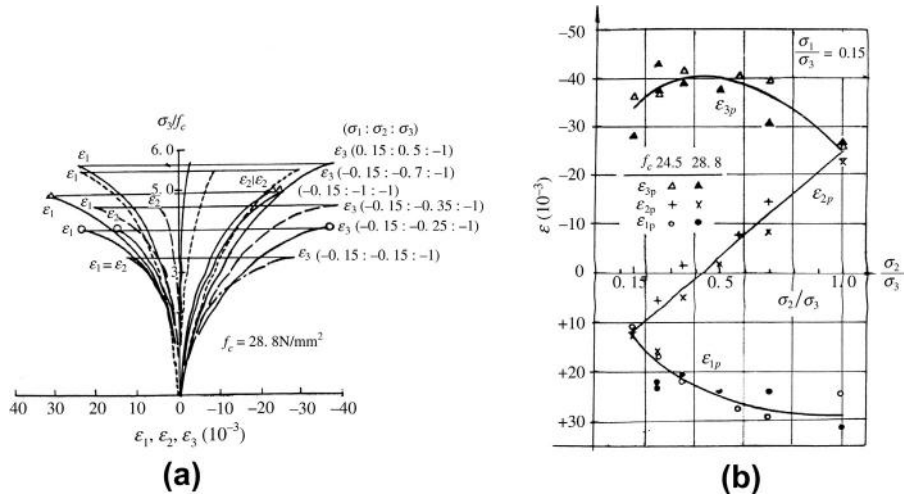


FIG. 5-9 Deformation of concrete under real triaxial compression state ($\sigma_1/\sigma_3 = 0.15$) [1-2]: (a) stress–strain curve, (b) peak strain

Table 5-2 Peak Strain of Concrete Under Real Triaxial Compression State (ϵ_{3p} , 10^{-3}) [1-2]

σ_1/σ_3	$\sigma_2/\sigma_3 =$	0.1	0.15	0.2	0.25	0.35	0.5	0.6	0.7	1.0
0.10	13.99							22.06		
0.15		26.37			36.65	41.64	37.62	40.50	39.52	25.58
0.20			51.37					46.48		27.12
0.25				69.70						

Note: Uniaxial compressive strength of the concrete is $f_c = 24.5 \text{ N/mm}^2$.

5.2.2.3 Triaxial tension–compressions (T/T/C, T/C/C)

The test of concrete under a triaxial tension–compression state, i.e. tension in one or two directions and compression in other directions, has technical difficulty to be conducted, and the relevant experimental data reported are limited with scatter [5-4,5-18]. The general regularity of it (Fig. 5-10) is concluded as below.

1. The triaxial tensile and compressive strengths of concrete under any stress ratio ($\sigma_1 : \sigma_2 : \sigma_3$) are lower than the corresponding uniaxial strength of concrete:

$$\begin{aligned} \text{T/T/C, T/C/C, } |f_3| &\leq f_c \\ f_1 &\leq f_t. \end{aligned} \quad (5-4)$$

2. The compressive strength (f_3) of concrete reduces quickly as the stress ratio $|\sigma_1/\sigma_3|$ increases.

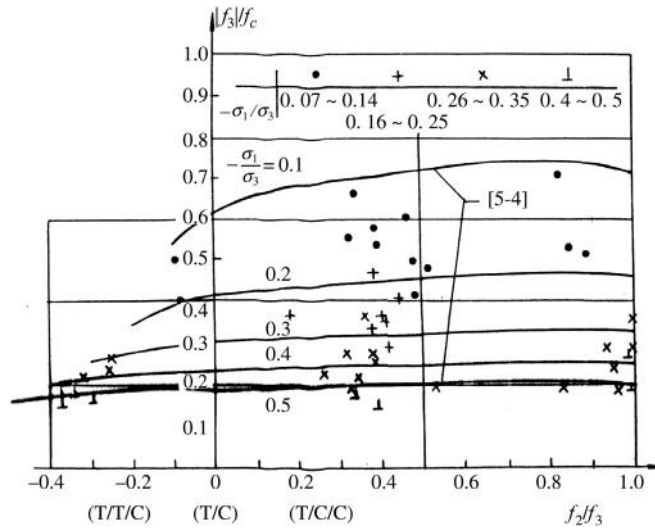


FIG. 5-10 Strength of concrete under triaxial tension-compression state [5-4]

3. The second principal stress (σ_2), whether it is tensile or compressive and regardless of the value of the stress ratio (σ_2/σ_3), has less influence on the triaxial compressive strength (f_3), of which the variation amplitude is less than 10%.

Most of the specimens loaded under a triaxial tension-compression state are broken at its failure, and the stress-strain curve (Fig. 5-11) is similar to that under uniaxial tension state. The plastic deformation of concrete develops slightly only when the stress approaches the ultimate strength. The peak principal tensile strain of the specimen at failure is $\epsilon_{1p} = (70-200) \times 10^{-6}$ and is slightly greater than the peak strain ($\epsilon_{t,p}$) of concrete under uniaxial tension, because of the influence

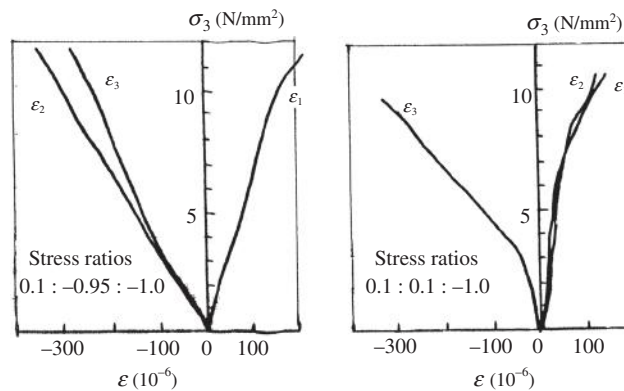


FIG. 5-11 Stress-strain curve of concrete under triaxial tension-compression state [1-2]

of the transverse deformation caused by the principle compressive stress σ_3 . Similarly, the plastic deformation of concrete in the direction of the principal compressive stress σ_3 also develops limitedly, and the corresponding peak strain is $|\varepsilon_{3p}| < 350 \times 10^{-6}$ and reduces as the principal tensile stress σ_1 increases.

When the specimen is loaded under the stress ratio $|\sigma_1/\sigma_3| < 0.05$, i.e. rather lower principal tensile stress, it fails in the pattern of columnar compressing or splitting into pieces (see Fig. 5-15). The principal compressive strain ε_{3p} of it develops obviously and reaches about 1000×10^{-6} at its failure, and the stress–strain curve is similar to that under uniaxial compression state.

5.2.2.4 Triaxial tensions ($\Pi/\Pi/\Pi$)

The state of triaxial principal tensile stresses ($\sigma_1 > \sigma_2 > \sigma_3 > 0$) of concrete appears very seldom in the practical structural engineering and the relevant experimental data are few. The tensile strength of concrete under the state of equally triaxial tension $\sigma_1 = \sigma_2 = \sigma_3 > 0$ given by the references [5-5] and [5-20] is

$$f_1 = f_{III} = (0.7 \sim 1.0)f_t. \quad (5-5)$$

And the ultimate strength (f_1) of concrete under biaxial (T/T) or triaxial tension ($T/T/T$) states is equal to or slightly lower than the uniaxial tensile strength of it (f_t). Possibly, this is because of the larger probability of defect and damage existed in the interior of the specimen.

Summarizing the multiaxial strength and deformation behavior of concrete under all the stress states, the general regularity can be briefly presented as below.

Multiaxial strength increases obviously ($|f_3| > f_c$) under the stress states of multiaxial compressions (C/C , $C/C/C$);

Multiaxial strength approaches to uniaxial tensile strength ($f_1 \approx f_t$) under the stress states of multiaxial tensions (T/T , $T/T/T$);

Multiaxial strength reduces ($|f_3| < f_c$ and $f_1 < f_t$) under the stress states of multiaxial tension–compression (T/C , $T/T/C$, $T/C/C$).

Multiaxial deformation — there are three categories for the shape of the stress–strain curve and the value of peak strain of concrete, which depend upon its stress state and failure pattern (see Table 5-4);

Tension type — the curve is sharp and similar to that under uniaxial tension, and the tensile strain is $\varepsilon_1 < 300 \times 10^{-6}$;

Biaxial compression type — the curve is similar to that under uniaxial compression, and the peak compressive strain is $|\varepsilon_3| \approx (2 \sim 3) \times 10^{-3}$;

Triaxial compression type — the curve is sharp at the beginning and turns gradually later, and is flattered on the peak part with a considerable value of peak compressive strain $|\varepsilon_3| \approx (10 \sim 50) \times 10^{-3}$.

Knowing and understanding the general regularity of concrete behavior under a multiaxial stress state is very helpful for learning the failure criterion and constitutive relation of concrete and for dealing with the affairs in the structural engineering

practice, such as design and calculation, analysis of engineering accident, strengthening measure.

5.2.3 Different materials and loading paths

The general regularity of multiaxial behavior of concrete introduced above is mainly based on the experimental results of the ordinary concrete (strength grade C20–C50) under monotonic and proportional loading. However, the relevant experimental data of the structural concrete of other kinds and under different loading path are limited up to now. Although some qualitative conclusions are available, the satisfactory regularity and accurate quantification about them need to be investigated further.

The experimental results of high-strength concrete ($\geq C50$) [5-23] show that the relative strength value (f_3/f_c) under multiaxial compression states (C/C and $C/C/C$) reduces as its strength grade (or f_{cu} , f_c) increases; the relative strength values (f_1/f_t and f_3/f_c) under biaxial tension (T/T) and tension–compression (T/C) states do not vary obviously with its strength grade.

Aerated concrete and light weight (aggregate) concrete are of brittle and lower strength. Although the biaxial compressive strengths of them are greater than their corresponding uniaxial compressive strength, the increased amplitudes of them are less than that of ordinary concrete [5-24,5-25].

The triaxial behavior of steel fiber concrete also has been investigated experimentally [5-25,5-26]. The relative ultimate strength (f_3/f_c) and the shape of stress–strain curve of steel fiber concrete under multiaxial compression states (C/C and $C/C/C$) approach that of ordinary concrete, while the relative strength (f_3/f_c) and peak strain of it under multiaxial tension–compression states (T/C , $T/T/C$, and $T/C/C$) are greater than the corresponding values of ordinary concrete. The influence of volume content of steel fiber (V_f , %) on the multiaxial strength and deformation of steel fiber concrete is similar to that on the uniaxial behavior of it.

A common regularity can be derived from the experimental results of these structural concretes under a multiaxial stress state: if the structural concrete is more brittle, i.e. the plastic deformation of it under loading develops less, the increased amplitude of its multiaxial compressive strength is less; on the contrary, the less brittle or more plastic deformation of the concrete, the larger the amplitude increase in multiaxial compressive strength.

It is very seldom that the three principal stresses at a point of concrete in a practical structure increase monotonically and proportionally ($\sigma_1:\sigma_2:\sigma_3 = \text{const.}$) from the beginning of its loading until its failure. The value and distribution of the internal forces of the structure vary continuously, because the load and support conditions vary and the plastic deformation and crack of the material occur and develop. Therefore, the principal stresses in three directions at a point have to experience various variable paths, even the stress changes from compressive into a tensile one or vice versa and the principal axes rotate. The variety of loading path and complications of experimental technique are difficulties in researching the multiaxial

behavior of concrete under different stress paths. The relevant experimental investigations have been reported [5-27–5-31], although limited, up to now, and some of the results and conclusions are introduced below.

The tests of concrete under biaxial compression state are conducted following the four paths (P1 to P4 in Fig. 5-12) of variable stress ratio and the results obtained are shown. It is demonstrated that the biaxial compressive strength of concrete experienced in the path of variable stress ratio is still consistent with the failure envelope of concrete under the path of constant stress ratio, if the stress level of concrete before changing the stress ratio is lower than 85% of the corresponding biaxial compressive strength ($\beta < 0.85$). In addition, the failure patterns of the specimens tested under these stress paths are same.

The tests of concrete under triaxial compression state with constant lateral compression ($\sigma_x = \sigma_y = \text{const.}$) are conducted following the two stress paths, shown in Fig. 5-13, until its failure. When the stress level of the specimen is lower and the internal microcrack is within the stably developing stage before changing the stress ratio, the multiaxial compressive strength of concrete after changing stress ratio is not related to the stress path experienced previously, and is consistent with that under monotonic and proportional loading ($\sigma_x:\sigma_y:\sigma_z = \text{const.}$). Also, the failure pattern of the concrete specimens tested under these stress paths is the same.

The strains of concrete specimens tested under biaxial compression state but experienced different stress paths should be different, and there are two examples

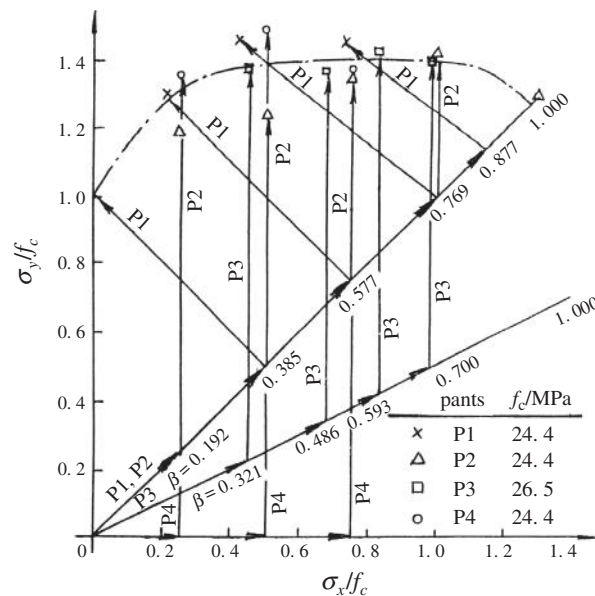


FIG. 5-12 Comparison of biaxial strengths of concrete tested under different stress paths [5-30]

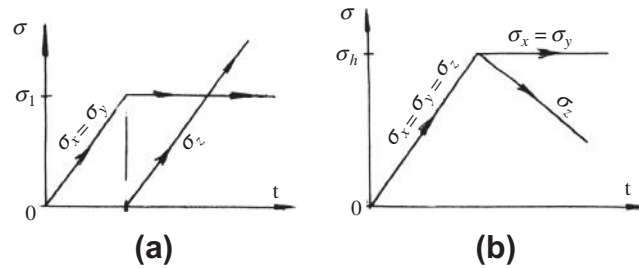


FIG. 5-13 Stress paths of specimen tested under triaxial compression with constant lateral compression [5-30]: (a) contraction type, (b) elongation type

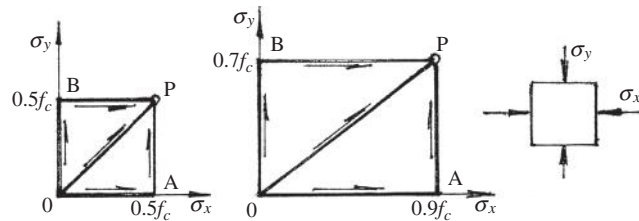


FIG. 5-14 Strain tests of concrete under biaxial compression with different stress paths [5-29]

shown in Fig. 5-14. The specimens experienced separately three stress paths, including OP (proportionally loading), OAP and OBP (uniaxial loading and succeeded by loading in another direction with constant lateral stress), and the principal strains of concrete (ε_x , ε_y) measured at stresses ($\sigma_x = \sigma_y = 0.5f_c$) and ($\sigma_x = 0.9f_c$, $\sigma_y = 0.7f_c$) are listed and compared in Table 5-3. Obviously, the strains of concrete at the same stress but experiencing different stress paths are considerably different. The main reasons for this are that the stress path or loading order have influence on the direction and development of internal microcracks in concrete, and the load acted previously confines and stagnates the development of the crack, which would be caused by the load acting on another direction.

Table 5-3 Comparison Between the Strains of Concrete Under Biaxial Compression and Experienced Different Stress Paths [5-29]

Stress Values		$\sigma_x = \sigma_y = 0.5f_c$		$\sigma_x = 0.9f_c, \sigma_y = 0.7f_c$	
Strain (10^{-6})		$-\varepsilon_x$	$-\varepsilon_y$	$-\varepsilon_x$	$-\varepsilon_y$
Path	OAP	740	350	1620	400
	OP	430	430	1000	500
	OBP	350	740	850	1100

These experimental data demonstrate that different principal strains of concrete are resulted when it reaches some values of multiaxial stresses but experienced different stress paths. In addition, the measured strains of concrete are different not only from that under monotonic and proportional loading, but also from the summation of the strains calculated individually by every principal stress, following the uniaxial stress–strain relation. Therefore, it is necessary to establish the multiaxial constitutive relation of concrete fitting for any variable stress paths, in order to represent the real behaviors of concrete material and structure.

The multiaxial behavior of concrete under repeated loading is also important for structural engineering. Two types of repeated loading test are reported in reference [5-31]: (1) the specimen under biaxial compression state is loaded and unloaded proportionally ($\sigma_x:\sigma_y = \text{const.}$), and the envelope of the stress–strain curve, the biaxial strengths, and the failure pattern obtained are consistent respectively with that under monotonically loading; (2) the specimen is loaded and unloaded only in one direction (σ_y) while the lateral stress is kept constantly ($\sigma_x = \text{const.}$), and the results obtained, including the envelope of stress–strain curve, unloading and reloading curves, residual strains, and hysteresis loop, are special and different from that under repeated uniaxial compression or under proportionally repeated biaxial compressions. The speciality can be consulted from the relevant reference and should be paid attention to.

As the multiaxial test of concrete under non-proportional loading is still limited so far, more important phenomena and regularity need to be explored continuously. For example, no experiment datum exists for the strength and deformation of concrete when the directions of its three principal stresses are varied or rotated. Therefore, more and deeper experimental investigations are needed for establishing the constitutive relation of concrete, fitting for any stress or strain paths.

5.3 Typical failure patterns and their boundaries

When concrete is loaded under a triaxial stress state with different tension–compression composition and stress ratios, five typical macro failure patterns (Fig. 5-15) can be found, because of the differences of the material deformation and the development and accumulation of microcracks and damage in the interior of the concrete.

5.3.1 Breaking in tension

When concrete is loaded under bi- and tri-axial tension or tension–compression state and the principal tensile strain (ϵ_I) reaches its ultimate value (ϵ_{Ip}), a crack occurs first on the weakest section and develops gradually, mainly because of the action of principal tensile stress σ_I . Finally, the specimen is suddenly broken into two pieces and the failure process and characteristic of it are the same as that for the prism specimen tested under uniaxial tension (see Section 2.4).

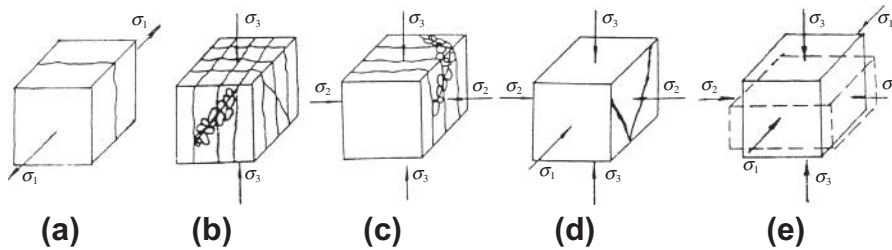


FIG. 5-15 Typical macro-failure patterns of concrete [5-4]: (a) breaking in tension, (b) columnar crushing, (c) splitting in pieces, (d) inclined shearing, (e) extruding and shifting

Generally, the broken surface of the specimen approximates a plane and is perpendicular to the maximum principal tensile stress σ_1 , and it is composed of the boundary of coarse aggregate and broken cement mortar. When the principal tensile stresses σ_1 and σ_2 are tensile and the ratio between them ranges from $\sigma_1/\sigma_2 = 0.5$ to 1.0, the broken surface may be at an acute angle with the axis of σ_1 , depending upon the random distribution of tensile strength of concrete.

5.3.2 Columnar crushing

When concrete is loaded under multiaxial compression or a tension—compression state and the absolute value of the principal compressive stress $|\sigma_3|$ is far greater than other principal stresses, the tensile strains (ϵ_1 and ϵ_2) occur in the two directions being perpendicular to the axis of σ_3 . After the strains reach and exceed their ultimate values, two sets of crack plane are formed and parallel respectively to the adjacent lateral surfaces of the specimen. As the crack planes extend and widen gradually, and finally run through the whole section, the cubic specimen is separated into a group of short columns and crushed (Fig. 5-15(b)).

The failed cubic specimen of edge length 100 mm is separated into 3–5 small columns in each side, and the edge length of them is about 20–30 mm or 1.5–2.0 times the size of coarse aggregate. The main crack planes separating the small columns are wider, and, besides, fine longitudinal cracks exist in the interior of the small columns. It shows that the boundary between coarse aggregate and cement mortar and the interior of cement mortar are damaged widely, and the failure characteristic is similar to that of the specimen under a uniaxial compression state (Table 2-8).

The main factor resulting in the pattern of columnar crushing is the principal compressive stress (σ_3), the other two principal stresses (σ_1 and σ_2) have mainly an influence on the lateral strain (ϵ_1 and ϵ_2) and also on the formation and development of the main crack plane. When σ_1 and σ_2 are both compressive, the lateral tensile strains are reduced and then the compressive strength of concrete is increased ($|\sigma_3| > f_c$, Fig. 5-8). On the contrary, when σ_1 and σ_2 are tensile, the lateral tensile strains are increased and the compressive strength of concrete has to be decreased ($|\sigma_3| < f_c$, Fig. 5-10).

5.3.3 Splitting into pieces

When concrete is loaded under a multiaxial compression or tension–compression state and the second principal stress (σ_2) is compressive and large enough to prevent from a forming tensile crack in its perpendicular direction, a larger tensile strain (ϵ_I) is caused in the direction of σ_1 under the common actions of σ_3 and σ_2 . Several crack planes paralleling with the σ_2 – σ_3 plane are formed successively, as the stresses increase. When the crack planes run through the whole section of the specimen, the failure pattern of splitting into pieces is presented (Fig. 5-15(c)).

The failed cubic specimen of edge length 100 mm is generally separated into 3–5 pieces. The main crack planes parallel macroscopically one another but with irregular slope and curve, due to the obstruction of coarse aggregate. The damage and small broken pieces are obvious near the cracked surface, but the coarse aggregates nearby are integral and none of them is split. The failure characteristic is also similar to that of the specimen under uniaxial compression state (Table 2-8).

It can be concluded from the analysis of the failure mechanism of concrete that the compressive strength (f_3) of the specimen under triaxial compressions (C/C/C) is certainly greater than that under biaxial compressions (C/C), and both strengths are certainly greater than that under triaxial tension–compression (T/C/C) (Fig. 5-8 and Fig. 5-10), even if the same failure pattern occurs.

5.3.4 Inclined shearing

When concrete is loaded under a triaxial compression state (C/C/C) and the principal stress (σ_1) is large enough to prevent the occurrence of splitting failure, but the difference between the principal stresses σ_1 and σ_3 or the shear stress $(\sigma_1 - \sigma_3)/2$ is larger, the inclined cracks appear on the surface of the failed specimen (Fig. 5-15(d)). The inclined cracks are of 1–3, and the direction of them is paralleling to σ_2 axis and at an angle of 20° – 30° with σ_3 axis. The marks of shear slide, pulverization, and crush can be seen on the inclined crack surfaces.

Some specimens under multiaxial stress state failed initially with several parallel crack planes and in the pattern of columnar crushing or splitting into pieces (Table 5-4), but the inclined crack also apparently appears afterwards on the surface of the specimen, if the test is continuous and the deformation of the specimen is increased further. This also happens for the prism specimen under uniaxial compression (Fig. 2-7), and it has been explained in Section 2.2.2 that the inclined crack is formed only when the stress–strain curve enters into its descending branch. Therefore, the inclined crack is a secondary failure pattern or final performance and is not related to the compressive strength of concrete (f_c or f_3), which depends only upon the longitudinal splitting crack of concrete.

5.3.5 Extruding and shifting

When concrete is loaded under a triaxial compression state and the stresses σ_1 and σ_2 are large enough, all the principal strains in three directions are contractive. The coarse aggregate and its boundary and the cement mortar between aggregates also mainly carry compressive stress, so the appearance and development of internal microcracks in concrete are delayed or prevented and the ultimate strength of it is considerably increased.

When high compressive stress is acted on concrete, parts of the cement mortar and weak coarse aggregate in it are locally crushed due to the non-uniform and even higher microscopic stress, and larger contraction and slide deformations of concrete are caused and the plastic deformation of the specimen increases significantly (Fig. 5-9 and Table 5-2). After the ultimate load is reached, macroscopic contraction deformation appears in the direction of the maximum compressive stress σ_3 , e.g. the edge length 70 mm of cubic specimen is compressed to 40–50 mm only. In the meantime, the specimen is extruded and expands out in both directions of σ_1 and σ_2 , and the cubic specimen is changed into a cuboid (Fig. 5-15(e)).

The concrete acted under common compressions in three directions occurs severely extruding and shifting, and the coarse aggregate and cement mortar in it are displaced considerably. The corners and edges of the specimen are loosened and spalled off during loading, because they are located outside of the loading plate and free of confinement. The material and construction in the interior of the concrete are seriously damaged under strong extruding. The failed specimen after testing is still an integral solid, but many irregular fine cracks exist on its surfaces and the residual strength of it under uniaxial compression is rather low.

These five typical failure patterns of concrete occur separately within the different scopes of multiaxial stress state, which can be determined, in principle, by the experimental data. The relevant suggestions provided in reference [1-2] are shown in Table 5-4 and Fig. 5-16.

These five failure patterns of concrete are distinguished and named according to the macro appearance of the failed specimen. Alternatively, if the dominant stress and crack characteristic of the specimen during the failure process are considered, two basic failure patterns of concrete are induced:

1. Principal tensile stress causes transverse tensile cracks and induces breaking in tension of concrete;
2. Principal compressive stress causes longitudinal splitting cracks and induces crushing of concrete, including the patterns of columnar crushing, splitting in pieces, inclined shearing, and extruding and shifting. The last failure pattern is a special one, because the longitudinal splitting crack in concrete is compacted by the lateral compressive stress and is not presented apparently.

The typical representatives of the basic failure patterns are uniaxial tension and compression, of which the failure characteristics are shown and compared in Table 2-8.

Table 5-4 Stress Scopes for Typical Failure Patterns [1-2]

Failure Characteristic		Breaking in Tension	Columnar Crushing	Splitting into Pieces	Inclined Shearing	Extruding and Shifting
Dominant stress		σ_1	σ_3	σ_2, σ_3	σ_1, σ_3	$\sigma_1, \sigma_2, \sigma_3$
Stress state	Uniaxial	$\sigma_1 > 0$	$\sigma_3 < 0$			
	Biaxial	T/T	$\sigma_1 \geq \sigma_2 > 0$			
		T/C	$\left \frac{\sigma_1}{\sigma_3} \right \geq 0.05$	$\left \frac{\sigma_1}{\sigma_3} \right < 0.05$		
		C/C		$\frac{\sigma_2}{\sigma_3} \leq 0.2$	$\frac{\sigma_2}{\sigma_3} > 0.2$	
	Triaxial	T/T/T	$\sigma_1 \geq \sigma_2 \geq \sigma_3 > 0$			
		T/T/C	$\left \frac{\sigma_1}{\sigma_3} \right \geq \left \frac{\sigma_2}{\sigma_3} \right \geq 0.1$	$\left \frac{\sigma_2}{\sigma_3} \right \leq \left \frac{\sigma_1}{\sigma_3} \right < 0.1$		
		T/C/C	$\left \frac{\sigma_1}{\sigma_3} \right \geq 0.05$	$\left \frac{\sigma_1}{\sigma_3} \right < 0.05$	$\left \frac{\sigma_1}{\sigma_3} \right < 0.05$	
			$\frac{\sigma_2}{\sigma_3} \leq 0.2$	$\frac{\sigma_2}{\sigma_3} > 0.2$		
	C/C/C		$\frac{\sigma_1}{\sigma_3} \leq \frac{\sigma_2}{\sigma_3} \leq 0.1$	$\frac{\sigma_1}{\sigma_3} \leq 0.15$ $\frac{\sigma_2}{\sigma_3} > 0.15$	$\frac{\sigma_1}{\sigma_3} =$ $0.15 \sim 0.2$	$\frac{\sigma_2}{\sigma_3} \geq \frac{\sigma_1}{\sigma_3} > 0.2$

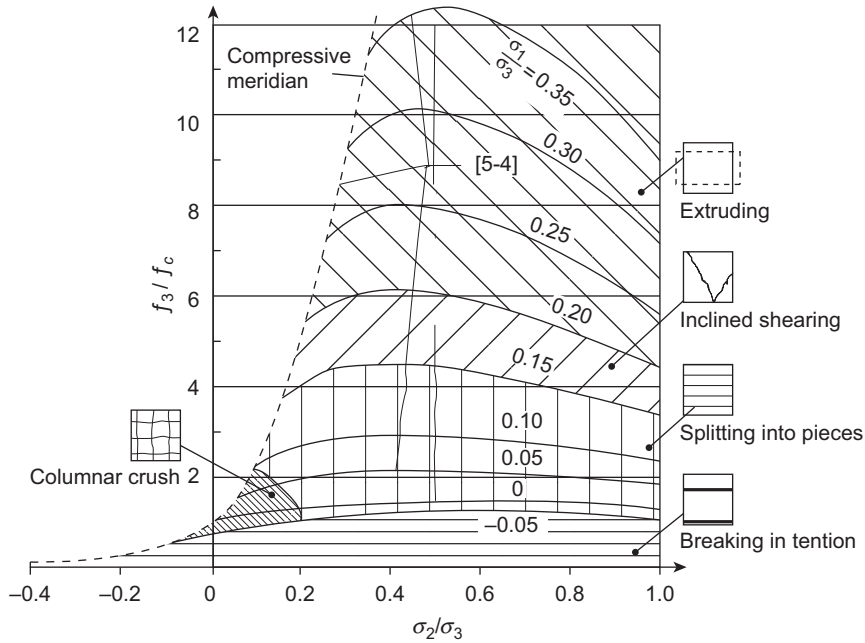


FIG. 5-16 Stress zones for various failure patterns of concrete [1-3]

5.4 Failure criterion

5.4.1 Shape of failure envelope and its expression

The experimental data of multiaxial strength (f_1, f_2, f_3) of concrete are plotted on the spatial Cartesian coordinates ($\sigma_1, \sigma_2, \sigma_3$) and the adjacent points of them are connected smoothly, the spatial curved failure envelope of concrete is obtained (Fig. 5-17(a)). The intersection line between the envelope and the coordinate plane is the biaxial failure envelope (Fig. 5-3(a)).

There is a hydrostatic axis in the space of principal stress, and it certainly passes through the origin of the coordinates. The perpendicular distances from any point on the hydrostatic axis to the three coordinate axes should be equal and the angles between the hydrostatic axis and the three coordinate axes are equal:

$$\alpha = \cos^{-1} \left(1/\sqrt{3} \right) \quad (5-6)$$

The distance between a point on the hydrostatic axis and the origin of the coordinates is called hydrostatic stress (ξ). Also, the summation of the projection lengths, on the hydrostatic axis, of the three principal stresses ($\sigma_1, \sigma_2, \sigma_3$) at any point in the space is called hydrostatic stress, i.e. $\xi = (\sigma_1 + \sigma_2 + \sigma_3)/\sqrt{3}$.

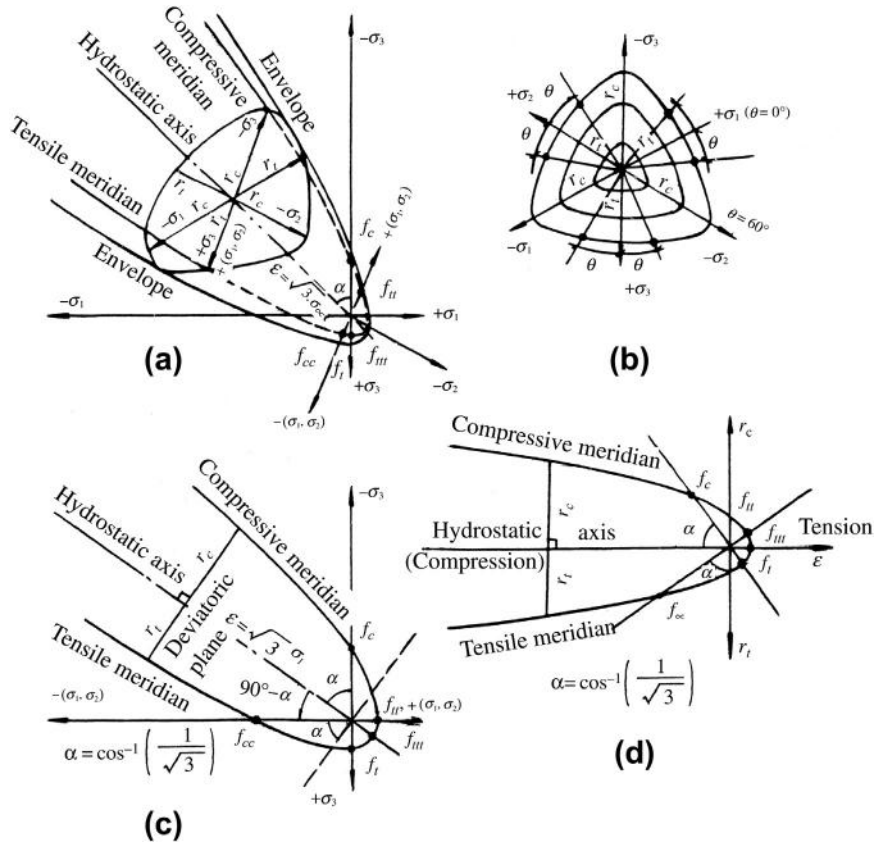


FIG. 5-17 Failure envelope of concrete and its expression: (a) spatial failure envelope, (b) deviatoric plane, (c) meridian plane, (d) meridian plane expressed by octahedral stresses

The deviatoric plane (Fig. 5-17(b)) is perpendicular to the hydrostatic axis and the projection lines of the three principal axes on it are at an angle of 120° to one another. It is easily proved that the summation of the three principal stresses at any point on same deviatoric plane is a constant, i.e. the first invariant of principal stress: $\sigma_1 + \sigma_2 + \sigma_3 = \text{const.} = I_1$. The intersection line between the deviatoric plane and the failure envelope is called as an envelope on deviatoric plane, and the envelopes at different hydrostatic stresses compose a family of closed curve.

The envelope on deviatoric plane is three-folded symmetrical, so the whole envelope can be obtained when an arc of 60° is known. The angle θ is given as 0° or 60° respectively for the positive or negative direction of the axis of each principal stress, and $0^\circ < \theta < 60^\circ$ for the other direction. The distance from a point on the envelope to the origin, i.e. hydrostatic axis, is called deviatoric stress (r), which gradually increases from the minimum (r_t) at $\theta = 0$ to the maximum (r_c) at $\theta = 60^\circ$, i.e. $r_t \leq r_c$.

There are several important points of characteristic strength located on the spatial failure envelope of concrete. The uniaxial compressive (f_c , obtained from the test with friction reducing measure) and tensile (f_t) strengths are located respectively in the negative and positive directions of the coordinate axes of three principal stresses. The equally biaxial compressive ($\sigma_1 = 0, f_2 = f_3 = f_{cc}$) and tensile ($\sigma_3 = 0, f_1 = f_2 = f_{tt}$) strengths are located on the equally divisional line of two axes on each of the three coordinate planes. And, the equally triaxial tensile strength ($f_1 = f_2 = f_3 = f_{ttt}$) is located alone in the positive direction of the hydrostatic axis. Otherwise, the triaxial strength of concrete under an arbitrary stress state ($f_1 \neq f_2 \neq f_3$) can be plotted as six points on the same deviatoric plane and with same angle θ (Fig. 5-17 (b)), when concrete is considered as an isotropic material and the three coordinate axes or principal stresses are substituted for one another.

The curved failure envelope of three dimensions is difficult to be drawn and is not convenient for understanding and application, so the envelopes of two dimensions on the meridian and deviatoric planes are usually used to replace it. The meridian plane contains the hydrostatic axis and one of the principal stress axes (e.g. σ_3 axis in Fig. 5-17(c)), and passes through the equally divisional line of two other axes (σ_1 and σ_2) of the principal stresses. The intersection curves between the meridian plane and the spatial failure envelope are called separately tensile ($\theta = 0^\circ$) and compressive ($\theta = 60^\circ$) meridians.

The stress state of tensile meridian is $\sigma_1 \geq \sigma_2 = \sigma_3$ and the corresponding angle on the deviatoric plane is $\theta = 0$, two characteristic strengths of concrete, i.e. uniaxial tension ($f_t, 0, 0$) and equally biaxial compressions ($0, -f_{cc}, -f_{cc}$), are located on it. On the other hand, the stress state of compressive meridian is $\sigma_1 = \sigma_2 \geq \sigma_3$ and the corresponding angle on the deviatoric plane is $\theta = 60^\circ$, two characteristic strengths, i.e. uniaxial compression ($0, 0, -f_c$) and equally biaxial tensions ($f_{tt}, f_{tt}, 0$), are located on it. The tensile and compressive meridians and the hydrostatic axis intersect at one point, i.e. the stress state of equally triaxial tensions ($f_{ttt}, f_{ttt}, f_{ttt}$). The perpendicular distances from the tensile and compressive meridians to the hydrostatic axis are respectively deviatoric stresses r_t and r_c .

When the figure in Fig. 5-17(c) is rotated counterclockwise an angle of $(90^\circ - \alpha)$ against the origin, the tensile and compressive meridians are presented in another coordinates, of which the abscissa and ordinate are respectively hydrostatic (ξ) and deviatoric (r) stresses (Fig. 5-17(d)). Consequently, the special failure envelope of concrete is expressed alternatively as the envelope curves on the meridian and deviatoric planes (Fig. 5-17(d) and (b)). And, the Cartesian coordinates (f_1, f_2, f_3) of any point on the spatial envelope can be changed and represented by the cylindrical coordinates (ξ, r, ϑ):

$$\left. \begin{aligned} \xi &= (f_1 + f_2 + f_3)/\sqrt{3} = \sqrt{3} \sigma_{oct} \\ r &= \sqrt{(f_1 - f_2)^2 + (f_2 - f_3)^2 + (f_3 - f_1)^2}/\sqrt{3} = \sqrt{3} \tau_{oct} \\ \cos\theta &= (2f_1 - f_2 - f_3)/(\sqrt{6} r) \end{aligned} \right\}. \quad (5-7)$$

When the coordinates in Fig. 5-17 (d) are reduced by $\sqrt{3}$ times, the hydrostatic and deviatoric stresses (ξ , r) are replaced respectively by the octahedral normal (σ_{oct}) and shear (τ_{oct}) stresses, and the corresponding tensile and compressive meridians and failure envelopes are obtained. There is an example shown in Fig. 5-18, in

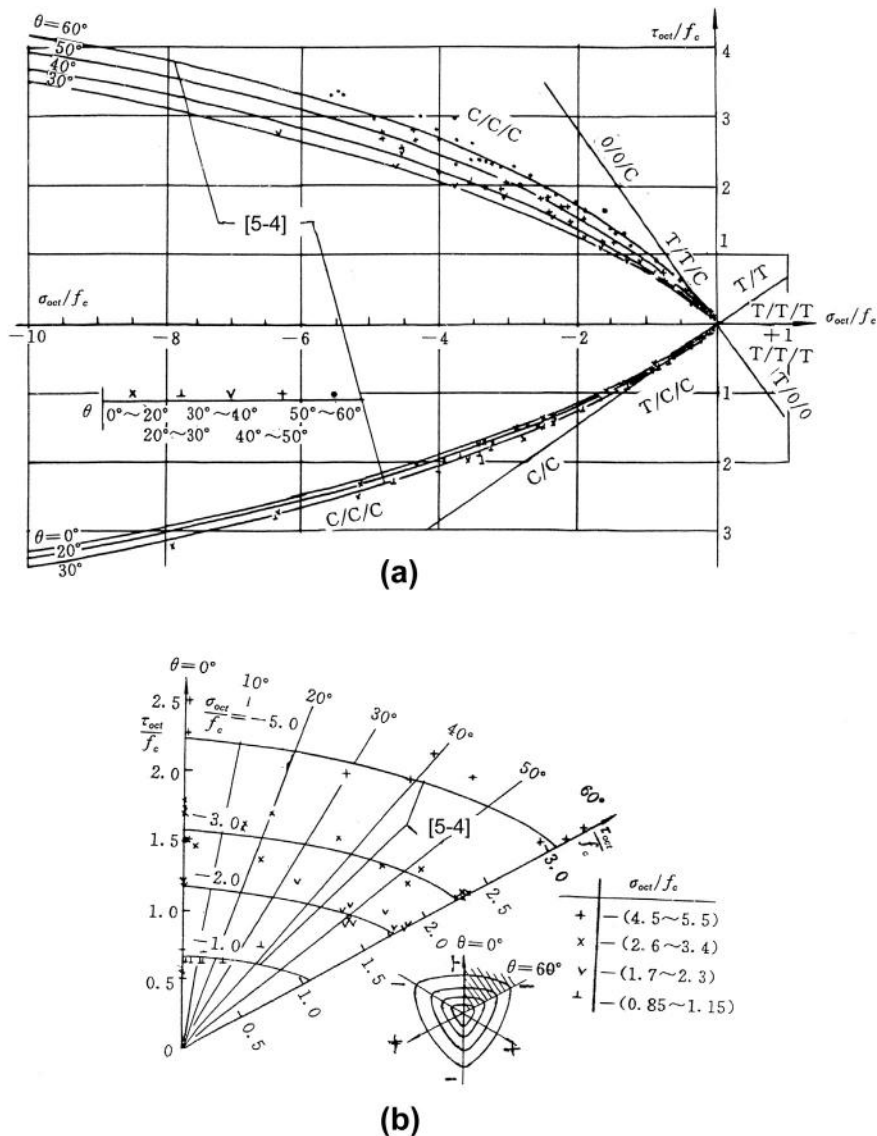


FIG. 5-18 Meridians and envelopes on deviatoric plane [1-2]: (a) meridians, (b) deviatoric plane

which the tensile and compressive meridians and envelopes on deviatoric plane are plotted, based on the experimental data.

The geometric characteristics of the spatial failure envelope of concrete are summarized as below, based on the experimental data at home and abroad:

1. The envelope is continuous, smooth, and convex;
2. The envelope is three-folded symmetrical;
3. The envelope is closed on the tension end of the hydrostatic axis and the peak point is the state of equally triaxial tension, while it is opened on the compression end and never intersects with the hydrostatic axis;
4. The value of deviatoric or octahedral shear stress at a point on the meridian increases monotonically with reducing rate and has a limit, as the algebraic value of hydrostatic or octahedral normal stress decreases;
5. The envelopes on the deviatoric plane are three-folded symmetrical, their sizes increase gradually and their shapes vary convexly from an approximate triangle ($r_t/r_c \approx 0.5$) to a circle ($r_t/r_c = 1$), as the algebraic value of hydrostatic or octahedral normal stress decreases.

5.4.2 Failure criterion

The spatial failure envelope of concrete can be described by a mathematic function, which is called a strength or failure criterion of concrete and used for judging if the concrete reaches its ultimate strength or failure condition. The failure criterion is the summarization of a large number of experimental data rather than a physical theory, but it can be used on relevant calculation with sufficient accuracy and is of great importance for the engineering practice.

More than ten failure criteria of concrete are suggested by the researchers at home and abroad [5-32—5-38,5-4] up to now, and they can be classified as three categories: (1) the point of view and calculation formula are learned from the classical strength theories of material; (2) the empiric formula is obtained regressively, based on the experimental data of multiaxial tests; (3) pure mathematic equation is derived theoretically basing on the geometrical characteristics of the failure envelope of concrete, and the values of the parameters in it are calibrated based on several characteristic strengths of concrete. These failure criteria of concrete also differ considerably from one another in expression, application scope, and calculation accuracy, and they should be carefully compared and selected during use. More details of these failure criteria can be found in references [5-32], [1-2] and others.

The failure and ultimate strength of various materials under multiaxial stresses are an important problem in different engineering fields, and many scientists have conducted a large number of experimental and theoretical researches on them since early history. The famous classical strength theories (failure criteria) suggested earlier for them include:

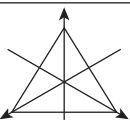
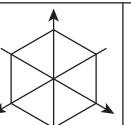
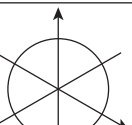
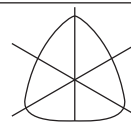
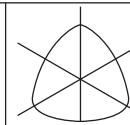
1. Maximum tensile stress criterion (Rankine, 1876);
2. Maximum tensile strain criterion (Mariotto, 1682);

3. Maximum shear stress criterion (Tresca, 1864);
4. Octahedral shear stress criterion (Von Mises, 1913);
5. Mohr-Coulomb criterion (1900);
6. Drucker-Prager criterion (1952).

The main characteristics of these classical criteria are as below. They have certain physical view points to explain the reason for failure and the variation regularity of strength for the particular material and are demonstrated experimentally. For example, Von Mises criterion fits for use in the plasticity theory of ductile metal (e.g. mild steel), and Mohr-Coulomb criterion fits for use in soil and rock mechanics. However, these criteria contain only one or two parameters in their mathematic expressions and the geometrical shapes of corresponding failure envelopes of them (Table 5-5) are rather simple and far different from that of concrete. Generally, these classical criteria can not be used for concrete and similar materials.

Various failure criteria, based on the relevant experimental data accumulated, are provided for concrete by many researchers. Several typical criteria among them are shown in Tables 5-5 and 5-6, and these criteria contain four or five parameters in their mathematic expressions to accurately simulate the spatial failure envelope of

Table 5-5 Classification of Meridians and Envelope on Deviatoric Plane of Various Failure Criteria [1-2]

Envelope on deviatoric plane					
Meridians	Regular triangle	Regular hexagon	Circle	Curve with three edges	Smooth and convex curve
C.M. ↑ T.M. → Parallel lines		Tresca (1)	Von Mises (1)		
C.M. ↑ T.M. → Inclined lines	Rankine (1)	Mohr-Coulomb (2)	Drucker-Prager (2)		Willam-Warnke (3)
C.M. ↑ T.M. → Smooth curve			Bresler-Pister (3)	Hsieh-Ting-Chen (4) Reimann (4)	Ottosen (4) Willam-Warnke (5) Kotsovos (5) Podgorski (5) Guo-Wang (5)

Note: The figure in the parentheses shows the number of the parameters in expression of the failure criterion.

Table 5-6 Initial and Unified Expressions for Failure Criteria of Concrete [1-2]

Failure Criterion	Number of Parameters	Initial Expression	Unified Expression
Reimann [5-14]	4	$\frac{\xi}{f_c} = a \left(\frac{r_c}{f_c} \right)^2 + b \left(\frac{r_c}{f_c} \right) + c$ $r = \varphi r_c$	$(1) \sigma_0 = A + B\tau_0 + C \tau_0^2$ $\sigma_0 = \frac{c}{\sqrt{3}} - \frac{b}{\phi} \tau_0 - \frac{\sqrt{3} a}{\phi^2} \tau_0^2$
Ottosen [5-34]	4	$a \frac{J_2}{f_c^2} + \lambda \frac{\sqrt{J_2}}{f_c} + b \frac{I_1}{f_c} - 1 = 0.$	$\sigma_0 = \frac{1}{3b} - \sqrt{\frac{1}{6}} \frac{\lambda}{b} \tau_0 - \frac{a}{2b} \tau_0^2$
Hsieh-Ting-Chen [5-35]	4	$a \frac{J_2}{f_c^2} + b \frac{\sqrt{J_2}}{f_c} + c \frac{\sigma_1}{f_c}$ $+ d \frac{I_1}{f_c} - 1 = 0$	$\sigma_0 = \left[\frac{1}{3d} - \frac{c}{3d} \frac{\sigma_1}{f_c} \right]$ $- \sqrt{\frac{1}{6}} \frac{b}{d} \tau_0 - \frac{a}{2d} \tau_0^2$
Podgorski [5-37]	5	$\sigma_{oct} - c_0 + c_1 \rho \tau_{oct}$ $+ c_2 \tau_{oct}^2 = 0$	$\sigma_0 = c_0 - c_1 \rho \tau_0 - c_2 f_c \tau_0^2$ $(2) \tau_0 = D + E \sigma_0 + F \sigma_0^2$
Bresler-Pister [2-34]	3	$\frac{\tau_{oct}}{f_c} = a - b \frac{\sigma_{oct}}{f_c} + c \left(\frac{\sigma_{oct}}{f_c} \right)^2$ $\theta = 0^\circ :$	$\tau_0 = a - b \sigma_0 + c \sigma_0^2$
William-Warnke(5) [5-33]	5	$\frac{\tau_{mt}}{f_c} = a_0 + a_1 \frac{\sigma_m}{f_c} + a_2 \left(\frac{\sigma_m}{f_c} \right)^2,$ $\theta = 60^\circ :$ $\frac{\tau_{mc}}{f_c} = b_0 + b_1 \frac{\sigma_m}{f_c} + b_2 \left(\frac{\sigma_m}{f_c} \right)^2$	$\tau_{ot} = \frac{a_0}{\sqrt{0.6}} + \frac{a_1}{\sqrt{0.6}} \sigma_0 + \frac{a_2}{\sqrt{0.6}} \sigma_0^2$ $\tau_{oc} = \frac{b_0}{\sqrt{0.6}} + \frac{b_1}{\sqrt{0.6}} \sigma_0 + \frac{b_2}{\sqrt{0.6}} \sigma_0^2$

Continued

Table 5-6 Initial and Unified Expressions for Failure Criteria of Concrete [1-2]—cont'd

Failure Criterion	Number of Parameters	Initial Expression	Unified Expression
Willam-Warnke(3) [5-33]	3	$\frac{\tau_m}{f_c} = r(\theta) \left(1 - \frac{1}{\rho} \frac{\sigma_m}{f_c} \right)$	$\tau_0 = \frac{r(\theta)}{\sqrt{0.6}} - \frac{r(\theta)}{\sqrt{0.6}\rho} \sigma_0, F = 0$ (3) $\tau_0 = G (\Phi(\sigma_0))^H$
Kotsovos [5-36]	5	$\theta = 0^\circ, \frac{\tau_{oct} t}{f_c} = a \left(c - \frac{\sigma_{oct}}{f_c} \right)^b$ $\theta = 60^\circ, \frac{\tau_{oct} c}{f_c} = d \left(c - \frac{\sigma_{oct}}{f_c} \right)^e$	$G = a, H = b, \phi = c - \frac{\sigma_{oct}}{f_c}$ $G = d, H = e, \phi = c - \frac{\sigma_{oct}}{f_c}$
Guo-Wang [5-4]	5	$\tau_0 = a \left(\frac{b - \sigma_0}{c - \sigma_0} \right)^d$ $C = C^t (\cos 1.5\theta)^{1.5} + C_c (\sin 1.5\theta)^2$	$G = a, H = d, \phi = \frac{b - \sigma_0}{c - \sigma_0}$

concrete. The initial expressions of these criteria are presented separately by different stress variables (Table 5-6):

1. Principal stresses f_1, f_2, f_3 ;
2. Stress invariants I_1, J_2, J_3 ;
3. Hydrostatic and deviatoric stresses ξ, γ, θ ;
4. Octahedral normal and shear stresses $\sigma_{oct}, \tau_{oct}, \theta$;
5. Average normal and shear stresses σ_m, τ_m, θ .

Nevertheless, these stress variables can be easily alternated with one another, as the basic formulas used are:

$$\left. \begin{aligned} \sigma_{0f_c} = \sigma_{oct} &= \frac{f_1 + f_2 + f_3}{3} = \frac{I_1}{3} = \frac{\xi}{\sqrt{3}} = \sigma_m \\ \tau_{0f_c} = \tau_{oct} &= \frac{\sqrt{(f_1 - f_2)^2 + (f_2 - f_3)^2 + (f_3 - f_1)^2}}{3} = \sqrt{\frac{2J_2}{3}} = \frac{r}{\sqrt{3}} = \sqrt{\frac{5\tau_m}{3}} \\ \cos\theta &= \frac{2f_1 - f_2 - f_3}{3\sqrt{2} \tau_{oct}} = \frac{2f_1 - f_2 - f_3}{2\sqrt{3}J_2} = \frac{2f_1 - f_2 - f_3}{\sqrt{6} r} = \frac{2f_1 - f_2 - f_3}{\sqrt{30} \tau_m} \\ \text{or } \cos 3\theta &= \frac{3\sqrt{3} J_3}{2J_2^{1.5}} = \frac{\sqrt{2} J_3}{\tau_{oct}^3} \end{aligned} \right\} \quad (5-8)$$

The initial expressions of these criteria are more variety and difficult to be compared with one another. If they are presented together in terms of relative octahedral strengths ($\sigma_0 = \sigma_{oct}/f_c$ and $\tau_0 = \tau_{oct}/f_c$), only three basic formulas are induced from them:

$$\left. \begin{aligned} \sigma_0 &= A + B\tau_0 + c\tau_0^2 \\ \tau_0 &= D + E\sigma_0 + F\sigma_0^2 \\ \tau_0 &= G[\phi(\sigma_0)]^H \end{aligned} \right\}. \quad (5-9)$$

The unified expressions of these criteria are shown in Table 5-6 as well.

In reference [1-2], a large number of the experimental data of multiaxial strength of concrete at home and abroad are collected and compared carefully with these failure criteria. When the evaluation criteria are taken as: (1) consistency between the experimental data and the calculated values; (2) application scope of stress state; and (3) reasonableness of geometrical shape of the theoretical failure envelope, the conclusions derived are that: criteria of Guo-wang, Ottosen and Podgorski are better, the criteria of Hsieh-Ting-Chen, Kotsovos, and Willam-Warke are second, but the Bresler-Pister criterion is worse.

When a reinforced concrete structure is analyzed by the finite element method, the failure criterion used for concrete should be reasonably selected to fit the scope of corresponding stress state and the requirement of accuracy asked. Among these

failure criteria of concrete, the criteria of Ottosen and Guo-wang are accepted respectively in the CEB-FIP Model Code [2-12] and the China Code [2-1].

5.4.3 Calculation charts for multiaxial strength

The failure criteria of concrete are expressed in the complicated mathematical formulas, and the multiaxial strengths of concrete are implicit in it and can not be calculated directly. Usually, a computer program is compiled for the criterion and contained within the total program of structural analysis. Alternatively, various charts are available in relevant design codes and references and can be used conveniently for determining the multiaxial strength of concrete. Normally, the strength values shown on these charts are slightly lower than the corresponding experimental data to ensure the structural safety. Sometimes, certain three-dimensional structures can be simplified into two-dimensional ones during their design or analysis, so the biaxial envelope of concrete is used more frequently in the engineering practice.

The chart for triaxial strength of concrete (Fig. 5-19) based on Ottosen criterion is provided in the CEB-FIP Model Code [2-12] and the code for design of prestressed

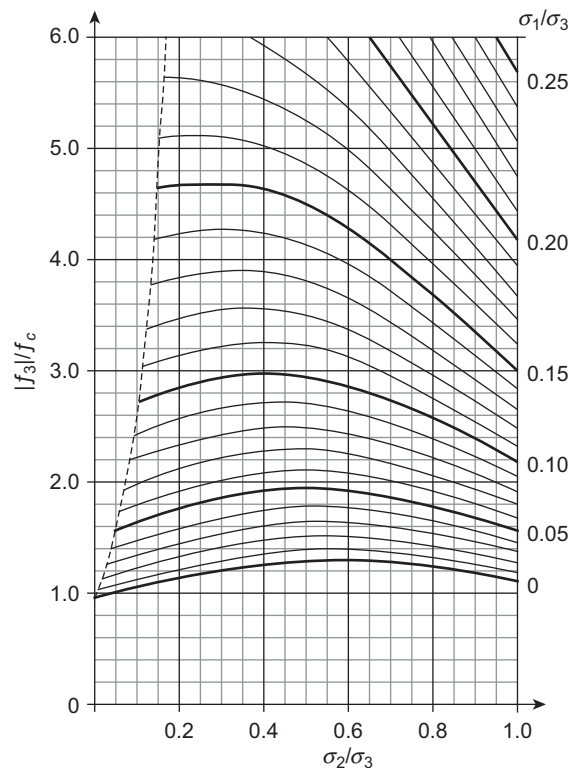


FIG. 5-19 Chart for triaxial compressive strength of concrete [2-12,5-39]

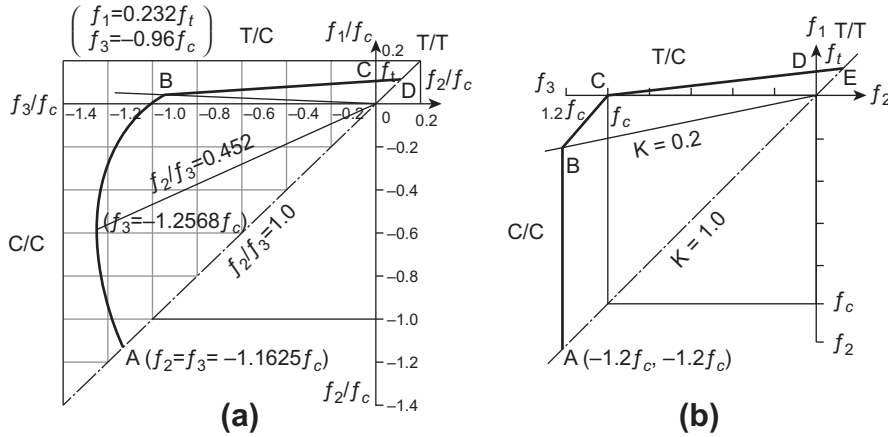


FIG. 5-20 Charts for biaxial strength of concrete: (a) Kupfer-Gerstle criterion [5-40], (b) Tasuji-Slate-Nilson criterion [5-41]

concrete reactor vessels [5-39]. The triaxial compressive strengths f_3 and f_1, f_2 can be consulted on the chart and then calculated after knowing the stress ratio σ_1/σ_3 and σ_2/σ_3 .

The chart for biaxial strengths of concrete shown in Fig. 5-20(a) is based on Kupfer-Gerstle biaxial failure criterion [5-40], which is widely used in engineering practice. Another chart for biaxial strength is shown in Fig. 5-20(b) and based on Tasuji-Slate-Nilson biaxial failure criterion [5-41], and it is composed of four straight lines linked together and is easy for use.

In the Chinese Code [2-1], the charts for both biaxial strength and triaxial compressive strength of concrete (Fig. 5-21) are given and the calculation rules for other stress states are suggested as well. The biaxial envelope in the chart is also composed of four straight lines and is slightly lower than the experimental one. The triaxial compressive strength (f_3) of concrete depends only upon the stress ratio σ_1/σ_3 and is not related to the second principal stress σ_2 to simplify the calculation, and its value is obviously lower than that in Fig. 5-19. The triaxial tensile-compressive strength (T/T/C, T/C/C) of concrete can be calculated by ignoring the stress σ_2 as well, so the strengths f_1 and f_3 can be found on the biaxial envelope (T/C quadrant in Fig. 5-21(a)). The triaxial tensile strength (T/T/T) of concrete of any stress ratio ($\sigma_1 : \sigma_2 : \sigma_3$) is simply taken as $0.9 f_t$.

5.5 Constitutive relation

The constitutive relation of concrete under simple stress state, i.e. complete stress-strain relations under uniaxial compression and tension, can be accurately measured during testing and described by a reasonable regression formula. Nevertheless, it

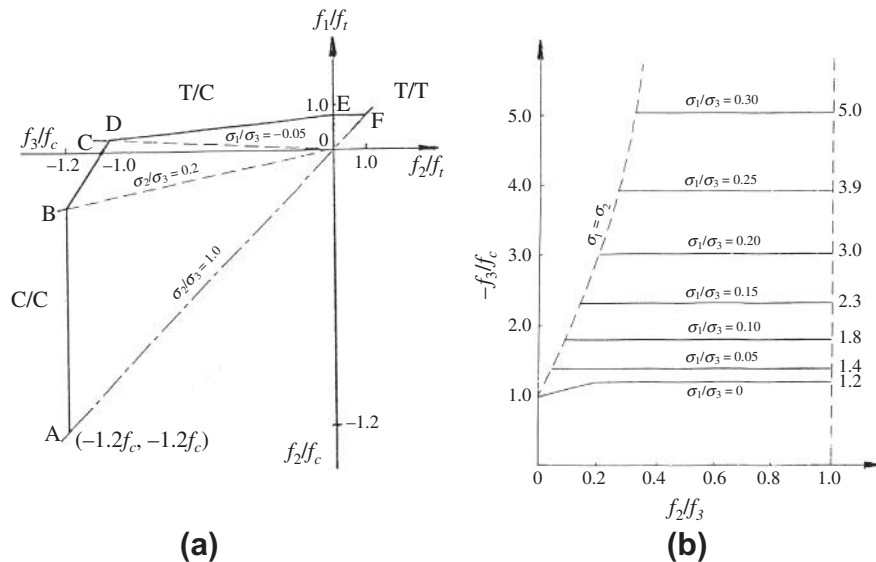


FIG. 5-21 Charts for multiaxial strength of concrete [2-1]: (a) biaxial envelope, (b) triaxial compressive strength

varies to a certain extent because of scatter of material property, variety of deformation compositions, and so many influencing factors of concrete.

The constitutive relation of concrete under multiaxial stress state is rather complicated. As the principal stresses are acted together in three directions, the normal and lateral deformations of concrete in these directions confine or promote one another, and the appearance and development of internal microcracks are strongly influenced. In addition, the ratios among the deformation components of concrete vary with the triaxial compressive–tensile stress state, and different cracking and failure patterns of concrete are caused. Therefore, the triaxial deformation of concrete varies significantly and complicatedly. On the other hand, the triaxial test method is not unified and the measuring technique of triaxial deformation of the cubic specimen is difficult, they result in considerable scatter of measured data. Consequently, establishing a reasonable triaxial constitutive relation for concrete is a difficult task.

As the multiaxial constitutive relation of concrete is necessary for calculation and finite element analysis of a structure, a variety of constitutive models are suggested by many researchers, based on their own experimental and theoretical researches. They can be classified into four categories, according to the understanding of the mechanical characteristics of concrete: (1) linear elasticity model; (2) non-linear elasticity model; (3) plasticity model; (4) model based on other mechanics. Among them, the first two are of elastic ones while the other two are of non-elastic ones; categories (1), (3), and (4) are learned respectively from the theories

of elasticity, plasticity, and other branches of mechanic theories, while category (2) is mainly obtained from the regression analysis of numerous experimental data.

These models differ from one another in many aspects, including theoretical basis, method and expression, application scope of stress state, and calculation accuracy. It is difficult to determine one unique constitutive model of concrete, which can be used for any structure, but the model should be carefully selected for a particular structure. Normally, the models of category (2) are used more widely in engineering practice, because they are based on the test result, expressed apparently, easily used, and calculated with sufficient accuracy.

5.5.1 Models of linear elasticity

This category of constitutive relation is the simplest and basic one for engineering material. The deformation (strain) of the material varies linearly during both loading and unloading (Fig. 5-22), and no residual deformation is presented after being totally unloaded. Therefore, a definite and unique relation is held between the stress and strain of the material, and the ratio between them is a constant, which is called the elastic modulus, of the material.

The linear elastic constitutive relation is the physical basis for Theory of Elasticity, and it is the most mature constitutive relation of material and also a special case of other categories of constitutive relation. Based on this, some finite element analysis programs of two- and three-dimensional structures, such as SAP, ADINA, and ANSYS, have been successfully used for many years in engineering practice.

Of course, the deformation characteristic of concrete, including stress–strain curves of it under uniaxial compression and tension and multiaxial stress state, is non-linear, in principle, the linear elastic constitutive relation can not be used for concrete structure. However, application of this category of constitutive relation is still an effective and quick measure for analysis of concrete structure under some situations, for example: (1) when the stress level of concrete is lower and internal microcracks and plastic deformation of it are limited; (2) before the structure, especially the prestressed concrete ones, is cracked; (3) when the structure of complicated configuration is analyzed preliminary or approximately; (4) when the structure is not sensitive to different constitutive relation of concrete. In fact, most reinforced concrete structures at home and abroad now are analyzed based on the

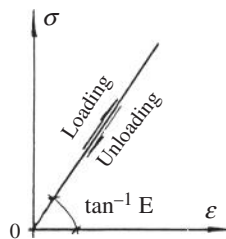


FIG. 5-22 Linear elasticity stress–strain relation

linear elastic constitutive relation of concrete, and then designed and constructed. It is demonstrated by engineering experience that these structures are generally of necessary, even slightly higher, safety and better serviceability. Many design codes for concrete structure, including [2-1] and [3-19], permit the use of linear elastic constitutive relation for analysis and calculation of it.

When directional difference of material behavior is considered, three linear elastic constitutive relations of different complications can be established.

5.5.1.1 Anisotropic constitutive model

Generally, there are six independent stress components, i.e. normal stresses σ_{11} , σ_{22} , and σ_{33} and shear stresses $\tau_{12} = \tau_{21}$, $\tau_{23} = \tau_{32}$, and $\tau_{31} = \tau_{13}$, at any point in a structure, correspondingly there are six strain components, i.e. normal strains ϵ_{11} , ϵ_{22} , and ϵ_{33} and shear strains $\gamma_{12} = \gamma_{21}$, $\gamma_{23} = \gamma_{32}$, and $\gamma_{31} = \gamma_{13}$ for it. If the elastic constant between any stress component and any strain component of a material is different from others, the general stiffness matrix of constitutive relation of the material is asymmetrical and contains $6 \times 6 = 36$ independent elastic moduli [1-3].

5.5.1.2 Orthogonal anisotropic constitutive model

When an orthogonal anisotropic constitutive material is concerned, the normal stress (σ_{ii}) acted causes no shear strain (γ_{ij}), and the shear stress (τ_{ij}) acted causes no normal strain (ϵ_{ii}) and no shearing strains (γ_{jk} , γ_{ki}) on two other planes. Therefore, the general stiffness matrix of the anisotropic constitutive model is dissolved into two matrices: the stiffness matrix of normal stress—strain is symmetrical and contains six elastic moduli, while the stiffness matrix of shear stress—strain is diagonal and contains three elastic moduli only. Then, the orthogonal anisotropic constitutive model contains a total of nine independent elastic moduli [1-3].

5.5.1.3 Isotropic constitutive model

The mechanical behavior of an isotropic material is the same in three directions and the constitutive relation of it is simplified and contains a total of only three elastic constants. These constants can also be expressed as well-known engineering quantities E , ν , and G , and only two among them are independent, because of

$$G = \frac{E}{2(1 + \nu)}. \quad (5-10)$$

Then, the isotropic constitutive model is established and is the same as the widely used in Theory of Elasticity.

All of these linear elasticity models can be found in detail in reference [1-3] or others.

5.5.2 Models of non-linear elasticity

The basic characteristic of non-linear elasticity constitutive relation of concrete can be explained by the uniaxial stress—strain curve shown in Fig. 5-23. The deformation of concrete increases with the stress and follows certain non-linear regularity,

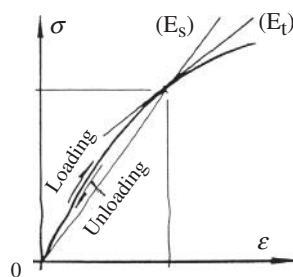


FIG. 5-23 Non-Linear elasticity stress—strain relation

and the stiffness of concrete decreases gradually. In addition, the deformation of concrete returns back along the loading curve during unloading and no residual deformation remains after being totally unloaded.

The advantages of this category of constitutive relation are: it reflects the main deformation characteristic of concrete under loading; the calculation formulas and parameter values of it are obtained from regression analysis of the experimental data; the calculation results are of sufficient accuracy when the concrete is loaded proportionally and monotonically; the expression of it is explicit and simple, and it can easily be understood and applied. Therefore, this category of constitutive relation of concrete is used most widely in engineering practice. However, the disadvantages of it are: it can not reflect the difference between loading and unloading; no residual deformation remains after unloaded. Therefore, this category of constitutive relation of concrete can not be used accurately for the conditions of unloading, loading—unloading cycle, non-proportionally loading, etc.

Many models of different expression and calculation method have been suggested and belong in this category of constitutive relation of concrete. When directional difference of concrete behavior is also considered, these models are classified as isotropic, orthogonal anisotropic and anisotropic models as well. Some typical models among them with their main characteristics are listed in Table 5-7, which include application scope of stress state, stress path, tangent or secant modulus, method for determining the parameter values, failure criterion used. More details of these constitutive models can be found in relevant references including [5-32], [1-2] and [1-3].

The Ottosen and Darwin-Pecknold models are clearly recommended in the CEB-FIP Model Code [2-12]. In Chinese design code [2-1], the orthogonal anisotropic model of non-linear elasticity or other constitutive relation demonstrated properly, but no specific model, is suggested.

5.5.3 Models of other categories

The classical theory of plasticity is established for the ideal elasto-plastic material, of which the uniaxial stress—strain relation is shown in Fig. 5-24. When the stress acted on the material is lower than its yield strength f_y , the strain increases

Table 5-7 Non-Linear Elasticity Constitutive Models of Concrete [1-3]

Category	Authors	Dimensions	Format of Moduli	Stress-Strain Curve	Loading Path	Method for Determining Parameter	Failure Criterion	Reference
Isotropic model	Kupfer-Gerstle	2 3C*	Secant	Ascending branch	Proportionally	Experimental simulation	Kupfer-Gerstle (Fig. 5-20(a))	[5-40]
	Romstad-Taylor-Herrmann	2	Tangent	Ascending branch	Proportionally	Experimental simulation	Broken-lines	[5-42]
	Palaniswang-Shah	3C*	Tangent	Before formation of unstable crack	Proportionally	Experimental simulation		[5-43]
	Cedolin-Crutzen-Dei Poli	3	Secant, tangent	Ascending branch	Proportionally	Experimental simulation	Broken-lines	[5-44]
	Ottosen	3	Secant	Complete	Proportionally	Equivalent uniaxial relation	Ottosen [5-34]	[5-45] [5-46]
Orthogonal anisotropic model	Lin-Nilson-Slate	2C*	Tangent	Ascending branch	Proportionally	Equivalent uniaxial relation	Broken-lines	[5-47]

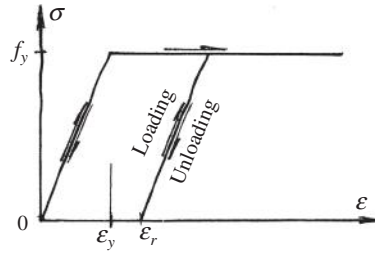


FIG. 5-24 Ideal elasto-plastic stress–strain relation

proportionally with the stress, the loading and unloading processes vary along the same inclined line, and no residual strain remains after totally unloaded. The stress of the material can not increase any more but keeps constant, when its yield strength is reached and its strain is increased further. Afterwards, the stress–strain line during unloading parallels with that before its yielding, but residual strain ϵ_r appears after being totally unloaded. When it is loaded again, the stress–strain line runs back along the unloading line with the same slope (stiffness of material).

This constitutive relation is mainly used for metal, e.g. mild steel, and the basic assumption and deformation regularity of it are demonstrated experimentally. The theoretical system of plasticity is formed based on the basic constitutive relation and the matured analytical methods [5-57] are provided, and the accurate results are obtained as it is applied in various engineering practices.

However, the construction and property of concrete material are obviously different from those of plasticity metal, and the considerable difference between the uniaxial compressive and tensile stress–strain curves of both materials is definite evidence. In order to use the theory of plasticity for concrete material, many scientists have reformed it and suggested various constitutive models of plasticity, e.g. perfect plasticity model [5-32], hardening plasticity model [5-58], plasticity model based on the spatial strain relaxation envelope, which corresponds to the spatial failure envelope of concrete [5-59], gradually fracturing model [5-60], and plastic-fracturing model [5-61]. Although these models improve on some aspects, e.g. stiffness degeneration and existence of descending branch for concrete, the material described by them is still different significantly from the actual behavior of concrete. In addition, their mathematical expressions are implicit and calculation processes are complicated, so they are not easily accepted and applied by structural engineers.

Other branches of mechanics developed latterly for various engineering materials are also used to establish the constitutive relation for concrete, e.g. models based on visco-elasto plasticity [5-62,5-63], endochronic theory [5-64], fracture and damage mechanics [5-65,5-66]. In addition, some models are composed of different theories, e.g. combined plasticity and damage mechanics [5-67], endochronic and damage mechanics [5-68], plasticity and fracturing theory [5-61]. Furthermore, there are other models, for example: model of plasticity theory based on fuzzy sets [5-69], and the model based on knowledge of material behavior with nerve networks [5-70].

Generally, these models follow the concept and method of the original theory to derive the corresponding expression for constitutive model of concrete, after introducing some simplification of its behavior. Then the values of the parameters in the expression are calibrated or directly given from some experimental data. However, the behavior of concrete calculated from these models is still different considerably from the actual behavior of concrete. In addition, these models seek theoretical accuracy, so their mathematical expressions are rather complicated and difficult to be widely accepted and applied by the structural engineers.

This page intentionally left blank

Combination Function of Reinforcement and Concrete

2

Reinforced concrete is a kind of composite material composed of concrete, which is the main body or matrix of it, and reinforcement of high tensile strength and different forms. Reinforced concrete is used most widely and successfully in structural engineering, because the behaviors of both materials fully complement each other.

Steel is a kind of ductile metal and its main element is iron. Steel reinforcement used in concrete structure is rolled into slender bars or fine wire. The external form and behavior index of the reinforcement are stable and its quality is guaranteed, because it is manufactured in modern industry and is examined systematically during processing. In contrast, concrete is brittle and the most of it is coarse with fine rocky aggregates, which are adhered integrally by cement after hydration. Most of the raw materials of concrete are provided locally and the mixing and manufacturing technique, quality control, and construction management of concrete structure are highly dependent, so the quality and behavior of concrete are deviated considerably.

The properties and mechanical behaviors of reinforcement and concrete are significantly different. Of course, the mechanical behavior of reinforced concrete, used as a composite material, is different from any one of both materials and is not a simple summation of them. However, the behavior of reinforced concrete is certainly dependent upon that of both materials and the relative cooperation of them, such as volumetric ratio, strength ratio, elastic modulus ratio, and form and detail of reinforcement. On the other hand, the effective composite form of both materials can be actively designed and constructed to satisfy the particular requirement of various engineering projects, when the variation regularity of the mechanical behavior of different composite form is known thoroughly.

The basic characteristic and main mechanical behavior of the composite material, i.e. reinforced concrete, is introduced in this part. The main contents of the five chapters in this part are separate: basic mechanical behavior of reinforcement, bond function between concrete and reinforcement buried in it, mechanical characteristics of structural sections reinforced longitudinally and transversely, and sectional analysis if deformation difference between reinforcement and adjacent concrete is a result. These are the basis for studying the behavior of reinforced concrete structural members, which are presented in later parts.

Mechanical Behavior of Reinforcement

CHAPTER OUTLINE

6.1 Reinforcement used in concrete structure.....	159
6.1.1 Reinforcement (diameter 6–40 mm)	160
6.1.2 High-strength wire (diameter 4–9 mm)	161
6.1.3 Shape steel.....	161
6.1.4 Ferrocement	162
6.1.5 Other substitutive materials.....	162
6.2 Stress–strain relation	163
6.2.1 Mild steel	163
6.2.2 Hard steel (wire).....	166
6.3 Deformation under action of cyclic loads.....	167
6.4 Behavior after cold-worked.....	172
6.4.1 Cold-stretching and age-hardening.....	173
6.4.2 Cold-drawn	175
6.5 Creep and relaxation	176
6.5.1 Kind of steel	178
6.5.2 Sustaining time of control stress.....	178
6.5.3 Stress level	178
6.5.4 Temperature	179

6.1 Reinforcement used in concrete structure

The main function of reinforcement buried in concrete structures is to carry the tensile force in it and to remedy lower tensile strength and deficient ductility of concrete material. Generally, slender bars and fine wires of high strength are widely used in most concrete structures. Shaped steel of various types are frequently used in some structures, in order to reduce the section size and weight, to enhance the bearing capacity and stiffness, to improve the detailed construction, and to accelerate the construction process of the structure. Other materials of high tensile strength can also be used in concrete structure to replace the steel reinforcement. Therefore, the generalized reinforcement in reinforced concrete structure includes materials of high tensile strength but with different properties and external form. The reinforcement used in engineering practice is now classified into several categories.

6.1.1 Reinforcement (diameter 6–40 mm)

The reinforcement used most in concrete structure is steel bars and their diameter usually ranges from 6 mm to 40 mm. The main chemical composition of structural steel is iron (>96%) and other compositions are carbon, manganese, silicon, sulfur, phosphorus, etc. When some metals are properly added in during smelting of steel to improve the mechanical behavior, structural steel of low alloy is obtained, e.g. series of manganese-silicon, silicon-titanium, manganese-silicon-vanadium.

Generally, the section of the reinforcement is circular, others are of ellipse, quasi-square, etc. The reinforcement is made into different appearances during its hot-rolling process: smooth circle (plain) surface for that of lower strength and spiral, λ , crescent, corrugated, and twisted shapes (Fig. 6-1) for that of higher strength, which are together called deformed (or ribbed) bars. The deformed surface is greatly helpful to enhance the bond strength between reinforcement and adjacent concrete, hence its strength can be utilized fully in the structure and the mechanical behavior of the structure is improved. In addition, different appearances of the reinforcement distinguish conveniently various categories and strengths of it.

In China, the reinforcement used for concrete structure is classified into several categories, according to its manufacturing technology, external appearance, and strength grade. Those suggested in the design code [2-1] are:

hot-roll plain bar HPB235 it means that the standard value of its yield strength is $f_{yk} = 235\text{N/mm}^2$. The same for those below;
hot-roll ribbed bar HRB335 and HRB400;
residual heat treated ribbed bar RRB400.

The reinforcement of HRB400 among them is recommended.

These reinforcements are of mild steel and a yielding plateau can be seen apparently on their complete stress-strain curve. The alloy compositions, contents of chemical elements, external appearance, mechanical behavior, and quality requirement of them can be found in relevant national standards [6-1–6-3].

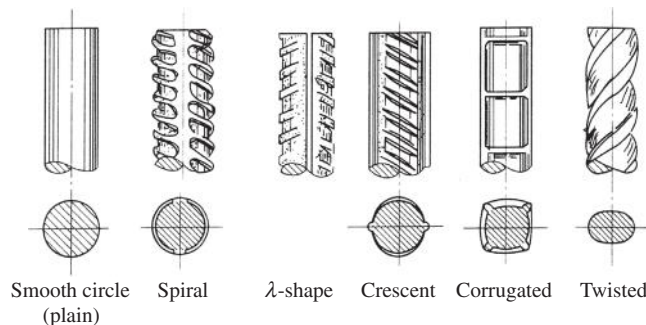


FIG. 6-1 Appearance of reinforcement

6.1.2 High-strength wire (diameter 4–9 mm)

As the wire of carbon steel experienced successively cold-drawing and heat treatment, the ultimate strength of it reaches a rather high value ($1500\text{--}1800\text{ N/mm}^2$), but no yielding plateau is obviously seen on its stress–strain curve. This kind of wire is called hard steel and is mainly used in prestressed concrete structures. In Chinese design code [2-1], the plain, spiral ribbed, or other deformed wires after stress relieved (diameter 4–9 mm) [6-4], steel strand twisted by 3–7 wires (diameter 3–6 mm) [6-5], and heat-treated steel (diameter 6–10 mm) [6-6] of high strength are suggested to be used in the structure.

However, steel rope is woven out of finer wire (diameter $<1\text{ mm}$) of even higher strength, but is seldom used in concrete structure, because of poor bond between it and adjacent concrete.

6.1.3 Shape steel

Various shape steels, including the angle, channel, I, plate, and tube steels, can be used in concrete structure, and different composite steel–concrete structures (Fig. 6-2) are formed. Mild steel of lower strength is generally used in these structures.

Shape steel can be used directly or welded into a compound section, and steel plate can be welded into I, box, or some complicated shapes or pressed or bent into some shapes. A variety of steel–concrete structures are frequently used as the columns of high-rise building and industrial workshops and shear-wall structures. When concrete is filled into a circle or square steel tube and the confined concrete formed has high compressive strength and ductility (see Section 9.3), this is usually used as the short columns of the lower floors in high-rise buildings, underground railways and garages, and other structures. And it can also be used for the main structure of arched bridges. The structure composed of shape steel beam and concrete flange is a reasonable scheme for the bridge of medium span.

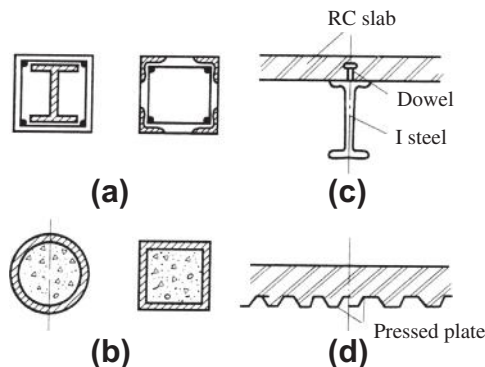


FIG. 6-2 Composite sections of shape steel-concrete: (a) shape steel, (b) tube (c), composite beam, (d) pressed plate

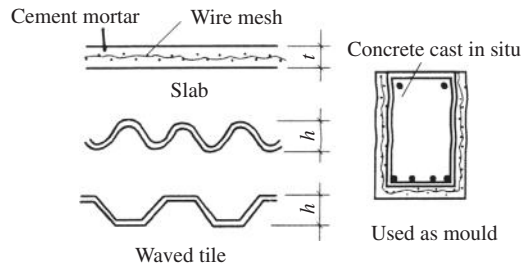


FIG. 6-3 Ferrocement

The pressed thin steel plate is often used as the bottom layer of concrete floors, and it serves the functions of both mold and tensile material.

6.1.4 Ferrocement

When fine steel wire is woven into mesh and used as the reinforcement, a kind of ferrocement plate is obtained after cement mortar is cast and hardened (Fig. 6-3). The ferrocement plate is of high cracking resistance because the fine wires distribute densely in two perpendicular directions. Ferrocement can be made into waved tiles, even ships, and other structures of complicated shape. It can also be used as the external layer of beams, columns, or other structures, and concrete is cast into it after other reinforcement is set up. The advantages of this kind of structure are of high cracking resistance during service stage and omitting other mold and its support during the construction stage.

6.1.5 Other substitutive materials

In principle, every material of high tensile strength can be used in concrete structure to substitute the steel reinforcement. In engineering history, cast iron and bamboo, of which the tensile strength is greater than 100 N/mm^2 , were used in practice. However, cast iron is of poor ductility and bamboo is of lower modulus of elasticity and is easily cracked and corroded, so the mechanical behaviors of the structural member reinforced with both materials are not satisfied. Therefore, they are not used any more now.

Various artificial fibers, e.g. glass and carbon yarns, are of very high strength (Table 4-5). When they are adhered with resin and made into bars or thin pieces, their strength is still greater than that of steel and they are of light weight, small size, and high corrosion resistance. Now, they are used in the concrete structure of offshore and other engineering and also used for strengthening the existing structure damaged. Sometimes, plastic is made into mesh and is used as the distributed reinforcement in concrete structure. However, some of the fiber materials are rather expensive and the elastic modulus of them is much lower than that of steel.

The steel and various substitutive materials of different strength grades, section shapes, sizes, and details, can be formed into various reinforced concrete structures,

of which the mechanical behaviors vary correspondingly. The main subject discussed later in this book is the concrete structure and its member reinforced with ordinary circle bar. Or, it may be called the ordinary reinforced concrete.

The mechanical behavior of the reinforced concrete structure other than the ordinary one can be similarly analyzed or estimated, according to the constitutive relation and detail of the substitutive materials used. In addition, proper specimens of the structure and its member are tested under loading if necessary, and the mechanical responses and regularity of them can be demonstrated and concluded.

6.2 Stress—strain relation

The stress—strain relation of reinforcement is measured from the test of the specimen, which is usually a piece of original one without any cutting. It is generally considered that the stress—strain curve of the reinforcement under compression is the same as that under tension, at least before its yielding and yield plateau. Therefore, the same values of the yield strength and the modulus of elasticity are taken for the reinforcement under both tension and compression.

The steel used in concrete structure is usually classified into two categories, i.e. mild and hard steels, depending upon whether or not yielding plateau appears clearly on the stress—strain curve.

6.2.1 Mild steel

The typical stress—strain curve of reinforcement of mild steel under tension is shown in Fig. 6-4, and several characteristic points on it reflect various physical phenomena before its failure.

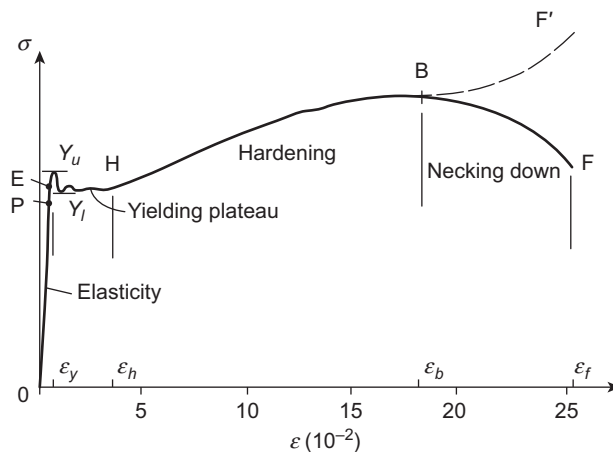


FIG. 6-4 Tensile stress—strain curve of mild steel

The stress and strain of the specimen increase proportionally from the start of loading until its proportional limit (Point P) on the curve. Afterwards, the strain increases more quickly than the stress does, and the stress-strain curve turns slightly. If the specimen is unloaded before the elastic limit (Point E), its strain runs back along the loading curve, and the origin is reached and no residual strain remains when it is totally unloaded. Therefore, the segment PE on the curve is a deformation zone of non-linear elasticity, but the stress increment within this zone is limited.

The strain of the specimen accelerates and the slope of the curve decreases after the elastic limit is passed. When the upper yield limit (Point Y_u) is reached, the stress of the specimen drops suddenly and a small peak is formed. Then, the lower yield limit (Point Y_l) is reached and the stress slightly increases again, when the strain is increased further. Afterwards, the curve enters the yielding zone and a stress plateau appears clearly, although the stress fluctuates slightly. The upper yield limit varies to a certain extent and depends upon the loading speed and the shape of the specimen (see Fig. 18-4), while the lower yield limit is relatively stable.

The stress-strain curve of the steel enters the hardening zone (H) after experiencing a large plastic deformation within the yield plateau, and the stress stably increases again until the ultimate strength (Point B) is reached. Afterwards, the tensile force decreases obviously as the strain increases further, and the section of a part of the specimen reduces apparently, and the necking phenomenon appears. Finally, the specimen is broken (Point F) at the middle of the necked part. The descending branch (BF) of the stress-strain curve is the result when the stress is calculated, using the original section of the specimen. If the tensile force is divided by the minimum area at the necked section, a continuously ascending branch (BF') is presented. When the elongation deformation, within the measuring length i.e. usually taken as 5 or 10 times the specimen diameter of the specimen after being broken is divided by the original length, the ultimate percentage elongation (δ_5 or δ_{10}) is obtained.

From the viewpoint of engineering application, the complete stress-strain curve of mild steel can be simplified into four zones including elasticity, yielding, hardening, and necking down ones. Consequently, the proportional, elastic, and upper and lower yield limits are merged into one point, i.e. yield limit (Y), and the elasticity zone (OY) before yielding is an inclined straight line and the yield plateau (YH) is a horizontal line ($f_y = \text{const.}$). The stress value of the yield limit is taken as that of the lower yield limit.

The main mechanical indices of the mild steel include yield and ultimate strengths (f_y, f_b), (initial) modulus of elasticity (E_s), and ultimate percentage elongation (δ_5 or δ_{10}). The steels of various alloy contents and strength grades show different values of these indices, and the indices of the qualified structural steels produced in China are listed in Table 6-1, and the typical stress-strain curves of them are shown in Fig. 6-5.

Comparing the mechanical indices of various steels, it is found that: (1) the higher the strength, the smaller the plastic deformation and ultimate elongation,

Table 6-1 Main Mechanical Indices of Structural Steels

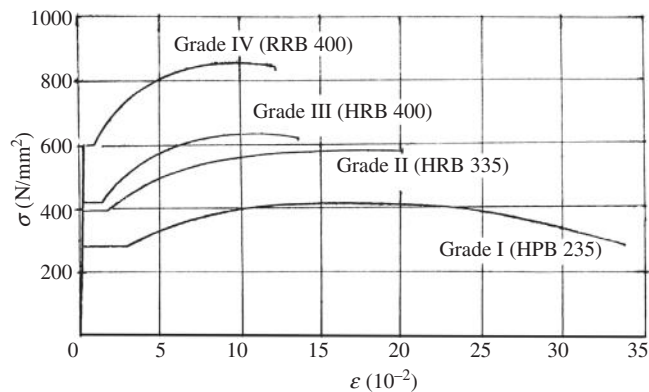
Category of Steel		Diameter (mm)	f_y (N/mm ²)	f_b (N/mm ²)	E_s (10 ⁵ N/mm ²)	δ_5 (%)
Hot-rolled bar	HPB235 (Q235)	8–20	235	370	2.1	25
	HRB335 (25MnSi)	6–50	335	490	2.0	16
	HRB400 (20MnSiV, 20MnSiNb, 20MnTi)	6–50	400	570	2.0	14
	RRB400 (K20MnSi)	8–40	400	600	2.0	14
Heat-treated bar	(40Si ₂ Mn, 48Si ₂ Mn, 45Si ₂ Cr)	6–10	(1250)	1470	2.0	6
Stress-relieved wire	Plain, spiral ribbed	4–9	(1340–1500)	1570–1770	2.05	4
	Deformed	5–7	(1340)	1570	2.05	4
Strand	3 or 7 wires	8.6–15.2	(1460–1580)	1720–1860	1.95	3.5

and the shorter the yield plateau; (2) the ratio between the ultimate and yield strengths of the mild steels is about:

$$f_b/f_y = 1.5 \quad \text{or} \quad f_y = 0.67f_b, \quad (6-1a)$$

$$\text{but } f_y \approx 0.85f_b \quad (6-1b)$$

for the hard steels.

**FIG. 6-5** Stress—strain curves of steel grades I to IV

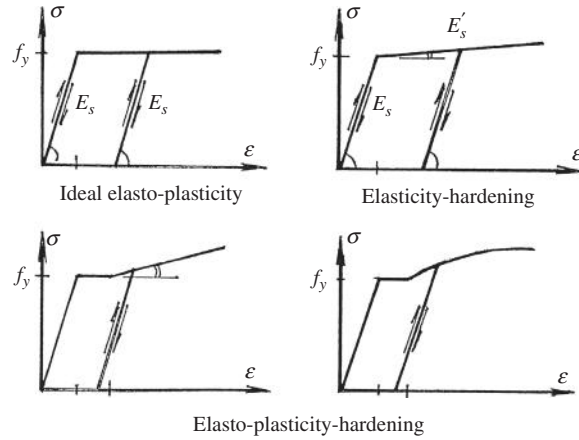


FIG. 6-6 Constitutive models for reinforcement (mild steel)

The mathematic models of the stress—strain relationship of the mild steel shown in Fig. 6-6 can be selected accordingly. The ideal elasto-plasticity model is the simplest one among them and is used widely in practice, because the strain of the reinforcement is normally less than 1% and has not entered into the hardening zone at failure of the structure. The model of elasticity hardening is of two straight lines linked at the yield point, and the stress—strain relation after yielded is simplified into a flatter line of slope taken usually as $E'_s = 0.01E_s$. The advantage of this model is uniqueness of the stress—strain relation. The elasto-plasticity hardening model of three lines or curve is slightly complicated but more accurate to describe the large deformation of the reinforcement.

6.2.2 Hard steel (wire)

The stress—strain curve of carbon wire, strands, and heat-treated steel of high strength is shown in Fig. 6-7. The stress and strain of the specimen increase proportionally after loading, and the proportional (elastic) limit is about $\sigma_e \approx 0.75f_b$. Afterwards, the strain accelerates and the slope of the curve decreases gradually. When the curve runs horizontally, the ultimate strength (f_b) is reached. Then, the curve descends slightly and the specimen is necked down and quickly broken. Its ultimate percentage elongation is only about 5–7%.

Obviously, there is no yield plateau on the stress—strain curve of hard steel wire. A nominal yield strength should be defined for hard steel and is used in the design of structure. In China, like other countries, the assumed yield point (Y) is taken as that corresponding to residual strain 0.2×10^{-2} after being unloaded, and the corresponding stress obtained from the experimental data is:

$$f_{0.2} = (0.8 \sim 0.9)f_b \quad (6-2)$$

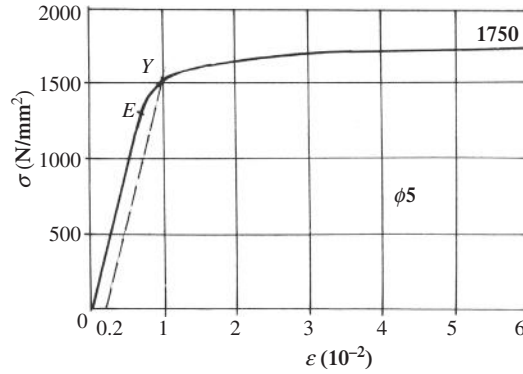


FIG. 6-7 Stress-strain curve of carbon wire of high strength

Therefore, the nominal yield strength of hard steel in Chinese Code [2-1] is taken as that shown in Eq. (6-1b). Other mechanical indices of hard steel are also listed in Table 6-1.

Ramberg-Osgood model [1-1] is used widely for the stress-strain relation of hard steel. When the elastic limit (σ_e, ϵ_e) and a reference point P $(\sigma_p, \epsilon_p = \sigma_p/E_s + e_p)$ of it are known in advance, the strain corresponding to any stress σ_s is determined by:

$$\left. \begin{aligned} 0 \leq \sigma_s \leq \sigma_e \quad \epsilon_s &= \frac{\sigma_s}{E_s} \\ \sigma_s > \sigma_e \quad \epsilon_s &= \frac{\sigma_s}{E_s} + e_p \left(\frac{\sigma_s - \sigma_e}{\sigma_p - \sigma_e} \right)^n \end{aligned} \right\}, \quad (6-3)$$

where $E_s = \sigma_e/\epsilon_e$ and the parameter is taken $n = 7-30$, depending upon the category of the steel.

According to the experimental data in China, the calculation formula [5-7] suggested for it is:

$$\epsilon_s = \frac{\sigma_s}{E_s} + 0.002 \left(\frac{\sigma_s}{f_{0.2}} \right)^{13.5} \quad (6-4)$$

6.3 Deformation under action of cyclic loads

When the repeated load (loading and unloading repeatedly, e.g. a lorry acting on a bridge) and reversed load (loading positively and negatively, e.g. seismic action) are acted cyclically on a concrete structure, the stress of a reinforcement in it should experience corresponding variations. As a single specimen of reinforcement is loaded repeatedly or reversely on a testing machine, the complete stress-strain

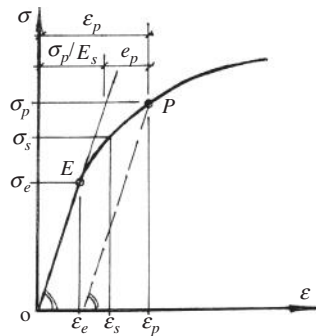


FIG. 6-8 Constitutive model for hard steel

curve of the specimen is measured and then the mathematic model of it can be simulated (Fig. 6.8).

The stress—strain curve of the reinforcement measured during repeated tension is shown in Fig. 6-9. When the reinforcement is loaded and unloaded before the yield point (Y), its stress and strain run along the straight line (OY) and no residual strain appears after being totally unloaded. After the reinforcement entered into the yield plateau ($\epsilon > \epsilon_y$), the unloading process is an inclined line (RO') paralleling with the initial loading line (OY) and the residual strain (ϵ_{res}) appears after being totally unloaded ($\sigma = 0$). And, the residual strain increases with the strain (ϵ_r) before unloading. When the reinforcement is loaded again, the stress and strain increments of it increase proportionally, i.e. ascend along the line $O'R$. If the reinforcement is loaded further, the stress—strain relation becomes curve $RH'B'F'$. Comparing with the original curve ($YRHB F$), the stress on segment RH' is increased, but the previous yield plateau disappears; the maximum stress (strength, at point B') approximates to the original ultimate strength (at point B) while the corresponding strain (ϵ_b) and ultimate elongation (δ_5) are reduced.

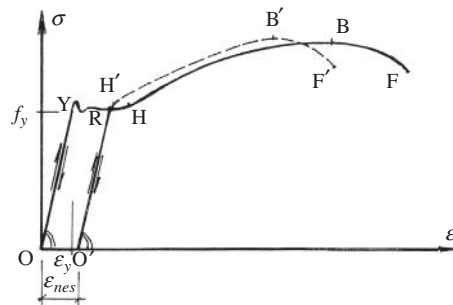


FIG. 6-9 Stress—strain curve of reinforcement under repeated tension

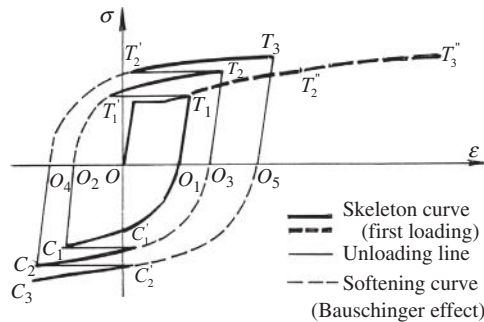


FIG. 6-10 Stress—strain curve of reinforcement under reversed tensile—compressive load

When the reinforcement specimen is loaded reversely, i.e. tensile and compressive stresses act alternately, and the maximum stress of every cycle is increased gradually, the stress—strain curve obtained is as shown in Fig. 6-10 [6-8—6-10]. After the tensile reinforcement entered into the yield plateau, it is unloaded from point T_1 until zero stress (line T_1O_1) and loaded reversely (compressive stress) from Point O_1 to Point C_1 (curve O_1C_1), then it is unloaded again from Point C_1 until zero stress (Point O_2) and line C_1O_2 is obtained. When the reinforcement is tensioned again, the stress—strain curve starts from Point O_2 and passes through Point T_1 , and reaches Point T_2 . When the reinforcement is successively unloaded, loaded reversely, and unloaded reversely again, the line T_2O_3 , curve $O_3C_1C_2$, and line C_2O_4 are obtained correspondingly.

When the loading curves in the same directions (tension and compression) are separately moved parallelly and linked together, two skeleton curves including tensile ($OT_1T_2''T_3''$, the black dashed line in Fig. 6-10) and compression ones are obtained. The skeleton curve in the direction of first loading (tensile one in Fig. 6-10) is consistent with the stress—strain curve of the same reinforcement tested under monotonic tension (Fig. 6-4), but both are obviously different from the skeleton curve in the negative direction (compression one). The main differences between them are that: the yield point during the first reverse loading is apparently lower and no yield plateau appears on the curve (O_1C_1), although the succeeding stress—strain curve is basically similar.

Therefore, when the steel is first loaded and entered into the yield plateau, its elastic limit during negative loading is apparently reduced, and the greater the strain reached during first loading, the more reduction in the elastic limit in the negative direction. This is called the Bauschinger effect [6-10]. The crystal lattice in the metal is of different directions and is deformed after loading, and the residual stress and strain of it exist after being totally unloaded, then plastic deformation occurs early under lower stress when it is loaded reversely.

The stress—strain curve of the reinforcement during unloading approximates a straight line regardless of tension and compression loads, and it parallels the initial

stress—strain line under first loading and the slopes of these lines, i.e. the modulus of elasticity, are equal. On the contrary, the stress—strain curve of the reinforcement during loading, including tensile or compressive load, is not a straight line because of the Bauschinger effect, except during first loading. Or, it is called softening segment.

Therefore, the complete stress—strain relation of the reinforcement under reversely loading can be described fully by three parts: skeleton, unloading and loading curves. Among them, the skeleton is taken as the complete stress—strain curve of the reinforcement under monotonic loading, the unloading curve is taken as an inclined line of slope E , but the loading curve or softening segment should be determined separately.

Cato model [6-9,1-1]. A local coordinate $(\sigma-\varepsilon)$, of which the origin is the starting point ($\sigma = 0$) of positively or negatively loading, is taken for the softening segment OA , and the ordinate and abscissa of Point A are respectively the maximum stress σ_s during last loading in the same direction and the strain increment ε_s from Point O to A (Fig. 6-11(a)). Therefore, the secant modulus of elasticity of segment OA is $E_B = \sigma_s/\varepsilon_s$, while the initial tangent modulus of elasticity of it is E . Let the relative coordinates be:

$$x = \varepsilon/\varepsilon_s \quad \text{and} \quad y = \sigma/\sigma_s,$$

and the equation is assumed for the experimental softening segment (Fig. 6-11(b)):

$$y = \frac{ax}{x + a - 1}. \quad (6-5)$$

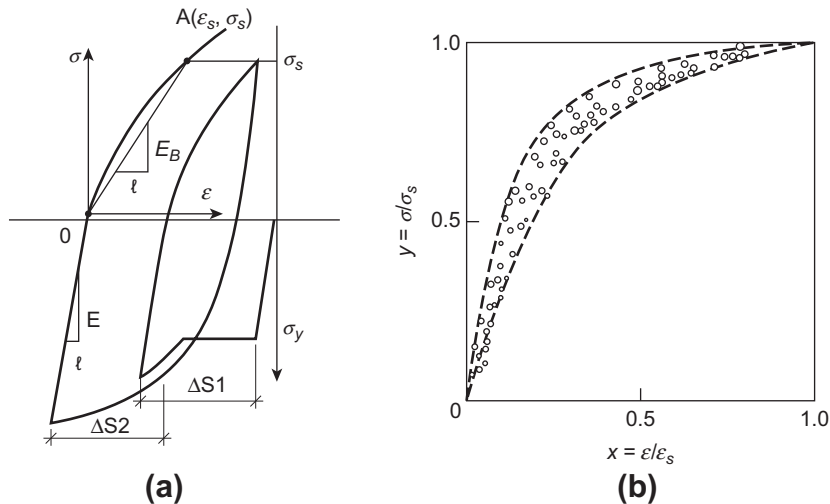


FIG. 6-11 Cato model for softening segment: (a) stress—strain curve under reverse loading, (b) shape of softening segment

When Eq. (6-5) is differentiated and let $x = 0$, the ratio between the initial slope of segment OA and the secant slope at Point A is obtained:

$$\begin{aligned} \left. \frac{dy}{dx} \right|_{x=0} &= \frac{a}{a-1} = \frac{E}{E_B} \\ \therefore a &= \frac{E}{E - E_B} \end{aligned} \quad (6-6)$$

The secant modulus of segment OA decreases gradually, i.e. stiffness degradation, at every loading as the plastic strain reached during last loading increases. According to the experimental data, the empiric value of the secant modulus of the softening segment is:

$$E_B = -\frac{E}{6} \log(10\epsilon_{res}), \quad (6-7)$$

where ϵ_{res} is accumulated strain on the skeleton within negatively loading history (Fig. 6-11(a)) :

$$\epsilon_{res} = \sum_i \Delta S_i \quad (6-8)$$

Kent-Park model [6-8]. The general formula of the stress-strain curve suggested by Ramberg-Osgood is:

$$\frac{\epsilon}{\epsilon_{ch}} = \frac{\sigma}{\sigma_{ch}} + \left(\frac{\sigma}{\sigma_{ch}} \right)^r, \quad (6-9a)$$

and the shape of the curve depends upon the value of r : it is a straight line and used for elastic material if $r = 1$; it includes two lines linked together and is used for ideal elasto-plastic material if $r = \infty$; it is one of the curve family transformed gradually when $1 < r < \infty$ (Fig. 6-12). The geometric characteristics of the family are: (1) every curve of them passes the point at $\sigma/\sigma_{ch} = 1$ and $\epsilon/\epsilon_{ch} = 2$; (2) the slope of

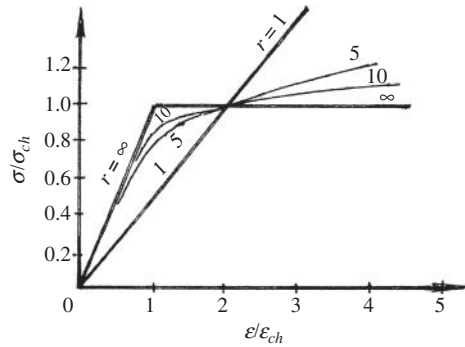


FIG. 6-12 Kent-Park model for softening segment [6-8]

the line is $dy/dx = 0.5$ when $r = 1$, while the initial slope of every curve equals $dy/dx = 1$ when $r \neq 1$.

Eq. (6-9a) is easily modified into:

$$\varepsilon = \frac{\sigma}{E} \left[1 + \left(\frac{\sigma}{\sigma_{ch}} \right)^{r-1} \right], \quad (6-9b)$$

where $E = \sigma_{ch}/\varepsilon_{ch}$ is the initial modulus of elasticity of reinforcement, σ_{ch} is the value of characteristic stress, which depends upon the plastic strain (ε_{ip}) caused within the previous stress cycles, and the empiric formula for calculation [1-1] is:

$$\sigma_{ch} = f_y \left[\frac{0.744}{\ln(1 + 1000\varepsilon_{ip})} - \frac{0.071}{(1 - e^{1000\varepsilon_{ip}})} + 0.241 \right] \quad (6-10)$$

when $\varepsilon_{ip} = 4-22 \times 10^{-3}$, where r is the parameter depending upon the number (n) of loading and unloading cycles:

$$\text{when } n \text{ is an odd} \quad r = \frac{4.49}{\ln(1 + n)} - \frac{6.03}{e^n - 1} + 0.297, \quad (6-11a)$$

$$\text{when } n \text{ is an even} \quad r = \frac{2.20}{\ln(1 + n)} - \frac{0.469}{e^n - 1} + 0.304. \quad (6-11b)$$

6.4 Behavior after cold-worked

Mild steel has a long yield plateau on its stress-strain curve and reaches the ultimate strength (f_b) after experiencing a large plastic deformation. However, only the yield strength of it can be used for structural design, but the ultimate strength (Eq. 6-1) can not be utilized, otherwise excessive deformation of the structure would occur if the corresponding strain is reached. On the other hand, the yield strength of mild steel will increase considerably, when it is stretched and enters into the yield plateau even strengthening zone and then unloaded, and the ultimate elongation of it is reduced corresponding but still satisfies the engineering requirement.

It is demonstrated by many engineering facts that the yield strength of mild steel is increased but the ultimate elongation is reduced after it was cold-worked, such as cold-stretched, -rolled, -twisted, -drawn, and larger plastic deformation was appeared, because the crystalline grain of the steel was distorted and deformed and, hence, its resistance was enhanced. This phenomenon is called cold-work strengthening. Furthermore, cold-stretching is a necessary procedure to straighten the reinforcement and also an additional examination for its quality during construction of the structure. Therefore, when the increased strength of mild steel is effectively utilized in the practical engineering, steel can be saved.

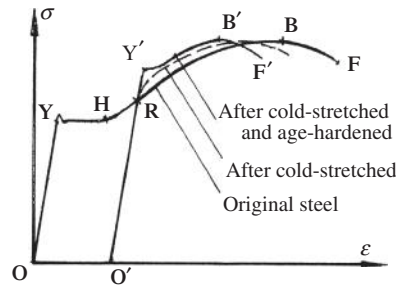


FIG. 6-13 Stress—strain relation of reinforcement after cold-stretching and age-hardening

6.4.1 Cold-stretching and age-hardening

When the reinforcement of mild steel is cold-stretched until exceeding the yield point and entering into the hardening zone and then is totally unloaded, the residual deformation (OO' in Fig. 6-13) is presented and the reinforcement is elongated. When the reinforcement is stretched again, the stress—strain curve obtained is shown as the dash line in the figure. It is seen that the yield strength approximately equals the stress value before unloading (Point R), which is called control stress of cold-stretching, and is higher than that before stretching; the yield plateau is not apparent and the modulus of elasticity is slightly reduced; the ultimate strength is approaching that of original steel, but the ultimate elongation is considerably decreased.

The main mechanical behavior, including yield strength (f_y), ultimate strength (f_b) and ultimate elongation (δ_{10}), of the reinforcement after cold-stretching depends upon the kind of original steel and the values of stress and elongation of it reached during stretching. The relevant data measured of various kinds of steel are listed and compared in Table 6-2. Generally, the yield strength of the reinforcement after stretching is increased by 20–35% over that of the original one, when it is stretched until elongation (3–5%). However, it should be mentioned that the compressive strength of the reinforcement after cold-stretching is not increased.

As the manipulation of cold-stretching is generally controlled by both stress and elongation of the reinforcement [6-11], the strength of the reinforcement and, then, the safety of the corresponding structure are guaranteed. In fact, when the wire rod (reinforcement) is mechanically straightened during the construction process, its plastic deformation also appears to a certain extent and the yield strength is increased correspondingly. When the yield strength of the reinforcement after straightening is determined from the reliable experimental investigation, it can be safely used in the design of the relevant structure [4-11].

The reinforcement after cold-stretching has no obvious yield plateau on its stress—strain curve. If the reinforcement is kept naturally for a period or heated artificially and then it is loaded again, the stress—strain curve $O'RY'B'F'$ shown in

Table 6-2 Comparison Between Behaviors of Reinforcement after Cold-Stretched and Age-Hardened and Original [6-11]

Kinds of Steel	Parameters of Cold-Stretching		f_y (N/mm ²)			f_b (N/mm ²)			δ_{10} (%)		
	Elongation (%)	Stress (N/mm ²)	Original Steel	After Stretched	After Stretched and Age-hardened	Original Steel	After Stretched	After Stretched and Age-hardened	Original Steel	After Stretched	After Stretched and Age-hardened
A5	4.00	478	—	478	525	—	—	570	—	20.4	15.7
16Mn	2.93	450	383	487	537	562	580	598	25.0	22.5	20.3
25MnSi	—	520	445	528	611	670	670	693	23.0	20.0	18.7
40Si ₂ V	1.71	750	705	758	853	930	936	942	15.3	13.4	13.0
45MnSiV	1.60	750	595	750	850	910	930	968	13.5	12.0	11.0
45Si ₂ Ti	2.30	750	—	750	844	—	957	956	—	11.7	12.8
44Mn ₂ Si	3.00	780	—	780	835	—	—	905	—	13.1	11.5

Fig. 6-13 is measured. It is seen that the yield plateau clearly appears again but with short length, the yield strength is increased once more and the ultimate strength is also increased slightly, but the ultimate elongation reduces further (Table 6-2). This phenomenon is called age-hardening (strengthening). Therefore, age-hardening is a succeeding process of cold-stretching for reinforcement, and it is helpful to improve its mechanical property.

Various kinds of steel need different age-hardening processes [6-11]. Ordinary, carbon steel (Grade I, A3 and A5) can be age-hardened under natural environment, and it takes generally two or three weeks, but takes less time under higher temperatures. Artificially heating accelerates the age-hardening process, for example, only two hours are needed under temperature 100°C . However, the age-hardening of low alloy steel (Grades II, III, IV) is very slow under natural environment, but it is accelerated under high temperature, e.g. it takes only half an hour under temperature 250°C .

6.4.2 Cold-drawn

When the reinforcement is stretched and passed through a die of hard metal, it is elongated and its diameter is reduced under common action of longitudinal tension and transverse compression, and its volume is decreased slightly. The original steel is normally wire rod of diameter 6 mm or 8 mm, its diameter is reduced by 0.5–2.0 mm after every cold-drawn, which is called cold-drawn wire of low-carbon steel.

Plastic deformation of the reinforcement occurs intensely and the crystalline grain in it is deformed and displaced considerably during the cold-drawing process, so its strength is greatly increased and the ultimate elongation is reduced correspondingly, and the stress–strain curve of it is similar to that of hard steel (Fig. 6-14). The cold-drawn wire is used widely in engineering practice in China to save steel used and to reduce the cost of the structure.

The main mechanical behavior of the cold-drawn wire, including nominal yield strength (f_y), ultimate strength (f_b) and elongation (δ_5 or δ_{10}), and modulus of

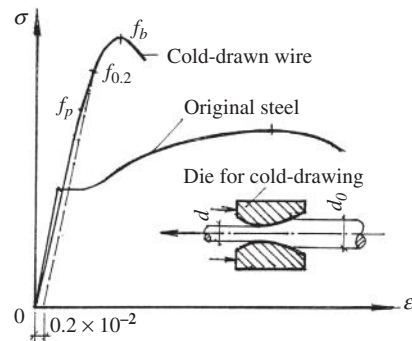


FIG. 6-14 Stress–strain curve of cold-drawn wire of low-carbon steel

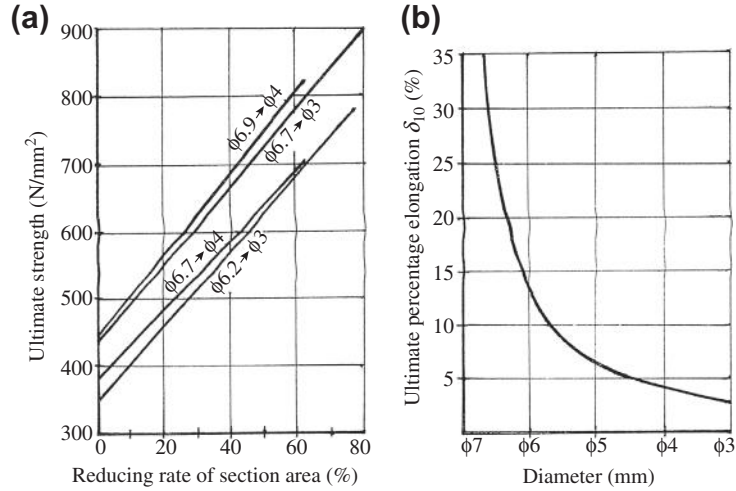


FIG. 6-15 Behavior of cold-drawn wire of low carbon steel [6-11]: (a) ultimate strength, (b) ultimate elongation (δ_{10})

elasticity, depends mainly upon the kinds of original steel and the reducing rate of its section area (Fig. 6-15), but is not apparently influenced by the number of cold-drawing.

According to the experimental data reported in China [6-11], the ultimate strength of cold-drawn wire of low-carbon steel reaches about 1.6–2.0 times that of original steel, and the ratios between the proportional limit and nominal yield strength with ultimate strength are respectively $f_p/f_b = 0.71$ – 0.84 and $f_{0.2}/f_b = 0.9$ – 1.0 . However, the ultimate elongation of its diameter of 3–5 mm is only $\delta_{10} = 2.5$ – 5.0% , i.e. 10–15% of that of the original steel, and the modulus of elasticity is decreased slightly.

The stress–strain relation of the cold-drawn wire of low-carbon steel is suggested in reference [6-12] as below:

$$\left. \begin{aligned} 0 \leq \varepsilon_s \leq \varepsilon_p \quad \sigma_s &= E_s \varepsilon_s \\ \varepsilon_s > \varepsilon_p \quad \sigma_s &= 1.075f_b - \frac{0.6}{\varepsilon_s} \end{aligned} \right\}, \quad (6-12)$$

where the strain corresponding to proportional limit is $\varepsilon_p = 2.5 \times 10^{-3}$.

6.5 Creep and relaxation

It is demonstrated experimentally that mild steel with an apparent yield plateau does not cause any creep or relaxation, when it is loaded constantly or repeatedly and its stress is lower than the elastic limit. However, the high strength and cold-worked

steels will cause plastic deformation under a higher stress level. When these steels are loaded and entered into non-elasticity zone, creep or relaxation occurs even under room temperature.

Creep and relaxation are different responses of plastic deformation of a material under sustained stress and their values can be converted into each other as introduced in Section 3.6.1. Creep of steel is the result when the crystalline grain in it is deformed and displaced with time under high stress. In engineering practice, the creep of steel causes gradually increasing deformation of a structure, especially the suspension structure of large span, and the relaxation of steel causes stress loss of the prestressed tendon (reinforcement) in a prestressed concrete structure and then its cracking resistance is reduced.

Usually, a long specimen of several meters or longer is used for measuring the relaxation of the steel. It is fixed at one end and stretched on the other end until the predetermined stress level (σ_0) and then fixed. Afterwards, the length of the specimen is kept constant but the stress in it is decreased gradually with time, and the stress difference or relaxation $|\Delta\sigma_r|$ is measured. Generally, the relaxation value ($\Delta\sigma_r/\sigma_0$) of the specimen sustained for 1000 hours is taken as the criterion. The experimental results of four kinds of steel are shown in Fig. 6-16.

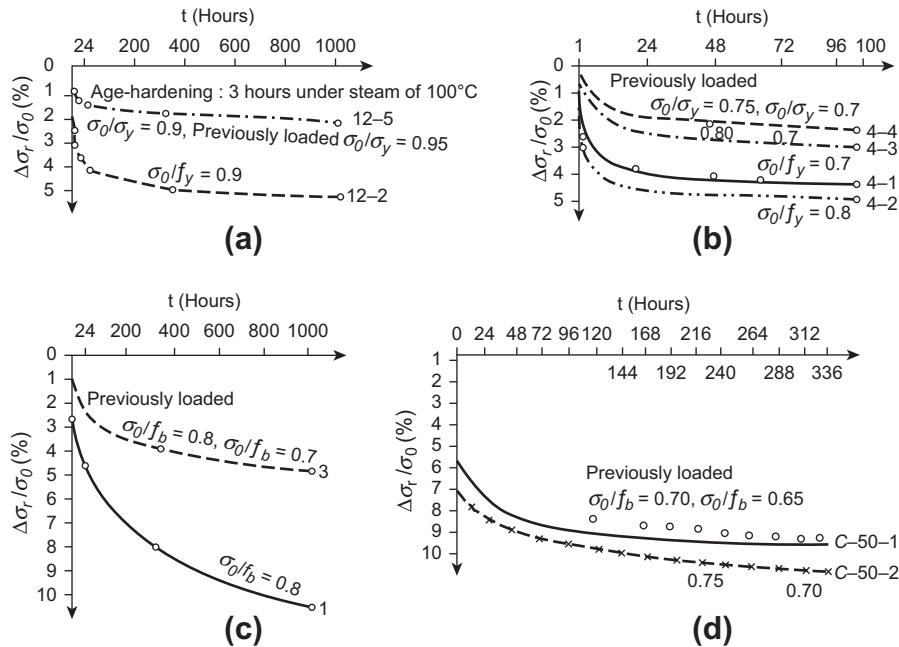


FIG. 6-16 Stress relaxation curves of various steels [6-13]: (a) cold stretched bar (16 Mn, $\Phi 12$), (b) cold-drawn wire of low-carbon steel ($\Phi 4$), (c) high-strength wire of carbon steel ($\Phi 5$), (d) strand wire (7 $\Phi 2.6$)

Table 6-3 Comparison Between Values of Stress Relaxations ($\Delta\sigma_r$) of Various Steels

Kind of Steel	Cold-Stretched Bar (Grades II–IV)	Cold-Drawn Wire of Low Carbon Steel	High-Strength Wire of Carbon Steel		Strand Wire
Control stress σ_0	$(0.85-0.95)f_y$	$0.7f_b$	$0.7f_b$	$0.8f_b$	$(0.65-0.70)f_b^*$
$\Delta\sigma_r/\sigma_0$ (%)	3.4–4.5	5.46	7.85	7.95	6–7*

*Note: The sustaining time of control stress is 1000 hours, but 336 hours for *.*

The main factors having influence on the relaxation of steel are discussed below.

6.5.1 Kind of steel

Mild steel shows no stress relaxation ($\Delta\sigma_r = 0$) when its stress is less than the elastic limit. The values of stress relaxation of other kinds of steel are listed in Table 6-3, and the order of them is successively cold-stretched bar, cold-drawn wire of lower-carbon steel, high-strength wire of carbon steel, and strand wire, according to the relaxation values from small to great.

6.5.2 Sustaining time of control stress

The stress relaxation of steel increases monotonically with sustaining time of the stress, and it appears quickly within the earlier period, e.g. about 50% within one day, and is slowed down later on. The increasing regularities of stress relaxation given by various researches (Table 6-4) are consistent, and some calculation formulas of logarithmic function are suggested in references, e.g. [1-1,2-12].

6.5.3 Stress level

The stress relaxation of steel increases non-linearly with the level of sustaining stress (σ_0/f_y or σ_0/f_b). A series of experimental data measured from the tests of

Table 6-4 Stress Relaxation Increases with Sustaining Time of Stress [1-1,2-12]

Sustaining Time of Stress	Hours	1	20	100	500	1000	3000	10000	100000
	Days					41.7	125	417	4167
Relative value	Guyon	0.29		0.71		1		1.25	1.36
	CEB-FIP MC90	0.25	0.55	0.70	0.90	1			
	REIS*	0.22				1	1.14		
	AREC*	0.24	0.48	0.61	0.90	1			

*REIS Railway Engineering Institute of Shanghai, AREC Academy of Railway Engineering of China.

Table 6-5 Stress Relaxation of High-Strength Wire of Carbon Steel Varies with Level of Sustaining Stress [1-1]

σ_0/f_b	<0.5	0.5	0.6	0.7	0.8
Relative $\Delta\sigma_r/\sigma_0$	0	1	3.38	5.60	8.50

Note: Stress relaxation of the specimen under sustaining stress $\sigma_0/f_b = 0.5$ is taken as 1.

Table 6-6 Stress Relaxation of High-Strength Wire of Carbon Steel Varies with Temperature

T (°C)	20	40	60	100
Relative $\Delta\sigma_r/\sigma_0$	1	≈ 2.0	≈ 3.2	≈ 7.0

Note: Stress relaxation of the specimen under temperature 20°C, stress $\sigma_0/f_b = 0.5$, and sustained time 1000 hours is taken as 1.

high-strength wire of carbon steel are given in Table 6-5, and they are consistent with that calculated by relevant formulas suggested in reference [2-12].

6.5.4 Temperature

It should be noticed that the stress relaxation of steel increases considerably with the environmental temperature as shown in Table 6-6.

In order to reduce the stress relaxation of the steel, and then to enhance cracking resistance and stiffness of the concrete structure, the main measure in engineering practice is using the special prestressing steel (wire) of low relaxation ($\Delta\sigma_r/\sigma_0 < 4\%$), and over-prestressing and re-prestressing technique during construction process (see Fig. 6-16) are also effective.

This page intentionally left blank

Bond Between Reinforcement and Concrete

CHAPTER OUTLINE

7.1 Function and composition of bond	182
7.1.1 Function and classification.....	182
7.1.1.1 Anchorage bond of reinforcement end	183
7.1.1.2 Bond between cracks.....	183
7.1.2 Composition.....	184
7.2 Test method and bond mechanism.....	186
7.2.1 Test method.....	186
7.2.1.1 Tension test	186
7.2.1.2 Beam test	187
7.2.2 Plain reinforcement	189
7.2.3 Deformed reinforcement	190
7.3 Influence factors	193
7.3.1 Strength of concrete (f_{cu} or f_t)	194
7.3.2 Thickness of concrete cover (c).....	195
7.3.3 Bond length of reinforcement (l)	195
7.3.4 Diameter and shape of reinforcement.....	196
7.3.5 Transverse stirrup (ρ_{sv}).....	197
7.3.6 Transverse compressive stress (q)	198
7.3.7 Other factors.....	198
7.4 Constitutive model for bond stress—slip	199
7.4.1 Calculation of characteristic values.....	200
7.4.1.1 Splitting stress (τ_{cr}).....	200
7.4.1.2 Ultimate bond strength (τ_u)	201
7.4.2 Equation for τ — s curve.....	201
7.4.2.1 Segmental model	201
7.4.2.2 Model of continuous curve	202

7.1 Function and composition of bond

7.1.1 Function and classification

The basic condition for reinforcement and concrete composing a composite structural material is the reliable bond and anchorage between them. If the reinforcement in a beam does not adhere with adjacent concrete along its length and without any anchorage on both its ends (Fig. 7-1(a)), it is free of force ($\sigma_s = 0$) and the beam will break soon after it is loaded slightly, as the beam acts like a plain concrete one. If the reinforcement in a beam does not adhere with adjacent concrete but the mechanical anchorages are set up at both ends (Fig. 7-1(b)), the stress in it is a constant ($\sigma_s = \text{const.}$) along its length when the beam is loaded, and the load-bearing capacity of the beam is enhanced greatly. However, the beam acts like an arch of two hinges rather than 'a beam', according to the stress distribution in the beam. Only when the reinforcement in a beam is adhered reliably with adjacent concrete along its length including both ends, does the stress of it vary with the bending moment on the section after the beam is loaded (Fig. 7-1(c)). Then, this fits the mechanical characteristic of a beam and a reinforced concrete beam is presented.

Analyzing the equilibrium condition of a segment of the reinforcement in a beam, the difference of normal forces at both ends of the segment is in equilibrium with the longitudinal shear stress on its periphery (Fig. 7-1(d)). The shear stress is the bond stress provided by the adjacent concrete:

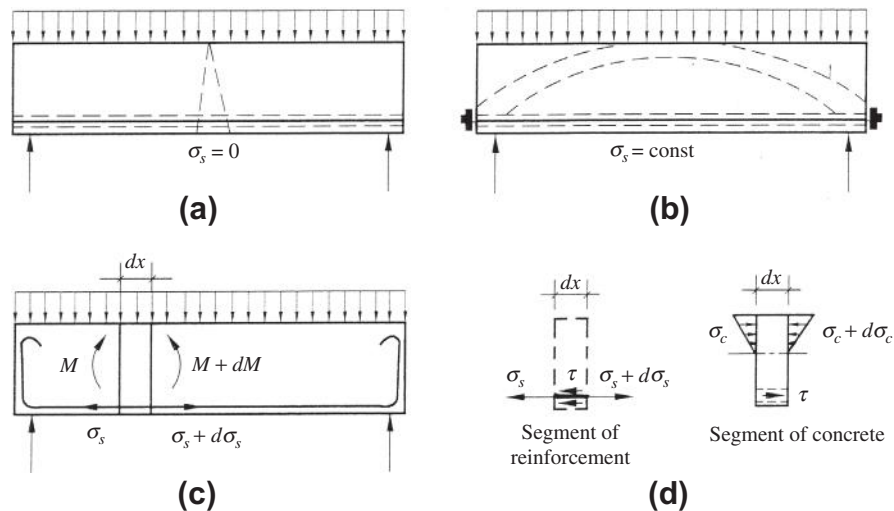


FIG. 7-1 Adhesion and anchorage of reinforcement in beam: (a) without adhesion and anchorage, (b) anchorages set up at both ends, but without adhesion along reinforcement, (c) reinforcement adhered reliably with adjacent concrete, (d) balance conditions

$$\tau = \frac{A_s d\sigma_s}{\pi d dx} = \frac{d}{4} \frac{d\sigma_s}{dx}, \quad (7-1)$$

where d and A_s are, respectively, the diameter and sectional area of the reinforcement. In the meantime, the longitudinal shear stress, i.e. the bond stress of opposite direction is acted to adjacent concrete by the reinforcement, and it has to be in equilibrium with the longitudinal forces of corresponding concrete segment.

According to the mechanical condition of a concrete structural member, the bond stress states are classified as two categories.

7.1.1.1 Anchorage bond of reinforcement end

For example: end of a reinforcement near the support of a simply supported beam, splice or cut of a reinforcement in beam span, extension of tensile reinforcement of a cantilever or beam-column joint (Fig. 7-2(a)). The normal stress at the end of the reinforcement is zero under these conditions, and it reaches its designed strength (yield strength f_y for mild steel) at the section not far away. Also, the distance between the section and the end is called development length. Therefore, the stress difference in the reinforcement segment is great ($\Delta\sigma_s = f_y$), and the bond stress on its periphery is high and varies greatly. If the reinforcement slides because of insufficient anchorage bond, its strength can not be fully utilized ($\sigma_s < f_y$) and the cracking and load-carrying capacities of the member should be reduced, or even the member may fail earlier. This is called bond failure, which is brittle and serious.

7.1.1.2 Bond between cracks

When the concrete in a tension member or in the tension zone of a flexural member under loading is cracked and out of work, the stress of the reinforcement in the

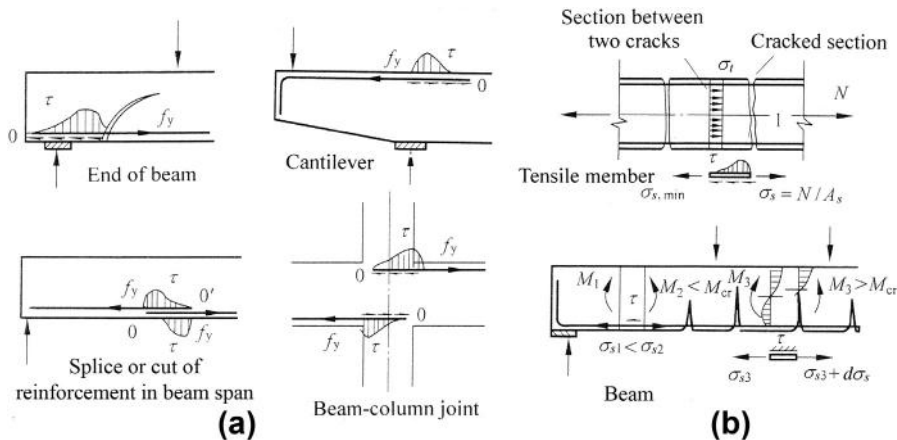


FIG. 7-2 Two categories of bond stress state: (a) anchorage bond of reinforcement end, (b) bond between cracks

cracked section increases. However, the concrete on the uncracked section still works and carries a certain amount of tensile force, the stress of the reinforcement in these sections is reduced. Therefore, the stress of the reinforcement varies along its longitudinal direction, and the bond stress on its periphery distributes corresponding (Fig. 7-2(b)). Then, the average stress (strain) of the reinforcement is high, although the stress difference is less within the segment between two cracks. It means that the average strain and total deformation of a reinforcement buried in concrete is respectively less than that of the reinforcement alone, because bond stress exists on its periphery. This is favorable to reduce the crack width of concrete and to increase the stiffness of a structural member (Chapters 12 and 13), and is called the effect of tension stiffening.

Therefore, when the normal stress of a reinforcement in a concrete structural member varies along its length, which is caused due to variation of internal force, cracking of concrete, or detailing requirement, the concrete surrounding it has to provide necessary bond stress (τ). Otherwise, if the bond stress is zero ($\tau = 0$), relative slip will occur between the reinforcement and adjacent concrete, larger cracking and deformation will appear in the member or joint, and the internal force (or stress) will redistribute, the structure may even fail earlier. In addition, the bond condition between reinforcement and adjacent concrete will be deteriorated under repeated action of the load, and it also has influence on the fatigue and aseismic behaviors of the structure (see Part 4). Therefore, the bond behavior between reinforcement and concrete has to be paid attention to in engineering practice.

On the other hand, bond behavior between reinforcement and adjacent concrete is a local stress state, the stress and strain there distribute complicatedly, local crack of concrete and relative slip between them do exist, and many factors have influences on it, so the hypothesis of plane section is not followed again and this is a difficulty in research work. Many experimental and theoretical investigations have been conducted on bond behavior but they are still not satisfactory up to now, so their application in engineering practice and the bond-slip constitutive relation used in finite-element analysis are mainly empirical.

7.1.2 Composition

The bond or slip resistance between reinforcement and adjacent concrete is composed of three parts [1-1,7-2]:

1. Chemical adhesion or adsorption is caused on the surface of reinforcement due to the action of cement gelation. The ultimate shear strength of it (τ_{ad}) depends upon the property of concrete and the rough level of reinforcement surface. When the reinforcement is forced and deforms greatly and after local slip occurred between it and adjacent concrete, the chemical adhesion loses.
2. Friction between reinforcement and surrounding concrete. This depends upon the friction coefficient between them and the radial compressive stress acted on the periphery of reinforcement, which is caused by shrinkage of the concrete and the action of load or reaction. Friction acts only after the adhesion lost.

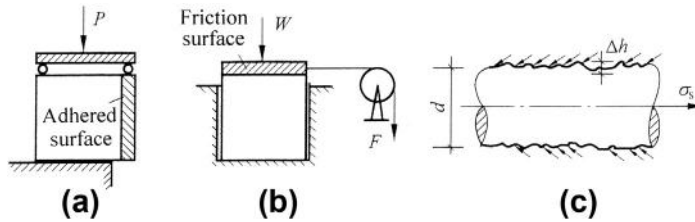


FIG. 7-3 Tests for parameters of bond between steel and concrete: (a) test of adhesion, (b) test of friction coefficient, (c) roughness and interaction on reinforcement surface

3. Mechanical interaction on rough surface of reinforcement or between ribs of the deformed reinforcement and concrete. This is the longitudinal component of inclined compression on rough surface of reinforcement (Fig. 7-3(c)), which is acted on by the surrounding concrete and the ultimate value of it is controlled by the shear strength of the concrete.

Actually, all of the three bond components are closely related to the levels of rough and corrosion of the reinforcement surface [7-3], and they are difficult to measure individually during testing and to be distinguished strictly from the experimental data. In addition, these components vary correspondingly when the reinforcement is at different loading stages and its slip develops, or under loading and unloading.

The steel plate is used to simulate the bond test of reinforcement (Fig. 7-3) in reference [7-2]. The roughness (Δh mm, Table 7-1) of the surface of the steel plate is caused due to different levels of corrosion and is measured before casting of concrete. The adhesion ($\tau_{ad} = P/A$) between the plate and concrete specimen is first measured (Fig. 7-3(a)), then the friction test (Fig. 7-3(b)) is conducted after failure of plate adhesion, and the measured adhesion and friction coefficient ($f = F/W$) are listed in Table 7-1. The experimental data of plain reinforcement are also listed in the table (last row) for comparison.

Table 7-1 Parameters of Roughness and Adhesion on Steel Surface [7-2]				
Levels of Corrosion	None	Slight	Serious	Extreme
Roughness Δh (mm)	0.025–0.040	0.05–0.17	0.17–0.34	0.23–0.66
τ_{ad} / f_{cu}	~0.02	~0.03	~0.035	~0.04
Friction coefficient f	0.20–0.25	0.26–0.30	0.40–0.50	0.45–0.60
Average bond strength of plain reinforcement $\frac{\tau_u}{f_{cu}}$	0.04	Increases gradually		0.14

7.2 Test method and bond mechanism

7.2.1 Test method

The stress state near the end of the reinforcement in a concrete structure is rather complicated and is difficult to be simulated accurately. There are two methods for the pull-out test of reinforcement, and different shapes and loading conditions of the specimens are used separately.

7.2.1.1 Tension test

This method was used earliest and the manufacture and testing of the specimen are simple. The specimen is generally of a prism and a reinforcement is buried in its center. When the specimen is tested, one end of it is supported on a steel plate with a hole in the center and the reinforcement end is clamped down by the test machine, then the tensile force is applied (Fig. 7-4(a)) until the reinforcement is pulled out or yielded.

The concrete near the loading end of the specimen is compressed locally and the stress state there is considerably different from that occurring near the reinforcement end in a structure, then the truthfulness of the testing result is doubtful. Alternately, the reinforcement near the loading end is locally separated from the surrounding concrete in the specimen (Fig. 7-4(b) and (d)). However, when the deformed reinforcement is used in the specimen and tested, the specimen frequently fails due to longitudinal splitting (see Fig. 7-9). Therefore, a spiral stirrup is set up in the specimen to ensure the deformed reinforcement being pulled out during testing (Fig. 7-4(c)). Up to now, the standard specimen and method of this kind of test, including transverse size (a/d) or thickness of concrete cover (c/d), buried and adhered length (l/d) of the reinforcement, and stirrup used, are not unified for different countries and organizations.

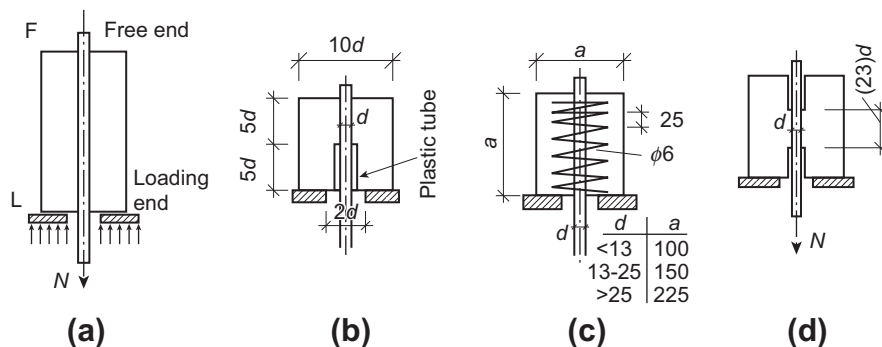


FIG. 7-4 Tension specimen for bond test: (a) used earlier, (b) RILEM-FIP-CEB, (c) CP 110 (British), (d) buried shortly

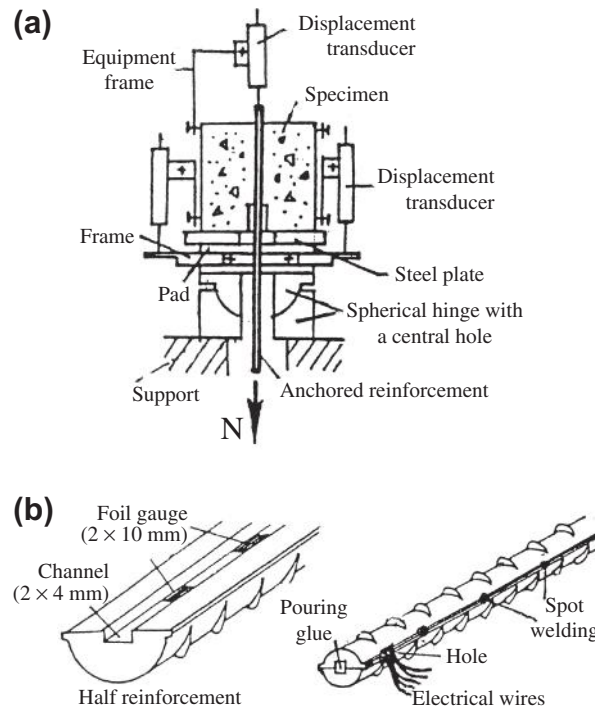


FIG. 7-6 Equipment and measurement of bond test [7-2]: (a) measuring equipment, (b) strain gauges sticking in interior of reinforcement

In order to measure the distribution of bond stress (τ) along the bond length but not to disturb the bond condition, the strain gauges have to be stuck in the interior of the reinforcement [7-7,7-2] (Fig. 7-6(b)). The reinforcement is machined into halves and a channel is milled on it for sticking the strain gauges, and the electrical wires are stretched out from a hole. After the channel is waterproofed, two halves of reinforcement are connected and spot-welded together, then the pull-out specimen is made after casting concrete. The bond stress can be calculated by Eq. (7-1) and the stress difference of the adjacent gauges is used, which are measured during testing, and the distribution of bond stress is then obtained.

The development of internal crack in the specimen is also investigated during the pull-out process [7-8,7-9]. Red ink is poured in advance into the small hole in the specimen, it permeates into the cracks after the specimen is cracked under loading, then the number and shape of the cracks can be clearly observed after the specimen is broken.

The ultimate bond strengths of plain and deformed reinforcements are significantly different, and the bond mechanism, slipping, and failure pattern of the specimens with both reinforcements are also different.

7.2.2 Plain reinforcement

The tensile force (N) or average bond stress ($\bar{\tau}$) and the slips at both ends of the plain reinforcement (S_l and S_f) are measured during the pull-out test and the experimental curves are shown in Fig. 7-7(a). The distributions, along the bond length, of normal stress (σ_s), the bond stress (τ) calculated, and the slips of the reinforcement vary as shown in Fig. 7-7(b), when the load (tension) increases.

After the specimen is loaded, the bond at the loading end of the reinforcement is failed soon and the relative slip (S_l) between the reinforcement and adjacent concrete is measured. In the meantime, only a part of the reinforcement near the loading end carries tension ($\sigma_s > 0$) and the distribution of bond stress is also limited within this part. The relative slip occurs only within the zone from the peak point of bond stress to the loading end of the reinforcement, the other part of the reinforcement is still adhered and free of slip. The tension zone of the reinforcement is gradually increased and the peak point of bond stress distribution moves towards the free end of the reinforcement, as the load (or $\bar{\tau}$) increases. Then, the slip zone of the reinforcement is spread and the slip at loading end (S_l) accelerates.

When the load is increased and $\bar{\tau}/\tau_u = 0.4 \sim 0.6$ is reached, the tension and slip zones of the reinforcement spread gradually, and the slip at loading end (S_l) accelerates obviously and $\tau-S_l$ becomes a curve, but the free end of the reinforcement is still not slipped. The distributed length of bond stress (τ) is spread and its peak point moves rapidly, and the shape of the curve changes from inclining to the right towards inclining to the left. When $\bar{\tau}/\tau_u \approx 0.8$, the free end of the reinforcement starts to

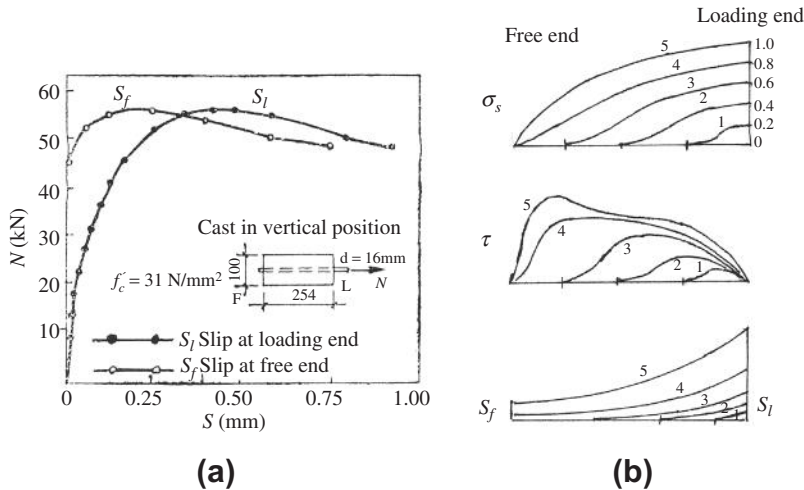


FIG. 7-7 Results of pull-out test of plain reinforcement: (a) $\tau-S$ curves, (b) distributions of stress and slip

slip, the bond near the loading end is damaged seriously and the bond stress there reduces, so uniform normal stress of the reinforcement is approached.

When the slip at the free end of the reinforcement reaches $S_f = 0.1\text{--}0.2$ mm, the load of the specimen reaches the maximum N_u and ultimate bond strength (τ_u , Eq. 7-2) is obtained. Afterwards, the slips of the reinforcement (S_l and S_f) increase quickly, the tension is carried by the friction and residual interaction on periphery of the reinforcement, then the adjacent concrete is crushed and its resistance reduces, and a descending branch of the $\bar{\tau} - S$ curve is formed. Finally, the reinforcement is pulled out gradually from the specimen, and some concrete dregs are adsorbed on its periphery.

The pull-out process of the reinforcement described above occurs only for the specimen of shorter bond length. If the bond length of the reinforcement is long enough, it will not be pulled out even after the loading end of it is yielded, when the specimen is loaded until $N_u = A_s f_y$. The minimum bond length of the reinforcement needed for this is called the anchorage length (l_a) [2-1], which is necessary to ensure the tensile strength of reinforcement is utilized fully in a structure. According to the equilibrium condition, the anchorage length can be calculated by

$$l_a = \frac{f_y}{4\tau_u} d^{\oplus}, \quad (7-3)$$

where τ_u is the average ultimate bond strength of reinforcement.

7.2.3 Deformed reinforcement

The typical bond stress-slip ($\bar{\tau} - S_l, -S_f$) curves measured from the pull-out test of deformed reinforcement are shown in Fig. 7-8(a). The distributions of normal stress (σ_s), bond stress (τ), and slip (S) of the reinforcement vary along its bond length as the load (or τ) increases, and they are shown in Fig. 7-8(b). The development process of the internal cracks in the specimen is shown schematically in Fig. 7-9 [7-10–7-14,7-2].

The deformed reinforcement differs mainly from the plain one in the transverse or inclined ribs on its periphery. When the deformed reinforcement is tensioned, its ribs compress the surrounding concrete (Fig. 7-9(a)) and the mechanical interaction between both increases greatly, so the bond mechanism is changed and this is favorable for anchorage behavior of reinforcement buried in concrete.

[⊕]This formula can also be used for deformed reinforcement. In Chinese Code [2-1], the basic formula for anchorage length required for tensile reinforcement is:

$$l_a = \alpha \frac{f_y}{f_t} d.$$

This is modified from Eq. (7-3), the tensile strength of concrete (f_t) is used to replace the average bond strength (τ_u) and a shape coefficient ($\alpha = 0.13\text{--}0.19$) of reinforcement is introduced to consider the variations of kind and surface shape of the reinforcement.

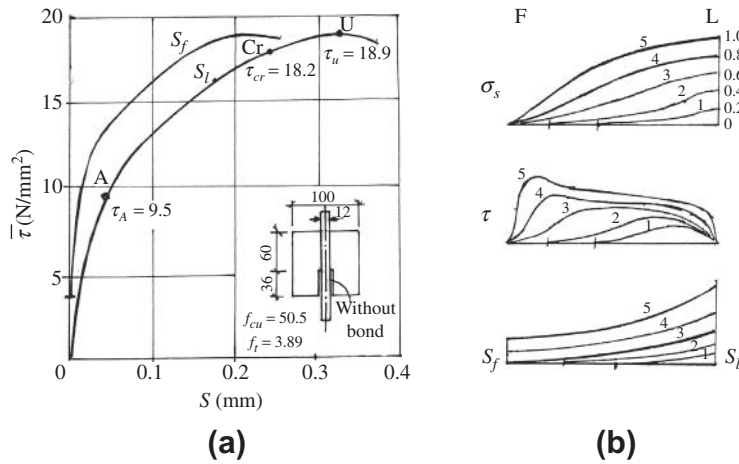


FIG. 7-8 Results of pull-out test of deformed reinforcement: (a) τ — S curves, (b) distributions of stress and slip

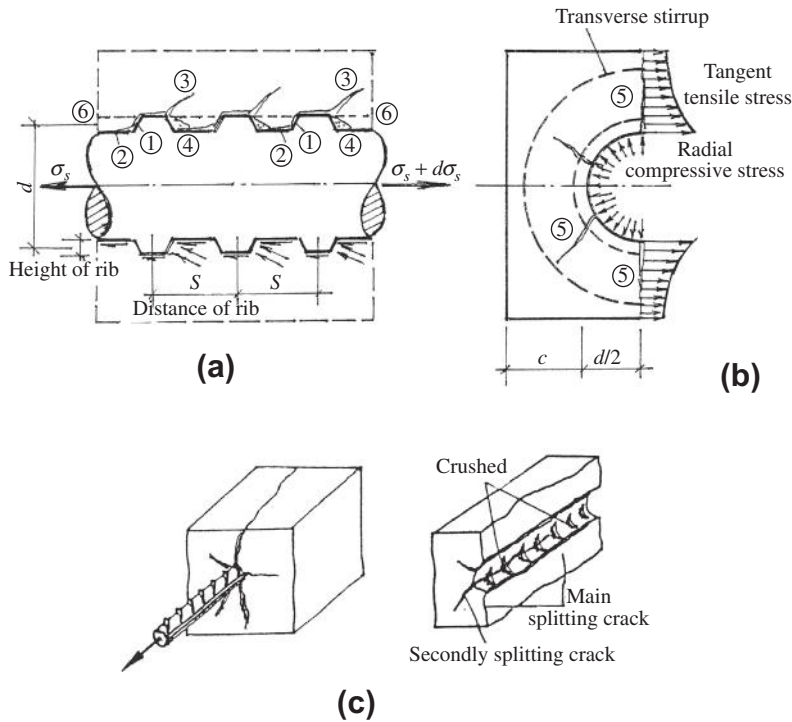


FIG. 7-9 Development process of internal cracks and bond failure of specimen with deformed reinforcement [7-2]: (a) longitudinal direction, (b) transverse section, (c) failure pattern

When a pull-out specimen without transverse stirrup is loaded, the bond near the loading end of the deformed reinforcement fails locally because of stress concentration and the slip (S_l) appears soon. As the load increases to $\bar{\tau}/\tau_u \approx 0.3$, the bond at the free end of the reinforcement also fails, and the slip (S_f) appears while the slip at the loading end accelerates. Comparing with that of plain reinforcement, the stress ($\bar{\tau}$), at which the free end of deformed reinforcement starts to slip, approximates but the ratio $\bar{\tau}/\tau_u$ reduces considerably, and the tension and slip zones of deformed reinforcement spread earlier over the whole buried length of it.

When the average bond stress reaches $\bar{\tau}/\tau_u = 0.4-0.5$, i.e. Point A on the $\bar{\tau} - S$ curve, the bond on the back of the rib near loading end of the reinforcement is failed, a tensile crack (1) (in Fig. 7-9(a)) appears there. Soon after, the crack extends towards the opposite direction of the load and a longitudinal slip crack (2) is formed on the surface of the reinforcement. As the load is increased slightly, the rib compresses the concrete near the rib tip, the crack (1) extends forwards and turns into an inclined crack (3), i.e. a cone crack, in the interior of the specimen. When the load is increased further, the cracks (1), (2), and (3) widen continuously and occur successively near each rib from the loading end until the free end of the reinforcement, the slips (S_l and S_f) develops rapidly and the slope of $\bar{\tau} - S$ curve reduces gradually. Comparing with that of plain reinforcement, the variation rate of normal stress σ_s of deformed reinforcement along its bond length is smaller, so the bond stress varies less.

After these cracks are formed, the tensile load is mainly transferred by the friction on the periphery and compressions on ribs of the reinforcement. As the compression on the front of the rib increases, a crushed zone (4) is formed there. The reinforcement ribs compress the surrounding concrete, and its transverse, i.e. radial, component causes tangent tensile stress in adjacent concrete (Fig. 7-9(b)). A radial-longitudinal crack (5) is formed when the tensile stress exceeds the ultimate strength of the concrete. This crack develops radially outside from the periphery of the reinforcement, and from the loading end until the free end of the reinforcement. When the load approaches the ultimate value (Point cr , $\tau_{cr}/\tau_u \approx 0.9$), the crack near the loading end extends to the surface of the specimen, which is visible to the naked eye. Then the crack extends longitudinally towards the free end, and the splitting sound is sent out and the slip of the reinforcement increases rapidly. The load is increased slightly and soon reaches the peak point (ultimate bond strength τ_u) and turns immediately into the descending branch, and then the specimen is split into two or three pieces (Fig. 7-9(c)). The mark of the reinforcement rib remains on the split surface of concrete, and the crushed dregs of concrete are absorbed on the front of the ribs of the reinforcement.

If the specimen is set up with transverse spiral stirrups or with thicker concrete cover ($c/d > 5$), the bond stress-slip curve measured is shown in Fig. 7-10. When the load is small ($\bar{\tau} < \tau_A$), the $\bar{\tau} - S$ curve is similar to that of the previous specimen, because the function of the spiral stirrup is limited. After the crack appears in the interior of the concrete, the spiral stirrups confine the development of the crack and the resistance is then enhanced. When the load is less slightly than the ultimate

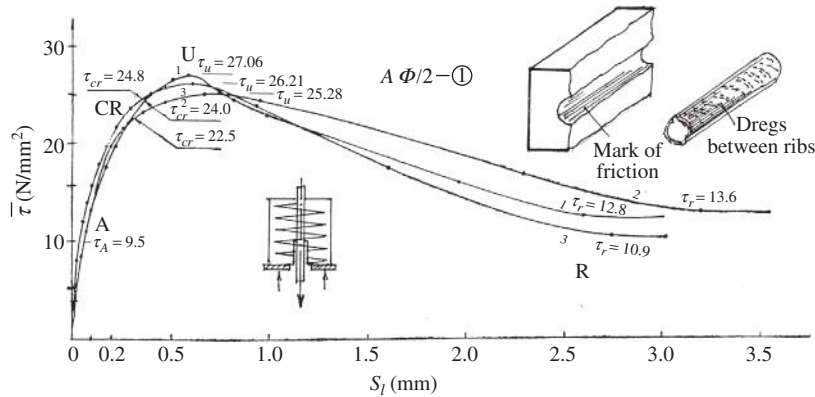


FIG. 7-10 $\bar{\tau}-S$ curve of the specimen with transverse spiral stirrup [1-1]

value, the reinforcement ribs compress strongly on the surrounding concrete and its radial component also causes a radial-longitudinal crack (5). However, the cracking stress (τ_{cr}) and corresponding slip (S_{cr}) increase greatly.

After the radial-longitudinal crack (5) appears, the stress in the transverse stirrup increases sharply and the expansion of the crack is then confined, so the specimen will not be split and the bond resistance is increased. When the reinforcement slips significantly and the crushed zone on the front of its ribs is enlarged gradually and develops successively along its bond length, the compression on the front of the rib is reduced and the descending branch of the $\bar{\tau}-S$ curve is formed. Finally, the concrete between ribs of the reinforcement is sheared off, and the reinforcement with concrete dregs filled in between the ribs is pulled out gradually (Point R). In the meantime, the friction still exists on the cylinder surface of the outside envelope of reinforcement ribs, and the residual resistance is about $\tau_r/\tau_u = 0.3$. The ultimate bond strength of this kind of specimen may reach $\tau_u = 0.4f_{cu}$ and is far greater than that of plain reinforcement (Table 7-1).

Four characteristic points can be defined on the complete bond stress-slip ($\bar{\tau}-S$, or $\tau-S$ represented latter) curve, which is obtained from the pull-out test of reinforcement, and they are individually: internally cracking (τ_A , S_A), splitting (τ_{cr} , S_{cr}), ultimate strength (τ_u , S_u), and residual strength (τ_r , S_r). These points divide the mechanical stages and can be used to establish the corresponding $\tau-S$ constitutive model.

7.3 Influence factors

The bond behavior between reinforcement and adjacent concrete and its characteristic values vary as many factors have influences on them.

7.3.1 Strength of concrete (f_{cu} or f_t)

When the strength of the concrete is enhanced, the chemical adhesion (τ_{ad}) and mechanical interaction between reinforcement and concrete increase as well, while the friction resistance is less influenced. In the meantime, the tensile (splitting) strength (f_t) of concrete also increases, so the internal cracking and splitting of the pull-out specimen are delayed and the bond strength and stiffness of it are increased as well (Fig. 7-11).

The experimental results show that the ultimate bond strength (τ_u) of reinforcement is approximately proportional to the tensile strength f_t (or compressive strength $\sqrt{f_{cu}}$) of concrete (Fig. 7-11(b)). Other characteristic values of bond stress (τ_A , τ_{cr} , and τ_s) are also proportional to the tensile strength of concrete (Fig. 7-12).

Some experiments [1-1] also show that the cement contents and water—cement ratio of concrete have a certain amount of influence on the bond behavior.

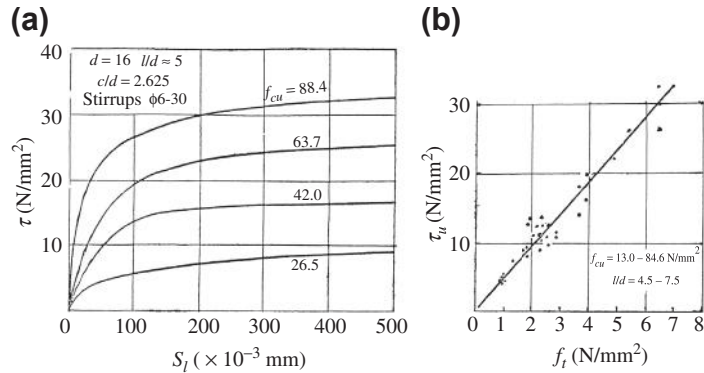


FIG. 7-11 Influence of concrete strength on bond behavior [1-1]: (a) τ - S curve, (b) τ_u - f_t

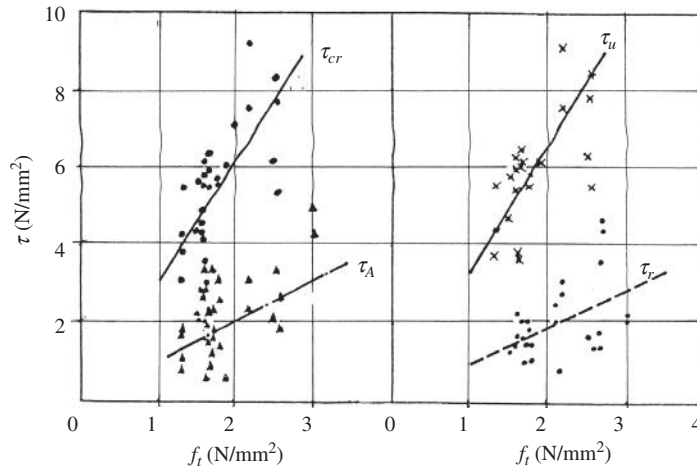


FIG. 7-12 Relation between characteristic values of bond stress and strength of concrete [1-1]

7.3.2 Thickness of concrete cover (c)

The thickness of concrete cover of the reinforcement is the minimum distance between the outside of it and surface of the specimen (c , mm). As the splitting resistance of surrounding concrete increases with the thickness, the splitting stress (τ_{cr}) and ultimate bond strength (τ_u) of the specimen are enhanced obviously (Fig. 7-13). However, if the thickness of concrete cover is even greater ($c > (5 \sim 6d)$), the specimen will not fail due to splitting but is pulled out along the outside of reinforcement ribs because of shearing off of concrete, so the bond strength will not increase further.

When there is more than one reinforcement on the section of a structural member, the pattern of bond failure is also related to the net space (s) between the reinforcements [7-15,7-16]. The member will fail in splitting of concrete cover when $s > 2c$, otherwise ($s < 2c$) it will fail in splitting along the net space (Fig. 7-14).

7.3.3 Bond length of reinforcement (l)

The longer the reinforcement is buried in concrete, the more non-uniform the distribution of the bond stress, and the smaller the ratio between the average and the actual maximum bond strengths (τ/τ_{max}). Therefore, the measured bond strength reduces as the bond length (l/d) increases (Fig. 7-15). When the bond length of reinforcement is $l/d > 5$, the average bond strength reduces slightly. If the bond length of reinforcement is even larger, it will not be pulled out but its loading end is yielded.

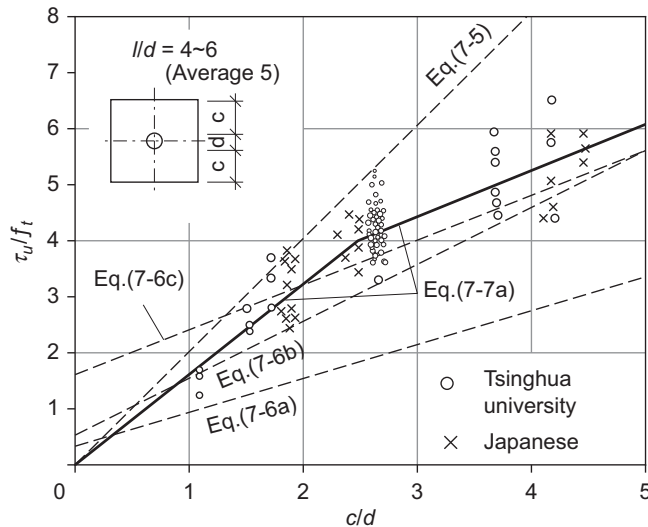


FIG. 7-13 Relation between bond strength and thickness of concrete cover

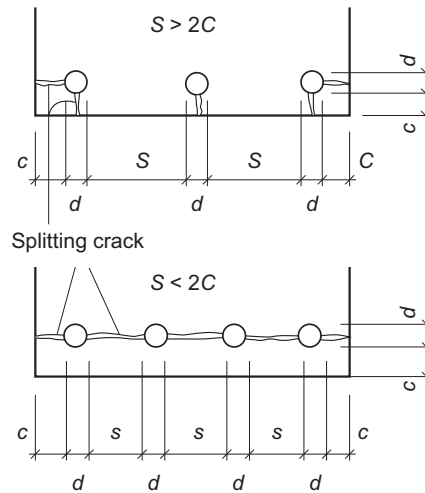


FIG. 7-14 Influence of net space of reinforcements on splitting cracks

Therefore, the experimental results of the specimen of bond length $l/d = 5$ are usually taken as a standard for the bond strength.

7.3.4 Diameter and shape of reinforcement

The adhered area of reinforcement is proportional to the periphery length of it and the tension is proportional to area of its section, so the ratio between the periphery

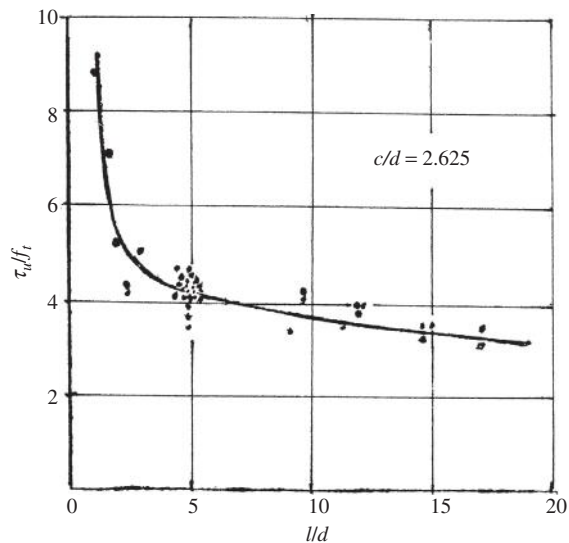


FIG. 7-15 Influence of bond length on bond strength [1-1]

and area ($\pi d / \frac{1}{4} \pi d^2 = 4/d$) represents the relative bond area of the reinforcement. The larger the diameter of reinforcement, the smaller the relative bond area of it, and this is unfavorable to ultimate bond strength. The experimental results given are that the bond strength varies slightly when $d \leq 25$ mm; bond strength possibly reduces by 13% for the reinforcement of diameter $d > 32$ mm; and the characteristic values of slip (S_{cr} , S_u , and S_r) increase apparently with the diameter of reinforcement ($d = 12\text{--}32\text{mm}$) [7-2].

The shape and size of the rib on the surface of deformed reinforcement are various (Fig. 6-1). The bond stress–slip curves for the reinforcements of spiral and crescent ribs are measured and compared in Fig. 7-16. They are seen that the ultimate bond strength of the reinforcement of crescent rib is smaller by 10–15% than that of spiral rib, and the slip of it occurs earlier and greatly but the descending branch of τ – s curve is flatter, so the post strength decreases slowly and the ductility is better, because the concrete between the crescent ribs is thicker and has higher shear resistance. In addition, the height of the crescent rib varies along the periphery and the radial compression is non-uniform, so the splitting crack is directional, i.e. linking line between two longitudinal ribs, during bond failure.

The geometric parameters, e.g. height, width, distance, and inclined slope, of reinforcement rib also have certain influence on the interaction of concrete. The experimental results [7-17] show that the shape of reinforcement rib has less influence on the ultimate bond strength but slightly greater influence on the slip.

7.3.5 Transverse stirrup (ρ_{sv})

When the transverse stirrup is set up in the pull-out specimen, the development of the radial-longitudinal crack is delayed and confined, so the splitting failure is prevented and the ultimate bond strength [7-18] and the characteristic slips (S_{cr} , S_u) are increased and the descending branch of τ – s curve is flatter, and the bond ductility is better.

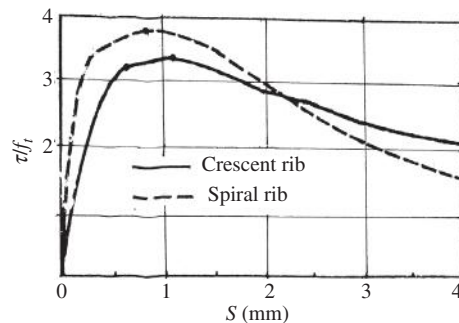


FIG. 7-16 τ – S curve of reinforcements of different ribs [7-2]

The content of the transverse stirrup is represented by the area rate of the stirrup on the splitting surface:

$$\rho_{sv} = \frac{A_{sv}}{cs_{sv}} = \frac{\pi d_{sv}^2}{4cs_{sv}} \quad (7-4)$$

where c is the thickness of concrete cover, d_{sv} , s_{sv} are the diameter and distance of the stirrup, respectively.

The stress increment from the splitting stress until the ultimate bond strength ($\tau_u - \tau_{cr}$) of the specimens is given in Fig. 7-17 and is increased with the transverse stirrup rate ρ_{sv} .

7.3.6 Transverse compressive stress (q)

The anchorage end of the reinforcement in a structural member is always acted by the transverse compression, e.g. reaction at the support or axial compression of the column in a beam-column joint. The friction acted on the boundary between the reinforcement and adjacent concrete is increased due to the action of transverse compression and is favorable for bond and anchorage.

The bond stress-slip curves of the reinforcement under the action of different transverse compressive stresses ($q = \text{const.}$) are shown in Fig. 7-18. It is seen that the ultimate bond strength and the corresponding slip increases to a great extent with the compressive stress. However, if the transverse compressive stress is excessively increased, e.g. $q > 0.5f_c$ [1-1], the splitting crack will occur in advance along the action plane of the compressive stress, and the ultimate bond strength is then reduced.

7.3.7 Other factors

All the factors influencing the quality and strength of concrete also have influences to a certain amount on the bond behavior between reinforcement and concrete, for

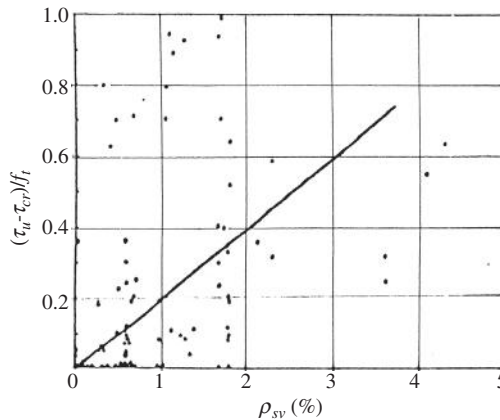


FIG. 7-17 Influence of transverse stirrup on bond strength [7-2]

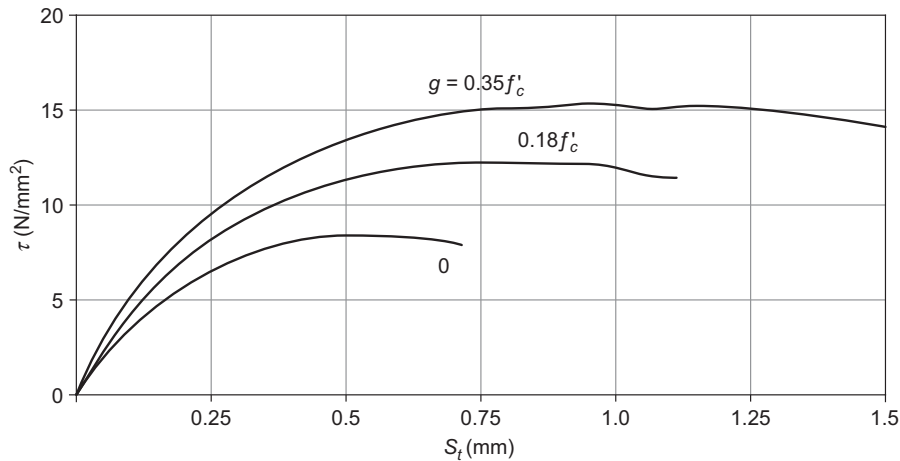


FIG. 7-18 Influence of transverse compressive stress on $\tau-S$ curve [7-19]

example: slump of fresh concrete, compacting quality, curing condition, various disturbances, the direction of the reinforcement being perpendicular to (e.g. beam) or paralleling (e.g. column) the direction of casting concrete, the reinforcement located on the top or bottom of the structural section.

In addition, the bond behavior introduced above is based on the pull-out test of tensile reinforcement, but the bond behavior of compressive reinforcement is generally better and is needed to be investigated by the push-in test. The reinforcement is transversely expanded during compression and is confined by the surrounding concrete, so the slip resistance of friction is increased and hence the bond strength is higher.

On the other hand, if the reinforcement is also under the action of the transverse load (e.g. dowel action in Chapter 14) besides the longitudinal tension, it may be torn out from the concrete, and the bond strength is seriously reduced so that even the premature failure of the structural member may be caused. And when the load is repeated or reversed many times, the bond strength and $\tau-s$ curve of the reinforcement will be degenerated, which will be introduced in Chapters 16 and 17.

7.4 Constitutive model for bond stress—slip

Sometimes, the bond stress—slip relation has to be used during design or analysis of reinforced concrete structures, for example: the bond element in non-linear finite element analysis, calculating for anchorage or splice length of the reinforcement, determining the tension stiffening after concrete cracked, calculating for slip deformation of the reinforcement in an aseismic member or joint, etc.

7.4.1 Calculation of characteristic values

7.4.1.1 Splitting stress (τ_{cr})

When the radial-longitudinal crack is formed in a structural member after the deformed reinforcement is tensed, this is an important index for critical bond condition, because the reinforcement is easily deteriorated then and the durability of the structure is harmed.

There are two ways to determine the value of splitting stress for tensile reinforcement. One of them is half-theoretical and half-empirical, the surrounding concrete of the reinforcement is simplified into a thick tube, and the calculation formula is approximately established based on elasticity or plasticity theory and the load acted on the tube is the compression between the transverse ribs of the reinforcement and adjacent concrete. For another way, the empirical formula is directly established using experimental data and regression analysis.

The assumption of the simplest theoretical method is that the tensile stress on the splitting surface is uniformly distributed and reaches the ultimate strength f_t when the concrete cover is split. If the angle between the compression of transverse rib and axis of the reinforcement is $\theta = 45^\circ$ (Fig. 7-19(a)),

$$\tau_{cr} \approx p_r = \frac{2c}{d} f_t \quad (7-5)$$

is easily derived, but the calculated result is apparently higher than the experimental data (Fig. 7-13).

After the calculation diagram and stress distribution are modified (Fig. 7-19(b) and (c)), the formulas can be derived correspondingly:

$$\text{reference [7-14]} \quad \frac{\tau_{cr}}{f_t} = 0.3 + 0.6 \frac{c}{d} \quad (7-6a)$$

$$\text{reference [1-1]} \quad \frac{\tau_{cr}}{f_t} = 0.5 + \frac{c}{d} \quad (7-6b)$$

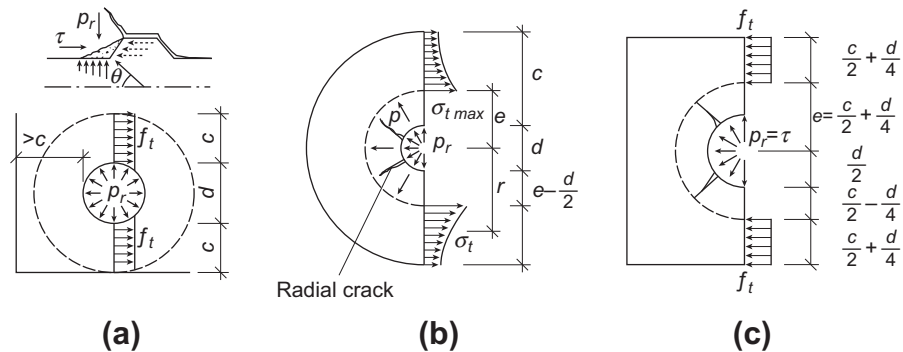


FIG. 7-19 Stress state of specimen during splitting: (a) $\theta = 45^\circ$, (b) Reference [7-14], (c) Reference [1-1]

Reference [7-2] suggests a formula as below according to the regression analysis of the experimental data:

$$\frac{\tau_{cr}}{f_t} = 1.6 + 0.7 \frac{c}{d} \quad (7-6c)$$

These formulas are the same in mathematical function but different in coefficient value. The calculated results of these formulas are compared with the experimental data in Fig. 7-13. It should be aware that τ_{cr} is slightly smaller than τ_u .

7.4.1.2 Ultimate bond strength (τ_u)

The average bond strength between reinforcement and concrete is usually calculated by the regression formula of experimental data. The main factors contained in various formulas are different, for example :

$$\left. \begin{array}{l} \text{reference [1-1]:} \\ \frac{c}{d} \leq 2.5 \quad \frac{\tau_u}{f_t} = \left(1.325 + 1.6 \frac{d}{l} \right) \frac{c}{d} \\ 2.5 < \frac{c}{d} < 5 \quad \frac{\tau_u}{f_t} = \left(5.5 \frac{c}{d} - 9.76 \right) \left(\frac{d}{l} - 0.4 \right) + 1.965 \frac{c}{d} \end{array} \right\} \quad (7-7a)$$

$$\text{reference [7-2]:} \quad \frac{\tau_u}{f_t} = 1.6 + 0.7 \frac{c}{d} + 20 \rho_{sv}, \quad (7-7b)$$

where ρ_{sv} is seen in Eq. (7-4). These formulas can be used for the reinforcement with short bond length ($l/d = 2-20$).

When the bond length of reinforcement is longer or the anchorage (or splice) length (l_a , Eq. 7-3) is needed to be calculated, other formulas should be used. The formula suggested in reference [7-20] can be used for $l/d \leq 80$:

$$\tau_u = \left(1 + 2.51 \frac{c}{d} + 41.6 \frac{d}{l} + \frac{A_{sv} f_y}{4.33 d_{sv} s_{sv}} \right) \sqrt{f_c}. \quad (7-8)$$

Other characteristic values of bond behavior, including initially cracking stress (τ_A), residual stress (τ_r), and various slips (s_A , s_{cr} , s_u , and s_r) are given by the researchers according to the experimental data of their own, and they are slightly different. The values suggested in reference [7-2] are:

$$\tau_A \approx \tau_r = f_t$$

$$\text{and } s_A = 0.0008d, \quad s_{cr} = 0.024d, \quad s_u = 0.0368d, \quad s_r = 0.054d.$$

7.4.2 Equation for τ – s curve

7.4.2.1 Segmental model

The bond stress–slip (τ – s) curve can be simplified into the models of multisegments, and several models of this kind, e.g. three [7-21–7-28], five [1-1,7-2], and six [7-22] segments (Fig. 7-20), are suggested already. Determining the values of

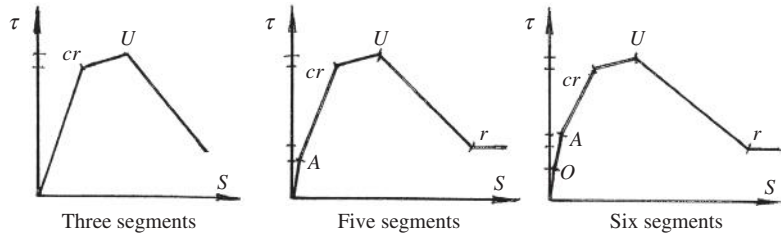


FIG. 7-20 τ - s models of multisegments

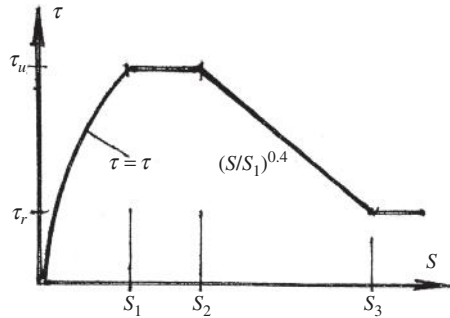


FIG. 7-21 τ - s model suggested in CEB-FIP Model Code

the characteristic bond stresses and slips and linking them with straight lines or simple curve, a τ - s constitutive model is composed. The CEB-FIP Model Code [2-12] suggests a model of four segments and is shown in Fig. 7-21 and the related parameters are listed in Table 7-2.

7.4.2.2 Model of continuous curve

When the equation of continuous curve is used to establish the bond stress-slip model, the values of tangent and secant bond stiffness obtained vary continuously

Table 7-2 Characteristic Values for τ - s Curve [2-12]

Confinement Condition, and Failure Pattern	Bond Quality	Bond Stress		Slip (mm)		
		τ_u	τ_r/τ_u	s_1	s_2	s_3
Without confinement, splitting failure	Good	$2\sqrt{f'_c}$	0.15	0.60	0.60	1.0
	Average	$\sqrt{f'_c}$				2.5
With confinement, pull out failure	Good	$2.5\sqrt{f'_c}$	0.40	1.0	3.0	Net space between transverse ribs
	Average	$1.25\sqrt{f'_c}$				

and definitely, which is convenient to be used in finite element analysis. The models of this kind are suggested in various references, such as:

$$\left. \begin{array}{l} \text{reference [7-23]:} \quad \tau = a_1 s - a_2 s^2 + a_3 s^3 \\ \text{reference [7-13]:} \quad \tau = (a_1 s - a_2 s^2 + a_3 s^3 - a_4 s^4) \sqrt{f_c} \end{array} \right\} \quad (7-9)$$

$$\left. \begin{array}{l} \text{and} \quad \tau = (a_1 s - a_2 s^2 + a_3 s^3 - a_4 s^4) \sqrt{\frac{c}{d}} f_t F(x) \\ \text{where} \quad F(x) = \sqrt{4 \frac{x}{l} \left(1 - \frac{x}{l}\right)} \end{array} \right\} \quad (7-10)^*$$

This is called as the position function, which represents the variation of τ — s relation at different buried (bond) depth of the reinforcement ($x = 0$ for its loading end and $x = l$ for its free end). Different forms of the position function are also suggested in other references, e.g. [7-22,7-23,7-2].

*Teng Zhiming, Lu Huizhong, Zhang Jinping. Inclined strut bond model for finite element analysis of reinforced concrete structure, 1988.

This page intentionally left blank

Mechanical Behavior Under Axial Force

8

CHAPTER OUTLINE

8.1 Compressive member	206
8.1.1 Basic equations.....	206
8.1.1.1 Geometrical (deformation) condition	206
8.1.1.2 Physical (constitutive) relation.....	207
8.1.1.3 Mechanical (equilibrium) equation.....	208
8.1.2 Analysis of stress and strain ($\epsilon_y < \epsilon_p$)	209
8.1.2.1 Before yielding of reinforcement ($\epsilon < \epsilon_y$)	209
8.1.2.2 After yielding of reinforcement but before reaching peak strain of concrete	210
8.1.2.3 After reaching peak strain of concrete ($\epsilon > \epsilon_p$)	210
8.1.3 Analysis of stress and strain ($\epsilon_y > \epsilon_p$)	210
8.1.3.1 Before reaching peak strain of concrete ($\epsilon \leq \epsilon_p$)	211
8.1.3.2 Descending stress of concrete but before yielding of reinforcement ($\epsilon_p < \epsilon \leq \epsilon_y$)	211
8.1.3.3 After yielding of reinforcement ($\epsilon > \epsilon_y$)	212
8.2 Tensile member.....	212
8.2.1 Basic equations for analysis	212
8.2.2 Analyses of stress and deformation within every stage.....	213
8.2.2.1 Before cracking of concrete ($\epsilon_t < \epsilon_{t,p}$).....	214
8.2.2.2 After cracking of concrete but before yielding of reinforcement ($\epsilon_{t,p} \leq \epsilon_t < \epsilon_y$)	214
8.2.2.3 After yielding of reinforcement ($\epsilon_t \geq \epsilon_y$).....	215
8.2.3 Minimum reinforcement rate	215
8.2.4 Tension stiffening.....	216
8.3 General regularity	218

After all the structures, including the one-dimensional members carrying various internal forces, e.g. axial force, bending moment, shear force, and torsion, and the two- and three-dimensional structures, are analyzed, the directions of principal stresses can be found easily. Either compression or tension is acted on these directions. When the reinforcement is set up in the direction of principal tensile stress, it can replace the cracked concrete and carries the tension on the section. When the

reinforcement is set up in the direction of principal compressive stress, the strength of the structure is also enhanced. Therefore, axial compression and tension are the simplest and basic mechanical conditions for reinforced concrete used as a composite structural material, and knowing well the general regularity of these conditions is the basis for understanding the behavior of other structure members.

8.1 Compressive member

8.1.1 Basic equations

A short column of reinforced concrete is shown in Fig. 8-1 and its section size ($b \times h$) and reinforcement used ($A_s = \mu bh$ and μ is the reinforcement rate) are known. Three equations should be established for accurately analyzing the whole processes of stress, deformation, and failure of the column under the action of central compression.

8.1.1.1 Geometrical (deformation) condition

The column is shortened under the action of central compression. However, the plane section before loading remains plane, i.e. the strain distribution on the section is uniform, after it is loaded until its failure. This is demonstrated by many experiments.

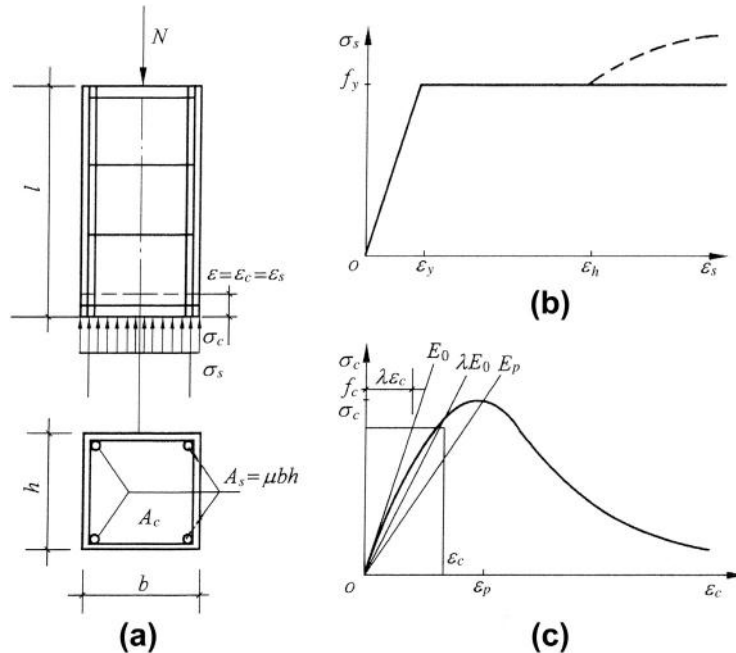


FIG. 8-1 Central compression column and constitutive relations of materials: (a) shape and reinforcement, (b) reinforcement, (c) concrete

When the longitudinal reinforcements are adhered well with the surrounding concrete and no slip occurs between them and when the outside of the reinforcements are surrounded with the ties, they will not buckle out and their concrete cover will not spall off even after they are yielded, the strains of the reinforcements and concrete in the column are equal to the strain of the column:

$$\varepsilon = \varepsilon_c = \varepsilon_s. \quad (8-1)$$

8.1.1.2 Physical (constitutive) relation

It is assumed that the constitutive relations of the reinforcement and concrete in a structure are respectively the same as that of the specimen of the same material obtained from the standard test. Now, the constitutive models of both materials are taken as shown in Fig. 8-1(b) and (c). The model for steel is:

$$\left. \begin{array}{ll} \varepsilon_s \leq \varepsilon_y & \sigma_s = E_s \varepsilon_s \\ \varepsilon_s > \varepsilon_y & \sigma_s = f_y = \text{const.} \end{array} \right\}, \quad (8-2)$$

where E_s, f_y are the modulus of elasticity and yield strength of the reinforcement.

The strain of the steel after yielding and entering into the hardening stage ($\varepsilon_h \approx 30 \times 10^{-3}$) is more than ten times the peak strain of the concrete (ε_p), so the stress-strain curve of the hardening stage is not necessary to be simulated.

The complete compressive stress-strain curve of concrete can be reasonably selected according to the property and strength grade of the material, and the equation (e.g. Eq. (2-6), Table 2-6) and relative parameters can be determined correspondingly. The non-linear stress-strain relation can be generally presented as

$$\sigma_c = \lambda E_0 \varepsilon_c \quad (8-3)$$

where $E_0 = d\sigma/d\varepsilon|_{\varepsilon=0}$ is the initial modulus of elasticity of concrete, λ is the plasticity coefficient of compressive strain of concrete, which is defined as the ratio between the secant modulus of elasticity (λE_0) at any strain (stress) and the initial modulus of elasticity, and is also the ratio between the elastic strain ($\lambda \varepsilon_c$) and total strain. Its value can be calculated from the equation of the stress-strain curve and is monotonically decreased as the strain increases:

$$\left. \begin{array}{ll} \text{when } \varepsilon_c = 0 \text{ and } \sigma_c = 0 & \lambda = 1.0 \\ \varepsilon_c = \varepsilon_p \text{ and } \sigma_c = f_c & \lambda = E_p/E_0 = 1/\alpha_a \\ \varepsilon_c > \varepsilon_p \text{ (descending branch)} & \lambda < 1/\alpha_a \\ \varepsilon_c \rightarrow \infty & \lambda \rightarrow 0 \end{array} \right\} \quad (8-4)$$

where α_a the parameter of ascending branch of the curve (Eq. 2-7).

When the strains of the reinforcement and concrete are equal (Eq. 8-1), the ratio between the stresses of both materials is:

$$\frac{\sigma_s}{\sigma_c} = \frac{E_s \varepsilon_s}{\lambda E_0 \varepsilon_c} = \frac{n}{\lambda} \quad \text{or} \quad \sigma_s = \frac{n}{\lambda} \sigma_c, \quad (8-5)$$

where the ratio between both moduli of elasticity is

$$n = \frac{E_s}{E_0}, \quad (8-6)$$

which is a constant of the material and is not related to the value of strain (stress), and it is quite important for the analysis of reinforced concrete structures.

It is seen from Eq. (8-5) that the ratio between the stresses of reinforcement and concrete increase gradually, as the strain of concrete increases and the value of λ reduces. However, equation (8-5) can only be used within the elastic stage of the reinforcement ($\epsilon_s < \epsilon_y$).

8.1.1.3 Mechanical (equilibrium) equation

There is only one equilibrium equation for the central compressive member:

$$N = N_c + N_s = \sigma_c A_c + \sigma_s A_s \quad (8-7a)$$

where N_c , N_s are the compressive forces carried, respectively, by the reinforcement and concrete.

The section area of the concrete can be approximately taken as¹

$$A_c = bh - A_s \approx bh^* \quad (8-8a)$$

and the section area of the reinforcement is:

$$A_s = \mu bh \approx \mu A_c. \quad (8-8b)$$

After Eq. (8-5) is substituted into Eq. (8-7a)

$$N = \sigma_c \left(A_c + \frac{n}{\lambda} A_s \right) = \sigma_c A_0 \quad (8-7b)$$

is obtained, where

$$A_0 = A_c + \frac{n}{\lambda} A_s^* \quad (8-9)$$

is called the converted section area of the member.

The converted section area of the member is composed of the area of the concrete (A_c) and the converted area of the reinforcement ($\frac{n}{\lambda} A_s$). Its physical meaning is that the composite section of two materials with different stresses is converted into a section of unique material of the same stress (σ_c). Actually, the conversion is only to increase n/λ times the area of the reinforcement. In addition, the converted area is also not a constant but increases as the strain is increased or the value of λ reduces.

¹The accurate equations should be respectively:

$$A_c = bh - A_s; \quad A_0 = bh - A_s + \frac{n}{\lambda} A_s = bh + \left(\frac{n}{\lambda} - 1 \right) A_s.$$

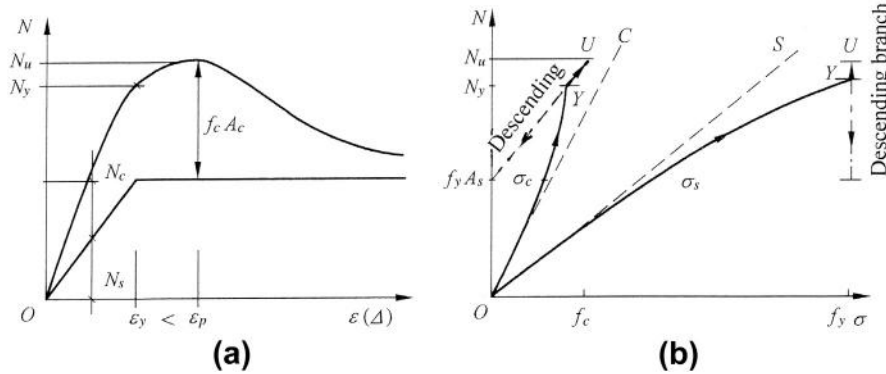


FIG. 8-2 Stress and deformation of column under central compression ($\epsilon_y < \epsilon_p$): (a) axial force-deformation (strain), (b) stresses in reinforcement and concrete

8.1.2 Analysis of stress and strain ($\epsilon_y < \epsilon_p$)

The responses of stress and strain of the concrete and reinforcement and the ultimate strength of a column under central compression are divided into several stages and can be calculated using these basic equations. When the yielding strain of the reinforcement (e.g. grade I or II) is less than the peak strain of the concrete ($\epsilon_y < \epsilon_p$), the behavior of the column is discussed first (Fig. 8-2).

8.1.2.1 Before yielding of reinforcement ($\epsilon < \epsilon_y$)

After the column is loaded and its strain increases gradually, the stress (σ_s) and compressive force (N_s) carried by the reinforcement increase proportionally. However, the stress (σ_c) and the compressive force (N_c) carried by the concrete also increase but with a reducing rate, because the plastic deformation of it appears and the modulus of elasticity is reduced gradually. Therefore, the fraction of the central force carried by the reinforcement (N_s/N) increases, while the fraction of the central force carried by concrete (N_c/N) decreases, as the central force is increased.

If both materials are of elastic and their moduli of elasticity are constants, the stresses of both are directly proportional to the central force, as shown by the dashed lines OS and OC in the axial force—stress diagram (Fig. 8-2(b)). However, after the plastic deformation of concrete appeared, its stress increased but with a reducing rate, so the stress of the reinforcement has to accelerate and the ratio between them (σ_s/σ_c) increases, as shown as the solid lines in the figure.

According to the equilibrium equation (8-7b) and Eqs. (8-3) and (8-1), the relation between the central force and the stress is

$$N = \sigma_c A_0 = \lambda \epsilon E_0 A_0, \quad (8-10)$$

and the deformation of the column is

$$\Delta = \epsilon l. \quad (8-11)$$

Then, the deformation of the column and the stresses of the reinforcement and concrete can be easily calculated for the column under different central compression.

8.1.2.2 After yielding of reinforcement but before reaching peak strain of concrete

When the reinforcement reaches its yielding point ($\varepsilon = \varepsilon_y$), the central compression should be:

$$N_y = \lambda \varepsilon_y E_0 A_0 = \lambda \varepsilon_y E_0 A_c + f_y A_s. \quad (8-12)$$

Afterwards, the stress of the reinforcement keeps a constant (f_y) although its strain continuously increases ($\varepsilon > \varepsilon_y$). Therefore, the increment of central compression is totally carried by the concrete, and the compressive stress of the concrete accelerates until its ultimate value (f_c). The ultimate central compression is reached at this time and is

$$N_c = f_c A_c + f_y A_s. \quad (8-13)$$

It means that both the concrete and reinforcement respectively reach their own ultimate strengths.

The slope of the N – ε curve of the column reduces gradually within this stage and the tangent at N_u is horizontal, but the curve is not continuous at N_y . The relation between the compression and strain of the column is:

$$N = \lambda \varepsilon E_0 A_c + f_y A_s. \quad (8-14a)$$

If the compression is known, the strain of the column can be calculated:

$$\varepsilon = \varepsilon_c = \frac{N - f_y A_s}{\lambda E_0 A_c} \quad (8-14b)$$

8.1.2.3 After reaching peak strain of concrete ($\varepsilon > \varepsilon_p$)

The stress of the reinforcement still keeps a constant (f_y) while the stress of the concrete (σ_c , or residual strength) reduces, as the strain of the column increases further. Therefore, the bearing capacity of the column reduces within this stage. When the strain increases greatly, the residual strength of the concrete is exhausted and the residual bearing capacity of the column is controlled by the reinforcement ($f_y A_s$).

The relation between the compression and strain of the column is the same as Eq. (8-14), but the value of λ should be taken from the descending branch of the stress–strain curve of the concrete.

8.1.3 Analysis of stress and strain ($\varepsilon_y > \varepsilon_p$)

If the column is reinforced with the reinforcement of higher-strength grade, e.g. III, IV, and the yielding strain of the reinforcement is greater than the peak strain of concrete ($\varepsilon_y > \varepsilon_p$), the mechanical stages and deformation process of the column under loading (Fig. 8-3) are quite different from those of the previous one ($\varepsilon_y < \varepsilon_p$).

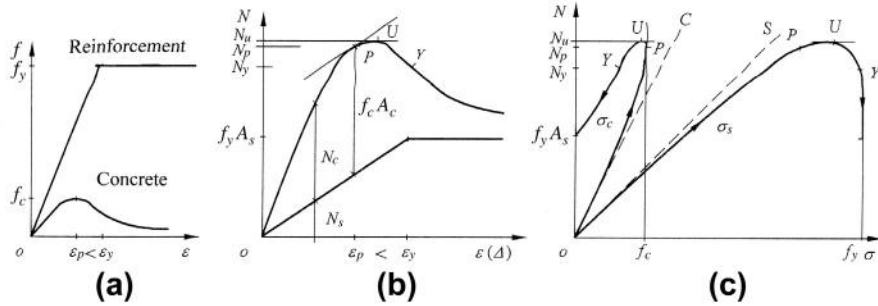


FIG. 8-3 Stress and deformation of column under central compression ($\epsilon_y > \epsilon_p$): (a) $\sigma-\epsilon$ curves of materials, (b) axial force-deformation (strain), (c) stresses in reinforcement and concrete

8.1.3.1 Before reaching peak strain of concrete ($\epsilon \leq \epsilon_p$)

The axial force-strain ($N-\epsilon$) and -stresses (σ_s and σ_c) curves of the column are not different from those of the previous column. In addition, the relation between the axial force and strain is also the same as Eq. (8-10):

$$N = \lambda \epsilon E_0 A_0 = \sigma_c \left(A_c + \frac{n}{\lambda} A_s \right).$$

When the strain of the column reaches the peak strain of the concrete (ϵ_p), the central compression is:

$$N_p = f_c A_c + \epsilon_p E_s A_s, \quad (8-15)$$

however this is not the ultimate (maximum) bearing capacity of the column.

8.1.3.2 Descending stress of concrete but before yielding of reinforcement ($\epsilon_p < \epsilon \leq \epsilon_y$)

The stress of the concrete reduces gradually when the strain $\epsilon > \epsilon_p$, while the stress (σ_s) and resistance (N_s) of the reinforcement increase continuously. Therefore, the bearing capacity of the column increases first then decreases afterwards, and the peak value of the compression is the ultimate strength of the column (N_u). The $N-\epsilon$ curve is continuous within this stage, and the tangent at N_p parallels that of the resistance of the reinforcement (N_s) and the tangent at N_u should be horizontal.

The ultimate strength of the column certainly exceeds the compression at the peak strain of the concrete, but is certainly smaller than the summation of the ultimate resistances of the concrete and reinforcement (Eq. 8-13), i.e.

$$N_p < N_u < f_c A_c + f_y A_s. \quad (8-16)$$

The accurate values of the ultimate strength and corresponding strain of the column have to be calculated analytically or digitally.

The reinforcement is yielding ($\epsilon = \epsilon_y$) after the peak value of compression appeared, and the compression at its yielding is

$$N_y = \lambda \epsilon_y E_0 A_c + f_y A_s \quad (8-17)$$

8.1.3.3 After yielding of reinforcement ($\epsilon > \epsilon_y$)

The stress of the reinforcement also remains constant while the residual strength of the concrete (σ_c) decreases continuously within this stage, the relation between the compression and strain of the column and the stress variations of the reinforcement and concrete are similar to that of the previous column (when $\epsilon > \epsilon_p$).

Comparing the mechanical behaviors of the two columns described above (Figs 8-2 and 8-3), even the simplest short column of reinforced concrete under central compression, the N - ϵ curve and the stresses of the reinforcement and concrete are non-linear and vary considerably with the indices of both materials, and the ultimate states and strengths of them are also different.

8.2 Tensile member

8.2.1 Basic equations for analysis

The shape and reinforcement of a tensile member of reinforced concrete is shown in Fig. 8-4(a), and its stress and deformation under the action of central tension have to be divided into stages and analyzed. The basic equations of the three categories are slightly modified as below.

Geometrical (deformation) condition. The reinforcement is adhered well with adjacent concrete before cracking, and the strains of both are equal:

$$\epsilon = \epsilon_s = \epsilon_t. \quad (8-18)$$

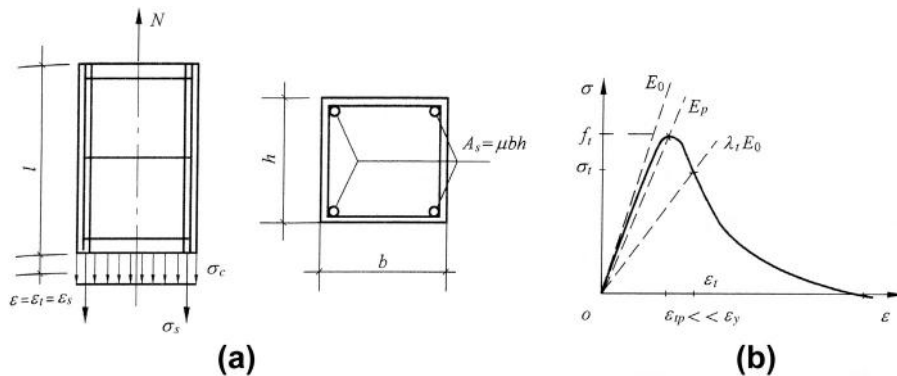


FIG. 8-4 Central tensile member: (a) shape and reinforcement, (b) complete stress-strain curve of concrete under tension

Physical (constitutive) relation. The constitutive relation of the reinforcement can be found above (Eq. 8-2), and the complete stress—strain curve of concrete under tension is shown in Fig. 8-4(b) and its expression is generally:

$$\sigma_t = \lambda_t E_0 \varepsilon_t, \quad (8-19)$$

where E_0 is the initial modulus of elasticity of concrete under tension. The experimental result shows that its value approximates that under compression and is usually taken as the same value; λ_t is the plasticity coefficient of tensile strain of concrete, which is defined as the ratio between the secant modulus of elasticity ($\lambda_t E_0$) and the initial modulus of elasticity. It can be calculated from the equation of tensile stress—strain curves of concrete, e.g. Eq. (2-20).

Similarly, when the strains of the reinforcement and concrete are equal, the ratio between the stresses of both is

$$\frac{\sigma_s}{\sigma_t} = \frac{n}{\lambda_t} \quad \text{or} \quad \sigma_s = \frac{n}{\lambda_t} \sigma_t, \quad (8-20)$$

where the ratio of elasticity moduli (n) is the same as the compressed column (Eq. 8-6).

Mechanical (equilibrium) equation is similar to that of a compressed column

$$N = N_t + N_s = \sigma_t \left(A_c + \frac{n}{\lambda_t} A_s \right) = \sigma_t A_0 \quad (8-21a)$$

8.2.2 Analyses of stress and deformation within every stage

The stress and deformation of the central tensile member vary with the tensile force and are shown in Fig. 8-5.

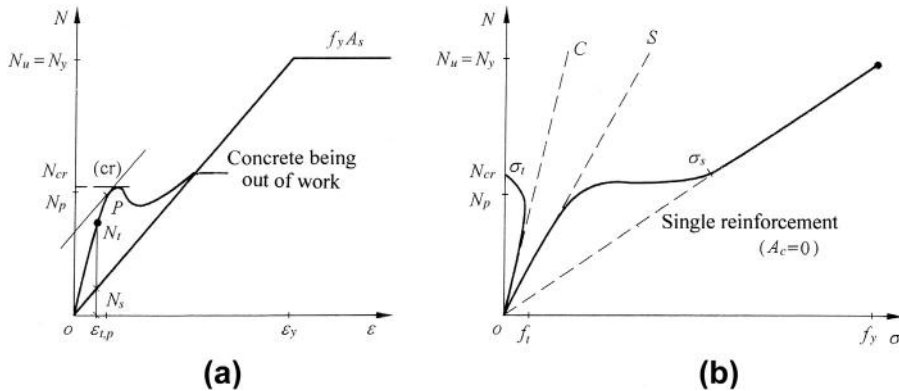


FIG. 8-5 Stress and deformation of central tensile member: (a) axial force-deformation, (b) stresses of reinforcement and concrete

8.2.2.1 Before cracking of concrete ($\epsilon_t < \epsilon_{t,p}$)

The stress of the reinforcement increases proportionally to the strain ($\epsilon_s = \epsilon_t$). The plastic deformation of concrete appears slightly before cracking, and correspondingly, the stress of concrete increases but at a reducing rate. The relation between the tensile force and strain of the member can be obtained from Eq. (8-21a), or

$$N = \lambda_t \epsilon_t E_0 A_0 = \lambda_t \epsilon_t E_0 \left(A_c + \frac{n}{\lambda_t} A_s \right). \quad (8-21b)$$

Therefore, the N – ϵ relation and the variations of stresses σ_s and σ_t of the tensile member are similar to that of the compressed column during the early stage.

8.2.2.2 After cracking of concrete but before yielding of reinforcement ($\epsilon_{t,p} \leq \epsilon_t < \epsilon_y$)

When the concrete reaches its tensile peak strain ($\epsilon_{t,p}$), the stress of the reinforcement is still low, i.e. about $20 \text{ N/mm}^2 \ll f_y$, and the central force then is

$$N_p = f_t A_c + \epsilon_{t,p} E_s A_s = f_t \left(A_c + \frac{n}{\lambda_t} A_s \right) \quad (8-22a)$$

Afterwards, the stress of the reinforcement increases continuously, but the tensile stress σ_t and resistance N_t of the concrete decrease quickly as the strain increases further, so a peak is formed on the tensile force–strain diagram. The tangent of the N – ϵ curve at N_p parallels to line N_s , i.e. the resistance of the reinforcement, and the tangent at peak is horizontal. Consequently, the ultimate value N_{cr} is the cracking force of the member and should be slightly greater than N_p , however

$$N_{cr} \approx N_p \quad (8-22b)$$

is generally taken.

The concrete is out of work ($\sigma_t = 0$) after cracking and the bond near the crack is locally failed, the geometrical condition (Eq. 8-18) is not held anymore. Only the reinforcement carries the central force on the cracked section, so

$$N = \epsilon E_s A_s = \sigma_s A_s. \quad (8-23)$$

The increment of central force ($N_{cr} - N_p$) from concrete reaching the peak strain ($\epsilon_{t,p}, f_t$) to being totally out of work is rather small, but the stress of the reinforcement increases suddenly (Fig. 8-5(b)). The line OS in the figure shows the tensile stress of the reinforcement if the concrete works together with, but it turns into another line which shows the reinforcement works alone. The stress increment of the reinforcement at this time is about:

$$\Delta \sigma_s \approx \frac{N_{cr}}{A_s} - \frac{n N_{cr}}{\lambda_t A_0} = \frac{N_{cr}}{A_c} \left(\frac{1}{\mu} - \frac{1}{\mu + (\lambda_t/n)} \right), \quad (8-24)$$

and its value is rather great because of $\lambda_t/n \gg \mu$.

8.2.2.3 After yielding of reinforcement ($\epsilon_t \geq \epsilon_y$)

When the reinforcement is yielding, the concrete ($\epsilon_y \gg \epsilon_{t,p}$) has been cracked seriously and can not carry any tensile force. Therefore, the force is totally carried by the reinforcement and its yielding is defined as the ultimate state of the tensile member, of which the strength is

$$N_u = N_y = f_y A_s, \quad (8-25)$$

if the hardening zone of the reinforcement is not considered.

The discussion above is only for the cracked section of the tensile member, and the analyses of the uncracked section and whole member can be seen in [Section 8.2.4](#).

8.2.3 Minimum reinforcement rate

After a reinforced concrete member is cracked under central tension and the concrete is out of work, the reinforcement in it carries the entire tension. Although the stress of the reinforcement suddenly increases during cracking of concrete but is still smaller than its yield strength ($N_{cr} < N_y$), the tension can be increased further until its yielding and the member is failed due to excessive deformation.

It is known from the above analysis that the cracking tension of the member (N_{cr} , [Eq. 8-22](#)) depends mainly upon the resistance of the concrete ($f_t A_c$), while the quantity of the reinforcement (A_s) has less influence on it. On the other hand, the ultimate tension of the member ($N_u = N_y$) depends entirely upon the resistance of the reinforcement ($f_y A_s$). Obviously, the relative ratio between both critical tensions varies with the quantity of the reinforcement, or the reinforcement rate (μ). When the reinforcement rate is reduced, the ultimate tension will proportionally reduce, but the cracking tension is decreased limitedly. If the reinforcement rate is too small ($\mu < \mu_{\min}$), the calculated ultimate tension of the member would be smaller than the cracking tension ($f_y A_s < N_{cr}$, [Fig. 8-6](#)). This kind of member is called less-reinforced, and the threshold is called the minimum reinforcement rate (μ_{\min}).

There is no difference between the less-reinforced and normal reinforced members and the concrete works together with the reinforcement under the central tension after loading but before cracking of the concrete. However, the reinforcement in the less-reinforced member will yield or even break and the member fails quickly soon after the concrete cracks because of excessive tension. Usually, this is not allowed to happen in engineering practice because of safety of the structure.

In order to avoid this unfavorable situation, $N_u \geq N_{cr}$ should be satisfied, i.e.

$$f_y A_s \geq f_t \left(A_c + \frac{n}{\lambda_t} A_s \right).$$

When $A_s = \mu_{\min} A_c$ is substituted into it, the μ_{\min} is obtained after modification:

$$\mu_{\min} = \frac{f_t}{f_y - \frac{n}{\lambda_t} f_t} = \frac{f_t / f_y}{1 - \frac{n}{\lambda_t} \frac{f_t}{f_y}}. \quad (8-26)$$

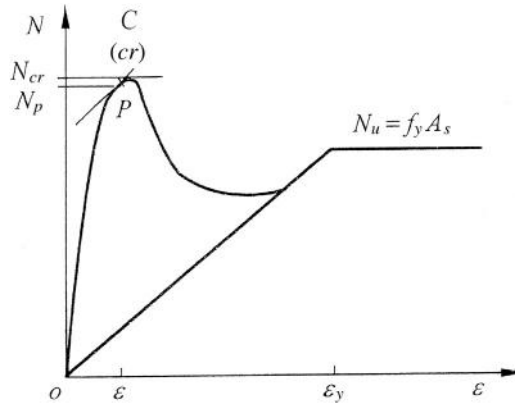


FIG. 8-6 Relation between tension and strain of less-reinforced member

This is the theoretical formula for calculating the minimum reinforcement rate of a central tensile member of reinforced concrete. In practice, the scatter of concrete property, the environmental situation, and the engineering experiences have to be considered and the value is modified [2-1,2-12]. Besides, the minimum reinforcement rate of flexural member can be found in Section 11.1.2.

8.2.4 Tension stiffening

After the concrete is cracked ($N > N_{cr}$) in a central tensile member of reinforced concrete, several cracks with approximate distance (l_{cr}) are formed (Fig. 8-7(a)). The concrete on the cracked section is out of work ($\sigma_t = 0$), and the tension is entirely carried by the reinforcement in it and its stress is σ_s . The bond between the reinforcement and concrete fails locally near the cracks and relative slip occurs between them, but the reinforcement and concrete on other parts of the member are still well adhered. Therefore, the stress or strain of the reinforcement varies along its axis, and it can be measured during testing (Fig. 7-6). Then, the average tensile stress of the concrete on every uncracked section ($\bar{\sigma}_t = (N - \sigma_s A_s)/A_c$) and the bond stress (τ) can be calculated by the equilibrium equation only, and they vary along the axis as well (Fig. 8-7(b)).

The stress of the reinforcement (σ_s) has the maximum value at the cracked sections, and it reduces gradually at other sections and reaches the minimum value ($\sigma_{s,min}$) at the middle section between two adjacent cracks. The strain of the reinforcement varies similarly. However, the tensile stress of the concrete ($\bar{\sigma}_t$) varies in opposite way, i.e. zero stress ($\bar{\sigma}_t = 0$) occurs near the cracked sections, and the maximum stress appears at the middle section between two adjacent cracks but is less than its tensile strength of the concrete ($\bar{\sigma}_{t,max} \leq f_t$).

The total elongation of central tensile member is the summation of the reinforcement strain along its axis:

$$\Delta = \int_0^l \epsilon_s dx = \int_0^l \frac{\sigma_s}{E_s} dx, \quad (a)$$

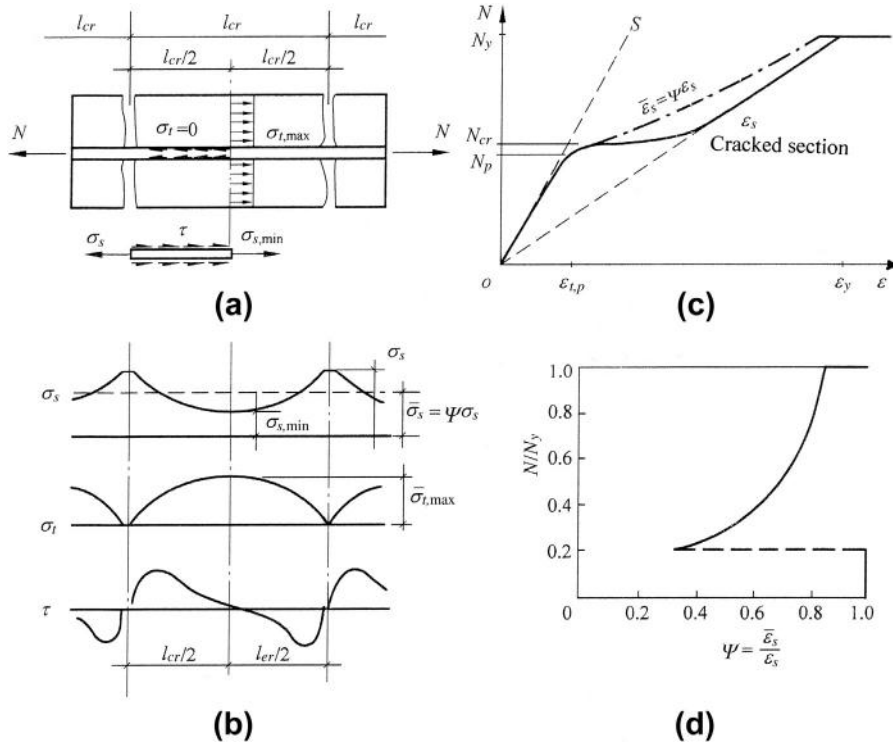


FIG. 8-7 Analysis of tension stiffening: (a) crack and equilibrium, (b) stress distribution, (c) variation of strain, (d) non-uniform coefficient of reinforcement strain

and the average strain and corresponding stress are:

$$\bar{\epsilon}_s = \frac{\Delta}{l} \quad \text{and} \quad \bar{\sigma}_s = \bar{\epsilon}_s E_s. \quad (b)$$

The reinforcement strain at the cracked section (ϵ_s) and the average strain between adjacent cracks ($\bar{\epsilon}_s$) increase with the central tension (N) and vary as shown in Fig. 8-7(c). The ratio between both strains is called the non-uniformity coefficient of reinforcement strain between cracked sections:

$$\Psi = \frac{\bar{\epsilon}_s}{\epsilon_s} = \frac{\bar{\sigma}_s}{\sigma_s} \leq 1 \quad (8-27)$$

The reinforcement is well adhered with concrete and its stress is the same along the whole length before cracking of the concrete ($N \leq N_{cr}$), so $\Psi = 1$. When the concrete is just cracking ($N = N_{cr}$), the reinforcement stress (σ_s) at cracking section increases suddenly, but the damaged area of bond is rather small and the tensile stress of the concrete between cracks is still high, so the minimum stress of the

reinforcement ($\sigma_{s,\min}$) is lower and the non-uniformity coefficient of strain is the minimum, i.e. about $\Psi = 0.10-0.25$. The reinforcement stress (σ_s) increases gradually with the central tension (N) and the bond is deteriorated more seriously, so the stress difference of the reinforcement between the adjacent cracks reduces and the value of Ψ increases continuously. When the reinforcement is just yielding ($\varepsilon_s = \varepsilon_y$), the value of Ψ is still less than 1; when the central tension ($N_y = f_y A_s = \text{const.}$) is maintained, the strain of the reinforcement increases further ($\varepsilon_s > \varepsilon_y$) and the value of $\Psi = 1$ (Fig. 8-7(d)) is reached as the bond between the reinforcement and concrete is failed along the whole length.

After the concrete is cracked, it is not related again to the strength of tensile member of reinforced concrete ($N_u = f_y A_s$). However, the concrete still causes the stress reduction of the reinforcement between cracks, so the average strain is surely smaller than the strain at the cracked section ($\bar{\varepsilon}_s < \varepsilon_s$) and the elongation of the member is decreased ($\Delta = \bar{\varepsilon}_s l < \varepsilon_s l$), or the stiffness of the member is increased. This is called tension stiffening. It also happens in the tension zone of a flexural member of reinforced concrete and is important to increase the stiffness and to reduce the crack width of the member, which will be discussed in detail in Chapters 12 and 13.

8.3 General regularity

According to the analysis of mechanical behaviors of the composite section of reinforcement and concrete under separate actions of central compression and tension, the general regularities can be summarized as below.

1. The stress state on a section of reinforced concrete redistributes continuously from start of loading until failure, and the non-linear process can be generally divided into several stages: elastic deformation — plastic deformation of concrete — cracking of concrete — yielding of reinforcement — ultimate state — residual (post-peak) behavior.
2. The mechanical responses of reinforced concrete, including deformation, cracking, yielding, ultimate strength, and failure pattern, vary considerably and depend not only upon the constitutive relations of concrete and reinforcement, but also upon the relative values of both materials, e.g. ratio of section areas (μ), ratio of elastic moduli (n), ratio of strengths ($f_c/f_y, f_t/f_y$), and the structural detail of the reinforcement.
3. Generally, the reinforcement and concrete in a member will not simultaneously reach their own strengths. Therefore, the strength of the member has to analyze and calculate following the constitutive relation of the material and the geometrical and equilibrium conditions of the member. If the ultimate resistances of both materials are simply added, unsafe consequences will sometimes result.
4. It is demonstrated from many experiments that the whole section or a part of the section under compression of a reinforced concrete member remains a plane

from the start of loading until failure. On the other hand, after the whole section or a part of the section of a reinforced concrete member is cracked under tension, the sections near the crack do not fit again the hypothesis of plane section, and the strain distribution on every section is different from one another.

However, when the internal forces and deformation of a structure are analyzed and the average deformation within a certain length (e.g. distance between cracks l_{cr}) is taken into account, the hypothesis of plane section can still be used conditionally.

5. The stresses of the reinforcement and concrete distribute non-uniformly along the axis after cracking of the concrete. The residual bond action and tensile stress of the concrete causes the phenomenon of tension stiffening, so the elongation of the reinforcement is reduced and this is favorable for increasing the stiffness and decreasing the crack width of the member.

These characteristics result due to the composition of concrete and reinforcement materials and are far more complicated than that of a single material. Therefore, the mechanical behavior of a reinforced concrete structure and its members can be comprehensively studied only when the loading history is divided into stages, the actual constitutive relations of materials and structural detail are considered, and the basic equations are used for analyzing. When a generalized reinforced concrete composed of various replacing materials of concrete and reinforcement is concerned, its mechanical behavior also follows the general regularity above and can be analyzed using the same principle and method.

This page intentionally left blank

Confined Concrete

9

CHAPTER OUTLINE

9.1 Column with spiral bar	222
9.1.1 Mechanical mechanism and failure process	222
9.1.2 Ultimate strength	224
9.2 Rectangular tied column	226
9.2.1 Failure process	226
9.2.2 Working mechanism of rectangular tie	229
9.2.3 Equation for complete stress–strain curve	234
9.2.3.1 Sargin model	234
9.2.3.2 Sheikh model	235
9.2.3.3 Digital calculation following loading history	235
9.2.3.4 Empirical formula	236
9.3 Steel-tube-confined concrete	238
9.3.1 Mechanical characteristic and mechanism	238
9.3.2 Calculation of ultimate strength	241
9.4 Local compression	244
9.4.1 Mechanical characteristic and mechanism	244
9.4.2 Calculation of strength	249
9.4.2.1 CEB-FIP model code model	250
9.4.2.2 Hawkins model	251
9.4.2.3 Empiric formulas	251

There are two basic forms of reinforcement in concrete structures. When the reinforcement is set up longitudinally in the member and runs parallel to the direction of its axial force or principal stresses, it is called directly reinforced. The longitudinal reinforcement provides tensile resistance or enhances compressive resistance for the member (see Chapter 8). When the separate ties or continuous spiral bar are set up transversely in the member or are perpendicular to its axial compression or principal compressive stress, it is called transversely or indirectly reinforced. The transverse reinforcement confines the transverse expansive deformation of the concrete surrounded by it and enhances the compressive strength in longitudinal (axial) direction.

Several kinds of transverse reinforcement, including continuous spiral (circle) bar, rectangular tie, steel tube, welded mesh, etc., are used in concrete structures.

The main function of them is to confine the transverse deformation of the concrete surrounded by them. In addition, when a concentrated load is locally acted on a concrete structure, the concrete under the loading area is also confined by the surrounding concrete. Actually, the confined concrete is under the condition of a triaxial compressive stress state, hence the strength and deformation ability of it is enhanced greatly. This is an important measure in the engineering practice to improve the mechanical behavior of a compressive member or compressive part in a structure.

9.1 Column with spiral bar

9.1.1 Mechanical mechanism and failure process

When a continuous spiral bar or separate welded circle ties are reinforced in a compressed member and the distance between the ties is small enough ($s < 80$ mm and $< d_{cor}/5$), the core concrete surrounded by them is effectively confined (Fig. 9-1) and its mechanical behavior is considerably improved and enhanced.

The compression—strain curve and stress state on the section of a plain or an ordinary reinforced concrete column ($\varepsilon_y < \varepsilon_p$; see Chapter 8) under central compression are described above. Although the longitudinal reinforcement (A_s) in the column enhances its compressive strength, it has less influence on the peak strain and descending curve of it (Fig. 9-2).

The compression—strain curve of the spiral column is shown in Fig. 9-2(a). When the strain of the column is smaller than the peak strain of the plain concrete ($\varepsilon < \varepsilon_p$), the transverse expansive deformation (or the Poisson's ratio, Fig. 2-7) of the concrete is rather small, so the tensile stress of the spiral bar is limited and it has less influence on the concrete. Therefore, the compression—strain curve is approaching that of the tied column, and the compression of the spiral column at $\varepsilon = \varepsilon_p$ also approximates the ultimate strength of the tied column (Eq. 8-13).

When the strain of the column is increased again ($\varepsilon > \varepsilon_p$), the concrete cover outside of the reinforcement (its area is $A_c - A_{cor}$) enters the stress descending branch and the longitudinal crack starts to appear and expand, so the cover spalls off gradually and its resistance has to be reduced. In the meantime, the core concrete

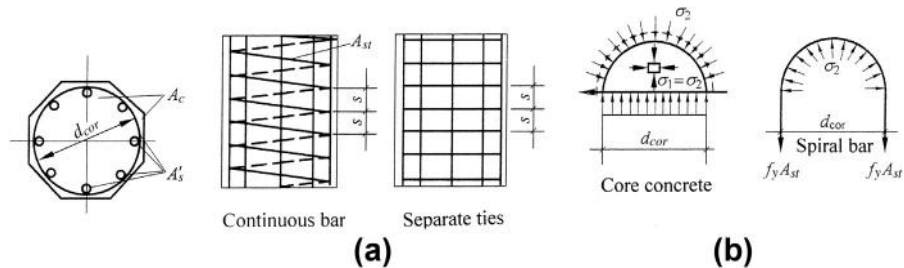


FIG. 9-1 Detail and confined stress of column with spiral bar: (a) reinforcement and structural detail, (b) confined stress

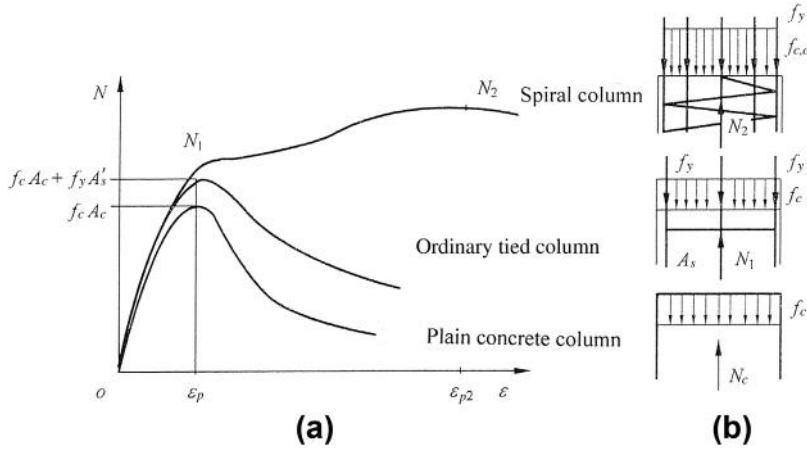


FIG. 9-2 Comparison between three kinds of column: (a) N - ϵ curves, (b) stress states

(area A_{cor}) expands outside because of an increase in the Poisson's ratio, and it exerts the radial compression (σ_2 in Fig. 9-1(b)) on the spiral bar. Correspondingly, the reactive compression of the spiral bar applies on the core concrete and the stress state of triaxial compression ($\sigma_1 = \sigma_2$) is formed, so its longitudinal strength is increased ($|f_3| > f_c$, see Chapter 5). Therefore, the total strength of the core and cover concretes still increases gradually with the strain.

When the strain of the column is increased further, the transverse expansion of the core concrete and the tensile stress of the spiral bar increase continuously. When the tensile stress of the spiral bar reaches the yielding strength (f_{yt}), the confinement stress of it (σ_2) reaches the maximum value. At this time, the longitudinal stress of the core concrete is still less than the triaxial compressive strength ($\sigma_3 < |f_3|$), so the central compression can be increased further. Afterwards, the tensile stress of the spiral bar (f_{yt}) keeps constant, and the core concrete expands continuously under the constant confinement stress. Until the longitudinal stress of the core concrete reaches the triaxial compressive strength (or compressive strength) of confined concrete ($f_{c,c} = |f_3|$), the column enters the ultimate state and its strength is N_2 . The longitudinal strain of the column is rather large, possibly $\epsilon_{p2} = 10 \times 10^{-3}$, during this time, and the residual compressive stress in the cover concrete is low, even if it is not totally spalled off.

Finally, the core concrete is extruding and shifting under triaxial compression (Section 5.3), its transverse expansion makes the column locally protrude, its longitudinal strain accelerates and the column is obviously shortened, the spiral bar is exposed or even broken, and a descending branch is formed on the N - ϵ curve of the column.

The increase in ultimate strength and, especially, the improvement of the deformation behavior are the main characteristics of the spiral column, and they are fully utilized in the engineering practice.

9.1.2 Ultimate strength

It is seen from the $N-\varepsilon$ curve of the spiral column that there are two critical values to control its ultimate strength:

1. Yielding of longitudinal compressive reinforcement and reaching compressive prism strength of concrete on whole section (N_1). The transverse strain of the concrete is small and the confinement action of the spiral bar can be neglected at this time, the calculation formula established is the same as Eq. (8-13):

$$N_1 = f_c A_c + f_y A_s \quad (9-1)$$

where A_c is the total area of the section, including the core and cover.

2. Reaching the compressive strength of confined core concrete ($f_{c,c}$) after yielding of the spiral bar (N_2). The cover concrete is already out of work as the strain of the column is considerable, but the yield strength of the longitudinal reinforcement maintains constantly (Fig. 9-2(b)):

$$N_2 = f_{c,c} A_{cor} + f_y A_s \quad (9-2)$$

where $f_{c,c}$ is the compressive strength of confined concrete, i.e. the strength of core concrete under triaxial compressive stress state ($|f_3|, \sigma_1 = \sigma_2$); A_{cor} is the area of core concrete which is calculated by the inside diameter of the spiral bar (d_{cor}).

If the volume rate of the transverse spiral bar is

$$\mu_t = \frac{\pi d_{cor} A_{st}}{\frac{\pi}{4} s d_{cor}^2} = \frac{4 A_{st}}{s d_{cor}}, \quad (9-3)$$

and it is multiplied by ratio between the strengths of spiral bar and concrete and the product obtained is:

$$\lambda_t = \mu_t \frac{f_{yt}}{f_c} = \frac{4 f_{yt} A_{st}}{f_c s d_{cor}}, \quad (9-4)$$

which is defined as the confinement index or the characteristic value of transverse reinforcement where: A_{st}, f_{yt} are the section area and yield strength of spiral bar, respectively; d_{cor}, s are the inside diameter and longitudinal distance of spiral bar, respectively.

Following the equilibrium condition (Fig. 9-1(b)), the maximum confined stress of the core concrete at yielding of the spiral bar is:

$$\sigma_1 = \sigma_2 = \frac{2 f_{yt} A_{st}}{s d_{cor}} = \frac{1}{2} \lambda_t f_c. \quad (9-5)$$

If the triaxial compressive strength of concrete is approximately calculated by the Richart formula (Fig. 5-7(a)):

$$f_{c,c} \approx f_c + 4\sigma_2 = (1 + 2\lambda_t)f_c, \quad (9-6)$$

and it is substituted into Eq. (9-2), the calculation formula for the ultimate strength is established:

$$\begin{aligned} N_2 &= (1 + 2\lambda_t)f_c A_{cor} + f_y A_s \\ &= f_c A_{cor} + 2f_{yt}\mu_t A_{cor} + f_y A_s. \end{aligned} \quad (9-7)$$

Obviously, the second term in the right hand of Eq. (9-7) is the contribution of the transverse spiral bar to the ultimate strength of the column. $\mu_t A_{cor}$ of the term and A_s of the third term represent respectively the converted longitudinal area of the spiral bar and the section area of the longitudinal reinforcement, so the coefficient 2 of the second term shows that the bearing efficiency of the former is double that of the latter, if the same material (strength) and volume (area \times s) are used for them. The actual value of the coefficient measured from the experiment ranges from 1.7 to 2.9 [1-1], and its average value is about 2.0.

It should be noted that the spiral bar enhances the ultimate strength of the column (N_2 , Eq. (9-7)) only when it is short enough ($H/d \leq 12$, H and d are respectively the height and depth of it) and is centrally compressed. The higher column will fail in buckling and mainly depends upon the elasticity modulus or deformation of it. When the column is eccentrically compressed, the compressive stress distributes non-uniformly on its section, even it is failed in the tensile zone. Therefore, Eq. (9-7) can not be used for these situations, because the confinement of the spiral bar is limited and the enhanced strength is doubtful.

The difference between the two critical strengths ($N_2 - N_1$) of the spiral column depends upon its confinement index (λ_t). If the spiral bar used is less and makes $N_2 < N_1$, it means that the strength enhanced by the confinement action of the spiral bar does not fully compensate the strength lost due to loss of concrete cover, so the column will fail at N_1 like an ordinary column. Therefore, when the spiral column is designed, the situation of $N_2 \geq N_1$ should be satisfied. After Eqs. (9-1) and (9-7) are substituted into it,

$$\lambda_t \geq \frac{A_c - A_{cor}}{2A_{cor}} \quad (9-8)$$

is obtained.

On the other hand, if the strength difference ($N_2 - N_1$) is too much, the concrete cover may reach, even exceed, its peak strain (stress) and the longitudinal crack is caused in it, even the cover spalls off under the service load. This does not satisfy the requirement of serviceability. Generally, the limit $N_2 \leq 1.5N_1$ [2-1] is suggested for the spiral column during design, so

$$\lambda_t \leq \frac{f_c(3A_c - 2A_{cor}) + f_{yt}A_s}{4f_c A_{cor}} \quad (9-9)$$

is obtained.

Eqs. (9-9) and (9-8) are the theoretical upper and lower boundaries of the confinement index for the spiral column. The boundaries given in the design codes of different countries are different, for example, the lower boundaries are separately:

$$\text{China [2-1]} \quad \mu_t A_{cor} \geq 0.25 A_s \quad (9-10a)$$

$$\text{U.S.A. [2-11]} \quad \lambda_t \geq 0.45 \left(\frac{A_c}{A_{cor}} - 1 \right) \frac{f_c}{f_y} \quad (9-10b)$$

9.2 Rectangular tied column

The applied scope of the spiral bar is limited, because its shape (circle) does not fit the single and composite (e.g. T and I shapes) rectangular sections of the structural member which are used most widely in engineering practice. The tie is set up parallel with the edges of a single rectangular section, while several ties are set up parallel with every edge of a composite rectangular section. Therefore, the rectangular tie is used most widely among the transverse bars.

The main functions of the tie reinforced in a column are: the longitudinal reinforcement together with it forms a skeleton to keep the correct shape and position during manufacturing; it carries the transverse stress, which is caused due to the shrinkage of concrete and the variations of environmental temperature and humidity, to prevent or reduce the developing of longitudinal crack during the service period; it reduces the unsupported length of the longitudinal reinforcement, of which the strength can be fully utilized during failure of the column; and it is also helpful for shear strength of the column. Therefore, the tie (transverse bar) is a composite portion necessary for a reinforced concrete structure.

In addition, the existing experimental investigation and the engineering experience, especially the survey of damaged structure after earthquake, demonstrate that more ties reinforced in the concrete member enhance the ductility and is favorable for the aseismic behavior. Therefore, one of the most simple, economical, and effective measures for strengthening the aseismic behavior of a structure is to increase properly and to improve the form of the tie in it.

9.2.1 Failure process

Many experimental and theoretical investigations [9-1–9-8] have been conducted on the mechanical behavior of the concrete confined by a rectangular tie. The complete compressive stress–strain curve of the confined concrete varies considerably as the main influence factor (confinement index λ_t) increases, it changes from the curve with an apparent single peak into the curve with a flatter top, as shown in Fig. 9-3.

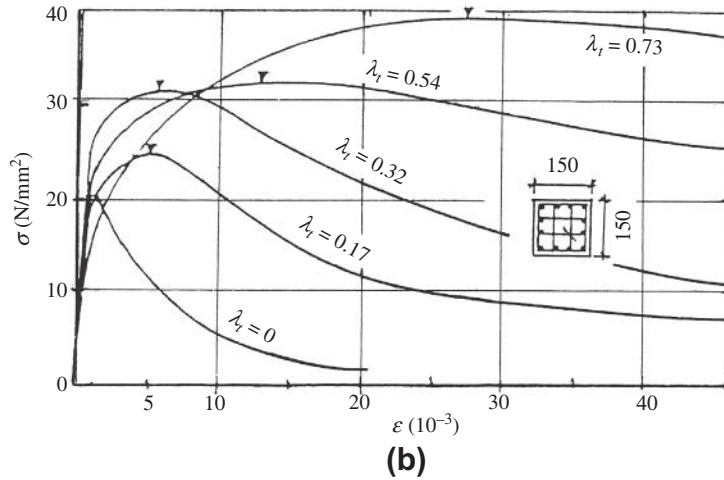
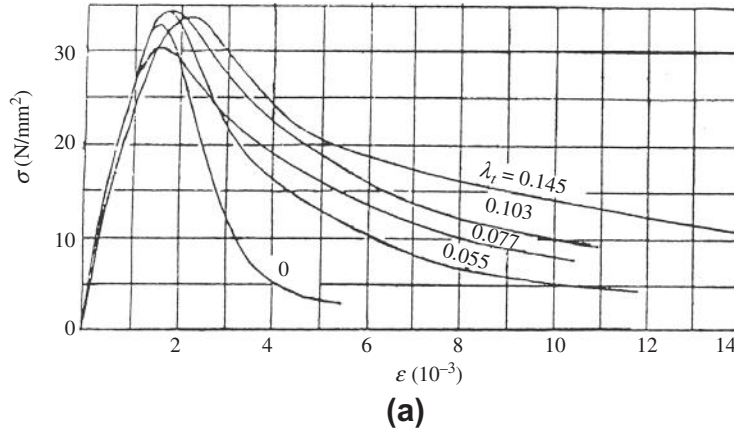


FIG. 9-3 Complete compressive stress—strain curves of concrete confined by rectangular tie: (a) ordinary tie [9-6], (b) composite ties [9-7]

Similarly, the confinement index for the rectangular tie in a member is also

$$\lambda_t = \mu_f \frac{f_{yt}}{f_c},$$

where μ_t is the volume rate of the transverse tie, i.e. the volume of the tie contained per volume of the confined concrete surrounded by the tie; f_{yt} and f_c are the tensile (yield) strength of tie and (uni-axial) compressive strength of concrete, respectively.

When the confinement index of the confined concrete is less ($\lambda_t \leq 0.3$), its stress—strain curve obviously has a peak and several characteristic points on it show the different mechanical stages (Fig. 9-4).

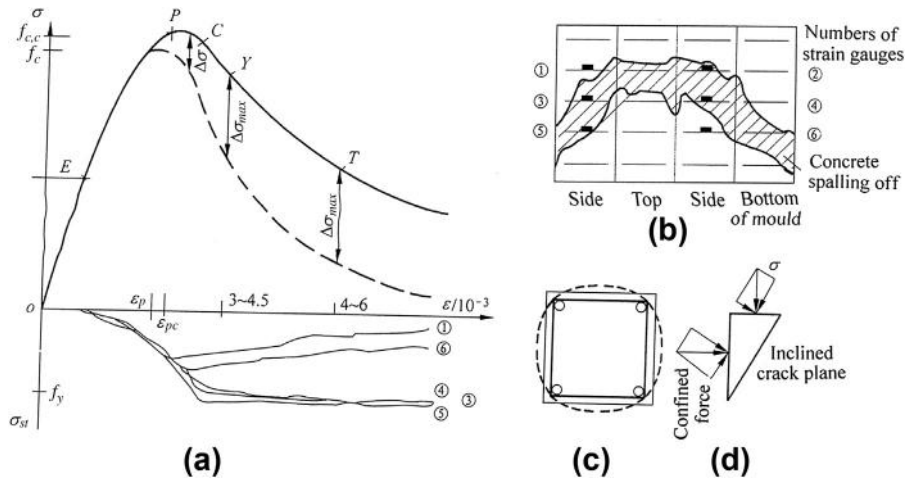


FIG. 9-4 Characteristic points on stress–strain curve of confined concrete ($\lambda_t \leq 0.3$):
 (a) stresses of specimen and tie, (b) cracks on four surfaces, (c) tie extruded, (d) equilibrium condition

The strain and stress of the specimen increase proportionally after loading. The plastic deformation of the concrete appears and the curve is slightly convex after the stress increases to $\geq 0.4f_{c,c}$ (Point E). When the stress is approaching the compressive strength of the plain concrete (f_c and $\epsilon_p = 1.5 - 1.7 \times 10^{-3}$), the strain of the tie is only $\epsilon_{st} = 0.4 - 0.6 \times 10^{-3}$ and its confinement action is limited, so the ascending branch of the stress–strain curve of the confined concrete approximates that of plain concrete. The peak (Point P) is reached as the stress increases slightly, the strain of the tie increases as well and reaches $\epsilon_{st} = 0.9 - 1.2 \times 10^{-3}$, but is not yielded yet. Therefore, the strength of the confined concrete increases ($>f_c$) with the confinement level of the ties.

The first vertical crack is visible (Point C) along the outside of the longitudinal reinforcement, as the stress–strain of the confined concrete is near the peak ($\epsilon = 0.85 - 1.11\epsilon_{pc}$). Afterwards, the crack expands and new cracks appear successively, so the residual strength of the concrete cover reduces, and the transverse strain of the confined concrete (ϵ') and the strain of the tie (ϵ_{st}) accelerate at the same time. After the longitudinal strain of the confined concrete reaches about $\epsilon = 3.0 - 4.5 \times 10^{-3}$ and the cracks run through the ties, some of them are yielding (Point Y) while the stress in other ties starts to descend. Therefore, the confinement of the tie on the confined concrete reaches the maximum at yielding of the tie, and the stress difference between the confined and plain concretes also reaches the maximum ($\Delta\sigma_{max}$, Fig. 9-4).

When the strain of the confined concrete reaches $\epsilon = 4 - 6 \times 10^{-3}$, the longitudinal short cracks link together and form an inclined critical crack (Point T). The ties passing through the critical crack are successively yielded, and their stresses keep

constantly (f_{yt}) while their strains increase further. Then, the core concrete protrudes out and presses the ties to horizontally bend outside (Fig. 9-4(c)), and the concrete cover starts to spall off and the longitudinal reinforcement and tie are exposed gradually. The sliding component of the longitudinal stress (σ) acted on the inclined crack is resistant by the component of the confined force of the tie and the residual shear strength of the concrete on the cracked plane (Fig. 9-4(d)), so a certain amount of residual strength still remains in the confined concrete.

When the specimen finally fails, the ties are yielded along the whole length one by one under the transverse compression of the core concrete, and some of them are even broken with a neck; the concrete cover is seriously cracked and spalled off; the longitudinal cracks distribute densely in the core concrete; and some pieces of mortar can be found but the coarse aggregate will not, generally, be broken on the critical inclined crack.

When the confined concrete is reinforced with more ties ($\lambda_t = 0.36 - 0.85$), the shape of the stress–strain curve (Fig. 9-3(b)) and the mechanical characteristics of it are different from that of the previous specimen with less tie ($\lambda_t \leq 0.3$). The slope of its ascending branch, i.e. the modulus of elasticity, may be smaller than that of the previous specimen, because the densely distributed ties may influence the casting quality of concrete cover and weaken the connection between the core and cover concretes. More ties surely strengthen the confinement of the core concrete, of which the triaxial compressive strength may be doubled and the peak strain (ϵ_{pc}) may be increased by ten times, or even more. And, the stress–strain curve of it ascends gradually, but has a flat terrace on the top instead of a sharp peak.

In addition, the longitudinal strains of the confined concrete ($\lambda_t \geq 0.36$) corresponding to the appearance of the first crack (Point C) and yielding of the tie (Point Y) approximate to that of the confined concrete with $\lambda_t < 0.3$, but both are smaller than the peak strain ($\epsilon \leq \epsilon_{pc}$), so both points are located on the ascending branch. When the confined concrete is failed, no critical inclined crack appears apparently, the longitudinal strain is considerable ($>10-30 \times 10^{-3}$) and the transverse deformation increases sharply, the ties protrude out like a circle and are exposed and few of them are broken, the longitudinal reinforcement is buckled and the concrete cover is almost totally spalled off, so the core concrete deforms greatly and protrudes locally. Therefore, the failure pattern of the concrete confined by the dense ties is similar to that confined by the spiral bar.

9.2.2 Working mechanism of rectangular tie

When the column with rectangular tie is acted on by a central compression, the straight part of the tie is bent horizontally (Fig. 9-5(a)) due to expansive deformation of the core concrete. As the flexural stiffness of the tie is less, its reaction, i.e. confined stress, on the core concrete is limited. On the other hand, the corner of the tie is stiff and deforms less, the concentrated force in the diagonal direction (45°) is composed of two tensions in perpendicular directions of the tie. Therefore,

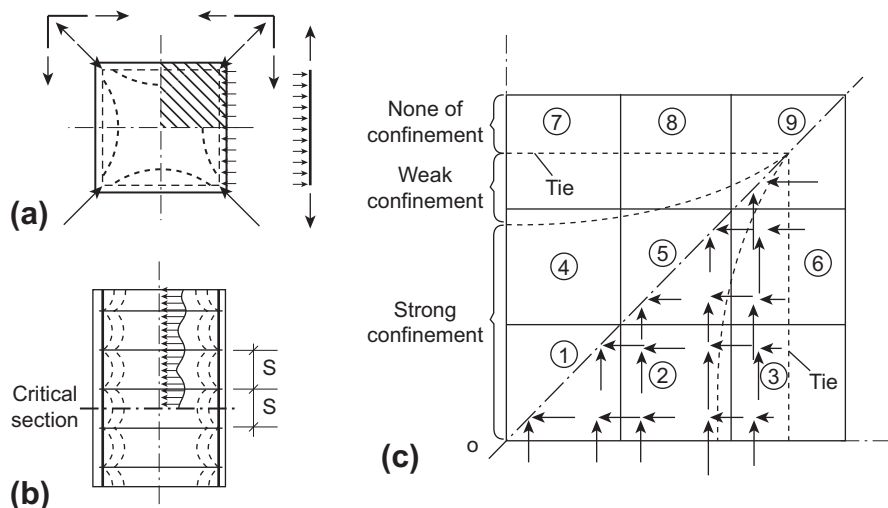


FIG. 9-5 Mechanical analysis of rectangular tie: (a) transverse, (b) longitudinal, (c) distribution of confined stresses [9-8]

the core concrete is strongly confined by the concentrated compressions at its corners and slightly confined by the distributed compression along its edges.

When the concrete column confined with rectangular (square) tie is loaded under longitudinal compression and is analyzed by the non-linear finite element method [9-8], the transverse stresses just before its failure distribute non-uniformly on the section and are shown in Fig. 9-5(c). The arrows on the figure show the direction and magnitude of the concrete stress of the section. The confined stresses are $\sigma_x = \sigma_y$ within the elements (1), (5), and (9) along the diagonal line, and they increase as the element nears its corner. However, the confined stresses are $\sigma_x \neq \sigma_y$ within the other internal elements (2) and (4), but their magnitudes are approaching that within the diagonal elements. When other elements having one or two edges exposed to outside are concerned, the confined stress is mainly acted in the direction of the tie in the element, e.g. σ_y within the elements (3) and (6) and σ_x within the elements (7) and (8), but the confined stress in another direction is less. The analysis of the stress distribution is consistent with the discussion above on the confinement of the tie.

The section of the column can be divided into three zones of different confinement level: (a) cover concrete (outside of the tie), i.e. the zone of none confinement; (b) middle part and the extensions towards the four corners, i.e. the zone of strong confinement, which is under triaxial compressive stress state ($\sigma_x \approx \sigma_y$) and this is the main factor causing an increase of strength of the confined concrete; (c) other zone between zones (a) and (b), i.e. the zone of weak confinement, which is located inside the straight parts of the tie and is basically under biaxial compressive stress state, so the strength enhanced there is limited. The area division of the

three zones depends first upon the quantity (λ_t), size and structural detail of the tie, and it also varies gradually as the central compression or deformation increases, i.e. zone of strong confinement reduces while the zone of weak confinement increases.

Usually, the ties are set up uniformly, i.e. with same distance (s), along the longitudinal axis of the column. The strongest confinement certainly occurs in the plane of the tie and the zone area of strong confinement reaches the maximum; while the weakest confinement occurs in the section between adjacent ties and the zone area of strong confinement reaches the minimum (Fig. 9-5(b)). The confined area and stress on other sections should be between the two sections. However, the ultimate strength of the column is only controlled by the weakest section, so the critical section should be the one between adjacent ties.

The strengthening of the rectangular ties on confined concrete varies with its quantity and structural detail as below.

Confinement index (λ_t). When more ties are reinforced in the column, larger confined stress is resulted in the core concrete and the compressive strength ($f_{c,c}$) and peak strain (ϵ_{pc}) of the confined concrete increases (Fig. 9-6). As introduced above, when the confined concrete with less tie ($\lambda_t \leq 0.3$) reaches the ultimate strength ($f_{c,c}$), the tie in it does not yield yet ($\epsilon_{st} < \epsilon_y$); while the ties in it are yielded already before the confined concrete with more ties ($\lambda_t \geq 0.36$) reaches the ultimate strength ($f_{c,c}$). Therefore, when the ultimate strength of confined concrete and the yield strength of the tie reach simultaneously, the corresponding boundary of confinement index should range between 0.3 to 0.36, and is about

$$\lambda_t \approx 0.32 \quad (9-11)$$

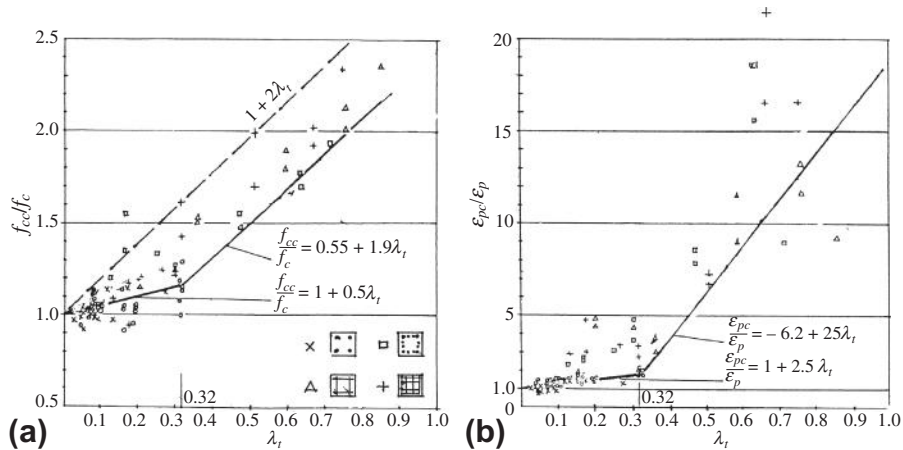


FIG. 9-6 Relations between behaviors and confinement index of confined concrete [9-7]:
(a) ultimate strength, (b) peak strain

from the experimental results. It is seen obviously in Fig. 9-6 that different variation rates are shown on both sides of $\lambda_t = 0.32$, i.e. $\lambda_t < 0.32$ and $\lambda_t > 0.32$.

It should be noticed that the coefficient in front of λ_t in Eq. (9-6) is 2 for the confined strength of the column with spiral bar, while the corresponding coefficient is less than 2 (Fig. 9-6(a)) for the confined strength of the rectangular tied column. It means that the confinement efficiency of the rectangular tie is far lower than that of the spiral bar.

Space of ties (s). This has influences on the confined area and stress of the critical section, i.e. the middle section between two adjacent ties. It is demonstrated experimentally [9-1,9-6] that the confinement is rather small if the space of ties is $s > 1.0 - 1.5b$ (where b is the width of the section). It is generally considered that the confinement is obvious only when $s < b$.

When the experimental results of two specimens with the same confinement index (λ_t) but different tie spaces (s and $2s$) are compared [9-7], the ascending branch of stress—strain curves, and compressive strengths ($f_{c,c}$) and peak strains (ϵ_{pc}) of both are less different, but the descending branch of the stress—strain curve of the specimen with the ties of smaller space (s) is obviously higher than that with the ties of larger space ($2s$). So, the ties with smaller space are favorable for ductility of the column.

Structural detail and shape of tie. The ties bound in a column are anchored well before failure of the column, and the confinement of it is not different obviously from that of the column with welded tie [9-6] (Fig. 9-7(a)).

The column of larger section is generally reinforced with more longitudinal bars and various composite ties are used (Fig. 9-7(b)). When the composite ties are horizontally bent under the compression of core concrete, their free lengths are shorter than that of the simple tie and the area of stronger confinement on the section is increased. Therefore, the strength and peak strain of the concrete confined with composite ties are slightly higher than that confined with the simple tie if the confinement indexes (λ_t) of both are equal, and also the ascending branch of the stress—strain curve of the former is flatter.

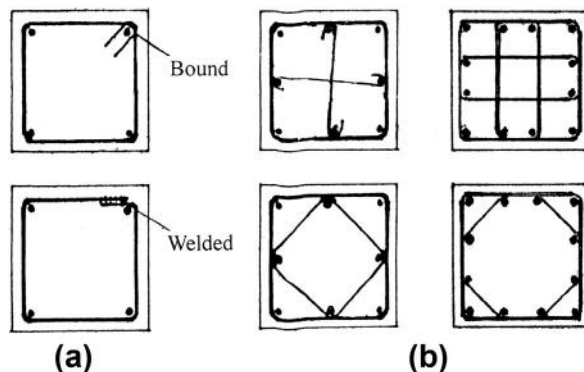


FIG. 9-7 Structural detail and shape of tie: (a) simple tie, (b) composite ties

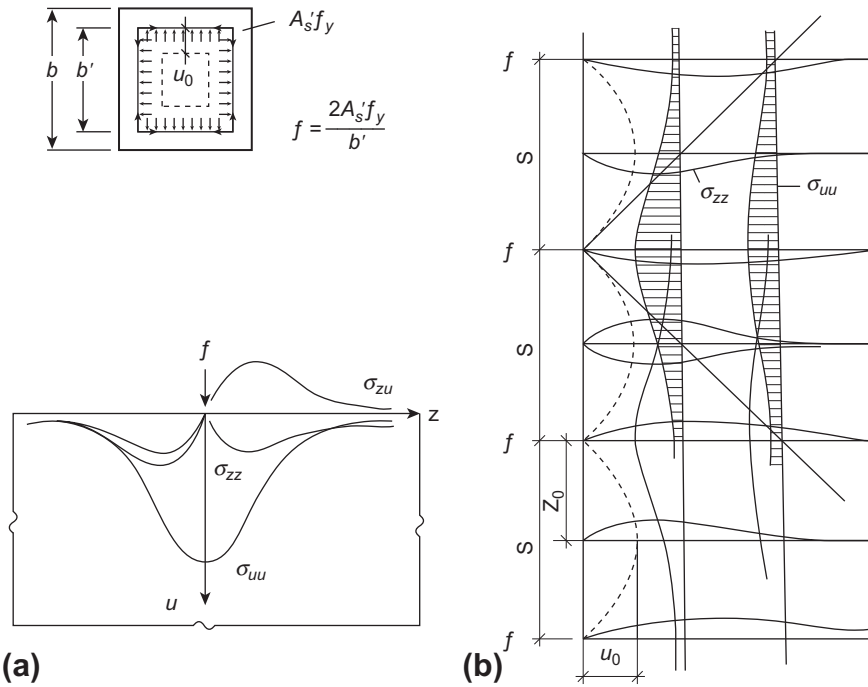


FIG. 9-8 Sargin model for confined concrete [9-4]

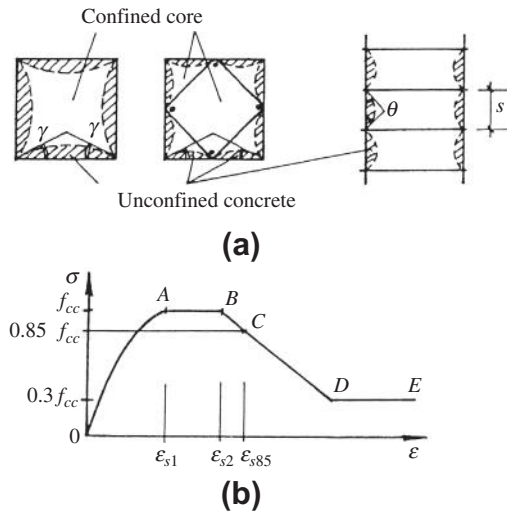


FIG. 9-9 Sheikh model for confined concrete: [9-11] (a) divisions of section, (b) complete stress-strain curve

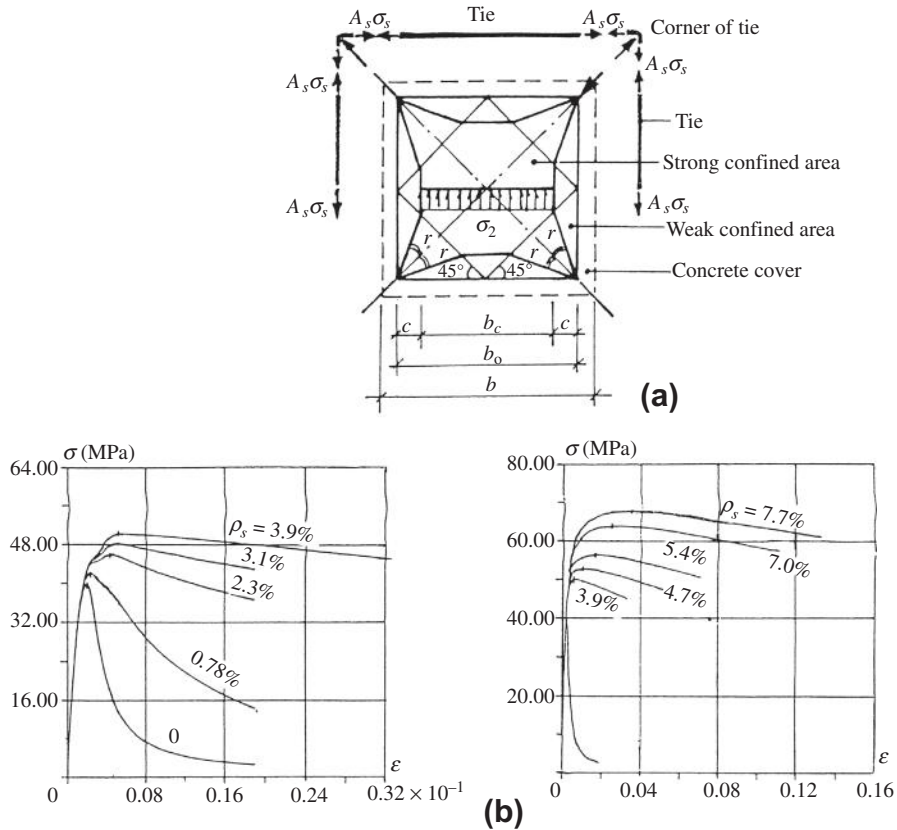


FIG. 9-10 Digital calculation following loading history [9-8]: (a) transverse calculation model, (b) calculated example ($b_0/b = 0.8$)

9.2.3 Equation for complete stress—strain curve

Several kinds of equations have been provided for the complete stress—strain curve of confined concrete and they are established in different ways, e.g. theoretical derivation, digital calculation, semi-theoretical and -empirical, and empirical ways. Some of the typical models are introduced below.

9.2.3.1 Sargin model (Fig. 9-8)

(1) It is assumed that the confined force (f) of the tie after yielded acts uniformly on the core concrete and its value is determined by the equilibrium condition. (2) The core concrete is considered as a semi-infinite elastic material and is acted on by the confined force (f) as a linear distributed load. The stresses in the concrete can be calculated by the Boussinesq equation, and the stress $\sigma_{uu} = 2fu^3/(\pi(z^2 + u^2)^2)$ among them is the transverse confined stress for core concrete, which varies with longitudinal

and transverse coordinates (z and u). (3) The minimum confined area $A_c = (b' - 2u_0)^2$ is called the critical core area and is located in the middle section between adjacent ties, in which the value of u_0 is solved from the condition of extreme value. (4) The triaxial compressive strength of the core concrete can be calculated by the Richart equation according to the confined stress of critical core section, and then the compressive strength of confined concrete is obtained:

$$f_{c,c} = f_c + \frac{16.4}{\pi} \rho'' f_y'' \frac{\xi^3}{(1 + \xi^2)^2} \quad (9-12)$$

where ρ'' and f_y'' are volumetric rate and yield strength of tie; $\xi = u_0/z_0$ is influence of tie space.

9.2.3.2 Sheikh model (Fig. 9-9)

(1) A section is divided into the effective confined core (area A_{eff}) and unconfined zones. The minimum area of the effective confined core (A_{ec}) appears on the middle section between adjacent ties. The parameters γ and θ and the areas A_{eff} and A_{ec} are given after regression analysis of the experimental data. (2) The compressive strength of the effective confined core concrete depends upon the volumetric rate of the tie (ρ_s) and its stress (f'_s) when the confined concrete reaches the ultimate state. When square ties are used and set up uniformly, the increasing coefficient of compressive strength of the core concrete is

$$\frac{f_{c,c}}{f_c} = k_s = 1 + \frac{B^2}{140P_{oc}} \left[\left(1 - \frac{nc^2}{5.5B^2} \right) \left(1 - \frac{s}{2B} \right)^2 \right] \sqrt{\rho_s f'_s}, \quad (9-13)$$

where B is the edge length of core area, n , c are the number and space of longitudinal reinforcement, respectively, s is the space of ties, and P_{oc} is the strength of core concrete if confinement is not taken into account.

(3) The complete stress-strain curve of confined concrete is given, and the ascending branch (OA) is a parabolic curve of second order and others (AB , BCD , and DE) are straight lines. The stress at point C is $0.85f_{c,c}$ and the residual strength is taken as $0.3f_{c,c}$, the strain values of the characteristic points (ϵ_{s1} , ϵ_{s2} , and ϵ_{s3}) are the functions of f_c , B , s , ρ_s , and f'_s , of which the calculation formulas can be found in reference [9-11].

Both constitutive models introduced above for confined concrete are based on the mechanical analysis and the main factors having influence on the confinement of tie are included. However, they are not analyzed following loading history and the basic assumption and mechanical model used are not totally reasonable. Therefore, they are used limitedly.

9.2.3.3 Digital calculation following loading history (Fig. 9-10)

(1) According to the distribution of confined stress on the section obtained from the non-linear finite element analysis (Fig. 9-5), the mechanical model for transverse stress analysis and divisions of different confinement on the section are suggested, the equilibrium condition of tie and confined concrete is derived, and the formula

for calculation of confined zone is given. (2) The tri- and uniaxial compressive stress—strain relations are determined respectively for the concretes in strong confined zone and unconfined zone including weak confined zone and cover, and the ratio between the transverse and longitudinal strains ($\varepsilon_2/\varepsilon$) of confined concrete is suggested. (3) The basic equations are established for the confined concrete:

$$\text{Strain } \varepsilon = \varepsilon_c = \varepsilon_n \quad (9-14a)$$

$$\text{Average stress } \sigma = (\sigma_c A_c + \sigma_n A_n) / b^2, \quad (9-14b)$$

where ε_c , σ_c , A_c are the longitudinal strain, stress, and area of the concrete in confined zone, respectively; ε_n , σ_n , A_n are corresponding values of the concrete in unconfined zone; b is the edge length of column section.

(4) These formulas consider the non-linear strain of concrete and some of them are coupled to one another, so the explicit solution of them is difficult to obtain.

Therefore, the digital calculation method is used and the computer program is compiled. When a longitudinal strain (ε) is given, the iterations are conducted following the predetermined flowchart [9-8] and all the equilibrium conditions, deformation compatibility, and constitutive relations of the materials are simultaneously satisfied, then the average stress on the section (σ), transverse strain (ε_2), stress of the tie (σ_{st}), confined stress of core concrete (σ_2), and other results are output. As the values of the longitudinal strain are input successively, the complete stress—strain curve and other physical quantities of the confined concrete are obtained. There is an example shown in Fig. 9-10(b), and the theoretical stress—strain curves agree well with the experimental ones.

9.2.3.4 Empirical formula

Several empirical stress—strain relations are suggested for the confined concrete, based on the regression analysis of relevant experimental results. They are presented in simple functions and are convenient for use in engineering practice.

The **Kent-Park model** is composed of an ascending curve and a descending branch of broken line (Fig. 9-11(a)). The compressive strength and peak strain of

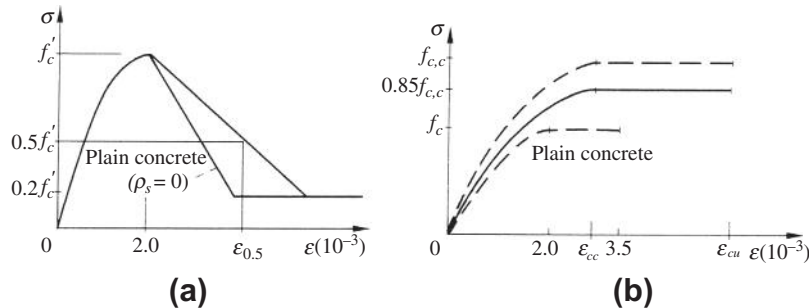


FIG. 9-11 Empirical constitutive models for confined concrete: (a) Kent-Part [9-12], (b) CEB-FIP Model Code [2-12]

the confined concrete are assumed to be the same as that of plain concrete ($f_{c,c} = f'_c$, $\varepsilon_{pc} = \varepsilon_p$). And, the ascending curve is also presented by the Hognestad formula: $y = 2x - x^2$ (Table 2-6), while the inclined line of the descending branch is determined by the strain at $\sigma = 0.5f'_c$:

$$\varepsilon_{0.5} = \left(\frac{20.67 + 2f'_c}{f'_c - 6.89} + \frac{3}{4} \rho_s \sqrt{\frac{b''}{s}} \right) \times 10^{-3} \quad (9-15)$$

where f'_c is the compressive strength of cylinder concrete (N/mm²), ρ_s is the volumetric rate of transverse ties to core concrete, which volume is calculated from outside to outside of tie, b'' is the width of confined core measured from outside to outside of tie, s is the longitudinal space of ties.

If $\rho_s = 0$ is taken in Eq. (9-15), only the first term remains on the right side, which is the corresponding strain in the descending branch of plain concrete (Fig. 2-14(c)). The last part of the descending branch is a horizontal line of residual strength $0.2f'_c$.

The **CEB-FIP Model Code model** (Fig. 9-11(b)) includes an ascending branch of parabolic curve of second order (Hognestad: $y = 2x - x^2$) and a horizontal line. The compressive strength and corresponding strain of the confiner concrete are calculated as below.

The confined stress of the tie acted on core concrete is (comparing with Eq. (9-5)):

$$\sigma_2 = \frac{1}{2} \alpha_n \alpha_s \lambda_t f_c. \quad (9-16a)$$

Two coefficients in it consider respectively the influences of the free length of tie or the number of longitudinal reinforcements (n) surrounded by tie and the distance (s) between ties:

$$\alpha_n = 1 - \frac{8}{3n}, \quad \alpha_s = 1 - \frac{s}{2b_0}. \quad (9-16b)$$

$$\text{when } \left. \begin{array}{ll} \sigma_2 \leq 0.05 f_c & f_{c,c} = f_c + 5\sigma_2 \\ \sigma_2 > 0.05 f_c & f_{c,c} = 1.125 f_c + 2.5\sigma_2 \end{array} \right\}$$

$$\varepsilon_{cc} = (f_{c,c}/f_c)^2 \times 2 \times 10^{-3} \quad (9-17)$$

$$\varepsilon_{cu} = 0.2 \frac{\sigma_2}{f_c} + 0.0035$$

The coefficient 0.85 in Fig 9-11(b) is introduced to consider the unfavorable influence of long-time loading.

Reference [9-7] suggests two sets of equation (Table 9-1) respectively for the stress-strain curve of confined concrete with different values of confinement index (λ_t). The ascending and descending branches are continuous at the peak point, and the values of the parameters in the equations are obtained from the experimental data at home (Fig. 9-6).

It should be mentioned that most of the constitutive models introduced above give only the stress-strain relation of confined core concrete surrounded by ties.

Table 9-1 Equations for Complete Stress–Strain Curve of Confined Concrete [9-7]

Confinement index	$\lambda_t \leq 0.32$	$\lambda_t > 0.32$
Compressive strength	$f_{c,c} = (1 + 0.5\lambda_t) f_c$	$f_{c,c} = (0.55 + 1.9\lambda_t) f_c$
Peak strain	$\epsilon_c = (1 + 2.5\lambda_t) \epsilon_p$	$\epsilon_{pc} = (-6.2 + 25\lambda_t) \epsilon_p$
Equations	$x \leq 1.0 \quad y = \alpha_{a,c} + (3 - 2\alpha_{a,c})x^2 + (\alpha_{a,c} - 2)x^3$	$y = \frac{x^{0.68} - 0.12x}{0.37 + 0.51x^{1.1}}$
$x = \epsilon/\epsilon_p, y = \sigma/f_{c,c}$	$x \geq 1.0 \quad y = \frac{x}{\alpha_{d,c}(x - 1)^2 + x}$	

Note: $\alpha_{a,c} = (1 + 1.8\lambda_t)\alpha_a$ and $\alpha_{d,c} = (1 - 1.75\lambda_t^{0.55})\alpha_d$ when the concrete is C20–C30, and α_a and α_d are the parameters for stress–strain curve of plain concrete (Table 2-7).

When the average stress–strain relation of a column is concerned, the average stress should be converted by Eq. (9-14), as the concrete outside of the tie, i.e. cover, is also considered. When the column has small section and the area of cover concrete occupies a great fraction of total section area, or the column is reinforced with less tie and the behaviors of the concretes within and outside of the tie are less different, the influence of cover concrete is not negligible.

The experiments of tie confining concrete under repeated load show that the deformation, cracking, and failure process of the specimen are similar to that under monotonic load, and its compressive strength ($f_{c,c}$) and peak strain (ϵ_{pc}) vary with the confinement index (λ_t) and are not obviously different from that of the latter. In addition, the envelope of stress–strain curve and the loci of common and stability points of the confined concrete are also similar to that under monotonic load, and the average ratios of similarity are:

$$\text{Locus of common point } \bar{K}_c = 0.893,$$

$$\text{Locus of stability point } \bar{K}_s = 0.822. \quad (9-18)$$

Comparing with the corresponding ratios for plain concrete (Eqs. (3-1) and (3-2)), \bar{K}_s of the confined concrete is slightly higher. The equations of stress–strain curve for tie confining concrete under repeated load can be found in detail in reference [9-13].

9.3 Steel-tube-confined concrete

9.3.1 Mechanical characteristic and mechanism

If the spiral bar in a concrete column is very closely spaced, and it is combined with the longitudinal reinforcement and the cover concrete is cancelled, the steel-tube-confined concrete or the concrete-filled steel tube is then formed. This is a special example of confined concrete.

Steel-tube-confined concrete has superior mechanical properties of high strength and better ductility, and also has many engineering advantages, such as smaller

sectional area, less weight (dead load), easy construction of structural joint, free of mold, without processing of reinforcement, quickly manufacturing, and reducing concrete quantity. Compared with steel structures, steel-tube-confined concrete has obvious advantages, including less steel consumed, greater stiffness, and less cost. Recently, steel-tube-confined concrete column is used widely in structural engineering and is frequently applied for the column carrying large axial load, for example, in high-rise buildings, single- and multi-storey workshops, frames of industrial equipment (e.g. iron-smelting furnaces, boilers for electrical power plants), underground engineering (e.g. railways, markets), arched bridges, and defense works. Better technical and economical benefits have been achieved so far.

Steel-tube-confined concrete member has been used in engineering practice for several decades and many theoretical and experimental investigations have been reported at home and abroad. [9-14–9-21] The typical mechanical behavior of short column ($L/D \leq 4$) of steel-tube-confined concrete under central compression is introduced below. The short column under eccentric compression, bending, shearing, torsion, and composition of bending-shearing-torsion, steel tube of non-circular section, and long column ($L/D > 4$) of steel-tube-confined concrete are also investigated and can be found in relevant references.

The main parameter of steel-tube-confined concrete is also the confinement index used for spiral column (Eq. 9-4), but using different calculation formula:

$$\lambda_t = \mu_t \frac{f_y}{f_c} = \frac{A_s f_y}{A_c f_c} \approx \frac{4t f_y}{d_c f_c} \quad (9-19)$$

where A_s , t are the sectional area and thickness of steel tube, respectively; A_c , d_c are the area and diameter of core concrete, respectively.

When $d_c \gg t$, μ_t approximates $4t/d_c$. Generally, the volumetric rate of steel tube ranges from $\mu_t = 0.04 - 0.20$, so $\lambda_t = 0.2 - 4.0$.

The typical axial force (average stress)—strain curve of short column of steel-tube-confined concrete under central compression is shown in Fig. 9-12, on which the mechanical characteristics of different stages are presented.

The specimen is within the elastic stage ($\sigma/f_{c,c} \leq 0.3 - 0.5$, segment OA on the curve) after being loaded, and the longitudinal stresses of the steel-tube-filled concrete are not high. The radial expansion of the steel tube is slightly greater than that of the filled concrete as the Poisson's ratio of steel is greater than that of concrete, so the latter is in radial tension if both are adhered well. At this time, the steel tube acts together with the filled concrete like the longitudinal reinforcement.

The longitudinal stress of the steel-tube-confined concrete is increased further and its strain accelerates as the load is increased, so the $N-\varepsilon$ curve is slightly convex then. When the radial deformation or Poisson's ratio of the concrete is greater than that of the steel tube, the concrete exerts the radial compressive stress (σ_r in Fig. 9-13(a)) on the steel tube. Therefore, the steel tube also carries a uniform tensile stress in tangent direction (σ_t) besides the longitudinal compressive stress (σ_z). However, the radial compressive stress is limited comparing with the stresses in the other two directions ($\sigma_r \ll \sigma_z, \sigma_t$).

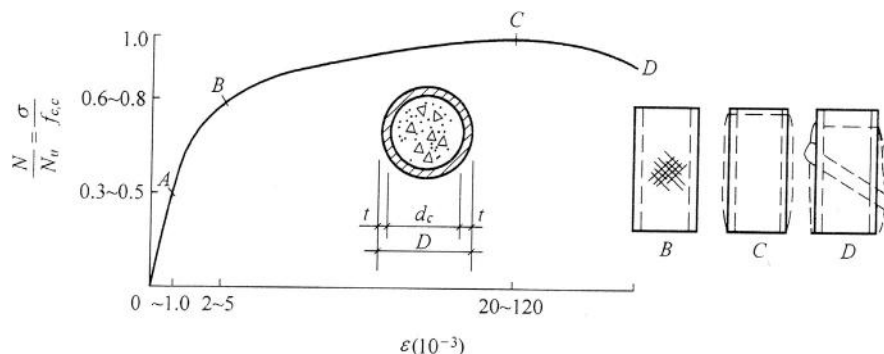


FIG. 9-12 Axial force—strain curve of steel-tube-confined concrete [9-18]

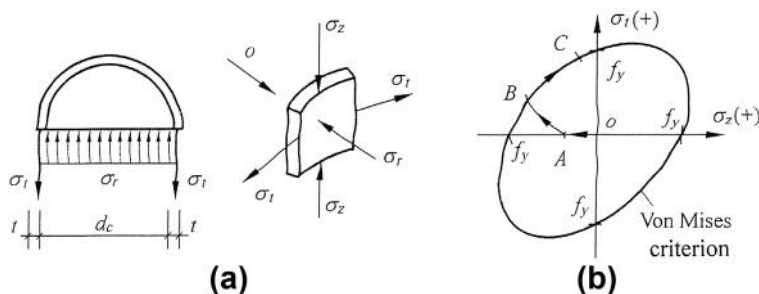


FIG. 9-13 Stress state and path of steel tube [9-18]: (a) stress state, (b) failure envelope and stress path

When the steel tube is initially yielded under common actions of the longitudinal and tangent stresses (Point *B*), the stress path experienced is *AB* in Fig. 9-13(b). During this, the core concrete is under a triaxial compression state but does not yet fail ($\sigma_r, \sigma_r, \sigma_c < |f_3|$). However, the yielding lines (or shear sliding lines in Fig. 9-12) appear on the surface of the steel tube, but no other change is obviously found on appearance of the specimen.

The steel tube enters the plastic stage (*BC*) afterwards ($N/N_u \geq 0.6-0.8$). The longitudinal deformation of the specimen increases quickly and the stresses of the steel tube move along the yield envelope (Von Mises criterion is generally taken, Fig. 9-13(b)), as the axial force increases slowly. It means that the longitudinal compressive stress (σ_z) reduces, while the tangent tensile stress (σ_t) increases. Although the longitudinal stress of the steel tube is reduced, the tangent stress enhances the confined stress ($\sigma_r = 2t\sigma_t/d_c$) acted on the core concrete, of which the triaxial compressive strength is, then, increased considerably. Therefore, the total strength of the specimen increases further.

When the axial force acted on the steel-tube-confined concrete reaches the maximum (Point *C*), the ultimate compression (strength N_u) is obtained. Then, the

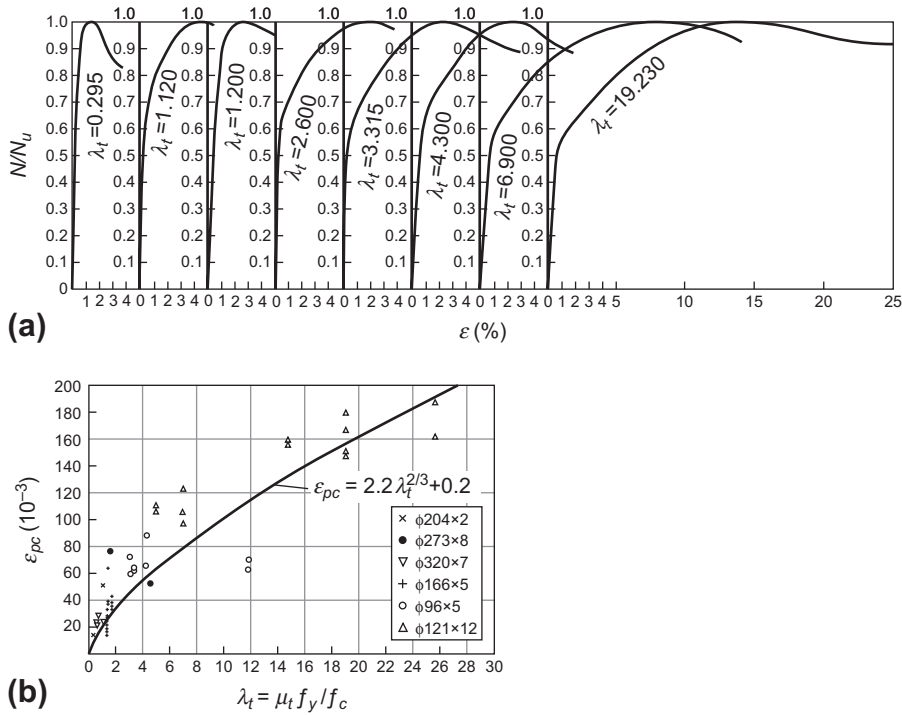


FIG. 9-14 Influence of confinement index on behavior of steel-tube-confined concrete [9-18]: (a) $N/N_u - \epsilon$ curve, (b) peak strain

longitudinal stress of the core concrete exceeds the triaxial compressive strength and reduces slowly, so the total strength of the specimen reduces gradually and a descending branch of $N-\epsilon$ curve is formed. Finally, the specimen is failed apparently in local buckling or convex (Point D in Fig. 9-12).

The axial force (stress)—strain curve and the peak strain of the steel-tube-confined concrete vary with the confinement index (λ_t) and are shown in Fig. 9-14. The higher the confinement index, the greater the plastic deformation (BC) after initial yielding of the steel tube, and the smaller the slope of the curve. The peak strain of steel-tube-confined concrete is so great and almost the same order as that of mild steel (Fig. 6-4 and Table 6-1). It demonstrates that the ductility of the steel-tube-confined concrete under compression is significant.

9.3.2 Calculation of ultimate strength

The ultimate compressive strength, i.e. average confined strength ($f_{c,c}$), of steel-tube-confined concrete increases with the confinement index and the relevant

experimental results are shown in Fig. 9-15. The basic calculation formula is theoretically established:

$$f_{c,c} = \frac{N_u}{A_c} = \frac{1}{A_c} (\sigma_{cp} A_c + \sigma_{zp} A_s), \quad (9-20a)$$

where the sectional areas of the core concrete and steel tube are respectively:

$$\left. \begin{aligned} A_c &= \frac{\pi}{4} d_c^2 \\ A_s &= \frac{\pi}{4} (D^2 - d_c^2) \approx \pi d_c t = \mu_t A_c \end{aligned} \right\} \quad (9-21)$$

σ_{cp} and σ_{zp} are the longitudinal compressive stresses of core concrete and steel tube under ultimate axial force (N_u), respectively.

The lateral confined compressive stress of the core concrete is $\sigma_r = 2t\sigma_{tp}/d_c = \mu_t \sigma_{tp}/2$, and its triaxial compressive strength is correspondingly presented as

$$\sigma_{cp} = f_c [1 + c(\sigma_r)] = f_c [1 + c'(\sigma_{tp})], \quad (9-22)$$

where c or c' are the coefficient depending upon σ_r or σ_{tp} and

$$c(\sigma_r) = 1.5 \sqrt{\sigma_r / f_c} + 2\sigma_r / f_c \quad (9-23)$$

is suggested in reference [9-18], σ_{tp} is the tangent tensile stress (strength) of steel tube during N_u and the relation between σ_{tp} and longitudinal compressive stress

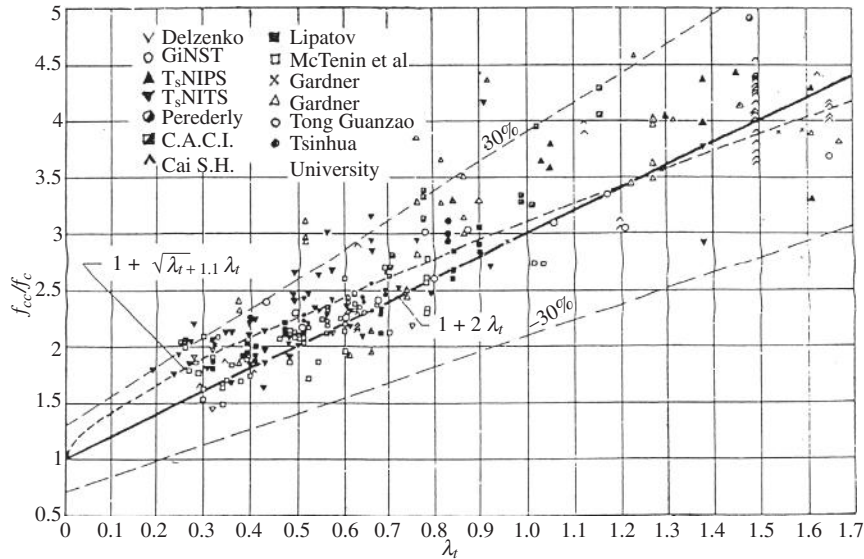


FIG. 9-15 Ultimate strength of steel-tube-confined concrete [9-20]

(σ_{zp}) following Von Mises criterion for steel under the biaxial stress state (Fig. 9-13(b)):

$$\sigma_{tp}^2 + \sigma_{zp}^2 + (\sigma_{tp} - \sigma_{zp})^2 = 2f_y^2. \quad (9-24)$$

After these formulas are substituted into Eq. (9-20),

$$\left. \begin{aligned} \text{or } f_{c,c} &= f_c \left[1 + c' \left(\sigma_{tp} \right) + \lambda_t \frac{\sigma_{zp}}{f_y} \right] \\ f_{c,c} &= f_c [1 + \alpha \lambda_t] \end{aligned} \right\} \quad (9-20b)$$

is obtained after being simplified.

There are two extreme conditions for steel-tube-confined concrete and the extreme values of ultimate compressive strengths are as below.

(1) The steel tube and core concrete reach simultaneously their own uniaxial compressive strengths in longitudinal direction, i.e. $\sigma_{zp} = f_y$ and $\sigma_{cp} = f_c$, while the tangent stress of the steel tube is $\sigma_{tp} = 0$ and, hence, the confined stress is zero ($\sigma_r = 0$). Therefore, the ultimate strength is:

$$f_{c,c,1} = f_c(1 + \lambda_t). \quad (9-25a)$$

(2) When the tangent stress of the steel tube reaches yield strength ($\sigma_{tp} = f_y$, but $\sigma_{zp} = 0$), the confined stress of the core concrete is the maximum ($\sigma_{r,max} = \mu_t f_y / 2$). Therefore, the ultimate strength is:

$$f_{c,c,2} = f_c(1 + \alpha_{max} \lambda_t). \quad (9-25b)$$

If $c(\sigma_r)$ in Eq. (9-22) is taken from the Richart formula (Eq.(9-6)), $\alpha_{max} = 2$ is derived.

The ultimate strength (N_u) of any steel-tube-confined concrete with a certain confinement index (λ_t) should be between the two extreme values and the ultimate stress state is also between the two extreme conditions. When Eq. (9-20b) is differentiated with respect to σ_{zp} or σ_{tp} and let to be zero, the stresses of the steel tube (σ_{zp} and σ_{tp}) under ultimate state are calculated (Fig. 9-16(a)). And, the parameter α varying with the confinement index (λ_t) is obtained (Fig. 9-16(b)):

$$\alpha = 1.1 + \frac{1}{\sqrt{\lambda_t}}. \quad (9-26a)$$

After the formula is substituted into Eq. (9-20b), the calculation formula of ultimate strength is established for steel-tube-confined concrete:

$$f_{c,c} = f_c \left[1 + \sqrt{\lambda_t} + 1.1 \lambda_t \right]. \quad (9-26b)$$

The theoretical values and experimental data are compared in Fig. 9-15 and Fig. 9-16(b).

The calculated results show that the tangent stress of the steel tube reaches uniaxial tensile strength ($\sigma_{tp} = f_y$) and the longitudinal stress of it is $\sigma_{zp} = 0$ under

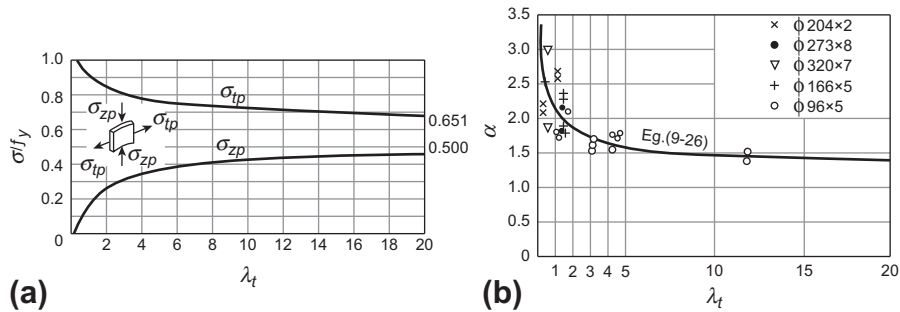


FIG. 9-16 Stresses and parameter value of steel tube under ultimate state [9-18]: (a) stresses of steel tube, (b) parameter α

ultimate state, only when the confinement index of steel-tube-confined concrete is rather small ($\lambda_t < 0.28$); the tangent stress (σ_{tp}) of the steel tube decreases and the longitudinal stress (σ_{zp}) of it increases under ultimate state, as the confinement index (λ_t) increases or the steel tube is strengthened. The convergent values of the stresses of the steel tube are $\sigma_{tp} = 0.651f_y$ and $\sigma_{zp} = 0.5f_y$, if the confinement index (λ_t) increases infinitely.

When the complete axial force (stress)—strain process is needed, the digital calculation should be conducted, or the general method of plasticity is used and the multiaxial constitutive relations of the steel and core concrete are introduced.

9.4 Local compression

9.4.1 Mechanical characteristic and mechanism

When a compression is transferred from one member to another in a structural system, the acted area of the concentrated load (A_l) is frequently smaller than the end or sectional area of the supporting member (A_b). There are many examples in engineering practice, e.g. a beam supported on top of a wall or column, a column supported on a base, a bridge supported on a pier, an anchorage plate of a prestress tendon supported on the end of a member, even the compression zone of a cracking section of a flexural member (Fig. 9-17(a)). These phenomena ($A_l < A_b$) are called local compression or bearing strength.

The shape of local area (A_l) acted with concentrated load is, most likely, rectangular or strip (its one side equals one edge of the supporting area). The local area may be located on the center (symmetric), middle (eccentric), edge or corner of the end surface of the supporting member (Fig. 9-17(b)). In addition, the end of the supporting member may be reinforced with spiral bar or welded wires (Fig. 9-17(c)) to strengthen the compressive strength of the confined concrete and to limit the crack, which would occur there.

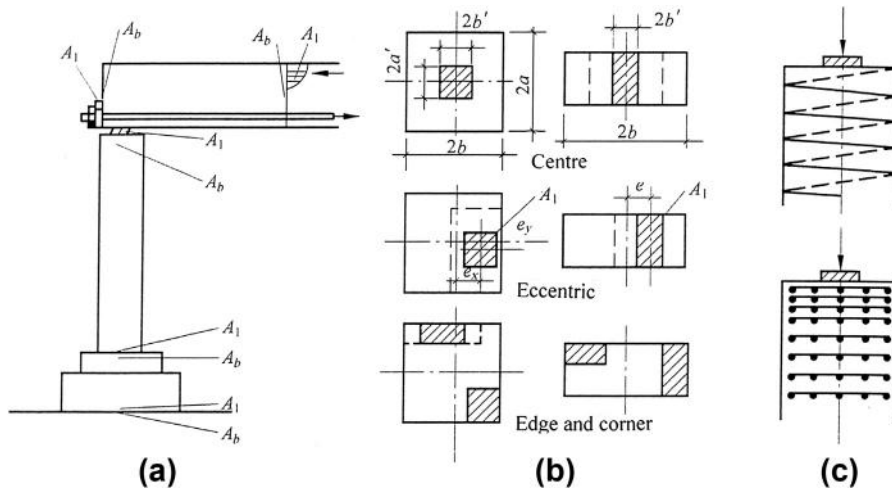


FIG. 9-17 Situations of local compression: (a) engineering example, (b) positions of compressed area, (c) local reinforcement

When the concentrated load is transferred to the supporting member via the local area (A_l), the stress and the strain of the concrete underneath are greater, so it is confined by the surrounding concrete within the area ($A_b - A_l$), which does not directly transfer the load. Therefore, the compressive strength of the local concrete within A_l is increased to some extent ($f_{cb} > f_c$). This phenomenon has been theoretically and experimentally investigated for many years at home and abroad, [9-22–9-29] and the research results have been adopted in the design codes of various countries.

A square column under the action of local compression is used here as a typical example to explain the mechanical characteristic and failure process (Fig. 9-18). Assuming the edge length of its section is $2b$ and the compression is acted on the local square area of edge length $2b'$, the part of the column outside of $\geq 2b$ from the loaded end can be considered being a uniform uniaxial compressive stress state, according to the San Venient Principle. However, a complicated stress state should exist near the loaded end within the range of $H \leq 2b$. The loci of principal stress obtained from elastic analysis are shown in Fig. 9-18(a): the vertical compressive stress (σ_z) decreases gradually along the central line from top to bottom; the horizontal stresses ($\sigma_x = \sigma_y$) are compressive on the upper part but change into tensile on the lower part, and the maximum tensile stress appears at $H = (0.6-1.0)b$ (Fig. 9-18(b)).

The compressed end of the column can be divided into three zones of different stress states: (1) Zone I is directly located under the loaded area ($2b' \times 2b'$), and the concrete there is expanded horizontally under the longitudinal compression but is confined by the surrounding concrete (zone II), so a triaxial compressive stress state is formed; (2) Zone II is the concrete surrounding zone I and carries the horizontal tensile stress due to the compression from zone I, so a bi- or triaxial

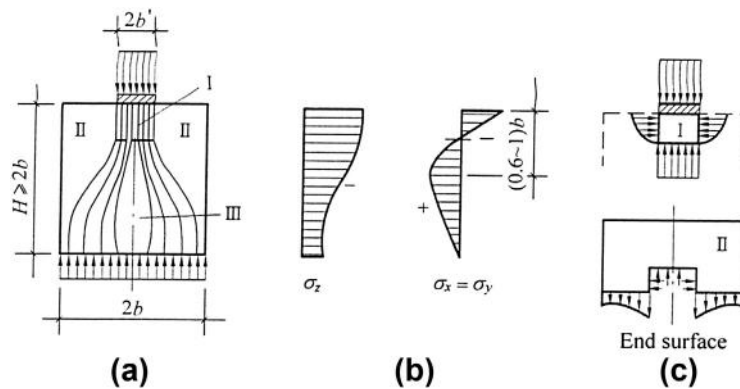


FIG. 9-18 Stress distribution on local compression end: (a) loci of principal stress and stress zone, (b) stress distribution along central line, (c) forces on zones I and II

tensile-compressive stress state is formed; (3) Zone III is within the scope of principal compressive stress loci and is of a triaxial tensile-tensile-compressive stress state. The shape, size, and stress value of these zones depend upon the shape of the column, area ratio (A_l/A_b), and position of local compression, and they decide the cracking, failure process, and local compressive strength (or bearing strength f_{cb}).

When the height of the column (or specimen) is greater than twice the width of its section ($H \geq 2b$), the local compressive strength of concrete and the subsiding deformation (δ) of the loaded surface increase monotonically with the area ratio (A_b/A_l), and three typical failure patterns may appear (Fig. 9-19) as follows.

1. Area ratio $A_b/A_l < 9$. After the specimen is loaded, the first crack appears vertically on the middle of the side surface and near the maximum tension in the upper part of zone III. The ratio between the cracking and ultimate loads is about 0.6–1.0 (see Fig. 9-22), and the greater the area ratio (A_b/A_l), the later the cracking. When the load is increased further, the crack widens and develops both downwards and upwards. Finally, the crack passes through, and the specimen is failed in splitting. However, the loaded area is not split as the friction and confinement exist under the load plate. Usually, a reversed pyramid is formed underneath the loaded area.
2. Area ratio $9 < A_b/A_l < 30$. After the specimen is loaded continuously, it is failed suddenly and split into several pieces once a crack occurs. The cracking load equals or is approaching the ultimate load (strength). When the test is observed very carefully, the crack starts first on the loaded surface and extends quickly downwards. It is seen that the failure of the specimen is controlled by the horizontal tensile stress in zone II and is caused by the compression outside of the concrete in zone I. However, the concrete underneath the loading plate is not split, but a reversed pyramid is also formed there.
3. Area ratio $A_b/A_l > 30$. The concrete volume (zone II) surrounding the loading plate is great enough and will not be split, as only low tensile stress is caused

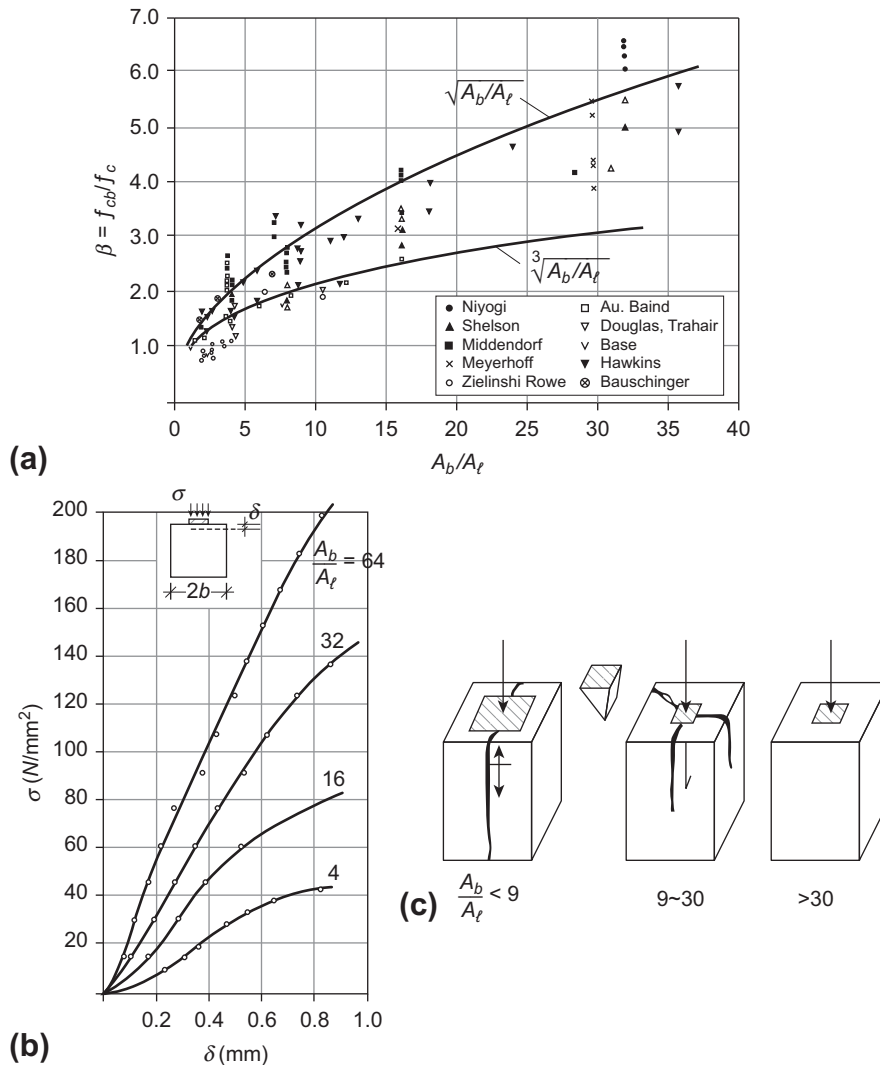


FIG. 9-19 Strength, deformation, and failure patterns of concrete under local compression: (a) ultimate strength [1-1], (b) deformation [9-29], (c) failure patterns ($H \geq 2b$)

there due to the local compression. The concrete underneath the loading plate (zone I) carries large triaxial compressive stresses, it makes the loading plate subside and the concrete shear off along the periphery of the plate, even some coarse aggregates are compressed and pulverized. Sometimes, the concrete near the loading plate is crushed and extruded out, just like the semi-infinite soil loses stability under a foundation. If the area ratio (A_b/A_l) is increased further, the local compressive strength of concrete converges gradually (Fig. 9-19(a)).

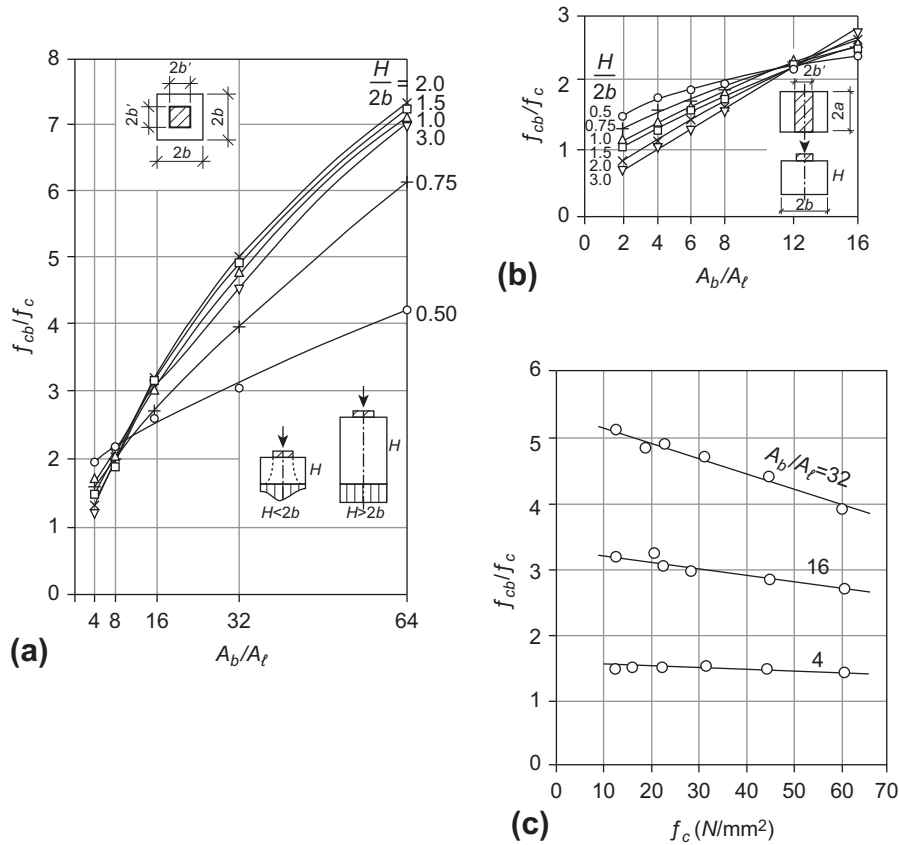


FIG. 9-20 Influences of main factors on local compressive strength: (a) height–width ratio (modified from reference [9-29]), (b) strip load [9-29], (c) strength of concrete [9-32]

Other factors having influences on the strength and failure pattern of concrete under local compression include the height–width ratio ($H/2b$) of the specimen, position and shape of loaded area, uniaxial compressive strength of concrete, size effect, pad material at the bottom, and quantity and detail of local reinforcement. These are discussed briefly below.

Generally, the height of the structural member under local compression is far greater than the sectional width ($H \gg 2b$) in engineering practice, while the height of the specimen tested is usually smaller ($H \leq 2b$). When the height–width ratio of the specimen is in the range of $H/2b = 1 - 3$, the stress distribution within the scope of $H = 2b$ varies less, and the local compressive strength–area ratio ($f_{cb} - A_b/A_t$) curves vary approximately (Fig. 9-20(a)). Therefore, the experimental results obtained from the specimens can be used for the structural member of $H/2b > 3$.

However, when the height of the specimen is smaller than the width ($H/2b < 1$), the reaction on its bottom is not uniformly distributed and the compressive stress in the

specimen concentrates more near the central line, so the crack occurs first at the bottom and develops upwards or the concrete surrounding the loading plate is split and fails [9-23,9-29]. The mechanical characteristic and failure pattern of the specimen are different from that under local compression introduced above, but are similar to the punching of a thin slab (see Section 14.4). The 'local compressive strength' of the specimens of $A_b/A_l > 10$ decreases quickly with the height (or $H/2b$) of the specimen.

When a compression is acted locally on a strip area of a specimen (Fig. 9-20(b)), a triaxial compressive stress state occurs only in a small area near the central part under the loading plate, but most of the specimens are of biaxial stress state and have less confinement on the loaded zone, comparing with the bidirectional confinement of the rectangular loading area (Fig. 9-20(a)). Therefore, the local compressive strength of the specimen increases with smaller amplitude. Generally, the specimen is failed due to the vertical crack occurring on the side surface, and the number and shape of the crack vary with the loading area (b'/b), which can be found in references [9-29] and [9-30].

When the loading area is deviated from the central line, even near the edge or corner, of the end surface of the supporting member (Fig. 9-17(b)), the stress distribution and confinement level of the concrete underneath are influenced and the local compressive strength reduces to a certain extent. This can be approximately treated during design: an effective supporting area (A_b) [9-31, 9-26] is taken based on the local compressed area (A_l), following the principles of concentricity and symmetry, and then the local compressive strength is calculated considering the confinement.

When the concrete of higher strength grade is used, the plastic deformation (Section 4.1) and relative value of triaxial strength (Section 5.2.3) reduce slightly, hence the increasing amplitude of local compressive strength decreases gradually (Fig. 9-20(c)) [9-32,9-33].

If the size of the specimen is increased but the shape and area ratio (A_b/A_l) are kept constant, the relative value of local compressive strength (f_{cb}/f_c) decreases [9-32]. This is consistent with the size effect for other mechanical behaviors of concrete.

When various transverse reinforcement (Fig. 9-17(c)) is set up within the concrete compressed locally, the development of internal crack is limited and the confined stress of the core concrete is enhanced, so the local compressive strength is obviously increased [9-26,9-34]. This is a major technical measure to improve the behavior of local compression. The working mechanism is similar to the concrete confined by the spiral bar or rectangular tie, and the detail and calculation method can be found in relevant references or design codes.

9.4.2 Calculation of strength

There are different ways to determine the local compressive strength of concrete. Of course, when the non-linear finite element method is used for analysis of three-dimensional structure following the loading history, the cracking load, development of crack, failure pattern, and local compressive strength of concrete can be obtained accurately. Generally, the local compressive strength of concrete does not need such

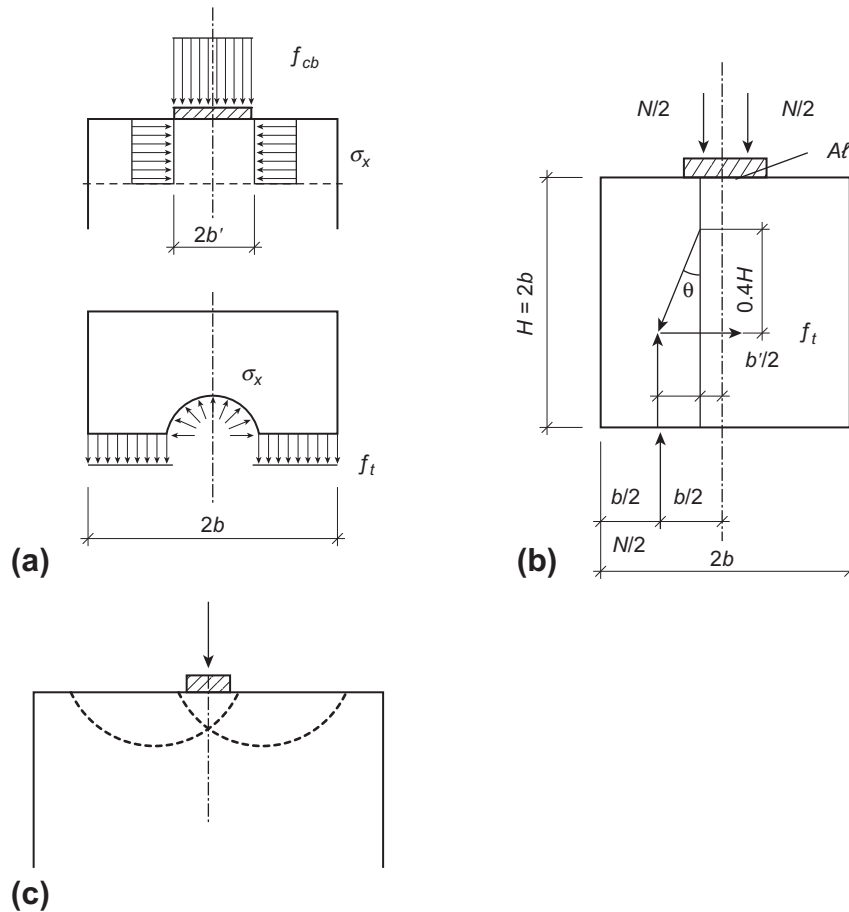


FIG. 9-21 Mechanical model for calculation of local compressive strength [2-12]:
(a) expanded splitting on top, (b) cracking at lower part of concrete, (c) crushing and losing stability on top

complicated calculation, and an approximate calculation of the simple mechanical model, even an empiric formula, is used for checking the calculation.

9.4.2.1 CEB-FIP model code model (Fig. 9-21)

Three possible failure patterns are separately checked as below.

1. Expanded splitting on top. The concrete under the loading plate is under triaxial compressive stress state and expands outside, so tensile stress is caused in the surrounding concrete (zone II). When the stress reaches the tensile strength of concrete there, the maximum confined stress (σ_x) and the corresponding local compressive strength (f_{cb}) can be calculated.

2. Cracking at lower part. The locus of the principal stress is simplified into a broken line within the scope of $H = 2b$ from top, and the horizontal tensile force $F_t = N \tan \theta / 2$ is obtained which is used to check the tensile strength of the concrete or splitting of the specimen, or to calculate the transverse reinforcement if necessary.
3. Crushing and losing stability. An empiric formula is suggested to prevent the concrete under the loading plate being crushed or subsided too much, if the local compressed area is too small.

After analyzing and simplifying, three calculation formulas are concluded and should be satisfied simultaneously:

$$\left. \begin{aligned} f_{cb} &= f_c \sqrt{A_b/A_l} \\ f_{cb} &= 1.92 f_t / \left[\frac{b'}{b} \left(1 - \frac{b'}{b} \right) \right] \\ f_{cb} &= 79 \sqrt{f_c} \leq 5 f_c \end{aligned} \right\} \quad (9-27)$$

9.4.2.2 Hawkins model [9-27,9-28]

It is suggested that a wedged pyramid of concrete is formed under the loading plate and moves downwards under the local compression during failure of the specimen, so the surrounding concrete is compressed transversely and tensile stress is caused along the ring direction which results in splitting of the specimen. The shear sliding surface of the pyramid is calculated by the Coulomb criterion, and then the calculation formula is established for the local compressive strength of concrete.

9.4.2.3 Empiric formulas

In the 19th century, Bauschinger (Germany) had suggested the calculation formula for the increasing coefficient of local compressive strength [1-1], basing on the experimental results of the cubic specimen (edge length 100 mm) of natural sandstone under local compression:

$$\beta = \frac{f_{cb}}{f_c} = \sqrt[3]{\frac{A_b}{A_l}}. \quad (9-28)$$

Many experiments have been conducted on local compressive strength of concrete at home and abroad since 1950 and they show that the theoretical value of Eq. (9-28) is obviously lower than the experimental data (Fig. 9-19(a) and Fig. 9-22). A calculation formula was derived based on the equilibrium condition during ultimate state [9-26], and a similar formula was adopted in some design code [9-35]:

$$\beta = \sqrt{A_b/A_l}. \quad (9-29)$$

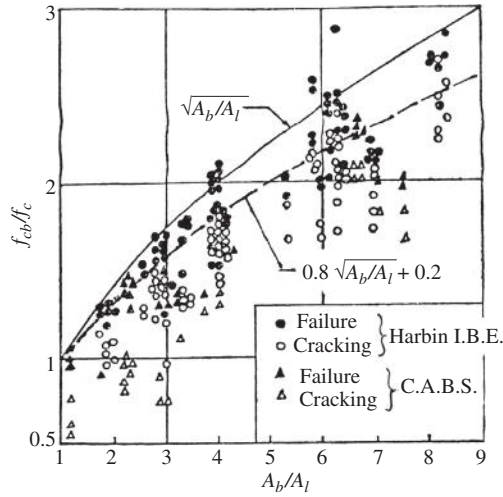


FIG. 9-22 Experimental results of local compression of concrete in China [9-31]

In addition, a lower calculation value is also suggested afterwards:

$$\beta = 0.8\sqrt{A_b/A_l} + 0.2 \quad (9-30)$$

In reference [9-29], the calculation formulas of increasing coefficient of concrete strength are also suggested for the structural member of square section ($b \times b$) under the central compression acted on different rectangular loading plates ($a' \times b'$):

Rectangular loading plate ($a' < b'$):

$$\beta = 0.42\left(\frac{b}{a'} + \frac{b}{b'} + 1\right) - 0.29\left[\left(\frac{b}{a'} - \frac{b}{b'}\right)^2 + 5.06\right]^{1/2}, \quad (9-31a)$$

Strip load ($b' = b$):

$$\beta = 0.42\left(\frac{b}{a'} + 2\right) - 0.29\left[\left(\frac{b}{a'} - 1\right)^2 + 5.06\right]^{1/2}, \quad (9-31b)$$

Square loading plate ($a' = b'$):

$$\beta = 0.84\left(\frac{b}{b'}\right) - 0.23. \quad (9-31c)$$

Mechanical Response of Deformation Difference

10

CHAPTER OUTLINE

10.1 Shrinkage of concrete	254
10.1.1 General analysis method	254
10.1.2 Practical calculation method	256
<i>Example 1. Calculating stress and cracking of symmetrically</i>	
<i>reinforced concrete member during uniformly shrinking</i>	<i>257</i>
<i>Example 2. Shrinkage difference of composite beam</i>	<i>258</i>
10.2 Difference of thermal deformation	259
<i>Example 3. Prestress analysis of aerated concrete slab after being</i>	
<i>autoclaved, assuming the temperature is uniformly distributed</i>	<i>259</i>
<i>Example 4. Analysis of a section with non-uniform temperature field ..</i>	<i>261</i>
10.3 Creep of concrete.....	263
10.3.1 Stress redistribution on section under sustained load.....	263
10.3.2 Stress state after unloaded.....	265

The major mechanical behaviors of steel reinforcement and concrete compensate each other, as the reinforced concrete is used as a composite structural material. On the other hand, the physical and mechanical behaviors of both materials are considerably different, and they do not always compensate, they may even be contradictory when they work together. For example, concrete will, but steel will not, expand or contract when the environmental humidity changes; the deformations of both materials are different when the environmental temperature changes; creep will occur in concrete but not in steel when the stress acted is sustained, etc. Therefore, the deformation differences between both materials in a structure are caused due to various reasons.

When the reinforcement and concrete are adhered well, the deformation difference between both certainly results in the redistribution of sectional stress and the internal forces of a statically indeterminate structure, and also the deformation and cracking under service load, even the ultimate strength, are influenced. Sometimes, an engineering accident may be caused. On the other hand, the deformation difference is favorable for the structure in some other conditions, e.g. the creep makes relaxation of thermal stress for massive concrete, a prestressed state may be established in a structure, utilizing the difference of thermal deformation.

The necessary concept, principle and method of analysis, and explanation of some important engineering phenomena are provided in this chapter for the

mechanical responses of structural members caused by the deformation differences between reinforcement and concrete.

10.1 Shrinkage of concrete

Water in concrete is lost during coagulating and shrinkage of concrete is the result. In addition, the volume of hardened concrete shrinks or expands as the environmental moisture changes (see Section 3.5). Therefore, the volume of structural concrete changes continuously during the service period.

The moisture exchanges between the concrete and the surrounding environment via the surface of the structure, so the moistures on the surface and in the interior of the structural concrete are different. Generally, a non-uniform moisture field and a corresponding shrinkage field of two or three dimensions are then formed. The differential equations can be established for moisture exchange between the concrete and surrounding environment similar to the basic equations of heat conduction (see Chapter 19). The moisture and, then, shrinkage of the concrete can be determined after the equations are solved or calculated by the finite element method. The shrinkage of one dimension and corresponding mechanical behavior of the structural member are introduced below.

10.1.1 General analysis method

If a concrete beam of rectangular section is reinforced asymmetrically, and the free shrinkage of the concrete occurs at time t and distributes constantly along its width but non-linearly along its depth ($\epsilon_{sh}(y)$, Fig. 10-1(a) (b)). The stress and strain on the section is generally analyzed as below.

1. Geometrical (deformation) condition. If there is no confinement on the section, the sectional deformation after concrete shrunk freely is non-linear (Fig. 10-1(c)). When the reinforcement is adhered well with the surrounding concrete and no slip occurs between them, the shrinkage deformation of the concrete is reduced due to the confinement of the reinforcement. In addition, the adjacent materials along the

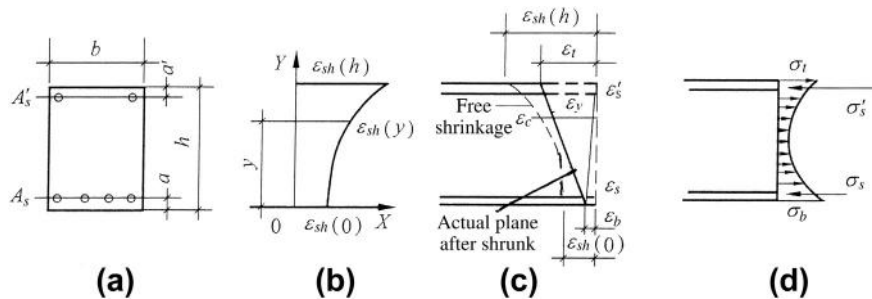


FIG. 10-1 Analysis of concrete shrinkage of structural member: (a) section, (b) free shrinkage, (c) sectional strain, (d) stress distribution

depth of the section are confined to each other and the ends of the beam are confined by other members connected or the supports, so the original section keeps a plane after concrete shrunk and the actual section at time t is an inclined plane.

As the shrinkage strains of the concrete at the top and bottom of the section (ε_t and ε_b) are taken as two basic unknowns, the shrinkage strain at y from the bottom is

$$\varepsilon_y = \frac{y}{h} \varepsilon_t + \frac{h-y}{h} \varepsilon_b. \quad (a)$$

Therefore, the tensile strain of the concrete there after shrunk equals the free shrinkage strain $\varepsilon_{sh}(y)$ minus the strain ε_y :

$$\varepsilon_c = \varepsilon_{sh}(y) - \varepsilon_y = \varepsilon_{sh}(y) - \left(\frac{y}{h} \varepsilon_t + \frac{h-y}{h} \varepsilon_b \right), \quad (10-1)$$

and the tensile strains of the concrete at top and bottom are respectively:

$$\varepsilon_{sh}(h) - \varepsilon_t \text{ and } \varepsilon_{sh}(0) - \varepsilon_b.$$

In the meantime, the strains of the upper and lower reinforcements are contractive:

$$\left. \begin{aligned} \varepsilon'_s &= \frac{h-a'}{h} \varepsilon_t + \frac{a'}{h} \varepsilon_b \\ \varepsilon_s &= \frac{a}{h} \varepsilon_t + \frac{h-a}{h} \varepsilon_b \end{aligned} \right\} \quad (10-2)$$

2. Physical (constitutive) relation. When the non-linear constitutive relation of concrete under uniaxial tension (e.g. Fig. 8-4) is taken, and the initial tangent elastic modulus is E_0 and the plasticity coefficient varying with the strain value is $\lambda_t (\leq 1.0)$, the tensile stress of the concrete is then obtained:

$$\sigma_c = \lambda_t \varepsilon_c E_0. \quad (10-3)$$

Usually, the compressive stresses of the reinforcements are far lower than their yield strength, so

$$\sigma'_s = \varepsilon'_s E_s \quad \text{and} \quad \sigma_s = \varepsilon_s E_s \quad (10-4)$$

are obtained, in where E_0 is elastic modulus of them.

3. Mechanical (equilibrium) equations. The stresses on the whole section have to be in equilibrium themselves and the resultant of them should still be zero:

$$\left. \begin{aligned} \sum X &= 0 \quad \int_0^h \sigma_c b dy = \sigma'_s A'_s + \sigma_s A_s \\ \sum M &= 0 \quad \int_0^h \sigma_c b y dy = \sigma'_s A'_s (h - a') + \sigma_s A_s a \end{aligned} \right\} \quad (10-5)$$

When the Equations (10-1) to (10-4) are substituted successively into Eq. (10-5), only two basic unknowns (ϵ_t and ϵ_b) exist for the shrinkage $\epsilon_{sh}(y)$ at any time t . After Eq. (10-5) is solved, the stresses on the section, i.e. tensile stress in concrete but compressive stress in the reinforcements, can be calculated easily (Fig. 10-1(d)). The curvature of the section is then:

$$\frac{1}{\rho} = \frac{\epsilon_t - \epsilon_b}{h}, \quad (10-6)$$

where ρ is the curvature radius of the section.

Afterwards, the deformations, i.e. deflection and angular rotation, of the structural member after shrinking can be calculated accordingly (see Chapter 13).

When the geometrical equation is established, two other physical quantities, e.g. the strain at center (ϵ_0) and curvature ($1/\rho$) of the section (similar to Fig. 10-7), can also be taken as the unknowns. If the environmental humidity is variable, the non-linear processes of stress and deformation of the member can be calculated gradually, as the shrinkage ($\epsilon_{sh}(y)$) is given successively for every increment of time or humidity. Generally, the digital method is used for analysis and is completed by computer.

10.1.2 Practical calculation method

If the free shrinkage of concrete ($\epsilon_{sh}(y)$) is linearly distributed along a section and constant elastic modulus of the concrete is assumed for every point on the section at same time, the practical calculation method based on the concept of prestressed concrete can be applied. The shrinkage of concrete ($\epsilon_{sh}(y) = \text{const.}$) occurring uniformly in a reinforced concrete beam (Fig. 10-2) is an example used here for explanation.

At first, it is assumed that the concrete shrinks freely and is not confined by the reinforcement in the section, so the reinforcement is longer than the concrete after shrinking and the difference between them is ϵ_{sh} per length. It is assumed again that a prestressed compressive stress $\epsilon_{sh}E_s$ is acted on the reinforcement only, and then the length of the reinforcements equal to the length of the concrete. The

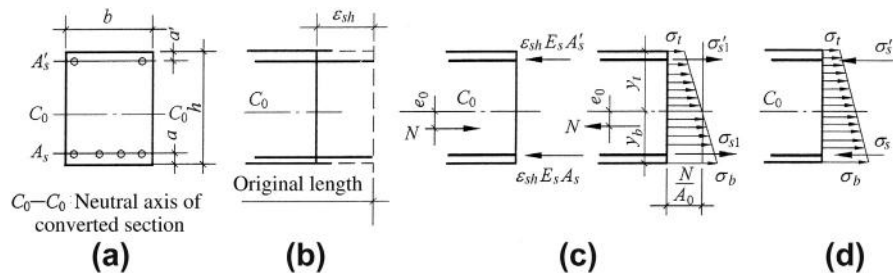


FIG. 10-2 Practical calculation for shrinkage of concrete beam: (a) section, (b) free shrinkage of concrete, (c) stress states at two stages, (d) stress distribution

compressive force should be acted on the center of gravity of both upper and lower reinforcements with the value of

$$N = \varepsilon_{sh} E_s (A'_s + A_s), \quad (10-7)$$

which is located at e_0 from the neutral axis of the converted section (see Chapter 8). However, the stress of the concrete is still zero at this time.

Secondly, an opposite force (tension) of same value is assumed to act at the same position of the converted section, and then the stress distribution on the converted section can be calculated easily. Afterwards, the stresses of the two stages on the section are added, and the final stress state of the section after concrete is shrunk is obtained (Fig. 10-2(d)).

Therefore, the values of tensile stresses of the concrete at top and bottom of the section are respectively:

$$\left. \begin{aligned} \sigma_t &= \frac{N}{A_0} - \frac{Ne_0 y_t}{I_0} \\ \sigma_b &= \frac{N}{A_0} + \frac{Ne_0 y_b}{I_0} \end{aligned} \right\}, \quad (10-8)$$

and the compressive stresses of the upper and lower reinforcements are respectively:

$$\begin{aligned} \sigma'_s &= \varepsilon_{sh} E_s - n\sigma'_{s1} = \varepsilon_{sh} E_s - n \left[\frac{N}{A_0} - \frac{Ne_0(y_t - a')}{I_0} \right], \\ \sigma_s &= \varepsilon_{sh} E_s - n\sigma_{s1} = \varepsilon_{sh} E_s - n \left[\frac{N}{A_0} + \frac{Ne_0(y_b - a)}{I_0} \right], \end{aligned} \quad (10-9)$$

where A_0 , I_0 are the area and moment of inertia of converted section, n is the ratio between elastic moduli of reinforcement and concrete, and y_t and y_b are the distances from top and bottom of section to neutral axis of converted section, respectively.

Example 1. Calculating stress and cracking of symmetrically reinforced concrete member during uniformly shrinking

Solution. The section and reinforcement of the member is shown in Fig. 10-3. If the free shrinkage strain of concrete (ε_{sh}) is uniformly distributed along its section, and

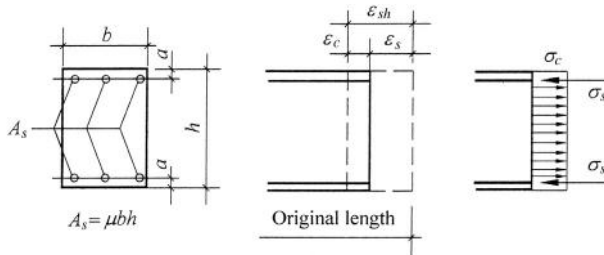


FIG. 10-3 Uniform shrinkage of symmetrically reinforced concrete member

the contractive strain of the member (ϵ_s) is reduced due to the confinement of the reinforcement.

When the contractive strain of the reinforcement (ϵ_s) is taken as the basic unknown, the tensile strain of the concrete should be $\epsilon_c = \epsilon_{sh} - \epsilon_s$ and the stresses of both are respectively $\sigma_s = \epsilon_s E_s$ and $\sigma_c = \lambda(\epsilon_{sh} - \epsilon_s)E_0$. The equilibrium equation is

$$\epsilon_s E_s A_s = \lambda(\epsilon_{sh} - \epsilon_s)E_0(bh - A_s) \approx \lambda(\epsilon_{sh} - \epsilon_s)E_0bh,$$

and the solutions obtained of it are

$$\epsilon_s = \frac{\lambda}{\lambda + n\mu} \epsilon_{sh} \quad \text{and} \quad \epsilon_c = \frac{n\mu}{\lambda + n\mu} \epsilon_{sh}, \quad (b)$$

where $n = E_s/E_c$ is the ratio between elastic moduli of reinforcement and concrete, $\mu = A_s/bh$ is the reinforcement content of section, and λ is the plasticity coefficient of tensile strain of concrete under corresponding stress.

Therefore, the compressive stress of the reinforcement and the tensile stress of the concrete are respectively:

$$\sigma_s = \frac{\lambda}{\lambda + n\mu} \epsilon_{sh} E_s \quad \text{and} \quad \sigma_c = \frac{\lambda n\mu}{\lambda + n\mu} \epsilon_{sh} E_0 \quad (10-10)$$

Obviously, the results are consistent with that calculated from the concept of pre-stressed concrete.

The higher the reinforcement content of the member, the stronger the confinement of the reinforcement, the less the shrinkage strain (ϵ_s) appears, and the larger the tensile stress (strain) of the concrete (σ_c, ϵ_c). If the reinforcement content of the member exceeds a limit value, the concrete will crack as the tensile stress reaches the tensile strength of the concrete (f_t). Let $\sigma_c \geq f_t$ in Eq. (10-10), the limit value is derived as below:

$$\mu \geq \frac{\lambda f_t}{n(\lambda \epsilon_{sh} E_0 - f_t)} \quad (10-11)$$

Example 2. Shrinkage difference of composite beam

A beam of width (b) is composed of the lower part of precast concrete (height $0.6h$) and the upper part of concrete cast in situ (height $0.4h$) (Fig. 10-4), if the

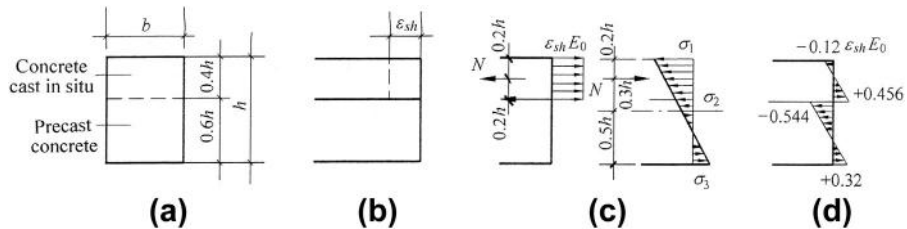


FIG. 10-4 Shrinkage difference of composite beam: (a) section, (b) shrinkage difference, (c) calculation of stress, (d) stress distribution

reinforcement is neglected. When the difference between free shrinkage strains of the upper and lower concretes is ε_{sh} , the stress and deformation of the beam is analyzed below.

Solution. It is assumed that the beam is separated into two parts and a tensile force ($N = 0.4bh\varepsilon_{sh}E_0$) is acted at the center of the upper concrete, and the tensile stress ($\varepsilon_{sh}E_0$) is caused there only, while the stress is still zero on the lower concrete. Afterwards, the two parts of same length are integrated together and a compressive force of same value is acted at the same position, and it is $e_0 = 0.3h$ (eccentricity) away from the center of the whole section. The stresses at top, connected plane, and bottom of the section are respectively calculated:

$$\begin{aligned}\sigma_1 &= -\frac{N}{bh} - \frac{0.5hNe_0}{I} = -1.12\varepsilon_{sh}E_0, \\ \sigma_2 &= -\frac{N}{bh} - \frac{0.1hNe_0}{I} = -0.544\varepsilon_{sh}E_0, \\ \sigma_3 &= -\frac{N}{bh} + \frac{0.5hNe_0}{I} = +0.32\varepsilon_{sh}E_0.\end{aligned}$$

After the stress states of the two stages (Fig. 10-4(c)) are added, the final stress distribution of the beam is obtained and shown in Fig. 10-4(d). In addition, the curvature of the beam after concrete shrink is

$$\frac{1}{\rho} = \frac{1.12\varepsilon_{sh} + 0.32\varepsilon_{sh}}{h} = 1.44 \frac{\varepsilon_{sh}}{h}.$$

10.2 Difference of thermal deformation

When the environmental temperature of a structure varies, especially if the structure is exposed to high temperature ($T > 200^\circ\text{C}$; see Chapter 19), a non-uniform temperature field with great gradient is formed on its section due to the thermal inertia of concrete. In addition, the linear expansion coefficients of reinforcement and concrete are different under the same temperature. Therefore, the difference in thermal deformations of them should appear considerably on its section.

The mechanical response of the deformation difference between the reinforcement and concrete on a section caused by temperature variation is similar to that caused by the shrinkage of concrete. The analytical concept and method of the latter described above can also be used for the former, and two examples are explained below.

Example 3. Prestress analysis of aerated concrete slab after being autoclaved, assuming the temperature is uniformly distributed

Solution. When the reinforced aerated concrete slab is manufactured, the mortar is mixed well and poured into the steel mold, and the strength of the aerated concrete will be reached only after cured under high temperature and pressure (usually

200°C, 15 atm., and about 24 hours) in the autoclave. When the slab is cooled down, the prestress is established certainly on its section due to the difference in thermal deformations between the reinforcement and aerated concrete, as the linear expansion coefficients of both materials are unequal (Table 4-4). This is called self-prestressing and is favorable for the cracking resistance of the slab, and an initial camber is obviously formed (Fig. 10-5).

The reinforcement is freely elongated (without stress) during heating, as the mortar of the aerated concrete is still a fluid. After the aerated concrete reaches a certain strength under high temperature (T_1), it is adhered well with the reinforcement, but both are still free of stress. When the slab is cooled down from T_1 to T_2 , the contractive deformations of both are unequal and the difference between them is

$$\Delta\epsilon_T = \epsilon_{sT} - \epsilon_{cT} = (\alpha_s - \alpha_c)(T_1 - T_2), \quad (10-12)$$

where ϵ_{sT} , ϵ_{cT} are contractive strains of reinforcement and aerated concrete during cooling, and α_s, α_c are linear expansion coefficients of reinforcement and aerated concrete.

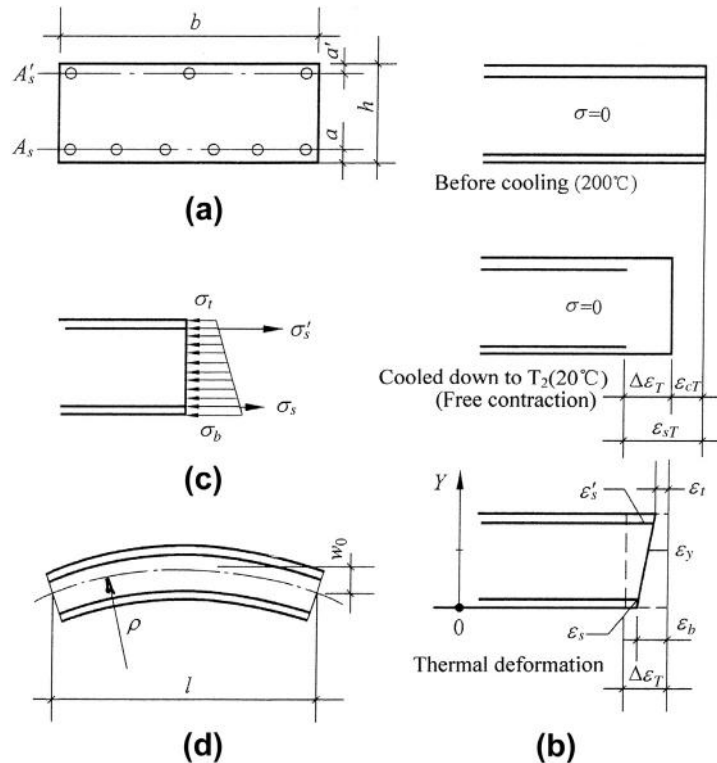


FIG. 10-5 Prestress analysis of aerated concrete slab: (a) section and reinforcement, (b) analysis of deformation, (c) stress distribution, (d) Initial camber

At this time, the relative slip between the reinforcement and aerated concrete is prevented due to the bond strength between them, so the reinforcement is tensed and elongated, while the aerated concrete is compressed and contracted (Fig. 10-5(b)). Comparing with Fig. 10-2(b) the deformation difference and the stress on the section of the aerated concrete slab are similar but just opposite from that caused by shrinkage of the concrete beam.

When the contractive strains at the top and bottom of the slab (ε_t and ε_b) are taken as the basic unknowns, the strain at y from the bottom of the slab is:

$$\varepsilon_y = \frac{y}{h} \varepsilon_t + \frac{h-y}{h} \varepsilon_b, \quad (c)$$

and the tensile strains of the upper and lower reinforcements are respectively:

$$\left. \begin{aligned} \varepsilon'_s &= \Delta \varepsilon_T - \left(\frac{h-a'}{h} \varepsilon_t + \frac{a'}{h} \varepsilon_b \right) \\ \varepsilon_s &= \Delta \varepsilon_T - \left(\frac{a}{h} \varepsilon_t + \frac{h-a}{h} \varepsilon_b \right) \end{aligned} \right\} \quad (d)$$

After the constitutive relations of aerated concrete and reinforcement (similar to Eqs (10-3) and (10-4)) are substituted into the equilibrium equations: $\sum X = 0$ and $\sum M = 0$ (similar to Eq. (10-5)), ε_t and ε_b can be resolved. Then, the stress distribution on the section is calculated and shown in Fig. 10-5(c), and the curvature and camber of the slab can be calculated by:

$$\frac{1}{\rho} = \frac{\varepsilon_b - \varepsilon_t}{h} \quad \text{and} \quad w_0 = \frac{l^2}{8\rho}. \quad (10-13)$$

Generally, the aerated concrete is autoclaved under temperature $T_1 = 200^\circ\text{C}$ and is cooled down to $T_2 = 20^\circ\text{C}$ after manufacture, and the linear expansion coefficients of it and reinforcement are respectively $\alpha_c = 8 \times 10^{-6}/^\circ\text{C}$ and $\alpha_s = 12 \times 10^{-6}/^\circ\text{C}$, so the strain difference between them after cooling is $\Delta \varepsilon_T = 720 \times 10^{-6}$ and, correspondingly, the prestress of the reinforcement is 150 N/mm^2 which is consistent with the measured value during testing [4-10]. The measured cambers are obviously visible and are 3.7–4.0 mm and 8.7–9.7 mm respectively for the reinforced aerated concrete slabs of span lengths 3.6 m and 6.0 m [4-10].

If the elastic modulus of the aerated concrete is considered as a constant, the concept of prestressed concrete can also be used for easy calculation. However, when the thermal stress of the structural member after autoclaving needs to be calculated accurately, it should be calculated and accumulated step by step following the time or temperature increments and the elastic moduli or constitutive relations of the aerated concrete and reinforcement varying with temperature have to be considered.

Example 4. Analysis of a section with non-uniform temperature field

Concrete is an inertia material of thermal conduction. When the environmental temperature is varied suddenly, e.g. a fire accident occurs and the temperature increases correspondingly, the temperature on the surface of the structure approaches that of the environmental temperature, while the temperature in its interior is still lower.

Therefore, a non-uniform temperature field is formed with severe variation on its section (Figs. 10-6 and 19-4). The temperature field varies continuously with the environmental temperature and time, and can be calculated by the method of heat conduction (see Section 19.2.3).

After the temperature distribution $T(y)$ on the section (Fig. 10-7(a)) is obtained, the free expansive strain $\varepsilon_{th}(y)$ of the concrete on the section can be calculated accordingly (Chapter 19). When the strain at the geometrical center of the section (ε_0) and the angular rotation per unit length of the member ($\theta = 1/\rho$) are taken as the basic unknowns, the difference between the confined deformation and the free expansive strain is

$$\varepsilon_c = \varepsilon_0 - \theta y - \varepsilon_{th}. \quad (10-14)$$

Therefore, the concrete is tensed when $\varepsilon_c > 0$, otherwise it is compressed when $\varepsilon_c < 0$.

When the constitutive relation of concrete under high temperature (Chapter 19):

$$\sigma_c = \phi(\varepsilon_c, T, t) \quad (10-15)$$

is introduced and the equilibrium equations:

$$\left. \begin{aligned} \Sigma X &= 0 \quad \int_{-h/2}^{h/2} \sigma_c b dy = 0 \\ \Sigma M &= 0 \quad \int_{-h/2}^{h/2} \sigma_c b y dy = 0 \end{aligned} \right\} \quad (10-16)$$

are established, the basic unknowns ε_0 and θ can be solved and the stress distribution on the section (Fig. 10-7(c)) and deformation of the structural member are then calculated.

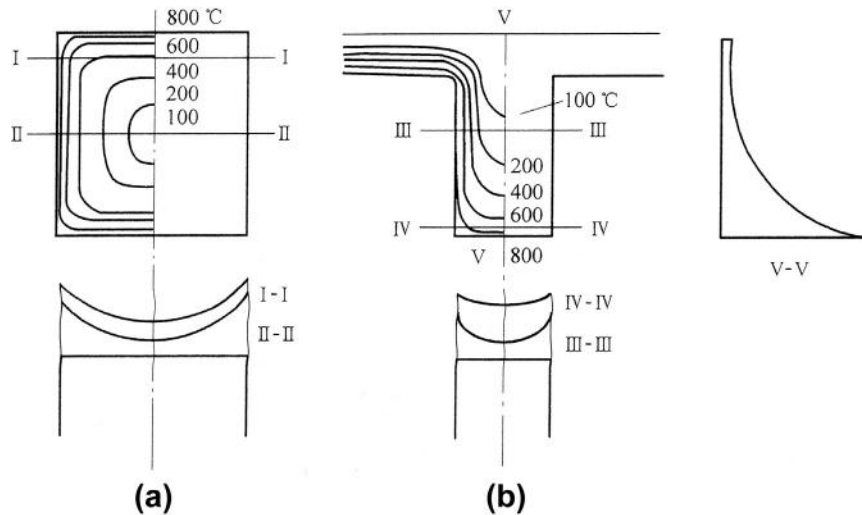


FIG. 10-6 Temperature field (two-dimensional) on section: (a) column with four surfaces exposed to fire, (b) beam with three surfaces exposed to fire

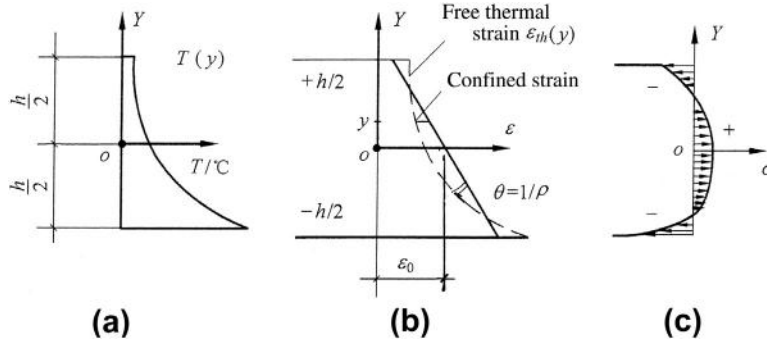


FIG. 10-7 Analysis of non-uniform temperature field: (a) temperature distribution $T(y)$, (b) strains on section, (c) stress distribution

When the member is reinforced, the area and constitutive relation of the reinforcement are introduced; when the member is acted with axial force (N) and bending moment (M), the equilibrium equations are modified; when the temperature field on the section is two-dimensional, the section is divided into networks, and the temperature and strain of every network are determined and then solved from the equilibrium equations.

10.3 Creep of concrete

Creep occurs in concrete under a sustained stress (Section 3.6), while it does not occur in steel (reinforcement) under normal temperature when the sustained stress is lower than its yield strength ($\sigma_s < f_y$). When a reinforced concrete structural member is used in a long period of service stage, the stress on its section will be redistributed and the additional deformation will be caused due to creep of the concrete. A centrally compressed column is analyzed as an example.

10.3.1 Stress redistribution on section under sustained load

The height, section area, and area of reinforcement of a reinforced concrete column are respectively l_0 , A_c , and A_s . If the initial stresses caused by creep of the concrete and the difference between thermal deformations of two materials are neglected, the stresses on the section should be zero before loading (age $t < t_0$), i.e. $\sigma_s = \sigma_c = 0$ (Fig. 10-8(a)).

When the column is loaded centrally (N) at age $t = t_0$, the strains of the concrete and reinforcement are equal, $\epsilon_{c0} = \epsilon_{s0}$, if they are adhered well. The stresses of both are respectively obtained from Eqs (8-7b) and (8-5):

$$\sigma_{c0} = \frac{N}{(1 + \frac{n\mu}{\lambda})A_c} \quad \text{and} \quad \sigma_{s0} = \frac{n}{\lambda} \sigma_{c0} = \frac{n}{\lambda + n\mu} \frac{N}{A_c}, \quad (10-17a)$$

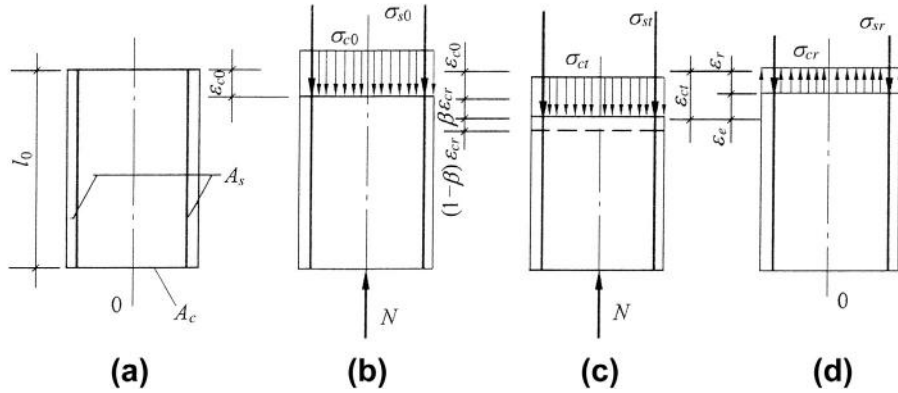


FIG. 10-8 Stress and deformation of a column under sustained load: (a) before loading ($t < t_0$), (b) after loading ($t = t_0$), (c) load sustaining ($t > t_0$), (d) after unloading, ($t > t_1 > t_0$)

and the strain of the column is also the strain of the concrete or reinforcement:

$$\epsilon_{c0} = \frac{\sigma_{c0}}{\lambda E_0} = \frac{\sigma_{s0}}{E_s}, \quad (10-17b)$$

where $n = E_s/E_0$, $\mu = A_s/A_c$, and λ is the plasticity coefficient of compressive strain of concrete.

When the central load ($N = \text{const.}$) is sustained later ($t > t_0$), the creep occurs in the concrete under compressive stress (σ_{c0}). Generally, the creep of plain concrete is calculated by

$$\epsilon_{cr} = \sigma_c \cdot C(t, t_0), \quad (e)$$

where $C(t, t_0)$ is the specific creep of the concrete (Eq. 3-23).

The creep of concrete (ϵ_{cr}) in the reinforced concrete column is confined by the reinforcement and is reduced to $\beta\epsilon_{cr}$ (Fig. 10-8(c)). This is similar to the situation of shrinkage strain of concrete discussed above (Example 1), and $\beta\epsilon_{cr}$ here corresponds to ϵ_s in Fig. 10-3, i.e. $\epsilon_s = \beta\epsilon_{cr}$, so

$$\beta = \frac{\lambda}{\lambda + n\mu} < 1.0 \quad (f)$$

is obtained referring to formula (b).

At this time, the total strain of the reinforcement, also of the column, is $\epsilon_{ct} = \epsilon_{c0} + \beta\epsilon_{cr}$, so the stress of the reinforcement is increased to

$$\sigma_{st} = (\epsilon_{c0} + \beta\epsilon_{cr})E_s. \quad (10-18a)$$

Correspondingly, the stress of the concrete has to be reduced and can be calculated by the equilibrium condition:

$$\sigma_{ct} = \frac{N - \sigma_{st}A_s}{A_c}. \quad (10-18b)$$

It is seen that the creep of the concrete (ε_{cr}) gradually causes the increase in column deformation (ε_{ct}) as the load is sustained, so the stresses on the section continuously redistribute, i.e. the compressive stress of the reinforcement increases while the compressive stress of the concrete decreases (or relaxes) (Fig. 10-9). Or, it is said that the compression of the concrete transfers gradually to the reinforcement, and the axial force carried by the reinforcement increases gradually.

10.3.2 Stress state after unloaded

When the central force ($N = \text{const.}$) is sustained until the age of t_1 and then is unloaded totally, the instantaneously recovered strain of the column is ε_e and the residual strain (contraction, Fig. 10-8(d)) of it is

$$\varepsilon_r = \varepsilon_{ct} - \varepsilon_e. \quad (g)$$

At this time, the external force is zero and the stresses on the section have to be in self-equilibrium, so the residual compressive stress of the reinforcement should cause tensile stress in the concrete.

The compressive stress of the concrete before unloading (σ_{ct}) is turned into tensile stress after unloading (σ_{cr}), which is related to the recovered strain (ε_e) (Fig. 10-9(b)):

$$\sigma_{cr} = \varepsilon_e \lambda_r E_0 - \sigma_{ct}. \quad (h)$$

Then, the equilibrium equation is established:

$$(\varepsilon_{ct} - \varepsilon_e) E_s A_s = (\varepsilon_e \lambda_r E_0 - \sigma_{ct}) A_c,$$

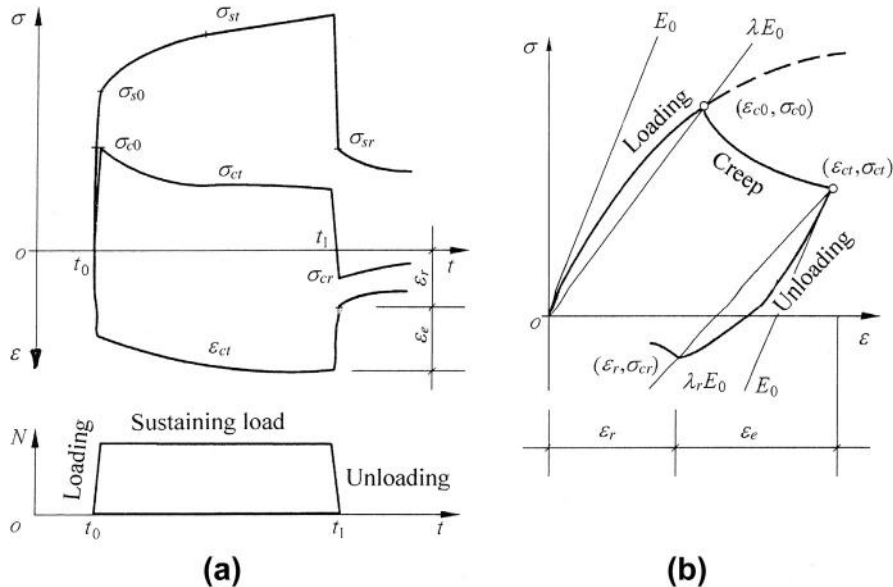


FIG. 10-9 Stress redistribution of centrally compressed column due to creep of concrete: (a) stress and strain varying with time, (b) stress-strain process of concrete

and the recovered strain can be solved:

$$\varepsilon_e = \frac{n\mu\varepsilon_{ct} + \sigma_{ct}/E_0}{\lambda_r + n\mu} \quad (10-19a)$$

and the residual strain is calculated by

$$\varepsilon_r = \frac{\lambda_r\varepsilon_{ct} - \sigma_{ct}/E_0}{\lambda_r + n\mu}. \quad (10-19b)$$

Therefore, the compressive stress of the reinforcement and the tensile stress of the concrete soon after unloading are respectively:

$$\left. \begin{aligned} \sigma_{st} &= \varepsilon_r E_s \\ \sigma_{cr} &= \mu \varepsilon_r E_s \end{aligned} \right\} \quad (10-20)$$

If the reinforcement content (μ) is rather high and the sustaining time of the load is very long, the creep of the concrete and the stress redistribution on the section of the column develop considerably, the tensile stress of the concrete after unloading may reach its tensile strength ($\sigma_{cr} = f_t$) and the transverse crack will occur along the periphery of its section. Therefore, it happens in engineering practice that some reinforced concrete columns, e.g. under silos, are still safe under significant axial forces even when sustained for a long period, but the tensile cracks appear transversely soon after unloading.

After the column is unloaded ($t > t_1$, $N = 0$), the post elastic effect (Section 3.6) and tensile creep of the concrete cause the residual strain (ε_r) to be decreased further, so the compressive stress of the reinforcement and the tensile stress of the concrete also reduce accordingly (Fig. 10-9).

Strength and Deformation of Structural Member

3

The reinforced concrete structure used most widely in engineering practice is mainly composed of one-dimensional members, of which the internal forces on the section are singly axial force, bending moment, shear force, or torque and the composition of them. Even the two- and three-dimensional structures are entirely or partly simplified and equivalent to a one-dimensional member. For example, a shear wall of a tall building is considered as a cantilever of narrow but deep section; a core tube of a high-rising building is considered as an eccentrically compressed member with box section; a folded plate structure is composed of eccentrically compressed plates; a diaphragm at the end of a shell structure is simplified to an eccentrically tensed member, etc.

When the reinforced concrete structure works under normal conditions, the strength, cracking, and deformation of its member, which carries different internal forces or their composition, are introduced in this part. In addition, the influences of main factors, principle of analysis, and calculation method of them are provided as well.

This page intentionally left blank

Strength of Member Under Compression and Bending

11

CHAPTER OUTLINE

11.1 Mechanical process and failure pattern.....	269
11.1.1 Rectangular beam with tensile reinforcement only.....	269
11.1.2 Suitably, less-, and over-reinforced beams.....	272
11.1.2.1 <i>Less-reinforced beam</i> ($\mu < \mu_{min}$).....	272
11.1.2.2 <i>Over-reinforced beam</i> ($\mu > \mu_{max}$).....	274
11.1.2.3 <i>Suitably reinforced beam</i> ($\mu_{min} < \mu < \mu_{max}$).....	275
11.1.3 Eccentrically compressed column (and tensed member)	275
11.2 Additional flexure of long column.....	280
11.3 General method for sectional analysis	283
11.4 Ultimate strength.....	289
11.4.1 Calculation formulas.....	289
11.4.1.1 <i>Equivalent rectangular stress diagram</i>	289
11.4.1.2 <i>Boundary of compressive depth</i>	292
11.4.1.3 <i>Calculation formulas</i>	293
11.4.1.4 <i>Eccentrically tensed member</i>	294
11.4.2 Member under biaxial bending.....	295
11.5 Members of various materials and structural details	298
11.5.1 High-strength concrete.....	298
11.5.2 Light-weight concrete	299
11.5.3 Reinforcements with different strengths	300
11.5.4 Reinforcement without yielding plateau.....	301
11.5.5 Reinforcements distributed along sectional depth	301
11.5.6 Non-rectangular sections.....	303

11.1 Mechanical process and failure pattern

11.1.1 Rectangular beam with tensile reinforcement only

A concrete beam of rectangular section is reinforced only on its tensile side, when it carries bending moment only (shear force $V = 0$). This is the most simple and basic reinforced concrete member, of which the mechanical process and responses have been tested and reported in detail. When the beam is simply supported on both

ends and two concentrated loads are symmetrically acted on its span, the middle part of the span is of pure bending and the main responses including distribution of average strain, position of neutral axis, strain (stress) of reinforcement, and curvature of the section are measured during testing. The typical results are shown in Fig. 11-1.

The mechanical process of a reinforced concrete beam can be divided into three stages from start of loading until failure, according to the deformation and cracking of the specimen observed during testing and to the analysis of the experimental data. The mechanical characteristics within each stage are individually presented below, consulting Figs. 11-1 and 11-2.

1. Stage I Before cracking of concrete ($M \leq M_{cr}$). When the beam is initially loaded and the bending moment is limited, the strain distributes linearly on the section and the stress of the concrete is proportional to its strain (Fig. 11-2(a)). As the reinforcement is located in the lower part of the section and its converted area is $nA_s > A_s$, the neutral axis is slightly lower down ($d_c > h/2$). The beam is of the elastic stage at this time, and the stresses of reinforcement and concrete and the curvature of the beam increase proportionally with the bending moment.

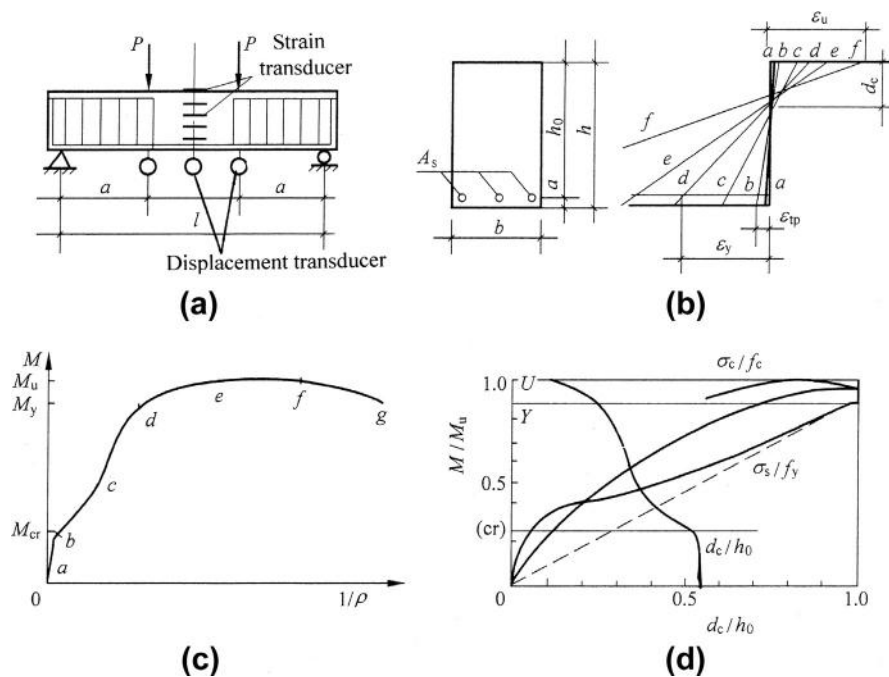


FIG. 11-1 Experiment on singly reinforced concrete beam of rectangular section: (a) specimen and loads, (b) strain distribution, (c) bending moment—curvature relation, (d) stresses of reinforcement and concrete and position of neutral axis

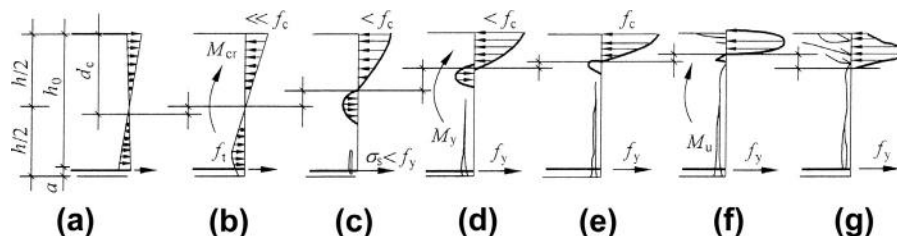


FIG. 11-2 Developments of sectional stress and crack of beam: (a) before cracking, (b) just cracking, (c) after cracking, (d) yielding of reinforcement, (e) after yield, (f) ultimate state, (g) descending branch

As the bending moment is increased, the plastic strain appears less in the concrete of tension zone of the beam, and a curved distribution of tensile stress is gradually formed there. However, the stress in the concrete of compression zone of the beam is far smaller than the compressive strength, so linear distribution of compressive stress is kept. Therefore, the neutral axis has to move up slightly in order to satisfy the equilibrium condition of horizontal forces on the section, and the curvature increases more. When the maximum tensile strain of the concrete reaches its ultimate value, the crack will appear soon on the beam, and a descending branch appears on the stress diagram of the tension zone (Fig. 11-2(b)). The bending moment of the beam at cracking is $M_{cr} \approx 0.2-0.3M_u$, where M_u is the ultimate strength of the beam.

2. Stage II Working with crack ($M_{cr} < M < M_y$). When the bending moment at mid-span reaches and exceeds the cracking moment, a crack is visible at the weakest section. The crack is fine and short and located near the bottoms of side surfaces and perpendicular to the axis of the reinforcement. A part of the concrete of tension zone on the cracked section is out of work then, so the tensile stress of the reinforcement is suddenly increased but is still far lower than the yield strength ($\sigma_s < f_y$). Therefore, the neutral axis moves up obviously, and the compressive stress of the concrete accelerates and distributes non-linearly (Fig. 11-2(c)), as the bending moment increases and the compressive area reduces.

The increment of bending moment within this stage, i.e. from cracking of the concrete until yielding of the reinforcement ($\Delta M = M_y - M_{cr}$), is greater than that of other stages. As the bending moment increases gradually within this stage, the existing crack slowly expands and extends upward and new cracks appear successively at a certain distance, the neutral axis moves up, and the stresses of the reinforcement and compressed concrete and the curvature increase continuously as well. Generally, the bending moment of a structural member is about $0.5-0.6 M_u$ during service period and is in the middle of this stage.

3. Stage III After yielding of reinforcement ($M \geq M_y$). When the tensile reinforcement just reaches the yield strength (f_y , Fig. 11-2(d)), the corresponding bending moment of the beam is $M_y \approx 0.9-0.95M_u$. The maximum stress of compressed concrete in the cracked section is still lower than its strength (f_c) during

that time, and the most part of the concrete on tension zone of the section is cracked and out of work, but a small part near the neutral axis is still tensed with little effect. Afterwards, the stress of the reinforcement (f_y) keeps constant, the increment of the bending moment depends upon only the increase in the internal arm of the section. As the strain of the reinforcement after yielding increases quickly and results in failure of the bond between the reinforcement and concrete near the cracked section, and the crack widens and extends upward and the compressive area reduces, so the internal arm is increased slightly. In the meantime, the compressive stress of the concrete increases quickly and reaches the maximum value (f_c) at the top of the section (Fig. 11-2(e)), but the corresponding bending moment is still lower than the ultimate value (M_u). When the bending moment is slightly increased further, the stress-strain curve of the concrete near the top enters the descending branch and the horizontal cracks appear nearby, and the ultimate bending moment of the beam (M_u) is reached (Fig. 11-2(f)). At this time, the vertical crack expands widely in the lower part and extends near the top of the section, and the compressed zone is limited, so the internal arm reaches the maximum.

If the test lasts longer, the strain of the reinforcement is increased further with constant stress, while the strain of the compressed concrete near the top is also increased with reducing stress. Therefore, the maximum compressive stress on the cracked section moves downwards and the internal arm reduces (Fig. 11-2(g)), and the bending moment descends slowly. Finally, one of the vertical cracks widens suddenly and extends obviously upwards, and more horizontal cracks appear and develop in the compression zone, then a triangular failure zone (similar to Fig. 3-6) is formed there and the concrete is gradually crushed and spalled off, so the residual strength of the beam decreases quickly and the beam is out of work soon.

11.1.2 Suitably, less-, and over-reinforced beams

The mechanical process of the concrete beam introduced above is of medium reinforced, and three characteristic points, i.e. cracking, yielding, and ultimate states are experienced successively. However, the mechanical behavior, failure pattern, and characteristic bending moments vary considerably with the reinforcement content ($\mu = A_s/bh_0$) (Fig. 11-3), and the beam can be divided into three categories.

11.1.2.1 Less-reinforced beam ($\mu < \mu_{min}$)

The cracking moment of a reinforced concrete beam is slightly greater than that of a plain concrete beam ($\mu = 0$), because the stress of the tensile reinforcement is rather low when the concrete in the tension zone is cracking. If the contribution of the reinforcement is neglected and the stress distribution on the section is simplified to a triangle on the compression zone and a trapezoid on the tension zone (Fig. 11-4), the cracking moment obtained (see Section 12.2) is

$$M_{cr} = 0.256f_tbh^2. \quad (a)$$

On the other hand, it is assumed that the tensile concrete is totally out of work when the tensile reinforcement is yielded, referring to Fig. 11-2, and the internal

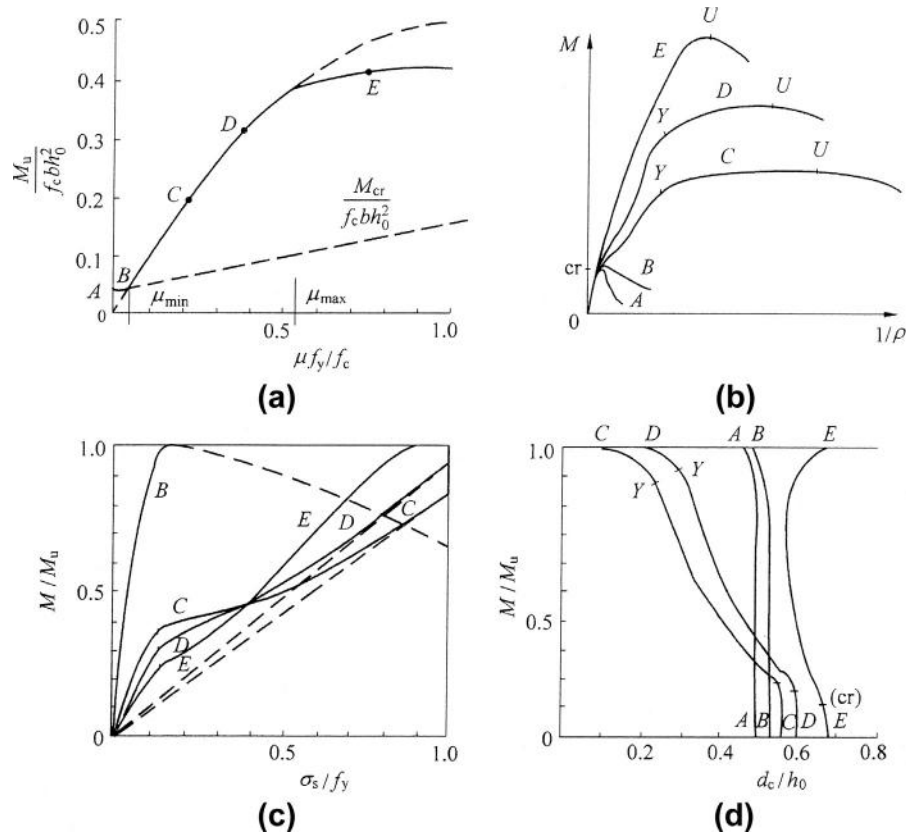


FIG. 11-3 Variations of mechanical behaviors of beams with different reinforcement contents: (a) ultimate bending moment, (b) bending moment—curvature relation, (c) stress of reinforcement, (d) position of neutral axis

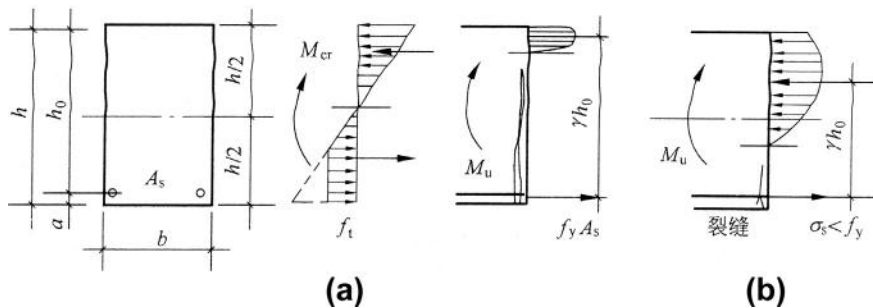


FIG. 11-4 Less- and over-reinforced concrete beams: (a) $\mu < \mu_{min}$ ($M_{cr} > M_u$), (b) $\mu > \mu_{max}$

arm on the section is γh_0 at the ultimate state, so the ultimate bending moment of the beam is

$$M_u = \mu b h_0 f_y \gamma h_0, \quad (b)$$

which is represented by a continuous curve (*OBCD*), including two dashed lines on both ends (Fig. 11-3(a)).

When the formulas (a) and (b) are substituted into $M_u \leq M_{cr}$, the reinforcement content

$$\mu \leq 0.256 \frac{f_t}{f_y} \frac{1}{\gamma} \left(\frac{h}{h_0} \right)^2 \quad (11-1a)$$

is derived. It means that the tensile reinforcement ($A_s = \mu b h_0$) is yielded even broken immediately after the cracking moment (M_{cr}) is reached, and the beam is cracked and failed simultaneously, because the reinforcement alone is not enough to resist the moment. This is the failure pattern of the less-reinforced concrete beam.

The less-reinforced concrete beam fails suddenly without warning, as it is controlled by tension of the concrete. The stress on the section, position of neutral axis, and curvature of the beam before failure are approaching that of the plain concrete beam (curves *A* and *B* in Fig. 11-3). Generally, the less-reinforced concrete beam should be avoided in engineering practice, so the minimum reinforcement content (μ_{min} , referring to Section 8.2.3) is provided for concrete beams in various design codes. The minimum reinforcement content is calculated by a simplified formula:

$$\mu_{min} = 0.45 \frac{f_t}{f_y} \quad (11-1b)$$

in Chinese code [2-1], and the similar formula or certain value depending upon the strengths of both materials is given in the codes of other countries.

If the reinforcement of a beam calculated by the ultimate bending moment (M_u) is less than $\mu_{min} b h_0$ (or $\mu < \mu_{min}$), the beam is usually reinforced with $\mu_{min} b h_0$. However, less-reinforced concrete ($\mu < \mu_{min}$) is still used for some structures, e.g. massive dams, in order to save steel, and so the safety of it has to be guaranteed in other ways.

11.1.2.2 Over-reinforced beam ($\mu > \mu_{max}$)

When the beam is heavily reinforced, the neutral axis of the converted section before cracking is located within the lower half and the compressive strain at the top is surely greater than the tensile strain at the bottom, so the cracking moment (M_{cr}) is increased but its relative value (M_{cr}/M_u) is decreased. After the tension zone of the beam is cracked, the crack slowly expands and extends upwards as the bending moment is increased. At this time, the neutral axis slightly moves upwards and the stress of the reinforcement increases suddenly with less amplitude, and the curvature is gradually increased without obvious turn (curves *E* in Fig. 11-3).

When the bending moment is increased further and the failure of the beam is approached, the concrete at the top reaches first the compressive strength and turns soon into the descending branch of the stress—strain relation, a horizontal crack appears near the top and the peak stress on the section moves downwards, the neutral axis moves downwards as well, but the stress of the reinforcement and the curvature are accelerated. Finally, the concrete in the compression zone is crushed as more cracks appear and develop, then the crushed zone is expanded downwards and a triangle failure zone is formed, but the tensile reinforcement does not yield yet ($\sigma_s < f_y$, Fig. 11-4(b)). Therefore, the ultimate strength of the beam is reached and decreased soon. This is the failure pattern of the over-reinforced concrete beam.

The failure of the over-reinforced beam is controlled by the compressed concrete, so the deformation (curvature) is small, the crack is not wide, and no warning obviously appears before failure. In addition, the ultimate moment (M_u) increases limitedly as even more reinforcements are put in the tension zone (Fig. 11-3(a)), so the strength of the reinforcement can not be utilized fully. Generally, the over-reinforced concrete beam is seldom used in engineering practice.

11.1.2.3 Suitably reinforced beam ($\mu_{min} < \mu < \mu_{max}$)

The mechanical process and failure pattern of the suitably reinforced beam have been introduced above (Figs 11-1 and 11-2). The failure of the beam is controlled by yielding of the tensile reinforcement, some warnings, including widening and extending of the tensile cracks, increasing of deformation and visible deformation, appear obviously from initially yielding of the reinforcement until final failure of the beam. Most beams used in engineering practice are of this category.

The stress, deformation, crack, and failure process of the suitably reinforced beam varies with the reinforcement content (e.g. curves B, C, and D in Fig. 11-3). When the reinforcement content is decreased and increased considerably, the beam is transferred respectively into the less- and over-reinforced ones. Therefore, the lower and upper boundaries of the reinforcement content are μ_{min} and μ_{max} respectively for the suitably reinforced beam, and μ_{min} is derived from the cracking moment (M_{cr} , Eq. 11-1b) while μ_{max} is determined by the boundary depth of the compression zone (x_b , see Section 11.3.1).

11.1.3 Eccentrically compressed column (and tensed member)

When a central force (N) and a bending moment (M) are acted together on section of the structural member, only normal stress (σ) is resulted in. The central force and bending moment can be equivalent to an axial force (N) acted eccentrically (eccentricity $e_0 = M/N$), and the central compression or tension ($e_0 = 0$) and pure flexure ($e_0 = \infty$) are obviously the special cases. Then, the member may be called the eccentrically compressed or tensed member, or the compressive- or tensile-flexural member.

This kind of structural member is used most widely in engineering practice, and many investigations have been conducted on it. The mechanical behavior of it varies

considerably with the main factors, including eccentricity, reinforcement content, and slenderness (l_0/h). A short column of rectangular section reinforced symmetrically ($A_s = A'_s$) is introduced below as an example to explain the behavior varying with the eccentricity.

The stress and strain distributions and the failure pattern of the eccentrically compressed column at ultimate state vary with the eccentricity as shown in Fig. 11-5 and Fig. 11-6 respectively.

The mechanical process and failure pattern of a centrally compressed column ($e_0 = 0$) is presented in detail in Section 8.1, the stress distributes uniformly on the section during failure, several longitudinal cracks appear and the concrete cover is spalled off into pieces, the reinforcements are yielded under compression and some of them are buckled within the adjacent ties. When the column is compressed

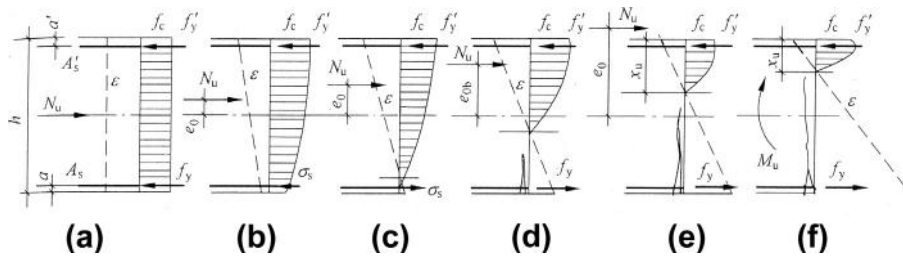


FIG. 11-5 Ultimate states of eccentrically compressed columns: (a) $e_0 = 0$, (b) $e_0 < e_{0b}$, (c) $e_{0b} < e_0 < e_{0cor}$, (d) $e_0 = e_{0b}$, (e) $e_0 > e_{0b}$, (f) $e_0 = \infty$

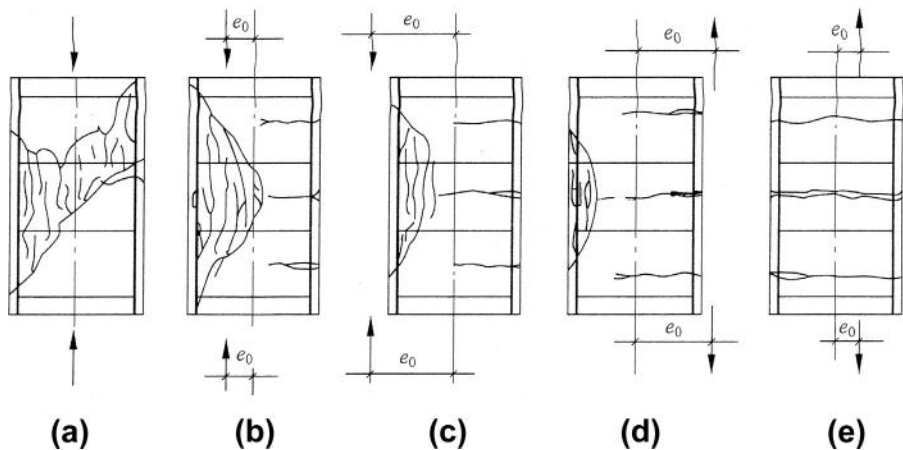


FIG. 11-6 Failure patterns of eccentrically compressed and tensed members: (a) central compression ($e_0 = 0$), (b) compression with smaller eccentricity ($e_0 < e_{0b}$), (c) compression with larger eccentricity ($e_0 > e_{0b}$), (d) tension with larger eccentricity ($e_0 > \frac{h}{2} - a$), (e) tension with smaller eccentricity ($e_0 < \frac{h}{2} - a$)

with small eccentricity ($e_0 < e_{\text{cor}}$, where e_{cor} is the core distance of the section), the compressive stress distributes non-uniformly on the whole section during failure, the concrete on the nearer side of the compression reaches first the compressive strength and the longitudinal cracks appear nearby, the reinforcement is yielded and buckled there, the concrete cover is spalled off gradually and the cracked zone expands towards the central line, and a triangle failure zone is finally formed. However, the compressive stresses of the reinforcement and concrete on the other side of the section are smaller than their strengths respectively, and no failure symptom is found there. When the eccentricity of the compression is $e_0 > e_{\text{cor}}$ but $< e_{0b}$, a triangle cracked zone of smaller area is also formed on the nearer side of the compression during failure, but a tension zone exists on the other side, and the concrete there is cracked and out of work and the tensile stress of the reinforcement is less than the yield strength ($\sigma_s < f_y$). In summary, the failure is controlled by compression of the concrete when the eccentricity of a column is $e_0 < e_{0b}$ (boundary eccentricity), and this is called a smaller eccentricity column or compression failed column.

When the column is compressed with larger eccentricity ($e_0 > e_{0b}$), the tension zone of the section and the tensile strain of the concrete are increased, the transverse crack appears first in the tension zone as the compression is increased, then the tensile stress of the reinforcement there increases suddenly and the neutral axis on the section moves towards the compression zone. Afterwards, the tensile reinforcement yields first and its strain increases quickly, the compression zone is reduced and the compressive stress of the concrete is increased and later reaches the required strength, so the column finally fails. The failure process and pattern is similar to that of a beam acted with bending moment only (Fig. 11-2), but the area of compression zone is larger due to the action of the compression, and the yielding moment (M_y) is nearer to the ultimate bending moment (M_u). This kind of failure pattern is controlled by yielding of tensile reinforcement, so it is called a larger eccentricity column or tension failed column.

The two failure patterns of the column described above transfer each other as the eccentricity changes gradually, and the boundary between them is found when the yielding of tensile reinforcement and the failure of compressive concrete on the section occur at the same time. The corresponding eccentricity (e_{0b}) is called the boundary eccentricity.

The ultimate axial force (N_u) and bending moment ($M_u = N_u e_0$) of the columns tested are plotted on a diagram and the envelope is obtained (Fig. 11-7(a)). The segment AD shows that the failure of the column is controlled by the compressive concrete, and the ultimate moment is certainly reduced as the axial compression increases, and, of course, the axial compression is reduced as the bending moment increases. On the other hand, the segment DF shows that the failure of the column is controlled by the tensile reinforcement, and the ultimate bending moment reaches the minimum when the axial compression is zero for a beam, but the ultimate bending moment is increased with the axial compression. Therefore, the axial compression is favorable for the ultimate strength of the column with larger eccentricity.

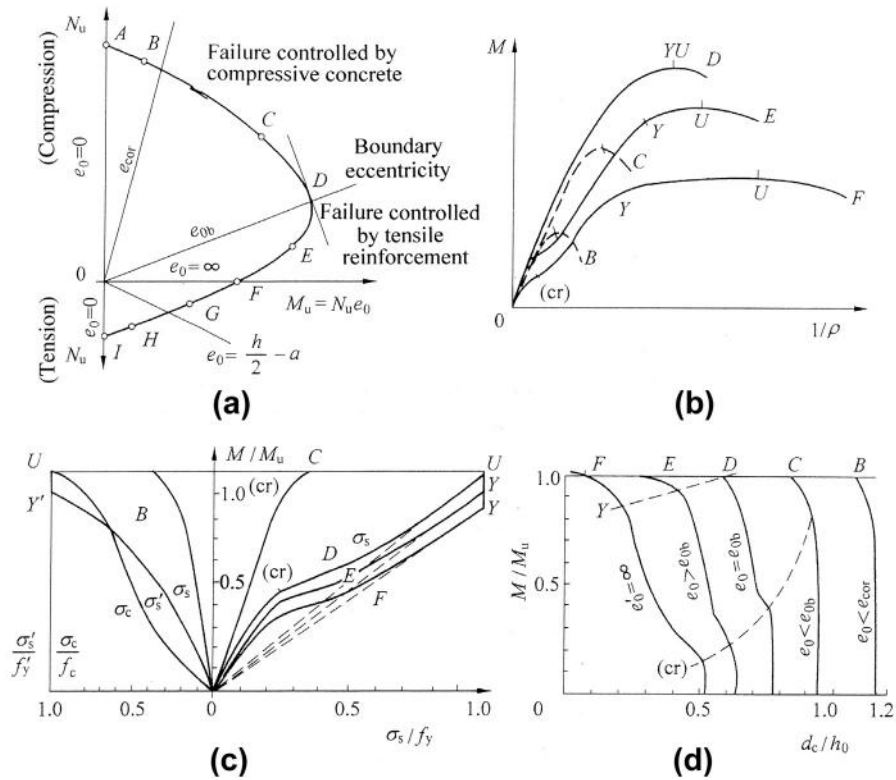


FIG. 11-7 Comparison of ultimate strengths and mechanical behaviors of columns with different eccentricities: (a) axial force-bending moment envelope, (b) bending moment—curvature relation, (c) stresses of reinforcement and concrete, (d) position of neutral axis

The compressed column with smaller eccentricity ($e_0 < e_{0b}$, e.g. curves C and D in Fig. 11-7) has greater compression zone (or d_c/h_0) on the section during failure, but the position of the neutral axis varies slightly as the compression increases during testing. The bending moment—curvature curves (M - $1/\rho$) of them are similar to the compressive stress—strain curve of plain concrete, the slope of the ascending branch reduces gradually without sudden change and even the concrete in the tension zone is cracked ($e_0 > e_{cor}$), and the curve descends quickly after peak point and poor ductility is shown. On the farther side apart from the compression on the section, the reinforcement (A_s) may be compressive or tensile but will not reach the yield strength under the ultimate state of the column.

When the column is compressed with larger eccentricity ($e_0 > e_{0b}$, e.g. curve E in Fig. 11-7), the variations of the neutral axis, reinforcement stress, and curvature of the section vary similar to that of the suitably reinforced beam (Fig. 11-3) as the axial

compression (N) increases. The column is transferred into the beam if the eccentricity increases infinitely.

When a central tension (N) and a bending moment (M) are acted together on a section of the structural member, they are equivalent to an axial tension (N) acted eccentrically ($e_0 = M/N$). The ultimate states of the member at failure (Fig. 11-8) are transferred from the central tension ($e_0 = 0$) to flexure ($e_0 = \infty$) as the eccentricity increases.

The mechanical process and failure pattern of the centrally tensed member have been analyzed above already (see Section 8.2), the concrete is cracked along the whole section and all the reinforcements are yielded (f_y) during failure. When the member is tensed with smaller eccentricity ($e_0 < \frac{h}{2} - a$) or the tension is acted between the upper and lower reinforcements, the crack occurs first at the tensile concrete with the maximum strain, which is located on the nearer side apart from the tension, and then gradually extends and expands, and the reinforcement on the same side (A_s) reaches the yield strength, as the tension is increased continuously. The concrete and reinforcement (A'_s) on the other side may be tensile ($e_0 < e_{cor}$) or compressive ($e_0 > e_{cor}$) at the beginning of loading, the concrete there is also cracked and the reinforcement is tensile but the stress is less than the yield strength ($\sigma'_s < f_y$) under the ultimate state. If the eccentricity of tension is $e_0 = \frac{h}{2} - a$, the stress of the reinforcement (A'_s) should be zero ($\sigma'_s = 0$) at ultimate state. When the member is tensed with larger eccentricity ($e_0 > \frac{h}{2} - a$) or the tension is acted outside of both reinforcements, the concrete and reinforcement on the other side should be compressive. The crack first occurs transversely and develops gradually on the nearer side of the tension and the reinforcement there (A_s) reaches the yield strength as the tension increases continuously. The compressed concrete on the other side is failed under ultimate state, and the failure process and pattern of the member are the same as that of the suitably reinforced beam (Fig. 11-2), but the compression zone on the section is smaller due to the tension acted. Therefore, the failures of all the centrally and eccentrically tensed members are controlled by yielding of the tensile reinforcement.

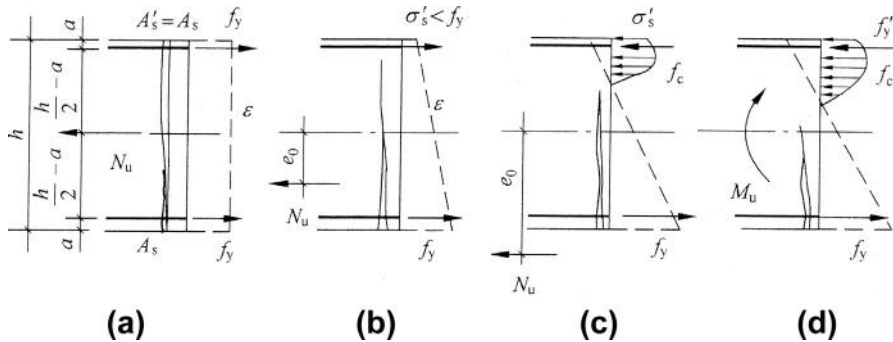


FIG. 11-8 Ultimate states of eccentrically tensed member: (a) $e_0 = 0$, (b) $e_0 < \frac{h}{2} - a$, (c) $e_0 > \frac{h}{2} - a$, (d) $e_0 = \infty$

The ultimate axial forces (N) and bending moments ($M_u = N_u e_u$) of the tensed members tested are plotted in Fig. 11-7(a), the segment FI is obtained and composed an integral envelope of axial force-bending moment (N_u-M_u) together with the segments DF and AD, which represent, respectively, the compressed members with larger and smaller eccentricities.

It should be mentioned that the mechanical behavior and failure patterns of the eccentrically compressed and tensed members described above are aimed only at the member symmetrically reinforced ($A_s = A'_s$). If the member is reinforced asymmetrically ($A_s \neq A'_s$) or the reinforcement content is too much or less, the mechanical behavior and failure pattern will change significantly. This has happened for the singly reinforced beam of rectangular section ($A'_s = 0$, $N = 0$, see Section 11.1.2), the different failure patterns, including less-, suitably, and over-reinforced, occur successively as the reinforcement content (or A_s) is increased greatly. Similarly, if the column is compressed with larger eccentricity ($e_0 > e_{0b}$) but the tensile reinforcement (A_s) is too much, it will not yield under the ultimate state and the failure of the column will be controlled by the concrete on the compression zone. In addition, the symmetrically reinforced member surely has a closed envelope being symmetrical about the N axis, as the positive and negative bending moments are acted respectively. Of course, the envelope is also closed but is asymmetrical about both the N and M axes, if the member is reinforced asymmetrically.

Of course, other important factors, e.g. the concrete and reinforcement of different kinds and strength grades, non-rectangular or asymmetrical section, long column (greater slenderness), various details of reinforcement, and loading path, also have certain influence on the mechanical behavior and failure pattern of the structural member, which have to be investigated and analyzed individually. Some of these problems will be discussed in Section 11.5.

11.2 Additional flexure of long column

When the ultimate state of the columns compressed with different eccentricities are introduced above (Fig. 11-5), it is assumed that the eccentricity ($e_0 = M/N$) keeps constantly from the start of loading until failure of the column, so the loading path is represented by a straight line in the $N-M$ envelope diagram (OA in Fig. 11-9(a)). Obviously, this is an ideal situation and is only true for the very short column. However, it is demonstrated experimentally that the loading path approximates a straight line, when the ratio between the height and sectional depth of the specimen is $l_0/h \leq 8$.

The actual column in engineering practice is rather high ($l_0/h > 8$), and the transverse deformation (deflection) should occur and increase gradually with the bending moment and axial force acted together [11-1,11-2]. When the column reaches the ultimate state (N_u), the deflection at the critical section (f in Fig. 11-9(b)) is called additional eccentricity, besides the initial eccentricity. The bending moment there

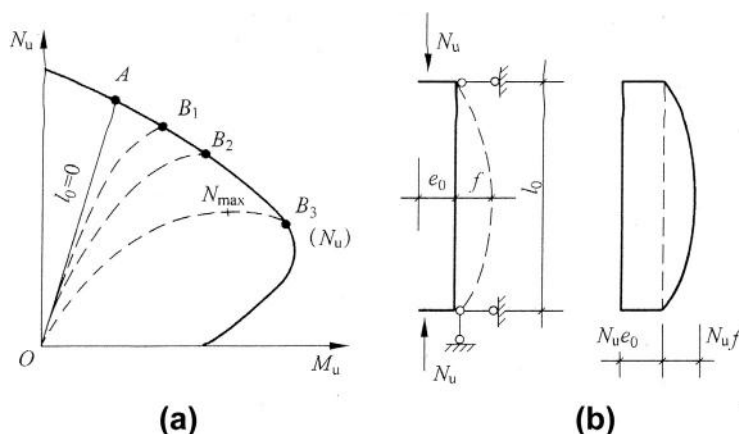


FIG. 11-9 Loading path and additional bending moment of long column: (a) N - M envelope, (b) additional bending moment of column supported by hinges

is actually $N_u(e_0 + f)$, and the additional bending moment caused by the axial force ($N_u f$) is also called the secondary bending moment or the secondary effect.

The loading path of a long column is a curve (OB) on the N - M envelope diagram, and the point of intersection (B) on the envelope corresponds to its ultimate state (Fig. 11-5). Compared with the short column, the ultimate bending moment is increased while the ultimate axial force is decreased for the longer column. Of course, the higher the column, the greater the additional eccentricity and the bending moment. Therefore, different loading paths (OB_1 , OB_2 , ...) and corresponding failure patterns are formed for the column of different height.

If the column is very high, the corresponding loading path deviates even farther from the line OA . When the axial force reaches the peak value (N_{max}) and, then, turns into the descending branch, the loading path is still within the envelope, so the concrete and reinforcement do not reach their strengths yet and no failure symptom can be found. However, the bending moment is increased continuously with the deformation (deflection), although the axial force is decreased gradually. Finally, the loading path intersects the envelope at point B_3 (Fig. 11-9(a)), and the column reaches the ultimate state. The column, of which the ultimate axial force is less than the maximum one experienced in the loading process ($N_u < N_{max}$), is called a slender column. It happened only in the experiments when $l_0/h = 30-40$ for the column of rectangular section ($b \times h$), but is seldom found in engineering practice.

Therefore, when the ultimate state and strength of a long column is discussed, the additional eccentricity and bending moment have to be considered. The appearance and increase of the additional eccentricity is the result of lateral deformation (deflection), so all the factors causing the deformation of the column have influences on the additional bending moment and ultimate strength. The factors mainly include: slenderness (l_0/h) and initial eccentricity; support condition and confinement level at

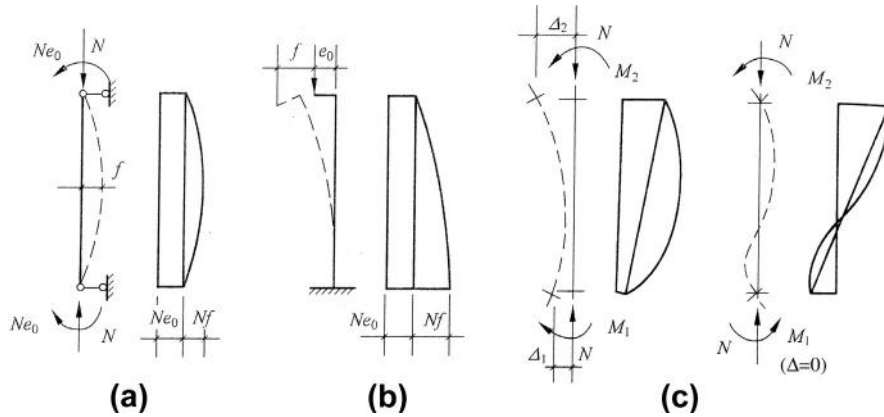


FIG. 11-10 Influence of support and confinement conditions at ends of column on additional bending moment: (a) hinged column, (b) cantilever column, (c) framed column

ends, i.e. displacement (Δ_1 , Δ_2), distribution¹ of bending moment of both positive and negative signs or single sign [11-1] (Fig. 11-10); constitutive relation of the materials and detail of reinforcement; initial eccentricity caused by non-uniformity of material and construction error; creep of concrete under sustained stress; etc.

The ultimate strength of the eccentrically compressed column can be accurately calculated only by non-linear analysis along the loading history. According to the mechanical conditions at both ends and the constitutive relations of the materials of the column, the sectional curvature ($1/\rho$) and deformation (f) are calculated first and the distributions of the internal forces are determined by digital iteration for every increment of axial force or deformation, then the complete curve of $M - N - f$ is obtained successively. This calculation needs many parameters and is time-consuming, so it is only used for some especially important or slender columns. The columns used generally in engineering practice can be calculated easily by the method with sufficient accuracy based on the experimental results [11-3].

When a column of height l_0 is support by two hinges at both ends and the curvature of the section at mid-height is $(1/\rho)_u$ under the ultimate state, the maximum deflection should be

$$f = \left(\frac{1}{\rho}\right)_u \frac{l_0^2}{\beta}, \quad (11-2a)$$

where the parameter β depends upon the distribution of the curvature along the height. For example, the parameter is $\beta = 8$, 9.6 , and $\pi^2 (\approx 10)$ respectively for the rectangular ($M = \text{const.}$), parabolic, and sine distributions, and the experimental datum is about 10.

¹It should be noted that the critical section of the column may be moved after the additional bending moment occurs.

The curvature at ultimate state is approximately taken as the boundary value between the failure patterns of the larger and smaller eccentricities $(1/\rho)_b$ and modified with two coefficients:

$$\left(\frac{1}{\rho}\right)_u = \left(\frac{1}{\rho}\right)_b \varsigma_1 \varsigma_2. \quad (11-3)$$

If the ultimate strain of the compressive concrete is $\varepsilon_u = 0.0033$ and amplified by a factor 1.25 considering creep effect and the yielding strain of the tensile reinforcement is taken as $\varepsilon_y = f_y/E_s = 0.0017$, the ultimate curvature $(1/\rho)_b$ is calculated and substituted successively into the two formulas above, the maximum deflection at mid-height of the column is derived as

$$f = \left[\frac{1.25 \times 0.0033 + f_y/E_s}{h_0} \right] \frac{l_0^2}{10} \varsigma_1 \varsigma_2, \quad (11-2b)$$

where the influence coefficients of slenderness and eccentricity are taken respectively from the experiment results:

$$\varsigma_2 = 1.15 - 0.01 \frac{l_0}{h} \leq 1.0$$

$$\text{and } \varsigma_1 = 0.2 + 2.7 \frac{e_0}{h} \leq 1.0, \quad (11-4)$$

$$\text{or } \varsigma_1 = 0.5 f_c \frac{bh}{N} \leq 1.0 \quad (11-4a)$$

for the symmetrically reinforced member.

The total eccentricity of the column at ultimate state is $e_u = e_0 + f = \eta e_0$, so the amplifying coefficient of the eccentricity [2-1] is:

$$\eta = \frac{e_0 + f}{e_0} \approx 1 + \frac{1}{1400 \frac{e_0}{h}} \left(\frac{l_0}{h} \right)^2 \varsigma_1 \varsigma_2, \quad (11-5)$$

where $h/h_0 = 1.1$ is taken.

The additional bending moment or eccentricity and ultimate strength of the eccentrically compressed long column have been investigated experimentally and theoretically in many countries, and various calculation methods, e.g. those listed in Table 11-1, are suggested already. However, the calculation principle and influencing factors considered for these methods are different significantly and can be found in the relevant design codes [2-11,2-12] and references [11-1,11-3].

11.3 General method for sectional analysis

When the section of a reinforced concrete member acted together with an axial force and bending moment is analyzed along the loading path, the basic assumptions used are as below.

1. A plane section of the member remains a plane from start of loading until failure. It is demonstrated experimentally that this assumption is accurately followed for

Table 11-1 Additional Bending Moment (Eccentricity) of Eccentrically Compressed Long Column

Reference	Calculation Formulas	Notes
U.K. CP110 [11-3]	$\left(\frac{1}{\rho}\right)_u = \frac{1}{175h} \left(1 - 0.0035 \frac{l_0}{h}\right) k_1$ $k_1 = \frac{N_0 - N}{N_0 - N_b} \leq 1.0$	N_0 ultimate strength under central compression, N_b ultimate strength at boundary failure
Germany DIN 1045 [11-3]	$f = h \frac{\lambda - 20}{100} \sqrt{0.1 + \frac{e_0}{h}} \text{ when } \frac{e_0}{h} \leq 0.3,$ $f = h \frac{\lambda - 20}{160} \geq 0 \text{ when } 0.3 \leq \frac{e_0}{h} \leq 2.5$ $f = h \frac{\lambda - 20}{160} \left(3.5 - \frac{e_0}{h}\right) \text{ when } 2.5 \leq \frac{e_0}{h} \leq 3.5$	$\lambda = \frac{l_0}{r} \leq 70$ r sectional radius of gyration.
Russia CH II II [11-3]	$\eta = \frac{1}{1 - \frac{N}{N_b}}$ $N_b = \frac{6.4E_0}{l_0^2} \left[\frac{J}{K_1} \left(\frac{0.11}{0.1 + \frac{1}{K_p}} + 1 \right) + nJ_s \right]$	N_b critical central force, E_0 initial modulus of elasticity of concrete, J inertia modulus of elasticity of concrete, J_s inertia moment of reinforcement area against centre, K_1 coefficient for influence of sustained load, K_2 coefficient for influence of prestressing on stiffness.
U.S.A ACI 318-95 [2-11]	<p>Increasing bending moment for design</p> $M_c = \delta_b M_{2b} + \delta_s M_{2s}$ $\delta_b = \frac{c_m}{1 - \frac{N}{\phi N_b}} \geq 1.0, \delta_s = \frac{1}{1 - \frac{\sum N}{\phi \sum N_b}} \geq 1.0$ $N_b = \frac{\pi^2 EI}{(l_0)^2},$ $c_m = 0.6 + 0.4 \frac{M_{1b}}{M_{2b}}$ <p>when $\frac{l_0}{r} < 34 - 12 \frac{M_{1b}}{M_{2b}}$ or < 22, the slenderness needs not to be considered;</p> <p>when $\frac{l_0}{r} > 100$, $P - \Delta$ analysis needs to be conducted along loading path.</p>	M_{2b}, M_{1b} absolute values of bending moments at both ends of the column ($M_{2b} \geq M_{1b}$) caused by load, which does not cause lateral displacement (Fig. 11-10(c)), $M_{2s} (M_{1s})$ similar to $M_{2b} (M_{1b})$ caused by load which apparently causes lateral displacement, $\sum N$ summation of axial forces of all columns in same storey, N_b critical axial force of a single column, $\sum N_b$ summation of critical axial forces of all columns in same storey, ϕ -reducing coefficient for ultimate strength.

Table 11-1 Additional Bending Moment (Eccentricity) of Eccentrically Compressed Long Column—cont'd

Reference	Calculation Formulas	Notes
Europe CEB FIP MC90 [2-12]	<p>Arbitrary column: $e = e_{01} + f$</p> $e_{01} = e_0 + e_a = \frac{M}{N} + e_a$ $f = 0.1k_1 l^2 \left(\frac{4}{\rho_e} + \frac{1}{\rho_1} \right)$ $k_1 = 2 \left(\frac{\lambda}{\lambda_1} - 1 \right) \text{ when } \lambda_1 \leq \lambda \leq 1.5\lambda_1$ $k_1 = 1 \text{ when } \lambda > 1.5\lambda_1$ <p>Farmed column: calculated separately, considering the mechanical situation of the frame and confinement condition at supports.</p>	<p>e_a initial eccentricity caused by default of the member, ρ_e, ρ_1 curvatures correspond respectively to eccentricities e and e_{01}, λ_1 boundary slenderness. Secondary effect can be neglected when $\lambda \leq \lambda_1$.</p>

the section without tension zone, but the section with tension zone only remains a plane before cracking of the concrete. After the concrete is cracked, the relative slip occurs and develops between the reinforcement and surrounding concrete nearby on both sides of the crack, so the plane section does not remain. However, from the point of view of engineering application, the assumption is still approximately satisfied, if the average strain within a length of the member along its axis, e.g. half of the sectional depth or the distance of the adjacent cracks, is considered.

2. The constitutive (stress—strain) relations of concrete and reinforcement measured from the standard tests are applicable for the structural member. Although the strain gradient, reciprocal influence between both materials, confinement of stirrups, size effect, different loading velocity, and sustaining time usually occur in the member, they are not considered during analyzing. It is also demonstrated experimentally that this simplification causes only a small error for the member of ordinary material and reinforcement detail.
3. Generally, the effects of time (or age of concrete) and environmental temperature and humidity on the member are not considered, so the internal stress and deformation states caused by shrinkage and creep of the concrete and variations of temperature and humidity are neglected.
4. The deformation of the member is small enough even under the ultimate states, and has no obvious influence on its calculation model and internal forces.

Geometrical (deformation) condition. When the section is loaded until the crack appears and develops, the neutral axis ($o-o$) moves gradually towards the same side of the compression and the compressive depth of the section (kh_0) is reduced. The concrete in tension zone is out of work after cracking except a small

part underneath the neutral axis ($y = 0 - y_t$). The angular rotation within a unit length of the member (φ), i.e. the curvature of the section ($1/\rho$) is

$$\varphi = \frac{1}{\rho} = \frac{\varepsilon_c + \varepsilon_s}{h_0} = \frac{\varepsilon_c}{kh_0}. \quad (11-6)$$

The strain at y_i from the neutral axis is

$$\varepsilon_i = \varphi y_i, \quad (11-7a)$$

so the concrete is compressive for $y_i > 0$ or tensile for $y_i < 0$. The compressive strain of the concrete at top of the section is

$$\varepsilon_c = \varphi kh_0, \quad (11-7b)$$

and the compressive strain of upper reinforcement and tensile strain of lower reinforcement are respectively:

$$\varepsilon'_s = \varphi(kh_0 - a) \quad \text{and} \quad \varepsilon'_s = \varphi(1 - k)h_0. \quad (11-7c)$$

Physical (constitutive) relation. Different stress–strain relations are, respectively, for the concrete under compression and tension (Chapter 2), and the stress–strain relation of tensile and compressive reinforcement depend upon the category and strength grade (Chapter 6):

$$\text{Concrete} \quad \sigma_c(\varepsilon_i), \quad \sigma_t(\varepsilon_i) \quad (11-8a)$$

$$\text{Reinforcement} \quad \sigma'_s(\varepsilon'_s), \quad \sigma_s(\varepsilon_s) \quad (11-8b)$$

Mechanical (equilibrium) equations. The equilibrium equations for axial forces and the moments against the center of tensile reinforcement are, respectively:

$$\left. \begin{aligned} \Sigma X = 0 \quad & \int_0^{kh_0} \sigma_c(\varepsilon_i)b(y)dy - \int_0^{y_t} \sigma_t(\varepsilon_i)b(y)dy + \sigma'_s A'_s - \sigma_s A_s = N \\ \Sigma M = 0 \quad & \int_0^{kh_0} \sigma_c(\varepsilon_i)b(y)(h_0 - kh_0 + y)dy - \int_0^{y_t} \sigma_t(\varepsilon_i)b(y)(h_0 - kh_0 + y)dy \\ & + \sigma'_s A'_s(h_0 - a') = N(e_0 + y_a) \end{aligned} \right\} \quad (11-9)$$

After equations (11-6) to (11-8a, -8b) are substituted into equation (11-9), only two unknowns (φ, k) are contained. Of course, two other unknowns, e.g. ε_c and ε_s or ε_c and k , may also be used.

After φ and k are solved from Eq. (11-9) and substituted into relevant formulas, the stress and strain distributions and curvature of the section are obtained. Then, the mechanical state and stage (Fig. 11-2) of the section can be judged and the crack and deformation can be calculated accordingly (Chapters 12 and 13). However, the explicit solution of Eq. (11-9) is hardly found because of the non-linear constitutive

relations of both materials and the cracks exist and develop. Generally, the equations are solved by digital method and the member is calculated along the loading path by computer.

Various calculation methods and different variations [11-4,11-5] are used for compiling computer programs. Among them the method, which assumes first a strain and then calculates the internal forces and curvature correspondingly, is easily and quickly conducted, and the complete curve, including descending branch of the bending moment-curvature relation of the section, can be directly obtained (Fig. 11-11).

The shape, size, and reinforcements of the section, the constitutive relations of concrete and reinforcement, and the axial force (N) and eccentricity ($e_0 = M/N$) are known in advance. The section is divided into narrow strips perpendicular to the symmetrical axis, and the stress and strain are assumed to be distributed uniformly within each strip. The compressive concrete strain (ϵ_c) of the top strip is selected as the basic variation, and is given successively following the equal or variable increment ($\Delta\epsilon_c$). The position of neutral axis or relative depth of compression zone (k) is taken as the iteration variation, the internal forces (N_i and M_i) are then calculated after iteration and output, when the allowable error is satisfied. The flow chart of the calculation is shown in Fig. 11-12.

In addition, the increment of compressive strain of concrete ($\Delta\epsilon_c$) may be adjusted to save the calculating time or to increase the calculation accuracy; the value of the allowable error ($[\Delta]$) is determined by the accuracy needed; the maximum compressive strain of concrete should be greater than the peak strain ($\epsilon_{\max} > \epsilon_p$) to obtain the descending branch of $M - 1/\rho$ curve and the ultimate strength (N_u, M_u); the output results and plotted curves are provided for necessary.

The general method described above can be used for analyzing any reinforced concrete member with various shape and reinforcement of the section and different constitutive relations of the materials used, and the mechanical behaviors and

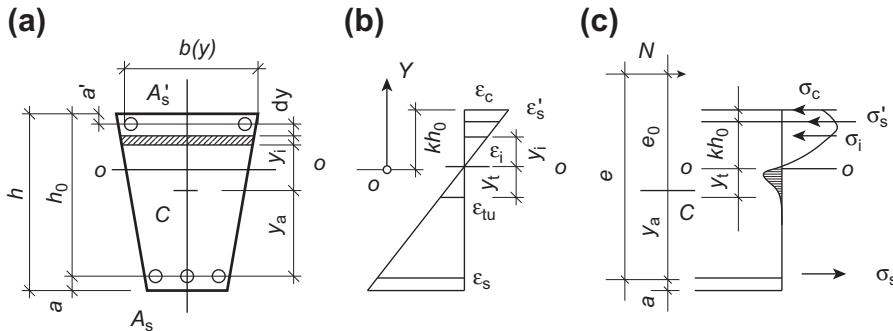


FIG. 11-11 Calculation model for symmetrical section: (a) section, (b) strain distribution, (c) stress distribution

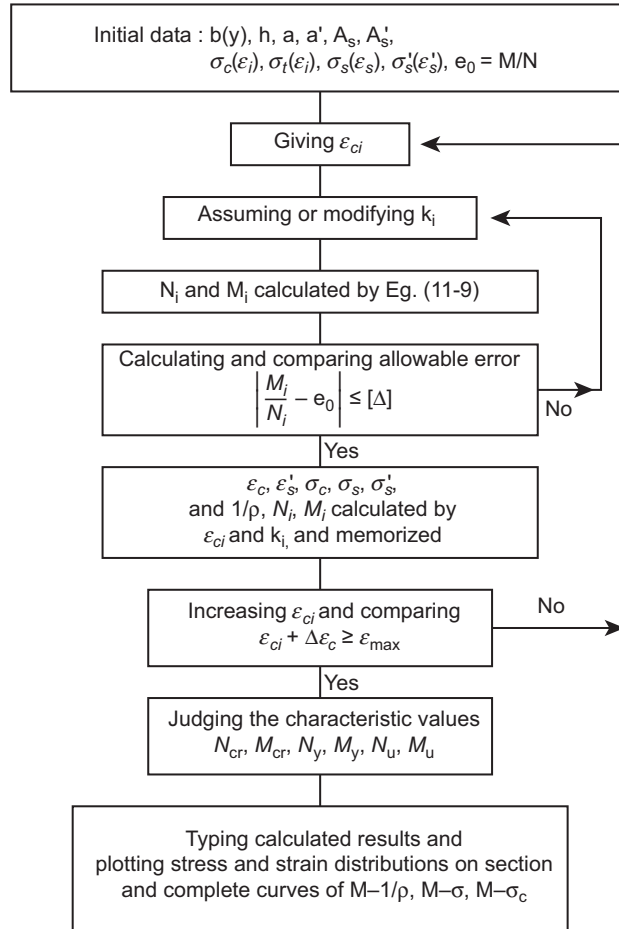


FIG. 11-12 Flow chart for sectional analysis

characteristic values along the complete loading history, including elastic stage, start and development of crack, yielding of reinforcement, ultimate state, and descending branch of the strength, are provided successively.

The sectional analysis along loading history is necessary only for the analysis along loading history of the structure, e.g. aseismic one, and numerous calculation works have to be conducted. Usually, only some characteristic values of the structure or its member, e.g. ultimate strength (N_u , M_u), crack width and the maximum deflection under service load, sectional stiffness used for analysis of statically indeterminate structure, are needed to be determined in engineering practice. Therefore, the practical methods used easily and directly should be provided, besides the general method.

11.4 Ultimate strength

11.4.1 Calculation formulas

The ultimate strength of an eccentrically compressed member of reinforced concrete is taken as the axial force (N_u) and bending moment ($\eta N_u e_0$) at failures of both tensile reinforcement and compressed concrete (larger eccentricity) or at failure of compressed concrete only (smaller eccentricity), and the basic calculation formulas are established based on the assumptions below.

1. The strains of the concrete and reinforcement on the section, including compression and tension zones, distribute linearly;
2. The tensile action of the concrete is neglected at the ultimate state, as the force and lever arm of the tensile concrete existing only underneath the neutral axis is limited;
3. The constitutive (stress—strain) relations of concrete and reinforcement measured from the standard tests are used for the analysis of structural member;
4. The internal stress and strain states caused by time (age) and environmental temperature and humidity are not considered.

Therefore, the strain and stress distributions on the rectangular section of an asymmetrically reinforced member at ultimate state are presented in Fig. 11-13(b) and (c). The maximum stress (strength) of the concrete in compression zone is γf_c , in which the value of γ is slightly greater than 1.0 (see Section 3.2), as the strain gradient exists on the section. Two important concepts are introduced in advance before the calculation formulas of ultimate strength are established.

11.4.1.1 Equivalent rectangular stress diagram

If the compressive depth is x_u and the strain at the top is ε_u on the section at ultimate state, the strain of compressed concrete apart y from the neutral axis should be

$$\varepsilon_c = \frac{\varepsilon_u}{x_u} y. \quad (c)$$

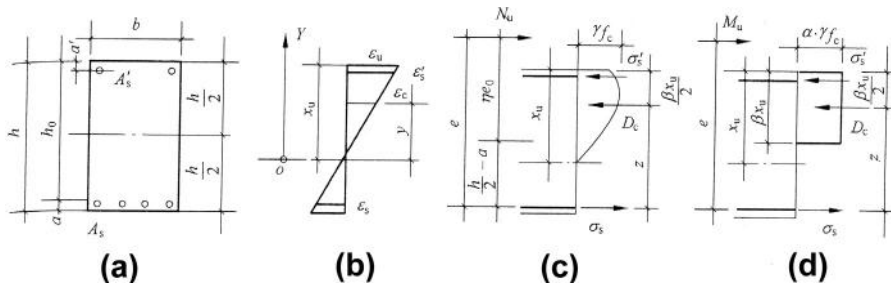


FIG. 11-13 Ultimate state and equivalent rectangular stress: (a) section, (b) strain distribution, (c) stress distribution, (d) equivalent stress

After it is substituted into the constitutive relation of concrete, the compressive stress $\sigma_c \left(\frac{\epsilon_u}{x_u} y \right)$ is obtained. Correspondingly, the volume of compressive stress block, i.e. total compressive force, on the compression zone is

$$D_c = \int_0^{x_u} \sigma_c \left(\frac{\epsilon_u}{x_u} y \right) b dy, \quad (d)$$

and the distance between the acting point of the force and top of the section is

$$\frac{\int_0^{x_u} \sigma_c \left(\frac{\epsilon_u}{x_u} y \right) b (x_u - y) dy}{D_c}. \quad (e)$$

In order to simplify the calculation, the curved stress diagram on compression zone is transferred to a rectangular one (Fig. 11-13(d)). When the volume (or area) and the gravity center, i.e. the total compression and its acting point, of the former coincide with that of the latter, both diagrams are totally equivalent. If the compressive depth of the rectangular stress diagram is βx_u and the uniform stress (strength) is $\alpha \gamma f_c$, the condition of equivalent should be as below:

1. The distance between the center of the rectangular diagram and top of the section ($\beta x_u / 2$) is equal to the value calculated by formula (e), so

$$\beta = \frac{2 \int_0^{x_u} \sigma_c \left(\frac{\epsilon_u}{x_u} y \right) b (x_u - y) dy}{D_c x_u} \quad (11-10a)$$

is obtained.

2. The areas of both stress diagrams are equal:

$$\begin{aligned} D_c &= \beta b x_u \cdot \alpha \gamma f_c, \\ \therefore \alpha &= \frac{D_c}{\beta \gamma b x_u f_c}. \end{aligned} \quad (11-10b)$$

There are three characteristic parameters (α , β , and γ) for the equivalent rectangular stress diagram. Among them α and β are the parameters obtained only from the transformation of the geometrical diagrams but are independent of the strength (γf_c). They mainly depend upon the shape of the complete stress—strain curve and the ultimate strain (ϵ_u) of the compressed concrete, and also vary with the sectional shape of the member, reinforcement content or compressive depth, confinements of longitudinal reinforcement and ties. Various provisions are provided in the design codes of different countries, and, in China [2-1] the values of these parameters are taken as below [11-6].

After several stress—strain curves of compressed concrete are selected and compared, the parabola of second order-horizontal model (Rüsch, Table 2-6) is taken as the stress diagram in compression zone (Fig. 11-14(a)), as it is used simply and the calculated results fit well with the measured strength of relevant specimens. The values of the characteristic parameters α and β are calculated according to the

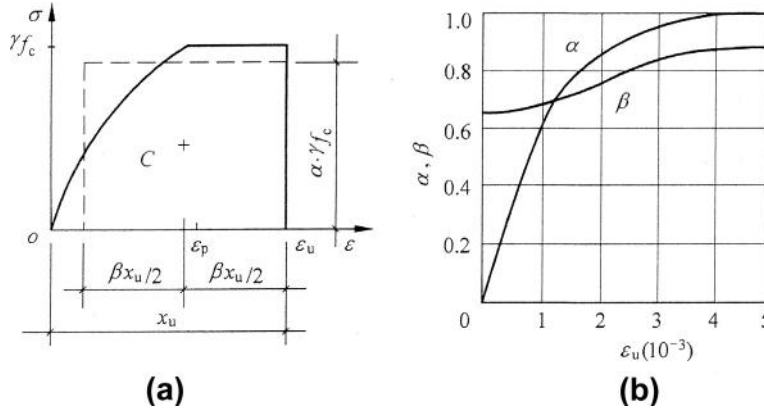


FIG. 11-14 Characteristic parameters for equivalent rectangular stress diagram: (a) equivalent of stress diagram, (b) values of α and β [11-6]

principle of equivalence, and they vary with the ultimate strain (ϵ_u) taken (Fig. 11-14(b)). If a very small value ($\epsilon_u \rightarrow 0$) is taken, the compressed concrete would be of elastic stage and the stress diagram would approach a triangle, so $\beta_{\min} = 2/3$ and $\alpha = 0$ are obtained; while a very large value ($\epsilon_u \rightarrow \infty$) is taken, the stress diagram would approximate a rectangle, so the values of both β and α approach 1.0.

The ultimate compressive strain of concrete is $\epsilon_u = 3-4 \times 10^{-3}$ for the flexural member of concrete grade C20–C50 and general reinforcement content, according to many experimental results [11-7]. The ultimate strain is slightly reduced for the eccentrically compressed member, as the compressive depth (x_u/h_0) is increased or the strain gradient is decreased. It is seen from Fig. 11-14(b) that the values of α and β do not vary much when $\epsilon_u > 3.0 \times 10^{-3}$. When the eccentricity of the compressed member is near the boundary between the larger and smaller ones, the relative depth of the compression zone on the section ranges from 0.4 to 0.7 and the average strain is about $\epsilon_u = 3.3 \times 10^{-6}$ at ultimate state. The values of the parameters are correspondingly

$$\alpha = 0.969 \quad \text{and} \quad \beta = 0.824, \quad (11-11a)$$

and they are rounded off to

$$\alpha\gamma = 1.0 \quad \text{and} \quad \beta = 0.8, \quad (11-11b)$$

after the value of γ is introduced. The calculated strength based on these values agrees well, with limited error, with the ultimate strength of the member tested of concrete grade \leq C50.

Alternately, the parameters are taken as

$$\left. \begin{aligned} \alpha\gamma f'_c &= 0.85f'_c \\ \beta &= 0.85 - 0.008(f'_c - 30) \end{aligned} \right\} \quad (11-12)$$

for the equivalent rectangular stress diagram in American code [2-11], in which f'_c is the compressive strength of concrete cylinder (N/mm^2), and the β value should range from 0.65 to 0.85.

11.4.1.2 Boundary of compressive depth

The failure patterns of eccentrically compressed members are transferred to each other as the eccentricity increases or decreases gradually. When the ultimate strain of the compressed concrete (ε_u) and the yielding strain of the tensile reinforcement (ε_y) of the member reach simultaneously at the ultimate state, this is the boundary of two failure patterns. Correspondingly, the compressive depth of the section can be calculated according to the assumption of the plane section (Fig. 11-15):

$$x_{0b} = \frac{\varepsilon_u}{\varepsilon_u + \varepsilon_y} h_0. \quad (\text{f})$$

The compressive depth is reduced to $x_b = \beta x_{ub}$ and the relative value is $\xi_b = \beta x_{ub} / h_0$, after the curved stress diagram is transferred to the rectangular one. After $\varepsilon_u = 0.0033$, $\varepsilon_y = f_y / E_s$, and $\beta = 0.8$ are substituted, the boundary of relative compressive depth is obtained

$$\xi_b = \frac{x_b}{h_0} = \frac{\beta \varepsilon_u}{\varepsilon_u + \varepsilon_y} = \frac{0.00264}{0.0033 + f_y / E_s}. \quad (11-13)$$

Therefore, when the equivalent rectangular stress diagram is used for calculation of the ultimate strength, the tensile reinforcement was yielded in advance and the compressive concrete fails later at ultimate state if $\xi \leq \xi_b$ or $x \leq x_b = 0.8x_{ub}$, so it should be a suitable-reinforced beam or a compressed member with larger eccentricity; while the compressive concrete fails first but the tensile reinforcement will

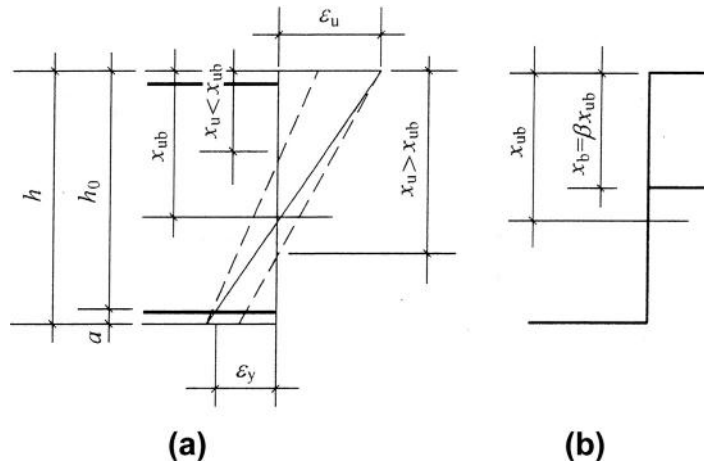


FIG. 11-15 Boundary depth of compressive zone: (a) position of neutral axis, (b) equivalent stress diagram

not yield ($\sigma_s < f_y$) at the ultimate state if $\xi > \xi_b$ or $x > x_b$, it should be an over-reinforced beam or a compressed member with smaller eccentricity.

The methods used to determine the boundary depth of compressive zone are similar in other countries [2-11,2-12], but the values taken for the ultimate strain of the concrete are slightly different and more safety is reserved.

11.4.1.3 Calculation formulas

After the equivalent rectangular stress diagram on the compression zone is determined, two equilibrium equations are easily established for the eccentrically compressed member of rectangular section at ultimate state (Fig. 11-16):

$$\left. \begin{aligned} \Sigma X = 0 \quad N_u &= f_c b x + \sigma'_s A'_s - \sigma_s A_s \\ \Sigma M = 0 \quad N_u \left(\eta e_0 + \frac{h}{2} - a \right) &= f_c b x \left(h_0 - \frac{x}{2} \right) + \sigma'_s A'_s (h_0 - a) \end{aligned} \right\} \quad (11-14)$$

The unknowns x and N_u can be solved for an eccentricity (e_0) given, and $M_u = \eta N_u e_0$ is then calculated and the ultimate axial force-bending moment envelope can be plotted correspondingly (Fig. 11-7(a)).

The values of the strength or stress of the materials in Eq. (11-14) are taken as below.

1. The compressive strength and strain of the concrete at the section edge near the compression reach respectively f_c (i.e. $\alpha\gamma = 1$) and $\epsilon_u > 3 \times 10^{-3}$ at ultimate state regardless of different failure patterns and eccentricities.

2. The stress of the reinforcement in compression zone (σ'_s) is calculated from the corresponding strain (ϵ'_s), which follows the assumption of plane section:

$$\sigma'_s = \epsilon'_s E_s = \frac{1.25x - d'}{1.25x} \epsilon_u E_s. \quad (11-15)$$

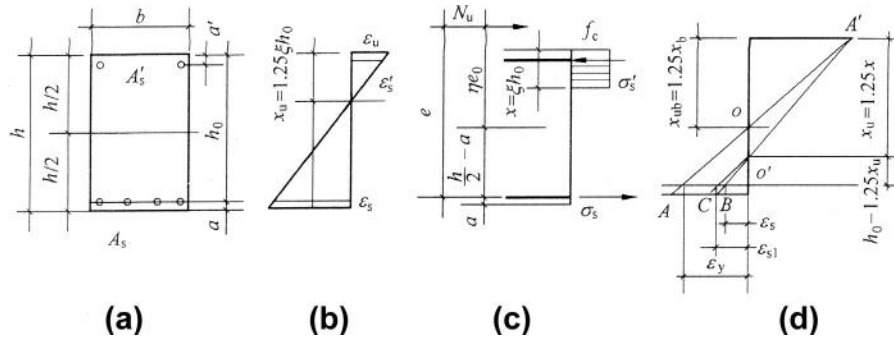


FIG. 11-16 Calculation of eccentrically compressed member of rectangular section: (a) rectangular section, (b) strain distribution, (c) stress state, (d) approximate stresses of reinforcements

When $x \geq 2a'$ and $\varepsilon_u > 3 \times 10^{-3}$, $\varepsilon'_s \geq 1.8 \times 10^{-3}$ is obtained, and the strain will be increased as creep of the concrete there is considered. Generally, the reinforcement in compression zone reaches the yield strength at ultimate state of the member, so

$$\sigma'_s = f_y \quad (11-16)$$

is used for calculation when $x \geq 2a'$.

3. The stress of tensile reinforcement (σ_s) should be calculated individually for different failure patterns of the member, which are distinguished by the boundary depth of the compression zone (x_{ub} or ξ_b):

When $x_u \leq x_{ub}$ or $\xi \leq \xi_b$, the failure of the member is controlled by yielding of the tensile reinforcement, so

$$\sigma_s = f_y; \quad (11-17)$$

when $x_u > x_{ub}$ or $\xi > \xi_b$, the failure of the member is controlled by the compressed concrete, while the stress of the tensile reinforcement does not yield ($\sigma_s < f_y$). However, the strain of the reinforcement also follows the assumption of plane section, and the stress is calculated by

$$\sigma_s = \varepsilon_s E_s = \frac{h_0 - 1.25x}{1.25x} \varepsilon_u E_s = \left(0.8 \frac{h_0}{x} - 1\right) \varepsilon_u E_s. \quad (11-18a)$$

When it is substituted into Eq. (11-14), an equation of third order of the unknown (x) is established, but it is solved with difficulty. Alternatively, the stress of the tensile reinforcement at ultimate state is calculated approximately. The strain distributions on the section are respectively $A'OA$ for the member at the boundary of two failure patterns and $A'O'B$ for the member with $x_u > x_{ub}$ (Fig. 11-16(d)). The stress (or strain ε_s) calculated by Eq. (11-18a) corresponds to the later situation. If the line $O'C$ is drawn and parallel to the line OA via point O' , the approximate value (ε_{sI}) is obtained from

$$\frac{\varepsilon_{sI}}{\varepsilon_y} = \frac{h_0 - 1.25x}{h_0 - 1.25x_b}.$$

Correspondingly, the stress of the reinforcement is

$$\sigma_s = \frac{h_0 - 1.25x}{h_0 - 1.25x_b} f_y = \frac{0.8 - \xi}{0.8 - \xi_b} f_y. \quad (11-18b)$$

Obviously, $\sigma_s = f_y$ when $\xi = \xi_b$, $\sigma_s = 0$ when $\xi = 0.8$, and $\sigma_s < 0$, i.e. compressive stress, when $\xi > 0.8$. Eq. (11-18b) can still be used for the last situation (smaller eccentricity).

11.4.1.4 Eccentrically tensed member

The initial eccentricity of an eccentrically tensed member of long length will not increase with the tension, even the eccentricity at ultimate state is less than the initial one ($\eta < 1$), so the ultimate bending moment is slightly smaller than the original

one. Therefore, the eccentricity of a tensed member is usually considered as a constant during loading ($\eta = 1$). According to the position or eccentricity of the tension, both the stress diagram at ultimate state and the failure pattern of the member are divided into two categories, and then calculated separately.

Tension with smaller eccentricity ($e_0 < \frac{h}{2} - a$). The whole section is cracked and the concrete is out of work at the ultimate state (Fig. 11-8(b)). Only if the tension is exactly acted at the resultant (or area) center of the upper and lower reinforcements, both reach the yield strength at the ultimate state. Otherwise, only the reinforcement on the tension side is yielded, while the reinforcement on other side is not yielded yet at the ultimate state. The calculation formulas are generally

$$\left. \begin{aligned} N_u \left(\frac{h}{2} - a' + e_0 \right) &= \sigma_s A_s (h_0 - a') \\ N_u \left(\frac{h}{2} - a - e_0 \right) &= \sigma'_s A_s (h_0 - a') \end{aligned} \right\} \quad (11-19)$$

Tension with larger eccentricity ($e_0 > \frac{h}{2} - a$). A compression zone should exist on the section of the member at ultimate state (Fig. 11-8(c)), and the stress distribution is similar to that of the eccentrically compressed member with larger eccentricity (Fig. 11-5(e)). The equilibrium equations established below are similar to Eq. (11-14), except the direction and position of axial force (N_u):

$$\left. \begin{aligned} N_u &= -f_c b x - \sigma'_s A'_s + \sigma_s A_s \\ N_u \left(e_0 - \frac{h}{2} + a \right) &= f_c b x \left(h_0 - \frac{x}{2} \right) + \sigma'_s A'_s (h_0 - a') \end{aligned} \right\} \quad (11-20)$$

The calculation of the eccentrically tensed member compensates the lower half of the ultimate axial force-bending moment envelope (curve FI in Fig. 11-7(a)).

11.4.2 Member under biaxial bending

When an axial (N) and two bending moments in the perpendicular directions (M_x and M_y) are acted together on a column, the eccentricities should be correspondingly $e_{0x} = M_x / N$ and $e_{0y} = M_y / N$ in both directions (Fig. 11-17(a)). This happens in engineering practice, e.g. the column at the corner of a building, the frame column supporting a water tower or pipeline, power transmission pole. This kind of structural member has been investigated experimentally and theoretically in many countries [11-8–11-12] and corresponding calculation and design methods are provided in various design codes.

It is demonstrated that the failure process of a compressed member with biaxial bending is similar to that with single bending. However, the neutral axis of the section ($o-o$) is not perpendicular to the acting plane of the compression with biaxial eccentricities (NC) ($\alpha + \theta \neq 90^\circ$), and the resultant of the deflections in two directions ($w_x + w_y = w$) is not placed in the plane NC ($\beta \neq \alpha$). When eccentric compression is increased, the transverse crack appears in the tension zone of the section, and

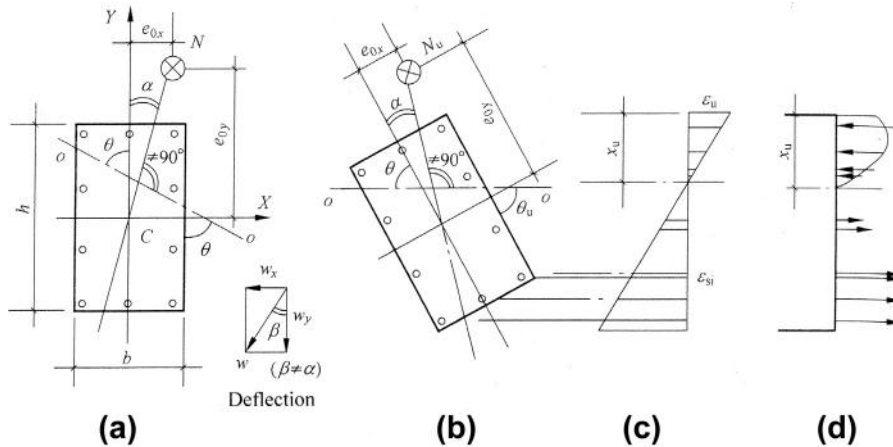


FIG. 11-17 Compressed member with biaxial bending: (a) axial force with biaxial eccentricities, (b) neutral axis, (c) strain distribution, (d) stress distribution

the neutral axis moves up and rotates ($\Delta\theta$) and the compression zone on the section is reduced gradually. Finally, the failure pattern of larger eccentricity occurs when the tensile reinforcement is yielded first and the compressive concrete fails later; or the failure pattern of smaller eccentricity occurs when the compressive concrete fails but the tensile reinforcement does not yet yield. The strain distribution under ultimate state also follows the assumption of plane section. When the general analysis method (Section 11.3) is used, the equilibrium equations $\sum N = 0$, $\sum M_x = 0$, and $\sum M_y = 0$ should be established referring to Fig. 11-17, and the unknowns N_u , x_u , and θ_u are solved after knowing the eccentricities e_{0x} and e_{0y} . Usually, the iterative calculation is needed and completed by computer.

When the section size and materials used for a reinforced concrete column are given, the ultimate strength (N_u , M_x , and M_y) with different eccentricities (e_{0x} and e_{0y}) can be measured during testing and the envelope is plotted correspondingly as shown in Fig. 11-18(a). The envelope intersects respectively with three coordinates at N_0 (strength of centrally compressed member), and M_{x0} and M_{y0} (respective ultimate bending moments in X and Y directions of the flexural member ($N = 0$)). In addition, the envelope intersects with two vertical coordinate planes, and two intersection curves show respectively the ultimate envelopes of axial force-bending moment in X and Y directions alone (N_0-M_{x0} and N_0-M_{y0} , similar to Fig. 11-7(a)). The points (M_{xb} , N_b) and (M_{yb} , N_b) on the curves represent respectively the members with boundary eccentricities in X and Y directions. The envelope also intersects with the horizontal coordinate plane, and the intersection curve ($M_{x0}-M_{y0}$) shows the envelope of the member under biaxial bending without axial force ($N = 0$).

The intersections between the envelope and the horizontal planes of different axial forces (N_u) are curves of a family. The curves should be the circles of different diameters for a column of circular section, i.e. the envelope is a rotating surface

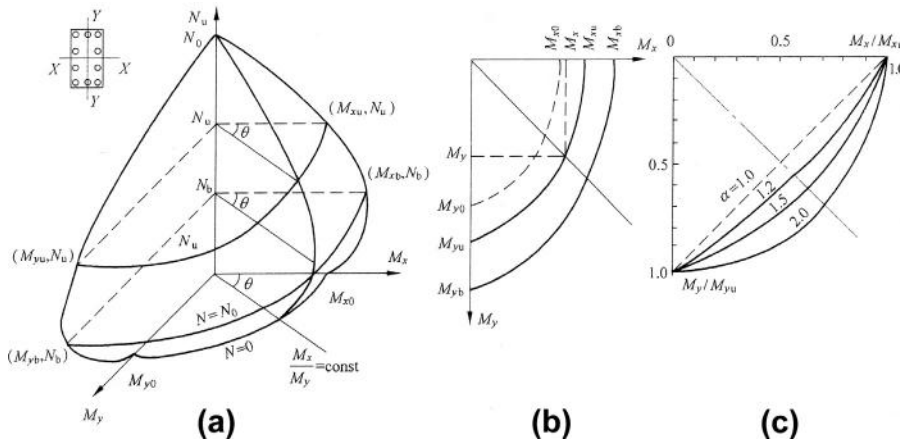


FIG. 11-18 Ultimate axial force-bending moment envelope for compressed member with biaxial bending (a) Spatial envelope (b) $M_x - M_y$ curves under constant axial force (c) $\frac{M_x}{M_{xu}} - \frac{M_y}{M_{yu}}$ curves

around the N_u axis. When the column of non-circular section, e.g. a rectangular one, is concerned, these curves are different to one another (Fig. 11-18(b)). However, if the relative values M_x/M_{xu} and M_y/M_{yu} are used for the co-ordinate, the curves obtained should intersect at 1 with the coordinate axes (Fig. 11-18(c)). Based on the experimental data the general expression [11-8] for these curves is

$$\left(\frac{M_x}{M_{xu}}\right)^\alpha + \left(\frac{M_y}{M_{yu}}\right)^\alpha = 1, \quad (11-21)$$

in which M_{xu} and M_{yu} are respectively the ultimate bending moments when the axial force (N_u) is acted with eccentricity in X or Y direction alone, and α is a coefficient depending upon N_u/N_0 , b/h of the section, content and position of the reinforcement, strengths and constitutive relations of the concrete and reinforcement. A certain calculation method [11-9] is suggested for α , and some constants between $\alpha = 1.15$ to 1.55 are given [11-8, 11-10]. Nevertheless, the value of α is surely less than 2, which corresponds to a circle.

Eq. (11-21) can be used for checking the ultimate strength of compressed member with biaxial bending. However, if the biaxial eccentricities $\eta_x e_{0x}$ and $\eta_y e_{0y}$ are known in advance, a simpler formula would rather be used in some design codes [2-1, 2-11]:

$$\frac{1}{N_u} = \frac{1}{N_{ux}} + \frac{1}{N_{uy}} - \frac{1}{N_{u0}}, \quad (11-22)$$

where N_{u0} is the ultimate strength of the column, if it is compressed centrally, N_{ux} (N_{uy}) is the ultimate strength of the column, if it is compressed with the eccentricity $\eta_x e_{0x}$ ($\eta_y e_{0y}$) alone.

Eq. (11-22) is the same formula used for calculation of a member of elastic material acted with N , M_x , and M_y together [11-11]. The calculated results approximate to the relevant experimental data of reinforced concrete columns and on the safe side.

The tensed member with biaxial eccentricities is less investigated, and the calculation method can be found in some references, e.g. [11-13].

11.5 Members of various materials and structural details

Various concretes and reinforcements of different kinds and strength grades, variety of sectional shapes, and different forms and details of the reinforcement are used for the members of reinforced concrete structures, and the mechanical behaviors and ultimate strengths of them vary significantly. Some situations happen frequently in engineering practice and are discussed briefly below.

11.5.1 High-strength concrete

The high-strength concrete ($f_{cu} \geq 50 \text{ N/mm}^2$) is more brittle and of sharp stress-strain curve under compression, and fails suddenly (see Section 4.1), compared with ordinary concrete. Comparing with the member of same section and reinforcement but different concrete of lower or medium strength, the characteristics of the flexural member of high-strength concrete are as below (Fig. 11-19). The stiffness before cracking of concrete and the bending moment at cracking (M_{cr}) are increased obviously; the stiffness of the section and the distance between cracks after cracking of both members are approached gradually; the bending moment at yielding of the tensile reinforcement (M_y) and the ultimate strength (M_u) are increased slightly; the ultimate compressive strain of high-strength concrete is slightly reduced ($\epsilon_u = 2.93 \times 10^{-3} \sim 3.28 \times 10^{-3}$), but the ultimate curvature ($(1/\rho)_u = \epsilon_u/x_u$, Fig. 11-13(b)) is increased as the depth of compression zone is decreased. However, when the post-yield resistance descends suddenly (point 4 in Fig. 11-19), the corresponding deflection, i.e. ductility of the member, is

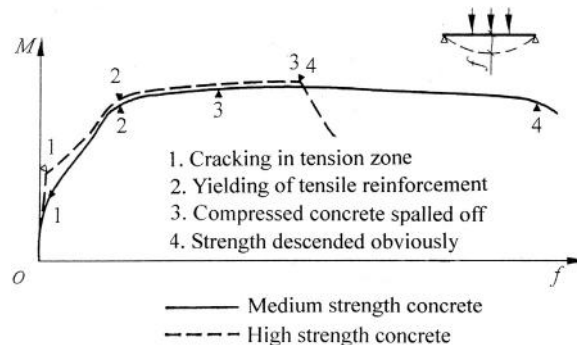


FIG. 11-19 Deflection of beam of high-strength concrete [4-1]

decreased obviously. If no longitudinal and transverse reinforcement is set up in the compression zone of the member, the high-strength concrete there is crushed suddenly with noise and the broken pieces are splashed down, and the residual strength descends sharply. Therefore, a certain amount of reinforcement should be set up in the compression zone, when the flexural member of high-strength concrete is designed.

The ultimate strength of the member of high-strength concrete can be calculated following the method and formulas introduced above, and the stress diagram on the compression zone of the section may be simplified to various diagrams [11-14], or uses the equivalent rectangular diagram. The parameters of equivalent rectangular diagram suggested in reference [4-2] are

$$\left. \begin{aligned} \alpha\gamma f_c &= f_c \\ \beta &= 0.8 - 0.005(f_{cu} - 50) \end{aligned} \right\}, \quad (11-23)$$

and the relative depth of boundary compression zone is also determined by Eq. (11-13) but $\varepsilon_u = 0.003$ is used. Alternatively, these values are taken as:

$$\left. \begin{aligned} C50 \sim C80 \quad \alpha\gamma &= 1 - 0.002(f_{cu} - 50) \\ \beta &= 0.8 - 0.002(f_{cu} - 50) \\ \varepsilon_u &= 0.0033 - (f_{cu} - 50) \times 10^{-5} \\ \varepsilon_0 &= 0.002 + 0.5(f_{cu} - 50) \times 10^{-5} \end{aligned} \right\} \quad (11-24)$$

in Chinese code [2-1].

11.5.2 Light-weight concrete

Light-weight (aggregate) concrete ($\rho \leq 1900 \text{ kg/m}^3$) is of smaller modulus of elasticity, sharp stress-strain curve, and fails suddenly (see Section 4.2). The mechanical behavior of the reinforced beam of light-weight concrete is similar to that of ordinary concrete, but shows larger deflection, wider crack, and quicker failure.

When the ultimate strengths of the flexural and eccentrically compressed members are calculated, the stress-strain curve of light-weight concrete is suggested as:

$$\left. \begin{aligned} 0 \leq \varepsilon \leq \varepsilon_0 \quad \frac{\sigma}{\sigma_u} &= 1.5 \left(\frac{\varepsilon}{\varepsilon_0} \right) - 0.5 \left(\frac{\varepsilon}{\varepsilon_0} \right)^2 \\ \varepsilon_0 \leq \varepsilon \leq \varepsilon_u \quad \sigma &= \sigma_u \end{aligned} \right\} \quad (11-25)$$

in Chinese code [4-13] (Fig. 11-20). The parameters of equivalent rectangular stress diagram $\beta = 0.769$ and $\alpha = 0.94$ are calculated accordingly, and then they are rounded off as

$$\beta = 0.75, \quad \alpha\sigma_u = 1.1f_c. \quad (11-26)$$

Afterwards, the equilibrium equations are established following Fig. 11-13(d), and the relative depth of the boundary compression zone (ξ_b) is also determined by Eq. (11-13) and $\varepsilon_u = 0.0033$ is used.

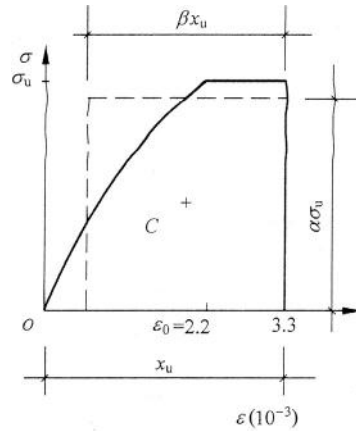


FIG. 11-20 Equivalent rectangular stress diagram for light-weight concrete

11.5.3 Reinforcements with different strengths

Sometimes, the reinforcements of different kinds and strength grades are set up in one structural member. If the reinforcements of two kinds, of which the yield strengths are $f_{y1} < f_{y2}$, are used in a beam, the mechanical process is shown in Fig. 11-21. The stresses of both reinforcements are approximately equal and vary similarly after loading and cracking of concrete, because the moduli of elasticity of the steels of various kinds are different slightly. Therefore, the stress in concrete, the curvature ($1/\rho$) and neutral axis (d_c/h_0) of the section also approximate to that of the beam reinforced with the same reinforcement.

After the reinforcement of lower strength (A_{s1}) is yielded first ($\sigma_{s1} = f_{y1}$ at M_{y1}), the yield strength of it keeps constant and the stress of another reinforcement (A_{s2}) accelerates, so the curvature and neutral axis vary rapidly. However, the deformation and crack of the beam increase stably, because the later reinforcement is not yielded yet ($\sigma_{s2} < f_{y2}$). When all the reinforcements are yielded ($\sigma_{s2} = f_{y2}$ at M_{y2}), the deformation increases quickly and the tensile crack widens and extends towards the

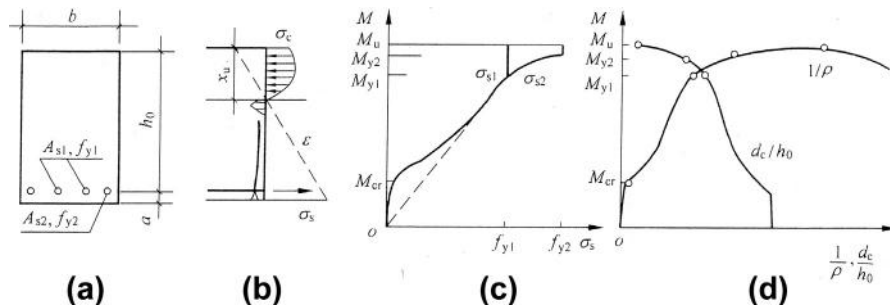


FIG. 11-21 Beam reinforced with reinforcements of different strengths: (a) section, (b) stress distribution, (c) stress of reinforcement, (d) curvature and neutral axis

compression zone. Afterwards, the bending moment increases slightly with the internal lever arm, although the total tensile force of the reinforcements in tension zone keeps constantly ($A_s1f_{y1} + A_s2f_{y2}$). Finally, the ultimate strength (M_u) is reached when the concrete in the compression zone is crushed.

Generally, the failure pattern and ultimate strength of the beam reinforced with different reinforcements are controlled by the total tensile force on the section, and the calculation formula is similar to Eq. (11-14).

11.5.4 Reinforcement without yielding plateau

Usually, the carbon steel wires of high-strength, steel strand, cold-drawn wire of low-carbon steel are used only in prestressed concrete structures. The stress-strain curves of them do not obviously show any yielding plateau (e.g. Fig. 6-7), and the nominal yield strength of them ($f_{0.2}$) is defined as the stress corresponding to the strain $\epsilon_{0.2} = 0.002 + (f_{0.2}/E_s)$. When a beam is reinforced with these kinds of reinforcements, the curvature and neutral axis of the section and cracks vary gradually without sudden turn, after the tensile reinforcement reaches the nominal yield strength. Afterwards, the stress of the tensile reinforcement increases continuously with the bending moment ($\sigma_s > f_{0.2}$). Finally, the ultimate bending moment of the beam (M_u) is reached when the concrete in compression zone is crushed (ϵ_u), but the tensile reinforcement does not necessarily reach the ultimate strength ($\sigma_s < f_b$).

When the ultimate strength (M_u) of the beam is calculated using the equivalent rectangular stress diagram [11-15], the boundary depth of compression zone on the section (referring to Fig. 10-15) should be

$$\frac{x_{ub}}{h_0} = \frac{\epsilon_u}{\epsilon_u + \epsilon_{0.2}} = \frac{0.0033}{0.0033 + \left(0.002 + \frac{f_{0.2}}{E_s}\right)}, \quad (11-27a)$$

$$\text{or } \xi_b = 0.8 \frac{x_{ub}}{h_0} = \frac{0.8}{1.6 + \frac{f_{0.2}}{0.0033E_s}}. \quad (11-27b)$$

When the stress of tensile reinforcement at ultimate state is taken as $\sigma_s = mf_{0.2}$ for a suitably reinforced beam, the amplifying coefficient suggested in reference [6-7] is

$$m = \frac{\sigma_s}{f_{0.2}} = 1.25 - 0.25 \frac{x_u}{x_{ub}}, \quad (11-28a)$$

where x_u is the calculated depth of compression zone at ultimate state (Fig. 11-13(d)). However, the coefficient used in Chinese code [2-1] is reduced to

$$m = 1.1 - 0.1 \frac{x_u}{x_{ub}}. \quad (11-28b)$$

11.5.5 Reinforcements distributed along sectional depth

The concrete member with high depth, e.g. shear wall in building, folded plate structure, box girder (Fig. 11-22), is reinforced with the reinforcements not only near top and bottom of its section (A'_s and A_s) but also distributed uniformly or

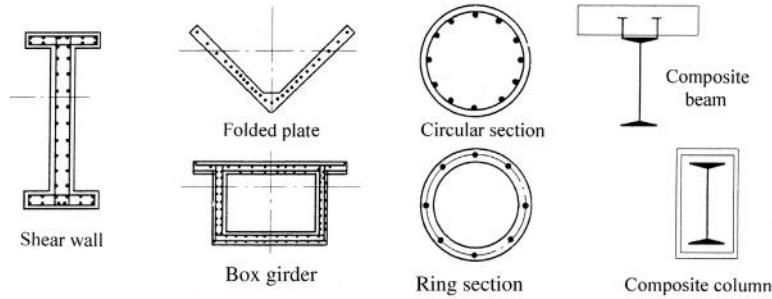


FIG. 11-22 Various members reinforced with reinforcements distributed along sectional depth

non-uniformly along its depth. The members of circular and ring sections are generally reinforced with the longitudinal reinforcements distributed uniformly along its periphery. The web of steel shapes within a composite concrete structure are reinforced continuously. When these members are loaded, the stresses (strains) of the reinforcements and web depend upon the distances apart from the neutral axis on the section. Therefore, they will not simultaneously, i.e. parts of them will but others will not, reach the yield strengths of their own under ultimate state of the member.

The reinforcements distributed separately along the sectional depth can be transferred into a continuous steel plate (web) with the same height and area (h_w and $A_w = h_w t$, Fig. 11-23(a)) during calculation. Correspondingly, the reinforcements distributed along a circle for the circular or ring section are transferred into a thin steel tube with the same diameter and area. The strain and stress on the section of the member at ultimate state are distributed as shown in Fig. 11-23(b) and (c), and the stress of the steel web or tube within ηx_u on both sides of the neutral axis

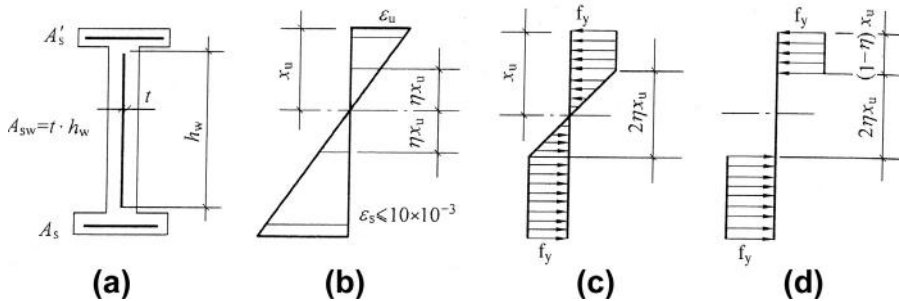


FIG. 11-23 Calculation for member with reinforcement distributed continuously: (a) section, (b) strain distribution, (c) stress distribution of reinforcement, (d) simplified stress diagram for reinforcements

is less than the yield strength ($\sigma_s < f_{yw}$). The value of η is determined by the assumption of plane section:

$$\eta = \frac{f_{yw}}{\varepsilon_u E_s}, \quad (11-29)$$

where f_{yw} is the yield strength of the reinforcement or steel web or tube, and ε_u is the ultimate strain of compressed concrete and 0.0033 is usually taken.

The ultimate strength of the member can be calculated by the equilibrium equations similar to Eq. (11-14). The equivalent rectangular stress diagram of concrete on the compression zone can also be used with the parameters $\beta = 0.8$ and $\alpha\gamma = 1$. The stresses of the reinforcements near the top and bottom of the section (A'_s and A_s) are calculated by Eqs (11-15) to (11-18). However, the maximum strain of the tensile reinforcement at ultimate state should be limited to, e.g.,

$$\varepsilon_{s\max} \leq 10 \times 10^{-3}, \quad (11-30)$$

in order to prevent too much high stress of the reinforcement and wide cracks of concrete occurring during the service period of the member. The calculation formulas derived for different sections are provided in detail in references [11-16,1-2].

If the reinforcements within ηx_u on both sides of the neutral axis are neglected (Fig. 11-23(d)), the calculation formulas established are even more simple and the induced error of the ultimate strength calculated is generally less than 2.5%.

11.5.6 Non-rectangular sections

The reinforced member of the rectangular section is manufactured most simply. However, various shapes of non-rectangular section, e.g. sharps of T, I, channel, box, trapezoid, triangle, circle, and ring, are designed in engineering practice to reduce the dead load (self weight of the structure) or to satisfy the special requirements of some functions. The mechanical behavior and failure process of the members of these sections are not obviously different from that of the rectangular one described above, and they can also be calculated using the general method for sectional analysis along the loading history (see Section 11.3).

Although the ultimate strength of the member of non-rectangular section can also be calculated using the same equivalent rectangular stress diagram on compression zone, the corresponding parameters of it (α , β , γ) should be changed with the variation of the sectional width ($b \neq \text{const.}$). For example, the strain distribution on the compression zone of the member of triangle section at ultimate state is shown in Fig. 11-24(b); the parameters calculated considering the variable width are:

$$\alpha = 0.922, \beta = 0.845, \quad \text{and} \quad \alpha\gamma \approx 1, \quad (11-31)$$

when the method introduced in Section 11.4.1 and the same compressive stress-strain relation of concrete (Fig. 11-14(a)) are used. Obviously, these parameters are different from those for rectangular section (Eq. (11-11a)).

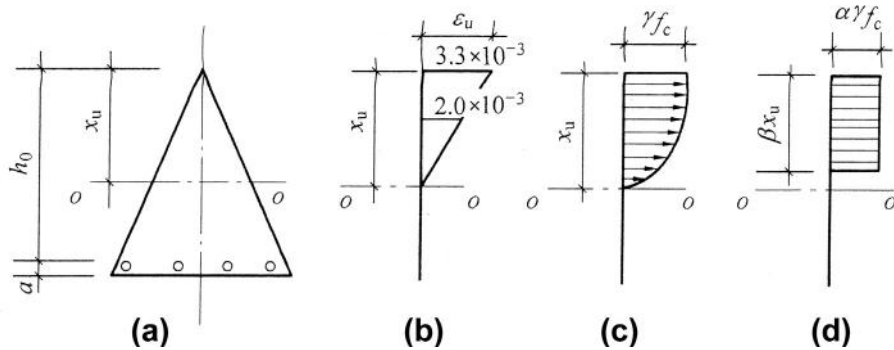


FIG. 11-24 Equivalent rectangular stress diagram for triangle section: (a) section, (b) strain distribution, (c) stress distribution, (d) equivalent stress diagram

The characteristic parameters of the rectangular stress diagram for other shapes of section may be approximately estimated referring to the parameters for rectangular and triangle sections, or accurately calculated using the same method ([Section 11.4.1](#)) after introducing the variation of sectional width.

Tensile Crack

12

CHAPTER OUTLINE

12.1 Cause and limitation of crack	305
12.1.1 Action of load.....	305
12.1.2 Non-loading factors	306
12.2 Internal force at cracking	309
12.3 Mechanism of cracking	311
12.3.1 Bond-and-slip method.....	312
12.3.2 Non-slip method.....	314
12.3.3 Comprehensive analysis	318
12.4 Calculation of crack width	322

12.1 Cause and limitation of crack

The tensile strength of concrete is rather low, and the concrete will be cracked in a structure when a small tensile strain (e.g. 100×10^{-6}) occurs. Therefore, the visible crack may appear on the surface of a concrete structure during construction and service periods, because of different reasons, e.g. quality of material, construction technology, environmental condition, action of load. When a reinforced concrete structure (without prestressing) is designed, it is known in advance that the structure will work with cracks in it under normal conditions, so the concrete cracks should be checked and limited properly. This is a special problem which will not happen for the structures of other materials, including steel, timber, and masonry.

Varieties of crack patterns of reinforced concrete are found in engineering practice, and the main reasons for these cracks can be divided into two categories.

12.1.1 Action of load

When a reinforced concrete structure is acted with load, one-dimensional tensile stress results on the transverse section of a member acted with bending moment or axial (tensile) force, and the principal tensile stress is formed in a member acted with shear force or torque or in two- and three-dimensional structures. Therefore, the cracks may occur perpendicular to the direction of principal tensile stress in these members (Fig. 12-1(a) and (b)). Usually, the cracks pass through the width of the

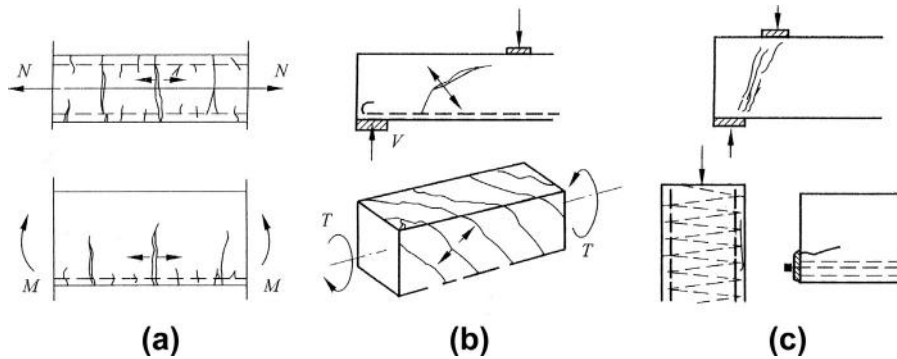


FIG. 12-1 Cracks on surface of structural member under action of internal force or load: (a) axial tension and bending moment, (b) shear force and torque, (c) compression

section, and different patterns and variable width of the cracks are presented on the surface of the member, if it is observed carefully. For example, short and more fine cracks are found near the position of reinforcement, besides the wider crack passing through the whole section for a tensed member with larger section; the width of a vertical crack in a deeper beam is variable, and it is narrower near the position of reinforcement but is wider on the web; the inclined crack near the end of a beam is also variable, and the maximum width appears near the middle of the section, but smaller width for other parts of the crack; etc.

A reinforced concrete structure and member can also be cracked under compressive load or stress. For example, the horizontal cracks occur in the compression zone of a beam under bending (Fig. 11-2); the inclined compressive cracks occur near the end of a beam between the concentrated load and the support (reaction); the longitudinal cracks appear outside of the spiral bars of the column; the cracks appear locally near the anchorage of prestressing tendon or concentrated compression (Fig. 12-1(c)). When the concrete is cracked under compression, the strain is generally greater than the peak strain (ϵ_p) of it, so it should be avoided during service period of a structure.

12.1.2 Non-loading factors

If the cement mixed in concrete has some deficiency in quality, e.g. stability, or the concrete is not cured properly or dries too quickly, many irregular cracks may appear on the surface of the structural member. If the concrete covers outside the longitudinal and transverse reinforcements are not thick enough, the cracks may form along the axes of the reinforcements (Fig. 12-2). Generally, these cracks caused by shrinkage of the concrete are of small width (0.05–0.1 mm) and shallow, and do not necessarily reach periphery of the reinforcement.

When the environmental temperature changes, the corresponding deformation of concrete is confined by the surrounding structure, and when the foundation of

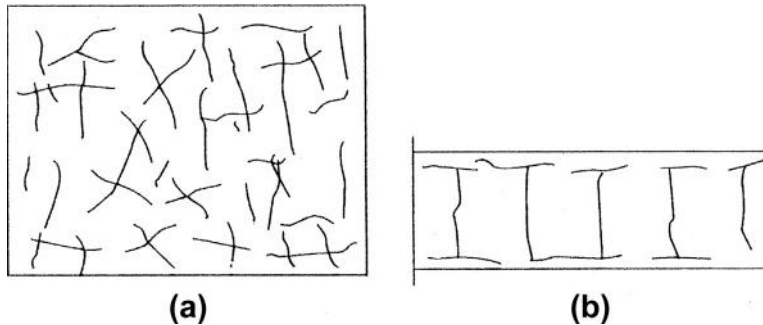


FIG. 12-2 Cracks caused by shrinkage of concrete: (a) on surface of slab, (b) outside of reinforcements

a structure is settled non-uniformly, the additional stress or redistribution of internal forces should occur and then the cracks may form in the structure. When a structure is exposed to high temperature, e.g. fire accident, and then cooled down, or when an outdoor structure experiences alternately summer and winter for many years, the irregular cracks may appear on the surface of them. In addition, after the reinforcement of an outdoor structure is corroded, a crack in the concrete may form along its axis.

Therefore, the concrete of a structure may crack due to different reasons, e.g. those listed above, and sometimes it is unavoidable. After the crack is formed and developed in the structural concrete, the behavior during the service period and durability of the structure may be influenced unfavorably as below.

1. Corrosion of reinforcement and reduction of durability of the structure (see Chapter 20). After the crack in the concrete is formed and developed, the part of reinforcement in the structure directly in contact with the environment for an outdoor structure, the surface layer of the reinforcement will be oxidized and corroded gradually and develops inside. The volume of the reinforcement is then increased and expands outside, so the concrete cover will be cracked, even spalled off, and a longitudinal crack is formed along its axis. Then, the corrosion of the reinforcement is accelerated. Therefore, the effective area of the reinforcement is reduced, the bond between it and concrete is deteriorated, and the ultimate strength and safety of the structure is finally decreased.
2. Permeability of the concrete structure is damaged and leakage of liquid or gas is caused. The service function of the hydraulic and container structures will be seriously deteriorated.
3. The deformation of a structure is increased as the stiffness reduces. The service function and appearance of some architectural details and members are influenced, e.g. opening of a door or a window is obstructed, the partition wall and finishing materials are deformed or even cracked.

4. Appearance and development of cracks in the structural concrete and local damage of other materials in a building may cause a sense of psychological unsafety for people. Sometimes, this is the main reason for strengthening or treating, although the structure is not necessarily unsafe.

Therefore, the cracks of structural concrete that appear possibly within the service period should be controlled in different ways. Many experimental and theoretical investigations have been conducted and corresponding results are reported in various countries, including surveys and statistics of cracks in existing structures, calculation of internal forces at cracking, development and mechanism of cracking, distance and width of the crack, development and influence of corroded reinforcement, influence of cracks on structural behavior. The calculation methods are suggested and the reinforcements for controlling cracks are given correspondingly. However, the calculation methods are mature only for the tensile and flexural members (Fig. 12-1(a)), which will be introduced below. The crack possibly caused by manufacturing or structural default and environmental condition is considered and treated during designing and manufacturing periods. The compressive cracks (Fig. 12-1(c)) should be avoided within service period, so this ought to be taken into account during design and calculation.

When a reinforced concrete structure member is designed following the Chinese code [2-1], the crack of the concrete should be limited separately in three levels [12-1] to fit the different requirements of service function.

Level I. The crack is not allowed strictly in the member, and tensile stress will not occur on its section under total design load, i.e.

$$\sigma_{sc} \leq 0. \quad (12-1a)$$

Level II. The crack will not appear, in the general case, in the member, and the tensile stress of concrete on the section is less than a fraction of the tensile strength under total load acted in short time and will not occur under the sustained load, i.e.

$$\text{Short time load } \sigma_{sc} \leq \alpha_{ct} \gamma f_t, \quad (12-1b)$$

$$\text{Sustained load } \sigma_{tc} \leq 0, \quad (12-1c)$$

where α_{ct} is the coefficient for limiting tensile stress, ranges from 0.3 to 1.0 and depends upon the working condition and environmental humidity of the member [2-1], and γ is the plasticity-dependent coefficient of concrete on tension zone (Eq. (3-7) and Eq. (12-6)).

Level III. The crack is allowed, sometimes it is unavoidable, for the member, but the maximum width calculated (Eq. (12-23)) should be limited:

$$w_{\max} \leq w_{\lim}. \quad (12-1d)$$

The allowable width of crack (w_{\lim}) is generally taken as 0.2–0.4 mm and depends upon the category of the working environment (see Table 20-4), load condition (static or vibrated), and kind of reinforcement used [2-1].

Of course, levels I and II are rarely achieved for an ordinary reinforced concrete member, as too much costs will be paid even if they are reluctantly achieved. Generally, prestressed concrete should be used for the member of levels I and II, while reinforced concrete is used only for the member of level III.

The crack limitation of structural concrete is similar in design codes of other countries. For example, the environmental condition is divided into five exposure grades in the CEB-FIP Mode Code [2-12], and tensile stress on the section is not allowed or the maximum crack width calculated is limited, generally $w_{lim} = 0.2\text{--}0.3$ mm. In ACI Code [2-11], the limits of the maximum crack width calculated are 0.4 mm and 0.33 mm respectively for the indoor and outdoor members. In some other countries, the limit of the maximum crack width is even wider (0.4–0.5 mm [1-1]).

12.2 Internal force at cracking

When the appearance of a concrete crack is checked or the distance and width of the crack are calculated for a concrete member, it is necessary to determine in advance the internal force, i.e. axial force and bending moment, at cracking, after the size and materials of the section are known.

The examples of centrally tensed members appearing in engineering practice are tensile members of a truss, circle water-pool, water pipe. Generally, these members are reinforced symmetrically, and the axial force at cracking of concrete is (Eq. 8-22):

$$N_{cr} = f_t \left(A_c + \frac{n}{\lambda_t} A_s \right) = f_t A_0, \quad (12-2)$$

where f_t is the tensile strength of concrete, A_0 is the converted sectional area of section, others are the same as in Eq. (8-22).

When the appearance of crack is limited following Eq. (12-1b), the tensile stress of concrete under axial force is calculated by

$$\sigma_{sc} = \frac{N}{A_0}. \quad (12-3)$$

The bending moment at cracking of concrete for a flexural member (M_{cr}) can be obtained accurately by the general method described in Section 11.3. However, many other factors have influence on cracking of concrete and the tensile strength of concrete scatters considerably, so an approximate method with sufficient accuracy is acceptable for calculation of the cracking moment in the engineering application.

The cracking moment of a beam of plain concrete (Fig. 12-3) is discussed first. The section of the beam keeps a plane before cracking of concrete. It is assumed that the maximum tensile strain at the bottom of the section reaches twice peak strain of concrete under uniform tension ($2\epsilon_{t,p}$), when the beam is just cracking. At this time,

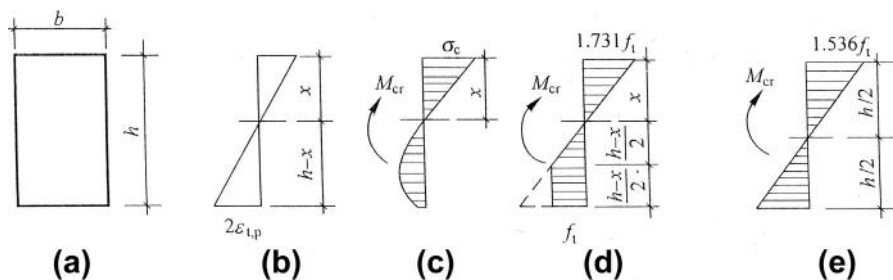


FIG. 12-3 Before cracking of plain concrete beam: (a) section, (b) strain distribution, (c) stress distribution, (d) stress distribution for calculation, (e) elastic stress diagram

the stress distribution is curved on the tension zone but it is a triangle on the compression zone, because the compressive stress is far smaller than the strength ($\sigma_0 \ll f_c$). When the stress diagram on tension zone is simplified into a trapezoid model (Fig. 2-27(a)) and the maximum tensile stress is taken as f_t , the maximum stress on compression zone of triangle diagram should be $\frac{x}{h-x} 2f_t$. Then, the equilibrium equation is established for the horizontal forces:

$$\frac{1}{2}bx\frac{x}{h-x}2f_t = \frac{3}{4}b(h-x)f_t,$$

and the solution of it is the compressive depth $x = 0.464h$. Correspondingly, the maximum compressive stress of concrete at the top of the section is $1.731f_t$ and the bending moment at cracking of the concrete of the beam is

$$M_{cr} = 0.256f_tbh^2. \quad (12-4)$$

If the beam is considered as an elastic material one and the stress distributes linearly on the section (Fig. 12-3(e)), the nominal flexural tensile strength, or modulus of rupture, of the concrete at cracking of the beam should be

$$f_{t,f} = \frac{M_{cr}}{bh^2/6} \approx 1.536f_t. \quad (12-5)$$

The ratio between $f_{t,f}$ and tensile strength (f_t) is called the plasticity-dependent coefficient of section modulus (γ). The value of the coefficient depends upon not only the stress distribution on the section but also shape, reinforcement content, strain gradient of the section, and the basic value for a rectangular section is taken as

$$\gamma_m = \frac{f_{t,f}}{f_t} = 1.55 \quad (12-6)$$

in Chinese code [2-1]. The values of coefficient for the sections other than the rectangular one, e.g. T, I, circular, ring shapes, range from 1.25 to 2.0 [12-3], because of different position of neutral axis and shapes of compression and tension zones.

The strain gradient on the section at cracking of concrete ($3.73\varepsilon_{t,p}/h$) reduces as depth (h) is increased, and the plasticity-dependent coefficient is also reduced. On the contrary, the coefficient increases as depth of the section is decreased, e.g. for a slab [12-4]. Reference [12-2] and Chinese code [2-1] suggest that the coefficient varies with the depth (h , mm) as below:

$$\gamma = \left(0.7 + \frac{120}{h}\right)\gamma_m, \quad (12-7)$$

and the depth value of the member (h) is taken 400 if $h < 400$ mm or 1600 if $h > 1600$ mm.

When a reinforced concrete beam is nearly cracking, the strain of concrete on the section is low and the stress distributes linearly on the compression zone. The bending moment at cracking of concrete can be calculated by the method of converted section, when the nominal strength $f_{t,f}$ is used for the tensile concrete and the tensile and compressive reinforcements are converted respectively into equivalent areas nA_s and nA'_s , using the ratio between the moduli of elasticity $n = E_s/E_0$ (Eq. (8-6)). Then, the position of neutral axis or the compressive depth (x), the moment of inertia (I_0), and the modulus of section against the tensile edge ($W_0 = I_0/(h - x)$) are calculated for the converted area (A_0 , Eq. (8-9)) of homogeneous elastic material. When the section is acted together with bending moment (M) and axial force (N , positive for tension and negative for compression), the stress at edge of tension zone on the section is calculated by:

$$\sigma_c = \frac{M}{W_0} + \frac{N}{A_0}, \quad (12-8a)$$

which can be used in Eq. (12-1a, b, c) for checking the appearance of cracking. Let $\sigma_c = f_{t,f} = \gamma_m f_t$ (Eq. (12-6)) in the formula, the internal forces at cracking (M_{cr} and N_{cr}) are determined. For example, the bending moment at cracking of a flexural member ($N = 0$) is

$$M_{cr} = \gamma_m f_t W_0. \quad (12-8b)$$

Similar methods are used in different design codes of other countries, in order to limit the tensile stress of concrete [12-2] under load or to calculate the internal forces at cracking when a reinforced member is designed.

12.3 Mechanism of cracking

After the tensile crack appears in a reinforced concrete structural member ($N > N_{cr}$, $M > M_{cr}$), its number increases and width widens gradually, and the distance between cracks reduces, as the load is increased. However, the cracks develop randomly to a certain extent, because the concrete is inhomogeneous and its behavior scatters considerably, and so many factors have influences on it. Therefore, the appearance of the crack on the surface of the member varies significantly and is

difficult to explain and analyze accurately, so various points of view and corresponding calculation methods are suggested so far.

12.3.1 Bond-and-slip method

At first, the bond-and-slip method [12-5] is suggested based on the experimental results of centrally tensed member of reinforced concrete. Afterwards, the complements and modifications are provided in later researches [12-6–12-11] following the basic concept.

When a tensed member is loaded and a crack nearly appears in the concrete ($N \approx N_{cr}$), the strains of the concrete and reinforcement in it are equal, while the stresses on them are respectively $\sigma_c \approx f_t$ and $\sigma_s \approx n f_t / \lambda_t$. And, both stresses distribute uniformly along the axis of the member. Therefore, the bond stress between them should be $\tau = 0$ (dash-dot line ①-① in Fig. 12-4(b)), and no slip will occur until then.

After the first crack appears at the weakest section ((1) in Fig. 12-4(a)), the concrete on the cracked section is out of work ($\sigma_c = 0$), the reinforcement there carries totally the axial force and its stress is increased suddenly to $\sigma_s = N_{cr}/A_s$, and the concretes on both sides of the crack are slipped locally. Therefore, the stresses of the concrete and reinforcement vary along the longitudinal axis of the member, and the bond stress on the boundary of both distributes corresponding as shown by the solid line (1) in Fig. 12-4(b).

It is seen (Fig. 12-4(b)) that the stress of the concrete at a distance (l_{min}) away from crack (1) keeps $\sigma_c = f_t$ and the stress of the reinforcement and the bond stress ($\tau = 0$) there are the same as that before cracking of concrete. This distance is called bonded length or transmitting length of bond stress and can be calculated by the equilibrium equation (Fig. 12-4(c)):

$$l_{min} = \frac{f_t A_c}{\tau_m \pi d} = \frac{d}{4\mu} \frac{f_t}{\tau_m}, \quad (12-9)$$

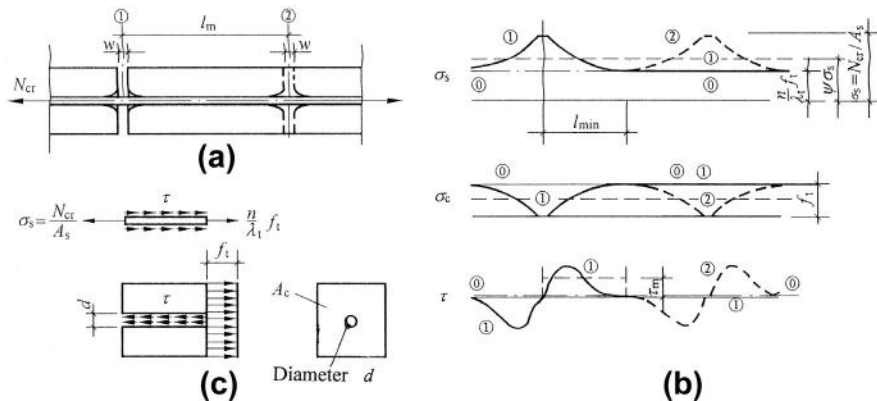


FIG. 12-4 Cracking and stress distribution of tensed member: (a) cracks, (b) stress distribution, (c) equilibrium condition

where τ_m is the average bond stress between reinforcement and concrete, f_t is the tensile strength of concrete, d , $\mu = A_s/A_c$ are the diameter and content of reinforcement on section, respectively.

The tensile stress of the concrete is $\sigma_c < f_t$ within the distance l_{\min} on both sides of crack (1), and generally, no crack will occur there. However, the cracks of the second batch (2) may occur at any section outside of the range, and usually also occur at the weaker section. After crack (2) appears, the variations of the stresses of the concrete and reinforcement and the bond stress along the axis are shown as the dotted curve (2) in Fig. 12-4(b), which is similar to the curve (1) after appearance of crack (1). If the space between two adjacent cracks is less than $2l_{\min}$, the tensile stress of the concrete there should be $\sigma_c < f_t$, and no crack will appear again. Therefore, the minimum and the maximum spaces between any two adjacent cracks should be l_{\min} and $2l_{\min}$ respectively. The actual space between cracks found in the experiments scatters considerably, and the average value of the space is about

$$l_m \approx 1.5 l_{\min}. \quad (12-10)$$

The space between the tensile cracks of concrete depends mainly upon the tensile strength of the concrete, content and diameter of the reinforcement, and the average bond strength between both materials. It is also found experimentally that the ratio f_t/τ_m varies less for the concretes of different strength grades; the space between the cracks tends to a constant when the reinforcement content (μ) is rather large, i.e. the ratio d/μ is rather small; the average space between the cracks is reduced by about 30%, comparing the deformed reinforcement with the plain one, as the former has higher bond strength. Then, the average space between the tensile cracks can be calculated by

$$l_m = \left(k_1 + k_2 \frac{d}{\mu} \right) \nu, \quad (12-11)$$

where k_1 , k_2 are parameters obtained from regression analysis of the experimental data, $k_1 = 70$ mm and $k_2 = 1.6$ are suggested in reference [12-11], ν is the parameter taking 1.0 for deformed reinforcement but 0.7 for a plain one.

The same method can be used to derive the calculation formula for the tensile cracks of flexural concrete member. The average space of the cracks can also be calculated by Eq. (12-11) but with different parameter values obtained from corresponding regression analysis. For example, $k_1 = 60$ mm and $k_2 = 0.6$ are suggested in reference [12-10], while $k_1 = 60$ mm and $k_2 = 2f_t\tau_m$ are suggested in reference [12-7].

According to the bond-and-slip method, the crack that appears is assumed to pass through the whole section with the same width, i.e. the crack widths near the boundary of the reinforcement and on the surface of the member are equal (Fig. 12-4(a)). Therefore, the crack width should be the difference between the elongations of the reinforcement and concrete within the space between adjacent cracks. Both strains

(stresses) of the reinforcement and concrete distribute non-uniformly along the length, and the average width of the crack is

$$w_m = (\bar{\epsilon}_s - \bar{\epsilon}_c) l_m, \quad (12-12)$$

where $\bar{\epsilon}_s$ and $\bar{\epsilon}_c$ are respectively the average strains of both materials.

The average strain of the reinforcement between cracks ($\bar{\epsilon}_s$) is certainly smaller than the strain of the reinforcement at cracked section ($\epsilon_s = \sigma_s/E_s$), and the ratio between them is called the non-uniformity coefficient of tensile reinforcement strain:

$$\psi = \frac{\bar{\epsilon}_s}{\epsilon_s} = \frac{\bar{\epsilon}_s E_s}{\sigma_s} \leq 1.0. \quad (12-13)$$

Generally, the average strain of the concrete is far less than the tensile strain of the reinforcement ($\bar{\epsilon}_c \ll \bar{\epsilon}_s$) and can be neglected during calculation. Therefore, the average width of the crack can be calculated simply by

$$w_m = \psi \frac{\sigma_s}{E_s} l_m, \quad (12-14)$$

12.3.2 Non-slip method

According to the bond-and-slip method, the space and width of the tensile crack depend mainly upon the ratio (d/μ) and average bond stress (τ_m), and equal width of the crack is assumed along the whole section. As the average bond strength of the deformed reinforcement is about four times that of the plain one (τ_u in Chapter 7), this would have significant influence on the crack. These conclusions and assumptions are obviously discrepant with the experimental results below.

Two series of the specimens of three beams each are reinforced respectively with the plain and deformed reinforcements (Fig. 12-5(a)). These beams are of rectangular section with the same size and approximate reinforcement content, but the diameters of the reinforcements used are considerably different (31.8 mm/12.7 mm = 2.5). The crack widths on surfaces of the beams at position of gravity center of the reinforcement are measured under the same bending moment, and the differences between them are rather small, e.g. 0.208 mm/0.191 mm = 1.089 and 0.223 mm/0.191 mm = 1.168, are much smaller than the ratio between the

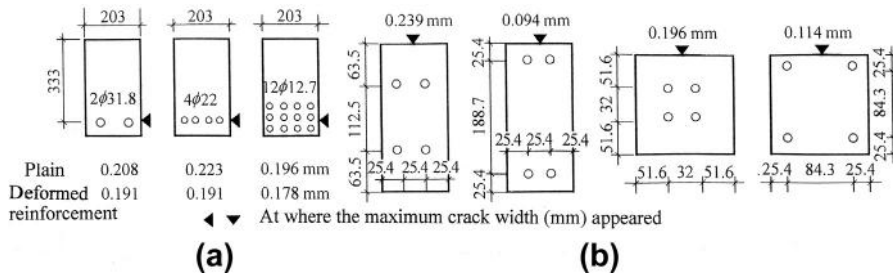


FIG. 12-5 Demonstration experiments and comparisons between crack width: (a) beam specimen [12-12], (b) central tensed specimen [12-14]

bond strengths of both reinforcements. These results show significant error for the conclusions of the bond-and-slip method.

Another series of specimens include four tensile members of same sectional area ($b \cdot h$) and reinforcements ($4\Phi 12.7$), but with different shapes (b/h) and concrete covers [12-14—12-16] (Fig. 12-5(b)). The crack widths of the specimens are measured at similar places on the surface under same axial tension, but they are considerably different, e.g. $0.239 \text{ mm}/0.094 \text{ mm} = 2.54$.

In addition, various effective methods are designed and conducted by the researches to measure accurately the configuration of the tensile concrete crack during testing. For example, some resin [12-17] or red ink [12-18] is poured with pressure into the tensile specimen to measure the deformation and relative displacement of the cracked surfaces [12-19]. Therefore, the deformations of the tensile crack are obtained in detail from these experiments (Fig. 12-6), including the variation of crack width along the section, the distribution of relative slip between the reinforcement and concrete, visible cracks on the surface and fine cracks in the interior. Some important conclusions about the crack pattern are then derived:

1. The cracked surface (section) is regularly curved and the crack width varies apparently along the section, i.e. the minimum width occurs at the periphery of the reinforcement while the maximum width appears on the surface of the member (Fig. 12-6(c)), and the latter is usually 3 or 7 times the former. Therefore, the experimental results deny the relevant assumptions of the

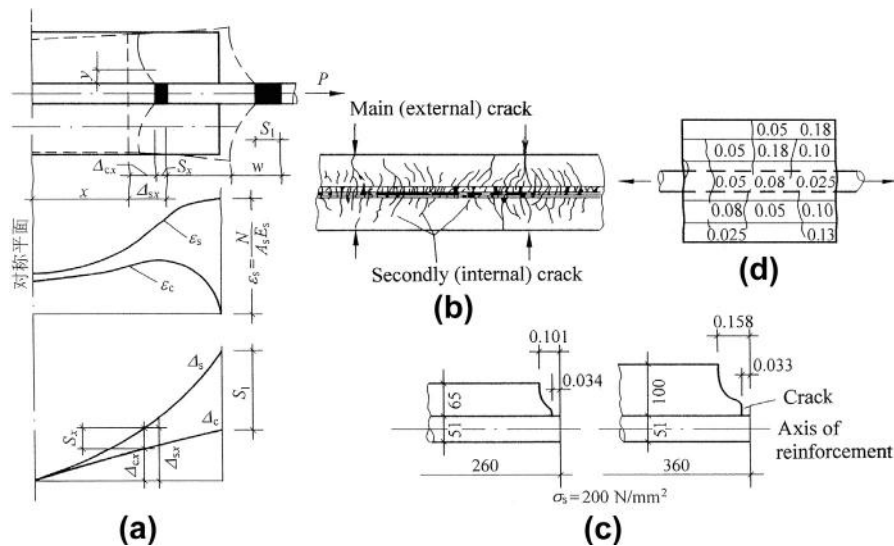


FIG. 12-6 External and internal cracks and deformation of tensile member: (a) deformation and relative slip of reinforcement and concrete [1-1], (b) internal and external cracks [12-18], (c) variation of crack width [12-18], (d) width of internal crack [12-14]

bond-and-slip method: the section after being cracked is separated into two parallel planes with equal crack width (Fig. 12-4(a)).

2. The width of the crack at the periphery of the reinforcement is rather small, so the relative slip between the reinforcement and concrete should be small too, even for the plain reinforcement.
3. Besides the main cracks appearing on the surface of the member with greater space and width and being perpendicular to the reinforcement, many internal inclined cracks, or secondary cracks, still occur near ribs of the reinforcement and extend outside (Fig. 12-6(b) and Fig. 7-9(a)). These cracks appear first near the cracked section and develop gradually inside as the tensile stress of the reinforcement is increased. The internal cracks are closely spaced and extend outside but do not reach the surface.
4. The deformation of the concrete surrounding reinforcement is complicated. The concrete inside and near the reinforcement carries tensile stress, which distributes longitudinally as consistent with σ_c in Fig. 12-4(b), if the local influence of internal cracks is not considered. However, the concrete near the surface of the specimen carries compressive stress on the sections near the crack, but carries tensile stress on the middle sections between two adjacent cracks (see Fig. 12-8(d)). The difference between the deformations of the concrete on surface layer and inside is the basic reason for the crack of the concrete being wider outside but narrower inside.

Many experimental results introduced above and others [1-1] query the validity of the bond-and-slip method, and are composed of the basis for the non-slip method. It is considered that the reinforcement content of the section (μ) and diameter of the reinforcement (d) have less influence on the space and width of the tensile crack. And, it is assumed that relative slip between the reinforcement and surrounding concrete at the cracked section is neglected, i.e. the width of the crack there is zero. The width of the crack on the surface of a member is proportional to the distance from there to the surface of the reinforcement, or the thickness of the concrete cover.

Analyzing the experimental data of tensile member and flexural beams of different sectional shapes (Fig. 12-7(a)), the calculation formulas are suggested in reference [12-16]:

$$\text{average space between cracks } l_m = 2t$$

$$\text{average width of cracks on surface } w_m = l_m \bar{\epsilon} = 2t\bar{\epsilon} \quad (12-15)$$

$$\text{the maximum width of cracks } w_{\max} = 2w_m = 4t\bar{\epsilon},$$

where t is the distance from position of the crack on surface to center of the nearest reinforcement, $\bar{\epsilon}$ is the average strain.

Many experiments of beam specimens are conducted and the crack widths on their surfaces are measured as shown in Fig. 12-7(b), and the calculation formulas are suggested for the maximum and average widths [12-12, 2-13]:

$$\text{deformed reinforcement } w_m = 1.67c\bar{\epsilon}, \quad w_{\max} = 3.3c\bar{\epsilon}, \quad (12-16a)$$

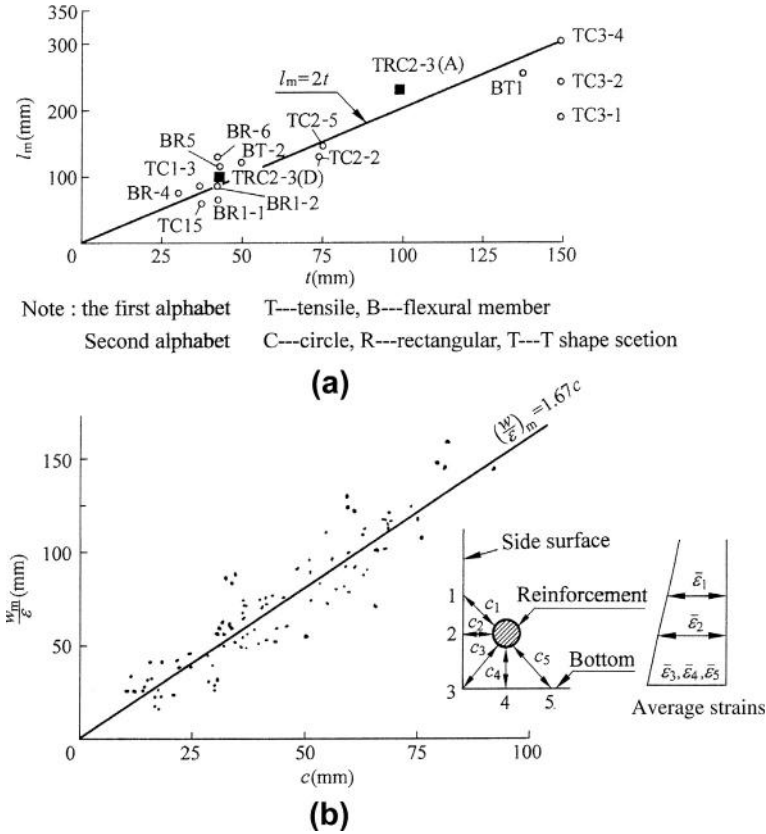


FIG. 12-7 Average space and width of concrete crack: (a) average space of crack [12-16], (b) average width of crack [12-12]

$$\text{plain reinforcement } w_m = 1.89c\bar{\epsilon}, \quad w_{\max} = 3.75c\bar{\epsilon}, \quad (12-16b)$$

where c is the distance from the position of the crack on the surface of the member to the periphery of the nearest reinforcement, $\bar{\epsilon}$ is the average strain calculated on the surface of the member, w_{\max} is the maximum crack width that appeared in 1% probability and about twice average width.

These two series of formulas Eqs. (12-15) and (12-16) show the same concept and qualitative conclusion but with different empirical parameters.

The distance from the surface of the member to the reinforcement inside (t or c) is considered as the most important factor having influence on space and width of the crack and is uniquely introduced into the calculation formulas for the non-slip method. More experiments [1-1] demonstrate that the conclusion fits well with the cracks when $c = 15-80$ mm, and explains well the phenomenon that narrower cracks appear near the reinforcement and wider cracks appear on further places,

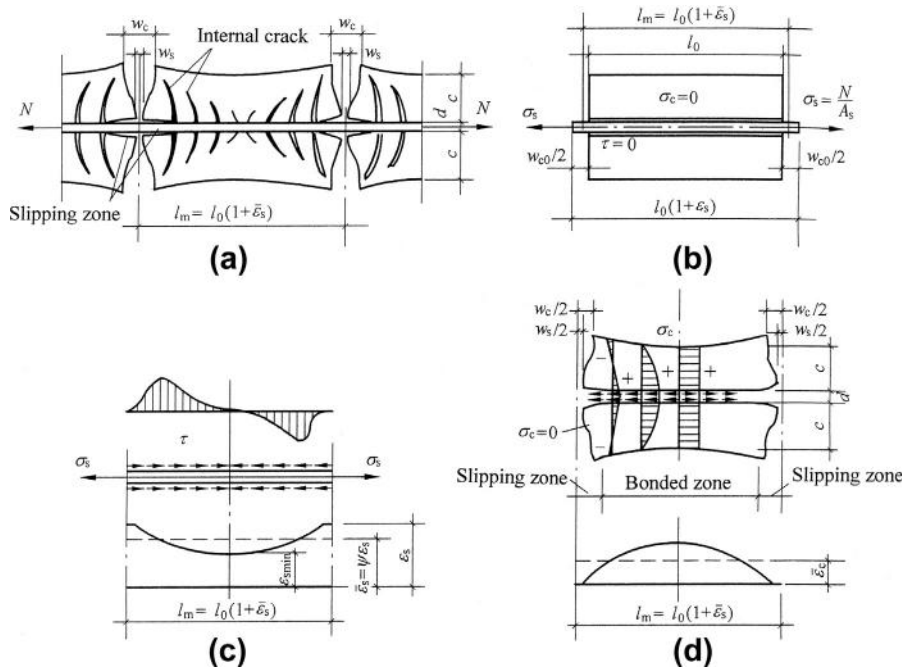


FIG. 12-8 Comprehensive analysis for crack of central tensile member: (a) deformation of concrete after cracking, (b) without bond, (c) stress (strain) distribution of reinforcement, (d) stress (strain) distribution of concrete

e.g. on web of the beam (Fig. 12-1(a), Fig. 12-9(c)). However, the crack width calculated by Eq. (12-15) or Eq. (12-16) is smaller by about 50% than the experimental one when $c < 15$ mm, and the calculated width is mostly larger than the experimental one when $c > 80$ mm, and larger error for larger value of c .

12.3.3 Comprehensive analysis

Micro- and fine-phenomena of the tensile crack of the reinforced concrete member are very complicated: the local stress distributed near the crack varies significantly; the bond stress and relative slip between the reinforcement and concrete are difficult to be determined accurately; so many factors have great influence on the crack; the formation, development, and extension of the crack are random to a certain extent and are controlled by non-homogeneity of the concrete material. Therefore, the space and width of the cracks measured both during testing and in the engineering practice deviate considerably. In addition, the difficulty of the experimental measurement and inadequate data collected cause more difficulty for theoretical analysis of the crack.

Both the bond-and-slip method and non-slip method contribute to reveal the regularity of the crack of tensile concrete. However, they emphasize differently the main influence factors, based on their own experiments. In addition, the formulas and results of their calculations are considerably different, and neither can completely explain all the experimental phenomena and data. Further researches combine reasonably both methods, not only the great influence of the distance between the reinforcement and surface crack (t or c) is considered, but also the assumption of the latter method, i.e. the relative slip and crack width at the boundary of the reinforcement are zero, is modified and the influence of bond-slip (d/μ) is introduced. Therefore, the general formula is given below for calculating the average space of tensile cracks:

$$l_m = k_1 c + k_2 \frac{d}{\mu}, \quad (12-17)$$

where the parameters k_1 and k_2 are calibrated differently based on various experiments [12-13,12-21,12-22,12-23].

The mechanism of cracking of tensile concrete can be generalized based on all the research results and a central tensed member is explained below as an example (Fig. 12-8).

The member is cracked under central tension ($N > N_{cr}$), and the crack width increases gradually with the tension. The number of cracks increases first but keeps constant later, so the space between the cracks tends to be stable. The average space between the cracks is $l_m = l_0(1 + \bar{\epsilon}_s)$ which is slightly longer than the original length (l_m). The deformation of a cracked section, the variation of crack width along depth of the section (h or c), and the space and distribution of the internal cracks are shown schematically together in Fig. 12-8(a).

The stress of the concrete at the cracked section should be $\sigma_c = 0$ and the stress and strain of the reinforcement there are respectively $\sigma_s = N/A_s$ and $\epsilon_s = \sigma_s/E_s$. If it is assumed that no bond exists between the reinforcement and surrounding concrete ($\tau = 0$), both can freely deform and the relative slip between them occurs. At this time, the concrete contracts freely after cracking and its length between two cracks recovers to l_0 , while the reinforcement is elongated uniformly along the axis and its total length between two cracks becomes $l_0(1 + \epsilon_s)$ (Fig. 12-8(b)). Therefore, the crack width of concrete would be a constant along depth of the section:

$$w_{c0} = \epsilon_s l_m = \frac{N l_m}{A_s E_s}, \quad (12-18)$$

which is called the crack width at non-bonded condition and is also the upper bound of the crack width.

It is demonstrated experimentally that the relative slip between the reinforcement and surrounding concrete occurs only on the local zone near the cracked section, while most of the reinforcement is bonded well with the surrounding concrete. Therefore, the stress of the reinforcement is decreased from the maximum value at the cracked section to the minimum value at the middle section between adjacent

cracks (Fig. 12-8(c)), as the bond stress of the concrete (τ) acts on its periphery. The average stress and strain of the reinforcement are, then, respectively:

$$\bar{\sigma}_s = \psi \sigma_s \quad \bar{\epsilon}_s = \psi \epsilon_s, \quad (12-19)$$

where ψ is the non-uniformity coefficient of the reinforcement strain between cracks.

Similarly, the bond stress of the reinforcement reacts on the surrounding concrete and confines free contraction of the concrete between cracks, so a complicated stress state is induced (Fig. 12-8(d)). The total tension or average tensile stress is zero at the cracked section, it increases with the distance from the cracked section to the section considered, and it reaches the maximum value at the middle section between adjacent cracks. In addition, the stress of the concrete on the whole cracked section is zero; on the section near the crack, it is tensile near the reinforcement and changes gradually into a compressive one near the surface; on the section far away from the crack, the tension zone near the reinforcement extends while the compression zone near the surface reduces; on the middle section between adjacent cracks, the concrete is generally tensile over the whole section with approximate stress ($\sigma_c < f_t$). Therefore, the surface layer of the member contracts greatly in longitudinal direction and wider crack (w_c) is formed there, while the concrete near the reinforcement contracts and the crack formed there is narrower ($w_s \ll w_c$), although local slip occurs. The difference between the crack widths ($w_c - w_s$) is compensated by the internal cracks near the reinforcement. The surface of the concrete is also flexed longitudinally, because the cracked section and crack width are curved along depth of the section.

Supposing the bond between the reinforcement and concrete are still well even after cracking, the relative slip would not occur ($w_s = 0$) and the crack width on the surface (w_c) would be the minimum, or the lower bound. Generally, the relative slip between the reinforcement and surrounding concrete occurs locally only near both sides of the crack, but does not occur on the most part along the longitudinal axis, so the actual crack width should be in between the upper and lower bounds.

It is verified that the reinforcement confines the development of the concrete crack due to the effect of the existent bond. The nearer the distance to reinforcement, the greater the confinement and the smaller the crack width. The crack width increases with the distance to the reinforcement (c or t , Fig. 12-7), as the confinement is weakened gradually. When the concrete is far away from the reinforcement, e.g. $c > 80-100$ mm, and is out of the effective scope of confinement, the crack width there will not vary again. The confinement of the reinforcement depends mainly upon its diameter and space and the bond condition with surrounding concrete. The mechanism analysis can be used to explain various phenomena of cracking presented above, e.g. Fig. 12-1(a) and Fig. 12-5.

The crack of a flexural concrete member can also be analyzed, using the same concept and method (Fig. 12-9). When the beam is cracked under the bending moment ($M > M_{cr}$), the compression and tension depths are respectively x and

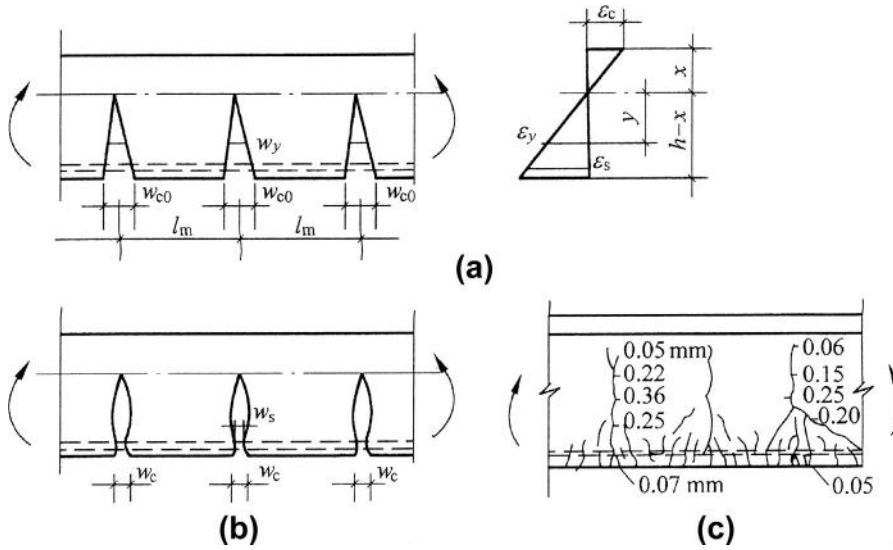


FIG. 12-9 Analysis of crack in a beam: (a) no bond at all ($\tau = 0$), (b) confinement of reinforcement, (c) crack measured in T beam

$(h-x)$ and the average space of the cracks is l_m . At first, no bond is assumed between the reinforcement and surrounding concrete ($\tau = 0$) and the concrete in the tension zone contracts freely after cracking, the crack width of the tensile concrete should be proportional to the distance to the neutral axis (y) or the average tensile strain calculated (ϵ_y):

$$w_y = \epsilon_y l_m = \frac{y}{x} \epsilon_c l_m, \quad (12-20a)$$

and the maximum crack width appears at edge of the tension zone:

$$w_{c0} = \frac{h-x}{x} \epsilon_c l_m. \quad (12-20b)$$

Afterwards, the effect of the bond stress between the reinforcement and surrounding concrete is considered. The confinement of the reinforcement causes a considerable reduction of the crack width at its periphery (w_s) and the crack width at other positions reduces correspondingly, because the confinement of the reinforcement weakens gradually as the distance increases. The final crack width varies as shown in Fig. 11-9(b), which is consistent with the measured results (Fig. 12-9(c)).

Therefore, the longitudinal reinforcements reinforced in web of the beam with larger depth are favorable to confine the development of crack there, and this is demonstrated by the experiments [12-24].

12.4 Calculation of crack width

Based on the available experimental results and analyses, various calculation methods are provided for the crack width of tensile and flexural concrete members under service load. Although the main factors used in these methods are consistent, the mathematical expressions and calculated results are different.

1. The calculation method and formulas [12-25,12-26] suggested in the Chinese design code [2-1] are as below. After the concrete in a member is cracked under load, the average space of the cracks within service stage is taken as (similar to Eq. (12-17)):

$$l_m = c_f \left(1.9c + 0.08 \frac{d_{eq}}{\rho_{te}} \right), \quad (12-21)$$

where c_f is the coefficient depending upon the internal force of a member (Table 12-1); c is the distance from the bottom of tension zone on the section to the outer edge of the reinforcement of out layer; d_{eq} is the equivalent diameter of tensile reinforcements of different diameters:

$$d_{eq} = \frac{\sum n_i d_i^2}{\sum v_i n_i d_i^2}, \quad (12-22)$$

n_i and d_i are the number and diameter of the i -th kind of reinforcement respectively; v_i is the relative coefficient of bond characteristics for the i -th kind of reinforcement, and 1.0 and 0.7 for deformed and plain reinforcements respectively; ρ_{te} is the reinforcement content (A_s/A_{te}) calculated by the effective area of tension zone (A_{te} , Table 12-1), and $\rho_{te} = 0.01$ if $\rho_{te} < 0.01$ is calculated.

The maximum crack width on surface of a member under sustained load is (similar to Eq. (12-12)):

$$w_{\max} = c_p c_t (\bar{\epsilon}_s - \bar{\epsilon}_c) l_m = c_p c_t c_c \bar{\epsilon}_s l_m.$$

Table 12-1 Parameters and Coefficients for Calculation of Crack Width [12-25]

Internal Force	Central Tension	Eccentric Tension	Bending or Eccentric Compression	Notes
c_f	1.1	1.0	1.0	$c_c = 1 - \frac{\bar{\epsilon}_c}{\epsilon_s} = 0.85$
c_p	1.9	1.9	1.66	
α_{cr}	2.7	2.4	2.1	For rectangular section
A_{te}	Bh	0.5bh	0.5bh	
σ_s	N/A_s	$N(e_0 - a' + h/2)/A_s(h_0 - a')$	$M/(0.87A_s h_0)^*$	

*Eccentrically compressed member has to be calculated in an another way.

After Eqs. (12-19) and (12-21) are substituted into it,

$$w_{\max} = \alpha_{cr} \psi \frac{\sigma_s}{E_s} \left(1.9c + 0.08 \frac{d_{eq}}{\rho_{te}} \right) \quad (12-23)$$

is obtained, where $\alpha_{cr} = c_p c_t c_c c_f$ is the coefficient of mechanical characteristic for the member; $c_p = w_{\max}/w_m$ is the ratio between the maximum and average crack widths, considering the deviations of crack space and width. The statistic value with 95% probability is shown in Table 12-1; c_t is the magnified coefficient of crack width under sustained load, due to shrinkage of the concrete and the creep of relative slip between reinforcement and concrete, and $c_t = 1.5$ is taken from the experimental data. $c_c = (\bar{\epsilon}_s - \bar{\epsilon}_c)/\bar{\epsilon}_s$ is the coefficient considering the influence of tensile strain of the concrete between adjacent cracks. $c_c = 0.85$ is taken from the experimental data. $\psi = \bar{\epsilon}_s/\epsilon_s$ is the non-uniformity coefficient of tensile strain of the reinforcement between adjacent cracks.

The value of coefficient ψ measured from the experiments of flexural member varies with bending moment as shown in Fig. 12-10. The value is the minimum when the member is just cracked ($M_{cr}/M = 1$), it increases gradually with the bending moment (M) or as the ratio M_{cr}/M decreases, and it tends to be 1.0 after the tensile reinforcement is yielded. The empiric formula after regression analysis is

$$\psi = 1.1 \left(1 - \frac{M_{cr}}{M} \right). \quad (12-24a)$$

when the cracking moment (M_{cr}) is expressed in the tensile strength of concrete (f_t) and the bending moment (M), at which the crack width is calculated, is expressed in the content (ρ_{te}) and stress (σ_s) of the tensile reinforcement, the formula is simplified properly and becomes [12-25]

$$\psi = 1.1 - \frac{0.65 f_t}{\rho_{te} \sigma_s}, \quad (12-24b)$$

where $\rho_{te} (= A_s/A_{te})$ and σ_s can be calculated following Table 12-1.

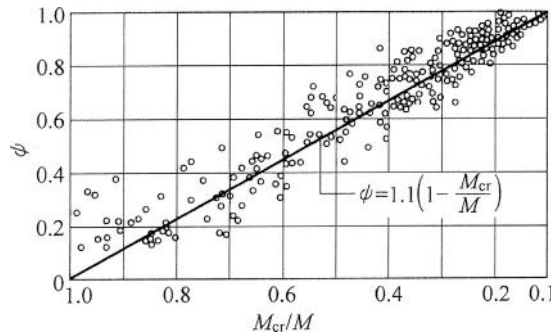


FIG. 12-10 Non-uniformity coefficient of tensile reinforcement strain [12-25]

It is experimentally demonstrated that Eq. (12-24b) can also be used for the centrally tensed and eccentrically tensed and compressed members.

2. In CEB-FIP Model Code [2-12], the tensile crack of a concrete member is calculated mainly based on the bond-and-slip method, and the formula is given for the crack width of concrete within effective confinement area of the reinforcement.

When the reinforcement content of a tensed concrete member is $\rho_{te} = A_s/A_{te}$ and the ratio between the elastic moduli of reinforcement and concrete is $n = E_s/E_c$, the axial forces carried respectively by the reinforcement and concrete just before cracking ($N \approx N_{cr}$) are (see Section 8.2):

$$N_s = \frac{n\rho_{te}}{1 + n\rho_{te}} N_{cr} \quad \text{and} \quad N_c = \frac{1}{1 + n\rho_{te}} N_{cr}. \quad (a)$$

The strains of both should be equal, i.e. $\varepsilon_{sr1} = \varepsilon_{cr1}$, where

$$\varepsilon_{sr1} = \frac{N_s}{E_s A_s}, \quad \varepsilon_{cr1} = \frac{N_c}{E_c A_{te}}, \quad (b)$$

and A_{te} is the effective area of tensile concrete (see Fig. 12-12).

Soon after the first crack appears ($N = N_{cr}$), the stress (strain) of concrete on the cracked section is zero, while the axial force is totally carried by the reinforcement and its stress and strain are respectively (Fig. 12-11(a)):

$$\sigma_{sr2} = \frac{N_{cr}}{A_s} \quad \text{and} \quad \varepsilon_{sr2} = \frac{\sigma_{sr2}}{E_s} \quad (c)$$

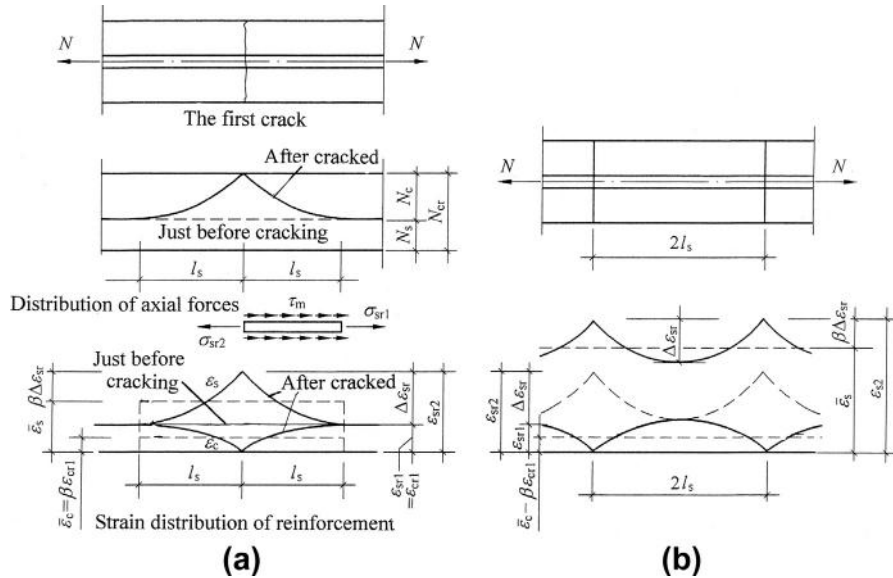


FIG. 12-11 Strain distributions for calculation of crack of tensile member [2-12]: (a) appearance of the first crack ($N = N_{cr}$), (b) crack developed stably ($N > N_{cr}$)

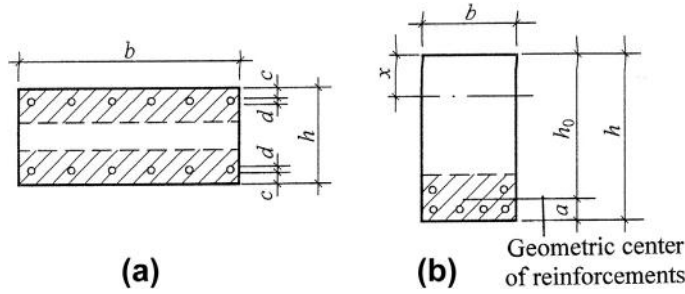


FIG. 12-12 Effective area of tensile concrete on section [2-12]: (a) tensed member, (b) flexural member

However, the stresses (strains) of the reinforcement and concrete out of the bonded length (l_s) on both sides of the cracked section are still the same as that before cracking. The stress difference of the reinforcement within the bonded length (l_s) is in equilibrium with the bond force, which is expressed as the average bond stress (τ_m):

$$\pi d_s \tau_m = (\sigma_{sr2} - \sigma_{sr1}) A_s = \frac{\sigma_{sr2} A_s}{1 + n \rho_{te}}. \quad (d)$$

Therefore,

$$l_s = \frac{d}{4} \frac{\sigma_{sr2}}{\tau_m} \frac{1}{1 + n \rho_{te}} \approx \frac{d}{4} \frac{\sigma_{sr2}}{\tau_m} \quad (12-25)$$

is obtained, where σ_{sr2} is the stress of the reinforcement on cracked section when the member is just cracked.

The strain difference of the reinforcement within the bonded length (l_s) is $\Delta \varepsilon_{sr} = \varepsilon_{sr2} - \varepsilon_{sr1}$. The average strains of the reinforcement and concrete there are respectively:

$$\bar{\varepsilon}_s = \varepsilon_{sr2} - \beta \Delta \varepsilon_{sr} \quad \text{and} \quad \bar{\varepsilon}_c = \beta \varepsilon_{sr1}, \quad (e)$$

and the difference between them is

$$\bar{\varepsilon}_s - \bar{\varepsilon}_c = (1 - \beta) \varepsilon_{sr2}. \quad (12-26)$$

The coefficient in these formulas is taken as

$$\beta = 0.6. \quad (12-27)$$

When the axial force is increased further ($N > N_{cr}$), the space of the cracks tends gradually to be stable and the maximum space is about $2l_s$ (Fig. 12-11(b)). At this time, the stress and strain of the reinforcement on the cracked section becomes:

$$\sigma_{s2} = \frac{N}{A_s} \quad \text{and} \quad \varepsilon_{s2} = \frac{\sigma_{s2}}{E_s}. \quad (f)$$

If the stress (strain) of the concrete between adjacent cracks distributes the same as that just cracking ($N = N_{cr}$), the average strain of the concrete there is still $\bar{\epsilon}_{c2} = \bar{\epsilon}_c$, and the stress (strain) of the reinforcement there distributes parallel with that just cracking and the maximum difference of the strain there is also $\Delta\epsilon_{sr}$. However, the average strain of the reinforcement and the difference between it and the concrete are respectively:

$$\begin{aligned}\bar{\epsilon}_{s2} &= \epsilon_{s2} - \beta\Delta\epsilon_{cr} \\ \text{and } \bar{\epsilon}_{s2} - \bar{\epsilon}_{c2} &= \epsilon_{s2} - \beta\epsilon_{sr2}.\end{aligned}\quad (12-28)$$

Therefore, the maximum width of concrete crack can be calculated and compared with the allowable value (w_{lim}):

$$w_{max} = 2l_s(\epsilon_{s2} - \beta\epsilon_{sr2}) \leq w_{lim}, \quad (12-29)$$

where ϵ_{s2} and ϵ_{sr2} are the strains of the reinforcement on the cracked section under axial forces N and N_{cr} and calculated by Eqs. (f) and (c) respectively.

The crack width of the flexural member can also be calculated by the above formulas, except the effective area of tensile concrete on section is taken differently (Fig. 12-12).

3. Simple and direct calculation is used in the U.S. code [2-12] to control the crack width of a flexural member. Basing on the statistic of many experimental data [12-27], the regression formula is given for the maximum width of concrete crack on bottom of a beam:

$$w_{max} = 11\beta\sigma_s\sqrt[3]{t_bA} \times 10^{-6} \text{ (mm)} \quad (12-30)$$

where σ_s is the stress of tensile reinforcement on cracked section or $0.6f_y$ (in N/mm^2); $\beta = \frac{h-x}{h_0-x}$ 1.2 or 1.35 is taken respectively for a beam or slab; t_b is the distance from the center of the reinforcements of lowest layer to bottom of the section (in mm);

$$A = A_{te}/n$$

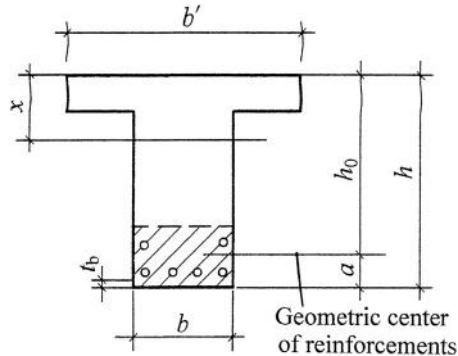


FIG. 12-13 Calculation parameters for crack width [2-11]

A_{te} is the area of concrete on the section, of which the gravity center coincides with the gravity center of tensile reinforcements (in mm, Fig. 12-13); n is the number of tensile reinforcements on the section.

The thickness of concrete cover near the bottom (t_b) and the average confinement area for every tensile reinforcement (A) are introduced into Eq. (12-30), so actually it is similar to the conclusions of the non-slip method.

However, a different parameter (z) is introduced in the relevant provision of the code [2-11] to substitute Eq. (12-30):

$$z = \sigma_s \sqrt[3]{t_b A} = \frac{w_{\max}}{11\beta} \times 10^{-3} \text{ (MN/m)}. \quad (12-31a)$$

The parameter should be limited for:

$$\text{indoor member} \quad z = \sigma_s \sqrt[3]{t_b A} \leq 30 \text{ (MN/m)}, \quad (12-31b)$$

$$\text{outdoor member} \quad z = \sigma_s \sqrt[3]{t_b A} \leq 25 \text{ (MN/m)}, \quad (12-31c)$$

which correspond respectively to limited crack width 0.4 mm and 0.33 mm.

This page intentionally left blank

Flexural Stiffness and Deformation

13

CHAPTER OUTLINE

13.1 Deformation of member and its limitation.....	329
13.1.1 Influences of structural deformation.....	329
13.1.2 Stiffness of section and deformation of member.....	331
13.2 Calculation of sectional stiffness	334
13.2.1 Effective moment of inertia	334
13.2.1.1 <i>Inertia moment of converted section</i>	
<i>before cracking of concrete</i>	<i>335</i>
13.2.1.2 <i>Inertia moment of converted cracked section</i>	<i>336</i>
13.2.1.3 <i>Effective inertia moment.....</i>	<i>336</i>
13.2.2 Analytical method for stiffness.....	337
13.2.3 Modification of tension stiffening.....	340
13.3 Calculation of deformation	342
13.3.1 General method.....	342
13.3.2 Practical methods.....	344
13.3.2.1 <i>Distribution of sectional stiffness.....</i>	<i>345</i>
13.3.2.2 <i>Deformation under sustained load</i>	<i>346</i>

13.1 Deformation of member and its limitation

13.1.1 Influences of structural deformation

Various loads acted on a structure cause corresponding deformations during the service period, e.g. deflection in mid-span of a beam or slab, angular rotation at the end of a beam, lateral displacement of a column or wall. The majority of a reinforced concrete structure is concrete, which has lower strength comparable with steel. Usually, the sectional size of a concrete structure is larger and the strain of concrete is less during the service period. In addition, the intersecting members are connected integrally in the structure. Therefore, the reinforced concrete structure generally has more stiffness and less deformation. Excessive deformation is seldom found in the structure and causes serious problems in engineering practice.

However, some situations appear to be accompanied by the development of a reinforced concrete structure, for example: the concrete of higher and higher

strength grade and the reinforcement of high strength are used in engineering practice, and their strains under service load are increased; the span of the beam or frame and the height of the column or wall are increased gradually; various hollow, box, and thin-wall sections are used widely for the structural member to reduce the weight (dead load). The deformation of the structure under these situations may increase considerably during the service period, especially after the concrete has cracked and under sustained load, which causes creep of concrete. Then, the excessive deformation of the structure causes deterioration of the service function, sometimes even the safety is affected.

The excessive deformation of a structure may cause unfavorable results as below [13-1].

1. The internal forces and bearing capacity of the structure are changed. For example: the additional eccentricity of a compressed member is increased, and the strength of it is then reduced; the dynamic response of a structure is intensified under the vibration of a machine or wind, or under the action of a movable load.
2. The service function of a building is obstructed. For example: the excessive deformation of the structure in a multi-storey industry building has obvious influence on the operation of precise machine, accuracy of machine-made detail, or quality of color printing; the excessive deformation of a crane beam may have influence on the movement of a crane or its usage life; the excessive deformation of a roof structure may cause damage to the waterproofer and water leakage; ...
3. The architectural details connected with the structure may be damaged. For example: the ceiling of a room is deflected or cracked; the light-weight partition supported on the structure is damaged locally; opening or closing of doors or windows is obstructed; ...
4. Psychological un-safety may be caused. For example: obvious deflection and bending of a beam or slab, lateral inclination of a column or wall, and trembling of a thin slab may cause psychological panic for people. Sometimes, this is the dominant factor needing proper treatment, even if the safety and service function of the structure are not really damaged.

Therefore, the maximum deformation of the member during the service period has to be checked and limited within the allowable value, when a concrete structure is designed. In Chinese Code [2-1], the allowable deformations are $1/200-1/300 l_0$ for the beam or slab of the general floor and roof and $1/500-1/600 l_0$ for the crane beam, where l_0 is the calculated span of the member. In USA Code [2-11], the deflection of a member during service period is limited within $1/180-1/480$ of its span or a certain value, or the inclined angle (in radians) of a column or wall is limited, according to different working conditions [13-1].

In addition, when the internal forces of a statically indeterminate structure are mechanically analyzed, the stiffnesses of the members have to be known in advance to satisfy the compatibility condition of deformation and to find the unknown redundants. When the non-linear analysis of a concrete structure, e.g. aseismic one, is

conducted along the loading history, the stiffness or curvature of every section of all the members and its variation are the premise and have to be known in advance. Therefore, the stiffness or bending moment—curvature relation of a section of the member has direct influence on the internal forces and their distribution of the structure.

13.1.2 Stiffness of section and deformation of member

The sectional stiffness and its variation of a reinforced concrete member can be determined directly and accurately from the bending moment—curvature curve measured during the corresponding test. The specimen is usually designed as a simply supported beam and two concentrated loads are acted symmetrically on its span, and the segment between the two loads is of pure bending (without shear force, $V = 0$). The beam is flexed, and the crack is formed and developed gradually in tension zone as the loads are increased. The section near the crack will not follow the hypothesis of the plane section. However, when the average strain of concrete measured within a certain distance, e.g. the space between adjacent cracks, is considered, the hypothesis is still fitted (Fig. 13-1). This will lead to only a small error for the calculations of stiffness and deformation of a structural member.

The strain transducers or gauges are set up on the middle segment with pure bending, the average compressive strain of concrete at the top of the section ($\bar{\epsilon}_c$) and the average strain of tensile reinforcement ($\bar{\epsilon}_s$) are measured separately during testing, then the average curvature of the section is calculated by

$$\frac{1}{\rho} = \frac{\bar{\epsilon}_c + \bar{\epsilon}_s}{h_0} \quad (13-1)$$

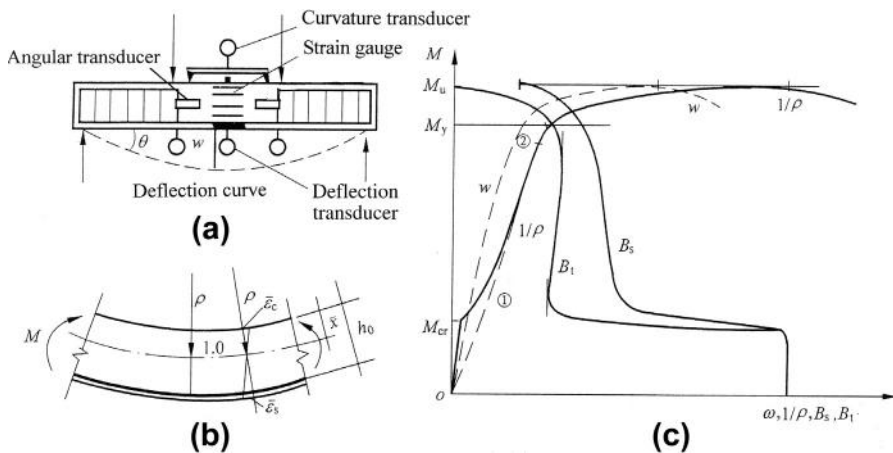


FIG. 13-1 Bending moment—curvature relation of beam: (a) specimen and measuring instruments, (b) average strain and curvature, (c) variations of curvature and stiffness

where ρ is the average radius of curvature and h_0 is the effective depth of the section.

Of course, the average curvature can also be measured by other instruments, e.g. the curvature transducer ($1/\rho = 8f/s^2$) or a pair of angular transducers ($1/\rho = (\theta_1 + \theta_2)/s$).

The typical relation between the bending moment and average curvature ($1/\rho$) of a suitably reinforced concrete beam is shown in Fig. 13-1(c) (similar to Fig. 11-1). The variation of the curve ($M-1/\rho$) represents the mechanical characteristics of the beam in different stages, which have been introduced above (Section 11-1). Two geometrical contraflexure points can be found on the curve. Soon after the beam is cracked ($M > M_{cr}$), the curvature increases and the slope of the curve decreases suddenly, and the curve turns obviously. Afterwards, the crack develops stably as the bending moment increases, and the curvature increases slower and the slope of the curve increases again, so the contraflexure point (1) appears. When the tensile reinforcement is approaching yielding, the curvature accelerates and the slope of the curve decreases quickly again, so the contraflexure point (2) is formed.

The deflection at mid-span of the beam is also measured during testing, the bending moment (or load)—deflection ($M-w$) curve plotted is similar to the bending moment—curvature ($M-1/\rho$) curve, but the slope of the former varies less and the former turns less near the cracking and yielding moments (M_{cr} , M_y).

According to *The Strength of Materials*, the relation between curvature and bending moment of a section of a structural member is derived:

$$\frac{1}{\rho} = \frac{M}{EI} = \frac{M}{B} \quad (13-2)$$

where $B = EI$ is the flexural stiffness of a section of elastic material, E is the elastic modulus of the material, and I is the inertia moment of the section.

The bending moment—curvature relation of a reinforced concrete member is non-linear, and the secant and tangent values of average flexural stiffness can be calculated separately from the $M-1/\rho$ curve:

$$B_s = \frac{M}{1/\rho} \quad \text{and} \quad B_t = \frac{dM}{d(1/\rho)}. \quad (13-3)$$

They vary with the bending moment as shown in Fig. 13-1(c).

Before cracking of concrete, the whole section of the reinforced concrete member works with small stress (strain), similar to an elastic material. The flexural stiffness of the section is $B_0 = E_c I_0$, where E_c is the elastic modulus of concrete and I_0 is the inertia moment of the converted section.

The secant stiffness of a member is $B_s = B_0$ before cracking of concrete, and it reduces monotonically after concrete cracks as the bending moment is increased. The secant stiffness reduces quickly when the cracking and yielding moments (M_{cr} , M_y) are just reached, i.e. the concrete is cracking and the tensile reinforcement is yielding respectively, but it is relatively stable between the two bending moments ($M_{cr} \rightarrow M_y$). The secant stiffness is rather low after the reinforcement is yielded ($>M_y$) and reduces continuously when the bending moment reaches the

ultimate value (M_u) and enters into the descending branch, although it is always greater than zero.

The tangent stiffness of a member is also $B_t = B_0$ before cracking of concrete but reduces sharply after concrete has cracked. There are two extreme values between the cracking and yielding moments ($M_{cr} \rightarrow M_y$), and they respectively correspond to the two contraflexure points on the $M-1/\rho$ curve. The tangent stiffness reduces quickly again after yielding of the reinforcement and reaches $B_t = 0$ at the ultimate moment (M_u), and it becomes a negative value when the bending moment enters into the descending branch. In all situations, $B_t \leq B_s$ is always held.

The bending moment at a different section of a reinforced concrete beam under load is variable, and the stiffness or curvature at the section varies correspondingly (Fig. 13-2). As the bending moment at the section increases with the load, the stiffness of the section and, then, its distribution along the span vary as well. Therefore, if the deformation of the beam is to be calculated accurately, non-linear distribution of the stiffness and its variation have to be considered. The general method for it is as below.

If the flexural curve of a beam is $w(x)$, the mathematical expression of the curvature is approximately:

$$\left(\frac{1}{\rho}\right)_x \approx \frac{d^2 w(x)}{dx^2}, \quad (13-4a)$$

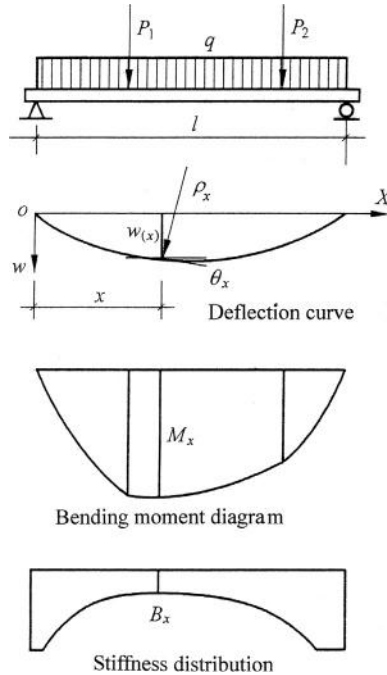


FIG. 13-2 Flexural curve and stiffness distribution of a beam

according to its definition. After Eq. (13-2) is substituted, the first and second order of integration of the equation give the deformations, i.e. angular rotation and deflection respectively, of the beam:

$$\theta = \frac{dw}{dx} = \int \left(\frac{1}{\rho} \right)_x dx = \int \frac{M_x}{B_x} dx \quad (13-4b)$$

$$w = \iint \left(\frac{1}{\rho} \right)_x dx^2 = \iint \frac{M_x}{B_x} dx^2. \quad (13-4c)$$

When the load and support conditions of a beam and the shape and material behavior of its section are known, the variations of the bending moment (M_x) and stiffness of the section (B_x) can be determined correspondingly, the deformation values can be obtained after integration of the equation. Generally, the beam is divided into several elements and the digital integration is conducted, because the stiffness of the section varies non-linearly.

13.2 Calculation of sectional stiffness

When the shape, size, and reinforcement of the section and the stress–strain relations of the concrete and reinforcement are known in advance, the complete bending moment–curvature curve can be calculated by the general analysis method (see Section 11.3) then the variable regularity of the sectional stiffness is known completely. The calculated result is accurate but has to be achieved through computing, so the method is usually used only for the structural analysis along the loading history.

The relevant problems that happen frequently in engineering practice are: e.g. checking the deflection of a member under service load, providing the sectional stiffness of the members for mechanical analysis of a statically indeterminate structure. Generally, the stiffness and deformation of the structural member are not necessary to analyze along the loading history, but only a simple calculation is needed for these situations.

The characteristics of the calculation are: the concrete crack exists in tension zone but the tensile reinforcement is not yielded yet, i.e. $M_{cr} < M < M_y$; the reinforcement and surrounding concrete between adjacent cracks are bonded locally, and tension stiffening results; the hypothesis of plane section is used for the average strain of the material on section. However, various methods suggested show different ways and formulas for calculation.

13.2.1 Effective moment of inertia

In the early stage of the application of a reinforced concrete structure, the mature method and formulas for homogeneous elastic material were used for design and calculation of the strength and deformation (stiffness) of it. In principle, the reinforcement on the section is converted into the concrete on the same section, based on the ratio between the elastic moduli of both materials. Then, an equivalent section of homogeneous material (concrete) is obtained, and the calculation formulas are easily

established for various purposes. This principle and method are still used now for some situations of calculation or design of concrete structure, e.g. before cracking of a prestressed concrete structure, stiffness analysis, checking fatigue strength [2-1].

The converted sections before and after appearance of the concrete crack on tension zone of the flexural or eccentrically compressed (tensed) member are obviously different (Fig. 13-3) and should be calculated separately.

13.2.1.1 Inertia moment of converted section before cracking of concrete

The concrete of a whole section works in compression or tension before cracking of the member. If the area of the tensile reinforcement is A_s , its converted area is nA_s and n is the ratio between the elastic moduli of both materials ($n = E_s/E_0$, Eq. (8-6)). Therefore, an additional area $(n - 1)A_s$ should be attached to the section at the same depth of the reinforcement, besides its initial area (A_s). The stress on the converted area of the reinforcement is the same as the stress of the concrete at the same depth ($\varepsilon_s E_0$). Then, the converted section of unique concrete is mechanically equivalent to the original section of reinforced concrete.

The total area of the converted section is then

$$A_0 = bh + (n - 1)A_s. \quad (13-5)$$

The compressive depth (x_0) is determined by the condition of equality in area moments of compression and tension zones against the neutral axis:

$$\frac{1}{2}bx_0^2 = \frac{1}{2}b(h - x_0)^2 + (n - 1)A_s(h_0 - x),$$

$$\text{and } x_0 = \frac{\frac{1}{2}bh^2 + (n - 1)A_sh_0}{bh + (n - 1)A_s} \quad (13-6)$$

is obtained. The inertia moment of the converted section is

$$I_0 = \frac{b}{3} [x_0^3 + (h - x_0)^3] + (n - 1)A_s(h_0 - x_0)^2 \quad (13-7)$$

and the stiffness of the section before cracking of concrete is

$$B_0 = E_0 I_0. \quad (13-8)$$

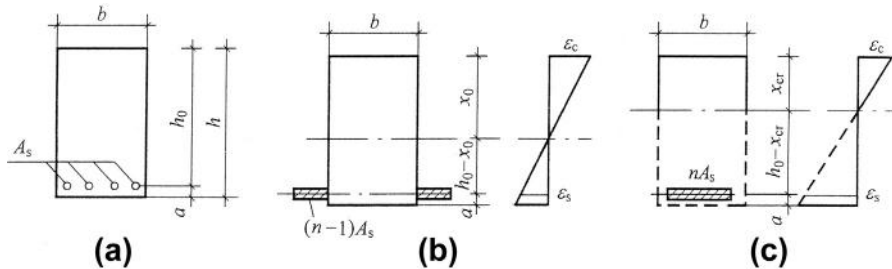


FIG. 13-3 Converted sections before and after cracking of concrete: (a) initial section, (b) before cracking, (c) after cracking

These geometrical characteristics of the converted section (A_0, x_0, I_0) can be used not only for the calculations of stiffness and deformation of the member, but also for checking the cracking (e.g. Eq. 12-8) and fatigue strength (see Section 17.4) of the member.

13.2.1.2 Inertia moment of converted cracked section

The concrete on the tension zone of the cracked section is assumed to be totally out of work and only the reinforcement there carries tensile force on the section, after the member is cracked. When the converted area of the reinforcement (nA_s) is placed on the same depth (h_0), the converted section of unique concrete is obtained (Fig. 13-3(c)).

The compressive depth of the converted cracked section can be determined similarly:

$$\frac{1}{2}bx_{cr}^2 = nA_s(h_0 - x_{cr}),$$

$$\text{and } x_{cr} = \left(\sqrt{n^2\mu^2 + 2n\mu} - n\mu \right) h_0 \quad (13-9)$$

is solved, where $n = E_s/E_0$ and $\mu = A_s/bh_0$.

Then, the inertia moment¹ and stiffness of the cracked section are respectively:

$$I_{cr} = \frac{1}{3}bx_{cr}^3 + nA_s(h_0 - x_{cr})^2 \quad (13-10)$$

$$\text{and } B_{cr} = E_0 I_{cr}. \quad (13-11)$$

Obviously, they are the minimum values of the section among all the sections of the beam, and also the minimum values of the cracked section before yielding of the reinforcement ($M_{cr} < M < M_y$).

13.2.1.3 Effective inertia moment

The sectional stiffness and inertia moment of a reinforced concrete beam reduce as the bending moment increases. The stiffness before cracking of concrete ($E_0 I_0$) is the upper bound, and the lower bound appears after the reinforcement yielded and the

¹In the early application of reinforced concrete structure, its member is designed following the concept of allowable stress of the material. The allowable stresses for tensile reinforcement and compressive concrete are respectively $[f_y/k_s]$ and $[f_c/k_c]$, where k_s and k_c are correspondingly the safety factors for the strengths of both materials. In order to guarantee safety of the structure, the formulas fitting for elastic material are used to calculate the stresses on its section, which are compared with the allowable stresses separately:

$$\sigma_s = \frac{nM(h_0 - x_{cr})}{I_{cr}} \leq \left[\frac{f_y}{k_s} \right] \quad \text{and} \quad \sigma_c = \frac{Mx_{cr}}{I_{cr}} \leq \left[\frac{f_c}{k_c} \right].$$

tensile concrete being totally out of work. The bending moment—curvature relation is relatively stable and the stiffness value (B_s , Fig. 13-1(c)) varies less during the service stage ($M/M_u = 0.5-0.7$), so they may be calculated approximately in the engineering application.

The simplest way used widely in the past is that the average stiffness of section of a structural member is taken as a constant, e.g.

$$B = 0.625 E_0 I_0. \quad (13-12)$$

This is also used now for analysis of the internal forces of a statically indeterminate structure.

When the deflection of a structural member ($M > M_{cr}$) is calculated, the design code of the USA [2-11,13-2] suggests that the effective inertia moment of its section is interpolated between I_0 and I_{cr} :

$$I_{eff} = \left(\frac{M_{cr}}{M} \right)^3 I_0 + \left[1 - \left(\frac{M_{cr}}{M} \right)^3 \right] I_{cr} \leq I_0. \quad (13-13)$$

In the formula, I_0 can also be calculated by the gross section of the concrete without considering the area of the reinforcement in it. The effective inertia moment calculated varies with the bending moment as shown in Fig. 13-4.

13.2.2 Analytical method for stiffness

After the segment of pure bending (without shear force) of a reinforced concrete beam is cracked and enters into the stably developing stage of crack under bending moment, the spaces between the cracks tend to be approximately uniform. The actual strains of every section distribute non-linearly and the neutral

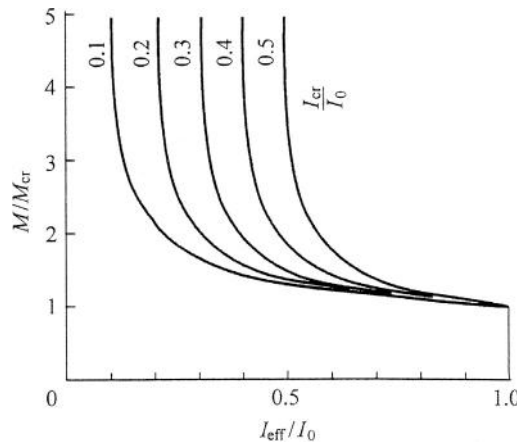


FIG. 13-4 Effective inertia moment calculated

axis is waved due to the influence of the cracks (Fig. 13-5(a)), and the minimum of the compressive depth (x_{cr}) appears at the cracked section. Therefore, the distributions of the compressive strain of the concrete at the top and the tensile strain of the reinforcement are also waved (Fig. 13-5(b)), and the average strains are $\bar{\epsilon}_c$ and $\bar{\epsilon}_s$ respectively and the maximum strains of them (ϵ_c and ϵ_s) appear at the cracked section as well.

The calculation formula for the average sectional stiffness of a structural member can be derived following the procedures below [12-6,12-10,13-3]:

1. Geometrical (deformation) condition. It is demonstrated experimentally that the average strain on the section still agrees with linear distribution (Fig. 13-5(c)), the distance from the corresponding neutral axis to the top is \bar{x} and the average curvature of it can be calculated by Eq. (13-1). In the equation, the average strain of the concrete can be approximately taken as $\bar{\epsilon}_c = \epsilon_c$ because the compressive strain of the concrete varies less in the longitudinal direction, while the average strain of the tensile reinforcement is taken as

$$\bar{\epsilon}_s = \psi \epsilon_s, \quad (a)$$

where ψ is the non-uniformity coefficient of tensile strain of the reinforcement between adjacent cracks and can be calculated by Eq. (12-24b).

2. Physical (constitutive) relations. The stress distribution on the cracked section during the service stage of the member is shown in Fig. 13-5(d), and the compressive

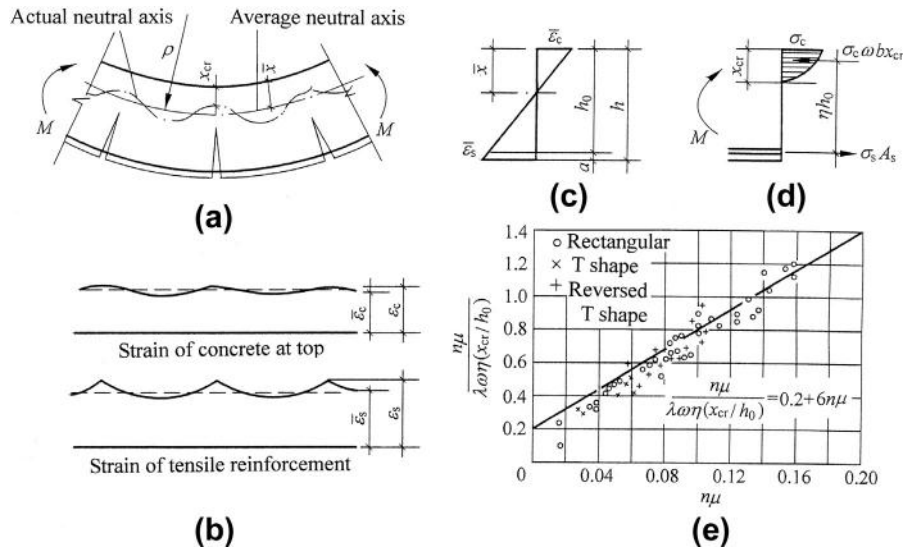


FIG. 13-5 Calculation of average stiffness of section: (a) cracks and neutral axis, (b) longitudinal distributions of strains, (c) average strains, (d) stresses on cracked section, (e) composite coefficient for average strain of compressive concrete [13-3]

stress of the concrete at the top and the tensile stress of the reinforcement can be calculated separately by Eqs (8-3) and (8-2):

$$\left\{ \begin{array}{l} \sigma_c = \varepsilon_c \lambda E_0 \approx \bar{\varepsilon}_c \lambda E_0 \\ \sigma_s = \varepsilon_s E_s = \frac{\bar{\varepsilon}_s}{\psi} E_s \end{array} \right. \quad \text{or} \quad \left\{ \begin{array}{l} \bar{\varepsilon}_c = \frac{\sigma_c}{\lambda E_0} \\ \bar{\varepsilon}_s = \frac{\psi \sigma_s}{E_s} \end{array} \right. \quad (b)$$

3. Mechanical (equilibrium) equations. Neglecting the stress of the concrete on the tension zone, the equilibrium equation is then established for the cracked section:

$$\left. \begin{array}{l} M = \omega \sigma_c b x_{cr} \eta h_0 \quad \sigma_c = \frac{M}{\omega \eta x_{cr} b h_0} \\ M = \sigma_s A_s \eta h_0 \quad \sigma_s = \frac{M}{\eta A_s h_0} \end{array} \right\}, \quad (c)$$

where ω is the integrality coefficient of stress block on compression zone, and η is the coefficient for lever arm on cracked section.

After Eqs (b) and (c) are substituted successively into Eq. (13-1), the average curvature of the section is obtained:

$$\frac{1}{\rho} = \frac{\psi M}{\eta E_s A_s h_0^2} + \frac{M}{\lambda \omega \eta x_{cr} E_0 b h_0^2} = \frac{M}{E_s A_s h_0^2} \left[\frac{\psi}{\eta} + \frac{n \mu}{\lambda \omega \eta \left(\frac{x_{cr}}{h_0} \right)} \right]. \quad (13-14a)$$

Therefore, the average stiffness (secant value) of the section is then

$$B = \frac{M}{1/\rho} = \frac{E_s A_s h_0^2}{\frac{\psi}{\eta} + \frac{n \mu}{\lambda \omega \eta (x_{cr}/h_0)}}, \quad (13-14b)$$

where A_s , E_s , h_0 , $\mu = A_s/bh_0$, and $n = E_s/E_0$ are definite values for a known member. However, the values of other parameters, including ψ , η , λ , ω , and x_{cr}/h_0 , vary with the bending moment and have to be determined in some other ways.

The coefficient ψ among them can be calculated by Eq. (12-24b).

As the level of bending moment of a member is about $M/M_u = 0.5-0.7$ and the crack develops relatively stably under service load, the coefficient for the lever arm on the cracked section varies less and usually ranges between $\eta = 0.83-0.93$. And, the larger the reinforcement content, the smaller the coefficient value, the average of it is taken approximately for calculation of the sectional stiffness of the member:

$$\eta = 0.87. \quad (13-15)$$

Other parameters are gathered up ($\lambda \omega \eta (x_{cr}/h_0)$) in Eq. (13-14) and do not appear independently, which is called the composite coefficient for the average strain of compressive concrete. Its value decreases as the bending moment increases, but is relatively stable under service load ($M/M_u = 0.5-0.7$). According to the experimental

results (Fig. 13-5(e)), it depends mainly upon the reinforcement content and the regression formula obtained is

$$\frac{n\mu}{\lambda\omega\eta(x_{cr}/h_0)} = 0.2 + 6n\mu \quad (13-16)$$

for the beam of rectangular section. And, the right side of the equation should be $0.2 + 6n\mu/(1 + 3.5\gamma_1)$ for the beams of doubly reinforced (where $\gamma_1 = (n - 1)A'_s/bh_0$ and A'_s being the area of the compressive reinforcement) and T or I shape sections (where $\gamma_1 = (b_f - b)h_f/bh$, and b_f and h_f being the width and thickness respectively of the compressive flange).

After Eqs (13-15) and (13-16) are substituted into Eq. (13-14(b)), the calculation formula for the average sectional stiffness of a beam is finally:

$$B = \frac{E_s A_s h_0^2}{1.15\psi + 0.2 + 6n\mu}. \quad (13-17)$$

When $M = M_{cr}$ is taken, $\psi = 0$ is obtained from Eq. (12-24a), and the maximum value of the average stiffness should be

$$B_0 = \frac{E_s A_s h_0^2}{0.2 + 6n\mu}. \quad (13-18)$$

Therefore, the relative stiffness (B/B_0) varies with the bending moment or ψ and the theoretical curve is shown in Fig. 13-6.

13.2.3 Modification of tension stiffening

The constitutive model of bending moment—curvature of a structural member (Fig. 13-7) is directly given in the CEB-FIP Model Code [2-12], and three basic stiffnesses are separately introduced:

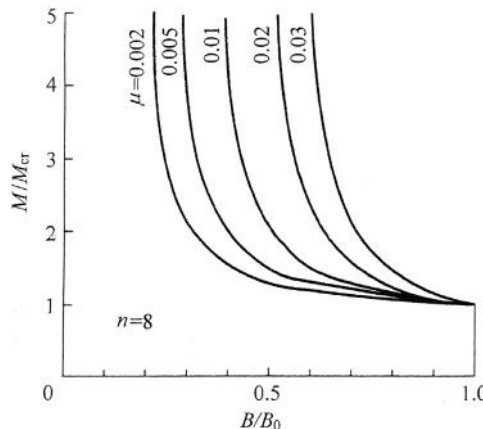


FIG 13-6 Sectional stiffness varying with bending moment

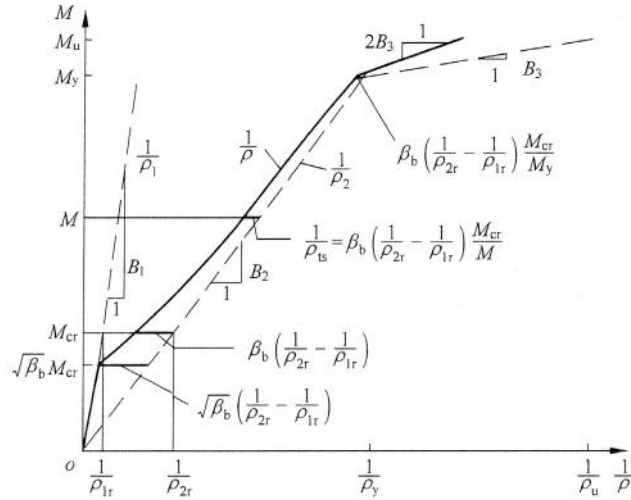


FIG. 13-7 Constitutive model for bending moment–curvature [2-12]

1. Before cracking of concrete in tension zone ($M \leq M_{cr}$)

$$\frac{M}{1/\rho_1} = B_1 = EI_0, \quad (13-19a)$$

2. After tensile concrete is cracked and out of work ($M \leq M_y$)

$$\frac{M}{1/\rho_2} = B_2 = EI_{cr}, \quad (13-19b)$$

3. After yielding of tensile reinforcement ($M_y < M \leq M_u$)

$$B_3 = \frac{M_u - M_y}{1/\rho_u - 1/\rho_y}, \quad (13-19c)$$

where I_0 and I_{cr} are calculated respectively by Eqs (13-7) and (13-10) and the curvatures at yielding of the tensile reinforcement and ultimate bending moment are separately:

$$\frac{1}{\rho_y} = \frac{\varepsilon_y}{h_0 - x_y} \quad \text{and} \quad \frac{1}{\rho_u} = \frac{\varepsilon_c}{x_u}, \quad (13-20)$$

where ε_y is the strain of tensile reinforcement at yielding, ε_c is the the maximum strain of compressive concrete at the ultimate state of the member, and x_y , x_u are the depths of compression zones at yielding and ultimate moments.

Considering the influences of shrinkage and creep of the concrete, non-uniform bond condition along the reinforcement, and variations of the loads, the cracking moment of the member is possibly lower than the calculated value (M_{cr}) and a modifying factor ($\sqrt{\beta_b}$) is introduced:

$$\sqrt{\beta_b} = \sqrt{\beta_1 \beta_2}, \quad (13-21)$$

where $\beta_1 = 1.0$ or 0.5 respectively for the deformed or plain reinforcement, $\beta_2 = 0.8$ or 0.5 respectively for the situation of the first loading or for the repeated loading or sustained load.

The average sectional curvature of a structural member is shown as a solid curve in Fig. 13-7, considering the effect of the tension stiffening of concrete (see Section 8.2.4). When the bending moment is divided into three stages, the average curvature can be calculated separately:

1. When $M < \sqrt{\beta_b} M_{cr}$ (before cracking of concrete)

$$\frac{1}{\rho} = \frac{1}{\rho_1} = \frac{M}{EI_0} \quad (13-22a)$$

2. When $\sqrt{\beta_b} M_{cr} \leq M < M_y$ (after cracking of concrete but before yielding of reinforcement)

$$\frac{1}{\rho} = \frac{1}{\rho_2} - \frac{1}{\rho_{ts}}, \quad (13-22b)$$

where $\frac{1}{\rho_{ts}}$ modification of curvature after considering the effect of tension stiffening:

$$\frac{1}{\rho_{ts}} = \beta_b \left(\frac{1}{\rho_{2r}} - \frac{1}{\rho_{1r}} \right) \frac{M_{cr}}{M}. \quad (13-23)$$

In the equation, the curvatures just before and after cracking of concrete ($M = M_{cr}$) are separately:

$$\frac{1}{\rho_{1r}} = \frac{M_{cr}}{EI_0} \quad \text{and} \quad \frac{1}{\rho_{2r}} = \frac{M_{cr}}{EI_{cr}}. \quad (13-24)$$

After Eq. (13-24) is substituted into Eq. (13-23), Eq. (13-22b) becomes as below:

$$\frac{1}{\rho} = \frac{M}{EI_{cr}} - \beta_b \left(\frac{M_{cr}}{EI_{cr}} - \frac{M_{cr}}{EI_0} \right) \frac{M_{cr}}{M}. \quad (13-22b)$$

3. When $M_y \leq M \leq M_u$ (after yielding of reinforcement but before ultimate state):

$$\frac{1}{\rho} = \frac{1}{\rho_y} - \beta_b \left(\frac{M_{cr}}{EI_{cr}} - \frac{M_{cr}}{EI_0} \right) \frac{M_{cr}}{M} + \frac{1}{2} \frac{M - M_y}{M_u - M_y} \left(\frac{1}{\rho_u} - \frac{1}{\rho_y} \right). \quad (13-22c)$$

13.3 Calculation of deformation

13.3.1 General method

After the relation between bending moment and average curvature ($M-1/\rho$) or the variation regularity of average stiffness (B) of the section is obtained by various methods, the non-linear deformation of the structural member with variable stiffness can be calculated by Eq. (13-4). Usually, the calculation based on the principle of virtual work is rather simple.

When the deformation of a beam (Fig. 13-8(a)) is needed, the internal forces on every section under the loads, including bending moment (M_p), axial force (N_p), and shear force (V_p), are calculated first, and then the corresponding sectional deformations, i.e. curvature ($1/\rho_p = M_p/B$), axial strain ($\epsilon_p = N_p/EA$), and shear strain (angle $\gamma_p = k V_p/GA$), are easily obtained.

It is assumed that a unit virtual load is acted at the place, where the deformation of the beam is wanted. For example, a unit concentrated load ($P = 1$) or a unit couple of forces ($M = 1$) is used respectively to find the deflection or angular rotation of the beam (Fig. 13-8(b)). Afterwards, the internal forces under the virtual load (\bar{M} , \bar{N} , and \bar{V}) are calculated correspondingly.

According to the principle of virtual work, the work done by the virtual load on the deformation of the beam should be equal to the total work done by the virtual internal forces on the corresponding sectional deformations of the beam. Therefore, the formula is established for calculation of the deflection at the mid-span of the beam:

$$1 \cdot w_c = \Sigma \int \frac{\bar{M}M_p}{B} dx + \Sigma \int \frac{\bar{N}N_p}{EA} dx + \Sigma \int \frac{k\bar{V}V_p}{GA} dx, \quad (13-25a)$$

$$\text{or } w_c = \Sigma \int \bar{M} \left(\frac{1}{\rho_p} \right) dx + \Sigma \int \bar{N} (\epsilon_p) dx + \Sigma \int \bar{V} (\gamma_p) dx. \quad (13-25b)$$

The second and third items on the right side of the formula show respectively the deflections caused by the axial force and shear force. Generally, the sectional curvature and deflection of the beam is decreased when the axial compression is acted

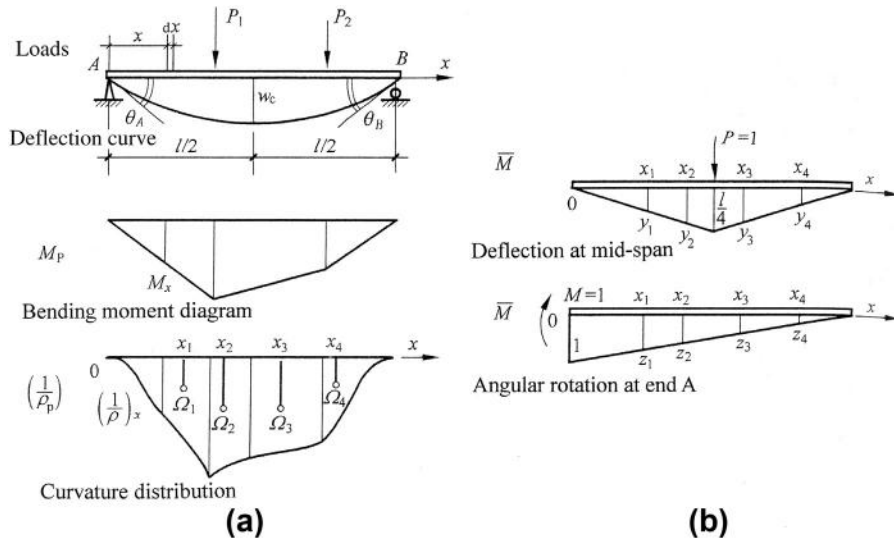


FIG. 13-8 Deformation calculation based on the principle of virtual work: (a) bending moment and curvature, (b) unit virtual load and bending moment

(Fig. 11-7(b)); the deflection caused by the shear force is negligible before cracking of the beam; the deflection at mid-span is increased after the inclined crack occurs near the end of the beam, and it reaches about 30% of the total deflection at ultimate state. Usually, the deflection of the beam caused by the axial and shear forces during the service period is possessed of a small fraction of the total deflection and may be neglected during calculation, so the formula is simplified into:

$$w_c \approx \int \bar{M} \left(\frac{1}{\rho_p} \right) dx, \quad (13-25c)$$

where $1/\rho_p$ is the average curvature of the beam section under load, varying with bending moment (M_p) diagram, \bar{M} is the bending moment under unit virtual load ($P = 1$).

As two concentrated loads are acted on the beam, the bending moment diagram of the beam is a fold line (Fig. 13-8a). Then, the curvature distribution is composed of three segments, which are taken correspondingly from the bending moment—curvature relation (or $M-1/\rho$ diagram). Because, the bending moment diagram (\bar{M}) caused by the virtual load is a straight or folded line (Fig. 13-8(b)), Eq. (13-25c) can be calculated easily by the multiply method of diagrams as below. For example, the curvature diagram ($1/\rho_p$) along the beam is divided into four parts and the area (Ω_i) and the position of geometric centre (x_i) of every part are determined in advance, the value of bending moment (y_i) at same position (x_i) is found on the bending moment diagram (\bar{M}) under the virtual load, then Eq. (13-25c) is equivalent to:

$$w_c = \sum_{i=1}^4 \Omega_i y_i. \quad (13-26a)$$

When the angular rotation at support of the beam is calculated, the virtual load acted there should be a couple of forces and a bending moment diagram of triangle is obtained (Fig. 13-8(b)). Then, the angular rotation can be calculated similarly by the same method:

$$\theta_A = \sum_{i=1}^4 \Omega_i z_i. \quad (13-26b)$$

If the bending moment—curvature relation of the section is simplified into a fold line of several segments, the curvature diagram along the beam under the load ($1/\rho_p$) is also composed of various fold lines. Then, the multiply method of diagrams is convenient and the calculation formula can be directly derived.

13.3.2 Practical methods

If it is only checked whether or not the deformation of a structural member is allowable, an even simpler method may be used.

13.3.2.1 Distribution of sectional stiffness

The bending moment of a structural member under load varies along its axis, and the average curvature or stiffness of the section varies correspondingly and even more complicatedly (Fig. 13-8(a)). This is the main difficulty for accurate calculation of deformation of a reinforced concrete member. If the sectional stiffness of a structural member is taken as a constant, e.g. the minimum stiffness at the section with the maximum bending moment ($B_x = B_{\min} = \text{const.}$), the curvature distribution of the member ($1/\rho_p = M_p/B_{\min}$) is certainly similar to the bending moment diagram, then the deformation of the member can be calculated easily by the principle of virtual work or multiply method of diagrams. Sometimes, the existing formulas for calculation of elastic deformation of the member with constant section can be used directly, e.g. the deflection at the center of a simply supported beam under uniformly distributed load (q N/m) is $w_c = \frac{5ql^4}{384B_{\min}}$. This simplification makes the calculated deformation somewhat larger, but usually no more than 10%, and is accepted in many design codes [2-1,2-11,2-12].

Generally, positive and negative bending moments exist together within the span of a continuous beam or frame beam (Fig. 13-9(a)), and various simplifications are used in different design codes. For example, the beam is divided into several segments with the same sign of bending moment [2-1], and the sectional stiffness in every segment is taken as a constant (Fig. 13-9(b)) and usually the minimum stiffness at the section with the maximum bending moment within each segment is used. Or, the sectional stiffness is taken as a constant within the whole span (Fig. 13-9(c)) [2-11], and the effective inertia moments ($I_{\text{eff}}^1, I_{\text{eff}}^c, I_{\text{eff}}^2$) at the section with the

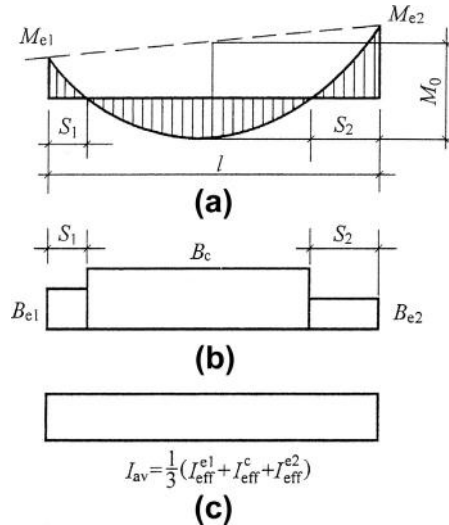


FIG. 13-9 Calculation value for sectional stiffness of continuous member: (a) bending moment diagram, (b) divisional stiffness, (c) average stiffness

maximum bending moment within the three segments of same sign are calculated separately (Eq. (13-13)) first and the average value (I_{av}) is then used.

If the inertia moments of the sections within position and negative bending moment segments are considerably different, e.g. a continuous member with T section, it is still suggested [13-4] that the sectional stiffness is taken as a constant within the whole span, but the weighted average of effective inertia moment should be used and calculated as below:

$$I_{av} = I_c \left[1 - \left(\frac{M_{e1} + M_{e2}}{2M_0} \right)^2 \right] + \frac{I_{e1} + I_{e2}}{2} \left(\frac{M_{e1} + M_{e2}}{2M_0} \right)^2, \quad (13-27)$$

where M_{e1} , M_{e2} are the bending moments at both ends of the member, M_0 is the bending moment at the center of the member as if it is simply supported (Fig. 13-9(a)), and I_c , I_{e1} , I_{e2} are the effective inertia moments calculated respectively at the sections of the center and both ends of the member.

13.3.2.2 Deformation under sustained load

Besides the deformation of a structural member occurs instantaneously under action of the load, it increases gradually as the load is sustained. It is demonstrated experimentally [12-19] that the deflection at the center of a beam increases continuously under the constant load sustained after six years, although the increasing rate is limited (Fig. 13-10). It is generally considered that the deflection of a concrete member tends to be stable after the load is sustained three years later.

When the load is acted continuously on a structural member, the concrete in the compression zone creeps, the crack of concrete in the tension zone extends and expands and more concrete there is out of work, the slip between the reinforcement and surrounding concrete develops, and the average strain of the tensile reinforcement is increased. These are the main reasons causing the increase in deformation under sustained load. In addition, the variation of environmental condition and the shrinkage of concrete also have certain influences. Therefore, the factors determining these conditions should have influences on the long-term deformation of the member, such as the raw materials, mixture, and curing of the concrete, concrete age at loading, reinforcement (especially compressive reinforcement) content, environmental temperature and relative humidity, sectional shape and size.

Many experimental data have been reported at home and abroad for the deflection of reinforced concrete beam (slab) under sustained load [12-10,13-5,13-6]. However, these data are deviated to a certain extent because of the differences of the specimens used and the experimental conditions.

If the deflection of a structural member occurring instantaneously under load is w_s and the deflection increases gradually but tends to be stable (w_l) as the load is sustained for a long time, the ratio between them is called a magnifying coefficient of deflection under sustained load:

$$\theta = \frac{w_l}{w_s}. \quad (13-28)$$

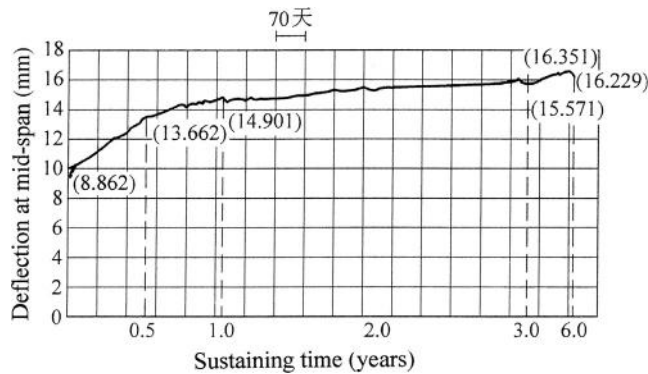


FIG. 13-10 Variation of deflection at center of beam under sustained load [12-10]

The relevant experimental results obtained in China are listed in Table 13-1, and the values of the coefficient given in the Chinese Code [2-1] are also listed. Generally, the coefficient is taken as $\theta=2$ for the singly reinforced (A_s only) beam of rectangular section. When the beam is doubly reinforced (A_s and A'_s) or there is a flange in the compression zone, the long-term deflection is decreased because of a reduction in concrete creep. By contrast, the deflection of the beam with a flange in the tension zone (section of reversed T shape) is slightly larger under sustained load.

The long-term loading tests of reinforced concrete member are also conducted abroad, and similar results are reported [13-5–13-8] and the average value give ranges $\theta = 1.85\text{--}2.01$. However, a higher reduction rate (Table 13-2) is suggested for the influence of the compressive reinforcement. In the USA Design Code

Table 13-1 Magnifying Coefficient for Deflection Under Sustained Load [12-10]

Sectional Shape	Singly Reinforced Rectangular Section	Doubly Reinforced, Rectangular Section	T Section	Reversed T Section
Tianjin University	1.51–1.89 ¹ (1.67) ²	1.51–1.74 ³	1.70–2.15	1.86–2.40
Southeast University	1.84–2.20 (2.03) ²	1.91 ³	1.89–1.94	2.41–2.65
Design code [2-1]	2.0	1.6 ⁴	2.0	1.2 × (value listed on left side)

Note:
¹ age at loading: 168 days,
² average value,
³ $\mu'/\mu = 0.44 - 1.0$,
⁴ used for $\mu'/\mu = 1$ only, or the interpolation should be used and $\theta = 2.0$ is taken for $\mu' = 0$.

Table 13-2 Reduction of Magnifying Coefficient of Deflection for Compressive Reinforcement [13-8]

μ'/μ	0	0.5	1.0
Reference [13-5]	1	0.64–0.76 (0.69)	0.47–0.76 (0.56)
Reference [13-6]	1	0.77–0.82 (0.80)	0.71–0.81 (0.78)
All experimental data	1	0.64–0.82 (0.72)	0.47–0.81 (0.64)

Note: the figures in the parentheses show the average value.

[2-11], the ratio between the deflections after five years under sustained load and occurring instantaneously is suggested as

$$\theta = \frac{2.4}{1 + 0.5p'}, \quad (13-29)$$

where $p' = A'_s/bh_0$ is the area ratio of compressive reinforcement.

Besides the practical calculation methods introduced above, the maximum span—depth ratio (l_0/h) [2-1,13-1] or the minimum sectional depth (h) [2-11] of the structural member, for which the stiffness (or deformation) requirement of the member is satisfied without checking calculation, is generally provided in the design code.

Strength of Member Under Shear Force

14

CHAPTER OUTLINE

14.1 Failure pattern and strength of beam without web reinforcement	350
14.1.1 Typical failure pattern (shear-compression)	350
14.1.2 Failure patterns of inclined compression and tension	354
14.1.2.1 Failure pattern of inclined compression (short strut)	354
14.1.2.2 Failure pattern of inclined tension	355
14.1.3 Ultimate shear strength	356
14.1.3.1 Shear-span ratio ($\lambda = a/h_o$)	356
14.1.3.2 Strength of concrete	358
14.1.3.3 Content of longitudinal reinforcement (μ , %)	358
14.2 Effect of web reinforcement and components of shear resistance	360
14.2.1 Effect of web reinforcement	360
14.2.2 Composition of ultimate shear strength	363
14.3 Calculation of ultimate shear strength	364
14.3.1 About finite element method	364
14.3.2 Empirical regression	365
14.3.3 Simplified mechanical models	369
14.3.3.1 Beam model	369
14.3.3.2 Truss model	370
14.4 Various members and mechanical conditions	373
14.4.1 Load acted on beam web	373
14.4.2 Beam of T section	374
14.4.3 Beam with variable section (depth)	376
14.4.4 Influence of axial force	377
14.4.5 Both positive and negative bending moments exist within shear span	378
14.4.6 Bracket	380
14.4.7 Punching of slab	382

14.1 Failure pattern and strength of beam without web reinforcement

Beam and column are used most widely in engineering practice and the main internal forces in them are axial force (N) and bending moment (M), which dominate the strength, deformation, cracking of concrete, and section size of them (Chapters 10–12). In addition, shear force is another important internal force and always exists together with bending moment ($V = dM/dx$) in the member. Generally, shear strength of the member is checked or the web reinforcement is designed only after the section is known in advance. However, shear force may be the dominant factor for sectional design in some situations, e.g. beam with smaller span-depth ratio, beam with thin web, shear wall in a tall building.

When a member is shear dominated, the stress state and mechanical behavior of it are more complicated than that of the flexural and compressive members and show some characteristics as below.

1. There is no member with pure shear ($M = 0$) alone, although few sections with pure shear ($V \neq 0$ but $M = 0$) may be found in the member, e.g. the section near support of a simply supported beam, the section at turning point between positive and negative bending moments of a continuous beam. When the segment of a member is of constant shear, the bending moment there should vary linearly. If the member is mainly failed due to the inclined crack, this should be influenced by the bending moment. Therefore, the shear strength of a member is essentially the strength under shear force and bending moment together.
2. The shear stresses at any position always occur in pairs in two perpendicular directions, and then a two-dimensional stress state is formed in a member with shear force.
3. The hypothesis of plane section is not held anymore, even for the member of elastic material.
4. The stress of the member redistributes obviously and continuously after cracking of concrete until failure (see Fig. 14-2) and does not fit again the stress distribution of a beam.
5. Usually, the member fails suddenly and is brittle with less ductility.

The mechanical behavior of the reinforced concrete member under the united action of shear force and other internal forces has been investigated experimentally and theoretically for many years at home and abroad [14-1–14-5]. Many results and conclusions are achieved and accepted in the relevant design codes, which are used widely in engineering practice. However, the mechanism and calculation accuracy of the shear resistance is still not perfect, because of the complicated stress state.

14.1.1 Typical failure pattern (shear-compression)

At first, the typical failure process under the joint action of shear force and bending moment is carefully examined for a simply supported beam of rectangular section reinforced with tensile reinforcement only (without web reinforcement) (Fig. 14-1).

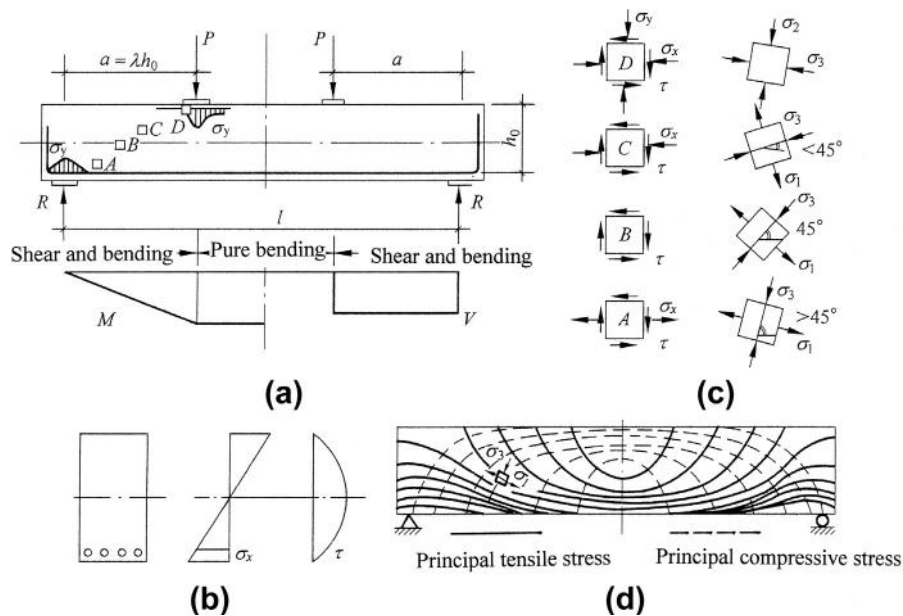


FIG. 14-1 Stress distribution on shear-bending segment: (a) specimen and internal forces, (b) sectional stress distribution (elasticity), (c) stress states and principal stresses, (d) loci of principal stresses

As two concentrated loads are symmetrically acted on the beam, the shear force at any section between the support and load is a constant ($V = \text{const.}$) and the bending moment there varies linearly. This segment is called a shear-bending one, and its length is called shear-span (a) and the ratio between the shear span and the effective depth of the section is called the shear-span ratio ($\lambda = a/h_0$).

According to *The Strength of Materials*, the two-dimensional stress state existing in the shear-bending segment (Fig. 14-1(b)) can be calculated simply as below: the horizontal normal stress distributes linearly on the vertical section and its value ($\sigma_x = M_y/I$) depends upon the bending moment and the distance to the neutral axis; the shear stress on the vertical section ($\tau = VS/bI$) distributes as a parabolic curve of second order. Of course, this is the simplified analyses for a beam of elastic material, and also fits the reinforced concrete beam before cracking. In addition, vertical normal stresses (σ_y), generally compressive stress, are formed locally and non-uniformly under the concentrated loads and near the supports.

Knowing the stress distributions (σ_x, σ_y, τ) within the shear-bending segment, the values and directions of the principal stresses (σ_1, σ_3) at any point there can be easily calculated, e.g. by the Mohr circle method, and their loci are then plotted (Fig. 14-1(c), (d)). If the load position or the shear-span (a), i.e. the ratio between bending moment and shear force ($M/V = a$), is changed, the relative values between the stresses σ_x, σ_y , and τ within the shear-bending segment varies

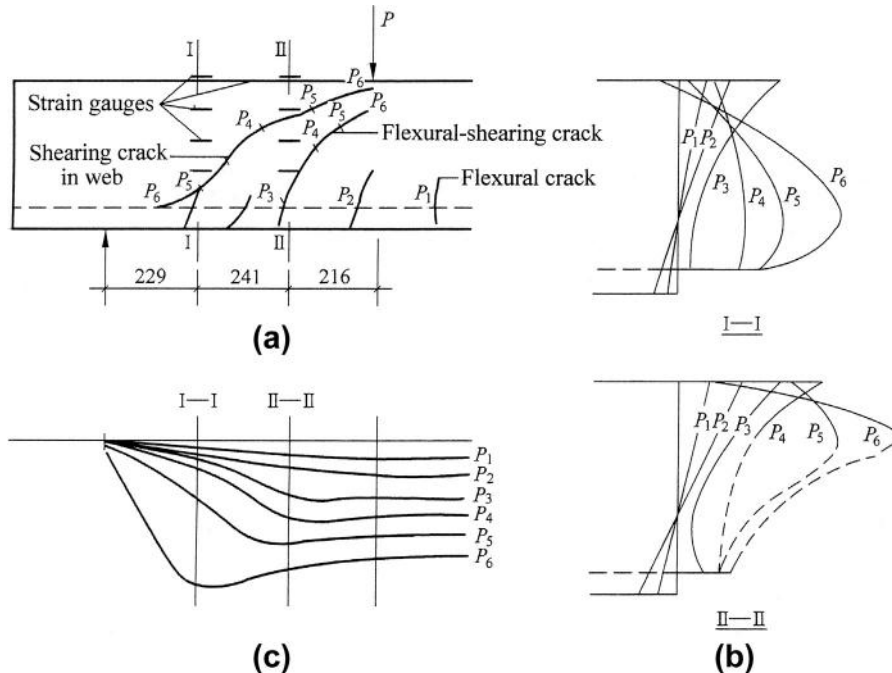


FIG. 14-2 Strain and stress distributions within shear-bending segment [14-6, 1-1]: (a) development of crack, (b) distributions of normal strain on sections, (c) distribution of tensile stress in longitudinal reinforcement

correspondingly, and various failure patterns with different ultimate strength will appear successively.

When a beam of medium shear-span ($\lambda = a/h_0 = 1-3$) is loaded continuously, the characteristics of stress state, deformation, cracking, and failure of the beam under shear force and bending moment are shown apparently (Fig. 14-2). In the early stage of loading, the stress in the beam is rather low and no crack appears in the concrete, the strain distribution on sections I-I and II-II approximates to the hypothesis of the plane section and the stress state in the beam approximates to that obtained from elastic analysis, and the tensile stress of the reinforcement on the section varies proportionally with the bending moment diagram.

The tensile crack appears first on the middle part, i.e. the pure bending segment (shear force $V = 0$), of the beam when the load reaches P_1 . The bending moment in the shear-bending segment increases with the load, the flexural (tensile) crack appears there near the bottom and is perpendicular to the beam axis when the load reaches P_2 . The crack gradually extends upwards with reducing slope as the load increases, and it is approximate to the locus of the principal compressive stress or is perpendicular to the direction of the principal tensile stress. This kind of crack

is called a flexural-shear crack. However, the strain distributions on the sections I—I and II—II are still approximate to the hypothesis of plane section.

When the load is increased to P_3 and P_4 successively, the new flexural-shear crack occurs while the existing crack extends upwards with reducing slope, and some cracks may pass through section II—II. In the meantime, an inclined crack of about 45° appears on the middle depth and about h_0 apart from the support, and it is called shear crack in web. At this time, the strain of concrete in the lower part of section II—II turns from tensile to a compressive one and the whole section is totally compressive, but the maximum compressive stress still exists at the top. Relative slip between the reinforcement and surrounding concrete occurs locally after the flexural-shear crack passes through, so the tensile stress of the reinforcement there is increased suddenly and is approaching that in the pure bending segment. Therefore, the longitudinal distribution of the reinforcement stress within the shear-bending segment turns from a triangle, which is similar to the bending moment diagram there, to a trapezoid, which is not again the stress state of a beam analyzed elastically.

When the load is increased further to P_5 and P_6 , the flexural crack in the pure bending segment is stagnated, while the flexural-shear crack in the shear-bending segment extends continuously upwards with reducing slope and the shear crack in web develops both upwards with reducing slope and downwards with increasing slope. When the upper end of the shear crack reaches underneath the loading plate and the lower end of it intersects perpendicularly with the tensile reinforcement, the critical inclined crack is then formed. The shape of these inclined cracks is consistent with the locus of principal compressive stress of the beam. At this time, the maximum compressive stress on sections I—I and II—II moves downwards, and the compressive stress at the top decreases obviously and even turns into a tensile one. The tensile stress of the longitudinal reinforcement is still low within a small length near the support, but the stress in another part of the shear-bending segment is approaching that in the pure bending segment with the maximum bending moment, and the stress of the reinforcement at the intersection between it and the critical inclined crack is even higher. It demonstrates that the load on the beam is transferred to the support via the curved compression lines, and the mechanical condition of the beam changes into several tied arches with variable section (Fig. 14-3).

When the load is increased further, the widths of these cracks are increased continuously but their number and shape do not change again. Finally, the compression zone near the loading plate and sectional top is reduced seriously, the concrete there reaches its biaxial compressive strength and then fails under the together action of normal (σ_x , σ_y) and shear (τ) stresses, and the horizontal cracks and failure zone are formed there. The lower end of the critical inclined crack near the reinforcement widens suddenly, and the horizontal tearing crack appears on the upper surface of the reinforcement. This kind of typical failure pattern is called a shear-compression one.

This kind of failure pattern of a beam can be simulated as a set of tied arches of variable section (Fig. 14-3(a)). The compression transferring lines of the main and secondary arches are consistent with the loci of principal compressive stress, and

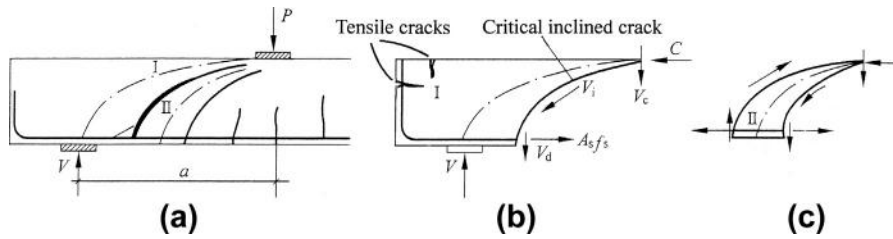


FIG. 14-3 Mechanical characteristics of shear-bending segment near support: (a) arch action, (b) main arch and shear components, (c) secondary arch

the stress of the tensile tie is divisionally uniform. The main arch should include the end of the beam, and the cracks may occur near the upper corner at the ultimate state due to the tensile stress caused by the inclined compression and corresponding eccentricity (Fig. 14-3(b)).

According to the equilibrium condition of the main arch at ultimate state, the main components of the shear strength (V_u), i.e. ultimate reaction at the support, of a reinforced concrete beam without web reinforcement are: shear resistance of the concrete above the upper end of the critical inclined crack (V_c), interaction between the aggregates on both sides of the crack (V_i), and the transverse resistance or dowel action of the longitudinal reinforcement (V_d). These three components share the total ultimate strength and are about 20–40%, 33–50%, and 15–25% respectively for a beam of rectangular section [13-2].

14.1.2 Failure patterns of inclined compression and tension

When the load position or shear span (a) is changed, different failure patterns (Fig. 14-4) will appear for the beam of the same size and materials. It means that the failure pattern on the end part of the beam depends mainly upon the relative value between the shear force and bending moment ($a = M/V$).

14.1.2.1 Failure pattern of inclined compression (short strut)

If the shear span of the beam is small enough or the concentrated load is closed to the support, e.g. $a/h_0 < 1$, the normal stress in vertical direction (σ_y) within the inclined strip between the loading and supporting plates is far greater than the horizontal normal stress (σ_x) and shear stress (τ) there. And, the direction of the principal compressive stress there parallels approximately to the linking line between the concentrated load and reaction at the support. When the load is increased gradually, an inclined crack appears first on the middle depth of the web and parallels the linking line. Afterwards, the crack extents both upwards and downwards along the same direction, and some other inclined cracks appear successively nearby. Finally, the middle part of the web is failed compressively in the inclined direction, and the failure pattern and mechanical model are consistent with that of an inclined short strut under the action of axial compression.

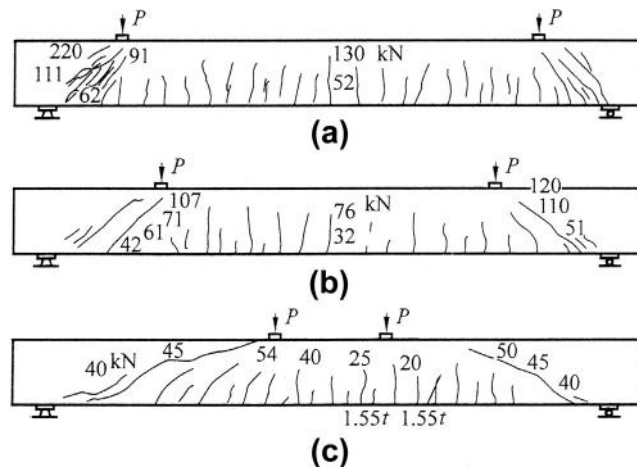


FIG. 14-4 Main failure patterns on beam end under shear force and bending moment: (a) inclined compression, (b) shear-compression, (c) inclined tension

14.1.2.2 Failure pattern of inclined tension

When the shear span of a beam is long enough ($3 < a/h_0 < 5-6$) and the concentrated load is far away from the support, the normal stress in the vertical direction (σ_y) there has a slight influence on the web. After the beam is loaded, the tensile crack appears first on the lower part of the pure bending segment, i.e. the middle part of the beam, and extends vertically. After the inclined shear crack of 45° slope occurred on the web of the shear-bending segment near the support, it extends quickly both upwards with reducing slope until shearing off the beam top and downwards with increasing slope until the tensile reinforcement and beam bottom. As the part of the beam beneath the inclined crack, together with the reinforcement, moves downwards under action of the load, the concrete cover near the beam end is torn away along the upper surface of the reinforcement (Fig. 14-4(c)). The inclined crack is dominated by the principal tensile stress of the beam and causes breaking in tension of concrete (see Section 5-3) and final beam failure.

The failure patterns of a reinforced concrete beam under shear force and bending moment transit successively from the inclined compression, and shear-compression to inclined tension as the shear span is increased. However, if the shear span is even longer, e.g. $\lambda > 6$, the failure of the beam is dominated by the bending moment only and the flexural failure pattern (Fig. 11-2) is formed in the pure bending segment, although the flexural-shear crack and shear crack in the web still occur in the shear-bending segment (shear span).

In addition, other failure patterns will occur in some special situations, for example: bond failure occurs near the end of the tensile reinforcement because of bond or anchorage default and excessive stress in the reinforcement caused after appearance of the inclined crack (Fig. 14-2(c)); local compressive failure occurs

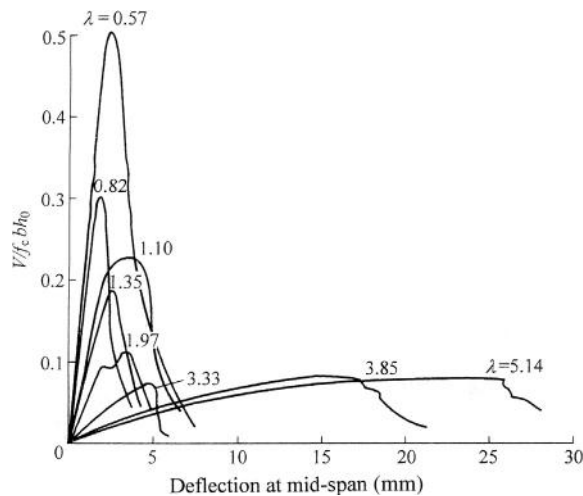


FIG. 14-5 Shear force–deflection curves [1-1]

in concrete near an extremely small area of the loading or supporting plate; splitting failure occurs in the shear span of very small length. These failure patterns are unusual for the beam under shear force and bending moment, and they should be avoided in engineering practice by taking proper measures.

The measured shear force (load)–deflection curves of the beams are shown in Fig. 14-5. The beam with small shear–span ratio fails suddenly in the failure pattern of inclined compression, its ultimate shear force (V_u) is rather high but with small deformation, so the curve has a sharp peak. The beam with medium shear–span ratio fails gradually and experiences successively the cracking of concrete, formation of critical inclined crack, and crushing of concrete near the top, so the deformation at ultimate state is relatively great. The beam with larger shear–span ratio fails suddenly without warning although the deflection at mid-span is not small due to longer flexural span, because the failure is controlled by the tensile strength of the concrete.

14.1.3 Ultimate shear strength

When a reinforced concrete beam without web reinforcement is acted under the concentrated load, its ultimate strength under shear force and bending moment depends upon many factors, among them the main ones are the shear–span ratio, strength of concrete, and content of longitudinal reinforcement.

14.1.3.1 Shear-span ratio ($\lambda = a/h_0$)

It is explained above that the shear–span ratio of a beam represents the stress state and relative values between various stresses on the failure zone, i.e. the shear-bending segment, near the end of the beam. When the shear–span ratio is increased, the ultimate strength (V_u/bh_0) reduces quickly (Fig. 14-6), as the failure pattern turns

14.1.3.2 Strength of concrete

The final failure of a beam under shear force is dominated by crushing or breaking of the concrete, so the ultimate strength varies certainly with the strength of the concrete. As the beam with different shear—span ratios fails in different patterns, its strength depends respectively upon compressive or tensile strength of the concrete, and the increasing rate of the strength (slope of the lines in Fig. 14-7) are obviously different, when the strength grade of the concrete (f_{cu}) used is increased.

The beam with smaller shear—span ratio ($\lambda < 1$) fails in the pattern of inclined compression which depends upon the compressive strength of concrete (f_c), so its ultimate strength (V_u) increases proportionally with the cubic strength of concrete (f_{cu}). The beam with larger shear—span ratio ($\lambda > 3$) fails in the pattern of inclined tension which depends upon the tensile strength of concrete (f_t), so its ultimate strength (V_u) increases slowly with the cubic strength of concrete. The beam with medium shear—span ratio ($\lambda = 1-3$) fails in the pattern of shear—compression which depends upon both the compressive strength of the concrete near the beam top and the aggregate interaction, being nearly the shear or tensile strength of concrete, along the critical inclined crack, so the increasing rate of its ultimate strength is in between the above two.

14.1.3.3 Content of longitudinal reinforcement (μ , %)

Beside the transverse force or dowel action (V_d , Fig. 14-3) is the direct shear resistance of the longitudinal reinforcement, the depth or area of the compression zone near beam top is increased with content (or area) of the reinforcement, so the ultimate strength of the beam under shear force is elevated indirectly (Fig. 14-8). However, the dowel action of the reinforcement is limited after the concrete cover near the beam end is torn off, and the reinforcement has less effect on the beam failed in

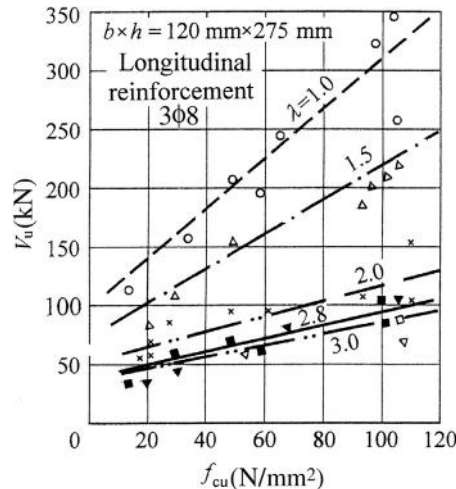


FIG. 14-7 Influence of concrete strength on ultimate shear strength [14-5]

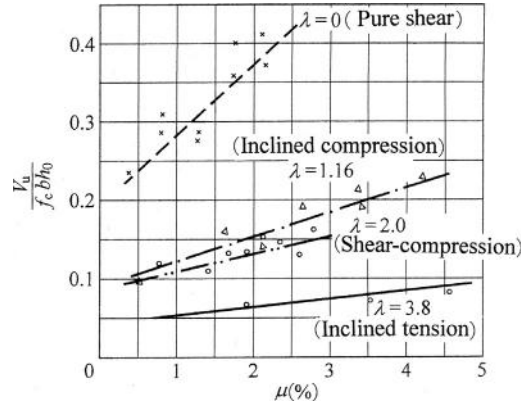


FIG. 14-8 Influence of reinforcement content on ultimate shear strength [1-2]

the pattern of inclined tension. Therefore, increasing reinforcement is not an effective measure for enhancing the ultimate shear strength of the beam.

Moreover, some other experiments show that the average ultimate shear stress (V_u/bh_0) reduces by 21–37% [14-2] when sectional depth of the beam is increased by 2 or 4 times but with other factors unchanged. The reason for this is that the aggregate interaction along the inclined crack is obviously reduced (see Eq. (14-9)), because the width of the crack at ultimate state increases with depth of the beam section.

The discussion and conclusion above are obtained based only on the experimental results of the simply supported beam acted with concentrated load. However, the beam acted with uniformly distributed load is widely used in engineering practice, and the mechanical state formed is certainly different: the shear force reaches the maximum while the bending moment is zero at the section near support of the beam, and the shear force reduces gradually to zero while the bending moment increases gradually to the maximum, as the section moves to the mid-span. Compared with the beam acted with concentrated load, the beam acted with uniformly distributed load does not have a shear-bending segment with constant shear force (shear span a), and the maximum shear force and the maximum bending moment will not happen together at any section. Therefore, the generalized shear–span ratio ($\lambda = M_{\max}/V_{\max}h_0 = l/h_0$) or the span–depth ratio (l/h_0) is used for the beam to reflect the relative value between shear force and bending moment.

A series of beams with the same section but different spans are tested under uniformly distributed load and also failed respectively in the typical patterns of inclined compression ($l/h_0 < 4$), shear–compression ($l/h_0 = 4 \sim 9$), and inclined tension ($l/h_0 = 9 \sim 20$) (Fig. 14-9(a)). Although the cracking and failure characteristics of these beams are consistent with that of the beam with concentrated load, the shear force on the section at the top of the critical inclined crack is not the maximum but

$$V = V_{\max} - qs, \quad (14-3)$$

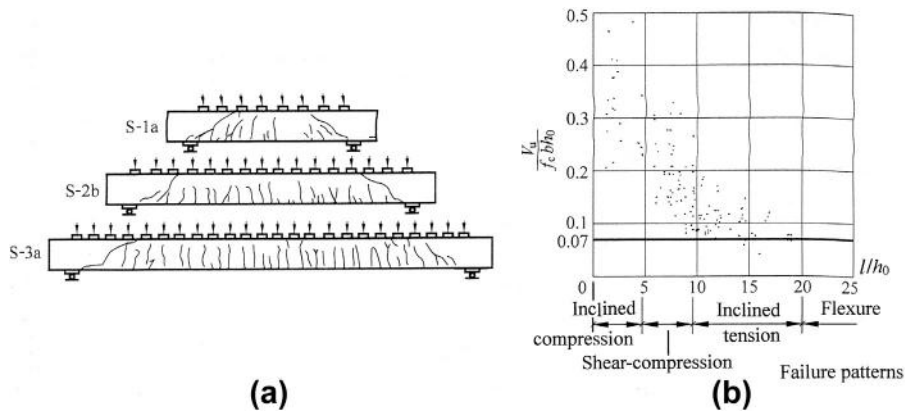


FIG. 14-9 Failure patterns and ultimate shear strength of beams acted with uniformly distributed load [14-5]: (a) failure patterns, (b) ultimate shear strength

where V_{\max} is the maximum shear force on the section near support, q is the uniformly distributed load, and s is the distance from support to the top of the critical inclined crack.

The ultimate strength under shear force of the beam acted with uniformly distributed load ($V_u / f_c b h_0$) decreases as the span—depth ratio increases (Fig. 14-9(b)), and the ultimate strength decreases quickly when $l/h_0 < 10$ but slowly when $l/h_0 > 10$. However, the beam of span—depth ratio $l/h_0 > 20$ will fail in the flexural pattern, which is controlled by bending moment only.

Other factors, such as position of load, sectional shape, and axial force, also have important influence on the ultimate shear strength of the beam and they will be discussed in detail later (Section 14.4).

14.2 Effect of web reinforcement and components of shear resistance

14.2.1 Effect of web reinforcement

If the ultimate strength of a beam without web reinforcement is not strong enough to resist the shear force and bending moment caused by the load acted, the transverse stirrups set in the web are rather effective. In addition, the web reinforcement is necessary to fix tightly the longitudinal reinforcement during manufacturing of the member, and it is also helpful to carry the thermal stress and to reduce the crack width during the long service period. Therefore, the web reinforcement is an essential part and occupies (15–25)% of the total steel used in the reinforced concrete member.

When the beam reinforced with web reinforcement is tested, the stress in the web reinforcement is rather low before cracking of concrete, so the web reinforcement

has less help to elevate the cracking load of the beam. When the beam is approaching the ultimate state, the stress distribution of every stirrup within the shear span is measured as shown in Fig. 14-10.

The vertical cracks appear first in the tension zone on the middle of the beam with larger bending moment as the load is increased, and they parallel with the web reinforcement and have little influence on its stress. When the load is increased, the tensile crack extends upwards with reducing slope and the flexural—shear crack is then formed in the shear span, and the shear crack in web occurs on the middle depth near the support and extends both upwards and downwards. After these inclined cracks intersect with the web reinforcement, the tensile stress of it increases suddenly. As the load is increased continuously, the inclined cracks widen and extend further and new cracks appear there, so the stress in web reinforcement varies correspondingly. Therefore, the tensile stress distributes non-uniformly in each web reinforcement, and the stress distribution and value of every web reinforcement in shear span are different from one another, because the stress at any point depends upon the position and width of the inclined crack nearby. In addition, the web reinforcement near the support possibly carries compressive stress due to the effect of the reaction there.

The web reinforcement is yielded first at the widest of the inclined crack and it can not obstruct any more the development of the inclined crack, although its yield strength (f_y) is maintained before failure of the beam. Afterwards, the web reinforcements nearby are yielded successively, and the inclined crack widens along its length and the aggregate interaction is weakened gradually. Finally, the concrete on the upper end of the critical inclined crack is crushed under the compressive and shear stresses together, and the failure pattern of shear—compression is formed similarly. Some of the web reinforcement is broken in tension with an obvious neck, which is found at the widest part of the inclined crack on the failed beam.

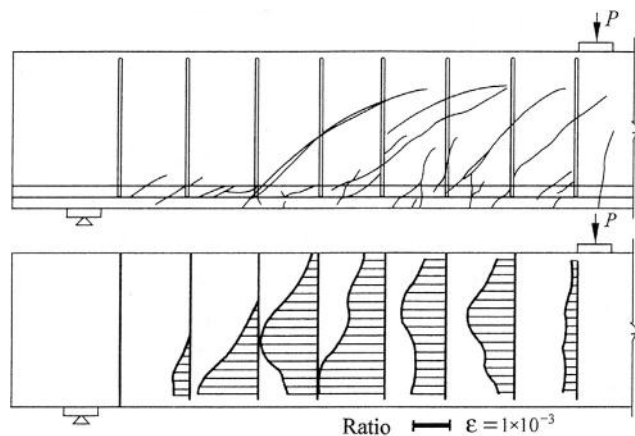


FIG. 14-10 Stress (strain) distribution of web reinforcements in shear span [14-8]

More longitudinal reinforcements are needed to resist the bending moment in mid-span of the beams of larger span and section, but only part of them has to be extended into the beam end and well anchored there, so others may be bent up or cut off appropriately, according to the bending moment diagram. Sometimes, the bent-up reinforcement enters the upper part of the section and passes through the support area, and can be used to resist the negative bending moment of a continuous beam. When the bent-up part of the reinforcement is set up properly and intersects with the inclined crack, the ultimate shear strength of the beam can be elevated considerably, because of not only the effect of the bent-up reinforcement itself but also development of the inclined crack being delayed and confined.

The bent-up reinforcement is also a kind of web reinforcement and acts similarly with the stirrups. It has less influence on appearance of the inclined crack, and its stress increases suddenly and distributes non-uniformly along the length, when the inclined crack passes through. The bent-up reinforcement intersected with the critical inclined crack may or may not reach the yielding strength depending upon the position and width of the crack.

Generally, the stirrups are set up perpendicularly with the longitudinal axis and reinforcement of the member for convenience of its manufacture. However, it can also be inclined and intersects at an angle of 30° – 45° with the longitudinal axis, which is approaching the direction of the principal tensile stress there, so it confines effectively development of the inclined crack [14-9]. Of course, all the stirrups should be anchored reliably in the concrete to ensure its strength is being used fully.

The shear resistance of the web reinforcements including stirrups and bent-up reinforcement is composed of two parts, i.e. shear force carried directly (V_s and V_b in Fig. 14-11) and the indirect effects as below. They confine the development

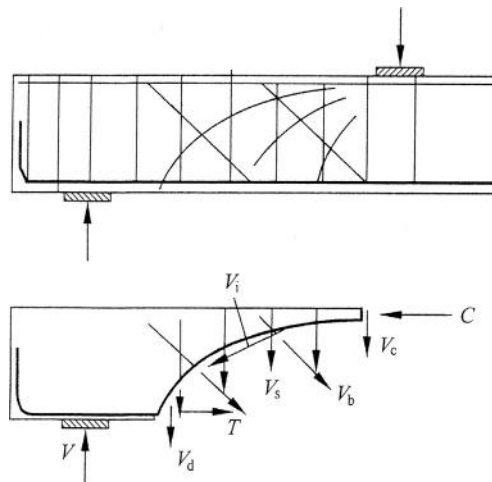


FIG. 14-11 Shear resistance of beam with web reinforcements

of the crack width, and the aggregate interaction (V_i) on the web is strengthened; they also confine the concrete cover near the beam end being torn off, and the dowel action (V_d) of the longitudinal reinforcement is increased; both web and longitudinal reinforcements compose a skeleton and confine the concrete inside. These are favorable for increasing the ultimate strength of the beam under shear force.

However, it should be clear that not all the stirrups and bent-up reinforcements near the beam end or in the shear span reach the yield strength at the ultimate state of the beam. Actually, the stress of every web reinforcement depends, to a great extent, upon position, width, and intersecting angle of the inclined crack intersected. In addition, it is also related to the failure pattern of the beam. For example, the stirrup near the support has less influence on the ultimate strength of the beam, if the pattern of inclined compression has occurred.

14.2.2 Composition of ultimate shear strength

The main components of ultimate strength of the beam under shear force (Fig. 14-11) are: shear resistance of compressive concrete on the upper end of the critical inclined crack (V_c), aggregate interaction of the concrete along the crack (V_i), transverse resistance (dowel action) of the longitudinal reinforcement (V_d), and tensile stresses, i.e. shear resistances, of the stirrup and bent-up reinforcements (V_s , V_b). The values and relative ratios of these components vary continuously within different stages (Fig. 14-12) when the load is increased and the cracks are formed and developed. The ultimate shear strength of the beam is the summation of them:

$$V_u = V_c + V_i + V_d + V_s + V_b. \quad (14-4)$$

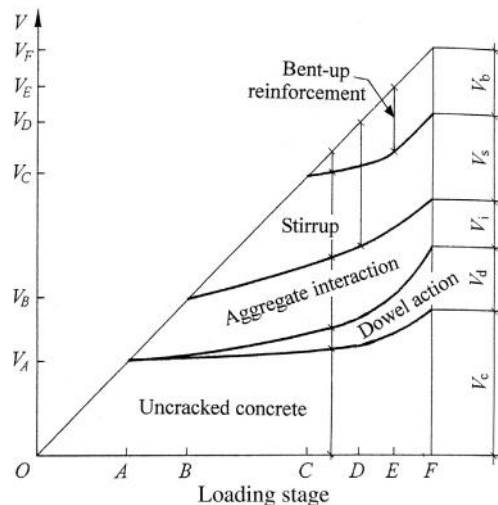


FIG. 14-12 Composition of ultimate strength [14-2,1-1]

The concrete carries almost all the internal forces and the stresses in the longitudinal and web reinforcements are rather low before cracking of the beam (OA in Fig. 14-12). After the flexural crack appears ($V \geq V_A$) and then the flexural–shear crack is formed (AB), the aggregate interaction of the concrete and the dowel action of the longitudinal reinforcement on the inclined crack take part in action as well. When the shearing crack appears on the web and develops, and then passes successively through the stirrup ($\geq V_B$) and bent-up reinforcement ($\geq V_C$), both web reinforcements start to work and undertake gradually more shear forces, as the inclined crack is effectively confined.

When the inclined crack develops continuously as the load is increased, one of the stirrups there yields first ($\geq V_D$) and others nearby may yield successively. The shear resistance of yielded stirrups keep constantly, and also the bent-up reinforcement keeps constant resistance after yielding ($\geq V_E$). In the meantime, the aggregate interaction of the concrete reduces as the inclined crack expands widely, but the dowel action of the longitudinal reinforcement and the shear resistance of the concrete on the upper end of the crack increase slightly. Finally, the beam is failed (V_u) when the concrete on the upper end of the crack reaches its biaxial strength under compressive and shear stresses together, and the dowel action of the longitudinal reinforcement acts downwards and tears off the concrete cover near the beam end.

The five components of the beam with web reinforcements share different ratios of shear resistance, which vary continuously during loading stages and depend upon strength of the concrete, numbers and positions of the longitudinal and web reinforcements. In addition, the position of load (shear–span ratio) or the failure patterns of the beam also have important influence. For example, the beam of longer shear–span shows longer inclined crack and more stirrups may be passed through, so they share more the ultimate shear of the beam.

14.3 Calculation of ultimate shear strength

14.3.1 About finite element method

The general method for the sectional analysis (Section 11.3), based on the hypothesis of plane section and uniaxial stress–strain relation of concrete, can not be used for the beam under the joint actions of shear force and bending moment, because the biaxial stress state exists especially near the beam end (shear span). In addition, the theoretical analysis of shear resistance is even more difficult because of various reasons, such as the variety of failure patterns, variations of position and shape of the inclined crack, variable direction and value of the aggregate interaction of the concrete along the inclined crack, complicated bond–slip relationship between longitudinal and web reinforcements and surrounding concrete, variable dowel action of longitudinal reinforcement, local stresses including vertical normal stress occurring near support and load.

In principle, non-linear finite element analysis of two dimensions can be used to analyze and predict accurately the whole process of a reinforced concrete beam

under shear force and bending moment, including stress distribution, deformation, appearance and development of crack, failure pattern, and ultimate strength. Actually, many theoretical analyses and calculation methods have been researched at home and abroad since the 1960s [14-10,1-3].

Generally, the procedure of finite element analysis includes: type selection of element, division of element (discretization), determination of constitutive relation for structural material, establishment of basic equation, and solution of equation series. When a reinforced concrete structure under shear force and bending moment is analyzed, some special problems [1-3], which have direct influence on the calculated accuracy, have to be considered and solved:

1. Bi- or triaxial failure criterion and constitutive relation of concrete (see Chapter 5); failure criterion of reinforcement under axial and transverse (dowel action) stresses together;
2. Treatment of concrete crack: e.g. single or smeared (uniformly distributed) crack occurring in an element; re-division element or not after concrete cracks; value and constitutive relation of aggregate interaction along inclined crack; principle and calculation of stress release during cracking and crack expanding of concrete;
3. Bond and slip between reinforcement and surrounding concrete: a special bond element without any volume is usually inserted in between the reinforcement element and surrounding concrete, and the physical models, e.g. springs in bi-directions, inclined springs, or others, and corresponding bond-slip relations (see Chapter 7) in longitudinal and normal directions, have to be given.

Various measures and methods are provided for these problems now, and the theoretical calculation is basically consistent with the experimental result for some reinforced concrete members. However, the generalized finite element program is not available for analysis of any reinforced concrete member with sufficient accuracy, because of so many influencing factors, complicated stress state, undefined crack, and variety of failure pattern. Therefore, various constitutive relations and calculation methods need to be complemented and improved.

Alternately, other methods based on the empiric statistics or simple mechanical model are used widely in the engineering practice in many countries, as the generalized calculation is rather complicated and not satisfied yet. These methods are easily used and the safety of the structure calculated is ensured, although the mechanism analysis, application scope, and calculation accuracy of them are somewhat inadequate.

14.3.2 Empirical regression

According to the statistic of 293 specimens of simply supported beam without web reinforcement tested under concentrated load at home and abroad [14-5], the ultimate shear strength (V_u) varies mainly with three factors, i.e. shear-span ratio ($\lambda = a/h_0$), compressive strength of concrete (f_c in N/mm^2), and content of

longitudinal reinforcement ($\mu = A_s/bh_0$), and the calculation formula obtained from the regression analysis is

$$\frac{V_u}{f_c b h_0} = \frac{0.08}{\lambda - 0.3} + \frac{100\mu}{\lambda f_c} \quad (14-5)$$

The average ratio between the experimental and calculated values is 1.033 with the deviation coefficient $c_v = 0.13$.

If these experimental data are presented only as the relation between the ultimate shear strength and single factor, i.e. shear—span ratio, Fig. 14-13 is plotted and the expressions of their upper and lower bounds are approximately:

$$\left. \begin{aligned} \frac{V_{u,\max}}{f_c b h_0} &= \frac{0.5}{\lambda} \\ \frac{V_{u,\min}}{f_c b h_0} &= \frac{0.12}{\lambda - 0.3} \quad (> 0.044) \end{aligned} \right\} \quad (14-6)$$

Considering the beam failing suddenly under shear force and bending moment together and considerable scatter of the experimental data, the beam should be designed with more safety than the beam failing under bending moment only, i.e. shear resistance is stronger than bending resistance. In addition, some unfavorable conditions, e.g. continuous beam and load acted on web (see Section 14.4), happen frequently in the engineering practice. Therefore, a formula giving lower ultimate shear strength is suggested:

$$\frac{V_c}{f_c b h_0} = \frac{0.175}{\lambda + 1} \quad (14-7a)$$

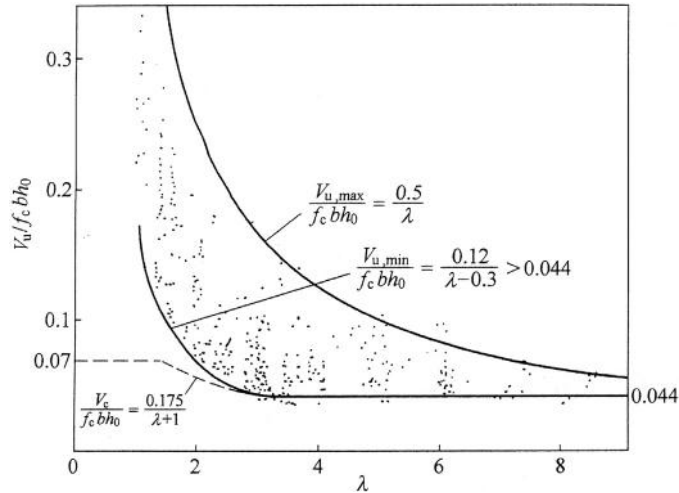


FIG. 14-13 Ultimate shear strength and its upper and lower bounds [14-5]

The formula is derived from the experimental results of the beam of lower strength grade of concrete ($\leq C50$). However, the increasing rate of the ultimate shear strength of the beam is less than that of compressive strength for the higher grade concrete (C50–C80), but the ultimate strength is approximately proportional to the tensile strength of the concrete. Therefore, $f_t = 0.1f_c$ is used and substituted into the formula, and

$$V_c = \frac{1.75}{\lambda + 1} f_t b h_0 \quad (14-7b)$$

is obtained and introduced into the Chinese Code [2-1] with two limits: when $\lambda < 1.5$, 1.5 is used in the formula and the maximum value of the coefficient in right hand is 0.7; $\lambda > 3.0$, 3.0 is used and the minimum value of the coefficient is 0.44.

As far as the beam without web reinforcement but acted with uniformly distributed load is concerned, the lower bound of the ultimate shear strength measured in the experiments (Fig. 14-9(b)) is

$$\frac{V_c}{f_c b h_0} = 0.07. \quad (14-8a)$$

Similarly, f_c in the formula is replaced by f_t , and the influence coefficient of the sectional depth (in mm)

$$\beta_h = \left(\frac{800}{h_0} \right)^{1/4} \quad (14-9)$$

is introduced, the formula becomes

$$V_c = 0.7 \beta_h f_t b h_0. \quad (14-8b)$$

In Eq. (14-9), $h_0 = 800$ mm or 2000 mm is used respectively if $h_0 < 800$ mm or > 2000 mm.

It is also demonstrated experimentally [14-4] that the inclined crack will not appear generally on the beam without web reinforcement under the service load, if the ultimate shear strength of it is calculated by Eq. (14-7) or Eq. (14-8).

The shear resistance of web reinforcement should be added to for the beam with it, which is used more widely in engineering practice. If the area of each stirrup is A_{sv} with space s (Fig. 14-14) and its tensile strength is f_{yv} , the shear resistance per unit

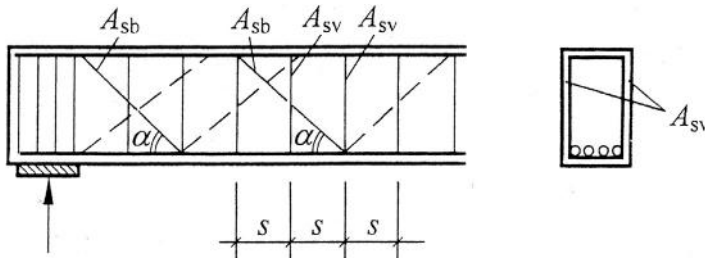


FIG. 14-14 Calculation of ultimate shear strength of beam with web reinforcement

length should be $V_s/s = A_{sv}f_{yv}/s$. And if the area of one bent-up reinforcement is A_{sb} of tensile strength f_y and its bent-up angle is α , the vertical component of its tensile resistance, i.e. shear resistance, should be $V_b = A_{sb}f_y \sin\alpha$. Therefore, the total ultimate shear strength of the beam can be calculated separately for different loads:

$$\text{concentrated load} \quad V_{cs} = \frac{1.75}{\lambda + 1} f_t b h_0 + \frac{h_0}{s} A_{sv} f_{yv} + 0.8 A_{sb} f_y \sin\alpha, \quad (14-10a)$$

$$\text{uniformly distributes load} \quad V_{cs} = 0.7 f_t b h_0 + 1.25 \frac{h_0}{s} A_{sv} f_{yv} + 0.8 A_{sb} f_y \sin\alpha. \quad (14-10b)$$

The coefficient 1.25 in the formula is introduced because of not only the direct shear resistance of the stirrups within projective length of inclined crack but also the indirect shear resistance due to confinement of the crack width. The reducing coefficient 0.8 in the formula is considered that the bent-up reinforcement does not necessarily reach the yield strength at ultimate state of the beam, because the inclined crack may intersect it at a different position. Generally, the ultimate shear strength calculated by these formulas is less than the experimental one [14-5].

The safety of the beam is ensured after calculation above, if the failure pattern of shear—compression or inclined tension would occur. However, if the failure pattern of inclined compression occurs on the web of the beam with a small shear—span ratio (λ) or span—depth ratio (l/h_0), the web reinforcement in the beam is not helpful. In order to increase the inclined compressive strength of the beam, a higher strength grade of concrete or larger sectional area should be used. Therefore, the minimum section of the beam has to be satisfied, e.g.

$$\left. \begin{array}{ll} h_w \leq 4b & V_u \leq 0.25 f_c b h_0 \quad \text{or} \quad b h_0 \geq \frac{V_u}{0.25 f_c} \\ h_w \geq 6b & V_u \leq 0.20 f_c b h_0 \quad \quad \quad b h_0 \geq \frac{V_u}{0.20 f_c} \end{array} \right\} \quad (14-11)$$

is suggested in the Chinese code [2-1], where h_w is the depth of web on section or effective depth of rectangular section (h_0).

When these formulas are used for the beam of high-strength concrete, another coefficient (β_c) should be introduced in right side of Eq. (14-11). The coefficient is taken as 1.0 and 0.8 respectively for concretes of grade $\leq C50$ and C80, and the linear interpolation can be used for concrete of grade C50—C80 in the Chinese Code.

In some other countries, the ultimate shear strength of a reinforced concrete beam is also calculated based on the regression analysis, but the statistical data, criterion of strength, and expression and parameters of calculation formula used are different considerably. For example, the shear force corresponding to formation of the critical inclined crack is used as the failure criterion in the USA Code [2-11], which is obviously lower than the ultimate strength or the maximum shear force

at failure of the beam. And, two components, i.e. concrete and web reinforcement, of shear resistance are also used:

$$V_u = \phi(V_c + V_s), \quad (14-12)$$

where $\phi = 0.85$ is a reducing factor considering the influences of variations of material strength and sectional size and inaccuracy of calculation.

The first component of shear resistance depends upon three main factors including $\sqrt{f_c}$, λ , and μ , among them cylinder compressive strength ($\sqrt{f_c}$) represents the tensile strength of concrete and the others are the same as above:

$$\lambda = \frac{M_u}{V_u h_0} \quad \text{but} \geq 1.$$

Then,

$$V_c = \frac{1}{7} \left(\sqrt{f_c} + \frac{120\mu}{\lambda} \right) b h_0, \quad \text{but} \leq 0.3 \sqrt{f_c} b h_0 \quad (14-13)$$

is given for the beams both with and without web reinforcement.

The component of shear resistance contributed by the stirrups and bent-up reinforcement is calculated by

$$V_s = \frac{A_{sv} f_{yv} h_0}{s} + A_{sb} f_y \sin \alpha \quad \text{but} \leq \frac{1}{1.5} \sqrt{f_c} b h_0, \quad (14-14)$$

in which the symbols used are the same as above.

14.3.3 Simplified mechanical models

14.3.3.1 Beam model

The shear resistance of the reinforced concrete beam was investigated first in Germany (Mörsch [14-1]) in the early 20th century, and the calculation formula was derived for the nominal shear stress (v) based on the elastic method. The main concept and design method based on it are still used in some countries. For example, the main concept is partly reserved in current Chinese Code [2-1], when the fatigue strength of the beam under shear force is checked.

The mechanical model for calculation is shown in Fig. 14-15. A short piece (length dx) of the beam is taken into account and bending moments acted on both sides are M and $M+dM$, respectively. It is assumed that the normal stress distributes triangularly on the compression zone of the section, and the normal stress of concrete is neglected and only the reinforcement is acted on the tension zone. Then, the nominal shear stress of the concrete on the neutral axis can be obtained from the equilibrium condition

$$v b dx = (C + dC) - C = \frac{dM}{z},$$

$$\text{so } v = \frac{dM}{b z dx} = \frac{V}{b z} \quad (14-15)$$

where V is the shear force on section, b is the breadth of beam section, and z is the internal lever arm on section, taking approximately $0.875 h_0$ [2-11].

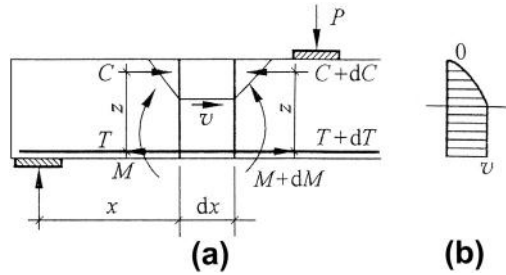


FIG. 14-15 Beam model: (a) calculation model, (b) distribution of shear stress on section

The shear stress at another position can be calculated similarly, and then its distribution on the section is obtained (Fig. 14-15(b)), i.e. a parabola of second order on compression zone and constant on tension zone or below neutral axis. Therefore, both the principal tensile and compressive stresses of concrete below the neutral axis equal the shear stress but with opposite sign ($\sigma_1 = \nu$, $\sigma_3 = -\nu$), and they act in the directions of $\pm 45^\circ$ respectively with the neutral axis.

The calculation formula can also be derived for the shear resistance of stirrups in the beam, based on the equilibrium condition (which is similar to that of Eq. (14-17) but $\theta = 45^\circ$ and $\alpha = 90^\circ$ are used):

$$\frac{V}{bz} = \frac{A_{sv}f_{yv}}{bs} \quad \text{or} \quad V = \frac{z}{s} A_{sv}f_{yv}. \quad (14-16)$$

Although the formula is similar to the corresponding items in Eqs (14-10) and (14-17) and the difference between them is the coefficient only, it is unreasonable however that the shear resistance of concrete is not taken into account again in this model.

14.3.3.2 Truss model

By end of the 19th century, Ritter (Germany) suggested first the truss model of parallel chords for calculation of shear strength of the beam with web reinforcement. Various modifications [1-1,14-1], e.g. the compressed upper chord being inclined, the inclination of compressed web bar being adjustable, are provided afterwards. This kind model is used now in many countries [2-12] because of its advantages: clear and simple mechanical concept and easy calculation.

The calculation principle of the truss model is shown in Fig. 14-16. It is assumed that all the bars of the truss are jointed with hinges, the compression zone of concrete on the top part and the longitudinal tensile reinforcement of the beam are considered respectively as the upper and lower chords, and the internal level arm is the vertical distance between both chords. The stirrups and bent-up reinforcements are considered as the tensed web bars with inclination α and the concrete on web is considered as the compressed web bars with inclination θ , which ranges generally from 18.4° to 45° .

When the internal force in the web reinforcement is calculated, an inclined section (ab) is assumed to be parallel with the compressed web bar of concrete

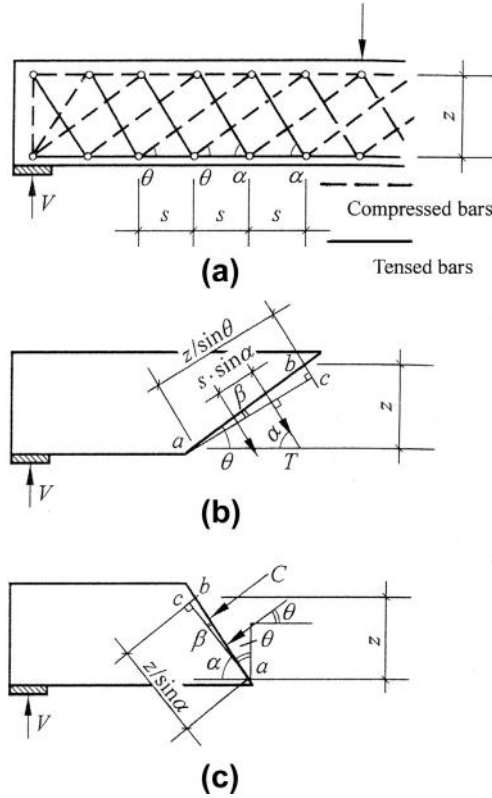


FIG. 14-16 Calculation of truss model: (a) mechanical model, (b) checking web reinforcements, (c) checking compressive web bar of concrete

(Fig. 14-16(b)), so the total tensile force (T) of the web reinforcements intersected acts only on the section and the vertical component is in equilibrium with the reaction at the support, i.e. shear force on the section.

Consequently, the angle between the inclined section and normal plane of the web reinforcement is

$$\beta = \theta + \alpha - 90^\circ \quad (a)$$

and the action length of the web reinforcements is

$$\overline{ac} = \frac{z}{\sin \theta} \cdot \cos \beta = z \frac{\sin(\alpha + \theta)}{\sin \theta}, \quad (b)$$

so the total tensile force of the web reinforcements on the section is

$$T = \frac{A_{sv} f_{yv}}{s \cdot \sin \alpha} \cdot z \frac{\sin(\alpha + \theta)}{\sin \theta} = \frac{A_{sv} f_{yv} z}{s} (\cot \theta + \cot \alpha). \quad (c)$$

According to the equilibrium condition of vertical forces,

$$V = T \sin \alpha = \frac{A_{sv} f_{yv} z}{s} \sin \alpha (\cot \theta + \cot \alpha) \quad (14-17)$$

is established and is then converted to a formula for calculation of area of the web reinforcement needed:

$$A_{sv} = \frac{Vs}{f_{yv} z} \frac{1}{\sin \alpha (\cot \theta + \cot \alpha)}. \quad (14-18a)$$

If the inclination of the compressed web bar of concrete is taken as $\theta = 45^\circ$, the formula is simplified as

$$A_{sv} = \frac{Vs}{f_{yv} z} \frac{1}{(\sin \alpha + \cos \alpha)}. \quad (14-18b)$$

The symbols used in these formulas are the same as above.

Similarly, when the compressive force in the web bar of concrete is calculated, an inclined section is assumed to be parallel with the web reinforcement (Fig. 14-16(c)), and

$$\beta = \alpha + \theta - 90^\circ \quad (d)$$

and

$$\overline{ac} = \frac{z}{\sin \alpha} \cos \beta = z \frac{\sin(\alpha + \theta)}{\sin \alpha} \quad (e)$$

are obtained successively. Then, the total compressive force of the concrete web is

$$C = \sigma_{cw} b z \frac{\sin(\alpha + \theta)}{\sin \alpha} = \sigma_{cw} b z \sin \theta (\cot \alpha + \cot \theta), \quad (f)$$

and the equilibrium equation is established

$$V = C \sin \theta = \sigma_{cw} b z \sin^2 \theta (\cot \alpha + \cot \theta). \quad (14-19)$$

Consequently, the average compressive stress of the concrete web is calculated and the strength of the concrete is checked as below

$$\sigma_{cw} = \frac{V}{b z} \frac{1}{\sin^2 \theta (\cot \alpha + \cot \theta)} \leq f_{cd2}. \quad (14-20)$$

However, the compressive strength used for web concrete is reduced, e.g.

$$f_{cd2} = 0.6 \left(1 - \frac{f_c}{250} \right) f_c \quad (14-21)$$

is suggested in Reference [2-12], because the stress state there is of biaxial tension–compression.

In the truss model above, the upper chord of concrete is assumed to carry compressive force only without shear force, the lower chord of reinforcement is assumed to carry longitudinal tensile force only without transverse force (dowel action), and the aggregate interaction is not taken into account. Obviously, these are not satisfied.

14.4 Various members and mechanical conditions

The structural members in engineering practice are not necessarily like the beams tested above, which is of rectangular section, simply supported, and acted only with shear force and bending moment. The experimental results, research conclusions, and calculation methods presented above do not fit other situations, such as non-rectangular or variable section, load acted not on top of the member, axial force also acted on the section, both positive and negative bending moments existing within the shear span. These situations have to be investigated separately and treated properly, because the stress state is more complicated and no unified theory or method can be used universally.

14.4.1 Load acted on beam web

Many reinforced concrete beams in various structural systems are actually loaded on its web at an even lower part (Fig. 14-17) rather than on top like the beam tested above. For example, the precast slab and the load on it are acting on protruding flange of the precast beam; the secondary beam in a monolithic structure and the load on it are transferred to the girder mainly via the uncracked concrete or compression zone of the section at the end of the secondary beam; the horizontal seismic and wind loads acted on a shear wall are transferred from top to bottom via the shear forces distributed continuously along every floor, which corresponds to the depth of a (cantilever) beam.

When the load is acted on the web or lower part of the beam, tensile normal stress occurs in a vertical direction ($\sigma_y > 0$) on the concrete higher than the loading position (Fig. 14-18(a)). This is just opposite to the situation that the compressive stress ($\sigma_y < 0$) occurs there, when the load is acted on top of the beam. As the vertical normal stress changes from a compressive to tensile one, the failure pattern of the beam is possibly alternated and its ultimate shear strength is reduced correspondingly [14-11,14-12], although other stresses (σ_x and τ) vary slightly.

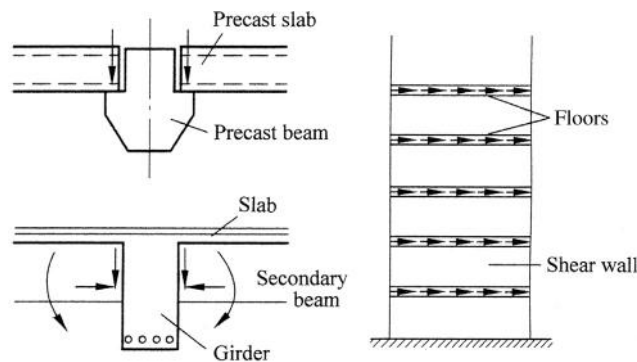


FIG. 14-17 Examples for beam loaded on web

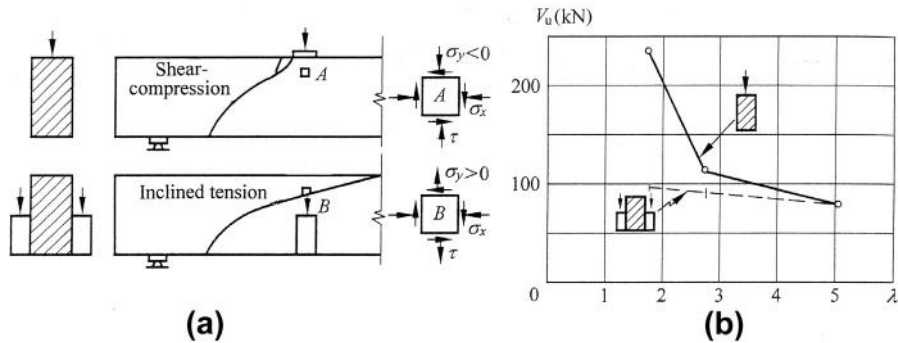


FIG. 14-18 Comparison between beams loaded on top and web: (a) stress state and failure pattern, (b) ultimate shear strength [14-11]

After a reinforced concrete beam without web reinforcement is loaded on a web with the shear–span ratio $\lambda \leq 3$, the inclined shear crack is formed on the web and then extends quickly through the loading section and beam top, so the beam is sheared off as a typical failure pattern of inclined tension. The ultimate load is about the same as the cracking load of the beam and is far smaller than that of the beam with the same shear–span ratio but loaded on top, because of changes of the vertical normal stress (σ_y) and principal tensile stress (σ_1). However, it is also demonstrated experimentally that the beams loaded on both web and top fail in inclined tension pattern and their ultimate shear strengths are less different if the shear–span ratio $\lambda > 3$ (Fig. 14-18(b)).

When the beam with web reinforcement is also loaded on a web or lower part, most stirrups within the whole span are tensed. The inclined cracks closely distribute before failure, the tensile stress (strain) of the stirrup distributes rather uniformly along its length, and the maximum stresses of the stirrups are approaching [14-8] (comparing with Fig. 14-10). Nevertheless, its ultimate shear strength is also less than that of the beam loaded on top, and the stirrups should be placed uniformly along the whole span during design.

14.4.2 Beam of T section

The beam of T section is used widely in the structural engineering. The stress distribution within its shear-bending segment varies with the ratio between the breadth of the flange and the thickness of the web (b_f/b) when other parameters are unchanged, and then the ultimate shear strength is influenced, even the failure pattern is changed. This is explained by two series of experiments below.

The first series of beams are of the same web thickness ($b = \text{const.}$) but with different flange breadth, and the maximum ratio between them is $b_f/b = 7$. If the ultimate shear strength of the beam of rectangular section ($b_f/b = 1$) is taken as 1, the strengths of other beams are shown in Fig. 14-19(a). It is seen that the strength of the beam of $b_f/b = 2$ is increased by about 20%, but the strength of the beam of

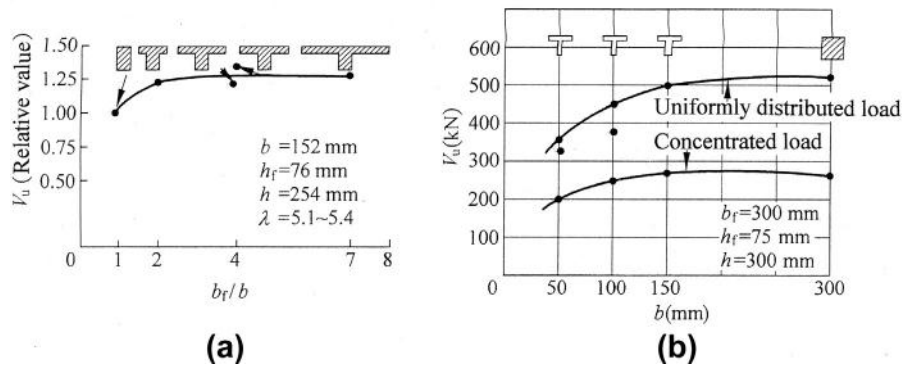


FIG. 14-19 Ultimate shear strength of T sectional beam: (a) influence of flange breadth ($b = \text{const.}$) [14-13], (b) influence of web thickness ($b_f = \text{Const.}$) [14-14]

even wider flange ($b_f/b > 2$) is hardly increased. This series of beams is tested under larger shear—span ratio ($\lambda = 5.1 \sim 5.4$) and fails in the pattern of inclined tension, so the ultimate shear strength of the beam is greater slightly than the shear force at cracking of concrete. According to elastic analysis, the inclined crack appears on web when the shear force reaches $V_{cr} = f_t b I / S_{\max}$, in which I is the inertia moment of its section and S_{\max} is the moment of sectional area on one side of the neutral axis about the axis. However, the ratio I / S_{\max} increases limitedly with the flange breadth. In addition, it is also demonstrated that only part, near the web, of the flange is fully acted together with the web, so the effective I / S_{\max} is even lower. Therefore, an increasing flange breadth of beam helps limitedly for the cracking shear force and ultimate shear strength.

Another series of beams with web reinforcement (stirrups) are of the same flange breadth (b_f) but with different web thicknesses ($b = 50 \sim 300$ mm), and the maximum ratio between them is $b_f/b = 6$. These beams are tested separately under concentrated load with a shear—span ratio of about 3.0 and uniformly distributed load, and the ultimate shear strengths measured are shown in Fig. 14-19(b). The strength of the beam of rectangular section ($b = 300$ mm) is about 40–50% higher than that of the beam of thinnest web ($b = 50$ mm). The beams of thicker web ($b \geq 150$ mm) fail in the pattern of shear—compression with approximate ultimate strengths, because the area and strength of the concrete on the upper end of the inclined crack and the resistance of the stirrups at the ultimate state are less different for both beams, although the aggregate interaction along the inclined crack on web varies with its thickness. The beams of thinner web ($b \leq 100$ mm) fail in the pattern of inclined compression and their ultimate shear strengths vary with the web thickness, because the principal compressive stress on web reaches the biaxial tension—compression strength of concrete which is lower than the uniaxial compressive strength of concrete, although the stirrups there are capable of carrying tensile force after the appearance of an inclined crack.

Accordingly, the ultimate shear strength of the beam of T section depends upon the shape and size of the section, longitudinal and web reinforcements, shear—span

ratio, transferring of failure pattern, etc. Generally, it should be safe if the ultimate shear strength of the beam of T section is calculated as that of a rectangular section only and the flange is neglected.

14.4.3 Beam with variable section (depth)

Various beams of variable section (Fig. 14-20) are used in structural engineering for different reasons, for example: increasing section (depth) at mid-span for higher strength or decreasing section near the end for less weight; making a slope on a roof for water drainage; a haunched beam for higher stiffness and strength. The failure patterns of inclined compression, shear-compression, and inclined tension will also occur successively for these beams, as the span—depth ratio of the beam or the shear—span ratio of concentrated load increases [14-15,1-1]. In addition, the experimental conclusion and calculation principle introduced above for the beam of constant section can also be used for them.

If the inclination of the top surface of the beam (α) is less, the critical inclined crack extends upwards and its upper end approaches to the section under the concentrated load at ultimate state, so the effective depth there is about h_0 and the ultimate shear strength also approximates to that of the beam of constant section and effective depth h_0 . However, if the beam with larger inclination (α) on the top surface is concerned, the upper end of the critical inclined crack will not reach the section near the concentrated load at ultimate state, so the effective depth there is less ($< h_0$) and the ultimate shear strength is reduced as well.

The critical inclined crack of the beam with inclined bottom generally passes through the section of the minimum depth (h_0) at the turning point of depth, and its failure pattern is shown in Fig. 14-20(b). The ultimate shear strength approximates that of the beam with constant section and effective depth h_0 . However, the vertical component of the longitudinal reinforcement ($A_s f_y \sin \beta$) is an additional component for shear strength of the beam and should be taken into account [14-15].

As the end part of a haunched beam is strengthened for both flexural and shear resistance, the critical inclined crack generally appears within the segment of constant section (effective depth h_0) at ultimate state and the ultimate shear strength of the beam can be calculated based on the depth h_0 .

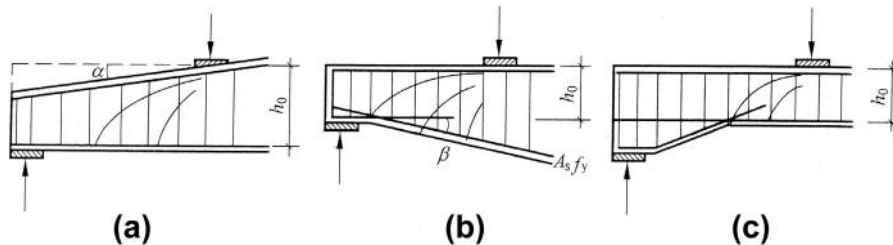


FIG. 14-20 Beams with variable section: (a) inclined top surface, (b) inclined bottom surface, (c) haunched beam

14.4.4 Influence of axial force

When the axial force, either compression or tension, is acted together with shear force and bending moment on a structural member, the longitudinal stress (σ_x) varies significantly, which causes changes of failure pattern and ultimate strength. The typical envelope of shear force (bending moment)—axial force obtained from the relevant tests is shown in Fig. 14-21 [14-5]. The axial force (N) is acted first on the member and maintained constantly during testing, then the transverse load is acted and causes corresponding shear force and bending moment until failure of the member.

When the member is acted only with axial force, the failure pattern of axial compression or tension will occur and the ultimate strength is easily determined. As the axial force is acted together with shear force and bending moment and varies from compression to tension, various failure patterns will appear successively. Usually, the pattern of shear—compression will occur in the shear-bending segment of the beam if axial force $N = 0$.

After the axial tension is acted first on the member, tensile cracks appear perpendicularly. Afterwards, the transverse load is acted and the bending moment is increased gradually, the crack on the top part of the member is closed and tensile stress of the reinforcement there (A'_s) is reduced and even turns into a compressive one, while the crack on the bottom part is widened and the tensile stress of the reinforcement there (A_s) is increased. In the meantime, the shear force is increased simultaneously and causes the existing crack to extend towards an inclined direction or the appearance of a new inclined crack. As the ratio between axial and shear forces (N/V) reduces, the inclination between the critical crack and member axis is decreased gradually, and two typical failure patterns, i.e. eccentric tension (Fig. 11-8(b)) and inclined tension (Fig. 14-4(c)), appear successively and can be distinguished clearly. The transverse load, also shear force (V_u) and bending moment, at the ultimate state of the member increase as the axial tension (N_u) is reduced.

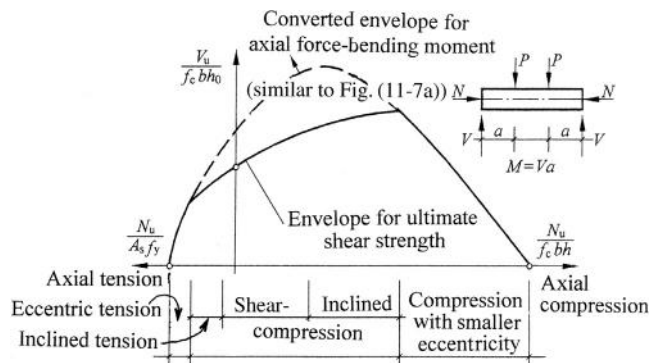


FIG. 14-21 Envelope of shear force—axial force and failure patterns

When axial compression is acted first on the member, the depth of the compression zone is increased while the tensile stress of reinforcement (A_s) is reduced under the bending moment caused by the transverse load. Therefore, appearance of the transverse tensile crack is delayed and the crack width is deduced. If the compression—strength ratio of the member ($N/f_c b h_0$) is larger enough, the flexural—shear crack and shear crack on web will not occur again, but the principal compressive stress increases considerably and the failure pattern of inclined compression will be formed. In addition, the ultimate strength (V_u) of the member is greater than that of the member without axial compression, and the maximum ultimate strength is found in the range of $N/f_c b h_0 = 0.3-0.5$. If the ratio ($N/f_c b h_0$) is even larger, the most part or the whole section of the member are compressed at the ultimate state and the failure pattern will be of smaller eccentricity (Fig. 11-5(c) or (b)), and the ultimate strength is decreased gradually.

The ultimate envelope of the axial force-bending moment ($N_u - M_u$, Fig. 11-7(a)) of a member can be converted into that of axial force—shear force ($N_u - V_u$, where $V_u = M_u/a$), which is shown as a dashed curve in Fig. 14-21. Both end parts of the envelopes coincide and represent respectively the failure patterns of eccentric tension and compression. However, the middle part of the solid envelope is lower than that of the dashed one, so the ultimate strength (V_u, M_u) is reduced, because the failure pattern is dominated by shear force rather than bending moment. On the other hand, if the member is strengthened to prevent the failure under shear force, it will fail in the pattern of larger eccentricity tension or compression depending upon axial force and bending moment, then the dash envelope is still valid.

An important conclusion is derived based on the experimental results and discussions above that the ultimate shear strength of a beam is increased when axial compression, including prestressing of tendons, is acted together, but is decreased when axial tension is acted together. This conclusion is introduced in various ways into the design codes of different countries. For example, the right side of calculation formula (Eq. 14-10) used in the Chinese Code [2-1] is added by an additional item, i.e. $+0.07N$ or $-0.2N$ respectively for the member with axial compression or tension, in where N is the axial force occurring simultaneously with the shear force. In the USA Code [2-11], the value of parameter λ in Eq. (14-13) is changed to

$$\lambda = \frac{M_u - \frac{N_u(4h-h_0)}{8}}{V_u h_0}$$

14.4.5 Both positive and negative bending moments exist within shear span

When concentrated and uniformly distributed loads are acted on a simply supported beam, the bending moment of the same sign, either positive or negative, occurs in the whole span including the failure zone at the ultimate state. However, when some other members, e.g. continuous beam, beam with a cantilever, frame beam and

column, are loaded until failure, both positive and negative bending moments exist together within each member. Usually, the negative bending moment at the support section turns gradually into a positive one at mid-span, and the maximum shear force and absolute value of bending moment happen together at the section near support.

The experiment of the beam with two cantilevers is introduced (Fig. 14-22) as an example. After the specimen is loaded, the tensile cracks appear first at the sections near support and mid-span with the maximum negative and positive bending moments respectively, and the stress distributions of the reinforcements near the top (A'_s) and bottom (A_s) are consistent with the diagram of sectional bending moment. Afterwards, the flexural-shear cracks and shear cracks on the web appear and extend gradually in both zones of negative and positive bending moments, as the load is increased. When these inclined cracks intersect with the longitudinal reinforcements, their tensile stresses increase suddenly and many short cracks appear along them due to bond damage. At this time, the stress distributions of the reinforcements do not fit again the diagram of bending moment, and the tensile zones of both reinforcements (A'_s and A_s) are expanded significantly and the stresses of them at section with $M = 0$ are obviously tensile. Therefore, this is not a beam model again, but the specimen works like a truss or the composition of normal and reverse arches with tensile ties.

The mechanical behavior of a member of this kind depends mainly upon the generalized shear-span ratio, i.e. the ratio between the bending moment and corresponding shear force at the section near support ($M^-/Vh_0 = a^-/h_0$) or concentrated load ($M^+/Vh_0 = a^+/h_0$). The failure patterns of inclined compression, shear-compression, and inclined tension also occur successively at ultimate state and the corresponding ultimate strength reduces gradually, as the generalized shear-span ratio of the beam is increased. When the beams have the same value

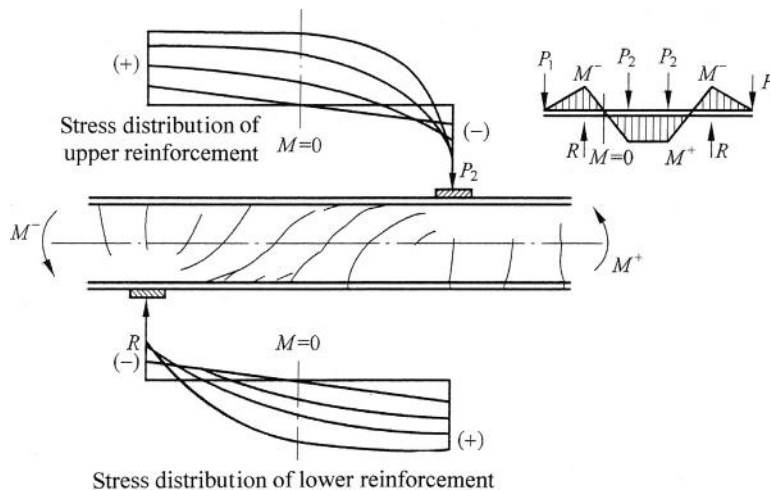


FIG. 14-22 Shear resistance of beam with two cantilevers

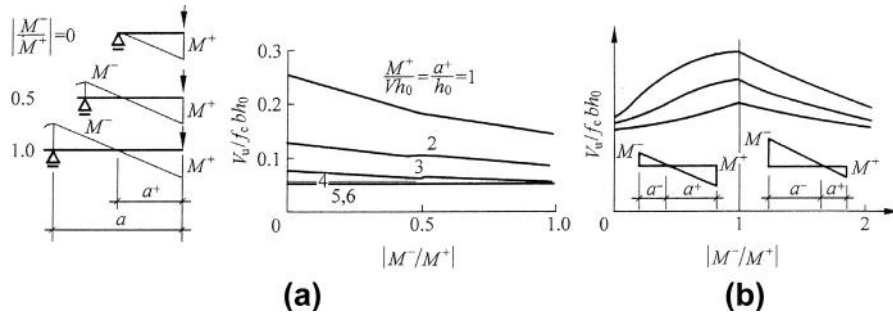


FIG. 14-23 Ultimate strength of beams with both positive and negative bending moments [1-2]: (a) equal generalized shear–span ratio (a^+/h_0), (b) Constant shear span length ($a^- + a^+ = a$)

as the generalized shear–span ratio (a^+/h_0) only in the shear span (a) (Fig. 14-23(a)), the tensile stress of upper reinforcement (A'_s) increases with the negative bending moment or ratio $|M^-/M^+|$, so the bond between reinforcement and concrete there is damaged seriously and the ultimate strength is decreased. However, the member with the generalized shear–span ratio $M^+/Vh_0 \geq 4$ fails in the pattern of inclined tension, and the influence of negative bending moment on ultimate strength is limited.

There is another situation. If the shear span of a beam is a constant ($a^- + a^+ = a = \text{const.}$, Fig. 14-23(b)), the summation of bending moments at sections near support and under concentrated load should be a constant too, i.e. $|M^-| + M^+ = Va = \text{const.}$ The bending moment at mid-span (M^+) reduces as that near support ($|M^-|$) is increased. Therefore, the shear span (a) of the beam can be divided into two segments of different shear–span ratios (a^-/h_0 and a^+/h_0). If $|M^-/M^+| < 1$, the shear–span ratio on the positive bending moment side is greater than that on the negative one, i.e. $a^+/h_0 > a^-/h_0$, so the ultimate strength is lower and failure of the beam occurs in the segment of positive bending moment. Contrariwise, the failure of the beam occurs in the segment of negative bending moment if $|M^-/M^+| > 1$ or $a^- > a^+$. Obviously, both shear–span ratios are equal when $|M^-/M^+| = 1$, and the maximum ultimate shear strength is found. Nevertheless, the ultimate strength of the beam under both situations is greater than that of the simply supported beam ($M^- = 0$ and a^+ reaches the maximum).

14.4.6 Bracket

The bracket is a protruding part of a structural member and used widely in the engineering practice to support another member placed on it. For example, the bracket of the column in an industrial workshop is used to support the roof girder or truss, and crane beam, even some equipment; the bracket of the wall or girder in a building is used to support the slab or beam. The bracket mainly carries the vertical load, and sometimes it also carries the horizontal load, e.g. wind and seismic ones, braking force of crane, shrinkage of concrete.

The tensile reinforcement near the top and horizontal stirrups is normally set up in the bracket, and sometimes bent-up reinforcement is also used (Fig. 14-24(a)). The bracket works mechanically like a short cantilever or a simple triangle truss composed of an inclined compression bar and a horizontal tie. If the distance between the vertical load and column surface is greater than the effective depth of the bracket ($a > h_0$), the bracket can be calculated and designed as a cantilever (beam) of same shear-span ratio (a/h_0). However, when the distance is smaller than the depth ($a \leq h_0$), its behavior and calculation are introduced briefly below.

The existing experiments [14-17–14-19] demonstrate that the protruding length of the bracket (a/h_0) dominates the internal stress state and, then, cracking of concrete and different failure patterns (Fig. 14-24(b)) as below.

Direct shear failure ($a \leq 0.1h_0$). Several inclined short cracks appear along the root of the bracket, and finally the bracket moves vertically downwards and fails, which is similar to that of the specimen under direct shear (Fig. 2-28(a)).

Inclined compression failure ($a = 0.1h_0 - 0.75h_0$). The vertical tensile crack appears first on top of the bracket and extends slightly downwards, when the load reaches 20–40% of the ultimate one. Then, the inclined crack occurs under the inside edge of the loading plate and develops downwards at about 40–60% of the ultimate load. As the load reaches 70–80% of the ultimate one, many short cracks occur parallel, near the inclined crack and extend and are connected gradually. Finally, the bracket fails like an inclined short strut under the loading plate. Actually, most brackets in engineering practice are of this kind.

Flexural-compression failure ($a = 0.75h_0 - h_0$). After the load on the bracket is increased, the vertical tensile crack appears first on top near its root, and then the inclined crack occurs under the inside edge of the loading plate and extends towards lower part of its root. The upper reinforcement is yielded under tension at about 80% of the ultimate load, and the vertical crack expands and extends quickly and the compression zone on the section of bracket root is decreased continuously. Finally, the bracket fails when the concrete there is crushed.

Besides the shear-span ratio (a/h_0), other factors, including strength of concrete, contents of stirrup and tensile reinforcement, and size of loading plate, also have an important influence on mechanical behavior of the bracket. In addition, the bent-up

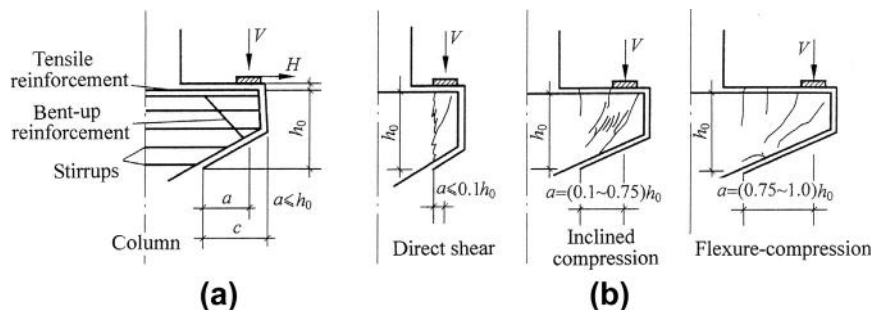


FIG. 14-24 Detail and failure patterns of bracket: (a) general detail, (b) failure patterns [14-18]

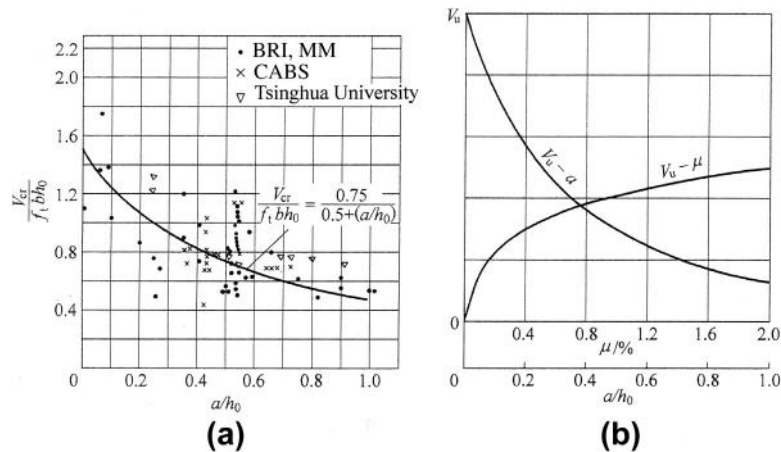


FIG. 14-25 Shear force at cracking and ultimate strength of bracket [14-18]: (a) shear force at appearance of inclined crack, (b) ultimate strength

reinforcement can limit the width of the inclined crack and cause an increase in the ultimate strength of the bracket, although it has less influence on the cracking strength.

The load or shear force corresponding to appearance of the inclined crack (V_{cr}) on the bracket reduces as the shear-span ratio (a/h_0) increases; the ultimate load or shear force of the bracket (V_u) also reduces as the shear-span ratio increases, but increases with the content of tensile reinforcement (μ) (Fig. 14-25). Usually when a bracket is designed, the sectional size is determined by the condition of cracking resistance or prevention of direct shear failure, and the tensile reinforcement and stirrups needed are calculated to satisfy the requirement of the ultimate strength.

14.4.7 Punching of slab

It frequently happens in engineering practice that a concentrated load is acted only on a small area of a reinforced concrete slab, for example: truck wheel on bridge slab, equipment on building floor, structural system of slab-column, and arbitrary foundation under column (Fig. 14-26). These slabs may fail locally under the concentrated load, i.e. a concrete pyramid together with the load or column is punched out from the slab. The mechanical characteristic and failure pattern of these slabs is like a multidirectional shearing. However, the load or reaction exists on the punching pyramid of the slab, which is similar to the beam acted with uniformly distributed load and failed under shear force, while no load exists on the failure zone of a beam acted with concentrated load.

The reinforced concrete slabs tested under one concentrated load have been conducted at home and abroad [14-20–14-23], and the process and pattern of punching failure are revealed in detail. Fig. 14-27 shows a square column and its foundation slab, which is supported elastically by many springs to simulate the soil base. The

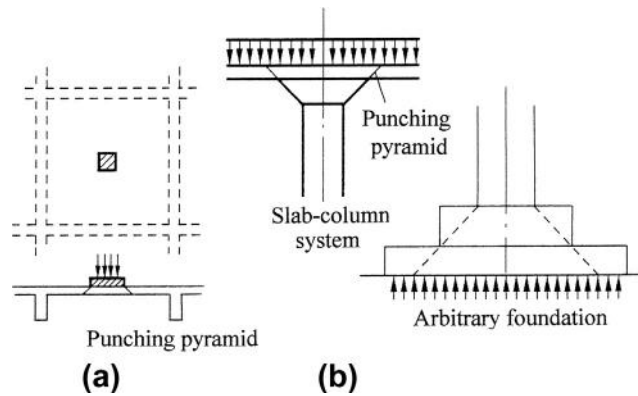


FIG. 14-26 Punching of slab: (a) concentrated load on slab, (b) continuously distributed load or reaction

foundation slab deforms less at an earlier stage of loading. When the load reaches 30–50% of the ultimate value, the flexural (tensile) cracks occur on the slab bottom along two perpendicular directions and extend outside from the middle part, and the deflection of the slab accelerates. As the load reaches 75–90% of the ultimate value, several cracks are visible on the side surfaces of the slab and slowly extend upwards from the bottom. The specimen fails suddenly at ultimate state, the column obviously settles down and four corners of the column bottom are slightly spalled off, and the concrete on the slab top surrounding the column bottom cracks and the middle part of the slab goes out (downwards) and is surrounded with punching cracks. Even the failure pyramid together with the column punches totally apart from the foundation slab, and some broken pieces of concrete are found on the inclined failure surfaces. The inclination between the punching surface (inclined crack) and slab plane is generally 40° – 48° . In addition, wider cracks possibly occur along the diagonal lines of the slab, while fine cracks appear on side surfaces (Fig. 14-27).

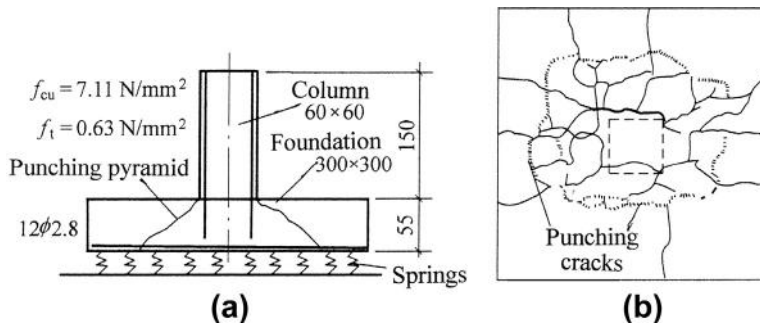


FIG. 14-27 Punching of elastically supported slab [14-23]: (a) specimen (M89), (b) cracks on bottom surface

The ultimate punching strength of a slab depends mainly upon its shape (flat, step, or trapezoid) and thickness, strength of concrete (f_t), and content of longitudinal reinforcement (μ). It should be noticed that the slab will fail in the flexural pattern under the load due to lack of longitudinal reinforcement.

When the slab is acted with a concentrated load and fails in the punching pattern, the stress state of concrete surrounding the load or column is even more complicated than that in shear span of a simple beam. Some solutions based on plastic limit analysis are explored in the references, but the practical method of accurate analysis is not currently available. Therefore, the relevant calculation formulas suggested in various design codes are empirical and mainly based on the experimental results.

The simplest formula [2-1] for calculation of the ultimate punching strength of a slab is

$$P_u = \beta u_m h_0 f_t \quad (14-22)$$

where u_m is the periphery length apart $h_0/2$ from the periphery of area acted with concentrated or local load on slab, h_0 is the effective depth of slab, f_t is the tensile strength of concrete, and β is the coefficient considering influences of shape (h_t/b_t) and position (in middle, by side, or at corner) of area acted with load on slab.

Other empirical formulas including more parameters are suggested in some references, for example

$$\left. \begin{aligned} [2-11] \quad P_u &= 0.167 \left(1 + \frac{2}{h_t/b_t} \right) \sqrt{f_t} u_m h_0 \\ [2-12] \quad P_u &= 0.12 \left(1 + \sqrt{200/h_0} \right) \sqrt[3]{100\mu f_t} u_m h_0 \\ [14-23] \quad P_u &= \left(A + B \frac{h_0}{b} \right) \sqrt{100\mu f_t} u_m h_0 \end{aligned} \right\}, \quad (14-23)$$

where h_t , b_t are the longer and shorter lengths of area acted with local load on slab, b is the shorter length (span) of slab, and A , B are empirical coefficients. Other symbols are the same as above.

Strength of Member Under Torsion

15

CHAPTER OUTLINE

15.1 Elasticity and plasticity solutions	386
15.2 Ultimate strength of member under torsion alone	390
15.2.1 Member without web reinforcement	390
15.2.2 Member with web reinforcement	392
15.2.3 Influence of contents of reinforcement and stirrup.....	393
15.3 Members with composite internal forces	395
15.3.1 Member with axial force and torsion	395
15.3.2 Member with shear force and torsion	395
15.3.3 Member with bending moment and torsion	397
15.3.4 Member with bending moment, shear force and torsion together.....	400
15.4 Calculation of ultimate strength	401
15.4.1 Empirical formulas	401
15.4.2 Truss model	403
15.4.3 Ultimate equilibrium of inclined twisted surface	405

In most structural systems of one-dimensional members, the section of the member is symmetrical about its vertical center axis and all the loads and reactions are acted within this symmetrical plane. Therefore, uni- or biaxial stress state is formed in the member, as the internal forces including axial and shear forces and bending moment are caused on its sections. However, if the axis of the member, loads, and reactions are not placed within the same (symmetrical) plane, another internal force, i.e. torsion, is certainly caused and the member should be of a triaxial stress state.

The torsional members that appear frequently in structural engineering are curved bridges, curved beam under balconies of theaters and stadiums, curved or spiral stairs, unsymmetrical sections, e.g. reversed L shapes, crane beam acting with braking force, etc. However, the member carried with torsion only is rare, but most members carry simultaneously with shear force and bending moment besides torsion and its sectional size and reinforcement mainly depend upon the former. In addition, the torsion should be avoided or reduced if possible during design of the structure.

The torsional member is of triaxial stress state and is acted together with other internal forces, so its mechanical behavior is even more complicated. Many

experimental and theoretical investigations have been conducted on this at home and abroad and corresponding results [15-1—15-8] are obtained, but the mechanism and calculation are still not perfect.

15.1 Elasticity and plasticity solutions

The simplest stress state is found for the torsional member when a torsion (T_e), without other internal force, is acted on an elastic member of circle section. It is demonstrated both experimentally and theoretically that the sectional plane of the member before loading maintains a plane after torsion acted, and the normal stress (σ) is zero and the shear stress (τ) distributes linearly along its radius (Fig. 15-1(a)):

$$\tau = \frac{T_e r}{I_0}, \quad (15-1a)$$

where $I_0 = \pi R^4/2$ is the inertia moment about sectional pole (center), R is the radius of section, and r is the distance from any point on section to the center.

The maximum shear stress occurs at $r = R$:

$$\tau_{\max} = \frac{2T_e}{\pi R^3}, \quad (15-1b)$$

or

$$T_e = \frac{\pi}{2} R^3 \tau_{\max} = W_{te} \tau_{\max}, \quad (15-1c)$$

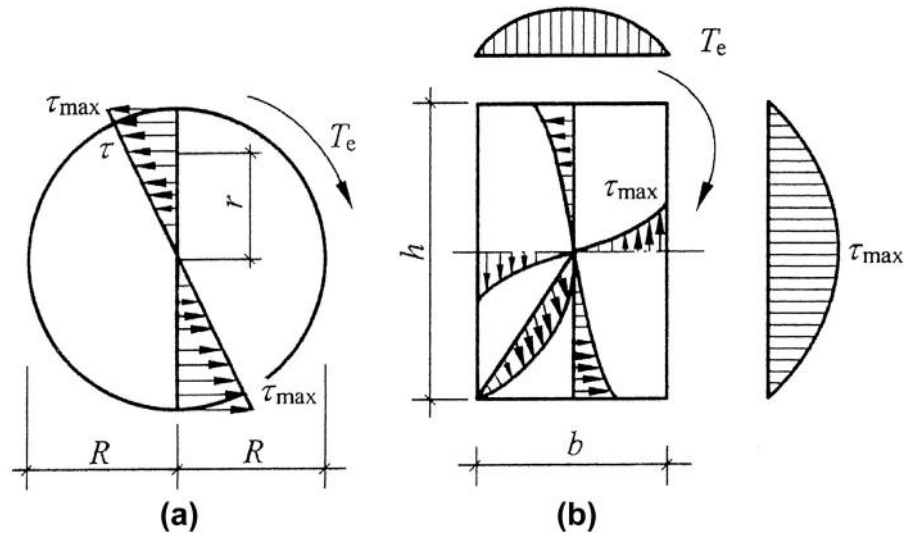


FIG. 15-1 Stress distribution of elastic member under torsion only: (a) circle section, (b) rectangular section ($h \geq b$)

where

$$W_{te} = \frac{\pi}{2} R^3 \quad (15-2)$$

is the elastic section modulus of a member with circle section under torsion.

However, when the member of rectangular section is acted with torsion only, its section is twisted and can not maintain again a plane, and the normal stress occurs correspondingly when the member is confined. In addition, the shear stress distributes non-uniformly on the section, and it is zero at the center and four corners and the maximum one occurs at the center of the longer edge of the section (Fig. 15-1(b)), which is obtained from the analytical solution of elasticity theory:

$$\tau_{\max} = \frac{T_e}{\alpha_e b^2 h} = \frac{T_e}{W_{te}}, \quad (15-3a)$$

or

$$T_e = \alpha_e b^2 h \tau_{\max} = W_{te} \tau_{\max}, \quad (15-3b)$$

where the elastic section modulus of a member with rectangular section under torsion is

$$W_{te} = \alpha_e b^2 h \quad (15-4)$$

and the coefficient α_e depends upon the ratio between sectional edge lengths (h/b , $h > b$) [15-9] and is listed in Table 15-1.

If a member of an ideal plastic material is concerned, the ultimate torsion (T_p) will reach only when shear stress at every point in it reaches the strength of the material (τ_{\max}). For example, the distributions of shear stress on the circle and rectangular sections at ultimate state are shown in Fig. 15-2, and their ultimate torsions are derived respectively based on the equilibrium condition:

$$\text{Circle section} \quad T_p = \frac{2}{3} \pi R^3 \tau_{\max} \quad (15-5a)$$

with plastic section modulus under torsion

$$W_{tp} = \frac{2}{3} \pi R^3, \quad (15-5b)$$

Table 15-1 Coefficient for Section Modulus of Rectangular Section Under Torsion										
h/b	1.0	1.2	1.5	2.0	2.5	3.0	4.0	6.0	10.0	∞
α_e	0.208	0.219	0.231	0.246	0.258	0.267	0.282	0.299	0.312	0.333
α_p	0.333	0.361	0.389	0.417	0.433	0.444	0.458	0.472	0.483	0.500
α_e/α_p	0.624	0.606	0.594	0.590	0.595	0.601	0.615	0.633	0.648	0.667
α_p/α_e	1.603	1.649	1.684	1.694	1.680	1.655	1.625	1.579	1.544	1.500

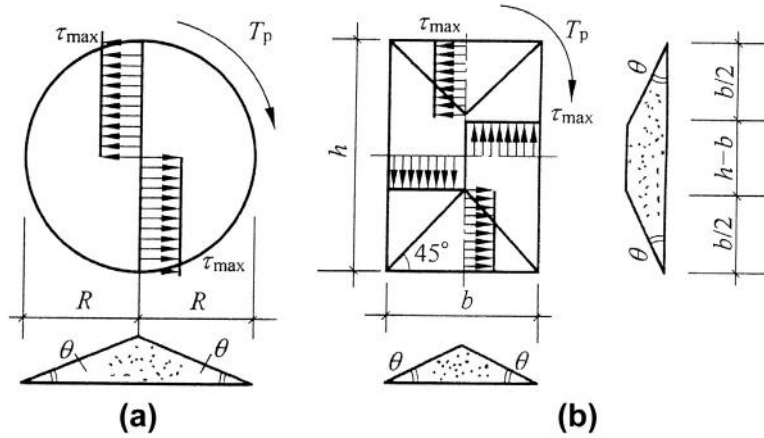


FIG. 15-2 Distribution of shear stress at ultimate state for ideal plastic member under torsion: (a) circle section, (b) rectangular section ($h \geq b$)

$$\text{Rectangular section} \quad T_p = \frac{1}{6}b^2(3h - b)\tau_{\max} \quad (15-6a)$$

with plastic section modulus under torsion

$$W_{tp} = \frac{1}{6}b^2(3h - b) = \alpha_p b^2 h, \quad (15-6b)$$

in which $\alpha_p = \frac{3-(b/h)}{6}$ is the coefficient for rectangular section and listed in Table 15-1 as well.

The ratio between the ultimate torsions or section moduli obtained from elastic and plastic calculations is $T_e/T_p = W_{te}/W_{tp} = \alpha_e/\alpha_p$, which is 0.75 for a circle section but variable for a rectangular section ranging from the minimum (about 0.590) to the maximum (2/3). Consequently, its reciprocal ($T_p/T_e = W_{tp}/W_{te} = \alpha_p/\alpha_e$) ranges from 1.5 to 1.694, and it is equivalent, in physical meaning, to the plasticity-dependent coefficient of section modulus for flexural member (see Section 12.2).

The analytical solution is given in the Theory of Plasticity for the torsional member of a non-circle section, and a practical analogue method of sand pile is also suggested to find the ultimate torsion [15-10] and is conducted as below. A plane of the same shape is manufactured to simulate a section of the member, then dry and loose sand is uniformly spread on it, until the sand pile does not elevate again and spare sand rolls down from it. If the slope of the sand pile formed is taken as the plastic ultimate stress ($\tan \theta = \tau_{\max}$) of the material, the plastic ultimate torsion of the member is double the volume of the sand pile, i.e.

$$T_p = 2V. \quad (15-7)$$

Similarly, Eqs. (15-5) and (15-6) are easily derived.

Of course, the analogue method of sand pile can also be used to calculate the plastic ultimate torsion for the composite rectangular sections, e.g. T, I, and reversed L shapes, used widely in structural engineering. For example, the shape of a sand pile for the member of T section is shown in Fig. 15-3(a), and its volume can be calculated by geometrical method and then the plastic ultimate torsion (T_p) is obtained.

Furthermore, the approximate calculation is also possible during engineering design. Usually, the composite section of a member is divided into several rectangles ($b_i \times h_i$, Fig. 15-3(b)), then the plastic section modulus of each one (W_{tpi} , Eq. (15-6)) is calculated separately and added together, so the approximate value of total plastic section modulus of the composite section under torsion is obtained

$$W_{tp} = \sum_i \alpha_{pi} b_i^2 h_i. \quad (15-8)$$

Comparing the shapes and volumes of both sand piles in Fig. 15-3(a) and (b), the difference between the accurate and approximate calculations is caused only at local parts near connections between rectangles divided. In addition, the volume calculated approximately is always smaller than that calculated accurately. Therefore, the ultimate torsion calculated approximately is on the safe side, and the same conclusion can also be drawn from comparison of shear flow diagrams.

The composite rectangular section can be divided into the compositions of different rectangles, e.g. Fig. 15-3(c), and the plastic section moduli and ultimate torsions obtained correspondingly should be different as well. Of course, the composition corresponding to the maximum value of ultimate torsion is selected. Generally, the rectangle with wider breadth on the section keeps integral first (e.g. Fig. 15-3(b)).

When the section of a member is of a closed box (Fig. 15-4(a)), the moment of shear stress at any point under action of torsion against the sectional center is of the same sign, i.e. either clockwise or anti-clockwise, so the plastic section modulus should be considerable. However, if it is calculated approximately and the section is divided into four rectangles (Fig. 15-4(b)), the shear stress flow will be limited within each rectangle and the direction of the shear stress near inside walls is

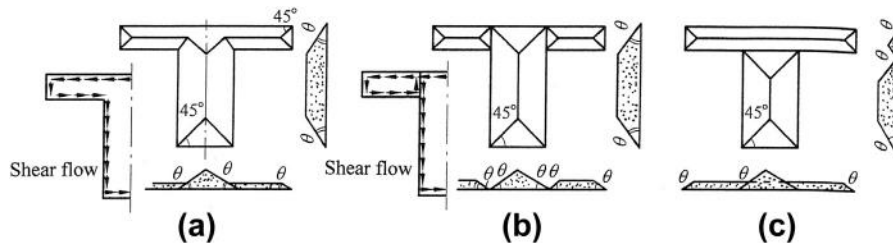


FIG. 15-3 Shape of sand pile (plastic ultimate torsion) for T section: (a) accurate calculation, (b) approximate calculation, (c) another approximate calculation

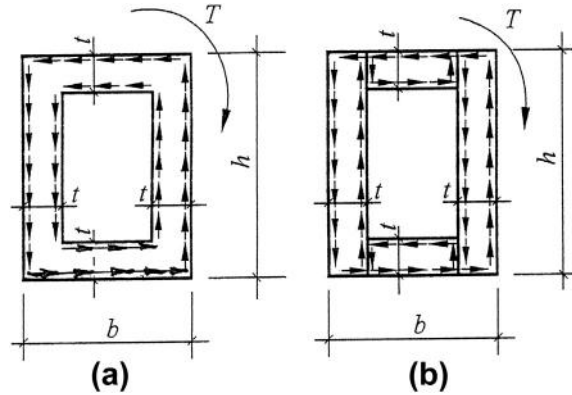


FIG. 15-4 Shear stress flow on box section: (a) integral section, (b) dividing into rectangles

opposite that near outer surfaces, so the total plastic section modulus obtained from Eq. (15-8) is far smaller than that should be. Therefore, the approximate method introduced above or Eq. (15-8) is unreasonable and can not be used for the member with a closed box section.

The existing experiments (see Fig. 15-7) show that the plastic section modulus and ultimate torsion of a member with box section can be calculated like that of a solid section, if its wall thickness is $t \geq b/4$. Because the area, shear stress, and lever arm in the middle of a solid section are relatively small, the torsion resistance there is limited and negligible. On the other hand, if the box wall is not thick enough ($t \leq b/10$), it can not prevent from buckling at the ultimate state, so it is not normally used in engineering practice. Then, the plastic section modulus under torsion of the box section with wall thickness $t = (\frac{1}{10} \sim \frac{1}{4})b$ can be calculated by interpolation, i.e. $W_{tp} = \alpha_p b^2 h (4t/b)$, which is still on the safe side [2-11] compared with the experimental data. Alternately, the Chinese Code [2-1] suggests that the plastic section modulus under torsion of a box section is taken as the difference between that of the solid section ($b \times h$) and hollow area ($b_n \times h_n$) calculated by Eq. (15-6), i.e. $W_{tp} = \alpha_p b^2 h - \alpha_{pn} b_n^2 h_n$.

15.2 Ultimate strength of member under torsion alone

15.2.1 Member without web reinforcement

When a plain concrete member of rectangular section is acted with torsion only (Fig. 15-5), the shear stress on the section distributes consistently with that obtained from the elastic analysis at the early loading stage, and the maximum shear stress appears at the center of the longer edge (mid-depth). In addition, the maximum principal tensile stress is $\sigma_1 = \tau_{\max}$ and occurs at the same point but with an inclination of 45° , because the shear stresses exist in pairs and the normal stress is neglected.

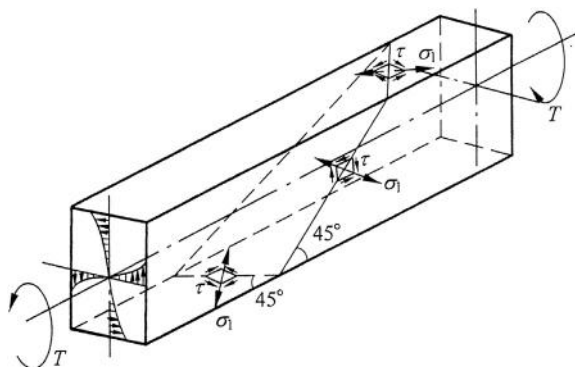


FIG. 15-5 Member of plain concrete under torsion only

The shear stress of the member increases with the torsion acted, and the plastic strain of concrete occurs slightly and the diagram of shear stress on the section (Fig. 15-1(b)) tends to plump up. When the maximum principal tensile stress of the concrete reaches the tensile strength, the inclined crack appears first on the middle of the side surface (longer edge of the section) and is perpendicular to the principal tensile stress. Afterwards, the inclined crack extends both upwards and downwards along the inclination of about 45° and then turns on the top and bottom surfaces (short edges of the section). After the three surfaces are cracked, the member is torn in two pieces along the fourth surface (longer edge of the section) with a twist failure surface (Fig. 15-5), but no crack is usually found on the other place. The appearance of the broken surface is consistent with the failure characteristics of concrete under tension (Table 2-8). Generally, the ultimate torsion is slightly greater, but by no more than 10%, than the cracking torsion of the member.

According to the statistic of experimental data at home and abroad, the ultimate torsion of a plain concrete beam of rectangular section ranges from

$$T_u = (0.7 \sim 0.8) W_{tp} f_t. \quad (15-9)$$

This is obviously greater than the theoretical value based on elasticity calculation ($T_e = (0.590-0.667) W_{tp} f_t$, Table 15-1), but it is smaller than the theoretical value based on plasticity analysis ($T_p = W_{tp} f_t$). Therefore, $T_u/T_e = 1.1-1.3$ but $< T_p/T_e = \alpha_p/\alpha_e = 1.5-1.694$ (Table 15-1) is obtained. This means that the plastic strain of the concrete develops to a certain extent but not fully before failure of the beam under torsion. In addition, the concrete in the member is of a biaxial tensile-compressive stress state, and the corresponding tensile strength is slightly smaller than the strength of concrete under uniaxial tension.

The experiments also show that the coefficient in Eq. (15-9) is slightly greater for the beam of lower strength of concrete (f_{cu}). To the contrary, the beam of higher-strength concrete has a slightly smaller coefficient and sharper inclination of the

critical crack at failure, because the plastic strain develops differently before failure for the concrete of different strengths.

15.2.2 Member with web reinforcement

In order to increase the shear resistance of a concrete member, both longitudinal reinforcements and transverse stirrups have to set up uniformly along the sectional periphery and member axis, respectively. The characteristics of deformation, cracking, and failure process of this kind of member under torsion are briefly presented below (Fig. 15-6).

After the torsion is acted and increased on the member, the stress distribution agrees well with that of elasticity analysis and the twisted angle increases proportionally but slowly before cracking of the concrete. When the principal tensile stress at mid-depth of lateral surface (longer edge of the section) reaches the biaxial tensile strength of the concrete, an inclined crack of 45° appears there and the stresses of the stirrup and longitudinal reinforcement intersected increase suddenly, and the twisted angle of the member increases quickly and the torsion-twisted angle ($T-\theta$) curve turns correspondingly, and a terrace may be formed there (Fig. 15-6(b)).

As the torsion is increased further, more inclined cracks appear parallel with the approximate distance and they expand gradually and extend to all four surfaces of the member, then multiple spiral cracks are formed on the surfaces. In the meantime, the cracks also extend inside from the surface and the concrete of the outer layer is gradually out of work, so the stirrup and longitudinal reinforcements share more portions of the torsion acted. Therefore, their stresses and the twisted angle of the member increase quickly, and the torsional stiffness of the member decreases correspondingly.

When some of the stirrups and longitudinal reinforcements intersected with the inclined cracks reach their yield strengths, the cracks widen more quickly and other

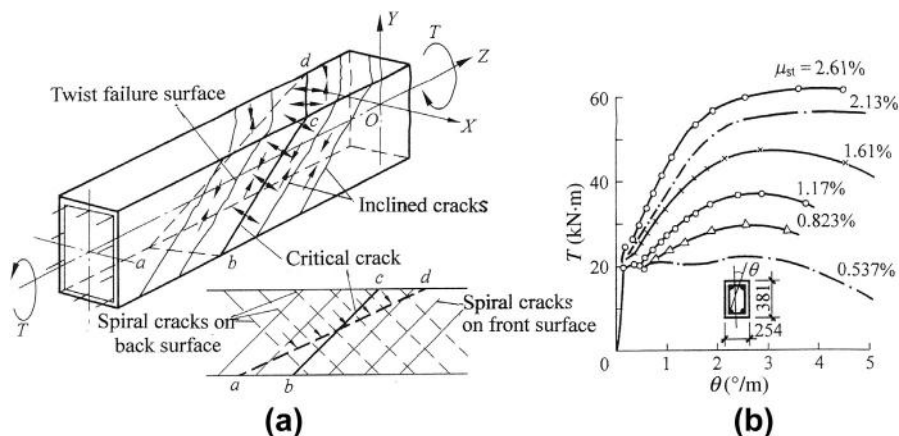


FIG. 15-6 Beam with web reinforcement under torsion: (a) cracks and failure surface, (b) torsion-twisted angle relation

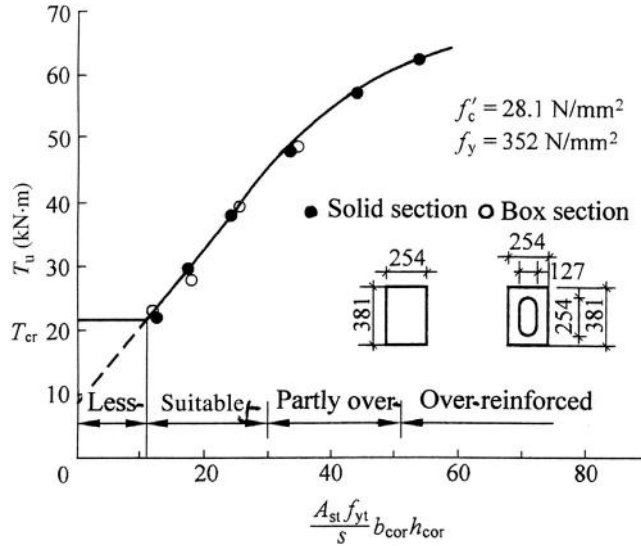


FIG. 15-7 Contents of reinforcements and ultimate torsion [15-11]

stirrups and longitudinal reinforcements nearby reach the yield strength as well, and more concrete of the outer layer is out of work and the twisted angle accelerates, so the $T-\theta$ curve tends gradually to flatten and the torsional stiffness of the member reduces correspondingly. Once one of the inclined cracks expands wider than others and the stirrups and longitudinal reinforcements intersected with it are yielded successively, it becomes the critical one and the torsion can not be increased again. Therefore, the $T-\theta$ curve turns horizontally and the ultimate torsion (T_u) is obtained. Afterwards, the critical inclined crack develops even wider and more concrete of the outer layer is out of work, then a descending branch of the $T-\theta$ curve is formed.

The final failure pattern of a reinforced concrete member under torsion only is an inclined twisted surface including the tensile cracks on three surfaces and a compressive strip near another surface (longer edge of the section) (Fig. 15-6(a)). It should be noticed that the spiral tensile cracks on the front and back surfaces are intersected normally (90°) from the front view, and the front crack (bc) on the failure surface is tensile, while the strip near the back on the failure surface (ad) is surely compressive.

15.2.3 Influence of contents of reinforcement and stirrup

When the member under torsion is reinforced properly with the stirrups and longitudinal reinforcements, the typical failure process described above will appear and the member is called one that is suitably reinforced. As the contents of both reinforcements are increased, the ultimate torsion (T_u) and torsional stiffness of the member will increase obviously (Fig. 15-7 and Fig. 15-6(b)). However, both

reinforcements contribute less for the torsion at cracking of the concrete, mainly because of smaller strains (stresses) of the concrete and reinforcements then. Nevertheless, the development of the inclined cracks is delayed and the twisted angle is reduced after cracking of the concrete, and the terrace on $T-\theta$ curve is shortened.

If the stirrups and longitudinal reinforcements are reinforced unsuitably in the member, some unfavorable situations will occur:

1. **Less-reinforced.** If the contents of both stirrup and longitudinal reinforcement in the member are too low and the torsion resistance carried by them is smaller than that of the plain concrete (T_{cr}) alone, the concrete is out of work soon after the inclined crack is formed under torsion, and the member fails quickly in a brittle twist. This is called the failure of less-reinforced. Generally, the minimum contents are given in various design codes [2-1,2-11] for both reinforcements to prevent the failure of this kind.
2. **Over-reinforced.** If the contents of both stirrup and longitudinal reinforcement in the member are too much, the stresses in them are rather lower after cracking of the concrete, and the inclined cracks develop and the stresses increase slowly with the torsion afterwards. Finally, the member fails quickly soon after the principal compressive stress of the concrete reaches the corresponding strength, while the stresses of both reinforcements are still lower than the yield strength. This is called the failure of over-reinforced. Therefore, the sectional size or concrete strength of the member should be elevated during design to prevent an unfavorable failure of this kind.
3. **Partly over-reinforced.** The principal tensile stress caused in the member under torsion has to be carried together by the stirrups and longitudinal reinforcements (Fig. 15-8), but can not be carried alone by either of them. The ratio between the strengths per unit length of them is

$$\zeta = \frac{A_s f_y / u_{cor}}{A_{st} f_{yt} / s} = \frac{A_s f_y s}{A_{st} f_{yt} u_{cor}}, \quad (15-10)$$

where A_s, f_y are the total area of longitudinal reinforcements set up along sectional periphery and their yield strength, A_{st}, f_{yt} are the total area of torsional stirrups in one

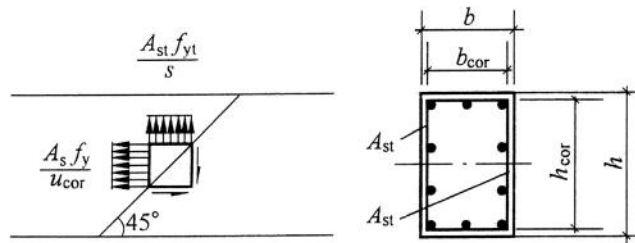


FIG. 15-8 Strengths per unit length of stirrups and longitudinal reinforcements

section and their yield strength, s is the distance of stirrups, $u_{\text{cor}} = 2(b_{\text{cor}} + h_{\text{cor}})$ is the peripheral length of sectional core, in which b_{cor} and h_{cor} are taken as the net distances between internal surfaces of stirrup in the Chinese Code [2-1].

It is demonstrated experimentally that the member fails under torsion in the pattern of suitable reinforced and both stirrups and longitudinal reinforcements are yielded already at ultimate state, when the ratio (ζ) ranges from 0.6 to 1.7. However, the stirrups in the member do not reach the yield strength at ultimate state and can not be utilized fully, if the longitudinal reinforcements is too low ($\zeta < 0.6$); while the longitudinal reinforcement can not be utilized fully if the stirrup is too low ($\zeta > 1.7$). Some experiments show that the ultimate torsion of a member reinforced with much longitudinal reinforcements but without stirrups is greater, by $<15\%$ only, than that of a plain concrete member. Both situations are called the failure of partly over-reinforced.

Therefore, not only shape and size of the section and total content of both stirrup and longitudinal reinforcement, but also the ratio between the contents of both should be determined properly, when the member under torsion is designed.

15.3 Members with composite internal forces

15.3.1 Member with axial force and torsion

As the member is acted with an axial compression or is prestressed by the tendons, the principal tensile stress of the concrete and tensile stress of the longitudinal reinforcement caused by the torsion should be reduced, so the cracking and ultimate torsions (T_{cr} , T_{u}) of the member is certainly increased. Contrary, both critical torsions of the member with axial tension and torsion together are certainly decreased.

Consequently, the influence of axial force on torsional strength of the member is considered in various design codes, but usually in an easy way, e.g. adding an extra resistance [2-1] or a modification coefficient [2-11].

15.3.2 Member with shear force and torsion

When shear force and torsion are acted separately on a member, the shear stress (τ_v or τ_T) is mainly caused on the section but with different distributions, which is shown in Fig. 15-9(a) based on elastic calculation. When shear force and torsion are acted together on a member, the composition of both shear stresses on the section is rather complicated. As the shear stress caused by shear force is zero ($\tau_v = 0$) at the top and bottom of the section, the shear stress there is dominated by torsion only ($\tau = \tau_T$); the shear stresses caused by shear force and torsion respectively can be added algebraically ($\tau = \tau_v + \tau_T$), if they act in the same direction, e.g. along lines I—I, II—II and III—III on the section; otherwise, both shear stresses should be added geometrically ($\vec{\tau} = \vec{\tau}_v + \vec{\tau}_T$) and both direction and value of the composed shear stress are changed, if they do not act in the same direction, e.g. along line IV—IV and other positions on the section.

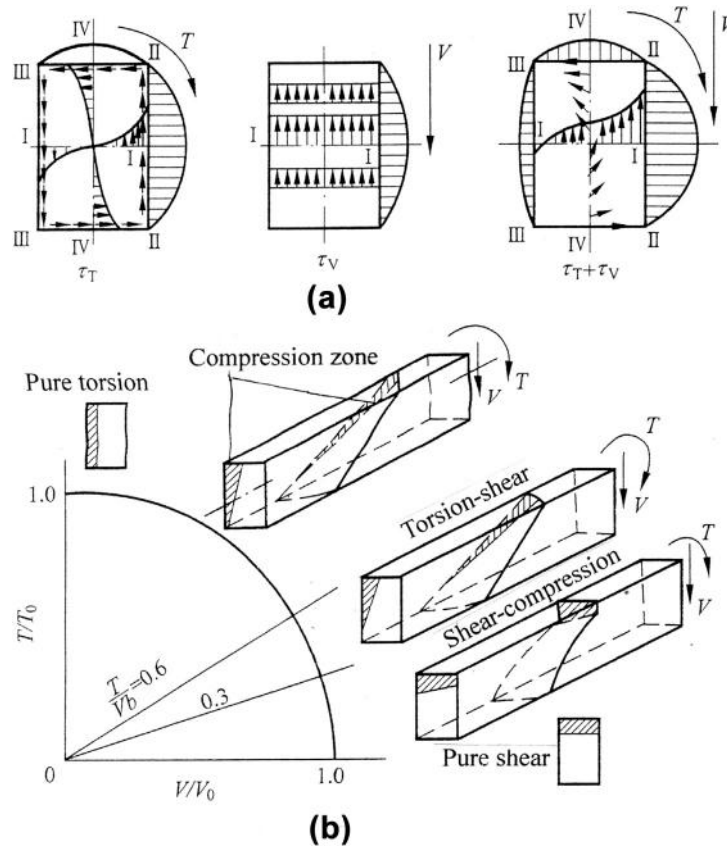


FIG. 15-9 Joint action of shear force and torsion: (a) distribution and summation of shear stresses, (b) failure patterns and envelope (member without web reinforcement)

In any case, the joint action of shear force and torsion always causes an increment in shear stress, and then principal tensile stress, of concrete on one of the side surfaces, so the torsion of the member at cracking (T_{cr}) is certainly reduced. In addition, the inclined cracks develop differently on both opposite surfaces after concrete cracks, and the ultimate torsion (T_u) of the member is also reduced. As the relative value between torsion and shear force acted (T/Vb) on the member varies, the composition of shear stress is different correspondingly and several failure patterns will appear successively (Fig. 15-9(b)).

1. Larger torsion—shear force ratio ($T/Vb > 0.6$). The inclined crack appears first on the side surface (longer edge of the section) of the member with the maximum shear stress, e.g. II—II in Fig. 15-9(a), as the principal tensile stress there reaches the tensile strength of the concrete. The inclined cracks extend to both top and bottom surfaces and a spiral crack is formed afterwards. When three sides

of the critical inclined crack are of tensile and another side (III—III) is torn away, the member fails and is broken into two pieces. The compression-zone on the twisted failure surface is trapezoid with wider top and narrower bottom as shown by the shadow in Fig. 15-9(b), while it is rectangular for the member acted with torsion only.

2. Smaller torsion—shear force ratio ($T/Vb < 0.3$). The tensile crack dominated by bending moment appears first on the bottom of the member and then extends upwards with different inclinations on both side surfaces and the flexural—shear cracks are then formed. Finally, the member fails in the pattern of shear—compression (see Section 14.1.1), but the compression zone on the section is a trapezoid near the top (Fig. 15-9(b)). However, the critical inclined cracks on both side surfaces are asymmetrical, and the crack extends higher and the compression depth is smaller for the side surface with larger shear stress, e.g. II—II.
3. Medium torsion—shear force ratio ($T/Vb = 0.3-0.6$). The cracks and failure pattern of this kind of member are in between the two situations introduced above and are transferred gradually. Generally, the inclined crack appears first on web of the side surface (II—II) with larger shear stress and, then, extends both upwards and downwards, even reaching the lower part of other side surface (III—III). Finally, the compression zone of a triangle is formed near the side surface (III—III) as the member fails. This is called torsion—shear failure.

The failure envelope of the member without web reinforcement under actions of shear force and torsion together approximates a circle (Fig. 15-9(b)) and is expressed as

$$\left(\frac{T}{T_0}\right)^2 + \left(\frac{V}{V_0}\right)^2 = 1, \quad (15-11)$$

where T_0 is the ultimate strength of the member under torsion only (shear force $V = 0$), V_0 is the ultimate strength of member under shear force and bending moment but without torsion ($T = 0$) (see Chapter 14).

15.3.3 Member with bending moment and torsion

When a reinforced concrete member is acted with torsion only, all the longitudinal reinforcements, regardless of being placed near the bottom, top, or lateral surfaces of the section, are tensile. However, the reinforcements are either tensile or compressive, depending upon their position on the section, in a member under bending moment only. When the member is acted with torsion and bending moment (e.g. positive one) together, tensile stress of the reinforcement (A_s) placed on flexural tension zone is increased while that of the reinforcement (A'_s) placed on flexural compression zone is decreased even turns in compressive stress, compared with the member under torsion only. Therefore, both reinforcements (A_s and A'_s) do not necessarily reach their yield strength (f_y and f'_y) at failure of the member.

Let the ratio between the ultimate strengths of both reinforcements on flexural—compression and —tension zones be

$$\gamma = \frac{A'_s f'_s}{A_s f_s}. \quad (15-12)$$

The ultimate envelope of bending moment—torsion for a symmetrically reinforced member ($\gamma = 1$) obtained from the relevant experiments is shown in Fig. 15-10(a), and it is composed of two parabolas being symmetrical about the T/T_0 axis and can be expressed by the regression formula

$$\left(\frac{T}{T_0}\right)^2 + \frac{M}{M_0} = 1, \quad (15-13)$$

where M_0 is the ultimate bending moment dominated by tensile reinforcement (A_s) when torsion $T = 0$.

The stresses of reinforcements on flexural—tension and —compression zones (σ_s, σ'_s) at ultimate state vary with the relative values of bending moment and torsion (Fig. 15-10(b)). Both of them reach tensile yield strength at ultimate state only when the torsion is acted alone, i.e. without bending moment ($M = 0$). When positive bending moment ($M > 0$) is acted as well, the reinforcement near the bottom of the section (A_s) certainly reaches the tensile yield strength ($\sigma_s = f_y$) at the ultimate state. However, the stress of the reinforcement near the top (A'_s) also reaches the tensile yield strength ($+f_y$) under torsion only ($M = 0$), but reduces gradually to zero and turns to a compressive one, even yield strength ($\sigma'_s = -f'_y$), as the bending moment is increased. Alternately, when a negative bending moment ($M < 0$) is acted together with torsion, the stress state at ultimate state changes correspondingly and the reinforcement near the top (A'_s) is always tensile and reaches yield strength.

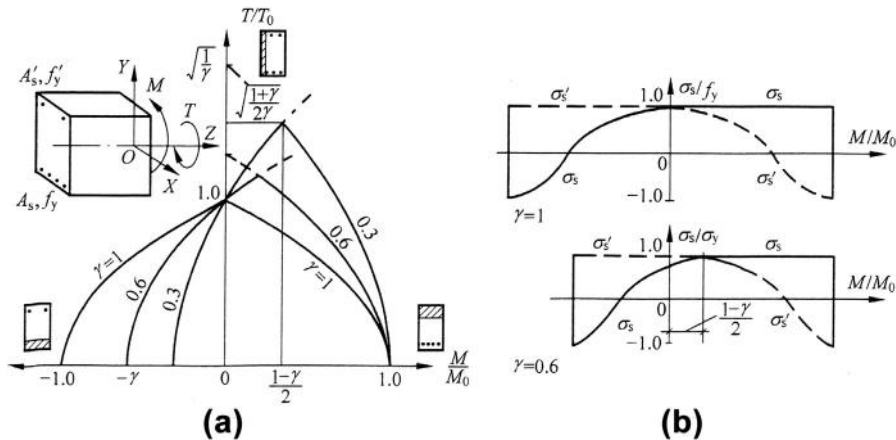


FIG. 15-10 Together actions of bending moment and torsion: (a) ultimate envelope, (b) stress of reinforcement at ultimate state

Therefore, the right half of the T - M envelope represents failure of the member dominated by the reinforcement near the bottom (A_s), while the left half represents failure of the member dominated by the reinforcement near the top (A'_s).

As far as an asymmetrically reinforced member ($\gamma < 1$) is concerned, the positive and negative ultimate bending moments (M_0 and $-\gamma M_0$) should be different, when no torsion is acted. If the member is acted with torsion only ($T_0 \neq 0$, $M = 0$), the reinforcement near the top of the section (A'_s) reaches, but the reinforcement near bottom (A_s) will not reach the yield strength at ultimate state. When a positive bending moment ($M > 0$) is added later, the stress of the reinforcement near the top (A'_s) is reduced while the stress of the reinforcement near the bottom (A_s) is increased, so more torsion can be acted further. Therefore, the ultimate torsion of the member increases with the bending moment acted, and its maximum value should appear together with a certain amount of bending moment (Fig. 15-10(a)). However, if an excessive bending moment ($+M$) is acted together with the torsion, the reinforcement near the top (A'_s) will not yield tensely, even be compressive, when the reinforcement near the bottom (A_s) is tensely yielded already at ultimate state. Consequently, the ultimate bending moment–torsion envelope of the member is surely asymmetrical, and its peak point corresponding to the maximum of ultimate torsion is located on the positive side ($M > 0$) and the deviation of the peak increases as the ratio between both reinforcements (γ) decreases.

The two parabolas located on the right and left sides of the peak point on T - M envelope are respectively dominated by the tensile yield of the reinforcements near the bottom (A_s) and top (A'_s), and their calculation formulas are separately given from the experimental investigation: [15-12]

$$\text{right parabola dominated by } A_s \quad \gamma \left(\frac{T}{T_0} \right)^2 + \frac{M}{M_0} = 1, \quad (15-14a)$$

$$\text{left parabola dominated by } A'_s \quad \left(\frac{T}{T_0} \right)^2 - \frac{M}{\gamma M_0} = 1. \quad (15-14b)$$

The extension of the right parabola intersects with the ordinate at $\frac{T}{T_0} = \sqrt{\frac{1}{\gamma}}$. In addition, intersection between both parabolas is also the peak point, at which

$$\frac{M}{M_0} = \frac{1 - \gamma}{2} \quad \text{and} \quad \frac{T_{\max}}{T_0} = \sqrt{\frac{1 + \gamma}{2\gamma}} > 1 \quad (15-15)$$

are obtained. It is clear that the maximum value of ultimate torsion of the member acted together with bending moment is greater than the ultimate value of the member acted with torsion only ($T_{\max} > T_0$).

If section of the member is narrow, i.e. ratio h_0/b is large, or the longitudinal reinforcements near lateral surface (longer edge of the section) (A_s^0) is too low, some of the reinforcements there reach first the yield strength when the member is acted together with torsion and bending moment. Usually, this leads to the torsional failure of the member. This kind of ultimate state can be approximated as a horizontal line

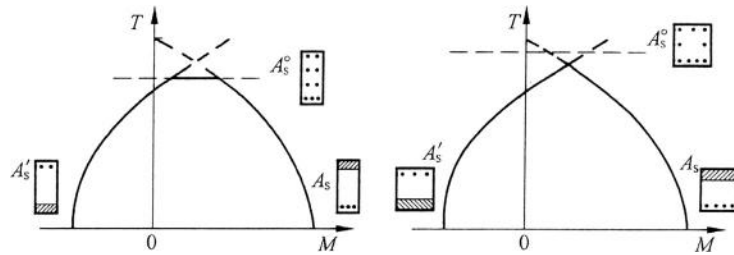


FIG. 15-11 Influence of longitudinal reinforcement near lateral surface on T – M envelope

and three segments are then formed on the envelope of bending moment–torsion (Fig. 15-11, left).

However, if the reinforcement there (A_s^0) is strong enough, the corresponding ultimate torsion would be greater than the maximum ultimate torsion dominated by the reinforcements near the top and bottom surfaces (Fig. 15-11 right), and the envelope will not be changed.

15.3.4 Member with bending moment, shear force and torsion together

The spatial ultimate envelope of a reinforced concrete member acting together with bending moment (M), shear force (V), and torsion (T) is shown in Fig. 15-12. The envelopes on the T – M plane are composed of two parabolas dominated respectively by the reinforcements near the bottom and top of the section, and the envelopes on the T – V plane are circular or elliptical, as introduced above. The simple expression for the spatial envelope is

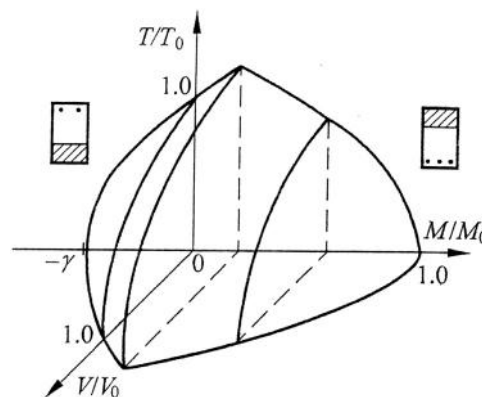


FIG. 15-12 Bending moment–shear force–torsion envelope [15-13]

$$\left(\frac{T}{T_0}\right)^2 + \left(\frac{V}{V_0}\right)^2 + \frac{M}{M_0} = 1. \quad (15-16)$$

If the member is of narrow section or is reinforced less near side surfaces (longer edges), the peak part of its envelope should be cut off [15-13] because of a reduction in the ultimate torsion strength.

15.4 Calculation of ultimate strength

It is mentioned above that the stress state is triaxial and the hypothesis of the plane section is not held for the member acted with torsion, so an accurate calculation of the member is rather difficult, especially as concrete is a non-elastic material and is easily cracked. Although the analysis method of finite element is well developed and the corresponding computer program is available, the calculated result is satisfied only for the member of elastic material. Therefore, the reinforced concrete member acted with torsion is designed in engineering practice mainly using the empiric formula based on the experimental results or the approximate calculation based on a simplified mechanical model.

15.4.1 Empirical formulas

Based on the experimental results of reinforced concrete members acted with torsion only, the empirical formula of ultimate strength (T_u) [15-6] is obtained regressively in China (Fig. 15-13)

$$\frac{T_u}{W_{tp}f_t} = 0.43 + 1.002\sqrt{\zeta} \frac{A_{st1}f_{yt}A_{cor}}{W_{tp}f_t s} + 0.5\sqrt{\zeta} \frac{A_{st2}f_{yt}A_{cor}}{W_{tp}f_t s}. \quad (15-17a)$$

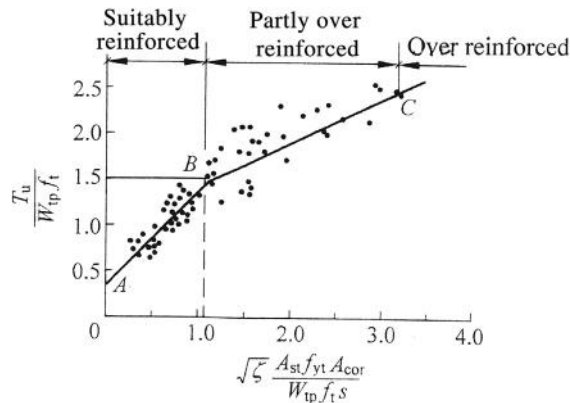


FIG. 15-13 Ultimate strength of member acted with torsion [15-6]

Or, the formula is simplified into two terms

$$\frac{T_u}{W_{tp}f_t} = 0.35 + 1.2\sqrt{\zeta} \frac{A_{st}f_{yt}A_{cor}}{W_{tp}f_t s}, \quad (15-17b)$$

where $A_{st1} + A_{st2} = A_{st}$, A_{st1} is total area of stirrups, within suitable reinforcement, of one section, A_{st2} is the corresponding area of stirrups, beyond suitable reinforcement, of one section, $A_{cor} = b_{cor} \times h_{cor}$. Other symbols are the same as above.

The intersection between two theoretical lines in Fig. 15-13 indicates the boundary between suitably and partly over-reinforced stirrups of the member.

Basing on this, the calculation and design methods are established correspondingly in the Chinese Code [2-1]. For example, the ultimate strengths of the member with rectangular section and acted together with shear force and torsion can be checked separately by the formulas below

$$T \leq 0.35\beta_t W_{tp}f_t + 1.2\sqrt{\zeta} \frac{A_{st}f_{yt} + A_{cor}}{s} \quad (15-18a)$$

$$V \leq 0.7(1.5 - \beta_t)f_t b h_0 + 1.25 \frac{A_{st}f_{yt}h_0}{s}, \quad (15-18b)$$

where β_t is the coefficient of reducing strength for the member acted together with shear force and torsion

$$\beta_t = \frac{1.5}{1 + 0.5 \frac{VW_{tp}}{Tbh_0}}, \quad (15-19)$$

and it takes $\beta_t = 0.5$ if $\beta_t < 0.5$ is calculated, while $\beta_t = 1$ is taken if $\beta_t > 1.0$ is calculated. When the member is acted with tension only ($V = 0$), $\beta_t = 1.0$ is obtained, so Eq. (15-18a) and Eq. (15-17b) are identical.

$$\text{In addition, if } \frac{T}{W_{tp}} + \frac{V}{bh_0} \leq 0.7f_t \quad (15-20)$$

is obtained, the concrete of the member will not crack under joint actions of shear force (V) and torsion (T), so the minimum longitudinal reinforcement and stirrup listed in the code are needed only. On the other hand, if

$$\frac{T}{0.8W_{tp}} + \frac{V}{bh_0} > 0.25f_c \quad \text{for } h_w \leq 4b \quad (15-21a)$$

$$\text{or } \frac{T}{0.8W_{tp}} + \frac{V}{bh_0} > 0.20f_c \quad \text{for } h_w \geq 6b \quad (15-21b)$$

is obtained, the principal compressive stress in the member will cause failure of the concrete, so the size of the section or compressive strength of the concrete should be increased.

When the member under torsion is designed with a non-rectangular section, e.g. T or I shape, the section is divided first into a composition of several rectangles like Fig. 15-3. The plastic section modulus of every rectangle (W_{tp} , Eq. (15-6b)) is

calculated separately and the torsion acted on the member is distributed to every rectangular sub-section following the ratio between the modulus of each one and the total modulus of the section (Eq. (15-8)), then each rectangle is calculated and reinforced correspondingly.

Similar calculation based on experimental data is also suggested in the code of the USA [2-11]. The maximum shear stress, i.e. principal tensile stress, in the member of plain concrete acted with torsion only is taken as $\tau_{\max} = \sigma_1 = \sqrt{f'_c}/2$ at its failure, where f'_c is the compressive strength of the concrete cylinder in N/mm². In addition, the coefficients in Eqs (15-4), (15-6), and (15-8) are taken uniformly as $\alpha_e = \alpha_p = \alpha_{pi} = 1/3$, so the section modulus of a composite rectangular section is approximately $\sum(b_i^2 h_i/3)$ and the ultimate torsion of the member of plain concrete should be

$$T_{cr} = \frac{1}{6} \sqrt{f'_c} \sum (b_i^2 h_i). \quad (15-22)$$

And, the basic formula for calculation of torsion resistance of a reinforced concrete member is

$$T_u = T_c + T_s = \frac{\sqrt{f'_c} \sum (\frac{1}{15} b_i^2 h_i)}{\sqrt{1 + \left(\frac{0.4V}{C_i T}\right)^2}} + \frac{\alpha_t A_{st} f_{yt} b_{cor} h_{cor}}{s}, \quad (15-23)$$

where T_c is the component of concrete for torsion resistance, and the numerator taking as $0.4T_{cr}$ (see Eq. (15-22)) and the denominator considering discount as shear force acted together, with $C_i = bh_0 / \sum(b_i^2 h_i)$ and bh_0 being the area of the web, T_s is the component of torsion resistance for stirrups, where $\alpha_t = (2 + h_i/b_i)/3$.

After the stirrup needed for a member under torsion is calculated from Eq. (15-23), the longitudinal reinforcement needed for the same member can be calculated below, based on the principle of equal volume:

$$A_s = 2A_{st} \frac{b_i + h_i}{s}. \quad (15-24)$$

In addition, it is also provided in the code of the USA that the torsion acted on a member can be neglected if $T_u \leq T_{cr}/4 = \sqrt{f'_c} \sum(b_i^2 h_i)/24$, or the section of the member should be increased to prevent the compressive failure of concrete if $T_s > 4T_c$.

15.4.2 Truss model

The truss model for analyzing the reinforced concrete member under torsion was suggested first by Rausch (Germany) as early as 1928, and it was improved and complemented later on and can be used for the member acted together with bending moment, shear force, and torsion [15-13–15-16]. However, some assumptions and simplifications introduced during establishment of the model are considerably different from real behavior of the member. The basic concept and calculation procedure of the model [15-13] are presented briefly as below.

When a reinforced concrete member of rectangular section is acted with torsion only, the section may be simplified into a box with four walls along which the shear stress flow per unit length is q , if the core in the middle of the section is neglected as it is of less torsion resistance. After the inclined spiral cracks occur parallel on the periphery, the member is simulated as a spatial truss (Fig. 15-14(a)), in which the longitudinal reinforcements are simulated as the tensile chords, the stirrups are simulated as tensile web bars, and the concrete belts between inclined cracks are simulated as compressive web bars. The internal forces of these bars are axial ones and respectively P , Q , and R , and P is in equilibrium with the component of R in direction Z and Q is in equilibrium with the component of R in direction X or Y at a joint (Fig. 15-14(b)).

The torsion resistance of the shear stress flow (q) on the section can be derived as

$$T = qh_{cor}b_{cor} + qb_{cor}h_{cor} = 2qA_{cor}. \quad (a)$$

If a triangle including an inclined crack is taken into account (Fig. 15-14(c)),

$$Q = qh_{cor} = \frac{A_{st}\sigma_{st}h_{cor} \cot \theta}{s}$$

or

$$q = \frac{A_{st}\sigma_{st}}{s} \cot \theta \quad (b)$$

is found. According to the equilibrium condition (Fig. 15-14(b)),

$$P = Q \cot \vartheta,$$

$$\text{i.e. } A_s \sigma_s \frac{h_{cor}}{u_{cor}} = qh_{cor} \cot \theta$$

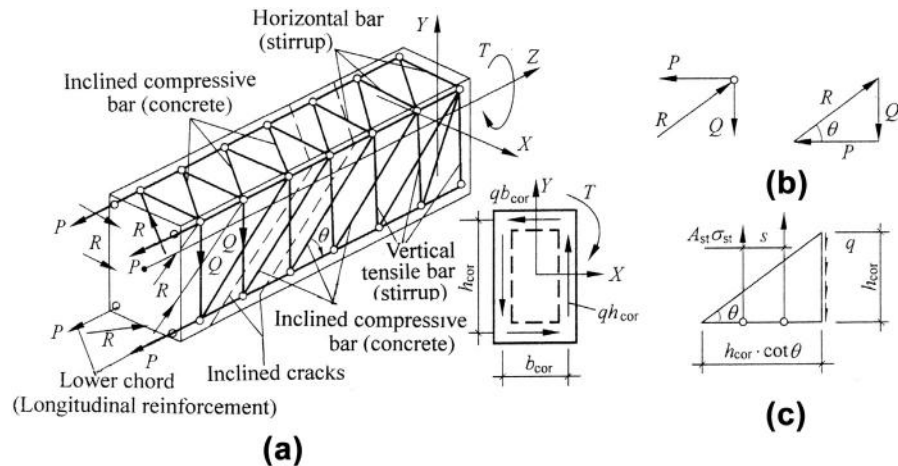


FIG. 15-14 Truss model for member under torsion: (a) calculation model, (b) equilibrium condition at a joint, (c) local equilibrium

is derived and

$$\cot \theta = \frac{A_s \sigma_s}{q u_{cor}} \quad (c)$$

is obtained. After formula (c) is substituted into formula (b),

$$q = \sqrt{\frac{A_{st} f_{st}}{s} \frac{A_s \sigma_s}{u_{cor}}} \quad (d)$$

is found and substituted again into formula (a),

$$T = 2A_{cor} \sqrt{\frac{A_{st} f_{st}}{s} \frac{A_s \sigma_s}{u_{cor}}}$$

or

$$T = 2\sqrt{\zeta} \sqrt{\frac{\sigma_{st} \sigma_s}{f_{yt} f_y}} \frac{A_{st} f_{yt}}{s} A_{cor} \quad (15-25)$$

is established, in which σ_{st} and σ_s are stresses of the stirrup and longitudinal reinforcement respectively at ultimate state and they are not necessarily reaching separately their yield strength ($\leq f_{yt}$, $\leq f_t$). Other symbols in these formulas are the same as above.

The term $\sqrt{\sigma_{st} \sigma_s / f_{yt} f_y}$ in the right side of Eq. (15-25) is equivalent to a coefficient in Eq. (15-18a). If the torsion resistance (T_c) of the core concrete and the interaction of aggregate along the inclined crack are added as well, the final formula is similar to Eq. (15-18a). Of course, various truss models have different assumptions and simplifications and a variety of expressions are suggested.

15.4.3 Ultimate equilibrium of inclined twisted surface

Russian researchers established first (1958) the equilibrium equations for the reinforced concrete member under torsion at ultimate state based on analysis of the failure characteristics. In addition, the calculation formula [15-17] was derived correspondingly and was then improved later on [15-18,15-13].

Experiencing successively appearance and development of concrete cracks and yielding of reinforcement, the reinforced concrete member of rectangular section under torsion fails finally and a twisted failure surface is formed and includes a tensile crack continuing spirally on three surfaces and a compressive strip along the fourth surface (longer edge of the section) (Fig. 15-6). There are several forces acting on the inclined twisted failure surface (Fig. 15-15(a)), and they include the tensile forces and transverse dowel actions of longitudinal reinforcement and stirrup, the normal and shear stresses (σ , τ) of concrete on the compressive strip, the aggregate interaction of concrete along the inclined cracked surface, and the shear stress flow of concrete within the uncracked core of the section.

The actions of normal and shear stresses on the compressive strip can be resolved into two perpendicular forces acting in the directions Z and Y , and one of them (N_z) is in equilibrium with the tensile force of the longitudinal reinforcements ($\sum Z = 0$) and the other one (N_y) is composed of a couple of torsion resistance together with tensile forces of the stirrups near opposite lateral surface. In addition, other couples

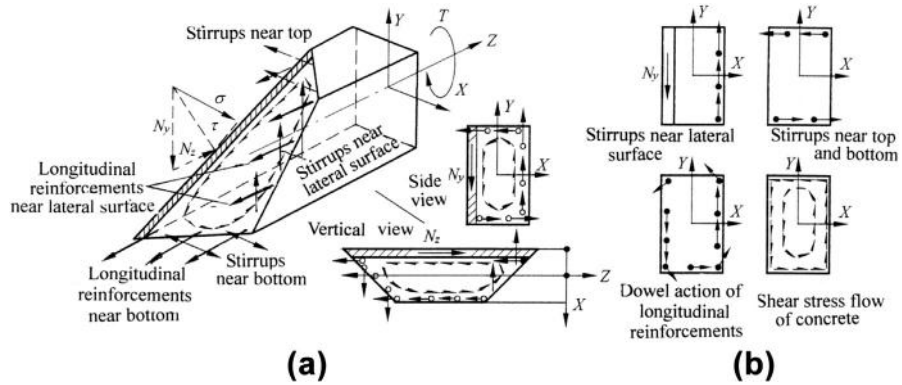


FIG. 15-15 Forces acted on inclined twisted failure surface: (a) forces acted, (b) composition of torsional couples

of torsion resistance on the inclined twisted surface are: tensile forces of the stirrups near top and bottom, dowel actions of both longitudinal reinforcements and stirrups, and shear stress flow of core concrete (Fig. 15-15(b)). After some assumptions or simplifications are properly made, the formulas for calculation of torsion resistance are derived based on the equilibrium equations and the parameters included can be calibrated from the relevant experimental data. The member acted together with bending moment and torsion is used here as an example.

When a reinforced concrete member is acted together with bending moment and torsion, various failure patterns, i.e. compression zone locating by top, bottom, right or left side of the section at ultimate state (Fig. 15-10, 15-11), may occur and each of them should be calculated separately.

The assumptions or simplifications used to establish the basic formulas are usually:

1. All inclinations of the spiral crack on three surfaces are 45° ,
2. The stresses of all the longitudinal reinforcements and stirrups passing through the inclined twisted surface reach the yield strength,
3. The compression zone at ultimate state is a narrow strip paralleling the nearer surface and the distance from its center to the stirrup on the opposite side is b_{cor} or h_{cor} ,
4. The torsion resistances of the dowel actions of longitudinal reinforcement and stirrup and the shear stress flow of concrete are neglected.

Assuming the compression zone being resulted by top of the member at ultimate state, the calculation model is taken as shown in Fig. 15-16 and two equilibrium conditions of the moments respectively against two axes, i.e. Z and X, at the center of the inclined twisted surface are then established:

$$\sum M_2 = 0 \quad T = A_{st}f_{yt} \frac{h_{cor}}{s} b_{cor} + A_{st}f_{yt} \frac{b_{cor}}{s} h_{cor}$$

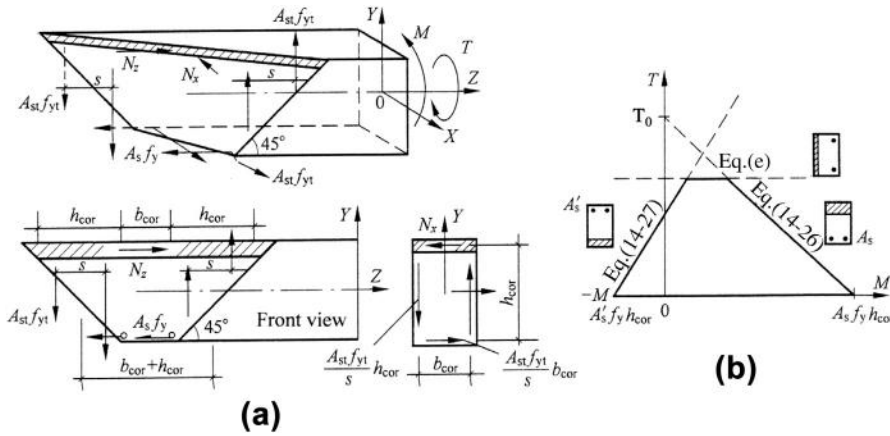


FIG. 15-16 Equilibrium analysis of inclined twisted surface of flexural-torsional member at ultimate state: (a) calculation model (compression zone on top part), (b) ultimate T - M envelope

$$= 2A_{st}f_{yt} \frac{b_{cor}h_{cor}}{s} \quad (e)$$

$$\sum M_X = 0 \quad M = A_s f_y h_{cor} - A_{st} f_{yt} \frac{h_{cor}}{s} (b_{cor} + h_{cor}), \quad (f)$$

where A_s is the area of tensile reinforcement near bottom of the section, and the other symbols are same as above.

Substituting Eq. (e) into Eq. (f),

$$M = A_s f_y h_{cor} - \frac{T}{2b_{cor}} (b_{cor} + h_{cor}) \quad (15-26a)$$

is obtained and it is shown as an inclined line on the ultimate bending moment-torsion envelope (Fig. 15-16(b)), of which two intersections on the abscissa and ordinate are separately:

$$M_0 = A_s f_y h_{cor} \quad \text{and} \quad T_0 = \frac{2A_s f_y b_{cor} h_{cor}}{b_{cor} + h_{cor}}. \quad (15-26b)$$

Similarly, when the negative bending moment and torsion act together on the member, the compression zone will result by bottom of the section at ultimate state, and the equilibrium formulas established correspondingly should be Eq. (e) and

$$M = A_{st} f_{yt} \frac{h_{cor}}{s} (b_{cor} + h_{cor}) - A'_s f'_y h_{cor}. \quad (g)$$

Therefore,

$$M = \frac{T}{2b_{cor}} (b_{cor} + h_{cor}) - A'_s f'_y h_{cor} \quad (15-27)$$

is obtained and it is another inclined line on the ultimate bending moment-torsion envelope.

If the compression zone on an inclined twisted surface of the member at ultimate state is located by side surface of the section, the ultimate torsion is not related to the bending moment, i.e. Eq. (e), and is shown as a horizontal line on the envelope of bending moment—torsion.

The calculated ultimate envelope of bending moment—torsion (Fig. 15-16(b)) is presented apparently as a folded line, which is controlled respectively by three formulas or failure patterns. The shape and size of the envelope calculated are different to a certain extent from that obtained from the experiments (Fig. 15-11), although they are macroscopically similar. Obviously, this is caused due to the errors of the assumption and simplification and the neglect of other components of torsion resistance.

Special Behaviors of Structural Members

4

The mechanical behaviors of the material and basic members presented in the previous chapters mainly deal with the normally working conditions of the reinforced concrete structure, which means that a static load acts monotonically on a specimen within a short time, e.g. several hours, under room temperature. Although these mechanical behaviors represent the main characteristics and generality of the structure, they do not fit well with the structure in engineering practice under various complicated environments and occasional conditions, for example:

- Non-statically loading vibrations of bridge and industrial building vibration under earthquake, instantaneous action of high-speed load, e.g. explosion, impact of heavy substance, ...
- Non-monotonically loading fatigue caused under repeated load, load sustained for a long time (years), ...
- Non-room temperature chimney and workshop sustaining high temperature (200—500°C), structure under fire accident, container for extra-low temperature, e.g. -80°C for storage temperature of liquefied petroleum gas, thermal stress caused by hydration heat of cement for a massive concrete structure,

Because the mechanical behaviors and constitutive relations of concrete material vary considerably under these unusual conditions, the special responses of the structure and its member appear differently and should be investigated separately. Only the seismic, fatigue, explosion, and fire resistances of reinforced concrete will be discussed in the following chapters, as space in this book is limited.

In addition, concrete structure has to work continuously for many years under the natural environment and service conditions after being built. As the temperature and humidity change alternately and the harmful environmental media cause physical and chemical erosions, various deterioration, damage, cracks and breaks of the materials will occur on the exterior and interior of the structure, and even its strength reduced. Then, the structure can not be used normally and safely within the predetermined service life, and this is called the failure of durability. This is another special and important problem in engineering practice and will be discussed briefly in the last chapter.

CHAPTER OUTLINE

16.1 Characteristics of structural behavior under earthquake	411
16.2 Ductility under monotonic load.....	413
16.2.1 Concept and expression of ductility	413
16.2.2 Calculation method.....	416
16.2.3 Angular rotation of plastic region	418
16.3 Hysteretic characteristic under reversed load of low cycles	421
16.3.1 General characteristics of hysteretic curves.....	421
16.3.2 Hysteretic curves under various conditions.....	426
16.3.2.1 Content of reinforcement.....	427
16.3.2.2 Compression—strength ratio	427
16.3.2.3 Shearing of short column.....	427
16.3.2.4 Shear wall.....	428
16.3.2.5 Bond-slip between reinforcement and concrete.....	430
16.3.2.6 Beam—column joint	432
16.3.3 Calculation model.....	434

16.1 Characteristics of structural behavior under earthquake

If enormous deformable energy accumulated within a long time in rock stratum of the earth crust releases suddenly, strong vertical and horizontal movements of the local ground are caused, this is an earthquake. The reason for the earthquake may be volcanic eruption, faulting of rock stratum, or ground depression. Usually, each earthquake lasts only a short period, e.g. several seconds or minutes. When the earthquake wave propagates quickly from its focus, of which the position on the ground is the earthquake center, to the surrounding via rock and ground, the foundations and super-structures of buildings there will shake irregularly and deform sharply.

The movement of a structure during earthquake is called seismic response, which includes displacement, velocity, and acceleration. In the meantime, the internal forces (stresses) and deformations result significantly and dynamically in the interior of the structure. When they reach or even exceed the corresponding limit of the structural member or its materials, various failure phenomena will appear to a

certain extent, e.g. cracking of concrete, yielding of reinforcement, obvious residual deformation, local damage, falling down of a member or its pieces, inclination or even collapse of the whole structure.

The ground near the earthquake center shakes violently with high frequency in vertical direction, but relatively weakly in the horizontal direction. Nevertheless, the vertical shake of the ground away from the earthquake center declines quickly and the peak value of vertical acceleration is only about $1/3-2/3$ of that of horizontal acceleration there. Therefore, the horizontal shake is the main factor causing strong responses and failure of structures for most buildings in the seismic area.

When a reinforced concrete structure experiences a strong earthquake, whether or not failure and the damage level of it depend mainly upon the earthquake parameters, including magnitude, intensity of the place located, sustaining period, the distance away from the earthquake center, kind of the ground, and velocity, acceleration (peak value), and characteristic of frequency spectrum of the ground movement, and they also depend upon the structural parameters, including the seismic resistance system, dynamic parameters, self weight, ductilities of the materials and members, detailing of the members and joints, etc.

According to the survey and statistics of damage conditions of concrete structures after earthquakes and the results of various experimental investigations [16-1-16-3,2-23], the main characteristics of the structure under earthquake are as below.

1. Seismic resistance and safety of the structure depend upon not only the static strength of it and its member, but also, to a greater extent, their deformable abilities and dynamic responses. The 'load' acted on a structure during an earthquake has not a definite value like a static one, but is a dynamic inertia action depending upon its acceleration response and its mass. When the structure is deformable and of better ductility, more seismic energy is dissipated and its response or 'load' is obviously reduced during the earthquake, so it is more safe and only slight damage is caused. On the contrary, when a structure is of greater stiffness, strength, and then, self-weight, serious damage or even failure may be caused during earthquakes because of poorer ductility. Therefore, the ductile structure of better seismic resistance is prior designed for the building within earthquake areas.
2. Working after yielding of reinforcement. When the intensity of an earthquake reaches or exceeds slightly that predicted, various damages of different levels will occur but collapse will not happen for the reinforced concrete structure designed following the principle and method of the Chinese Code [16-1]. The damage appearing includes wider cracks of concrete appearing on the critical parts of the members and their joints, part of the reinforcements being yielded, residual deformation of the member being obvious, surface layer of the member locally breaking and spalling off. Therefore, the 'normal' work condition of the structure is in its latter mechanical state, and even enters the descending branch of its strength, when the predicted earthquake occurs.

3. Seismic load acts reversely. The structure shakes reversely in the horizontal direction during an earthquake, and it is equivalent to the horizontal load acting alternately in positive and negative directions. Generally, the seismic load acting on a structure is reversed only several decade times (low cycles) because of the short periods of earthquakes and the damper of the structure itself. Then, the internal forces of the structure, mainly bending moment and shear force and sometimes also axial force and torsion, alternate positively and negatively during earthquakes. Therefore, the hysteretic characteristic of the reinforced concrete member under reversed load has to be investigated properly, and the corresponding model is important for analysis of the structure along the process of an earthquake.
4. Considerable deformation. The considerable deformation, e.g. lateral displacement of a column or wall, of the structure may be induced under an earthquake. This causes unfavorable effects on the structure itself, e.g. secondary ($P-\Delta$) effect and increase in additional bending moment, buckling under compression, overturning, impact between the members on both sides of a construction gap. In addition, the architectural and other non-structural members in the building, e.g. partition wall, decoration, ceiling, glass curtain wall, and elevator track, may also be damaged or failed, and their service functions are lost. Therefore, the total deformation and the relative displacement between adjacent storeys of a structure under an earthquake should be controlled during its designing.

16.2 Ductility under monotonic load

16.2.1 Concept and expression of ductility

Various mechanical responses of the structure and its members and materials appear successively during different loading stages, such as elastic deformation, initiation and development of plastic strain, appearing and spreading of concrete crack, yielding and entering hardening zone of reinforcement, neutral axis drifting on section, crushing and spalling off of concrete. When the generalized force–deformation ($F-D$) relations of them are plotted out, e.g. $\sigma-\epsilon$ curve in Fig. 2-7 and $M-1/\rho$ curve in Fig. 11-1, the geometrical characteristics corresponding to these responses should be formed on the curves. Therefore, the shape and variation of the force–deformation curve shows apparently the macroscopic behavior of the structure or its material.

The generalized force–deformation ($F-D$) relation has a particular physical concept and corresponding curve shape for different objects discussed, for example:

- Materials: stress–strain ($\sigma-\epsilon$) curves of concrete under compression (Fig. 2-7) and tension (Fig. 2-22), tensile curve of reinforcement (Fig. 6-4), bond–slip ($\tau-s$) curve between reinforcement and concrete (Fig. 7-7 and 7-8);
- Sections of structural member: bending moment–curvature ($M-1/\rho$) curve of flexural member (Fig. 11-1), torsion–twisted angle ($T-\theta$) of torsional member (Fig. 15-6);

- Structural members: load—deflection at mid-span ($P-w$) of beam, load—angular rotation ($P-\theta$) at support, axial force—deformation ($N-\delta$) of column, axial force—lateral displacement at mid-height ($N-w$) of column under eccentric compression, shear force—deflection at mid-span ($V-w$) of beam;
- Structures: horizontal load—lateral displacement at top floor ($P-\Delta$) and horizontal load—relative displacement between adjacent storeys ($P-\delta$) of shear-wall or frame structure.

All of these force—deformation ($F-D$) curves may be generalized into two kinds of typical shapes (Fig. 16-1). One of them shows apparently a peak at the maximum strength and descends suddenly afterwards, while another one shows a long plateau near the maximum strength which does not reduce sharply, even experiencing a considerable deformation. Generally, they are called, respectively, brittle and ductile ones.

The ductile structure used in engineering practice has important advantages:

1. The ductile structure fails slowly with obvious presages, so it works more reliably and safely.
2. When an unpredictable load or situation occurs, e.g. occasional overload, load acting reversely, environmental temperature elevated suddenly, settlement of foundation, and the additional internal forces are induced correspondingly, the ductile structure presents strong bearing ability and resistance.
3. The ductile structure is favorable to achieve fully the redistribution of internal forces for a statically indeterminate structure, so its ultimate strength is increased and the materials used are utilized fully.
4. When a dynamic load, e.g. vibration, earthquake, or explosion, is acted, the ductile structure carries less inertia force and absorbs more dynamic energy, so it damages less and is repaired easier.

Consequently, it is very important to judge if the structure is brittle or ductile. In order to measure and compare the ductility of a structure or material, a quantitative index should be determined. Generally, the ductility or ductility ratio is used and defined as the ratio between the ultimate (D_u) and initially yielding (D_y)

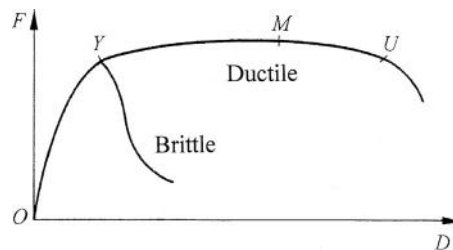


FIG. 16-1 Two kinds of typical force—deformation curves

deformations when the ultimate strength of the structure or material is basically maintained, i.e.

$$\beta_D = \frac{D_u}{D_y} \quad (16-1a)$$

When the generalized deformation (D) is determined as a particular one, the corresponding ductility ratio is obtained, such as ductility ratio of sectional curvature ($\beta_{1/\rho}$), ductility ratio of structural deflection (displacement) (β_w), ductility ratio of angular rotation (β_θ), ..., i.e.

$$\beta_{1/\rho} = \frac{(1/\rho)_u}{(1/\rho)_y}, \quad \beta_w = \frac{w_u}{w_y}, \quad \beta_\theta = \frac{\theta_u}{\theta_y}, \dots \quad (16-1b)$$

It is generally considered that the required ductility ratio is $\beta = 3 - 4$ for the aseismic structures of reinforced concrete.

The characteristic points (Y and U) are determined easily and their values (D_y and D_u) are obtained definitely for an ideal $F-D$ curve (Fig. 16-2(a)), but there is no authentic point for Y and U on a general $F-D$ curve of reinforced concrete. For example, the bending moment—curvature relation of a flexural member is a continuous curve (Fig. 16-2(b)), as it experiences successively elastic stage, cracking of concrete (cr), initial yielding of tensile reinforcement (Y), the maximum strength (highest point M), descending branch, crush and spall off of concrete (U). It is seen that the segment from point Y to M and U is continuous with less variation

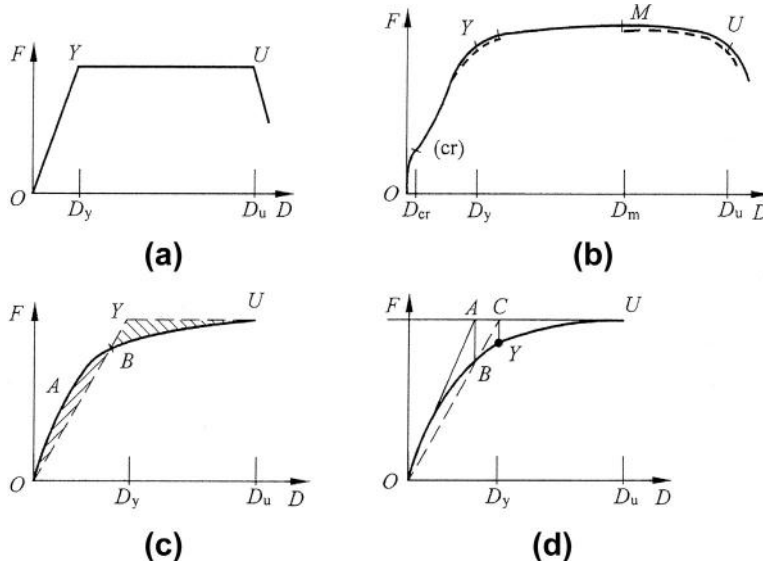


FIG. 16-2 Determinations of initially yielding (Y) and ultimate (U) points: (a) ideal curve, (b) general curve (e.g. $M - 1/\rho$), (c) equal energy, (d) geometrical method

of basic strength, but there is no exact turning point for Y and U . If the values of D_y and D_u are determined by naked eye within certain ranges (dashed lines in the figure), the ductility ratio (β_D) obtained may be rather different.

There is no unified method to determine exactly the initial yielding (Y) and ultimate (U) points on an arbitrary curve till now. The methods used more for determination of the initially yielding point are: (1) equal energy method (Fig. 16-2(c)) drawing a broken line $OY-YU$ to replace the original $F-D$ curve and let total areas under both be equal to each other or area OAB equals area YUB ; (2) geometrical method (Fig. 16-2(d)) drawing successively the horizontal line passing through U , tangent line OA from O , vertical line AB , straight line OBC , and vertical line CY , and Y is assumed to be the initially yielding point and D_y is obtained then.

The methods used more for determination of the ultimate point are: (1) the point corresponding to be maximum strength reduced by 15%, or $F_u = 0.85F_M$ on the descending branch; (2) the point at which compressive strain of the concrete reaches the ultimate value, e.g. $\epsilon_u = 3 \times 10^{-3} - 4 \times 10^{-3}$.

Other methods are also used for determination of the characteristic points (Y and U) or values (D_y and D_u), for example: examining the shape of the $F-D$ curve and estimating by the naked eye; calculating increasing rate of the deformation increment (ΔD) for constant force increment (ΔF) and deciding. However, it should be noticed that various methods used for determinations of D_y and D_u for the same $F-D$ curve certainly give different values of ductility ratio.

16.2.2 Calculation method

The ductility ratio has to be tested and measured particularly for a complicated structure or special member, while it can be calculated following the method and formula demonstrated for a simple beam or column used widely.

When the section and reinforcements of an eccentrically compressed member are known in advance, the strain distributions on the section at initial yielding of the tensile reinforcement (ϵ_y) and at ultimate strain of compressed concrete (ϵ_u) can be calculated following the general method for sectional analysis (see Section 11.3) and shown in Fig. 16-3. The sectional curvatures are respectively

$$\left(\frac{1}{\rho}\right)_y = \frac{\epsilon_y}{h_0 - x_y} = \frac{f_y}{E_s h_0 (1 - \xi_y)}$$

$$\left(\frac{1}{\rho}\right)_u = \frac{\epsilon_u}{x_u} = \frac{\epsilon_u}{\xi_u h_0},$$

and the ductility ratio is

$$\beta_{(1/\rho)} = \left(\frac{1 - \xi_y}{\xi_u}\right) \frac{\epsilon_u E_s}{f_y}, \quad (16-2)$$

where ξ_y and ξ_u are the relative depths of compression zones on section, respectively, at initial yielding of reinforcement and ultimate strain of compressive concrete, following the basic assumptions and formulas introduced in Section 11.3.

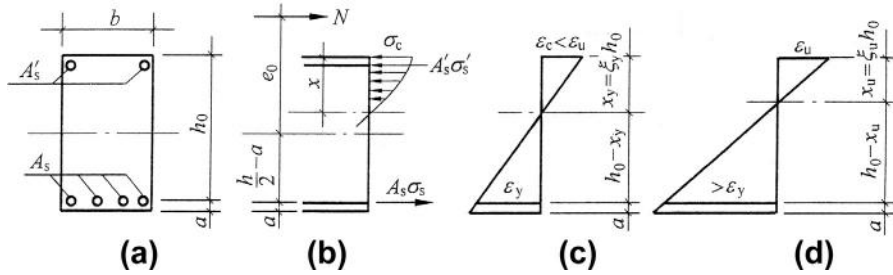


FIG. 16-3 Calculation of sectional ductility ratio for an eccentrically compressed member: (a) section and reinforcements, (b) load and stress distribution, (c) strain distribution at yielding of reinforcement, (d) strain distribution at ultimate strain of concrete

Determining load and internal forces of a structural member and bending moment—curvature ($M-1/\rho$) relation of its section, the deformations at initial yielding of reinforcement and ultimate state, e.g. deflections w_y and w_u , angular rotation θ_y and θ_u , can be calculated based on the principle of virtual work (see Section 13.3.1), and the corresponding ductility ratios (β_w, β_θ) are obtained easily (Eq. (16-1).)

The ductilities of various reinforced concrete members have been experimentally investigated in China [16-4–16-6] since the 1970s. The main results including main parameters of wide range: compressive strength of concrete $f_c = 16 - 130 \text{ N/mm}^2$, strength grades of reinforcement I, II, III, and IV, content of reinforcement $\mu = 0.48 - 4.84\%$, and relative compressive depth of section $\xi = 0.03 - 1.133$, are given in reference [16-4]. In addition, the empirical formulas related are suggested there.

If the ultimate deformation (D_u) of a structural member is taken as that at the maximum strength (D_M), the sectional curvatures at initially yielding (Y) and ultimate (U) points can be calculated separately by the regression formulas below:

$$\left(\frac{h_0}{\rho}\right)_y = \varepsilon_y + (0.45 + 2.1\xi) \times 10^{-3} \quad (16-3)$$

$$\left(\frac{h_0}{\rho}\right)_u = \varepsilon_u + \frac{1}{35 + 600\xi} (\xi < 0.5) \quad (16-4a)$$

$$\text{or } = \varepsilon_u + 2.7 \times 10^{-3}, (0.5 \leq \xi < 1.2) \quad (16-4b)$$

in which the maximum strain of concrete on compression zone at the ultimate state is

$$\varepsilon_u = (4.2 - 1.6\xi) \times 10^{-3} \quad (16-5)$$

and ξ is the relative depth of compression zone at ultimate state, assuming rectangular stress block there ($\beta x_u/h_0$ in Fig. 11-13(d)).

Correspondingly, the regression formulas suggested for calculations of ductility ratios of sectional curvature and deflection and angular rotation of a member are respectively:

$$\beta_{(1/\rho)} = \frac{1}{0.04 + \xi} (\xi \leq 0.8) \quad (16-6)$$

$$\text{and } \beta_w = \beta_\theta = \frac{1}{0.045 + 1.75\xi} (\xi \leq 0.5) \quad (16-7a)$$

$$\text{or } = 1.1 (\xi > 0.5). \quad (16-7b)$$

Obviously, the ductility ratios of the deflection and angular rotation are smaller than those of sectional curvature of the same structural member, i.e. $\beta_w \approx \beta_\theta < \beta_{(1/\rho)}$.

Based on the experimental results and calculation model (Fig. 16-4) and formulas presented above, the influences of main factors on the ductility ratio of structural member may be concluded below. (1) When the content of tensile reinforcement ($\mu = A_s/bh_0$) and the axial compression or compression—strength ratio (N/f_cA) are increased, the ductility ratio decreases as the relative compressive depth at ultimate state (ξ) is increased; (2) When the reinforcement in compression zone (or $\mu' = A'_s/bh_0$) and the strength of concrete (f_c) are increased, the ductility ratio increases as the relative compressive depth at ultimate state is reduced; (3) When the yield strength of tensile reinforcement (f_y) is increased, the yield curvature $\left(\frac{1}{\rho}\right)_y$ is increased as well but the ductility ratio (Eq. 16-1b) is reduced. In addition, if the stirrups are set up closely and the confined concrete is formed in a structural member, the ductility ratio may increase considerably with the ultimate strain of compressed concrete (ϵ_u).

A series of measures of calculation and detailing are provided in the Chinese Code [2-1,16-1] to satisfy the necessary ductility for reinforced concrete member of an aseismic structure [16-7,16-8], although no definite value of ductility ratio required is assigned. For example, ‘column being stronger than beam’, ‘shear resistance being higher than bending resistance’, and ‘joint being stronger than member’ are desired in principle during design, and brittle failure should be avoided during earthquake; the compressive depth on section at ultimate state (ξ), compression—strength ratio (N/f_cA), content of reinforcement (μ), and reinforcement of high-strength should be limited in a certain range; the minimum content of reinforcement (μ_{\min}) should be increased, the anchorage length of reinforcement should be extended, and more stirrups should be set up, etc.

16.2.3 Angular rotation of plastic region

When a reinforced concrete beam is acted with load and the maximum bending moment caused is greater than the yield one but is less than the ultimate one ($M_y \leq M < M_u$), the tensile reinforcement reaches or keeps the yield strength and a plastic region is formed within the length of ($l_{pl} + l_{pr}$) on both sides of the

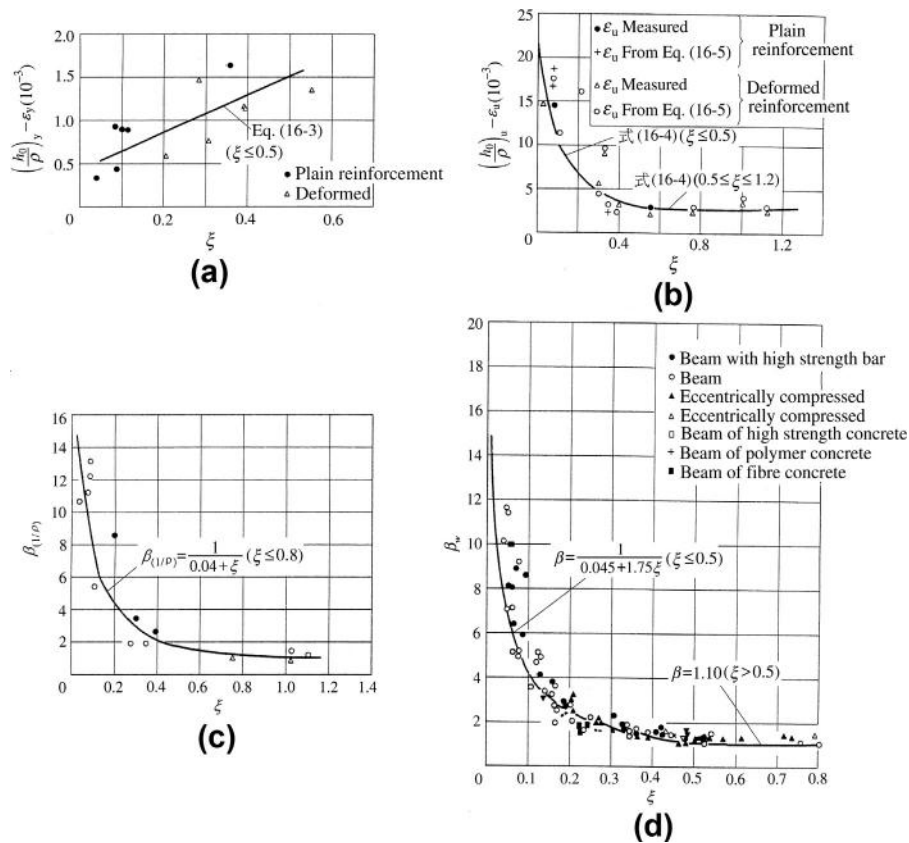


FIG. 16-4 Experimental results for ductility of an eccentrically compressed member [16-4]: (a) curvature at yielding of reinforcement, (b) ultimate curvature, (c) ductility ratio of curvature, (d) ductility ratio of displacement

maximum bending moment (Fig. 16-5). The sectional curvature in this region is far greater than that of the other section and a local angular rotation should appear there ($\theta_p = \theta_c$). This is also called the angular rotation of a plastic region (or hinge).

The length and angular rotation of the plastic region surely increase with the load and corresponding maximum bending moment. When the ultimate load or bending moment (M_u) of the member is reached, the ultimate (θ_u) is obtained.

After the plastic rotation is formed in a reinforced concrete structure of one-dimensional members, the deformation is significantly increased as a direct consequence. For example, a rotated displacement occurs at the top of a cantilever member ($\theta_p l$, Fig. 16-5(b)); the total displacement and relative displacement between adjacent floors of a frame structure are induced after plastic rotations appear on bottom of the columns. These additional displacements may cause serious $P-\Delta$

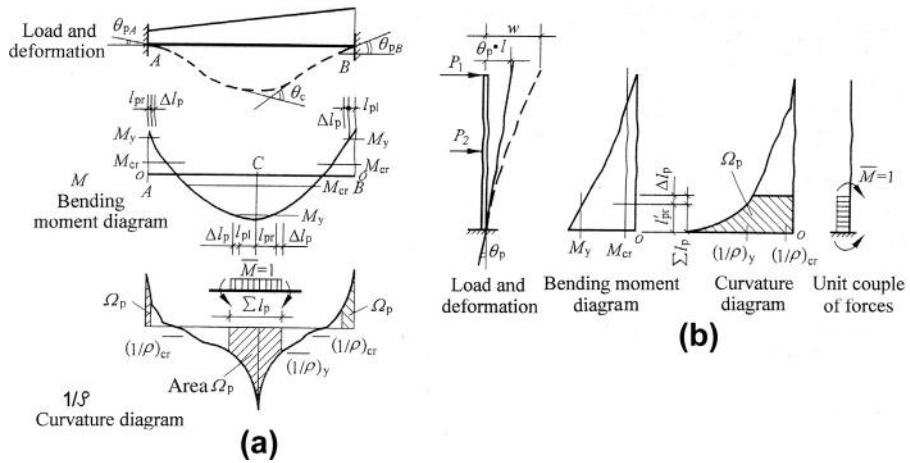


FIG. 16-5 Region of plastic deformation and angular rotation: (a) fixed-end beam acted with distributed load, (b) cantilever acted with concentrated loads

effect for column and wall, and the ultimate strength of the structure is reduced considerably. On the contrary, appearance and development of the plastic rotation advance favorably redistribution of internal forces for a statically indeterminate structure, and the ultimate angular rotation is necessary for checking calculation of whether the internal forces are fully redistributed.

The angular rotation of plastic region (θ_p) and ultimate angular rotation (θ_u) of a member can be calculated as below based on the principle of virtual work (see Section 13.3). A pair of couple of forces ($\bar{M} = \pm 1$) are assumed to be acted oppositely on both sides of the plastic region (Fig. 16-5), the area of curvature diagram ($1/\rho$) within the plastic region (Ω_p) is the plastic angular rotation:

$$\theta_p = \Omega_p, \quad (16-8)$$

according to the basic equation (Eq. (13-26)) established. However, the bending moment (M), length of plastic region (l_p), and bending moment—curvature relation ($M - 1/\rho$) of the member have to be known in advance. Similarly, the ultimate angular rotation (θ_u) is also obtained from the corresponding bending moment diagram and others at ultimate state.

The length of plastic region (l_p) of a member depends mainly upon the shape of the bending moment diagram and the value of the maximum bending moment ($M > M_y$) acted. If the lengths of the plastic region on the left and right sides of the section with the maximum bending moment are respectively l_{pl} and l_{pr} , and the nearby slipping regions (Δl_p) of the reinforcement caused after yielded should be added, so the total length of plastic region is

$$l_p = l_{pl} + l_{pr} + \Delta l_{pl} + \Delta l_{pr}. \quad (16-9)$$

Generally, the concept of equivalent length of the plastic region (or hinge) is used for simplifying calculation, and the sectional curvature ($1/\rho$) within the length is assumed to be a constant and is determined by the maximum bending moment there ($M > M_y$). When the equivalent length on each side of the maximum bending moment is l_p , the plastic angular rotation of the member will be:

$$\text{at mid-span or middle support} \quad \theta_p = \frac{2l_p}{\rho}, \quad (16-10a)$$

$$\text{at fixed end} \quad \theta_p = \frac{l_p}{\rho}. \quad (16-10b)$$

Similarly, the ultimate rotation should be correspondingly

$$\theta_u = \frac{2l_p}{\rho_u} \text{ or } \frac{l_p}{\rho_u}. \quad (16-11)$$

According to the statistics of experimental data of China [16-4], the equivalent length of plastic region (hinge) ranges

$$l_p = (0.2 \sim 0.5) h_0 \quad (16-12)$$

and the average value is about $l_p = h_0/3$. Various empirical formulas are also suggested by the researchers abroad, for example:

$$\text{Corley [16-9]} \quad l_p = 0.5h_0 + 0.2 \frac{z}{\sqrt{h_0}}, \quad (16-13a)$$

$$\text{Mattock [16-10]} \quad l_p = 0.5h_0 + 0.05z, \quad (16-13b)$$

$$\text{Sawyer [2-22]} \quad l_p = 0.25h_0 + 0.075z, \quad (16-13c)$$

where z is the distance from the section with the maximum bending moment to that with zero or support.

In addition, the empirical formula of the ultimate angular rotation (in radian) is also suggested in reference [16-4] (Fig. 16-6):

$$\theta_u = \frac{1}{65 + 1000\xi} (\xi \leq 0.5), \quad (16-14)$$

where ξ is the same as in Eq. (16-5).

16.3 Hysteretic characteristic under reversed load of low cycles

16.3.1 General characteristics of hysteretic curves

When the structure works under the seismic load during an earthquake, the internal forces also alternate positively and negatively (Fig. 16-7(a)), so the mechanical behavior should be investigated from the corresponding experiment under reversed

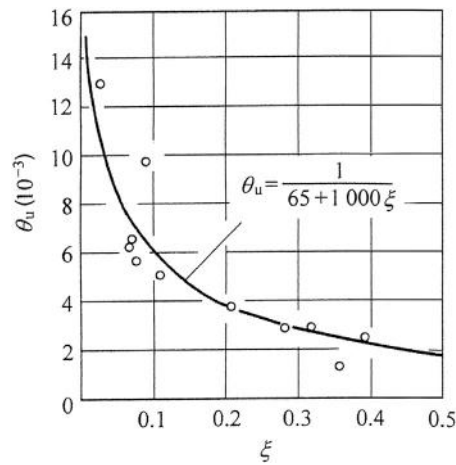


FIG. 16-6 Ultimate angular rotation [16-4]

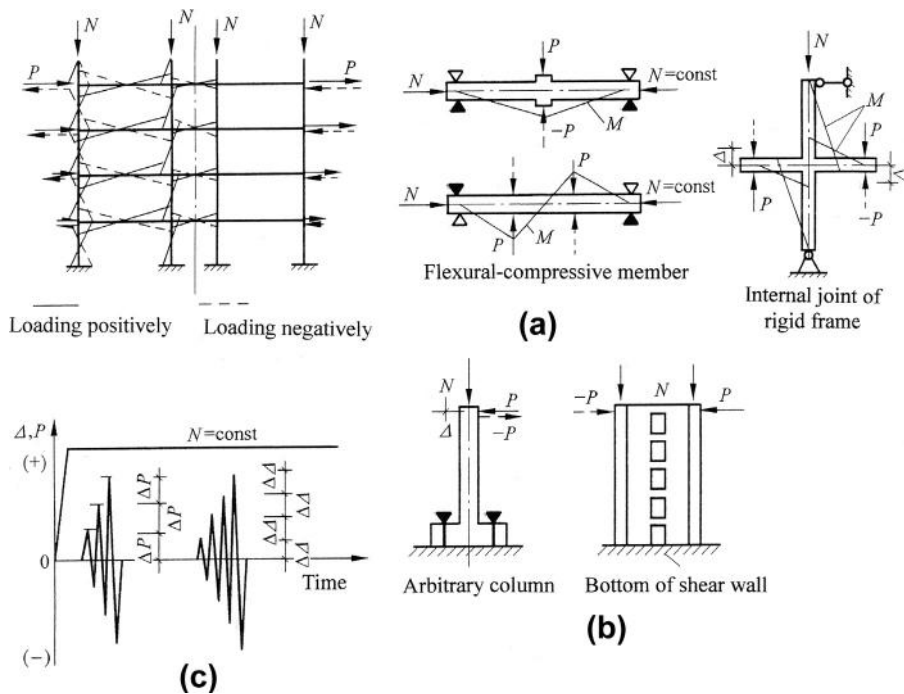


FIG. 16-7 Test of specimen under reversed load of low cycles: (a) load and internal force of frame structure, (b) tests of structural members and joints, (c) loading procedure

load of low cycles [16-11,16-12]. The model of the whole structure may be tested on a shaking table fed with various seismic waves, or the pseudo-dynamic test controlled by computer or on-line computer test is conducted on it to simulate the process of an earthquake. However, more frequently only the critical part of the structure, e.g. a column, a beam, a joint, or a part of rigid frame or shear-wall (Fig. 16-7(b)) is tested, and the prototype or its model on a certain scale is used and manufactured. Usually, the specimen is loaded statically but the internal forces are similar to that happening during an earthquake. For example, the axial force (N) is loaded first on the specimen and keeps constantly; the transverse loads are then acted reversely with equal increments (ΔP); after the reinforcement is yielded, the transverse loads are controlled by equal increments of displacement ($\Delta \Delta$) until failure of the specimen (Fig. 16-7(c)).

A hysteretic curve ($P-\Delta$) measured from the test of reinforced concrete member under compression and bending is typically shown in Fig. 16-8, and the orders of positively ($+P$) and negatively ($-P$) loadings are represented respectively by the odd and even numbers. The shape of the hysteretic curve shows the aseismic characteristics of the member as below.

Although the cracks of tensile concrete and the plastic strain of compressive concrete of the member appear already before yielding of the tensile reinforcement, the deformation (Δ) is limited and the slope of $P-\Delta$ curve varies slightly in this stage, so the residual deformation after each unloading is less and the hysteretic loop composed after each positively-and-negatively loading cycle does not reveal obviously. However, the mechanical behavior at this stage is not the key characteristic for an aseismic structure.

As the reversed load is acted continuously after yielding of the reinforcement, the tensile cracks of concrete expand and extend gradually and tensile strain of the

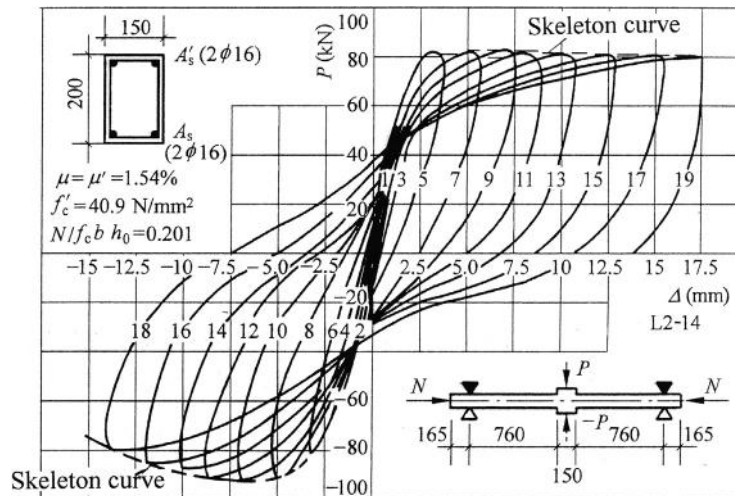


FIG. 16-8 Hysteretic curve of member under compression and bending [16-11]

reinforcement and compressive strain of the concrete increase and accumulate after each loading cycle, so the total deformation (Δ) increases considerably but the strength (P) changes less. In addition, some features are presented on the loading and unloading curves as below.

Loading curve. The slope decreases gradually as the load (P) increases within each loading curve; the slope of the loading curve is less than that of the previous one in the same direction, i.e. positively or negatively loading, and this shows the stiffness degradation of the member after reverse loading; a contra flexure appears on the loading curve after the load is reversed several times, and this is called the pinch effect (Fig. 16-9), of which the level gets more serious after successively loading.

Unloading curve. The unloading curve is rather sharp and the recovered deformation (Δ) of the member is less at the beginning; the recovered deformation increases gradually as the load is decreased, and this is called the delay of recovered deformation; the slope of the unloading curve decreases as the reversely loading cycle increases, and this also shows the stiffness degradation of the member under reverse unloading; the residual deformation exists obviously after totally unloading ($P = 0$) and accumulates successively after every loading—unloading cycle.

The hysteretic loop of load—deformation ($P-\Delta$) of a structure or its member obtained after each cycle of positively and negatively loading-and-unloading shows different shapes (Fig. 16-9), including (1) a closed diamond with parallel sides for the member of an ideal elasto-plastic material and (2) a convex curve for loading but a straight line for unloading for the Bauschinger material. However, the hysteretic loop is generally an olive (3) or pinch (4) for the reinforced concrete structure and its members, and its plentiful or pinch level depends mainly upon different internal forces, materials used, content of reinforcement, and cycles of load reversed.

The pinch effect appears frequently on the hysteretic loops of reinforced concrete structures, especially after total deformation occurs considerably at a later stage.

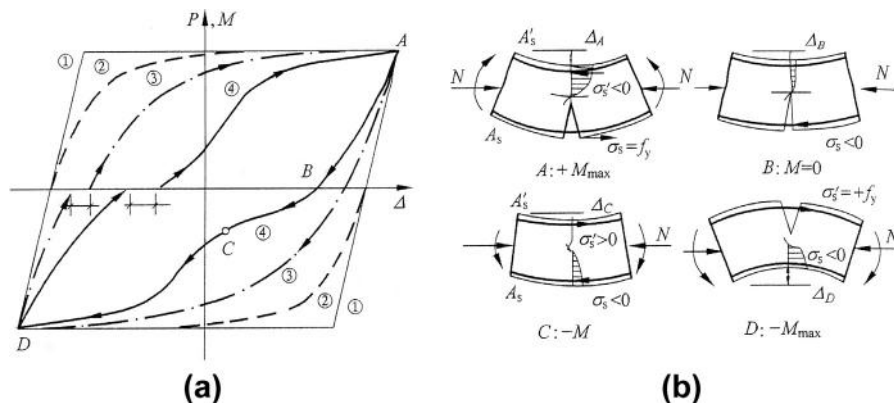


FIG. 16-9 Shapes of hysteretic loop and pinch effect: (a) shapes of hysteretic loop, (1) diamond, (2) Bauschinger, (3) olive, (4) pinch, (b) stress state, deformation, and crack

A reinforced concrete member acted with axial compression and bending moment (Fig. 16-9(b)) is used as an example to explain the pinch effect. When the maximum bending moment in the positive direction ($+M_{\max} > M_y$) is reached, i.e. at point A on the hysteretic loop, the tensile reinforcement near the bottom (A_s) is yielded already and the plastic strain appears considerable, so the crack in the concrete there expands widely and the bond nearby fails and relative slip occurs between the reinforcement and adjacent concrete; after the load (P) is totally released ($M = 0$) but the axial compression (N) is maintained, i.e. at point B on the hysteretic loop, the residual deformation ($\Delta_B > 0$) exists and the crack does not close yet, and the residual stress is compressive ($\sigma_s < 0$) but the residual strain is tensile for the reinforcement near the bottom (A_s), while both residual stress and strain are compressive for the concrete on the upper part of the section; when the load ($-P$) is acted in a negative direction ($M < 0$), the concrete and reinforcement (A'_s) on the upper part of the section turn gradually to tension from compression while the reinforcement near the bottom (A_s) is yielded with no concrete there, carries compression, so the deformation of the member (Δ) increases quickly and the $P-\Delta$ curve is flattened; when the reinforcement near the bottom (A'_s) is yielded compressively and the crack there is closed gradually, so the concrete there starts to be compressed and the increasing rate of the deformation (Δ) is slowed down or the slope of the $P-\Delta$ curve is increased, then a contra flexure, i.e. point C, is formed on the curve; when the negative load is increased further, the plastic strain of concrete (on the lower part of the section) under compression is increased while the reinforcement on upper part of the section (A'_s) is yielded tensely and the concrete there is cracked, so the stiffness of the member is reduced again and the deformation (Δ) turns to a negative one from a positive one; as the bending moment reaches the minimum (or $-M_{\max}$, at point D), the tensile crack expands widely and the reinforcement (A'_s) is yielded with considerable slip on the upper part of the section. This is, in brief, the process of a pinch effect for a reinforced concrete member.

Accordingly, the level of pinch effect of hysteretic curve for a reinforced concrete member depends mainly upon the crack width expanded of the tensile concrete, elongated strain of reinforcement, relative slip between reinforcement and adjacent concrete, accumulation of residual (plastic) strain of compressed concrete, and variation of neutral axis on section. The slope of the diagonal line (line AD or from $+M_{\max}$ to $-M_{\max}$) represents the total stiffness of the member, and the area surrounded with the hysteretic loop shows the energy dissipation by the member experiencing one cycle of positive and negative loading-and-unloading. Apparently, the hysteretic loop of more fullness is favorable for the aseismic structure.

If the peak points of all cycles of reversed loading-and-unloading are linked successively, the corresponding skeleton curve is obtained (Fig. 16-8). When the skeleton curve is compared with the load-deformation ($P-\Delta$) curve measured from the monotonically loading test of the specimen with similar parameters [16-11], both shapes are similar to each other and the variation regularities of various indices of them are also similar but with different values (Fig. 16-10): the maximum (ultimate) strength reduces by no more than 10%, the yielding and ultimate

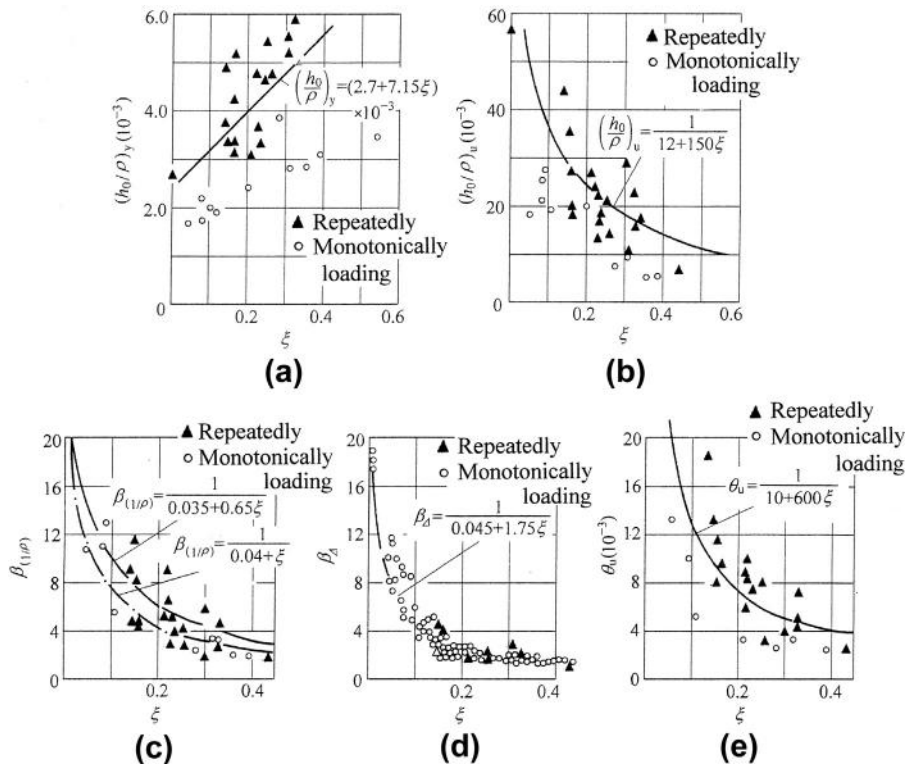


FIG. 16-10 Comparison of behavior indices between skeleton curve under reversely loading and load-deformation curve under monotonic loading: (a) yielding curvature, (b) ultimate curvature, (c) ductility ratio of curvature, (d) ductility ratio of displacement, (e) ultimate angular rotation

curvatures $((1/\rho)_y$ and $(1/\rho)_u$) increase greatly but the ductility ratios of curvature and displacement ($\beta_{(1/\rho)}$ and β_Δ) increase slightly, and the ultimate (plastic) angular rotation (θ_u) increases obviously. These differences result due to the reasons, such as: alternative changes of tensile and compressive stresses in concrete and reinforcement, alternative opening and closing of concrete cracks, alternative changes of the direction of bond stress between reinforcement and adjacent concrete, and bond failure and residual deformation accumulated continuously, as the member is acted with reversely loading-and-unloading many times.

16.3.2 Hysteretic curves under various conditions

The hysteretic curve of reinforced concrete members or joints under action of various load or internal forces varies with its section, materials, reinforcements, and detailing, and some examples are introduced below.

16.3.2.1 Content of reinforcement

The hysteretic curve shown in Fig. 16-8 is measured from the test of a symmetrically reinforced concrete member with contents of the reinforcements ($\mu = \mu' = 1.54\%$), whereas the hysteretic curves measured from the members with different contents of reinforcements ($\mu = \mu' = 0.467\%$ and 2.54%) are respectively shown in Fig. 16-11. It is easily seen that the hysteretic characteristic and ductility of the member is apparently improved for the member with greater content of reinforcement ($\mu = \mu'$). For example, the area surrounded by each hysteretic loop, i.e. the capacity of energy dissipation, is increased, the pinch effect is released, and the stiffness is increased. Of course, these are favorable for seismic resistance of the structure.

16.3.2.2 Compression—strength ratio

The compression—strength ratio of the member shown in Fig. 16-8 is $n = N/f_c b h_0 = 0.201$, and the hysteretic curves measured from the members with greater ($n = 0.367$) and smaller ($n = 0$) compression—strength ratios are shown respectively in Fig. 16-12. As the specimen (L2-13) is a flexural member with zero compression ($N = 0$), its hysteretic curve is more plump and the skeleton curve does not descend even after the concrete is failed locally under compressive stress caused by bending moment, because the reinforcements on upper and lower parts ($A_s = A'_s$) of the section still sustain together the bending moment. So the ductility of the flexural member is the best among these members. However, the specimen (L2-21) is tested under higher compressive—strength ratio, serious pinch effect appears on the hysteretic curve after a few cycles of reversely loading and the skeleton curve descends soon after the peak point, so it shows poor ductility.

16.3.2.3 Shearing of short column

When a short column is acted together with a shear force (V), axial force (N), and bending moment (M) and the shearing failure (Chapter 14) is finally resulted, the

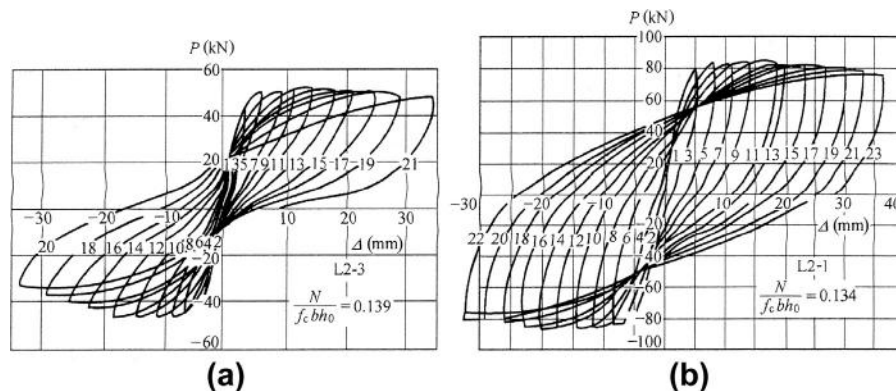


FIG. 16-11 Hysteretic curves of load—deformation of a member with different contents of reinforcement [16-11]: (a) $\mu = \mu' = 0.467\%$, (b) $\mu = \mu' = 2.54\%$

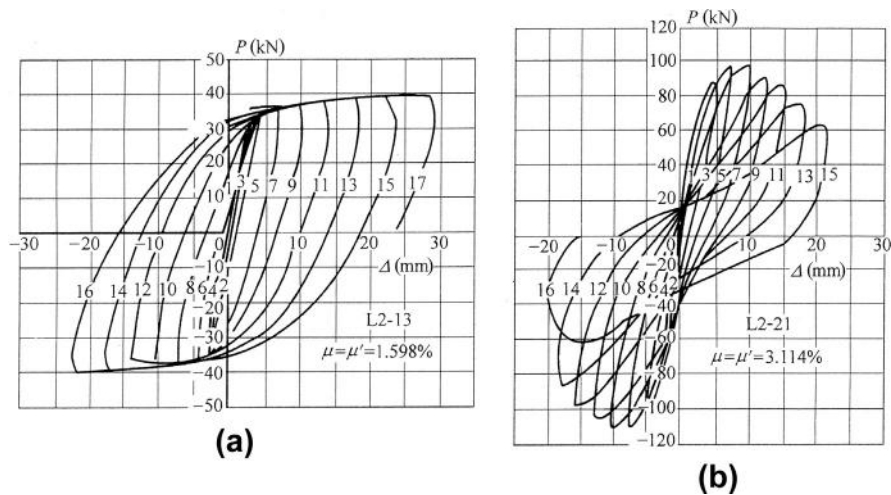


FIG. 16-12 Hysteretic curves of load—deformation of members with different compression—strength ratios [16-11]: (a) $n = N/f_c b h_0 = 0$ ($\xi = 0$), (b) $n = N/f_c b h_0 = 0.367$ ($\xi = 0.419$)

typical hysteretic curve and skeleton curve of load—deformation measured are shown in Fig. 16-13. Actually, the yielding point, in physical meaning, does not exist for this kind of failure of reinforced concrete member. However, the nominally yielding point and corresponding values can still be determined (see Fig. 16-2) properly based on shape of the skeleton curve, and the ductility ratio is calculated accordingly.

When the load (P), i.e. shear force and bending moment, is acted reversely and increased successively after the axial compression (N) is acted in advance and keeps constant, the cracks of X shape appear and develop on the member and the pinch effect is presented much more obviously on the hysteretic curve. In addition, the member fails and the skeleton curve drops suddenly with poor ductility ratio. Generally, the ultimate strength of the member under reversely loading is less by 10–15% than that under monotonic loading. The hysteretic characteristic of the member is even poorer, if the member is of smaller shear—span ratio (a/h_0), greater compression—strength ratio ($N/f_c b h_0$), and less content of stirrup. On the contrary, the hysteretic characteristic of the member gets to be improved.

16.3.2.4 Shear wall

A shear wall or coupled shear walls with many openings may not work differently from a vertical cantilever (column). However, the sizes and positions of the openings dominate the mechanical behavior and failure pattern of the coupling beams and walls, and have considerable influence on the hysteretic curve. There are two examples in Fig. 16-14 showing the hysteretic curves of horizontal load—lateral

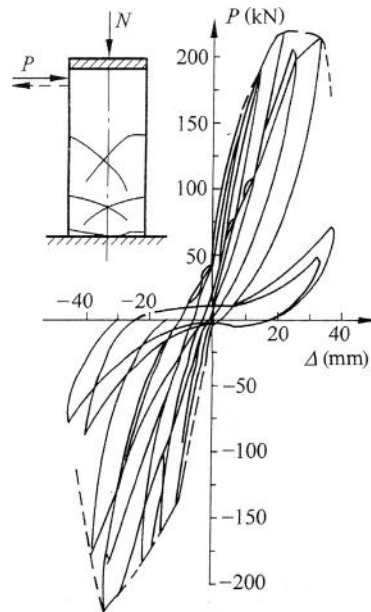
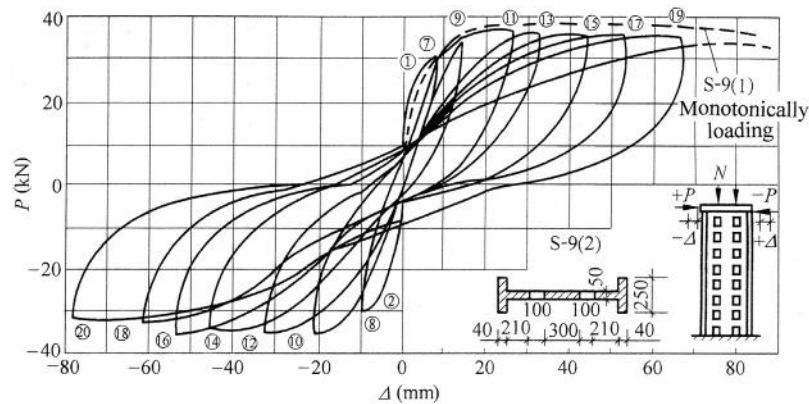


FIG. 16-13 Hysteretic curve of short column under shear failure [16-12]

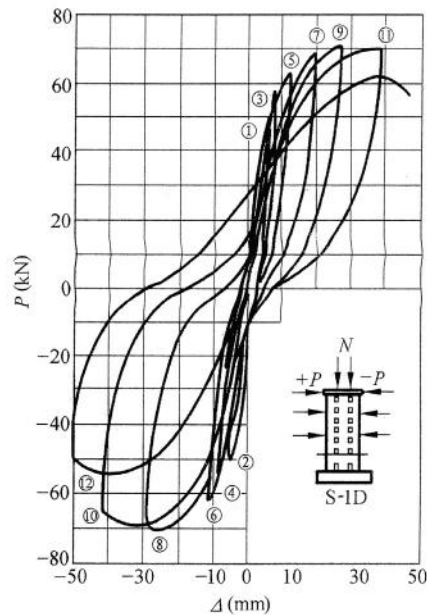
displacement ($P-\Delta$) for the shear wall with openings. The differences between the hysteretic curves and skeleton curves of both shear walls are closely related to the failure process and pattern.

The specimen S-9(2) is of shear-span ratio $a/h_0 = 2.42$ and is acted reversely with a horizontal load (P) at the top besides the vertical compression ($N = \text{const.}$). A flexural crack appears first at the end of a coupling beam, and then several flexural cracks occur horizontally and successively at the bottom and above on the wall. When the tensile reinforcement of the wall is yielded and a plastic hinge is formed at the bottom, the lateral displacement at the top (Δ) increases considerably but the strength (or load) varies slightly, so the skeleton curve bends gently and better ductility is presented apparently. Finally, the compressive concrete on the bottom is crushed and the wall fails in flexural pattern, as the plastic hinge there deforms reversely under positive and negative bending moments.

Another shear wall (S-1D) is acted reversely with three horizontal loads on one side distributed like a reversed triangle, and the generalized shear-span ratio is only 1.38. As the loads (P) are increased after each cycle, a flexural crack appears horizontally first on the bottom of the wall and then the tensile reinforcement there is yielded. Afterwards, an inclined critical crack forms on the lower part of the wall and the wall fails suddenly in shear pattern near the first floor, so the strength reduces, or the skeleton curve descends, immediately with poor ductility.



(a)



(b)

FIG. 16-14 Hysteretic curves of load–displacement at the top of shear walls with openings [16-13]: (a) flexural failure, (b) shearing–flexural failure

16.3.2.5 Bond-slip between reinforcement and concrete

When a reinforced concrete member is acted reversely with positive and negative bending moments during an earthquake, the longitudinal reinforcement in it certainly sustains reversed compression and tension. The hysteretic curve of bond stress–slip (τ – s) shown in Fig. 16-15(a) is measured from the test of a bonded

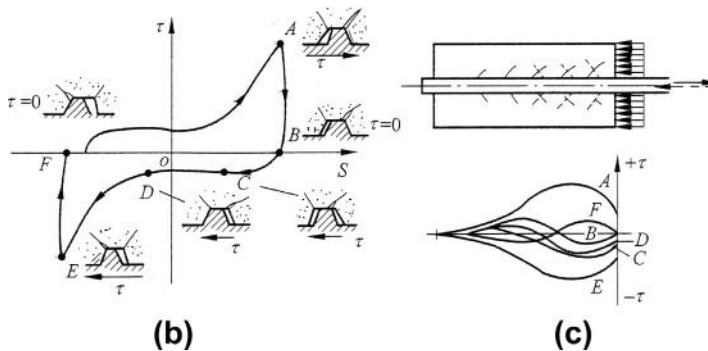
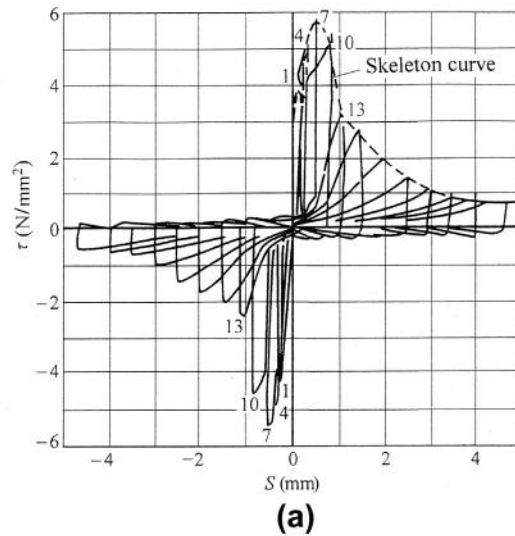


FIG. 16-15 Hysteretic curve of bond stress—slip: (a) hysteretic curve [16-14], (b) deformation and crack of concrete near transverse rib on surface of reinforcement [1-1], (c) cracks and distribution of bond stress [1-1]

reinforcement under reverse loadings of tension and compression. The skeleton curve obtained is similar to the $\tau-s$ curve measured from the test of monotonically loading (Fig. 7-10), but the average bond strength (τ_u) of a deformed reinforcement obtained is reduced by about 14%. In addition, the bond strength of a plain reinforcement is reduced seriously under reversely loading, so the plain reinforcement is not recommended to be used in an aseismic structure.

The pinch effect found on the hysteretic curve of bond stress—slip ($\tau-s$) between reinforcement and concrete is more serious than that appearing for a general structural member (e.g. Figs 16-11—16-14): the unloading line of every cycle almost runs parallel with the ordinate and the recovered slip is few even the bond stress is totally released ($\tau = 0$); when the specimen is loaded oppositely and the bond stress reaches

about $\tau = 0.2\tau_{\max}$, the residual slip recovers totally and the opposite slip then appears considerably, so a long plateau is presented obviously; afterwards, the slip increases with the bond stress.

The formation of the slip plateau on the hysteretic curve is a successive process (Fig. 16-15(b)): when the specimen is loaded positively, e.g. towards the right, until the maximum bond stress (τ_{\max} , point A) of one cycle, the concrete in front of the transverse rib of the reinforcement is crushed locally and an inclined internal crack appears and develops near the tip of the rib, while a gap exists behind the left side of the rib (Fig. 7-9); when the specimen is unloaded (AB), an opposite friction is acted on the reinforcement, so the reversed deformation is small and the inclined crack will not change; when the specimen is loaded reversely, i.e. towards the left, the deformation of concrete and the slip of the reinforcement are recovered gradually (BC); after the friction on surface of the reinforcement ($\approx 0.2\tau_{\max}$) is overcome, the rib of the reinforcement moves towards the left and a slip plateau (CD) appears gradually; when the rib of the reinforcement passes the gap and reaches and compresses the concrete on the left side, the stress is increased (DE) and the inclined crack expands gradually near the left tip of the rib, while the inclined crack near the right tip of the rib is closed. When the specimen is unloaded and reloaded reversely again, the process is repeated similarly.

As a bonded reinforcement is acted reversely with tension and compression, the transverse ribs on its surface move reversely and compress alternately the concrete on both sides, then the crushed areas and the inclined cracks develop gradually. In the meantime, the damaged area extends inside from the loading end, or the cracking section of a member, and the inclined cracks of X shape appear successively in the interior of the member (Fig. 16-15(c)). In addition, the distribution of bond stress on the surface of the reinforcement varies correspondingly, as the tensile and compressive loads change alternately and the local damage is accumulated continuously. Therefore, the bond behavior between reinforcement and adjacent concrete in a structural member is obviously deteriorated under reversely loading.

16.3.2.6 Beam—column joint

The joint connecting beams and columns in a reinforced concrete frame structure is an important part during an earthquake, because the maximum values of shear force and bending moment happen together and the damage is easily resulted there under seismic load, and additional damage or even collapse of the structure may be caused after its failure. Therefore, the joint should be designed carefully, and the principle of 'joint being stronger than members' is usually followed, according to the Chinese design code [16-1]. There are various joints, including middle, side, and corner joints, connected with different beams and columns in the frame, and they have to be investigated separately under reversely loading of low cycles [16-15–16-19]. A hysteretic curve of load—displacement at the beam end measured from a middle joint in a frame structure is shown in Fig. 16-16(a) as an example.

The core zone of a joint works under multi-axial stress state, as the axial forces, bending moments, and shear forces are acted simultaneously at ends of the beams

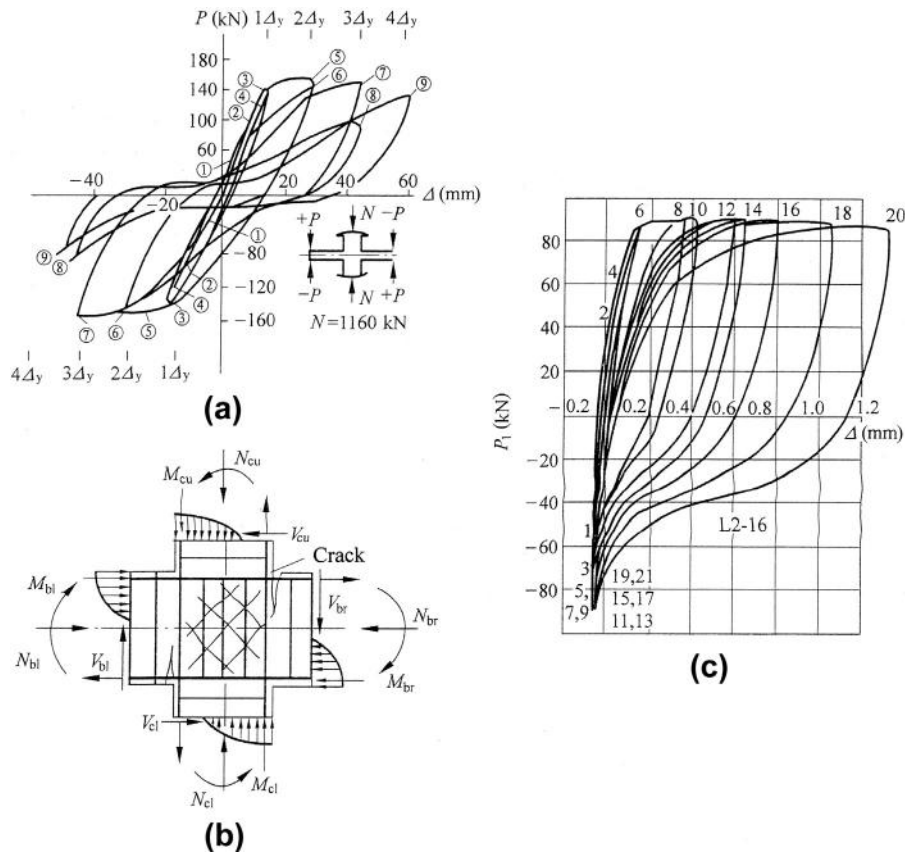


FIG. 16-16 Hysteretic curve and mechanical condition of beam-column joint: (a) hysteretic curve [16-12], (b) mechanical condition of middle joint, (c) hysteretic curve of reinforcement deformation on outer layer of joint [16-11]

and columns connected (Fig. 16-16(b)). The stress of concrete there is approaching that calculated elastically and the stress of stirrups there is rather low before cracking of concrete. When the load is increased and 60–70% of the strength of the joint is reached, a diagonal crack appears within the core zone and the stress of stirrups there increases suddenly. As the load is increased further and acted reversely for several times, two series of diagonal cracks crossing each other are formed and expand continuously, and the stirrups there are yielded successively. In the meantime, the longitudinal reinforcements in beams and columns are yielded tensely and the plastic hinges are formed near their ends, and the slipping areas between the reinforcements and concrete extend gradually into the interior of the joint, so the deformation (Δ) of the joint increases quickly and its stiffness decreases. The concrete in the core zone is acted with alternative tensile and compressive stresses in a diagonal

direction, the diagonal cracks open and close alternately and the pinch effect is resulted seriously on the hysteretic curve (Fig. 16-16(a)). Finally, the concrete in the core zone is crushed and spalled off and the strength reduces. The ultimate strength and hysteretic behavior of a beam-column joint depend mainly upon the ratio between internal forces of beams and columns connected, compression-strength ratio of the column, content and anchorage of longitudinal reinforcement, detailing of stirrup.

The hysteretic curve of load-deformation ($P-\Delta$) of longitudinal reinforcement in beam and column near the joint is asymmetrical (Fig. 16-16(c)). When the reinforcement is yielded tensely under bending moment, the crack of concrete nearby expands widely and the slipping area of the reinforcement extends into the joint zone, so the elongated deformation ($+\Delta$) results. On the contrary, when the reinforcement is compressed thereafter, the crack of concrete nearby is closed and compressed and the opposite slip of the reinforcement is slight, so the compressive deformation of it is limited although the pinch effect still appears.

16.3.3 Calculation model

A series of non-linear responses of reinforced concrete structure occur successively and the internal forces, cracking of concrete, and yielding of reinforcement in it vary reversely under earthquakes. In order to analyze dynamically the mechanical responses of the structure or its member following the process of an earthquake, an accurate constitutive relation, or mathematic model of load-displacement of the material and section used, e.g. $\sigma-\epsilon$, $M-1/\rho$, or $P-\Delta$, has to be known in advance.

The calculation model of sectional behavior of a structural member can be established following the general method introduced in Section 11.3, of which the principles used are: (1) giving the stress-strain relations ($\sigma-\epsilon$) of concrete and reinforcement and the bond-slip relation ($\tau-s$) between them under reverse loading; (2) assuming the member section maintaining a plan after loading and determining the relative relations of various strains on the section; (3) establishing the equilibrium equations for the external and internal forces acting and solving the unknowns. Usually, the structural member is divided into several segments along its axis and each segment is transversely divided again into several strips, then the basic equations are derived and the digital calculation is conducted and completed by computer. This method can be used for any members acted with various internal forces and the result obtained is accurate, but it should be calculated particularly for each member, which takes more calculation.

The method used widely in engineering practice is as below. The bending moment-curvature relation ($M-1/\rho$) is given directly for section of the member based on the experimental result or theoretical calculation, then the internal forces and deformation of the structure are analyzed by the non-linear finite element method. In order to simplify the calculation, various approximate $M-1/\rho$ models are suggested in reference [16-11], among them Clough's degrading stiffness model of three lines (Fig. 16-17) is used frequently.

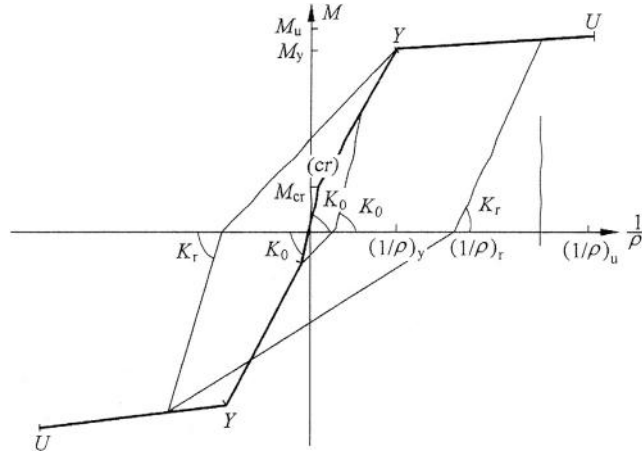


FIG. 16-17 Clough's $M-1/\rho$ model of degrading stiffness [16-11]

The main points of hysteretic rule of Clough's $M-1/\rho$ model are:

1. Skeleton line is three-folded and is linked successively with four characteristic points, i.e. origin (0, 0), cracking of concrete (M_{cr} , $(1/\rho)_{cr}$), yielding of tensile reinforcement (M_y , $(1/\rho)_y$), and ultimate state (M_u , $(1/\rho)_u$) of the member.

2. Unloading lines are taken as the inclined ones and their slopes (K_r) vary with the value of bending moment or corresponding curvature $(1/\rho)_r$ at the start of unloading. Considering the degrading stiffness of the member after yielding of the reinforcement, the slope is calculated by the formula:

$$\text{when } M \leq M_y \quad K_r = K_0, \quad (16-15a)$$

$$\text{or } M_y < M \leq M_u \quad K_r = \left(\frac{(1/\rho)_y}{(1/\rho)_r} \right)^\zeta \cdot K_0, \quad (16-15b)$$

where K_0 is the elastic stiffness of the member before cracking of concrete, and ζ is the empirical coefficient. The average value $\zeta \approx 1.5$ can be used, as the experimental value ranges from 0.8 to 1.8.

3. Reloading lines start from the residual curvature $(1/\rho)_r$ after totally unloading ($M = 0$) and link linearly with the highest point reached in the last loading cycle. If the highest point reached does not exceed the cracking or yielding point (M_{cr} or M_y), the reloading line should link with the characteristic point and, then, go toward the skeleton.

This model reflects to a certain extent the main characteristics, e.g. stiffness degraded and pinch effect, of the member under reverse loading and is easily used for calculations. Based on this model, other models are also suggested for improvement (complement and modification), for example, the influence of additional deformation caused by slip of the reinforcement within the joint zone, influences of axial and shear forces acted on the section, and aggregate interaction on the

cracked face of concrete are considered. Consequently, the accuracy of the calculated result is improved while more calculation is needed.

Comparing with the measured hysteretic curves, e.g. Figs. 16-11 to 16-16, these models are of the first approximation and are obviously simplified. Nevertheless, when these simplified models are used for analysis of hysteretic behavior of a reinforced concrete structure or its member, the calculated results may be still satisfied, because (1) earthquake action is highly random and undetermined, (2) appearing and developing of concrete crack and slipping of reinforcement are scattered significantly, and (3) error of the $M-1/\rho$ model is not so sensible for the calculated results in some conditions.

Fatigue Resistance

17

CHAPTER OUTLINE

17.1 Fatigue of concrete	438
17.1.1 Experimental results and expression.....	438
17.1.2 Influence factors and calculation formula	441
17.2 Fatigue of reinforcement.....	443
17.3 Fatigue of bond between reinforcement and concrete	446
17.4 Fatigue of structural member and its checking calculation	449
17.4.1 Fatigue under bending moment	450
17.4.2 Fatigue under shear force.....	454

Usually, after a reinforced concrete structure designed in accordance with ultimate load-bearing capacity is put in service for many years, the load actually acted may occasionally exceed the one designed, but it is seldom in engineering practice that the structure fails due to an occasional overload only. However, when the structure is acted with the load being smaller than the designed one but is repeated thousands of times, it may fail suddenly after accumulation of internal damage. Sometimes, the latter situation is even more dangerous than the former one.

When a structure is failed under the repeated load, or internal forces, being smaller than the ultimate one during monotonically load, this phenomenon is called fatigue of the structure. Many examples happen frequently in structural engineering: bridge or crane beam and its supporting structure are acted on with vertical and horizontal loads of the vehicles or crane; the structure of industry building is acted with periodic, e.g. rotating of an eccentric block or reciprocating movement of rocker arm, or random vibration; a hydraulic dam or offshore structure is slapped with waves. These loads acting on the structure may repeat several million times within the service period.

Generally, fatigue failure of a material or structure occurs after the load is repeated for 10^4 – 2×10^6 times. If the structure fails when the load is repeated less than 1000 times, this is called fatigue of low cycles, e.g. the structure under an earthquake (Chapter 16). On the other hand, if the structure does not fail after the load is repeated 10^7 times, it is generally considered that it will not fail even if the load is repeated more times, or the fatigue failure will never occur at all. Therefore, it is important to determine the fatigue limit (or strength) for a material or structure, i.e. the maximum bearing capacity of it as the fatigue failure will not occur.

The fatigue of a structure is a long process and generally is caused by accumulation of internal damages. Usually, the micro-defects, e.g. micro-cracks, porosity, and interface and impurity of low strength, initially exist in the interior of the structural material, the stress concentration occurs nearby under action of the load and corresponding damages appear, develop, and accumulate continuously after the load is acted repeatedly many times, then the effective area of the material for resistance is reduced and the eccentric stress and stress concentration are emphasized unfavorably. Finally, the material and structure fail suddenly as its bearing capacity is reduced gradually.

The fatigues of reinforced concrete structure and its materials have been experimentally investigated at home and abroad [17-1–17-5] for many years. Because the fatigue of a material depends mainly upon its internal microstructure and many factors have influence on it, the fatigue strength or life (repeating times of the load) of the structure measured from the tests is scattered considerably.

17.1 Fatigue of concrete

17.1.1 Experimental results and expression

The stress–strain curve of a concrete prism under action of repeated compression is shown in Fig. 17-1. When the compressive stress repeated on the specimen is smaller than the fatigue strength of concrete, e.g. $\sigma_1, \sigma_2 < f_c^f$ in Fig. 17-1, the area of a hysteretic loop composed of each reloading and unloading cycle is reduced gradually as the repeating time of the load (n) increases, and the stress–strain curves of reloading and unloading tend to be fixed and the residual strain after being unloaded will not increase further after a certain amount of times of load repeating. This shows that deformation and internal structure, including development of crack, of the concrete material tend to be stable and excessive deformation and failure of the specimen will not occur even when the load is repeated more times.

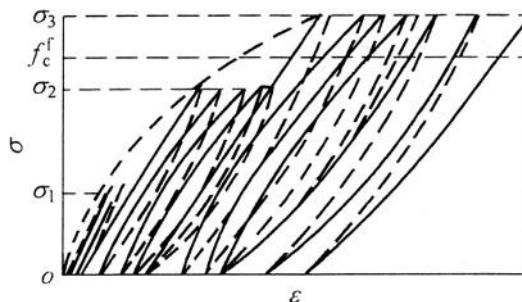


FIG. 17-1 Stress–strain curve of concrete under repeated compression [1-1]

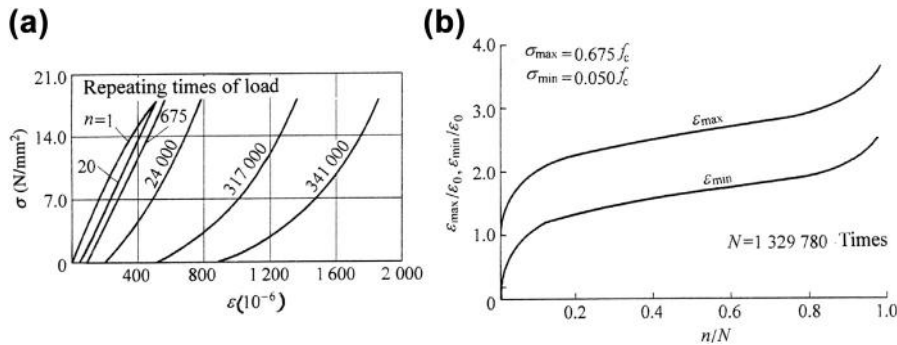


FIG. 17-2 Variation of concrete strain under repeated stress: (a) stress–strain curves at different times of repeated load [17-2], (b) increases of the maximum and minimum strains [17-1,17-4]

When the compressive stress repeated is greater than the fatigue strength of concrete, e.g. $f_c > \sigma_3 > f_c^f$ in Fig. 17-1, the specimen will fail after the load is repeated N times, which is called the fatigue life of the concrete, in the range of σ_{\min} to $\sigma_{\max} = \sigma_3$. Correspondingly, the variation regularity of the stress–strain curves (Fig. 17-2) is generally as below. When the load is repeated less than 20 times ($n < 20$), the area of the hysteretic loop reduces gradually after each reloading and unloading cycle, and the reloading and unloading curves tend to be a straight line. When the load is repeated more than 10^4 times ($n > 10^4$), the creep and internal micro-crack of concrete develop gradually, the reloading and unloading curves tend to be convex towards the abscissa (strain axis), and the total and residual strains (ϵ_{\max} and ϵ_{\min}) of each loading cycle increase continuously and the slope of the curves or the stiffness of the specimen reduce gradually. Finally, the specimen fails suddenly when the load is repeated N times (fatigue life), because the internal damages are accumulated, the cracks develop and link together, and the deformation of the specimen accelerates and diverges.

The strains (ϵ_{\max} and ϵ_{\min}) of concrete specimen at the maximum and minimum stresses (σ_{\max} and σ_{\min}) are measured during repeatedly loading test and they vary with repeating time of the load as shown in Fig. 17-2(b). In addition, an acoustic instrument may be used for measuring the wave speed in the specimen, which also varies with repeating time of the load.

Analyzing these experimental data, the fatigue process of concrete can be divided into three stages:

1. Besides the original crack, a new crack is formed in the weak part of the specimen and the strains accelerate when $n/N < 0.1$;
2. The cracks develop stably and the strains increase slowly when $n/N = 0.1-0.9$;
3. The cracks expand unstably and the strains diverge when $n/N > 0.9$, in which n is repeating time of the load and N is the fatigue life or the repeating time of load at failure of the specimen.

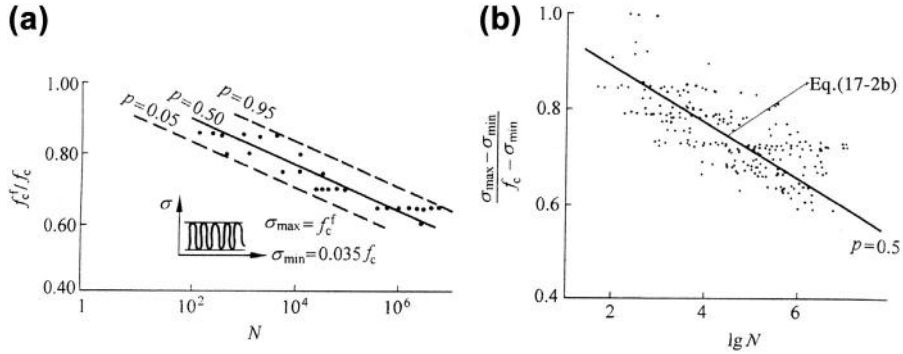


FIG. 17-3 *S-N* or *S-N-P* diagram for fatigue strength of compressed concrete [17-1]: (a) *S-N-P* diagram, (b) *S-lgN* diagram

The experimental results of fatigue tests can be plotted in two ways. When the variation amplitude of stress (S , e.g. $f_c^f = \sigma_{\max}$) and the fatigue life (N or $\lg N$) are respectively taken as the ordinate and abscissa, the $S-N$ diagram of fatigue strength (e.g. Fig. 17-3), or Wohler diagram, is obtained for the material. Another expression is the Goodman diagram as shown in Fig. 17-6(b). Because of considerable scatter of the experimental data, the fatigue strength of concrete can also be expressed in terms of failure probability (p) and the $S-N-P$ diagram is then obtained, in where the contour of $p = 0.5$ represents the average value of the fatigue strength.

According to the experimental data and viewpoints of different researchers, the variation amplitude of stress during fatigue test (S) is expressed by various stress indices, e.g. stress difference $f_t = \sigma_{\max} - \sigma_{\min}$ [2-11], stress ratio $\rho_f = \sigma_{\min}/\sigma_{\max}$ [2-1], and other, i.e. $(\sigma_{\max} - \sigma_{\min})/(f_c - \sigma_{\min})$, σ_{\max}/f_c^f , etc.

The experimental results and analyses introduced above are based on the fatigue test with constant amplitude, i.e., the maximum and minimum loads (stresses) repeated are kept constant during testing, and most fatigue tests conducted at home and abroad till now are of this kind. Actually, the load acted on a structure or the stress of its material is always variable, even significantly varied within service time in engineering practice. Therefore, the fatigue test with variable or random amplitude (e.g. Fig. 17-4) should be conducted and investigated.

Usually, the Palmgren-Miner hypothesis is used for determining the fatigue strength of a material under variable stress amplitude. The whole loading and unloading process is treated as a composition of k kinds of constant stress amplitude, and the material will fail due to fatigue when

$$\sum_{i=1}^k \frac{n_i}{N_i} = 1.0 \quad (17-1)$$

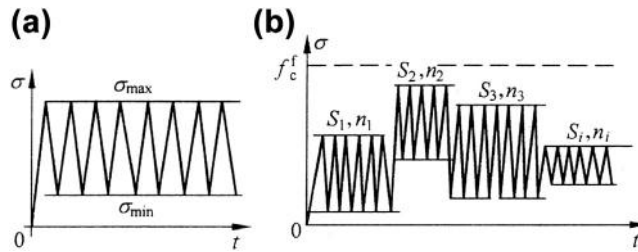


FIG. 17-4 Fatigue tests with constant and variable amplitudes: (a) constant amplitude, (b) variable amplitude

occurs according to the principle of successive accumulation of fatigue damage, in which n_i repeating time of i th constant stress amplitude, N_i fatigue life (time) of the material under i th constant stress amplitude alone.

Several results of fatigue tests with variable stress amplitude are reported [17-1,17-5], but the conclusions given are not consistent. Some of them conclude that the equation is reasonable, but others consider that the constant in the right side of the equation should be smaller than 1.0 or the appearing order of different stress amplitudes should be taken into account. However, this equation is still adopted widely in available design codes of many countries [2-1,2-11,2-12].

17.1.2 Influence factors and calculation formula

The main factors, having influence on the fatigue strength (f_c^f) or life (N) of concrete, are as below besides the stress amplitude (S).

Stress gradient. When the concrete prisms are compressed repeatedly with different eccentricities (e), the S — N diagram measured is shown in Fig. 17-5. It is

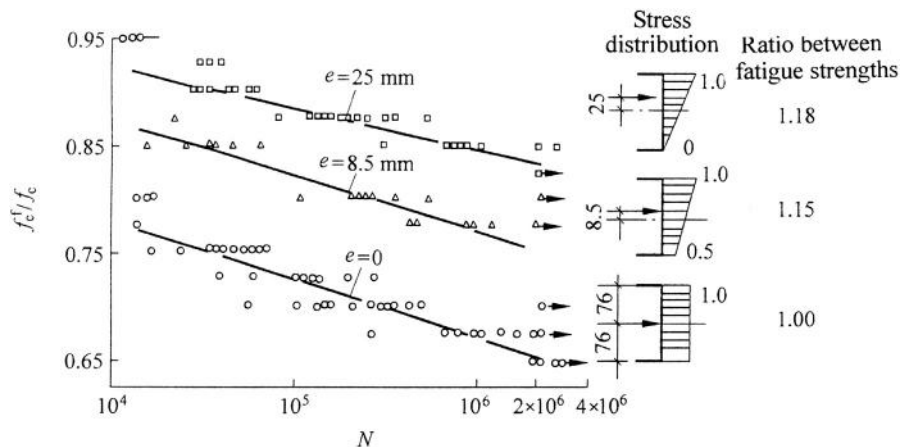


FIG. 17-5 S — N diagram for concrete prisms with different stress gradients [17-6]

demonstrated that the fatigue strength of concrete increases with the stress gradient on its section. When the stress gradient of the prism is zero, the whole section of it is compressed uniformly with high stress, so greater probability of concrete damage appearing earlier and developing much quicker is caused and the fatigue strength should be reduced correspondingly.

Material composition and manufacture technique. It is generally considered that many factors, including content of cement, water—cement ratio, kind of aggregate, curing condition, age at loading, of concrete do not have direct influence on its fatigue strength. However, these factors have obvious influence on the compressive strength (f_c) of concrete, which influences indirectly the fatigue strength. For example, high-strength concrete contains less defects in the interior and has a higher relative value of fatigue strength [17-7], while light-weight (aggregate) concrete contains many porosities and more defects in the interior and has lower relative value of fatigue strength [17-8].

Loading frequency. The loading frequency during the fatigue test usually ranges from 100 to 900 times per minute, which has no obvious influence on the fatigue strength of concrete. Nevertheless, the fatigue strength or life of concrete will reduce if the loading frequency is too low, e.g. 4 times per minute, as larger creep is caused.

Fatigue strength under tension. It is experimentally demonstrated [17-9] that the relative fatigue strength of concrete under tension (f_t^f/f_t), including axial (f_t , Eq. (2-9)), splitting ($f_{t,s}$, Eq. (2-10)), and flexural tension, i.e. modulus of rupture ($f_{t,f}$, Eq. (2-11)), is consistent with that under axial compression (f_c^f/f_c). However, the fatigue strength of concrete under reversed tensile and compressive loads is smaller than that under a repeated tensile load.

Various kinds of simplified formula or diagram are provided for checking the fatigue strength of structural concrete in the design codes of different countries. Some of them give the fatigue strength of concrete for predetermined times of repeated stress, e.g. $N = 2 \times 10^6$ or $N = 4 \times 10^6$ (Fig. 17-6(a)), or give the fatigue life (N) for predetermined variation amplitude of repeated stress (σ_{\max} , σ_{\min}), e.g. Fig. 17-6(c). In addition, the Goodman diagram gives the allowable variation amplitude of repeated stress (σ_{\max} , and σ_{\min}), according to the required fatigue life of the concrete, e.g. $N = 10^6$ (Fig. 17-6(b)).

Some researchers also suggest different formulas for the calculation of fatigue strength or life of concrete, for example:

$$\text{Aas - Jacobson (Sweden)} \quad \lg N = \frac{1 - (\sigma_{\max}/f_c)}{\beta(1 - \sigma_{\min}/\sigma_{\max})} \quad (17-2a)$$

$$\text{with } \beta = 0.0685$$

$$\text{Kakuta - Okamura (Japan)} \quad \lg N = 17 \left[1 - \frac{\sigma_{\max} - \sigma_{\min}}{f_c - \sigma_{\min}} \right]. \quad (17-2b)$$

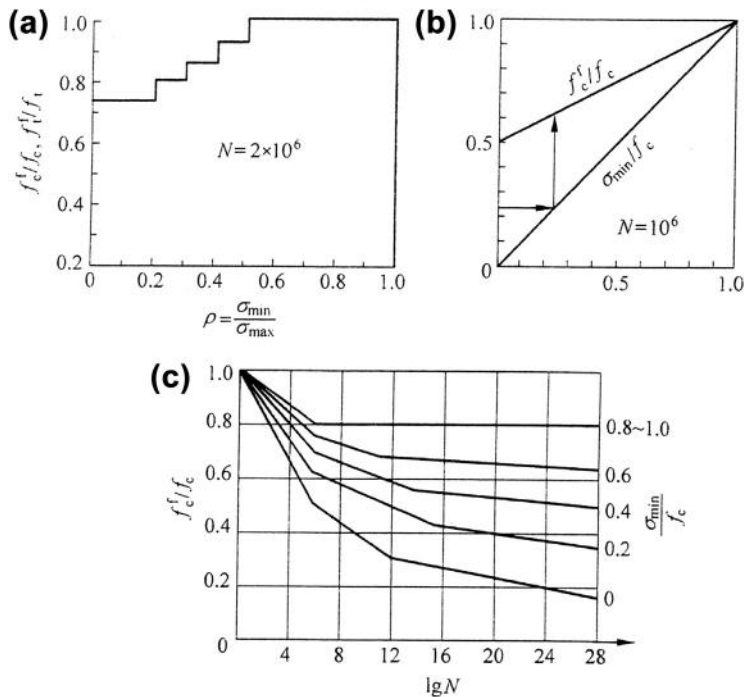


FIG. 17-6 Diagrams for calculation of fatigue strength of concrete: (a) Chinese Code [2-1], (b) ACI Committee 215 [1-1], (c) CEB-FIP Model Code [2-12]

17.2 Fatigue of reinforcement

The fatigue strength or life of a reinforcement (steel) is also expressed by $S-N$, $S-N-P$, or the Goodman diagram, e.g. Fig. 17-7, based on the experimental results.

There are three kinds of specimens used for fatigue test of reinforcement: (1) taken from original plain or deformed reinforcement; (2) standard specimen with smooth surface turned from original reinforcement. Both can be directly tested under repeated loading and unloading cycle on the testing machine; (3) reinforcement is buried reliably in the tension zone of a beam, on which two concentrated loads act symmetrically and repeatedly.

The experimental results show that the fatigue strength obtained from the original reinforcement is the lowest among them. The fatigue strength of the reinforcement in a beam is slightly higher, and its fatigue fracture occurs near the cracked section within the maximum bending moment region of the beam. Generally, the fracture occurs initially at the rib root or factory mark on the surface of the reinforcement. Therefore, the smooth standard specimen eliminates most defects on the surface after being worked, and the fatigue strength is almost doubled.

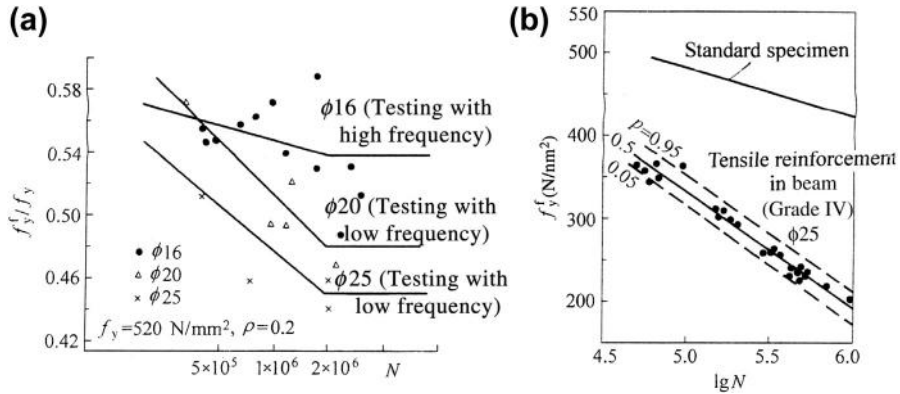


FIG. 17-7 Fatigue strength of reinforcement: (a) original reinforcement [1-1], (b) reinforcement in beam and standard specimen [17-1]

The reinforcement fails suddenly under repeated load after the fatigue life is reached and the fracture surface observed is shown in Fig. 17-8(a). The process of fatigue failure can be divided into three stages:

1. Initial formation of crack. Some defects, e.g. impurity, fine crack or gap, carving mark, and rust stain, are caused on the surface and in the interior of the reinforcement, during the processes of smelting, rolling, and cold working. Consequently, stress concentration occurs near these defects or at the rib root on the surface under the repeated stress, and the crack is initially formed there when the stress exceeds the corresponding strength and causes slipping of steel crystal in the reinforcement.
2. Expansion of crack. As the stress acted repeats more and more, the initial crack expands gradually and the damage caused accumulates, then the effective area on the section of the reinforcement is reduced. In the meantime, the cracked area on the section is smoothed down by friction and a darker color appears there under repeated loading and unloading.
3. Fatigue fracture. When the effective area remaining on the section of the reinforcement is deduced continuously and can not carry anymore the stress acted,

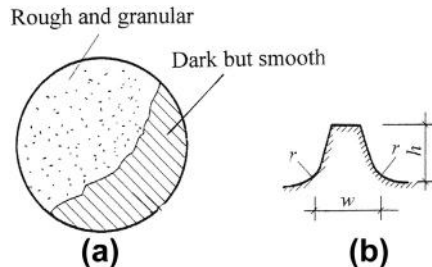


FIG. 17-8 Fracture surface of reinforcement after being fatigued: (a) fracture surface, (b) shape of rib on outer surface

the reinforcement fractures suddenly. The fracture area on the section looks fresh and bright and rough granules appear on it.

The available results of fatigue test with variable stress amplitude show that the Palmgren-Miner hypotheses (Eq. (17-1)) based on damage accumulation can also be used for reinforcement although with some argument.

The first factor having influence on fatigue strength or life of reinforcement is also the variation amplitude of stress acted (S), but various indices related are selected by different researchers. Other factors are mainly as below.

Appearance and diameter. The ratio between the radius at the root and height of the rib (r/h , Fig. 17-8(b)) in the surface of a reinforcement has considerable influence on the coefficient of stress concentration nearby, e.g. 1.5 to 2.0 [17-1]. Therefore, the fatigue strength increases with the ratio (r/h). The probability of internal defect increases and, then, the fatigue strength reduces as the diameter of the reinforcement increases (Fig. 17-7(a)).

Strength grade. As the strength grade of reinforcement is elevated, the absolute value of fatigue strength, e.g. $f_y^f = \sigma_{\max}$ or Δf_y^f , is increased (Fig. 17-9(a)) as well,

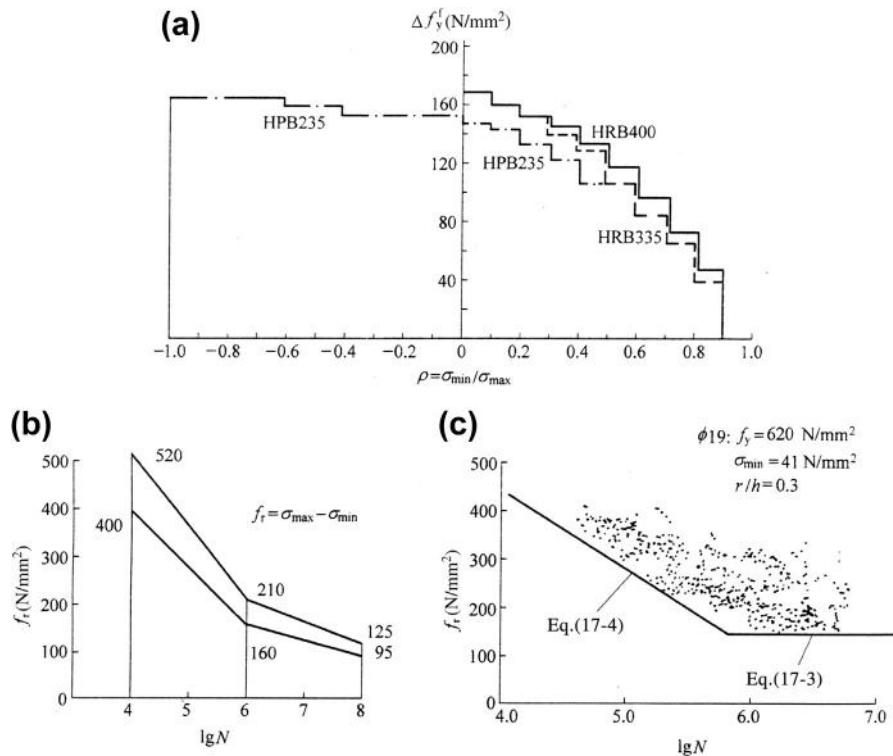


FIG. 17-9 Diagram for calculation of fatigue strength of tensile reinforcement: (a) Chinese Code [2-1], (b) CEB-FIP Model Code [2-12], (c) USA AASHTO [17-1]

while its relative value, e.g. f_y^f/f_y or $(\sigma_{\max} - \sigma_{\min})/f_y$, is decreased. Consequently, the steel wire and strand of high strength used for prestressed concrete follow the regularity [17-10].

Processing and environment. Additional damage will be locally caused in the reinforcement after processing, e.g. bending, welding, and mechanically splicing, or sustaining corrosion in air or seawater. Consequently, stress concentration nearby is aggravated after the reinforcement is stressed, so its fatigue behavior is deteriorated. Some experimental results report that the fatigue strength of the reinforcement may be reduced by about 50%.

Frequency of loading. The machines used for fatigue testing of material are different in frequency of repeatedly loading, and 200–600 cycles/min and 5000–10,000 cycles/min are respectively called low and high frequencies. The latter one gives slightly higher value of fatigue strength of reinforcement, because of shorted time of testing and less damage accumulation.

Various expressions of formula or diagram (Fig. 17-9) are provided for checking fatigue strength or life of the reinforcement in the structural member in the design codes of different countries. The formulas in Fig. 17-9(c) are

$$f_r = \sigma_{\max} - \sigma_{\min} = 145 - 0.33\sigma_{\min} + 55(r/h) \quad (17-3)$$

$$\lg N = 6.1044 - 591 \times 10^{-5} f_r - 200 \times 10^{-5} \sigma_{\min} + 103 \times 10^{-3} f_b - 8.77 \times 10^{-5} A_s + 0.0127 d(r/h), \quad (17-4)$$

where d is the diameter of reinforcement in mm, A_s is the sectional area of reinforcement in mm^2 , σ_{\max} , σ_{\min} , and f_b are the maximum and minimum stress repeated, and tensile strength of reinforcement in N/mm^2 , r and h (see Fig. 17-8(b)).

17.3 Fatigue of bond between reinforcement and concrete

When a load is acted repeatedly on a reinforced concrete structure, the tensile reinforcement in it is also stressed and released repeatedly, and the bond stress acted reciprocally on the interface between reinforcement and concrete near anchorage ends and cracked sections vary correspondingly. Therefore, various damages are caused and accumulated, relative slip between both is increased, and bond stiffness and average bond strength are decreased gradually, as the load is repeated continuously. These are referred to as degradation of bond.

The degradation of bond between reinforcement and concrete has great influence on mechanical behavior of the reinforced concrete structural member during the service period, e.g. tensile crack widens, stiffness reduces, and deformation increases. More seriously, some structural members, especially reinforced with plain bars only, will fail earlier than expected, because the load-carrying capacity is reduced after the load is repeated many times. For example, the concrete inside the end hook of the reinforcement is crushed and considerable slip is then caused, an inclined crack is formed afterwards and expands quickly (Chapter 14) and the stirrups nearby are

broken, so the member fails suddenly as the concrete on the compression zone of the section is crushed [17-11].

The tension specimen (Fig. 7-4) is normally used for bond test of reinforcement under repeated load [17-12–17-14], and a consistent conclusion is derived, although the material, shape, detail, and loading method of the specimens are different from one another. A typical S – N diagram obtained for the ultimate bond strength between reinforcement and concrete (τ_u^f) is shown in Fig. 17-10(a). The bonded length of the specimen used is $l = 3d$, and the minimum value of average bond stress acted repeatedly during testing is $\tau_{\min} = 0.1\tau_u$, in which τ_u is the average bond strength under monotonic loading. The experimental results show that the bond strength (τ_u^f/τ_u) reduces monotonically as the repeated times of load, i.e. fatigue life (N), increases, e.g. $\tau_u^f/\tau_u = 0.75$ – 0.85 when $N = 1000$ and $\tau_u^f/\tau_u = 0.6$ – 0.7 when $N = 10^6$. Of course, the fatigue bond strength ($\tau_u^f = \sigma_{\max}$) increases with the minimum bond stress (τ_{\min}) acted repeatedly, and vice versa. However, the strength of the concrete ($f_c = 23.5$ – 48 N/mm²) and the diameter of the reinforcement ($\Phi 8$ – $\Phi 28$) do not have obvious influence on the fatigue bond strength.

The bond between plain reinforcement and adjacent concrete is mainly dependent on friction resistance on the interface. However, the friction resistance is easily damaged under repeated load, so the fatigue bond strength (τ_u^f/τ_u) reduces correspondingly and degradation appears seriously.

The average bond stress vs. relative slip relation (τ – s) between reinforcement and concrete under repeated load is shown in Fig. 17-11 and is similar to the compressive stress–strain curve of concrete (Fig. 17-1). A hysteretic loop is formed on the figure after each loading and unloading cycle, and its area reduces successively and tends to be stable after a certain amount of loading cycles. The relative slips at the loaded and free ends increase successively (Fig. 17-10(b)) when the maximum load (or τ_{\max}) is reached in every loading cycle. After the load is released totally ($\tau = 0$) in every loading cycle, the relative slips remain increased with reducing increment and tend to be stable. If the maximum load repeated (or τ_{\max}) is increased, the area of hysteretic loop and relative slips after the loading and

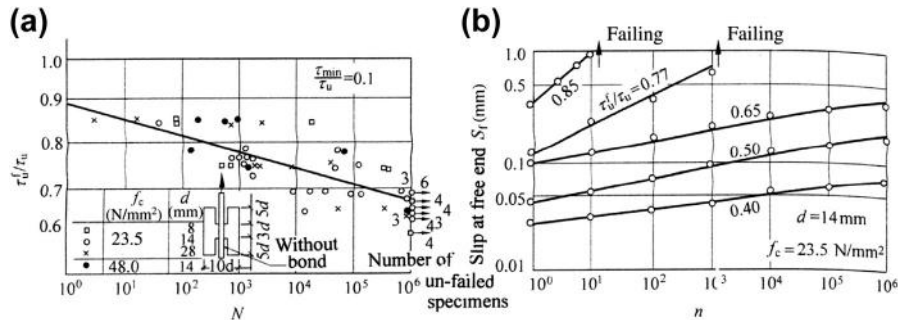


FIG. 17-10 Fatigue bond strength between reinforcement and concrete [1-1]: (a) S – N diagram, (b) slip at free end

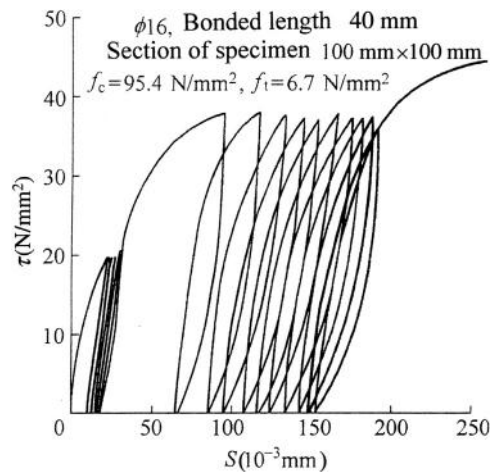


FIG. 17-11 τ - s curve under repeated load [1-1]

unloading cycle are newly increased as well. If the average bond stress of the reinforcement under repeated load is greater than the fatigue bond strength, the relative slips increase suddenly (Fig. 17-10(b)) and the concrete surrounding the reinforcement is split or the reinforcement is pulled out gradually from it after many times of load repeated (N), then the specimen is failed.

The distributions of tensile (σ_s) and bond (τ) stresses and local damage near the rib of the reinforcement experienced each loading and unloading cycle is schematically shown in Fig. 17-12(a). When the specimen is loaded until the maximum value (point A in the figure, or τ_m), the tensile stress at the loaded end of the reinforcement also reaches the maximum and the reinforcement there moves towards the right side,

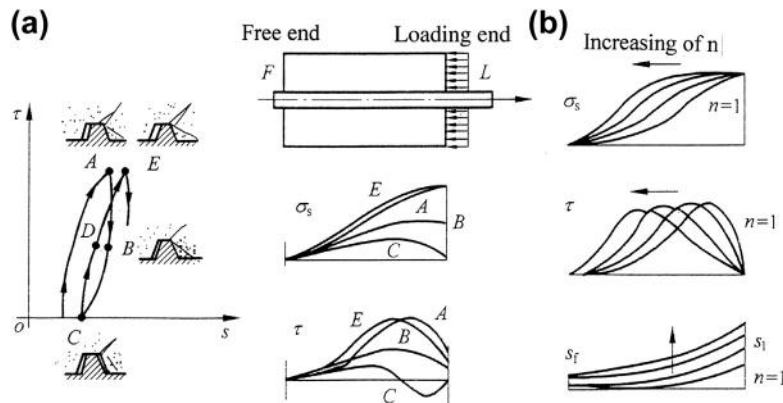


FIG. 17-12 Analysis of bond behavior of specimen under loading and unloading cycle: (a) one cycle of loading and unloading, (b) after n times of load repeated

and the concrete in front of the rib is crushed and an inclined crack occurs or develops at the right tip, while a gap remains behind, e.g. on left side of the rib. When the specimen is unloaded until point *C* via point *B*, the deformation and inclined crack in front of the rib recover slightly only and the gap behind the rib shrinks slightly, so the residual slip is considerable. The tensile stress at the loaded end of the reinforcement should be zero after unloading (point *C*), and the corresponding strain of the reinforcement nearby shrinks mostly and the residual stress is less, while the left part near the free end of the reinforcement is confined by the opposite friction from the bonded concrete and the tensile stress (σ_s) these will not be released totally. Therefore, the tensile stresses at both loaded and free ends of the reinforcement are zero then, and the maximum stress appears in the middle of the bonded length. Correspondingly, the bond stresses on right and left parts of the reinforcement are of opposite directions. When the specimen is reloaded until point *E* (τ_m) via point *D*, the tensile stress at the loaded end of the reinforcement again reaches the maximum, so the concrete on right side of the rib is crushed more, the inclined crack there develops more, and slip of the reinforcement and the gap behind the rib increase as well. In the meantime, the region with higher tensile stress expands within the loaded length and the peak point of bond stress moves towards the inside, e.g. towards the left side.

As the load is repeatedly acted even more times, the deformation and damage of the concrete adjacent to the reinforcement accumulate and extend gradually from the loaded end towards the free end, and the slipping zone near the loaded end is elongated. Therefore, the total deformation and slip of the specimen increase continuously, and the distributions of tensile (σ_s) and bond (τ) stresses of the reinforcement vary correspondingly (Fig. 17-12(b)). This is the reason and mechanism of degradation of bond behavior between reinforcement and concrete under repeated load.

The bond degradation is closely related to the microscopic stress state and local damage near the interface between two materials and is scattered and influenced by many factors, so the quantitative analysis with accuracy is difficult, but some empirical formulas [16-14] are provided for reference.

It should be emphasized that the bond degradation between reinforcement and concrete is not recoverable once it has occurred. If a structure experienced in advance several times overload and the bond degradation was caused already under higher stress state (σ_{\max} , τ_{\max}), its mechanical behavior during service period is influenced afterwards, e.g. greater deformation and slip, wider crack and smaller stiffness, even though the repeated load later causes a lower stress state ($\sigma < \sigma_{\max}$, $\tau < \tau_{\max}$). This should be paid attention to in engineering practice.

17.4 Fatigue of structural member and its checking calculation

Generally, tensile cracks may exist in the concrete during the service stage for an ordinary reinforced concrete (RC) structure, and it surely causes degradation of mechanical behavior and reduction of fatigue strength under repeated load. In order

to improve the fatigue property and ensure safety, prestressed concrete is frequently used for the structure carrying mainly dynamic and repeated loading, e.g. bridge and crane beam. Usually, prestressed concrete is divided into two categories: entirely prestressed concrete (PC), in which no tensile stress will appear in the concrete ($\sigma_c < 0$) under service load, and partially prestressed concrete (PPC), in which tensile stress ($\sigma_c > 0$, but $< f_t$), even a fine crack, is allowed in concrete under service load.

The fatigue behavior of these structures has been experimentally investigated at home and abroad and many conclusions are reported [17-11, 17-14–17-19]. If the reinforced and prestressed concrete structures are not cracked under bending moment and axial and shear forces during service stage, the stresses of concrete, reinforcement, and stirrup in it vary with limited amplitude under repeated load and fatigue failure will not happen at all, even the load repeated numerous times. Generally, the fatigue failure occurs only for the structure or its member cracked under service load, and ‘no crack, no fatigue’ is held.

17.4.1 Fatigue under bending moment

The bending moment at cracking of a flexural reinforced concrete member under repeated load (M_{cr}^f) is certainly smaller than that under monotonic load (M_{cr} , Chapter 12), and the ratio between them (M_{cr}^f/M_{cr}) depends mainly upon the fatigue strength of tensile concrete (f_t^f/f_t), which reduces as the repeated times of loading (or fatigue life N) increases. Generally, when $N \geq 2 \times 10^6$, $M_{cr}^f = (0.5–0.6) M_{cr}$ for an average structural member.

Usually, a flexural specimen of reinforced concrete or partially prestressed concrete is cracked already under the bending moment when the maximum value (P_{max}) reaches during the first loading, so it works with cracks in (Fig. 11-2) until fatigue failure when the load is acted repeatedly.

The results of fatigue test of a partially prestressed concrete beam are illustrated as an example shown in Fig. 17-13. The specimen is of I section (Fig. 17-14), and the tensile reinforcement used is of grade IV after being cold-stretched ($3 \Phi 14, f_y = 750 \text{ N/mm}^2$) and is pretensioned with control stress 520 N/mm^2 . The effective prestress of it reduces to 280 N/mm^2 after stress lost when the specimen is tested. When the specimen is loaded first to $M = 0.625M_u$, where M_u is the ultimate bending moment of the beam under monotonic load, the flexural (tensile) crack appears already in it. Then, the specimen is unloaded to the lower bound ($M_{min} = 0.077M_u$) and reloaded to the upper bound ($M_{max} = 0.423M_u$), and the load is acted repeatedly 2.05×10^6 times. Afterwards, the upper bound of the load is increased until $M_{max} = 0.5M_u$ and repeated for 2.04×10^6 times. Furthermore, the upper bound of the load is increased, again until $M_{max} = 0.635M_u$, then the specimen fails in fatigue after the load repeated 0.78×10^6 times and one of the tensile reinforcement is broken. The total time of the loading–unloading cycle is 4.87×10^6 times.

The mechanical behavior of the beam varies gradually under repeated load with constant amplitude (Fig. 17-13). When the load is repeated continuously, the

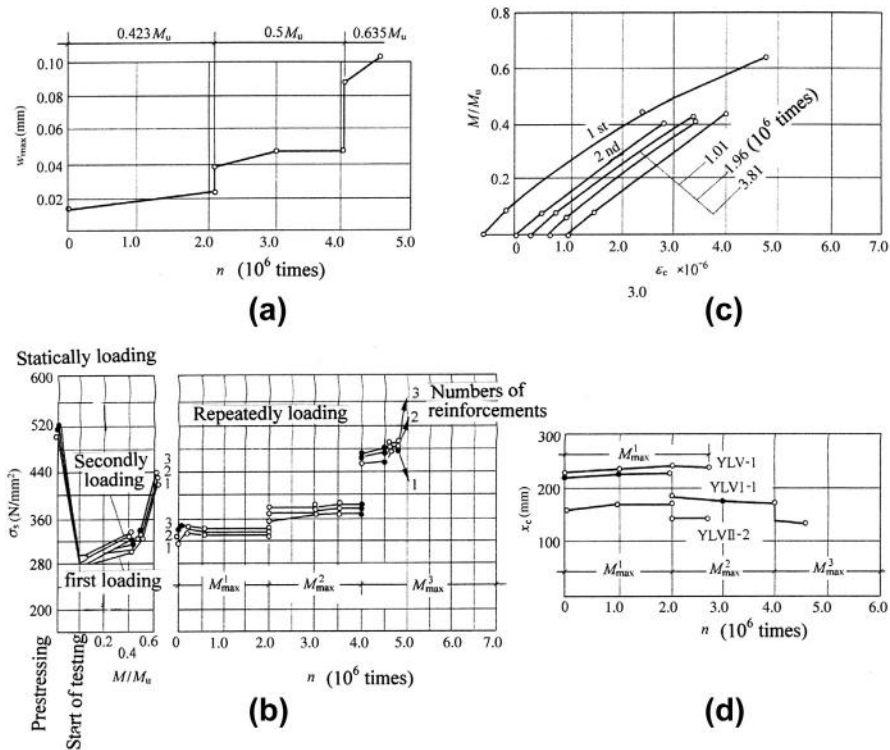


FIG. 17-13 Results of fatigue test of a partially prestressed concrete beam under bending moment [17-18]: (a) crack width, (b) stress of reinforcement, (c) compressive strain of concrete, (d) depth of compression zone on section

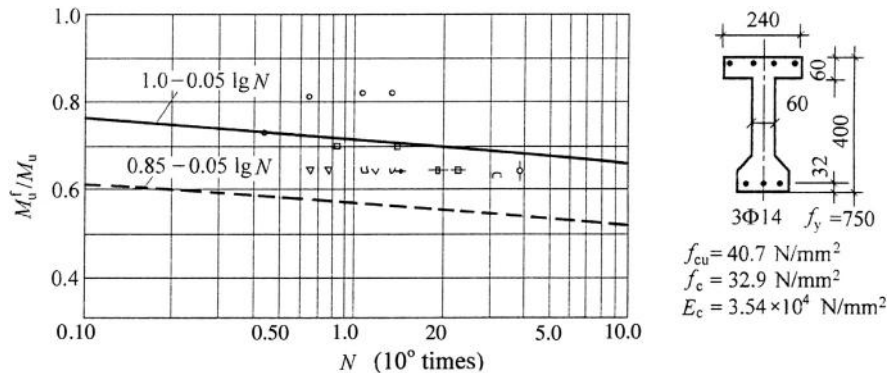


FIG. 17-14 S-N diagram for partially prestressed concrete beam under bending moment [17-18]

existing cracks widen slightly (W_{\max}) and tend to be stable, but new cracks appear and widen gradually between the existing cracks, because fatigue strength of tensile concrete reduces. When the load in succeeded cycle reaches the upper bound (P_{\max} or M_{\max}), tensile stress of the reinforcement (σ_s), compressive strain of the concrete at extreme fiber ($\bar{\epsilon}_c$), relative slip between the reinforcement and concrete, and deflection of the beam increases correspondingly. And, residual strain of the concrete and residual deflection of the beam after unloading ($P = 0$ or $M = 0$) increase as well. The variation regularities of them are consistent with that of the deformation of compressed prism (Fig. 17-1) and the bond-slip relation of the reinforcement ($\tau-s$, Fig. 17-11), as the load is acted repeatedly.

The strain distribution on sectional depth is measured, and the position of the neutral axis or average depth of compression zone (x_c) on the section is then determined at the maximum load acted after a certain amount of loading cycles (Fig. 17-13(d)). It is demonstrated that the average strain on section still follows approximately the plane section hypothesis and the compression depth varies less after the load acted is repeated many times.

As the upper bound of the repeated load is increased, but $M_{\max} < M_u^f$, later on, the deformation, crack, stresses of reinforcement and concrete of the beam are increased while the stiffness and compressive depth of the section are decreased correspondingly. When the load is repeated again with the same upper bound, these indices vary slightly and tend to be stable as well. Comparing these stable indices with the corresponding values during the first loading, the increasing or decreasing amplitude of them depends mainly upon the upper bound of the repeated load (or M_{\max}/M_u), materials used, content of reinforcement, prestressing level, and sensitivities of these indices themselves. For example, tensile stress of the reinforcement and deflection at mid-span of the beam are increased respectively by 1–3% and 1–8% only, while compressive strain and crack width of the concrete are increased respectively by 12–18% and 0–50%, after the beam is acted with the load, or corresponding bending moment $M_{\max} = 0.423M_u$, repeated 2×10^6 times. If the beam were of reinforced concrete without being prestressed, the increasing amplitudes of these indices should be much greater under the same repeated load.

When the upper bound of the repeated load acted is increased and the fatigue strength (M_u^f) of the beam is reached, the beam fails after the load repeated a certain amount of times (N). Actually, the fatigue failure of most specimens is a gradual process as below. At first, one of the tensile reinforcements in the beam is broken due to tensile fatigue, then suddenly the stress of other reinforcements increases, concrete cracks expand, and neutral axis moves upwards and compression zone reduces on the section (Fig. 17-13). After the load is repeated again several thousands times, the damage in concrete accumulates continuously and other tensile reinforcements are broken successively in fatigue, so the load-carrying capacity of the beam is reduced. The possibility of all the tensile reinforcements broken simultaneously in fatigue is rare. Therefore, the repeated times of the loading cycle, at which the first reinforcement is broken, is usually taken as the fatigue life of the beam (N).

The experimental results obtained at home and abroad demonstrate that most flexural members of reinforced and partially prestressed concrete failed in fatigue are dominated by breaking of the tensile reinforcement. Only a few of them, e.g. with high content of reinforcement or special sectional shape (e.g. reversed T), fail due to fatigue of the compressive concrete. The fatigue limit or strength of the partially prestressed concrete beam under bending moment is presented in Fig. 17-14, in which $S = M_u^f/M_u$ and fatigue life (N) are used respectively for the ordinate and abscissa, in where M_u is the ultimate bending moment of the beam under monotonic loading.

Normally, a reinforced or partially prestressed concrete member under repeated load is designed first as if the load is acted monotonically and statically and its sectional size and reinforcement are then determined according to the methods of ultimate state design (see Chapters 11–15). In addition, the fatigue strength of the member is checked afterwards, although different principles and methods of calculation may be used.

Values of repeated loads. When lower and upper bounds of the stress acting repeatedly on the structural material are calculated, the values of the minimum and maximum loads acting on the structure should be determined in advance. Usually, the minimum load includes weight of the structure itself and other dead loads acting, and also effective action of prestressing if any. On the other hand, the maximum, or fatigue load used is slightly lower than the standard value of total load, [2-1] because the load repeated many times in engineering practice is certainly smaller than the designed value of total load, which is used for calculation of its ultimate strength and an over-load coefficient is included.

Requirement for fatigue checking. The maximum stresses (σ_{\max}) acting on the reinforcement and concrete of a structure under fatigue load should satisfy the requirement [2-1] below, in which the fatigue strength is measured from the same material (Figs 17-9 and 17-6) acted with the repeated stress of the same variation amplitude (between σ_{\min} to σ_{\max}):

$$\text{Reinforcement} \quad \sigma_{\max} - \sigma_{\min} \leq \Delta f_y^f \quad (17-5a)$$

$$\text{Concrete} \quad \sigma_{\max} \leq f_c^f. \quad (17-5b)$$

Calculation of stresses under fatigue load. When the stresses acted repeatedly between σ_{\min} and σ_{\max} on the material of a structure under fatigue loads or corresponding bending moments (M_{\min} , M_{\max}) are calculated, the converted section method (Fig. 13-3) is usually used with the basic assumptions below: (1) plane section being kept even after concrete is cracked, (2) stress is distributed triangularly on compression zone, (3) tension of the concrete below neutral axis being neglected, (4) ratio between the elastic moduli of reinforcement and concrete being $n^f = E_s/E_c^f$, where E_c^f used being smaller than the ordinary one (E_c) [2-1].

After the converted section of a member is determined, position of the neutral axis (X_{cf} , Eq. (13-9)), inertia moment (I_{cf} , Eq. (13-10)), and stresses

(σ_{\min} and σ_{\max}) of the materials under repeated load can be calculated easily following the general method for homogeneous elastic material.

17.4.2 Fatigue under shear force

When a reinforced concrete beam without web reinforcement is loaded repeatedly and fatigue failure occurs in the pattern of inclined crack dominated by shear force (Chapter 14), the ultimate value of shear force (V_u^f) is about 60% of that under monotonic loading (V_u) [17-15].

As far as a reinforced or partially prestressed concrete beam with web reinforcement is concerned, the shear force (V_{cr}^f) at appearance of inclined crack under repeated load is also smaller than that under monotonic load (V_{cr}). The ratio V_{cr}^f/V_{cr} depends mainly upon the fatigue strength of tensile concrete (f_t^f/f_t), which decreases as the repeated time of loading, or fatigue life, (N) is increased. The stress of web reinforcement in the beam is rather low before appearance of the inclined crack, so web reinforcement has only a slight influence on delaying of concrete cracking.

The results of fatigue test of a partially prestressed concrete beam dominated by shear force are shown in Fig. 17-15, and section, material, and prestressing of the

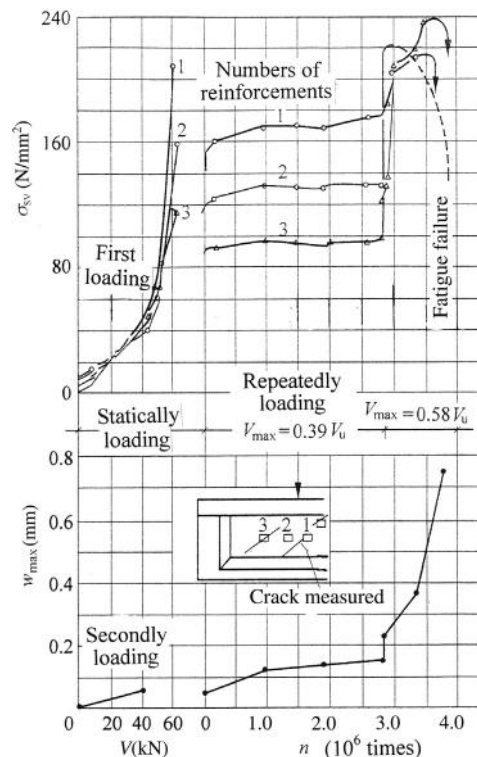


FIG. 17-15 Fatigue test of partially prestressed concrete beam failed in inclined crack [17-18]

specimen used are the same as the previous one (Fig. 17-13). When the specimen is loaded first until $V = 0.58V_u$, in where V_u is the ultimate shear force of the same specimen under monotonic loading, an inclined crack appears in the shear span (near beam end). Then the specimen is unloaded and loaded again repeatedly 2.81×10^6 times ranging from lower to upper bounds, which correspond respectively to $V_{\min} = 0.071V_u$ and $V_{\max} = 0.39V_u$. Afterwards, the upper bound of the repeated load is increased until $V_{\max} = 0.58V_u$, and the specimen fails with a critical inclined crack after the load is repeated 1.34×10^6 times and the stirrup there is fatigued and broken. The total time of load repeated is 4.15×10^6 .

When the beam is loaded first, tensile stress of the stirrup is only $\sigma_{sv} < 30 \text{ N/mm}^2$ and most shear force is carried by the concrete before the appearance of the inclined crack, but the tensile stress increases obviously and the portion of shear force carried by concrete reduces correspondingly after formation of the inclined crack. In addition, the tensile stress of every stirrup (σ_{sv} , Fig. 17-15) within the shear span varies considerably with the position located, distance from the inclined crack, and crack width nearby. The inclined crack does not close after being unloaded totally ($V = 0$), and the residual stress of the stirrup is $30\text{--}60 \text{ N/mm}^2$.

When the beam is loaded repeatedly with equal amplitude, the stress of stirrup (σ_{sv}) and the width of inclined crack (w_{\max}) under the upper bound of load (or V_{\max}) vary similarly with residual stress and crack width under the lower bound (or V_{\min}). They increase obviously at an early stage (less n) but tend gradually to be stable later on. However, if the upper bound of the repeated load is increased later, the stress, inclined crack, and deformation of the beam are increased immediately and also tend to be stable later on.

Finally, fatigue failure of the beam occurs suddenly after the load is repeated N times with upper bound or fatigue limit ($V_{\max} = V_u^f$). However, there are two categories for the beam failing with critical inclined crack. Generally, one of the stirrups intersected with the inclined crack is broken first in fatigue, and greater crack width and higher stress in adjacent stirrups are caused suddenly. Afterwards, the adjacent stirrups are broken successively, the inclined crack expands and extends both upwards and downwards, and the compression zone on the section is reduced gradually, as the load is repeated further. Finally, the beam fails soon after the concrete on compression zone reaches the fatigue strength under actions of compressive and shear stresses together. Another category of fatigue failure appears usually for the beam with less content of reinforcement. The longitudinal reinforcement of the beam is broken in fatigue under tensile stress and dowel action (shear stress) together, after the stirrup is broken first and the inclined crack is expanded. This causes final failure of the beam, but no obvious failure symptom is found on compression zone of concrete.

The relation between the fatigue limit of shear resistance ($S = V_u^f/V_u$) and the fatigue life (N) of the partially prestressed concrete beam is shown in Fig. 17-16, in where V_u is the ultimate shear strength of the beam under monotonically loading.

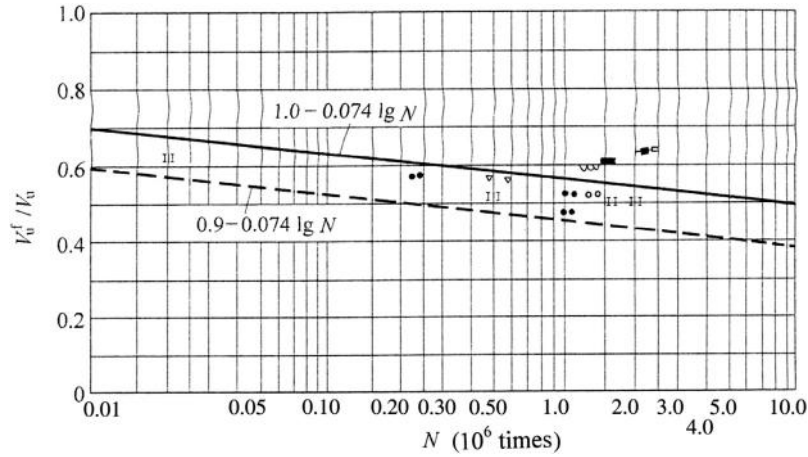


FIG. 17-16 *S-N* diagram of shear strength for partially prestressed concrete beam [17-18]

A structural member dominated by shear force and acted with repeated load is usually designed first and the sectional size, reinforcement, and stirrup are determined to satisfy the ultimate strength, following the method of ultimate state (Chapter 14). Afterwards, the fatigue of shear resistance of the beam is checked, and different principles and methods of calculation may be used.

Values of repeated loads. The same as that used for checking the fatigue of bending resistance (Section 17.4.1).

Requirement for checking. If appearance of the inclined crack is not allowed for a prestressed concrete member, the maximum principal (tensile) stress of concrete under the maximum repeated load should satisfy:

$$\sigma_{c1}^f \leq f_t^f. \quad (17-6)$$

As cracking of concrete is allowed for a reinforced concrete member under service load, the nominal shear stress (v^f) on flexural tension zone calculated following the stress distribution on the section (Fig. 14-15, Section 14.3.3) is also the principal tensile stress of concrete (σ_1). The fatigue strength of the stirrup is not necessary to be checked for the beam if the shear stress under repeated load is

$$v^f \leq 0.6f_t^f. \quad (17-7)$$

However, if the shear stress $v^f > 0.6f_t^f$ exists in both end parts of the member, the fatigue strengths of stirrup and bent reinforcement there should be checked.

Calculation of stress under fatigue load. Usually, the simplified formula based on the beam or truss model (see Section 14.3.3) is used for calculation, but different formulas are provided in the design codes of various countries.

Explosion Resistance

18

CHAPTER OUTLINE

18.1 Characteristics of explosion resistance of structures	457
18.2 Behaviors of materials under high-speed loading	461
18.2.1 Testing equipment and method.....	461
18.2.2 Reinforcement	463
18.2.3 Concrete	465
18.3 Behaviors of structural members	468
18.3.1 Flexural member	468
18.3.2 Compressive member	472

18.1 Characteristics of explosion resistance of structures

Various explosion accidents happen frequently in daily life, although the probability of explosion is rather low for an ordinary structure. However, huge amounts of energy, released instantaneously after an explosion has occurred nearby, will cause serious damage or even collapse of structures, and this may cause loss of life and property and sometimes even social unrest.

Explosion happening in structural engineering may be classified into four kinds:

- Fuel explosion, e.g. containers and pipes for gasoline, kerosene, or other fuels, workshop and storehouse for producing combustible material and chemical products;
- Industrial dust explosions on the workshop of flour or textile mills are sometimes full of the dust of tiny particles, which may suddenly catch fire or even explode under certain conditions of temperature and pressure;
- Explosion of conventional or nuclear weapon during war-time, sudden attack from a car-bomb;
- Directional explosion designed specially for removing an existing or damaged structure.

Actually, most of these explosions occur unexpectedly for various reasons, but many others are artificial incidents.

The explosion is the physical phenomenon that the energy stored initially in a substance is released instantaneously after triggering off under certain environmental

conditions. The explosions of different substances are triggered by under different conditions, and various processes and destructive power are induced correspondingly. The property and effect of the explosion is explained below, and the nuclear explosion [18-1], having most power, is used as an example.

After a nuclear bomb is ignited in the air, very high pressure, being much greater than normal (p_0 , N/mm^2), is induced instantaneously in the reaction zone near the explosion center. Therefore, an airflow with high pressure quickly pushes on from the center to the surrounding area, and the wave front is seen as a wall of high pressure. When the wave front reaches a distance away (R_z) from the explosion center in time t_z , the pressure reduces correspondingly to p_z (Fig. 18-1(a)). At this time, the over pressure ($\Delta p_z = p_z - p_0$) there is the maximum and reduces gradually inside but still $\Delta p > 0$, where this is called a compressed zone. In addition, a sparse zone is formed as the place being even nearer the center and the pressure there is lower than the normal air pressure ($p_z - p_0 = \Delta p_z < 0$), because of inertia of the moving air and no energy supplement there. The compressed and sparse zones are linked and compose together the air blast wave of explosion.

The air blast wave pushes on outside from the explosion center with a speed greater than the speed of sound. Then, the radius and areas of both compressed and sparse zones increase continuously with time (t), while the peak pressure of the wave front (p_z or Δp_z) decreases gradually. As the wave front moves far away from the explosion center after a certain time period, the pressure at the center increases and turns to the normal air pressure (p_0).

If a structure is located at R_z away from the explosion center and the wave front reaches there in t_z seconds after the explosion, the air pressure elevates instantaneously to the peak value (p_z) from the normal air one (p_0). Afterwards, the compressed zone reaches and the overpressure (Δp_z) there reduces gradually to zero as the wave front moves continuously outside and experiencing a period t^+ .

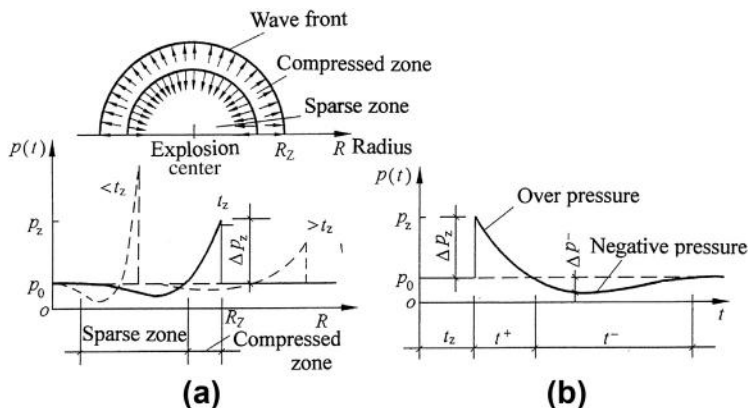


FIG. 18-1 Blast wave of nuclear explosion in air [18-1]: (a) pressure distribution along pushing radius, (b) $p-t$ curve at place apart R_z from explosion center

Successively, the sparse zone with negative pressure comes until the air blast wave totally passes through, and normal air pressure is recovered there. The curve of air pressure and time relation at the position is shown in Fig. 18-1(b), and the times taken for the over- and negative pressures are respectively t^+ and t^- .

According to experimental investigations, the peak value of overpressure (Δp_z), the maximum negative pressure (Δp^-) and time periods (t^+ and t^-) of an air blast wave are the functions of $\sqrt[3]{Q}/R$ varied monotonically, where R is the distance from the explosion center and Q is the explosion equivalent, i.e. the weight of trinitrotoluene (TNT) used. For example, when a hydrogen bomb of $Q = 10^9$ kg is ignited and exploded on the ground, the explosion parameters of the air blast wave measured are as shown in Table 18-1.

If a nuclear explosion were to occur, the air blast wave caused pushes on quickly outside with overpressure and can destroy any structure nearby on the ground. If the overpressure in the horizontal direction is $\Delta p_z = 0.1 \text{ N/mm}^2 = 100 \text{ kN/m}^2$, i.e. about 1 atm. only, it is equivalent to several hundred times wind load in an average place (e.g. 0.5 kN/m^2) or several decades of seismic load, so no structure can survive. In addition, other destructive effects also include: (1) the radiations of ray and high temperature are caused instantaneously after the explosion, and they spread out with the velocity of light and may last several tens of seconds, so the structure will sustain the impact of high temperature and may catch fire; (2) the broken pieces from damaged structures may splash out and impact other structures; (3) explosion on the ground usually causes strong shock and the underground structure may suffer serious damage, etc.

Another category of structural problem, being similar to the explosion, that happens in engineering practice is impact. For example, a missile or airplane may impact a containment of a nuclear power plant or other building, a car may impact various buildings and structures, a ship or naval vessel may impact a bridge pier, or harbor and offshore structures, a pile is impacted by the hammer, a falling weight impacts a structure below, etc.

When a structure suffers a sudden strike under occasional explosion or impact, some mechanical characteristics are shown obviously as below.

1. Particularity of the load. Usually, the load of these kinds is acted occasionally and instantaneously but a single time only, and its value is extremely large but not definite. Therefore, the design philosophy specially for these structures should be

Table 18-1 Parameters for Air Blast Wave of Hydrogen Bomb (10^9 kg)

t_z (s)	0.6	0.8	3.5
R_z (km)	1.1	1.5	2.6
Δp_z (N/mm ²)	0.6	0.3	0.1
Δp^- (N/mm ²)	0.030–0.013		
t^+ (s)	1.4–2.1		
t^- (s)	5.9–6.8		

different from that under ordinary loads. For example, the requirements for designed safety or reserved strength may be reduced, the structure entering into the plastic or yielding state and appearing greater crack and deformation even local damage is allowable under the design load, but its collapse should be avoided and protective function should be reserved.

2. Dynamic responses of structure. When an air blast wave or weight impact is acted on a structure, the pressure–time curve (Fig. 18-1(b)) is considered as a dynamic load of pulse type and is usually simplified into the composition of elevated and decay pressures (Fig. 18-2(a)). Therefore, the structure will vibrate during and after the load is acted, and the internal forces and deformation vary regularly with time, e.g. Fig. 18-2(b), which is called the dynamic responses of the structure. Consequently, the maximum internal force can be determined and the safety or damage level of the structure can be checked or estimated correspondingly. Of course, the dynamic responses of a structure have to be specially analyzed and depend upon not only the value and acting time of the load but also the weight, or mass M , and the dynamic parameters of the structure itself, including the period of free vibration (T) and damping ratio dominated by the stiffness and its variation.

3. Material loaded or deformed with high rate. The straining rate of the material in a structure ($\dot{\epsilon}$ in 1/s) is rather low under normally loading. When a structure is tested destructively in a laboratory, the average straining rate of the material is only $0.5\text{--}5 \times 10^{-6}$ /s, if the ultimate strain is 3000×10^{-6} and testing period ranges from 10 minutes to 2 hours. Generally, the standard test takes 1–3 minutes for the basic mechanical behaviors of concrete and reinforcement materials, so the average straining rate is about $10\text{--}200 \times 10^{-6}$ /s.

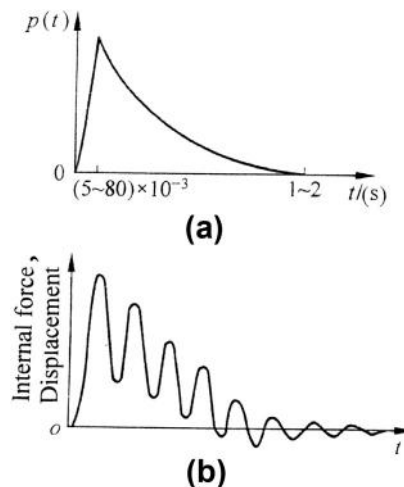


FIG. 18-2 Dynamic response of structure under explosion load: (a) load–time curve, (b) dynamic response of structure

Table 18-2 Typical Values for Straining Rate of Structural Materials Under Various Conditions [18-2]

Kind of Load	Traffic	Gas Explosion	Earthquake	Piling	Nuclear Explosion
$\dot{\epsilon}$ (1/s)	(1–100) $\times 10^{-6}$	(50–500) $\times 10^{-6}$	$(5–500) \times 10^{-3}$	$(10–1000) \times 10^{-3}$	$25–400 \times 10^{-3}$
Airplane Impact	Weight Impact	Impact with Extra High Speed	Standard Test of Material		Structural Test*
			Concrete*	Reinforcement*	
$(50–2000) \times 10^{-3}$	1–50	$100–10^6$	$10–20 \times 10^{-6}$	$50–100 \times 10^{-6}$	$0.5–5 \times 10^{-6}$
*Data given by the author.					

If the peak overpressure of an air blast wave is acted on a structure at $t_z = 5–80 \times 10^{-3}$ s after nuclear explosion and the maximum strain of the material is $\epsilon = 2000 \times 10^{-6}$, the average straining rate should be $\dot{\epsilon} = 25–400 \times 10^{-3}$ /s, which is several thousand times higher than that during the standard test of the material. Actually, the straining rate of a structural material in engineering practice varies significantly under various dynamic or impact loads, some typical values, for example, are shown in Table 18-2. Thereafter, the mechanical behaviors, including strength and deformation, of the structure and its materials are influenced considerably.

4. Particularity of the structure. Most possibly, the ordinary structures on the ground would be totally ruined within the effective range of a nuclear explosion, so the defense works and shelters have to be built underground if necessary. Of course, the stress wave is strong in soil or rock layer of the ground under the dynamic action of an air blast wave, and the load acted and internal forces of the underground structure have to be analyzed correspondingly. The structure with longer span is usually designed into an arch or thick shell, while the structure with shorter span is designed into a frame of slab–beam–column. Generally the section size and depth–span ratio of these members are rather great, and their strength is dominated mainly by shear force. In order to reduce the size and to increase the efficiency of the underground structure, structural materials of high strength are preferred.

18.2 Behaviors of materials under high-speed loading

18.2.1 Testing equipment and method

The test with high-speed loading or deforming for a specimen can not be achieved on an ordinary hydraulic testing machine. Therefore, special loading equipment is necessary to investigate the mechanical behavior of a structural material under a high straining rate. The equipment developed and manufactured in Tsinghua

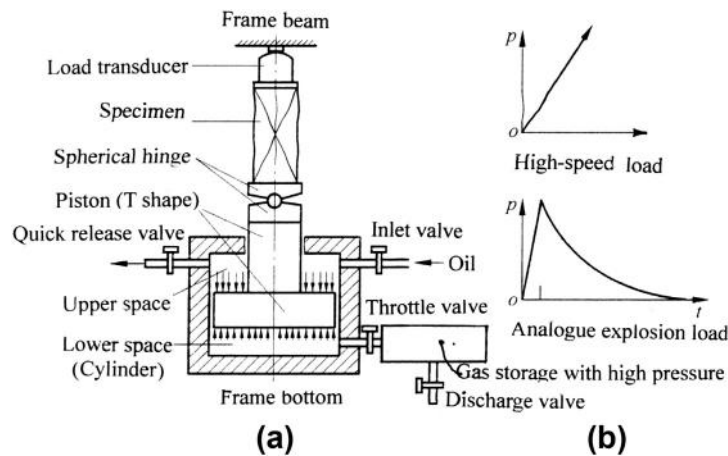


FIG. 18-3 Testing equipment for high-speed loading of material specimen: (a) structural scheme, (b) two categories of loading test

University is shown schematically in Fig. 18-3, and the maximum compression is 1500 kN, the shortest time of elevating pressure is 4×10^{-3} s, and the maximum straining rate of a specimen is $\dot{\epsilon} = 500 \times 10^{-3}/s$.

The testing equipment mainly includes the loading frame, major cylinder, gas storage with high pressure, pipes, and various valves and their control system. The loading frame is composed of four loading screws and upper and bottom beams, and the major cylinder is placed between them. There is a piston of T shape in the cylinder, and the upper and lower spaces of different area are formed in it. The lower cylinder is connected with the gas storage with high pressure via pipes and valve, and the spherical hinge, specimen, and load transducer are successively put on the upper end of the piston before testing.

Two categories of loading test can be conducted on this equipment (Fig. 18-3(b)):

1. High-speed loading (deforming). The upper space of the major cylinder is emptied out in advance. When the oil or gas is entered with high speed into the lower cylinder via the gas storage with high pressure, the piston moves immediately upwards and the specimen is compressed quickly.
2. Analogue explosion load. At first, the upper and lower spaces of the cylinder are filled separately with oil and gas, e.g. nitrogen used usually, and the pressures in both spaces are adjusted so as to keep balance of the piston. When the quick release valve is opened suddenly, the oil with high pressure in the upper cylinder releases out immediately and the gas quickly enters into the lower cylinder from the storage. Therefore, the piston rises and quickly compresses the specimen and an ascending branch of loading is formed. As the discharge valve is opened slightly later, the gas pressure in the storage, also in the lower cylinder, reduces continuously and a descending branch of loading is then formed as well. When

the oil and gas pressures respectively in the upper and lower spaces of the cylinder and the opening times and levels of the quick release and discharge valves are selected properly, the values and periods of loading (ascending) and unloading (descending) can be controlled and the load-time ($p-t$) curve needed is achieved.

The load transducer on the upper end of the specimen and the displacement transducers or strain gauges on the lateral surfaces of the specimen are connected with the vibrator oscilloscope via a dynamic strain instrument. The starting order and time of various valves and the starting time and recording velocity of the oscilloscope are properly set up in advance, then the stress and strain of the specimen varies with time during testing, i.e. $\sigma-t$ and $\varepsilon-t$ curves, can be recorded automatically. Afterwards, the stress-strain or compression-deformation ($N-\delta$) curve of the specimen is then determined consequently.

A similar testing equipment is also developed and manufactured for the tensile specimen under high-speed loading, of course the load exerted is tension only rather than compression.

18.2.2 Reinforcement

The tensile specimens of reinforcement are tested with different loading (straining) rates ($\dot{\varepsilon}$) and corresponding stress-strain curves are given. The typical measured curves of two grades of reinforcement are shown in Fig. 18-4, where t_y represents the time-span from the start of loading until yielding of the specimen.

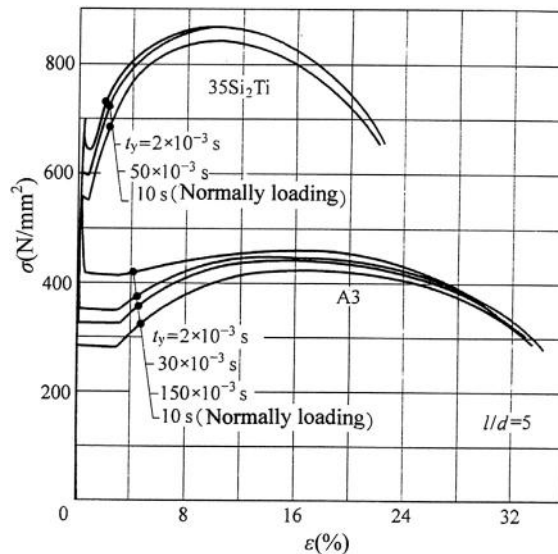


FIG. 18-4 Stress-strain curves of reinforcement under different loading rate [18-3]

According to the experimental results, the general regularities of mechanical behavior of the reinforcement, or steel, are concluded as below, when the loading or straining rate ($\dot{\epsilon}$) of the specimen increases or the loading time-span (t_y) reduces:

1. A sharp peak appears apparently at the upper yielding point. The greater the loading rate, the higher and the sharper the peak, and even the peak is higher than the ultimate strength (f_b) under standard test. However, the value measured at the peak point, i.e. upper yielding strength, scatters considerably and the succeeding value at the yielding plateau is much smaller than it, so it can not be utilized as the strength index for design in engineering practice.
2. The yield strength (f_y^{imp}) determined by the yielding plateau increases obviously and monotonically with the loading rate, while the ultimate strength (f_b^{imp}) increases slightly only by no more than 5–10%. Therefore, the ratio between the ultimate and yield strengths (f_b^{imp}/f_y^{imp}) reduces as the loading rate increases.
3. The deformation behaviors of the reinforcement, including modulus of elasticity (E_s), length of yielding plateau, and ultimate percentage elongation (δ), do not obviously vary with the loading rate.
4. The necking before failure and the necked percentage and appearance of broken surface after failure of the reinforcement under high-speed loading are not different obviously from that under standard test.
5. If the initial stress ($0.5\text{--}0.7 f_y$) is acted before high-speed loading, the strength measured is not influenced obviously.

Consequently, the main variation of mechanical behavior of the reinforcement under high-speed loading or deforming is the increment of yield strength, while the deformation behavior including ductility is not damaged. This is of particular advantage for use in the anti-explosion structure. The available test results at home and abroad [18-2,18-3] report the yield strength (f_y^{imp}/f_y) for the reinforcements of various grades and categories under high-speed loading, e.g. Fig. 18-5, and some of them are accepted in the design codes of different countries, e.g. Reference [2-12].

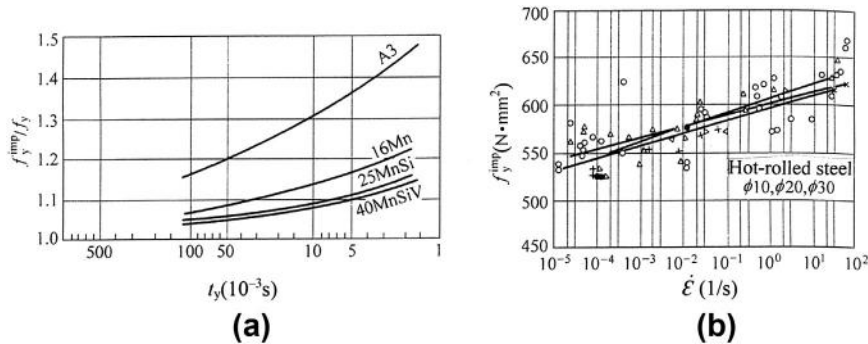


FIG. 18-5 Yield strength of reinforcement under different loading rate: (a) reference [18-3], (b) reference [18-2]

The experimental results show that the higher the strength grade of reinforcement (f_y , f_b), the smaller the increasing amplitude of the strength under high-speed loading. When the loading rate of the specimen corresponds to $t_y = 8-40 \times 10^{-3}$ s or the straining rate ranges $\dot{\epsilon} = 50-250 \times 10^{-3}$ /s, the increasing percentages of the yield strength are respectively 30% (Grade I), 13% (Grade II), 8% (Grade III), and 6% (Grade IV) for various reinforcements in China, compared respectively with that obtained from the standard test. However, the strengths of the reinforcement of even higher grade ($f_y > 600$ N/mm²) and the high-strength steel wire without obvious yielding plateau increase limitedly under high-speed loading, so no increased strength can be used during design.

18.2.3 Concrete

The stress—strain curve of concrete prism specimen are measured under compression with different loading rates (or $\dot{\epsilon}$) and is shown in Fig. 18-6, where t_c represents the time-span from the start of loading until the maximum stress or strength (f_c^{imp}) is reached.

The general regularities of the mechanical behavior of compressed concrete varying with the loading rate are concluded as below.

1. The compressive prism strength of concrete (f_c^{imp}) increases monotonically with the loading rate.
2. The shape of stress—strain curve ($\sigma-\epsilon$) measured does not vary obviously for the specimens with different loading rates. Nevertheless, the strain at peak point

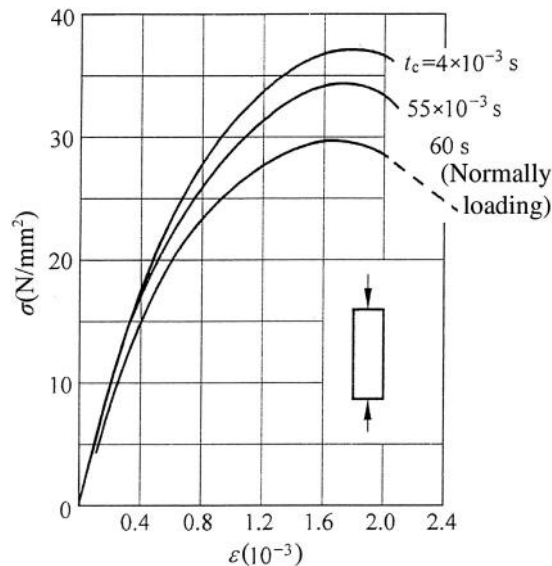


FIG. 18-6 Stress—strain curves of concrete under compression with different loading rate [18-6]

(ϵ_p^{imp}) and the modulus of elasticity (E_c^{imp}) of concrete also increase monotonically with the loading rate, and the increasing amplitude of the former is less than 10% and that of the latter is slightly higher but less than that of the compressive strength (Fig. 18-7).

3. The Poisson's ratio of concrete does not vary obviously with the loading rate.
4. The concrete under high-speed loading fails more brittle than that under normally loading and some broken pieces of high-strength concrete often splash out, although the failure pattern is similar under different loading rates.

There are many experimental results [18-2,18-4–18-7] reported on the compressive strength and modulus of elasticity of concrete under high-speed loading, and some of them are shown in Fig. 18-7. Although the general conclusions given are similar, the defined values are rather scattered. For example, as far as the difference between the concretes of high strength and middle or lower strength is concerned, reference [18-6] suggests that the increasing amplitudes of concrete strength under high-speed loading are basically identical for the concrete ranging from $f_c = 20 \text{ N/mm}^2$ to $f_c = 100 \text{ N/mm}^2$ (Fig. 18-7(a)), while reference [18-2] considers obvious differences even between the concretes of $f_c = 20 \text{ N/mm}^2$ and $f_c = 50 \text{ N/mm}^2$ (Fig. 18-7(b)). Actually, the different results are caused possibly due to the different testing equipment and method used by the individual researcher.

Summarizing all the experimental data, a quantitative conclusion is approximately drawn: as the loading or straining rate is increased every 10 times, the compressive strength of concrete is increased by 10%.

The compressive strength (f_c^{imp}) and modulus of elasticity (E_c^{imp}) of concrete under different loading or straining rate are also expressed as the calculation formulas

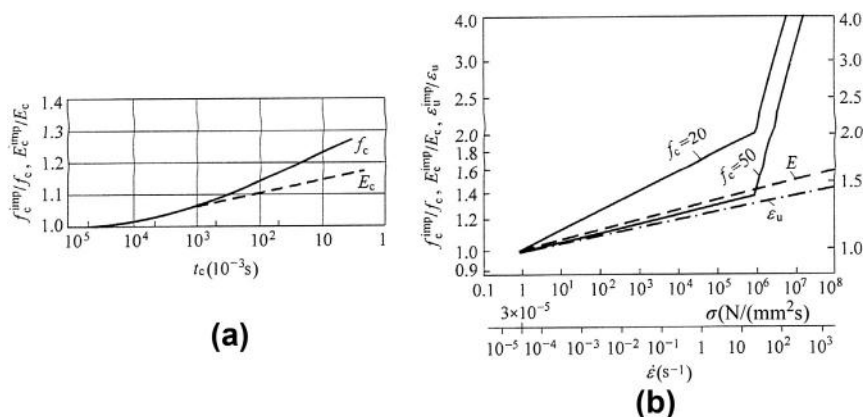


FIG. 18-7 Compressive strength and deformation of concrete under different loading rate: (a) reference [18-6], (b) reference [18-2]

besides the diagram and curve. According to the experimental data given in reference [18-2], the CEB-FIP Model Code suggests the formulas below:

$$\left. \begin{aligned} |\dot{\epsilon}| \leq 30/s \quad f_c^{imp} &= f_c \left(\frac{\dot{\epsilon}}{\dot{\epsilon}_0} \right)^{1.026\alpha_s} \\ |\dot{\epsilon}| > 30/s \quad f_c^{imp} &= \gamma_s f_c \left(\frac{\dot{\epsilon}}{\dot{\epsilon}_0} \right)^{1/3} \end{aligned} \right\} \quad (18-1)$$

$$\text{and} \quad E_c^{imp} = E_c \left(\frac{\dot{\epsilon}}{\dot{\epsilon}_0} \right)^{0.026} \quad (18-2)$$

where $\dot{\epsilon}$ -straining rate of concrete in 1/s,

$$\begin{aligned} \dot{\epsilon} &= 30 \times 10^{-6}/s, \\ \text{other parameters} \quad \alpha_s &= \frac{1}{5 + 0.9f_c}, \quad \log \gamma_s = 6.156\alpha_s - 2. \end{aligned} \quad (18-3)$$

In reference [18-7], the compressive strength of a concrete specimen measured under standard test is $f_c = 37.43 \text{ N/mm}^2$ and the straining rate tested of the specimen ranges from $10\text{--}20,000 \times 10^{-6}/s$, and the empirical formulas are suggested below for the compressive strength and modulus of elasticity of concrete under different straining rates ($\dot{\epsilon}$):

$$f_c^{imp} = f_c \left[1 + 0.0622 \lg \left(\frac{\dot{\epsilon}}{\dot{\epsilon}_0} \right) \right] \quad (18-4)$$

$$E_c^{imp} = E_c \left[1 + 0.0452 \lg \left(\frac{\dot{\epsilon}}{\dot{\epsilon}_0} \right) \right], \quad (18-5)$$

where $\dot{\epsilon}_0 = 10 \times 10^{-6}/s$ is taken.

The tensile strength and modulus of elasticity of concrete are also experimentally investigated under high-speed loading and some of the results are shown in Fig. 18-8. It is generally concluded that the variation regularity of tensile behavior of concrete is similar to that of the compressive one, as the loading rate increases. However, the increasing amplitude of tensile strength is slightly greater ($f_t^{imp}/f_t > f_c^{imp}/f_c$), that of tensile peak strain is approximate ($\epsilon_t^{imp}/\epsilon_t \approx \epsilon_c^{imp}/\epsilon_c$), and that of modulus of elasticity is slightly smaller ($E_t^{imp}/E_t < E_c^{imp}/E_c$), comparing respectively with that under compression. In addition, the related formulas are given for calculation in some references [2-12, 18-2, 18-7].

The available experimental data [18-2, 18-10] demonstrate that the loading rate has only negligible influence on the bond strength between plain reinforcement and concrete, while the bond strength between deformed reinforcement and concrete

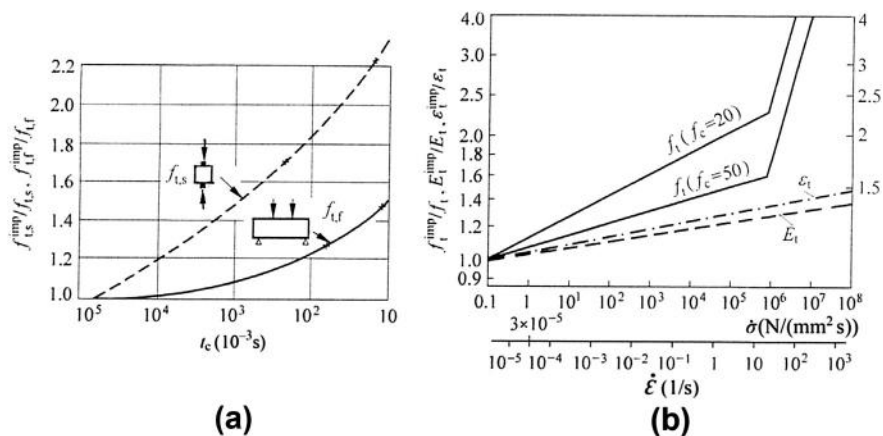


FIG. 18-8 Tensile strength and deformation of concrete under different loading rate: (a) splitting and flexural tensions [18-8], (b) central tension [18-2]

is obviously influenced and related to the strength grade of the concrete. In addition, some empirical formulas are given in the reference. The qualitative conclusion derived [18-1] shows that the increasing amplitude of the bond strength under high-speed loading is greater than that of the tensile strength of the reinforcement. Therefore, the same anchorage and splice lengths of the reinforcement in a concrete structure under normal loading can also be used for that under high-speed loading, and the bond safety of the reinforcement is guaranteed.

18.3 Behaviors of structural members

18.3.1 Flexural member

The responses of a reinforced concrete beam under high-speed loading or deforming also have to be experimentally investigated, using special loading equipment and measuring instruments. The beam specimens reported in reference [18-11] are tested separately under two kinds of high-speed loading: (1) loading with constant deforming rate: the ultimate strength and failure pattern of the specimens are determined, when the time-span is $t_y = 50 \times 10^{-3}$ s from start of loading until yielding of the tensile reinforcement; (2) analog explosion load (Fig. 18-3(b)) — the residual behaviors of the specimens after explosion are examined, when the peak value of explosion load is taken as 85–95% of the load corresponding to yielding of the tensile reinforcement in the specimen under high-speed loading and the ascending and descending branches of loading respectively take about 50×10^{-3} s and 1 s.

The typical curve of load (or resistance)-deflection at mid-span ($P-w$) of the reinforced concrete beam under high-speed loading test with constant deforming

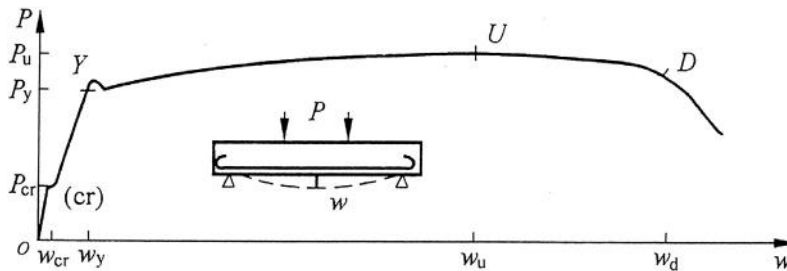


FIG. 18-9 Load—deflection curve of beam under high-speed loading [18-11]

rate is shown in Fig. 18-9. The macroscopic appearance of it is quite similar to that under normal loading (Fig. 11-1), and the special geometric points on the curve obviously present the mechanical stages and characteristic of the specimen.

When the concrete in the tension zone does not crack yet and the load—deflection ($P-w$) relation is linear in the early stage of loading, the beam is within the elastic stage. The load—deflection curve turns suddenly under load P_{cr} and even an apparent plateau appears there for a beam with rather low content of reinforcement, when the tensile concrete is cracked. Usually, the cracking load (P_{cr}) or bending moment (M_{cr}) of the beam under high-speed loading is greater by 13–33% than that under normal loading, because the tensile strength of concrete is increased with loading rate. Afterwards, the beam works continuously but with cracks in it.

The stiffness of the beam (P/w or dP/dw) before and after cracking of concrete under high-speed loading are slightly greater respectively than that under normal loading, because the modulus of elasticity of concrete is increased as well.

When the tensile reinforcement in the beam is yielded under high-speed loading, the load (also resistance) appears first as a peak value and slightly descends later, which corresponds to the peak of upper yielding point of reinforcement alone (Fig. 18-4). In addition, the smaller the content of tensile reinforcement in the beam, the higher the yielding peak formed. Usually, the yielding load (P_y) or bending moment (M_y) of the beam is taken as the lower value post peak (Point Y), which is still greater than that under normal loading. However, the corresponding deflection (w_y) is approximate for the beams under different loading rate.

The deflection of the beam accelerates as the load increases slightly after yielding of the reinforcement. Correspondingly, the strain of tensile reinforcement increases continuously, the tensile crack of concrete expands and extends upwards, and the area of compression zone on the section is reduced. Consequently, the compressive strain of concrete at extreme fiber increases and later reaches the peak strain (ϵ_p^{imp}), and enters into the descending branch of stress, so horizontal cracks appear gradually on the compression zone. In the meantime, the distance between the tensile reinforcement and the resultant of compressive concrete on the section, i.e. lever arm, increases slowly but decreases later on, so the value of bending

moment (resistance) varies limitedly and a long and flat curve of plastic deformation is then formed. The top (Point U) on the curve is the ultimate load (P_u) of the beam, and the ultimate bending moment (M_u^{imp}) is easily calculated. As the beam is deformed further, the compression zone on section expands downwards and more concrete there is cracked horizontally, crushed and spalled off, so the bending moment (resistance) of the beam is apparently reduced (Point D) and the load–deflection (P – w) curve suddenly turns downwards.

Comparing the mechanical indices of the reinforced concrete beam measured under high-speed loading with that under normal loading, some conclusions can be drawn as below.

The ultimate strength (bending moment) of the beam under high-speed loading increases obviously and the increasing amplitude depends mainly upon the strength grade of the reinforcement used, e.g. $M_u^{imp}/M_u = 1.25$ (for grade I), 1.07–1.16 (grade II), 1.06–1.12 (grade III), or 1.06 (grade IV) [18-11], which is approximately consistent with that of yield strength of reinforcement (f_y^{imp}/f_y).

However, no difference is found obviously between the beams with the same parameter but tested separately under high-speed loading and normal loading, as far as the deformation indices are concerned, including the ultimate strain of compressive concrete, the deflections at the maximum load (w_u) and the start to descend obviously (w_D), ductility ratios (w_u/w_y , w_D/w_y), and others.

The load–deflection curves of flexural members (Fig. 18-10) under high-speed loading, like that under normal loading, vary with different content of tensile reinforcement ($\mu = A_s/bh_0$). Because the reinforcement contents of these beams tested are much smaller than the upper boundary ($\mu_{\max} \approx 0.42 f_c/f_y$ for the steel 35 Si₂Ti used), they fail certainly in the pattern of being suitably reinforced (Section 11.1.2) which is controlled by the tensile reinforcement. When the reinforcement content of the beam is increased, the load at yielding of reinforcement (P_y) and the ultimate load (P_u , or strength M_u) almost increase proportionally, while the plastic deformation after yielding of reinforcement and the ductility ratio reduce correspondingly.

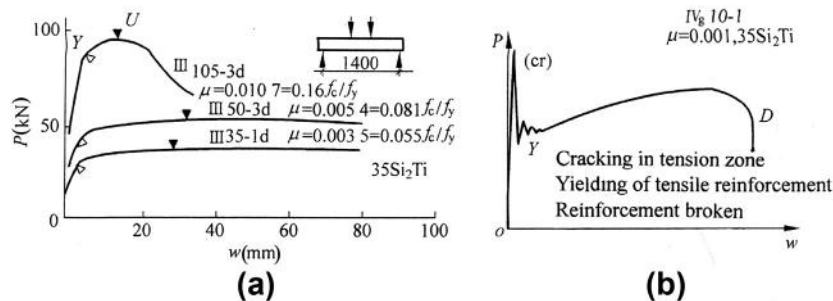


FIG. 18-10 Load–deflection curves for beams with different reinforcement contents under high-speed loading [18-11]: (a) $\mu = 0.0035$ – 0.0107 , (b) $\mu = 0.001$

When the reinforcement content of the beam is too low (e.g. $\mu = 0.001$ in Fig. 18-10(b)), the load at cracking of tensile concrete (Point P_{cr}) is higher than that at yielding (Point Y) and also at breaking (Point D) of the tensile reinforcement. The maximum load acted drops sharply soon after the first tensile crack occurred on the critical section, but no crack appears later on another section of the beam. The reinforcement at cracked section deforms significantly and is necked prior to being broken. At this time the maximum strain of concrete on compression zone of the critical section is only about 2000×10^{-6} and no failure symptom is observed there.

On the other hand, the results of another category of high-speed loading test, i.e. under analogue explosion load (Fig. 18-3(b)), demonstrate that the beam is certainly safe and the deformation and crack caused during and after testing are limited only, if the stress of tensile reinforcement under the peak load during testing is smaller than the yield strength (f_y^{imp}). Usually, the maximum width of concrete crack under the peak load is 0.2–0.4 mm, varying with strength and content of the tensile reinforcement used. And, the residual width of the crack is smaller than 0.1 mm after test of the beam, and the higher the content of the tensile reinforcement, the smaller the crack width, e.g. 0.03–0.04 mm only for the beam of reinforcement content $\mu = 0.015$. In addition, the crack width of the beam is not increased even if the explosion load is repeated several times. For example, the beam reinforced with the cold-stretched steel of grade IV (45MnSiV) is acted successively six times the explosion load and the maximum stress experienced by the tensile reinforcement reaches 770 N/mm^2 , the residual width of concrete crack finally accumulated is still less than 0.2 mm.

Accordingly, when a reinforced concrete beam is designed or checked for its explosion response, the principles below are usually followed.

Flexural strength. The calculation method and formulas used for the beam under normal (static) loading also fit for that under high-speed loading, but the strengths of reinforcement and concrete (f_y^{imp} , f_c^{imp}) there varying with the loading or straining ($\dot{\epsilon}$) rate have to be considered. It is demonstrated that the ultimate bending moment calculated (M_u^{imp}) of the beam is smaller than the experimental one, so the calculation method can be used safely and even more safely for the beam with less content of reinforcement. In addition, the bending moments at cracking of concrete (M_{cr}^{imp}) and yielding of reinforcement (M_y^{imp}) of the beam can also be calculated following same principle.

Stiffness and deformation. When the sectional stiffness or curvature and the deformation of beam at cracking or yielding are calculated, the corresponding methods for the beam under normal loading can also be used. However, the values of the moduli of elasticity and characteristic strains of the reinforcement and concrete used in the calculation should be modified to fit the loading or straining rate that occurs.

Limitations of reinforcement content. The flexural member should be designed with enough plastic deformability, in order to prevent total collapse and to improve the shock resistance of it under explosion. The basic and effective measure used

popularly in engineering practice is to control strictly the reinforcement content for the section, i.e. the maximum content (μ_{\max}) should be reduced while the minimum content (μ_{\min}) should be increased, compared with that of the beam under normally loading (Section 11.1.2). The limitations of reinforcement content suggested in reference [18-11] are

$$\left. \begin{aligned} \mu_{\max} &= 0.3 \frac{f_c}{f_y} \\ \mu_{\min} &= (0.14 \sim 0.30)\% \end{aligned} \right\}, \quad (18-6)$$

where the greater value of μ_{\min} is used for the beam of high-strength concrete and reinforced with the reinforcement of lower strength, and vice versa.

Enhancement of structural detail. For example, more compressive reinforcements and closer stirrups are set up properly in the beam, so the plastic deformability is then enhanced favorably, although the ultimate strength is increased limitedly. In addition, the anchorage and splice lengths of the reinforcement are extended; the reinforcement and stirrup within a joint and nearby between beams and columns are enhanced; the concrete cover of deformed reinforcement is increased. These measures are certainly favorable for collapse resistance of the structure and should be carefully considered during design.

The shear resistance of the reinforced concrete beam under high-speed loading or straining should be considered seriously. If failure of the beam is dominated by shear force, different patterns like that of the beam under normally loading, including inclined compression, shear-compression, and inclined tension, may also occur and depend upon the shear-span ratio (a/h_0). The ultimate shear strength of the beam is obviously elevated, and the increasing amplitude (V_u^{imp}/V_u) varies with the failure pattern that occurs and is consistent respectively with that of the compressive (f_c^{imp}/f_c) or tensile (f_t^{imp}/f_t) strength of concrete.

Usually, when the ultimate shear strength of a beam under high-speed loading or straining is calculated or checked, the same method and formulas fitting for that under normal loading can be used, and, of course, the strengths of the materials depending upon the loading or straining rate should be introduced. It is noticed that the error and lower value taken in the calculation (e.g. Fig. 14-13, Eqs. (14-7) and (14-8) in Section 14.3.2) are also included in the calculated result. When the beam is designed, it should be guaranteed that the cracking of tensile concrete and yielding of tensile reinforcement of the beam under bending moment occur prior to the failure with inclined crack under shear force and more shear resistance is reserved for safety, in order to satisfy the plastic deformability needed for the structure under explosion.

18.3.2 Compressive member

The mechanical behaviors of centrically and eccentrically compressed members of reinforced concrete are also experimentally investigated under high-speed loading

or deforming. Two categories of loading are reported in the reference [18-12]: (1) high-speed loading with constant deforming rate of the specimen and the time-span being $t_y = 40\text{--}50 \times 10^{-3}$ s from the start of loading until the maximum load or yielding of tensile reinforcement; (2) analog explosion loading and the time-spans of ascending and descending compressions being respectively 50×10^{-3} s and about 2 s.

The axial force—strain curve of the centrally compressed member measured during high-speed loading with constant straining rate is shown in Fig. 18-11 and is compared with that measured during normal loading. It is seen that the shapes of both curves are similar, and the peak compression of the former is obviously higher than that of the latter while the corresponding strains ($\varepsilon = 2300\text{--}3000 \times 10^{-6}$) are different slightly.

When the eccentrically compressed member is tested under high-speed loading with constant deforming rate, two typical failure patterns of the smaller and greater eccentricities (Section 11.1.3) may also occur successively as the eccentricity of the load (e_0/h) increases. The mechanical behavior and failing process of both patterns are similar respectively to that of the centrally compressed member (Fig. 18-11) and flexural member (Fig. 18-9). In addition, the failure appearance and boundary eccentricity of the member are consistent separately with that under normal loading. The ultimate strength of the member varies with the loading or deforming rate and increases similarly with the strength of the material, while the characteristic deformations and plastic deformability of the member approximate to that of the member acted statically with the same eccentricity.

When the reinforced concrete member is tested under analog explosion loading, the main conclusions obtained [18-12] are as below. If the peak compression acted centrally during testing ranges from 50% to 80% of the ultimate strength (N_u^{imp}), no crack is found on the surface of the member after tested. And, if the member is tested again under normal loading, the ultimate strength (compression N_u) measured is not necessarily smaller than that of the member without previous loading. However, if the peak compression reaches $0.95N_u^{imp}$ during analog explosion testing,

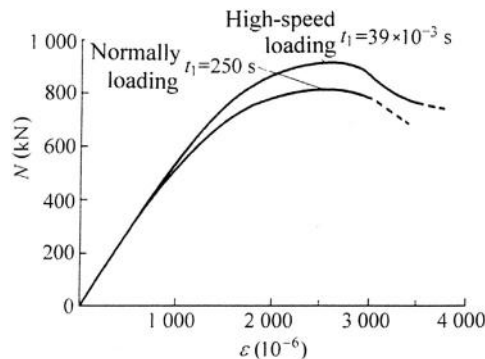


FIG. 18-11 Axial force—strain curves of columns acted with centric compression [18-12]

the member fails within the descending branch of loading at 70×10^{-3} s post peak compression. This is called delayed failure, which often occurs for the compressed specimen of plain concrete under analog test of explosion load. Therefore, the explosion load with slowly descending branch after the peak pressure should be treated very carefully in engineering practice.

When the member is eccentrically compressed first under the analog explosion loading and the peak compression experienced is smaller than $0.8N_u^{imp}$, the residual width of the concrete crack measured after testing is less than 0.03 mm. If the member is tested again under high-speed loading with constant deforming rate until its failure, the ultimate strength measured is not obviously different from that of the member without previous loading (N_u^{imp}).

The general conclusions can be derived as below from these experimental results. The ultimate strength of a reinforced concrete column increases obviously under high-speed loading or deforming and the increasing amplitude mainly depends upon that of the strength of reinforcement (f_y^{imp}/f_y) or concrete (f_c^{imp}/f_c) under the same straining rate, while its deformation behavior and failure pattern are not different obviously from that of the column under normal loading. When the ultimate strength and deformation of the column are calculated, the corresponding formulas fitting well for the column under normal loading can also be used, but the strength and modulus of elasticity of the material have to be modified for different loading or straining rates. It is demonstrated that results calculated in this way are on the safe side.

CHAPTER OUTLINE

19.1 Characteristics of fire resistance of structures	475
19.2 Temperature field on section	479
19.2.1 Temperature–time curve	479
19.2.2 Thermal behaviors of materials	481
19.2.3 Basic equation for heat conduction and determination of temperature field	485
19.3 Mechanical behaviors of materials at elevated temperature	487
19.3.1 Behavior of reinforcement	487
19.3.2 Basic behavior of concrete	491
19.4 Coupling constitutive relation of concrete	499
19.4.1 Upper and lower bounds of compressive strength	500
19.4.2 Thermal strain under stress and transient thermal strain	501
19.4.3 Short-term creep at elevated temperature	504
19.4.4 Coupling constitutive relation	505
19.5 Behavior and calculation of structural members at elevated temperature	505
19.5.1 Flexural and compressive members	505
19.5.1.1 <i>Flexural member</i>	505
19.5.1.2 <i>Central compressive member</i>	507
19.5.1.3 <i>Compressive–flexural member</i>	508
19.5.1.4 <i>Influences of different load-temperature paths</i>	511
19.5.2 Statically indeterminate structure	513
19.5.3 Analysis and approximate calculation	516

19.1 Characteristics of fire resistance of structures

Generally, the concrete structure works under normal temperature within the construction period and long service life, and its environmental temperature has a low value, e.g. less than 80°C or 100°C, and fluctuation. The structure can satisfy the requirements of safety and service performance, when it is designed following the current codes [2-1,2-11,2-12]. However, if the environmental temperature elevates suddenly too much or varies periodically many times, the structure may fail as its service performance deteriorates or strength decreases, sometimes it may be destroyed locally or even collapse totally.

Owing to the temperature change, the thermal problems that occur usually in structural engineering can be classified into three categories:

1. Temperature changes periodically or occasionally beyond the normal value.

For example as a high-rise or long-span building is concerned, the temperature on its surface exposed to the sun increases when there is sunshine and decreases after sun-set, and the air around the building increases in summer and decreases in winter, then the temperature difference appears periodically in the interior of the structure and its internal force should redistribute correspondingly, and more deformation and cracks may be caused. In addition, the non-uniform temperature field [19-1] will be formed in a massive hydraulic structure (i.e. dams, etc.), because of accumulation of the hydration heat of cement in concrete during the hardening process and the temperature variation caused by the circumferential water, air, and sunshine. Although the maximum temperature reached in the interior of the structure is not too high (generally less than 60°C), the strain induced by the temperature change (e.g. $\pm 30^{\circ}\text{C}$) is much greater than the value of the ultimate tensile strain of concrete. Therefore, it is sufficient to cause cracking of the concrete in a large area and water leakage may result, then the service function and safety of the structure are damaged.

2. High-temperature action lasts for a long time under normal working conditions of the building.

For example, some structures in metallurgy and chemical industry workshops work under radiation of high temperature all year round, and the temperature on their surface may reach 200°C or even higher. When a chimney spurts smoke of high temperature, the temperature may reach $500\text{--}600^{\circ}\text{C}$ at the internal lining and $100\text{--}200^{\circ}\text{C}$ on the external surface. In the reactor vessel and containment structures of a nuclear power plant, the temperature of concrete may reach 120°C or even higher at local positions.

3. High-temperature impact in a short time is caused by occasional accidents.

For example, a building fire may last a few hours and the maximum temperature of the fire may reach 1000°C or even higher within one hour only. If a chemical or nuclear explosion or an accident of nuclear plant occurs, the temperature may reach several thousands centigrade or even higher within a short time counted in seconds or milliseconds.

These thermal problems in structural engineering have different temperature ranges and variation rules, which cause considerable differences in the material and structure behaviors and damage levels of the structure. Correspondingly, different design codes [19-2—19-6,3-19] are suggested for various structures in home and abroad, in which the general instruction, design and calculation methods, and material used and structural details are included. This chapter mainly deals with the third category of the structural thermal problem, and the mechanical behaviors and analyses of the structure and its materials under fire or high temperature are introduced in detail. The method and conclusion given can also be used as a reference for other categories of structural thermal problems.

As serious fire accidents occur frequently every year worldwide due to various natural, technical, and manmade reasons, enormous natural resources, social property, and human life are lost, and it may cause serious social unrest. Moreover, the harmfulness of building fires gets more and more seriously, as human society develops quickly and people and property are more highly concentrated in modern cities.

In order to prevent or reduce losses in fire accidents, many effective measures are presented based on the experience and lessons learnt from previous fires and the experimental investigations and theoretical research completed. These measures may be generalized into two respects: (1) Preventing fire accidents from occurring and spreading. For example, when a building is designed [19-7], the circumference space and road for a fire-truck should be reserved sufficiently, the material used and detailing are selected to satisfy the fire-endurance grade required, the equipment and furniture in the rooms would be better made of incombustible material and a refractory coating should be sprayed upon the combustibles, an automatic alarm and sprinkler should be installed, etc. (2) Enhancing the fire resistance of architectural and structural members. For example, large furnaces are built specially for testing and measuring the endurance limit of the full-scale members, the structural material is selected reasonably and the structural detail is improved, an insulated material is set up on the member surface, experimental and theoretical researches are conducted systematically on the thermal-mechanical behavior, the design and calculation methods are developed correspondingly, etc.

Several kinds of material have been used in structural engineering. Timber structure itself is a combustible, and it can not prevent a fire and even enhances the fire after being lightened up. Although steel structure is not a combustible, the temperature of steel member rises quickly under a fire accident and then the load-bearing capacity is reduced and the local buckling is caused or even the whole structure can collapse, because heat conducts very quickly in steel and the structural members are usually composed of thin-wall-shaped steels and plates. However, the main part of reinforced concrete is concrete which is a material of heat inertia and the main structural members usually have thick sections. So, the temperature in the interior of the member elevates slowly under fire accidents and the temperature rise of the reinforcement is delayed by the outer cover. Therefore, the strength of the material loses less and the load-bearing capacity of the member decreases slowly, and the fire-resistant behavior and the endurance limit of the reinforced concrete structure are much better than that of steel and timber structures.

Of course, if the fire continues for a long time, the damage and failure phenomena of different levels will appear successively in the concrete structure: cracking and loosening on the surface, damage to the edge and corner, explosive spalling of the cover, reinforcement bared, deflecting of the member, surface layer separating gradually from the main body, and damage area penetrating into the interior of the member, and finally local holes, cave in, and collapse of the structure may result.

When a fire accident occurs in a building, the structure acted as the load-bearing and support system should keep sufficient strength and endure a longer time under fire, in order for the rescue of victims, injured and died people, and to save important

property. Therefore, it is considered that the structure is failed under fire, if one of the three limit states [19-8,19-9] below is reached:

1. **The limit state of load-bearing capacity.** The load-bearing capacity of the structure reduces continuously under fire accident (at elevated temperature). The limit state reaches when the service load can not be supported any more, because of the structural collapse, or instability, or excessive deflection (e.g. 1/30 of the clear span).
2. **The limit state of obstructing fire.** The integrity of the structure is damaged under fire, so the fire spread and smoke flow can not be stopped again when wide cracks and holes are formed.
3. **The limit state of heat insulation.** When the temperature on the surface unexposed to fire of the structural member increases too much (e.g. 140°C for average value or 180°C for the maximum value), it may cause fire in adjacent rooms and the fire spreads.

When a structural member (e.g. slab, wall) or an architectural member (e.g. partition, door, window) reaches one of the three limits under the fire following the standard temperature time curve (Eq. 19-1, Fig. 19-2), the duration time of it is called its endurance limit (in hours). According to the Code of Fire-Prevention of Building [19-7], a building can be classified into four grades depending upon its importance, and a minimum endurance limit (0.5–4 hours) is stipulated for different members.

In order to measure practically the endurance limit of various members, special furnaces should be built correspondingly, in which gas or oil is used and sprayed into it and the temperature should elevate following the standard temperature–time curve after a fire is lighted. When a structural member is tested, it is installed first in the furnace and the service load is applied and maintained constantly, then the fire is lighted and the temperature inside elevates continuously until one of the limit states is reached. If the furnace is not available, the thermal behavior and endurance limit of various structural and architectural members of different material and size may be consulted from relevant literature [19-8,19-9] and can be used as a reference during design.

According to the existing results of the experimental and theoretical researches and the experience of the engineering practice, the behaviors of reinforced concrete structures at elevated temperature (under fire) are considerably different from that under normal temperature. The characteristics of them are as follows [19-10].

1. **Temperature distributed non-uniformly in the interior.** The temperature on the surface of the structure rises very quickly under fire but the temperature in the interior increases slowly, because the thermal conductivity of concrete is rather low. So, a non-uniform temperature field is formed in the structure, especially a large temperature gradient appears at its outer layer. Besides, the temperature field varies continuously as long as the fire lasts. The main factors determining the temperature field of a structure are the temperature–time process and duration of the fire, the shape and size of its members, and the thermal behavior of the concrete material. However, the internal forces, deformation, and small

crack of the structure have less influence on the temperature field. On the contrary, the temperature field of the structure influences significantly on the internal forces, deformation, and bearing capacity of it. Therefore, the analysis of the temperature field of a structure can be conducted independently and should be conducted in advance of the mechanical analysis of it.

2. **Serious deterioration of the material behavior.** The values of the strength and elastic modulus of concrete and reinforcement at elevated temperature decrease considerably and the deformations of both materials increase correspondingly. Besides, the external damage phenomena of concrete, e.g. cracking, loosening, and spalling off, appear successively and become gradually more severely as the temperature increases. This is the main reason that causes serious reductions of the bearing capacity and the endurance limit of the structure and its member at elevated temperature.
3. **Coupling effect of stress—strain—temperature—time.** When a structure under normal temperature is analyzed mechanically, only the stress—strain relation of the material is necessary. However, the value and duration of high temperature have a strong influence on the strength and deformation of the material. Furthermore, different heating and loading history cause unequal values for the strength and deformation of the same material, a coupling effect is then composed of four factors: stress, strain, temperature, and time for the concrete. Therefore, in order to analyze accurately the behavior of the structure at elevated temperature, it is necessary to develop a corresponding coupling thermal-mechanical constitutive relation for concrete. Of course, this causes more work and difficulty for analyzing the structure and its member.
4. **Redistributions of stress on member section and internal force of structure.** The non-uniform temperature field of a member section inevitably results in unequal temperature strain and stress redistribution on it. The thermal deformation of the material in a statically indeterminate structure under high temperature is restrained by the adjacent material and structure of different temperature and the joint or support, so the redistributions of internal forces (i.e. bending moment, shear force, and axial force) are serious. In addition, the temperature field of a structure varies with the temperature and duration of the fire and the internal forces of the structure redistribute correspondingly, so both thermal and mechanical analyses of it are dynamic process.

19.2 Temperature field on section

19.2.1 Temperature—time curve

When a fire accident occurs in a building, the fire generally experiences several stages, i.e. fire lighting up, spreading out, and declining and going out. It is also possible under some situations that the fire declines and burns again repeatedly

before it goes out eventually. The whole process usually takes a few hours but, sometimes, may last several days, e.g. if the fire accident occurs in an underground space. If the fire reaches higher temperature and lasts a longer time, more serious losses will result. The seriousness of a fire accident depends mainly upon following factors: (1) thermal behavior of building material, (2) property, quantity, and distribution of all the combustibles in the room, (3) area and shape of the room and areas and positions of the window and door, and (4) air flow and ventilation conditions.

The direct effect is heating the surface of a structure if a fire acts on it, so the temperature—time ($T-t$) curve of the fire is the basic and the most important condition for the thermal analysis of the structure. The actual variation of a fire temperature can be illustrated by a series of experimental results of wood burning in a full-scale room. The first and second figures near each curve (in Fig. 19-1) show respectively the quantity of wood (in kg/m^2) burning in the room and the percent between the area of window and door holes on the wall and the gross area of the wall. It is seen that the temperature reaches quickly (within 10–40 minutes) the maximum value after the wood is lighted up and a longer period of declining and going out is succeeded afterwards.

Up to now, some theoretical and empirical formulas [19-5,19-9] are available for calculating the temperature—time curve of a simple fire based on the main parameters. However, more complicated conditions exist in engineering practice, e.g. different combustibles are mixed and their quantities and distributions are irregular in the room, air flow and ventilation vary considerably, and even the combustibles in the room can not be predicted during the design of the building. Therefore, the temperature—time curve of a fire accident is random to a great extent. In order to unify the requirement of fire resistance of the structures and to establish objectively a comparative base, some research institutions and organizations suggest several

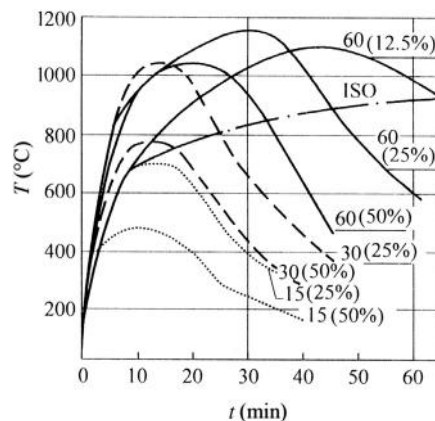


FIG. 19-1 Temperature—time curves measured from tests of burning wood [19-8]

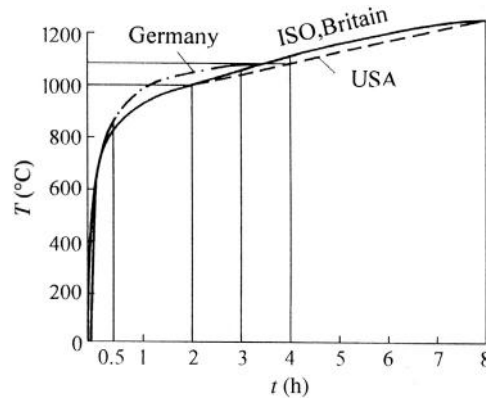


FIG. 19-2 Standard temperature–time curve for fire accident [19-8]

standard temperature–time curves of fire (Fig. 19-2). Among them the standard curve suggested by the International Standard Organization (ISO) for fire-resistance test of structure is used most widely and expressed as

$$T - T_0 = 345 \lg(8t + 1), \quad (19-1)$$

where T_0 is the initial temperature and 20°C is usually taken, and T is the temperature at t minutes after the fire has been lighted.

These curves show obviously the monotonic heat process without a cooling stage, and they are approaching one another except a few, but none of them is identical with the actual fire occurring in a building (e.g. Fig. 19-1). However, the standard temperature–time curve can be used as a criterion to conduct the fire-resistance test and thermal analysis and to check the fire-endurance limit for a structure or its members, in order to ensure the same fire-resistance capacity or to offer a comparable fire-resistance safety for different structures and their members.

19.2.2 Thermal behaviors of materials

When the temperature field of a structure is theoretically analyzed and the basic equation of heat conduction (Eq. 19-8) is established, it is necessary to know in advance the basic thermal parameters of the material, which include coefficient of heat conductivity (λ), specific heat capacity (c), and mass density (ρ). Besides, another basic thermal parameter of the material is linear expansion coefficient (α) or the thermal expansion strain (ϵ_{th}), which influences only the thermal strain and stress of the structure but is unrelated to its temperature field. Of course, the values of these parameters are different for various materials and vary non-linearly with the temperature elevation.

The thermal behavior of concrete varies considerably and mainly depends upon the chemical composition and mineral texture of its raw material, mixing ratio, water content, etc., and the experimental data of the thermal parameters measured are deviated. The experimental results (Fig. 19-3) are shown as some examples, but they exhibit the general values and variation regularity for the thermal parameters of concrete.

When a prismatic concrete specimen is heated monotonically, its length and corresponding thermal strain (ε_{th}) increase and depend mainly upon the aggregate in it. Usually, the thermal strain of the concrete with light-weight aggregate is much smaller than that of ordinary concrete. When the testing temperature $T < 200^{\circ}\text{C}$, the solid components of the concrete, including coarse aggregate and hardened cement mortar, expand due to elevated temperature and shrink simultaneously due

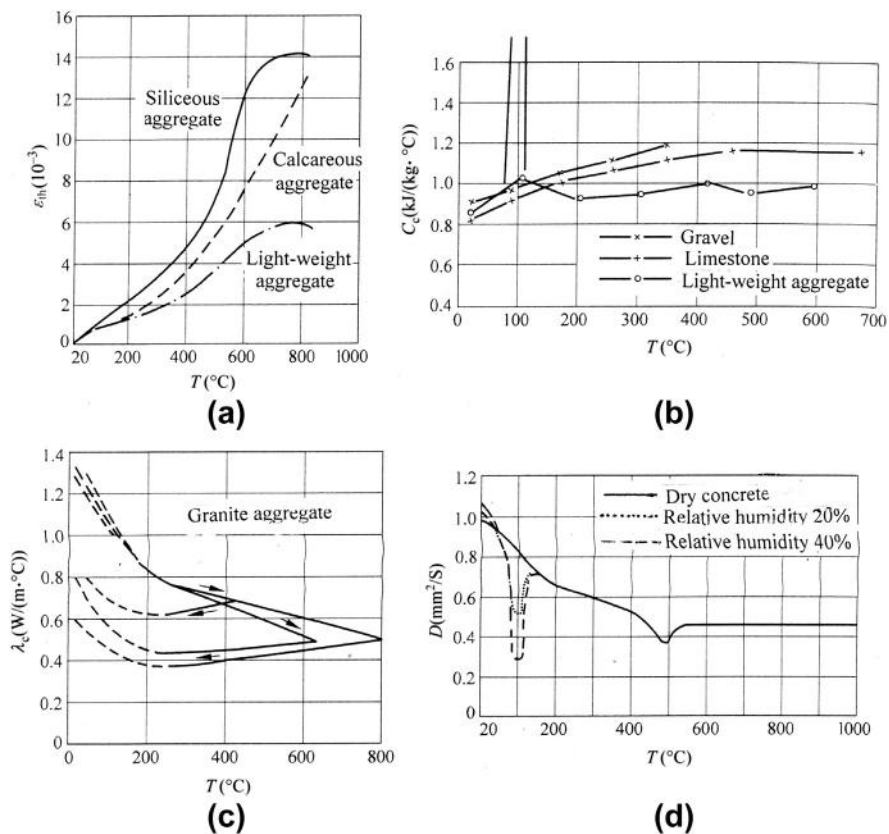


FIG. 19-3 Experimental results of thermal parameters of concrete [19-6]: (a) thermal expansion strain, (b) specific heat capacity, (c) coefficient of heat conductivity, (d) heat diffusivity

to water loss. Both factors compensate and cause smaller strain (elongation, e.g. $\varepsilon_{th} = 0.8 \times 10^{-3} - 1.5 \times 10^{-3}$ at 200°C). When $T = 300 - 600^\circ\text{C}$. The solid components expand continuously and the cracks on the boundary of aggregate appear and extend gradually, so the thermal strain increases quickly, e.g. $\varepsilon_{th} = 6 \times 10^{-3} - 9 \times 10^{-3}$ at 500°C . When $T > 600^\circ\text{C}$, the increasing rate of the thermal expansion strain slows down or even ceases, possibly because the crystal of mineral component within the aggregate varies and the internal damage of concrete accumulates. The thermal strain may reach $\varepsilon_{th} = 10 \times 10^{-3}$ or even more at this time.

Fitting with the definition, the **average value of linear expansion coefficient** of concrete can be calculated based on the measured thermal strain:

$$\bar{\alpha}_c(T) = \frac{\varepsilon_{th}}{T - T_0}. \quad (19-2)$$

Its value varies non-linearly with temperature and ranges usually from $6 \times 10^{-6}/^\circ\text{C}$ to $30 \times 10^{-6}/^\circ\text{C}$.

When the concrete specimen is cooled down to the initial temperature soon after heating to the predetermined temperature, the thermal strain (elongation) reduces gradually but does not vanish completely (Fig. 19-18). Therefore, a residual strain (elongation) of the concrete exists and depends upon the maximum temperature ever reached. If the concrete experiences several heating-cooling cycles, the thermal strain varies correspondingly [19-11].

The **mass heat capacity** or **specific heat capacity** (c in $\text{J}/(\text{kg} \cdot ^\circ\text{C})$) is defined as the quantity of heat (J) absorbed per unit mass (kg) of a material when its temperature elevates 1°C . The value of specific heat capacity of concrete (c_c) increases gradually with temperature and tends to be stable when $T > 600^\circ\text{C}$. However, a sharp peak appears near $T = 100^\circ\text{C}$, because the water contained in the interior of concrete evaporates suddenly and a lot of steaming heat is absorbed. Generally, the different aggregates of concrete have less influence on the specific heat capacity.

The **thermal conductivity** or **coefficient of heat conduction** (λ in $\text{J}/(\text{h m}^\circ\text{C})$ or $\text{W}/(\text{m}^\circ\text{C})$) of a material is defined as the quantity of heat (J) passing through per unit area (m^2) with uniform temperature per unit time (h) and under the condition of per unit temperature gradient ($^\circ\text{C}/\text{m}$). The value of the coefficient of heat conduction of concrete (λ_c) reduces obviously as the temperature is elevated, and it reduces almost linearly when $T > 200^\circ\text{C}$ but it varies considerably with the water content when the temperature nears 100°C . If the concrete is cooled down after heating, the coefficient of heat conduction will reduce further but slightly, rather than increase (recover). The coefficient of a light-weight concrete is far smaller, e.g. may be less than half that of ordinary concrete.

The **mass density** is also called **volume density** (ρ in kg/m^3), and it is defined as the mass of a material per unit volume. The mass density of concrete (ρ_c) reduces slightly at elevated temperature as the water contained loses gradually, however, it usually is taken as a constant during calculation.

The **heat diffusivity** (Fig. 19-3(d)) is a derived thermal parameter for a material and is defined as $d = \lambda/c\rho$ (Eq. 19-8) in m^2/h . The value of heat diffusivity of

concrete (d_c) reduces gradually as the temperature is elevated, but a deep valley appears near $T = 100^\circ\text{C}$, which corresponds to the sharp peak of specific heat capacity (c_c , Fig. 19-3(b)).

The values of these thermal parameters of concrete vary considerably. If the accurate values of them are needed for a particular concrete, the only way is to produce specially certain specimens and to measure experimentally. When no reliable datum is available, the formulas [19-12] shown below can be used for calculation of these parameters for concrete with siliceous aggregate:

$$\left. \begin{array}{ll} 20^\circ\text{C} \leq T \leq 700^\circ\text{C} & \varepsilon_{th,c} = -1.8 \times 10^{-4} + 9T \times 10^{-6} + 2.3T^3 \times 10^{-11} \\ 700^\circ\text{C} < T \leq 1200^\circ\text{C} & \varepsilon_{th,c} = 14 \times 10^{-3} \end{array} \right\} \quad (19-3)$$

$$20^\circ\text{C} \leq T \leq 1200^\circ\text{C}$$

$$\left\{ \begin{array}{l} c_c = 0.215 + 1.59T \times 10^{-4} - 6.63T^2 \times 10^{-8} \quad (\text{kcal}/(\text{kg}^\circ\text{C})) \quad (19-4) \\ \lambda_c = 1.72 - 1.72T \times 10^{-3} + 0.716T^2 \times 10^{-6} \quad (\text{kcal}/(\text{hm}^\circ\text{C})) \quad (19-5) \\ \rho_c = 2300 \quad (\text{kg}/\text{m}^3) \quad (19-6) \end{array} \right.$$

where $1 \text{ kcal} = 4.1868 \times 10^3 \text{ J}$. Besides, the calculation formulas for concrete with calcareous aggregate can be found in the same reference [19-12]. The representative values of the thermal parameters may take as: $\bar{\alpha}_c = 10 \times 10^{-6}/^\circ\text{C}$, $c_c = (0.84-1.26) \times 10^3 \text{ J}/(\text{kg}^\circ\text{C})$, and $\lambda_c = 1.63-0.58 \text{ W}/(\text{m}^\circ\text{C})$.

The thermal behavior of steel varies similarly at elevated temperature [19-5,19-13]. The thermal expansion strain ($\varepsilon_{th,s}$) increases nearly linearly and the average value of linear expansion coefficient ($\bar{\alpha}_s$) varies less, the specific heat capacity (c_s) increases gradually and slightly, and the mass density (ρ_s) varies slightly, but the coefficient of heat conduction (λ_s) reduces nearly linearly with considerable amplitude, as the temperature increases. The values of these parameters for various kinds of steel are in the range of:

$$\left. \begin{array}{ll} \bar{\alpha}_s = (12 \sim 15) \times 10^{-6} & 1/^\circ\text{C} \\ c_s = (0.42 \sim 0.84) \times 10^3 & \text{J}/(\text{kg}^\circ\text{C}) \\ \lambda_s = 52.3 \sim 27.9 & \text{W}/(\text{m}^\circ\text{C}) \\ \rho_s = 7850 & \text{kg}/\text{m}^3 \end{array} \right\}. \quad (19-7)$$

The representative values of them are successively: $14 \times 10^{-6} (1/^\circ\text{C})$, $0.52 \times 10^3 (\text{J}/(\text{kg}^\circ\text{C}))$, $34.9 (\text{W}/(\text{m}^\circ\text{C}))$, and $7850 (\text{kg}/\text{m}^3)$. It is seen that the specific heat capacity of steel is smaller than that of concrete ($c_s < c_c$), while the coefficient of heat conduction of steel is several tens of times higher than that of concrete ($\lambda_s \gg \lambda_c$).

Generally, the reinforcement or wire is spread in the interior of a reinforced or prestressed concrete structure and only possesses of a few percentages ($< 3\%$) of the total volume. When the temperature field is theoretically analyzed, it is usually considered [19-6,19-12] that the structure is composed of homogeneous material (plain concrete) only and the reinforcement contained is neglected. The result

obtained satisfies the accuracy required in engineering practice and is on the safe side, i.e. slightly higher temperature is given, compared with that calculated in consideration of existing reinforcement.

19.2.3 Basic equation for heat conduction and determination of temperature field

Generally, the temperature field of a structure at elevated temperature is not influenced by its internal force and deformation and can be analyzed first and arbitrarily. According to the principle of energy conservation, the sum of the heat quantity, which enters into or goes out from a micro-cube ($dx dy dz$) of mass density (ρ) via its surface and generates in its interior, should be equal to the heat quantity respectively absorbed because of the temperature elevated or released because the temperature reduces in the micro cube. Therefore, the basic equation of heat conduction is established:

$$\left[\frac{\partial}{\partial x} \left(\lambda \frac{\partial T}{\partial x} \right) + \frac{\partial}{\partial y} \left(\lambda \frac{\partial T}{\partial y} \right) + \frac{\partial}{\partial z} \left(\lambda \frac{\partial T}{\partial z} \right) \right] dx dy dz + q_d dx dy dz = c \rho \frac{\partial T}{\partial t} dx dy dz \quad (19-8a)$$

or

$$\frac{\partial T}{\partial t} = \frac{1}{c \rho} \left[\frac{\partial}{\partial x} \left(\lambda \frac{\partial T}{\partial x} \right) + \frac{\partial}{\partial y} \left(\lambda \frac{\partial T}{\partial y} \right) + \frac{\partial}{\partial z} \left(\lambda \frac{\partial T}{\partial z} \right) \right] + \frac{q_d}{c \rho}, \quad (19-8b)$$

where T is the temperature of the micro cube in $^{\circ}\text{C}$, c , λ , and ρ are the thermal parameters of the micro cube, of which the definitions and values are introduced above, q_d is the heat quantity generated per unit volume of the micro cube itself per unit time (s), and t is time in s.

The basic equation can be used for analysis of any three-dimensional structure. The linear member, such as beam and column used most popularly in practice, is generally assumed that the temperature is identical along its axis-line and its temperature field is then simplified into the two-dimensional one on its section. In addition, the planar member, such as wall and slab, is generally assumed that the temperature is identical along its plane, then its temperature field is simplified further into the one-dimensional one along its thickness.

When the temperature of a structure varies with time (t), Eq. 19-8 should be solved at different times or external temperatures and series of temperature fields are obtained successively. This is called dynamic or transient heat conduction. Whereas the temperature of an external medium does not vary with time ($\partial T / \partial t = 0$) and the material of the structure itself does not generate any heat quantity ($q_d = 0$), Eq. (19-8) is then simplified into:

$$\frac{\partial}{\partial x} \left(\lambda \frac{\partial T}{\partial x} \right) + \frac{\partial}{\partial y} \left(\lambda \frac{\partial T}{\partial y} \right) + \frac{\partial}{\partial z} \left(\lambda \frac{\partial T}{\partial z} \right) = 0, \quad (19-9)$$

and only one solution is obtained. This is called static or stable heat conduction.

In order to find the solution of the equation of heat conduction (Eq. (19-8) or Eq. (19-9)), the initial and boundary thermal conditions of the structure have to be determined in advance, besides knowing the thermal parameters of its material. The initial condition is the temperature distribution of the structure at initiation ($t = 0$), which is usually assumed to be uniform and is equal to the environmental temperature (T_0) before a fire accident occurs. The boundary condition of the structure depends upon its environment and the heat exchange with the medium surrounded, and is generally divided into four categories [19-1]: (1) the temperature on its boundary (surface) is a function of time $T = f(t)$, e.g. Eq. (19-1); (2) the quantity of heat flow passing through its boundary is a function of time $-\lambda \partial T / \partial n = f(t)$; (3) the quantity of heat flow passing through the boundary is proportional to the temperature difference ($T - T_a$) in which T_a is the temperature of the air surrounded; (4) the temperature and the quantity of heat flow at the boundary vary continuously when it is contacted with other solid materials. The basic methods for solving these problems of various thermal boundaries may consult relevant monographs [19-1, 19-14].

When the temperature field of a concrete structure under a fire accident or at elevated temperature is analyzed, there are not only the variable heating process and the thermal parameters of the material varying non-linearly with the temperature, but also the complicated boundary conditions. Therefore, the accurate solution of the partial differential equation of heat conduction is very difficult to find out analytically. Nevertheless, several methods are usually used now to find the solution in accordance with the required accuracy for structural engineering:

1. The temperature field of a structure is assumed approximately to be a one- or two-dimensional one and the basic equation Eq. (19-8) is simplified into a linear and stable heat conduction, the analytical solution can be derived more easily;
2. The method of finite-element or difference analysis, or both combined, is used and the computer program is compiled correspondingly, then the numerical solution is obtained after numerous calculations on the computer. This method is used most widely now and several universal programs for the thermal analysis of a structure are available on the market;
3. The full-scale specimen is produced specially and the standard thermal test is completed, then the temperatures at key points can be measured and the temperature field can be derived;
4. The temperature fields of some particular conditions are provided on relevant design codes or handbooks [19-6, 19-10, 19-12, 19-15] and may be expressed as various charts or tables (e.g. Fig. 19-4), which may be utilized directly or indirectly. Although, this method is very easy and convenient, the conditions given, e.g. shape and size of structural section, material of concrete, temperature–time curve and time lasted, are limited and the temperatures given are of less accuracy.

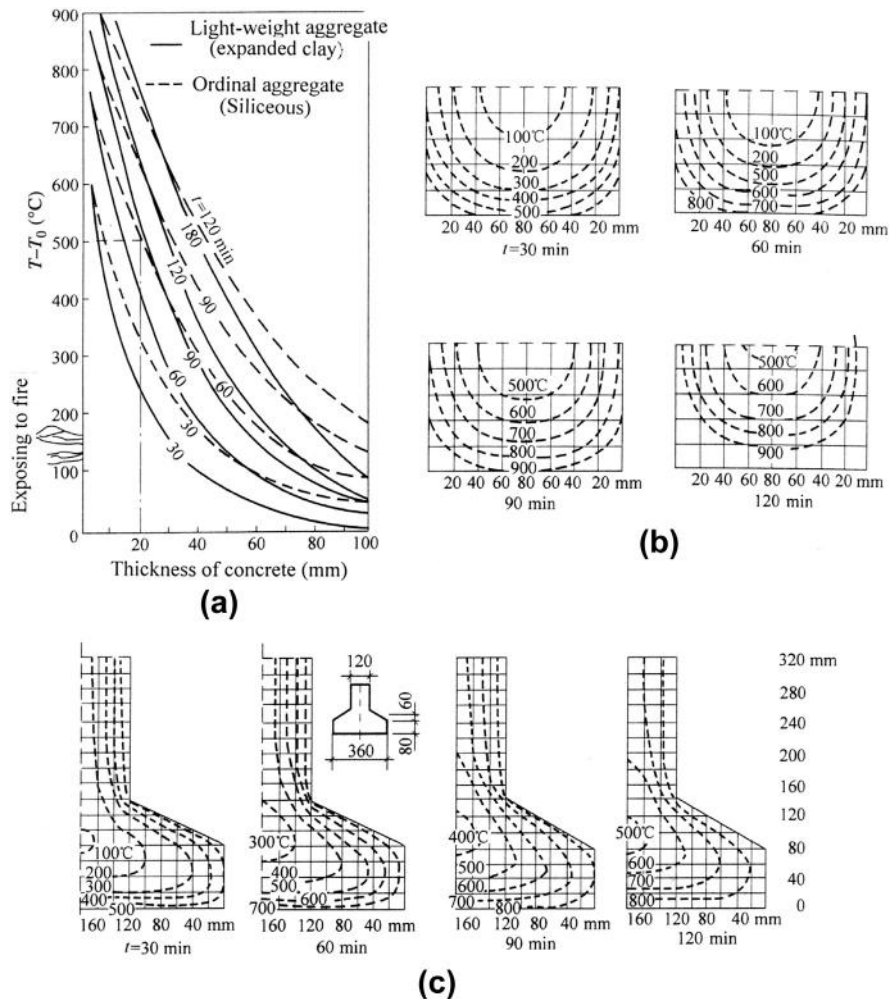


FIG. 19-4 Temperature field (contour) of structural section [19-6]: (a) plate with one surface exposed to fire, (b) lower part of rectangular section ($b = 160\text{mm}$, $h = 320\text{mm}$, siliceous aggregate), (c) lower part of I-shape section (siliceous aggregate)

19.3 Mechanical behaviors of materials at elevated temperature

19.3.1 Behavior of reinforcement

A special heating—loading testing machine is necessary for testing and measuring the mechanical behavior of steel at elevated temperatures. The specimen is set up in the furnace and heated freely (stress $\sigma = 0$) to the predetermined temperature

(T , °C) and maintained constantly, then it is loaded (stretched) until its failure and the tensile force—elongation or stress—strain (σ — ϵ) curve is recorded simultaneously. The curves of the steels (reinforcements) of various kinds and strength grades at different temperatures are shown in Fig. 19-5.

The tensile force—elongation (or σ — ϵ) curve of the hot-rolled steel (grades I to IV) tested under normal temperature shows apparently a long yielding plateau. When the testing temperature is $T < 200^\circ\text{C}$, the yielding plateau can still be found on the curve but the corresponding yield strength reduces slightly ($f_y^T < f_y$). However, the yielding plateau is hardly identified and the yield strength is difficult to be determined when the testing temperature is even higher ($T > 250^\circ\text{C}$). In addition, the ultimate strength of steel, i.e. the peak value of the curve, reduces obviously as the testing temperature increases ($f_b^T < f_b$).

If the specimen under normal temperature is stretched further after the ultimate strength is reached, it should be necked locally and broken soon into two pieces. The area on the necked section is reduced considerably and the length of the necked zone is about twice the original diameter of the specimen. When the specimen is tested until failure under high temperature, the tensile force or nominal stress calculated by the original area of the specimen decreases gradually after the ultimate strength is reached. After the specimen is cooled down, it is found that the length of necked zone at failure increases with the temperature tested. When the testing temperature is $T \geq 800^\circ\text{C}$, the steel is softened and the specimen is stretched much longer and finer, and no neck can be found on it.

The yield and ultimate strengths of the reinforcements of various steels at elevated temperatures obtained from the stretching tests are shown in Fig. 19-6, in which the ratios between them and corresponding strengths at normal temperature (f_y^T/f_y , f_b^T/f_b) are expressed respectively. Generally, the strengths of the reinforcements of hot-rolled steel (grades I to IV) loss less when $T \leq 300^\circ\text{C}$, and the strength of a few specimens at certain temperature is even slightly higher than that at normal temperature; the strength reduce sharply when $T = 400$ – 800°C ; the strengths are rather low at $T = 800^\circ\text{C}$ and higher temperature and usually less than 10% of that at normal temperature. As far as the high-strength wire, used mostly for prestressed concrete, is concerned, the strength loses even more seriously at elevated temperature: it reduces obviously at $T = 200^\circ\text{C}$ and sharply at $T = 400$ – 600°C , and it is only 5% of that at normal temperature when $T = 800^\circ\text{C}$.

The elastic modulus of reinforcement varies similarly as its strength does at elevated temperatures. The elastic modulus reduces limitedly when $T \leq 200^\circ\text{C}$ but quickly when $T = 300$ – 700°C , and it is rather low at $T > 800^\circ\text{C}$ and usually no more than 10% of that at normal temperature (Fig. 19-7).

The stress—strain curve of reinforcement at elevated temperature is suggested as a simple geometrical diagram and corresponding calculation formula is given in some references, such as an inclined line succeeded by a horizontal line (elasto-plastic relation) [19-16], two straight lines of different slopes linked together [19-13], or an inclined line succeeded by a hardening curve [19-10]. Besides, a complete stress—strain curve (Fig. 19-8), including an inclined line (elastic stage), an

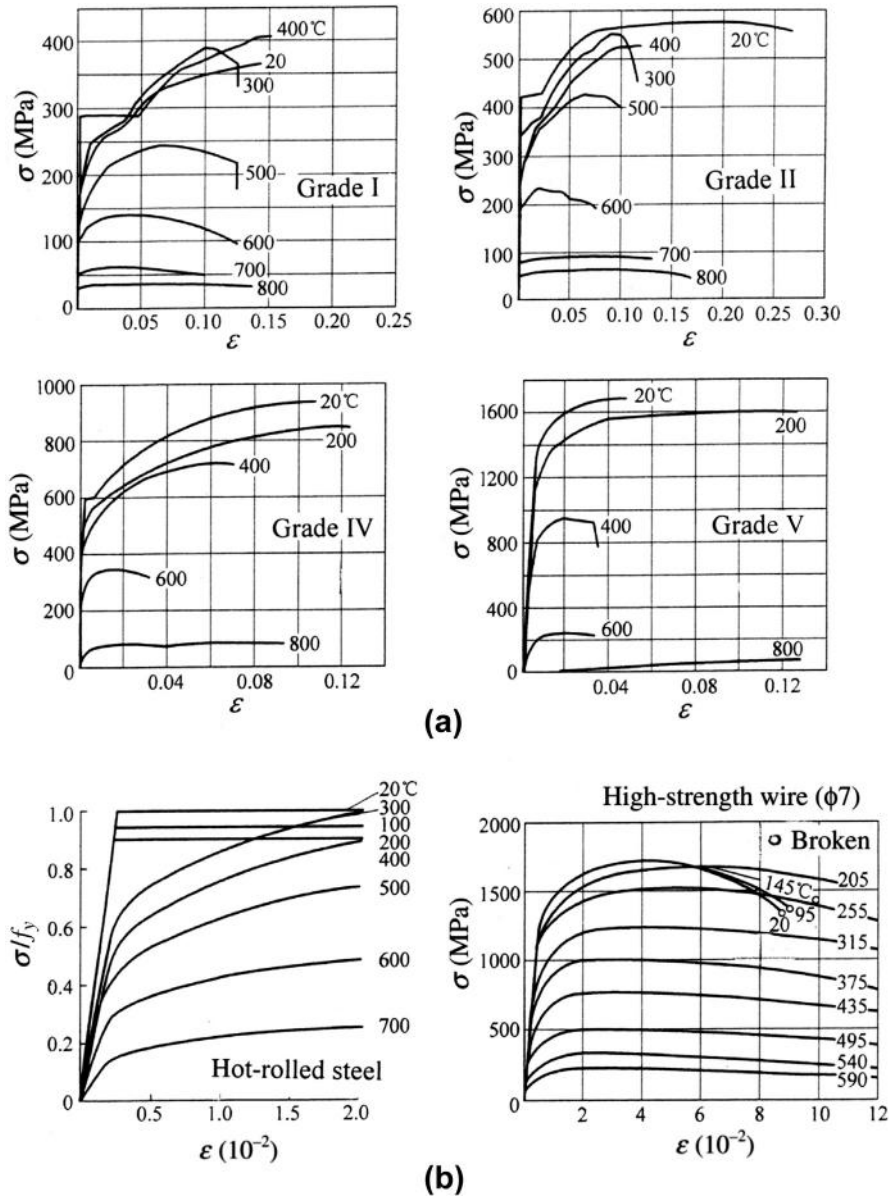


FIG. 19-5 Stretching curves of various steels at elevated temperature: (a) reference [19-13], (b) reference [19-6]

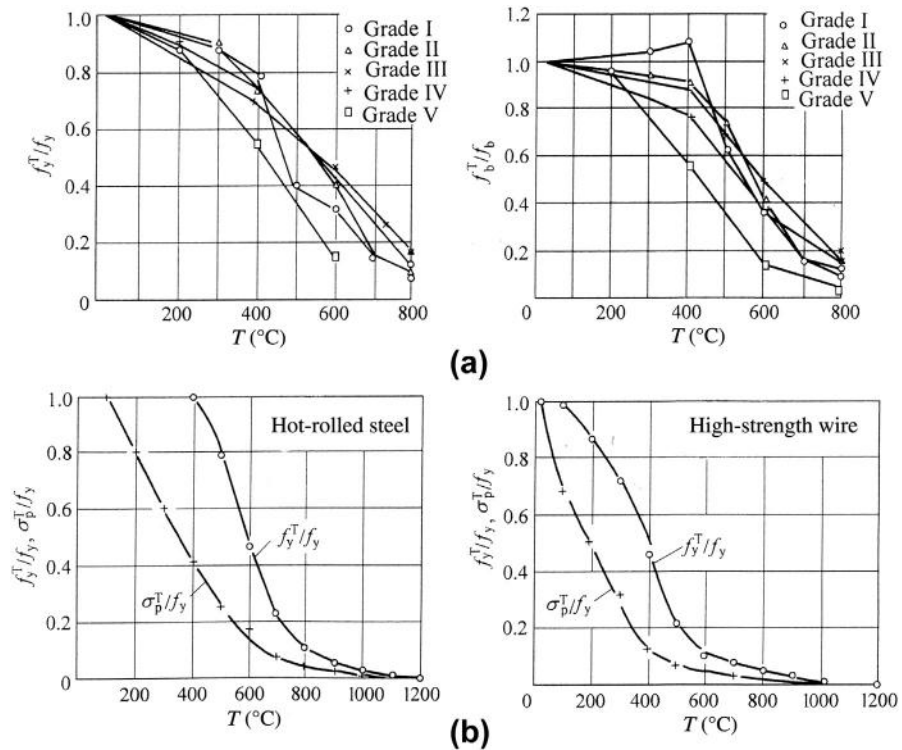


FIG. 19-6 Yield and ultimate strengths of reinforcements at elevated temperature: (a) reference [19-13], (b) reference [19-12]

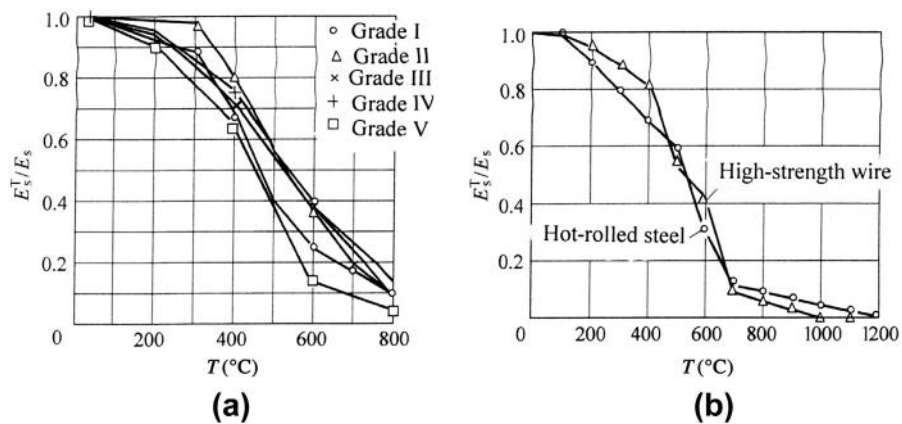


FIG. 19-7 Elastic modulus of reinforcement at elevated temperature: (a) reference [19-13], (b) reference [19-12]

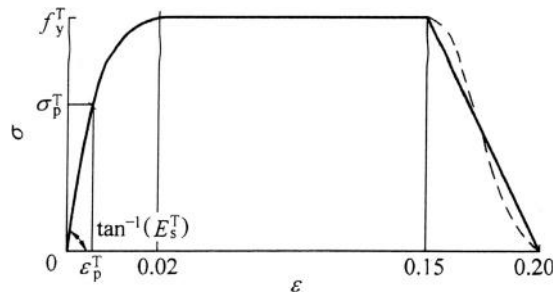


FIG. 19-8 Stress—strain relation of reinforcement at elevated temperature [19-12]

elliptical curve (hardening), a horizontal line (plastic stage), and a descending branch, and all the formulas and parameters for calculation are provided in reference [19-12].

The other mechanical behaviors of reinforcement at elevated temperature are also introduced in relevant references [19-6,19-13]. For example, the creep of reinforcement appears with considerable value in short time (counted in hours or minutes) under constant temperature and stress, different deformation (strain) and strength of it are presented when it experiences various orders of heating and loading.

19.3.2 Basic behavior of concrete

The basic mechanical behavior of concrete varies significantly at elevated temperature and many results of experimental investigations are reported in various references [19-10,19-16–19-20]. Generally, the furnace used for testing is specially designed and produced by the researches themselves and is put on the working table of an ordinary testing machine before the thermal test, then the specimen is set up into the furnace and heated to and maintained constantly at the predetermined temperature, and finally the specimen is loaded monotonically until failure and the strength and deformation are measured simultaneously. Because concrete is a material of thermal inertia, the specimen should be heated and kept constant for a long time before loading, if the temperatures at the surface and interior are needed to be uniform. For example, when a concrete cube with edge length 100 mm is heated to 700°C on its surface within 30 minutes, it takes 6 hours under constant temperature in the furnace as the temperature at its center reaches 680°C [19-18].

The mechanical behavior of concrete varies considerably and mainly depends upon not only the material factors, including the chemical composition and texture of raw material, mixing ratio, and water content, but also the testing equipment and method used, such as thermal function of the furnace, shape and size of the specimen, heating velocity and period maintained under testing temperature, and measuring instrument and method used for experimental data. The measured data of the specimens of one series are rather scattered under the same testing condition.

The most important index of mechanical behavior is the cubic compressive strength for concrete (f_{cu}^T at elevated temperature and f_{cu} at room temperature), which

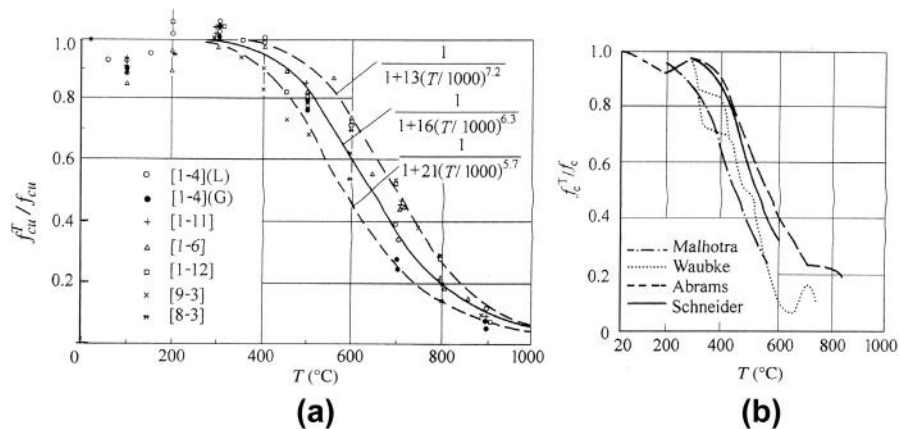


FIG. 19-9 Cubic compressive strength of concrete at elevated temperature: (a) reference [19-10], (b) comparison between different experimental results [19-6]

varies with temperature as shown in Fig. 19-9 and the variation regularity is generally as follows:

1. $f_{cu}^T/f_{cu} = 0.88\text{--}0.94$ when the testing temperature $T = 100^{\circ}\text{C}$. The free water contained in the concrete evaporates gradually and the capillary crack and porosity are formed in the interior, and the vapor pressure in the crack causes tensile stress in the surrounding material. In addition, the stress concentration occurs at the tip of the crack and accelerates the crack expanding after the specimen is loaded. So, the compressive strength of concrete reduces slightly.
2. $f_{cu}^T/f_{cu} = 0.98\text{--}1.08$ when $T = 200\text{--}300^{\circ}\text{C}$. The compressive strength then is usually higher than that at $T = 100^{\circ}\text{C}$ and even than that under normal temperature. The possible reasons for this are that the adhesive action of the cement particles is enhanced and the stress concentration near the crack is relaxed as the combined water in the cement gelation starts to release during then.
3. f_{cu}^T/f_{cu} decreases obviously when $T \geq 400^{\circ}\text{C}$ (Table 19-1). The thermal deformation difference between the aggregate and the hardened cement mortar increases continuously, the crack is caused and expanded on boundary of the aggregate, and the water in the calcium hydroxide and others yielded during cement hydration releases with considerable volume expansion, so the cracks in the interior expand and extend gradually and the strength reduction is caused sharply.

Table 19-1 Relative Cubic Compressive Strength of Concrete at Elevated Temperature

T ($^{\circ}\text{C}$)	400	500	600	700	800	900
f_{cu}^T/f_{cu}	0.90–0.98	0.75–0.85	0.50–0.70	0.30–0.50	0.15–0.28	0.05–0.12

4. When $T > 600^\circ\text{C}$, the quartz components in the un-hydrated cement particles and the aggregates decompose, and the crystal is formed and accompanied with considerable expansion. Then the cracks also appear in the interiors of some aggregates and expand further as the temperature increases, so the compressive strength of concrete reduces sharply.
5. When $T > 800^\circ\text{C}$, only little the compressive strength remains, but it is not necessarily guaranteed sometimes. Usually, the specimen is broken into several pieces at the end of testing and can not be integrally taken out from the furnace.

The thermal action results in the strength loss and deformation behavior deterioration of concrete and the main reasons can be summarized as: (1) crack and porosity form in the interior of concrete after water evaporated; (2) thermal behavior of the coarse aggregate and the hardened cement mortar are different, and it causes the deformation difference and internal stress between them and results cracking on their boundary; (3) coarse aggregate expands and cracks itself under higher temperatures. These internal damages of concrete develop and accumulate continuously, and tend to be more serious as the temperature increases.

Various factors have influence on the compressive strength of concrete at elevated temperatures, and it is generally realized according to the available experimental investigation:

- The concrete of siliceous aggregate (e.g. granite) has slightly lower strength than that of calcareous aggregate (e.g. limestone) has, and the concrete of light-weight aggregate has much higher strength (f_{cu}^T/f_{cu}) than that of ordinary aggregate [19-17] under the same temperature;
- The higher the strength at normal temperature (f_{cu}), the smaller the relative strength (f_{cu}^T/f_{cu}) at elevated temperature;
- The specimen of high-strength concrete ($> \text{C60}$) may spall off and break suddenly when $T > 400^\circ\text{C}$;
- The strength reduces with the heating velocity, and the strength is lost continuously as the time lasts longer under high temperature, but most of the strength loss appears already within the first two days;
- The strength reduces gradually as the damage accumulates, when the heating—cooling cycles are repeated, but most of the strength loss appears already after the first cycle;
- The compressive strength of concrete at normal temperature after a heating—cooling cycle is slightly smaller than that at the maximum temperature experienced, and it shows that new damage, depending upon the cooling velocity, occurs during the cooling stage after being heated.

The compressive stress—strain curve of concrete prism or cylinder at elevated temperature tends to be flatter and flatter and its peak obviously drops and moves toward the right-hand as the testing temperature increases (Fig. 19-10). It means that the prism compressive strength (f_c^T) decreases and the correspondingly peak strain (ϵ_c^T) increases considerably, and the modulus of elasticity decreases sharply

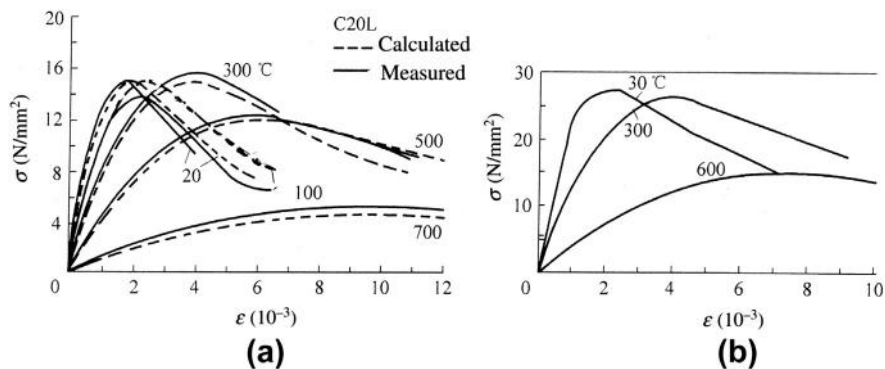


FIG. 19-10 Complete stress–strain curve of compressed concrete at elevated temperature: (a) reference [19-10], (b) reference [19-19]

at elevated temperature. Also, the similar curves are found for the concretes of different aggregates and strength grades.

The deformation process from the start of loading till failure of the prism specimen can be divided into three stages: (1) when $\sigma/f_c^T < 0.3-0.5$, the strain of concrete increases approximately linearly with the stress, although many cracks are formed already in the specimen during heating and before loading; (2) when $\sigma/f_c^T = 0.5-1.0$, the plastic strain of concrete develops quickly and the slope of the stress–strain curve decreases gradually because many cracks are expanded or formed newly on its surface and in the interior, and the curve tends to be flatter on the top part and the tangent of the curve is horizontal at the maximum stress (peak point f_c^T); (3) passing the peak, the strain of concrete increases ($\epsilon > \epsilon_p^T$) continuously and the cracks develop further while the stress decreases slowly, and a descending branch is formed stably. The final failure pattern of the concrete prism at elevated temperature is similar to that under normal temperature. An inclined main crack appears clearly on the surface with wider breaking belt but smaller slope, and many thermal cracks distribute irregularly on other part of the surface.

The ordinate and abscissa of the peak point on the stress–strain curve of concrete at elevated temperatures are respectively the prismatic compressive strength (f_c^T) and corresponding strain (ϵ_p^T), which vary with the testing temperature as shown in Fig. 19-11. It is found that the prismatic compressive strength (f_c^T/f_c) of concrete varies similarly but is smaller than that of the cubic compressive strength (f_{cu}^T/f_{cu}), whereas the peak strain (ϵ_p^T) increases considerably as the testing temperature increases.

The initial elastic modulus of concrete at elevated temperature (E_0^T), just like that under normal temperature [0-2], is defined as the ratio between the stress $\sigma = 0.4f_c^T$ and corresponding strain ϵ or the secant slope at this point on a measured stress–strain curve. In addition, the secant modulus at peak stress is the ratio between the prismatic compressive strength and the corresponding peak strain, i.e. $E_p^T = f_c^T/\epsilon_p^T$. Both moduli of concrete reduce monotonically as the testing

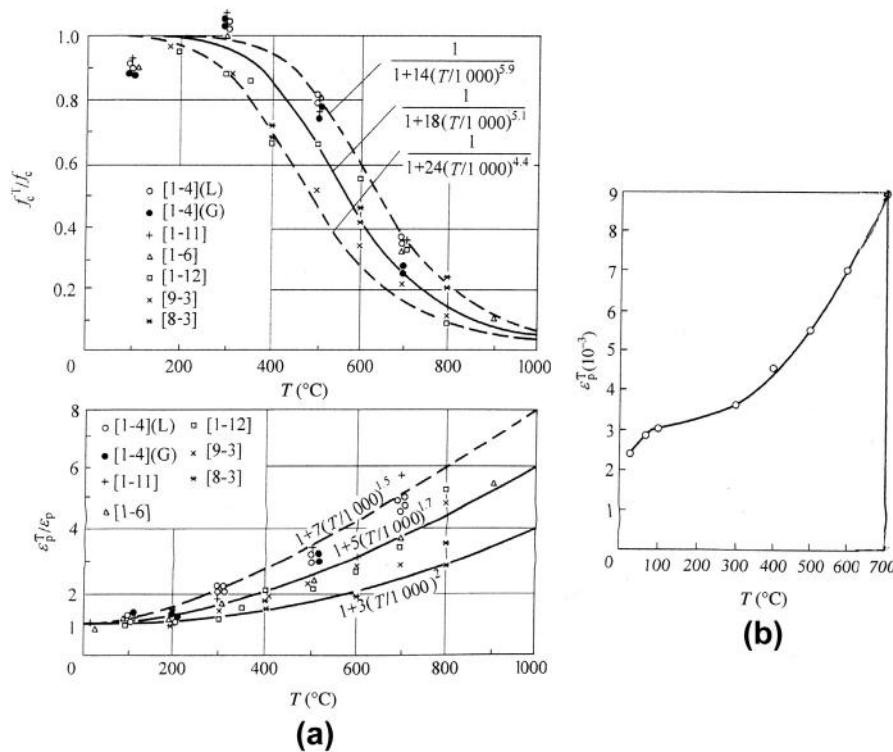


FIG. 19-11 Prismatic compressive strength and peak strain of concrete at elevated temperature: (a) reference [19-10], (b) reference [19-19]

temperature increases (Fig. 19-12), and the relative values of both approach each other ($E_0^T/E_0 \approx E_p^T/E_p$). Some experimental investigation [19-20] demonstrates that the elastic modulus of concrete, like its strength, varies slightly during cooling after being heated (Fig. 19-12(b)), and it also means that the damage caused during heating does not recover during cooling.

Poisson's ratio of concrete (ν) reduces as the testing temperature increases ($> 50^{\circ}\text{C}$) and reaches less than half of the initial value at $T = 400^{\circ}\text{C}$, and it keeps the low value obtained at elevated temperature and also it does not recover during cooling (Fig. 19-12(b)).

The splitting testing method and the cubic specimen of edge length 100 mm are used for measuring the tensile strength of concrete at elevated temperature. The tensile strength of concrete decreases considerably (Fig. 19-13) as the testing temperature increases, and the range of its relative value (f_t^T/f_t) against temperature is listed in Table 19-2. Generally, the specimen approaches failure and is hardly loaded at all when $T \approx 900^{\circ}\text{C}$. It is noticed that the tensile and compressive strengths of concrete vary differently at elevated temperature, and the ratio between them (f_t^T/f_c^T) is not a constant and its minimum value occurs in the range $T = 300\text{--}500^{\circ}\text{C}$.

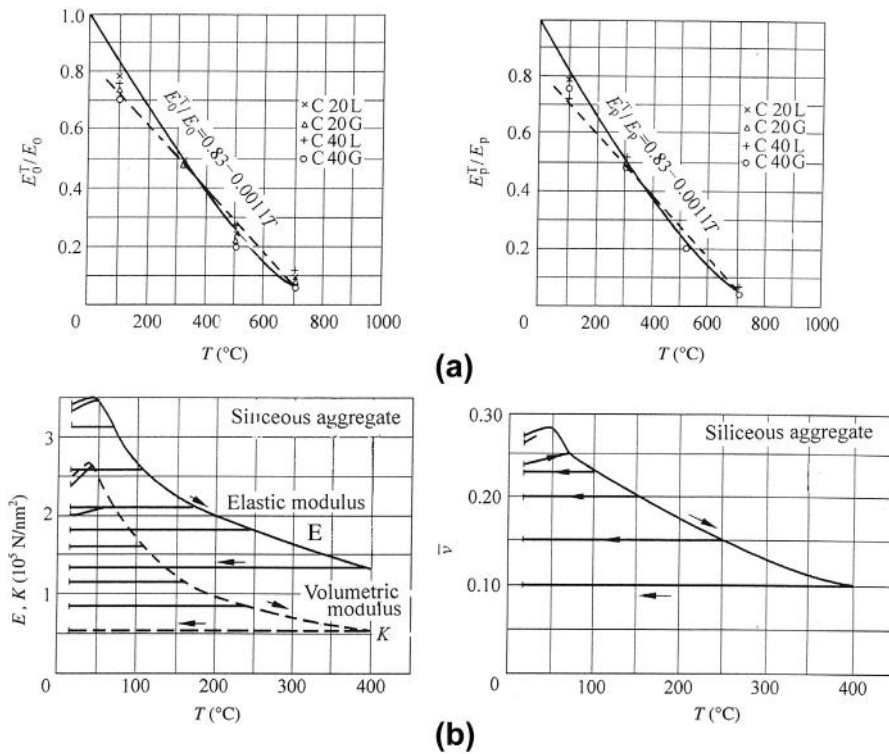


FIG. 19-12 Elastic modulus and Poisson's ratio of concrete at elevated temperature: (a) reference [19-10], (b) reference [19-20]

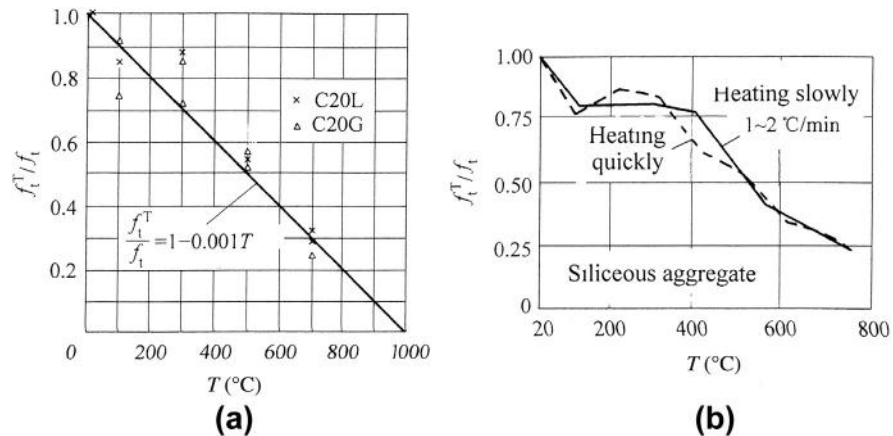


FIG. 19-13 Tensile strength of concrete at elevated temperature: (a) reference [19-18], (b) reference [19-6]

Table 19-2 Tensile Strength of Concrete at Elevated Temperature

$T (^{\circ}\text{C})$	100	300	500	700	900
f_t^T / f_t	0.78–0.90	0.66–0.88	0.52–0.60	0.24–0.32	

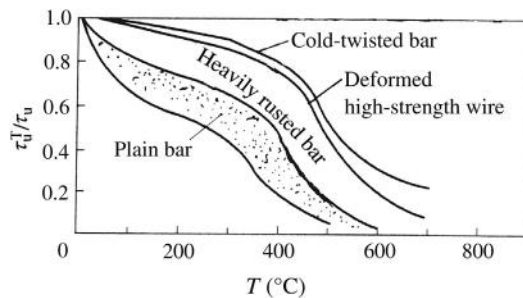
The bond strength (τ_u^T) between reinforcement and concrete reduces also monotonically as the testing temperature increases (Fig. 19-14) and varies similarly to the tensile strength of concrete (f_t^T). The bond strength considerably depends upon the surface shape and corrosion level of the reinforcement. Obviously, the bond strength of the plain bar loses most and even more than the tensile strength of concrete does under same temperature.

The stress–strain relation of concrete at elevated temperature is necessary for thermal or fire resistance analysis of the concrete structure. Because the tensile strength of concrete is rather low under normal temperature and is not guaranteed at elevated temperature, the tensile action of concrete is generally neglected during structural analysis. When the compressive stress–strain curves of concrete at different temperatures are expressed uniformly on the coordinate of relative values (σ/f_c^T and ϵ/ϵ_p^T), they can be uniquely simulated by one equation, for which various functions are suggested in the relevant reference [19-12,19-16,19-18].

The theoretical curves and the corresponding compressive strength (f_c^T/f_c) and characteristic strains (ϵ_p^T and ϵ_u^T) of concrete at elevated temperature given in reference [19-12] are shown in Fig. 19-15. The equation for the ascending branch is suggested as

$$\sigma = \frac{3 \left(\epsilon / \epsilon_p^T \right)}{2 + \left(\epsilon / \epsilon_p^T \right)^3} f_c^T, \quad (19-10)$$

and the descending branch may be taken as a reasonable curve or simply as a straight line between the peak (ϵ_p^T, f_c^T) and ultimate ($\epsilon_u^T, 0$) points.


FIG. 19-14 Bond strength between reinforcement and concrete at elevated temperature [19-21]

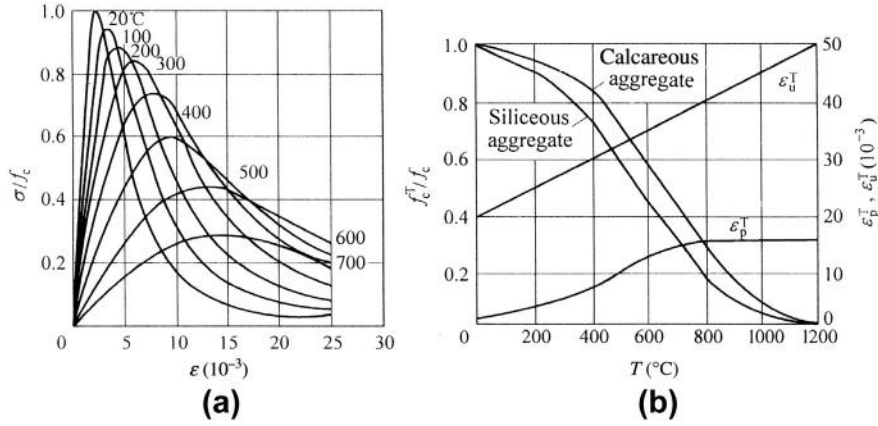


FIG. 19-15 Theoretical stress–strain curves for compressed concrete at elevated temperature [19-12]: (a) stress–strain curves, (b) ultimate strength and strains

The calculation formulas suggested in reference [19-10] are:

$$f_c^T = \frac{f_c}{1 + 18 (T/1000)^{5.1}} \quad (19-11)$$

$$\epsilon_p^T = \left[1 + 5 (T/1000)^{1.7} \right] \epsilon_p \quad (19-12)$$

for the prismatic compressive strength and corresponding peak strain of concrete at elevated temperature, and the equations for the ascending and descending branches of stress–strain curve are the same as for that under normal temperature (Eq. (2-6)) but with different values of the parameters included:

$$\left. \begin{aligned} \frac{\epsilon}{\epsilon_p^T} \leq 1 \quad \sigma &= \left[2.2 \left(\frac{\epsilon}{\epsilon_p^T} \right) - 1.4 \left(\frac{\epsilon}{\epsilon_p^T} \right)^2 + 0.2 \left(\frac{\epsilon}{\epsilon_p^T} \right)^3 \right] f_c^T \\ \frac{\epsilon}{\epsilon_p^T} \geq 1 \quad \sigma &= \frac{\left(\frac{\epsilon}{\epsilon_p^T} \right)}{0.8 \left(\frac{\epsilon}{\epsilon_p^T} - 1 \right)^2 + \left(\frac{\epsilon}{\epsilon_p^T} \right)} f_c^T \end{aligned} \right\}. \quad (19-13)$$

The calculated curves are compared with the experimental results in Fig. (19-10(a)).

These equations can also be used for calculating the elastic modulus of concrete at elevated temperature and the results obtained are shown as a solid curve in Fig. 19-12(a). Alternatively, the solid curve can be simplified into a

straight line shown as a dashed line in the same figure, of which the calculation formula is

$$T = 60^{\circ}\text{C} \sim 700^{\circ}\text{C} \quad \frac{E_0^T}{E_0} = \frac{E_p^T}{E_p} = 0.83 - 0.0011 T. \quad (19-14)$$

19.4 Coupling constitutive relation of concrete

When a concrete structure is constructed completely and then used for service, the structure should carry various dead and live loads and sustain frequently or occasionally temperature variation. This is a complicated load (or internal force)—temperature long-term history, and the redistribution of internal force of the structure during the heating and cooling process is also included. In the meantime, the concrete in the structure experiences correspondingly a complicated stress—temperature path, i.e. both increase or decrease simultaneously or alternately, and every point of the concrete has a particular stress—temperature path.

When the stress and temperature of the concrete vary from the initial condition to certain values, there may be many different paths and generally it should be an irregular path, e.g. (*OCP*) in Fig. 19-16. If the stress and temperature increase proportionally, a special path (*OP*) is resulted, but it is seldom in engineering practice. In addition, there are two extreme but important paths as below:

1. Path of loading under constant temperature (T — σ , *OAP* in Fig. 19-16). The concrete is heated first and maintained at a certain value of temperature and then is loaded. The tests of various concrete behaviors at elevated temperature, which are introduced above, are of this path.
2. Path of heating under constant stress (σ — T , *OBP* in Fig. 19-16). The concrete is loaded first and maintained at a certain value of stress and then is heated. For

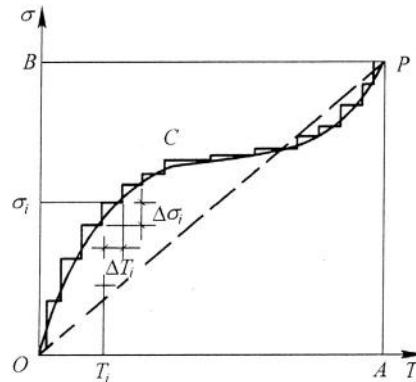


FIG. 19-16 Different stress—temperature paths [19-22]

example, a fire accident occurs in a building, in which the structure is loaded already.

An arbitrary stress–temperature path can be simulated approximately by finite steps of stress and temperature increments. All the ordinate increments are the path of loading ($\Delta\sigma$) under constant temperature (T), while all the abscissa increments are the path of heating (ΔT) under constant stress (σ). Therefore, it is necessary to investigate first the mechanical behavior of concrete under these two basic paths, in order to determine the strength and deformation of concrete under an arbitrary stress–temperature path.

19.4.1 Upper and lower bounds of compressive strength

The cubic compressive strengths of concrete measured experimentally under different stress–temperature paths [19-10,19-23] are plotted in Fig. 19-17. It is demonstrated that the linking line of the experimental data measured from the path of loading under constant temperature ($T-\sigma$) is the lower envelope among different paths, i.e. the lower bound of the compressive strength of concrete at elevated temperature. Whereas the linking line of the experimental data measured from the path of heating under constant stress ($\sigma-T$) is the upper envelope, i.e. the upper bound of the compressive strength of concrete at elevated temperature, the compressive strength of concrete measured under other stress–temperature

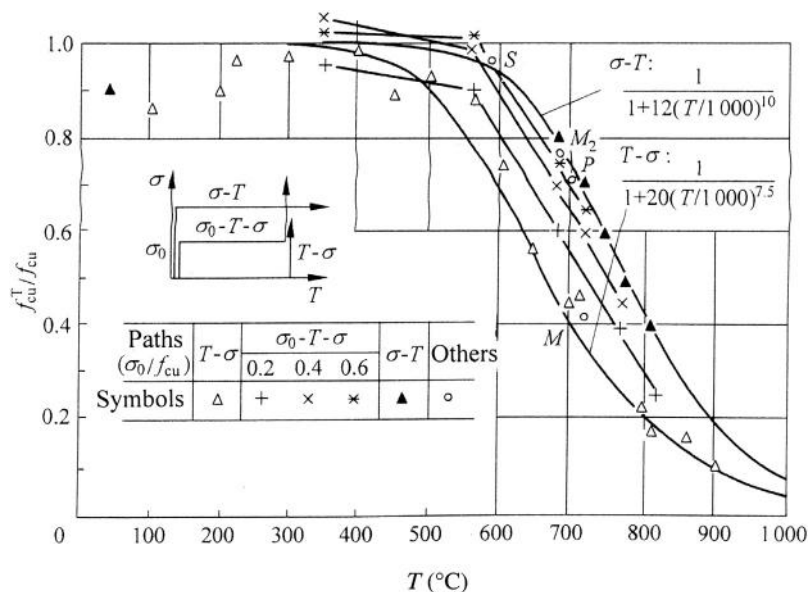


FIG. 19-17 Upper and lower bounds of cubic compressive strength of concrete at elevated temperature [19-10]

paths, e.g. initially loading ($\sigma_0/f_{cu} = 0.2-0.6$) - heating (from room temperature to $350-820^\circ\text{C}$) - reloading until failure path ($\sigma_0-T-\sigma$), is located between the upper and lower bounds.

The ratio between the upper and lower bounds of the compressive strength of concrete is usually 1.4–2.5, and the maximum difference between them reaches $0.20-0.35 f_{cu}$ within the range of $T = 600-800^\circ\text{C}$. The formulas for calculation of the upper and lower bounds are suggested in reference [19-10].

It is demonstrated by many experiments and is generally agreed that the compressive strength of concrete under the path of heating under constant stress ($\sigma-T$) is higher than that under other paths. The main reasons for this are that the compressive stress acted on in advance effectively confines the freely expanding deformation and crack of concrete and mitigates the bond failure on the boundary between the aggregate and hardened cement mortar during heating, and the compressive stress also reduces the volume expansion resulted by crystallizing of the aggregate and dehydrating of the cement hydration products at higher temperature.

19.4.2 Thermal strain under stress and transient thermal strain

The thermal deformation of concrete during heating and cooling varies significantly with its stress condition (Fig. 19-18). When the concrete specimen is heated freely

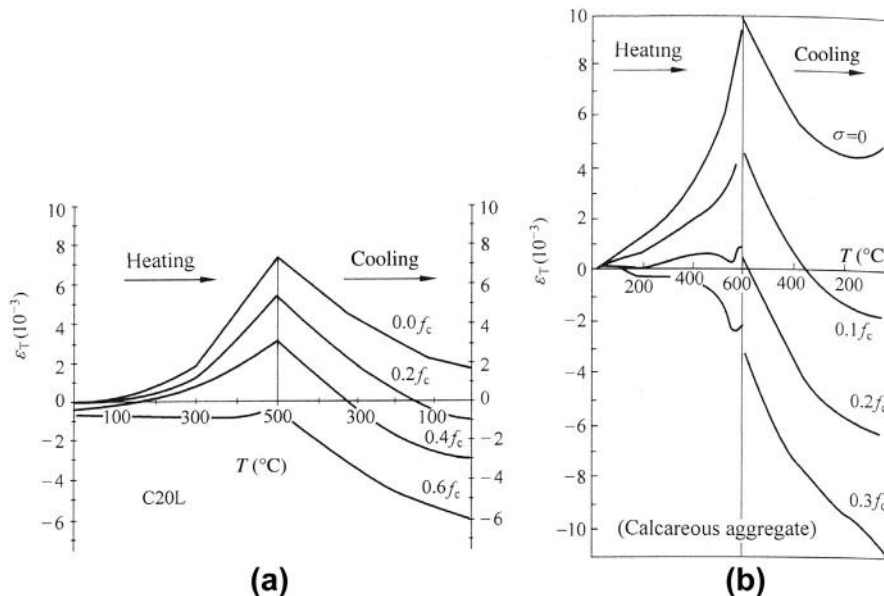


FIG. 19-18 Strains of concrete during heating and cooling under constant stress: (a) reference [19-22], (b) references [19-24,19-25]

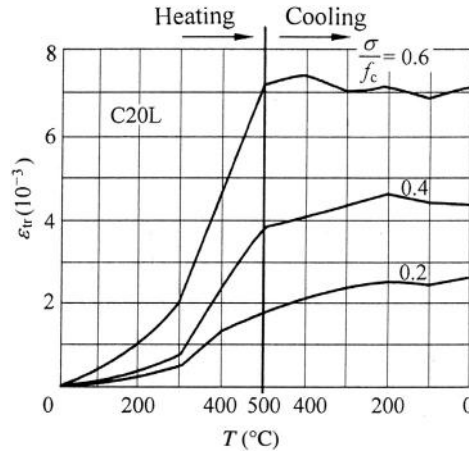


FIG. 19-19 Transient thermal strain of concrete [19-22]

($\sigma = 0$), the thermal expansion is ϵ_{th} at elevated temperature as the same as shown in Fig. 19-3(a), and a residual deformation (elongation) is left after being cooled down to normal temperature. However, when the specimen is compressed (stress σ) first under normal temperature and a contracted strain should be caused; if the specimen is then heated to the same temperature as the previous one under the constant stress (σ), the expansion (increment) and total strains (ϵ_T) measured are respectively much smaller than that of the freely heated specimen. If the constant stress (σ) acted is even higher ($0.6f_c$ in Fig. 19-18), a contraction strain (negative) will appear during heating and is opposite that of the freely heated specimen.

On the other hand, the recoverable strains of the specimens under different values of constant stress are always contracted during cooling and the corresponding strain–temperature curves measured are approximately parallel to one another. The residual strain of the specimen is generally contracted after cooling down to the normal temperature, but its value varies considerably with the constant stress acted.

The difference¹ between the free expansion strain (ϵ_{th} at $\sigma = 0$) and thermal strain under stress (ϵ_T at σ) of concrete at same temperature is defined as the transient thermal strain [19-23], i.e.

$$\epsilon_{tr} = \epsilon_{th} - \epsilon_T \quad (19-15)$$

Substituting the values of ϵ_{th} and ϵ_T measured (Fig. 19-18(a)) into the equation, Fig. 19-19 is plotted. It is seen that the transient thermal strain accelerates during

¹The difference is called load-induced thermal strain (LITS) in reference [19-24] and it is considered that it is composed of two parts, i.e. ‘transient thermal strain’ and ‘basic creep’, but the former one is the main part.

heating and is approximately proportional to the stress level (σ/f_c) acted, but it is nearly constant during cooling.

The transient thermal strain (ϵ_{tr}) of concrete appears instantaneously with considerable value during heating under compressive stress, and its value is far greater than the peak strain of concrete under normal temperature and also the short-term creep at elevated temperature (Fig. 19-21). Therefore, the transient thermal strain is the key composition of the thermal strain of concrete under various heating—loading paths and has considerable influences on deformation and stress relaxation (or redistribution) of the concrete, and it should be taken into account for the analysis of the structure at elevated temperature. However, the mechanism of the transient strain of concrete is not clear till now. Possibly when the concrete is headed under certain stress, the chemical and physical reactions occur in the cement hydrates and cause the variations of microstructure of the cement mortar and volume change of the internal holes in the interior of the concrete.

The difference between the strain values of concrete experiencing different stress—temperature paths can be illustrated by the experimental results of the two extreme paths. For example, when the concrete prism reaches $T = 500^\circ\text{C}$ and $\sigma = 0.6f_c$ from the initial conditions ($T = 20^\circ\text{C}$ and $\sigma = 0$), the specimen tested under the path of loading under constant temperature ($T-\sigma$, OAP in Fig. 19-20) experiences successively freely heating strain (OA) and instantaneous strain under loading at constant temperature (AP) and the total strain is PR (elongation), while the specimen tested under the path of heating under constant stress ($\sigma-T$, OBQ) experiences successively the strain under loading at normal temperature (OB) and thermal strain during heating under constant stress (BQ) and the total strain is RQ (contraction). Obviously, the two total strains obtained from the different stress—temperature paths may have opposite sign and the difference between them ($\Delta\epsilon = PQ$) is rather considerable. If the specimen reaches separately

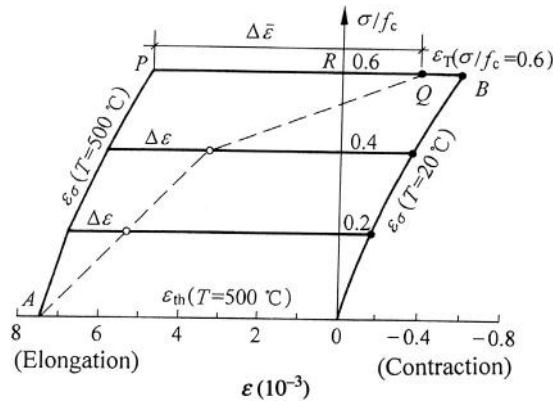


FIG. 19-20 Deformations of concrete experiencing two extreme stress—temperature paths [19-22]

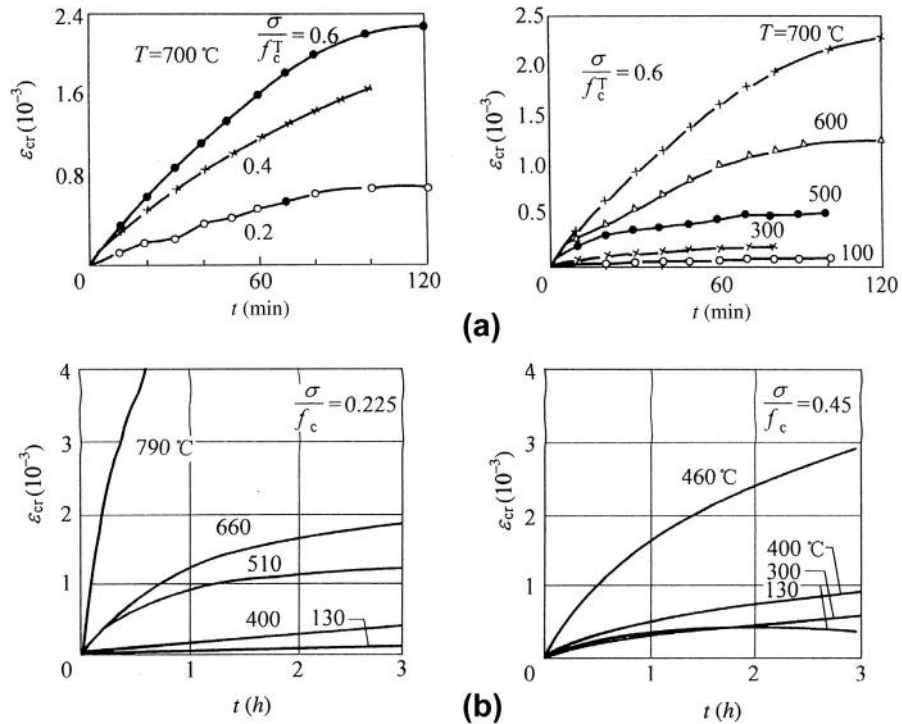


FIG. 19-21 Short-term creep of concrete at elevated temperature: (a) reference [19-23], (b) reference [19-6]

$\sigma/f_c = 0-0.6$ and $T = 500^\circ\text{C}$, the total strains should be AP and AQ respectively for both extreme paths.

19.4.3 Short-term creep at elevated temperature

Another kind of thermal deformation of concrete related to stress state is short-term creep (ϵ_{cr}), i.e. the strain increases with time (t counted in hours or minutes) under constant stress and temperature (Fig. 19-21).

The short-term creep of concrete under constant stress and temperature increases quickly within the initial stage ($t < 60$ min) but slowly later on, and it will still increase slightly after a few days. The short-term creep increases almost proportionally to the stress level ($\sigma/f_c^T \leq 0.6$) acted and accelerates with the temperature acted.

The short-term creep, counted in minutes, of concrete at elevated temperature is far greater than the long-term creep, counted in months or years, of concrete under normal temperature. Nevertheless, the absolute value of the short-term creep of concrete is still smaller than that of other thermal strains (ϵ_{th} , ϵ_T , and ϵ_{tr}) introduced above.

19.4.4 Coupling constitutive relation

According to the resolution of an arbitrary stress–temperature path (Fig. 19-16), the strain of concrete caused under stress and temperature acted together is composed of three components [19-23,19-10], including the strain caused under the path of loading under constant temperature (ε_σ , Fig. 19-10), the strain caused under the path of heating under constant stress (ε_T , Fig. 19-18), and the short-term creep caused under constant stress and temperature (ε_{cr} , Fig. 19-21). Therefore, the total strain of concrete under compression is

$$\varepsilon = -\varepsilon_\sigma(\sigma, T) + \varepsilon_T(\sigma/f_c, T) - \varepsilon_{cr}(\sigma/f_c^T, T, t) \quad (19-16)$$

$$\text{or } \varepsilon = -\varepsilon_\sigma(\sigma, T) + \varepsilon_{th}(T) - \varepsilon_{ir}(\sigma/f_c, T) - \varepsilon_{cr}(\sigma/f_c^T, T, t) \quad (19-17)$$

when Eq. (19-15) is substituted.

The components of thermal strain of concrete in the equation can be measured individually from the corresponding tests as above, or they can be calculated by the empiric formulas suggested in relevant references, e.g. [19-10] and [19-26]. However, these four components of thermal strain of concrete under stress and temperature are merged into two or three components for simplicity in some references [19-22].

The constitutive relation of concrete at elevated temperature has to deal with the coupling ones between the four factors, i.e. stress (σ), strain (ε), temperature (T), and time (t), so it is much more complicated than stress–strain relation of concrete under normal temperature. In addition, the values of the thermal strains are considerable while the strength is rather low at higher temperature, the thermal and mechanical behavior is scattered significantly, a great variety of stress–temperature paths occur at different positions of a structure, etc. Therefore, it is difficult to establish accurately the constitutive relation for concrete under any possible stress–temperature paths, and more research on it is needed.

19.5 Behavior and calculation of structural members at elevated temperature

19.5.1 Flexural and compressive members

19.5.1.1 Flexural member

When a floor system in a building experiences a fire accident, usually only one surface, either bottom or top, of the slab and three surfaces, including bottom and two sides, of the rectangular beam are exposed to fire and high temperature, but another surface of them keeps the room temperature before the fire or is exposed to much lower temperature than the fire. When the fire simulation test [19-27] is conducted under the path of heating under constant load following ISO standard temperature–time curve, the full-scale specimen of the slab or simply supported beam is put into the special furnace and then loaded and heated successively until

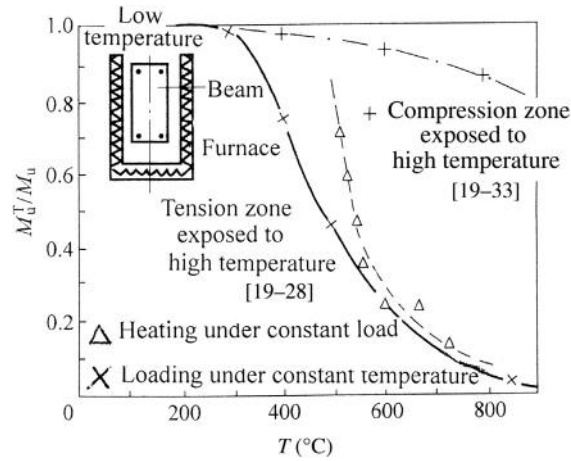


FIG. 19-22 Ultimate bending moment-temperature of concrete beam with three surfaces exposed to high temperature

failure, and the ultimate temperature under certain load level or the fire endurance (hours) of the specimen is obtained. Of course, the ultimate strength (or load) of the specimen at certain temperature can also be tested and measured under the path of loading under constant temperature in the similar way.

Three series of concrete beam [19-28,19-29] of rectangular section reinforced symmetrically are tested in the furnace with three surfaces exposed to high temperature, and all the results measured are plotted in Fig. 19-22.

When the specimen with tension zone exposed to high temperature is tested under the path of loading under constant temperature, the strengths of the materials (f_y^T , f_c^T) reduce already before loading and depend upon the maximum temperature reached there after heating and maintained. As the load is increased continuously afterwards, the tensile stress of the reinforcement in the beam increases gradually and reaches its strength at elevated temperature ($\sigma = f_y^T$), then the crack on the critical section expands quickly and the deflection increases suddenly, so the failure of the specimen is caused. The ratio between the ultimate bending moments measured separately at elevated temperature and under normal temperature (M_u^T/M_u) reduces as the testing temperature increases, and its variation regularity is approaching that of the yield strength of the reinforcement (f_y^T/f_y , Fig. 19-6). After the tested specimen is cooled down to room temperature, it is found clearly that many thermal cracks spread widely on the surface, the tensile crack on the critical section extends towards the compression zone and closes to the top surface, the concrete in the compression zone near the critical section is crushed within a small depth but longer length in the longitudinal direction, and the specimen is bent obviously with great residual deflection.

When the specimen with tension zone exposed to high temperature is tested under the path of heating under constant load, the stress state (σ_s , σ_c) established under

the action of initial load or bending moment varies slightly during heating because of the redistribution of the stress and move of the neutral axis on section at elevated temperature. In the meantime, the strength of the material reduces continuously as the temperature increases and depends upon its position on the section and the temperature actually reached (temperature field). Once the yield strength of the tensile reinforcement is reduced to the value of current stress ($f_y^T = \sigma_s$), the specimen is failed soon after the crack on the critical section expands and extends quickly and the concrete in the compression zone is crushed. The ultimate temperature of the specimen under certain load is then obtained. It is seen in Fig. 19-22 that the ultimate bending moment–temperature curve of the specimen tested under the path of heating under constant load is always above that tested under the path of loading under constant temperature.

Another series of the specimen is also tested under the path of loading under constant temperature, but the three surfaces exposed to high temperature are the two side ones and the compression one, rather than the tension one. This simulates obviously a beam acted with a negative bending moment or a segment near the middle support of a continuous beam. Because the tensile reinforcement is located near the top of the specimen, its strength losses less as the temperature there is rather low even after heating to 800°C on other surfaces. On the other hand, the concrete in the compression zone is located on the lower part of the specimen and exposed directly to high temperature, its strength (f_c^T) reduces significantly and a much greater area of compression zone on the critical section is needed to keep equilibrium with the tensile force of the reinforcement at ultimate state. Therefore, the lever arm on the section and then the ultimate bending moment (M_u^T) of the specimen reduce correspondingly, but with limited amplitude (Fig. 19-22). It is concluded that the ultimate strength of the beam with compression zone exposed to high temperature (fire) is much greater than that with tension zone exposed to high temperature.

In addition, the ultimate strength at elevated temperature and fire-endurance of a flexural member of reinforced concrete also vary with the kind and property of the aggregate, thermal parameters of the concrete, shape and size of the section, thickness of the concrete cover, reinforcement rate, and etc.

The ultimate shear strength (V_u^T) of a flexural member also reduces as the test temperature increases, but the relative value (V_u^T/V_u) is greater than that of the ultimate bending moment (M_u^T/M_u) at elevated temperature, because it depends mainly upon the strength of the concrete near middle depth and compression zone, including inside of the section with lower temperature. Some specimen would fail in shear pattern with an inclined critical crack under normal temperature, but fails actually in the flexural pattern at elevated temperature [19-28].

19.5.1.2 Central compressive member

The ultimate strength of a reinforced concrete column under central compression reduces monotonically at elevated temperature. When the specimen is tested with all periphery exposed to high temperature and under the path of heating under

constant load, the ultimate temperature (T_u) or fire endurance (t_u) reduces as the initial load level (N_u^T/N_0) increases [19-30,19-31]. The relation between the ultimate temperature (T_u) and compression (N_u^T/N_0) of a column is similar to that between the ultimate temperature and prismatic compressive strength (f_c^T/f_c) of the plain concrete (Fig. 19-11) and depends mainly upon the kind of aggregate, sectional size, concrete cover, strength of the concrete, and reinforcement content.

When a reinforced concrete column of rectangular section is tested under the path of loading under constant temperature and with three surfaces exposed to high temperature [19-32,19-33], it bends up gradually towards the surface of higher temperature during free heating because of the temperature distributed non-uniformly on the section, and the maximum deflection appeared at its mid-height is also the initial eccentricity during loading. After central compression is acted on the specimen, the compressive strain of concrete in the higher-temperature zone is greater than that in the lower-temperature zone because of different values of elastic modulus there, so the specimen will bend up towards the surface of low temperature, i.e. just being opposite to that occurring during heating. If the temperature maintained during loading is $T > 400^\circ\text{C}$, the specimen fails with the pattern of smaller eccentricity, i.e. the concrete in the higher-temperature zone is crushed but tensile cracks appear transversely in the lower-temperature zone, and the specimen finally bends up towards the surface of lower temperature. The ultimate strength of the specimen (N_u^T) reduces as the test temperature increases, but the reduction amplitude is smaller than that of the specimen with all four surfaces exposed to high temperature.

19.5.1.3 Compressive—flexural member

When a structure system of one-dimensional members experiences a fire accident, most of the members are acted together with axial compression and bending moment and with three or one surface exposed to the fire, e.g. column and wall. In addition, the beam and slab of the floor system acted with vertical load and bending moments are caused correspondingly under normal temperature, and the axial compressions are also resulted when their axial expansions during fire are constrained by the adjacent members without exposing to fire. Usually, the axial compression is very beneficial to the ultimate strength of the flexural member at elevated temperature.

The ultimate strength of a concrete column of rectangular section and reinforced symmetrically reaches the maximum value (N_0) when it is compressed centrally ($e_0 = 0$) under normal temperature (20°C). The ultimate strength (N_e) reduces as eccentricity of the axial compression (e_0/h) increases no matter whether the eccentricity is located on the right or left side by the sectional center. Therefore, a symmetrical envelope line is obtained on the ultimate compression—bending moment diagram (Fig. 19-23).

A series of compressive—flexural (or eccentric compressive) members are tested under the path of loading under constant temperature and with three surfaces exposed to high temperature, and the results measured are plotted in Fig. 19-23. A non-uniform temperature field is caused in the specimen and the mechanical

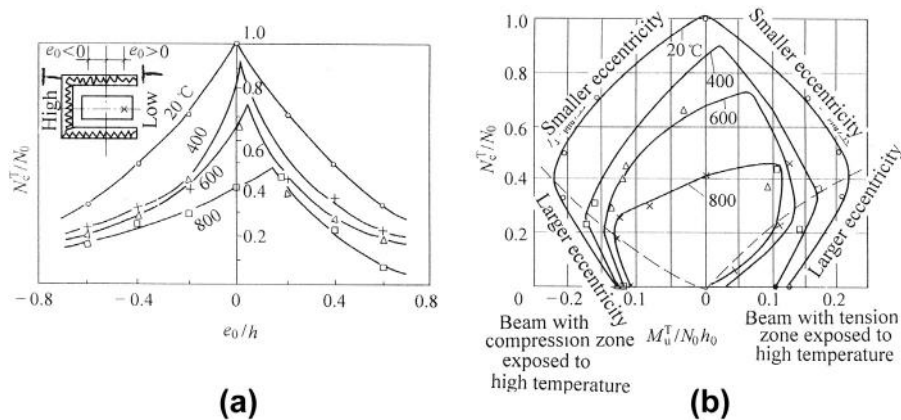


FIG. 19-23 Ultimate strength of eccentric compressive member under different temperature: (a) ultimate compression and eccentricity [19-4,19-29], (b) ultimate compression—bending moment envelope [19-29]

behavior of the concrete deteriorates correspondingly during heating, so a non-uniform strength field should be formed on the section before loading and the center of the strength has to move towards the surface of low temperature. Therefore, among all the specimens tested under the same temperature, the ultimate strength of the specimen compressed centrally (N_e^T , $e_0 = 0$) is not the maximum, the ultimate strength increases gradually as the compression moving towards the surface of low temperature ($e_0 > 0$) and reaches the maximum as the eccentricity $e_0 = e_u^T$, then the ultimate strength reduces gradually when $e_0 > e_u^T$. The eccentricity, with which the compression acted, is called the optimum one (e_u^T) for the specimen at elevated temperature, when the ultimate strength (N_u^T) reaches the maximum value.

The optimum eccentricity should be zero ($e_u^T = 0$) for the member of symmetrical section tested under normal temperature, and it moves gradually towards the surface of low temperature ($e_u^T > 0$) as the test temperature increases. Therefore, a peak appears at the optimum eccentricity on the corresponding ultimate compression—eccentricity ($N_e^T/N_0 - e_0/h$) curve and the two branches of the curve are obviously unsymmetrical about the peak. The right branch descends more quickly than the left one and represents the ultimate strength of the member controlled by concrete crush near the surface of low temperature (the failure pattern of smaller eccentricity) or controlled by yielding of the tensile reinforcement near the surface of high temperature (the failure pattern of greater eccentricity), depending upon the eccentricity. On the other hand, the left branch of the curve represents the ultimate strength of the member controlled by concrete crush near the surface of high temperature or by yielding of the tensile reinforcement near the surface of low temperature, depending also upon the eccentricity.

Similarly, the ultimate envelope of compression—bending moment of the member ($N_e^T/N_0 - M_u^T/N_0 h_0$) is also symmetrical about the ordinate axis under normal

temperature but unsymmetrical at elevated temperature (Fig. 19-23(b)). The peak point of the envelope moves downwards and towards the right hand, as the test temperature increases. In addition, the boundary between the failure patterns of smaller and greater eccentricities varies as well with the temperature, and the eccentricities at the boundary points (e_b^T) on both the right and left hands are not symmetrical and equal any more.

The deformation and failure processes of an eccentric compressive member with three surfaces exposed to high temperature are much more complicated than that under normal temperature, and the additional eccentricity at ultimate state varies considerably. When the member is heated freely ($N = 0$) on the three surfaces, it bends up towards the surface of high temperature because of non-uniform temperature field formed on the section. After the member is compressed under the constant temperature, the deformation depends upon eccentricity of the load and distributions of the stress acted and the elastic modulus of concrete at elevated temperature on the section. When the eccentricity of the compression is located on the low-temperature zone ($e_0 > 0$), the member also bends up towards the surface of high temperature, i.e. the same direction during heating, so the total deformation should be the summation of both. While the eccentricity of the compression is located on the high-temperature zone ($e_0 < 0$), the member should bend up towards the surface of low temperature, i.e. just the opposite direction during heating, so the total deformation should be added algebraically and may change sign (positive or negative) as the compression increases. Finally, the direction and value of deformation of the eccentric compressive member at ultimate state depend mainly upon the test temperature and the eccentricity of the compression and are introduced in detail in reference [19-29].

There are also some structural members of rectangular section with two adjacent surfaces exposed to high temperature during fire accidents, e.g. corner column and side beam in a building or other members with two other adjacent surfaces connected with walls or slabs. Obviously, the temperature distribution and mechanical behavior of this kind of member at elevated temperature is quite different from that of the member with three or one surface exposed to high temperature, in which one symmetrical axis always exists. The available experimental investigation on this kind of member [19-34–19-36] demonstrates that an asymmetrical temperature field in two perpendicular directions [19-10] is formed during heating on two adjacent surfaces and the non-uniform behaviors of the concrete and reinforcement on the section are caused correspondingly, so the member bends up differently in biaxial directions. In addition, the existed deformation and crack develop asymmetrically in both directions and vary complicatedly during loading, even the compression is acted centrally or eccentrically in one direction only (Fig. 19-24). Finally, the neutral axis on the critical section is inclined to the two perpendicular symmetrical axes and the compression zone is a triangle or trapezoid at the ultimate state, and the member fails in the pattern of biaxial eccentric compression even if the load is acted centrally.

The ultimate strength and failure pattern, i.e. of either smaller or greater eccentricity, of the eccentric compressive member with two adjacent surfaces exposed to

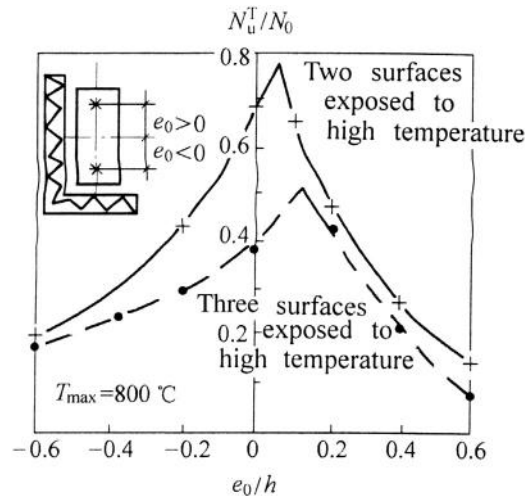


FIG. 19-24 Ultimate strength of eccentric compressive member with two adjacent surfaces exposed to high temperature [19-34]

high temperature vary with the eccentricity and are similar respectively to that with three surfaces exposed to high temperature, and the ultimate strengths of the members tested under both conditions are compared in Fig. 19-24. Although the temperature distributed on the section is asymmetrical in two perpendicular directions and the deflection in the direction of short side of the section during heating and loading is greater than that in the direction of the long side of the section, the ultimate strength of the member with two adjacent surfaces exposed to high temperature is always greater than that with three surfaces exposed to high temperature, because the area with high temperature on the section is smaller and the overall strength of the material losses is less. The difference between them is even greater when the failure pattern, i.e. of smaller eccentricity, is controlled by the concrete crushed in the compression zone.

19.5.1.4 Influences of different load-temperature paths

When a fire accident occurs in a building, the various structural members and their sections should experience a considerable variety of load–temperature paths, which have influences to different extents on the ultimate strength and fire endurance.

The compression between the eccentric compressive members tested respectively under the path of heating under constant load and the path of loading under constant temperature with three surfaces exposed to high temperature demonstrates [19-34] that the members bend up towards the same direction and fail in the same pattern, and the depths of crushed concrete and tensile crack on their critical sections are approached. However, the ultimate envelope of compression–bending moment corresponding to the path of heating under constant load is similar to but on the

outside of that corresponding to the path of loading under constant temperature, i.e. the fire resistance of the former is better than that of the latter. Especially, the difference between them is even greater when their failure pattern is of smaller eccentricity, mainly because the compressive strength of concrete at elevated temperature is higher under the path of heating under constant load (Fig. 19-17).

In addition, some other thermal conditions, e.g. high temperature sustained constantly and cooling down to room temperature after heating, occur frequently during the whole process of fire accidents in engineering practice, besides the two basic load–temperature paths introduced above. Four thermal conditions of the specimens selected as below [19-37–19-39] are tested with three surfaces exposed to high temperature:

1. The specimen is loaded until failure under room temperature and is used as a criterion for comparison.
2. The specimen is heated first to 800°C (in chamber of the furnace) and maintained for 10 minutes, and then it is loaded until failure.
3. The specimen is heated to 800°C and maintained ($\pm 25^\circ\text{C}$) for two hours, and it is then loaded until failure.
4. The specimen is heated to 800°C and maintained for 10 minutes, afterwards it is cooled down to room temperature and takes usually 16–20 hours, and then it is loaded until failure.

The ultimate envelopes of compression–bending moment of the eccentric compressive specimens of reinforced concrete tested under these thermal conditions are shown in Fig. 19-25, and it is demonstrated that the ultimate strengths of the specimens ever experienced high temperature are obviously reduced, compared with those that never experienced high temperature.

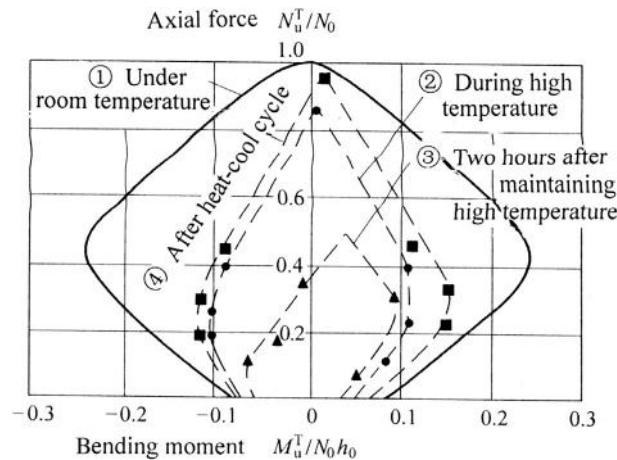


FIG. 19-25 Comparison between ultimate strengths of eccentric compressive specimens tested under different thermal conditions [19-37]

Comparing the specimens tested separately under the path of loading under high temperature (2) and under the path of loading after heating—cooling cycle (4), they fail in the same pattern if the eccentricity $e_0 \leq 0.2h_0$, i.e. either the pattern of smaller eccentricity controlled by compressive strength of the concrete or the pattern of greater eccentricity controlled by tensile strength of the reinforcement in low-temperature zone, so their ultimate strengths are less different from each other because the strengths of the concrete (f_c^T) and the reinforcement ($\approx f_y$) of both specimens are approaching respectively. However when the eccentricity $e_0 > 0.2h_0$, the specimens tested under both thermal conditions fail in the pattern of greater eccentricity controlled by tensile strength of the reinforcement in high-temperature zone, so the ultimate strength of the specimen tested under high temperature (2) reduces considerably because the tensile strength loses much ($f_y^T \ll f_y$), while the ultimate strength of the specimen tested after the heating—cooling cycle (4) reduces less because the tensile strength of the reinforcement (f_y) is recovered already.

As the specimen tested under thermal condition (3) is heated to high temperature and maintained for two hours before loading, the high temperature is spread widely on the section and the temperature of the reinforcement is elevated as well and approximates to that on the surface of the specimen, so the concrete of more area and the reinforcement are deteriorated seriously, the deformation increases highly, and the ultimate strength of the specimen drops significantly. Therefore, the relevant ultimate envelope is abruptly reduced and inclined and thermal condition (3) is the most unfavorable one among the four conditions tested.

19.5.2 Statically indeterminate structure

Most structures of reinforced concrete in engineering practice are statically indeterminate and their internal forces should be redistributed at elevated temperature or during a fire accident, so the behavior and failure process of them are different considerably from that of the structure under normal temperature. Although some investigations on this topic have been reported till now, the experimental data provided are not complete. Nevertheless, the continuous beams and frames of reinforced concrete [19-28,19-40,19-41] are tested at elevated temperature and the redundant reactions of the specimens are measured during testing, so the redistribution process of internal force is obtained and this is helpful to know clearly the important characteristics of the statically indeterminate structure at elevated temperature.

For example, a continuous concrete beam of rectangular section of two spans is reinforced symmetrically (No. TCB 1-2 in reference [19-28]) and two concentrated loads ($P_0 = 20 \text{ kN} \approx 0.5P_u$, P_u being the ultimate load of the beam if tested under normal temperature) are acted first on one-third point of each span near the side support (Fig. 19-26). Afterwards the beam is heated continuously on the bottom and two side surfaces under the constant loads, three plastic hinges appear successively at the sections on the middle support and under the loads when the test temperature reaches $T_u = 743.2^\circ\text{C}$, then the beam fails as a movable mechanism is formed. Another

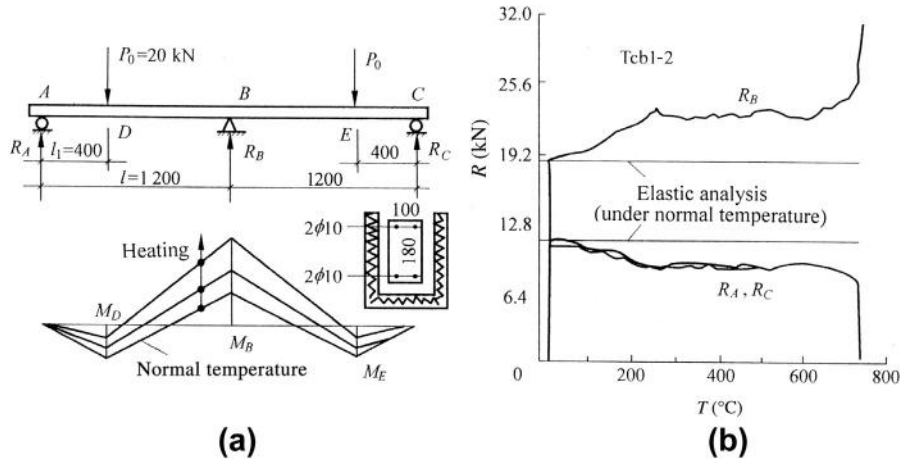


FIG. 19-26 Continuous beam of two spans tested under path of heating under constant load [19-28]: (a) specimen, load, and bending moment diagram, (b) reactions at supports varying with temperature

continuous beam (No. TCB 1-1) is loaded to $P_0 = 10 \text{ kN} \approx 0.25P_u$ only before heating and is failed when the test temperature reaches $T_u = 950^{\circ}\text{C}$. The failure process and pattern of both beams are similar although their ultimate temperature is different.

When the continuous beam is loaded under normal temperature, the measured reactions at the supports, and also the bending moment on every section, are less different ($< 2\%$) from that calculated elastically. However after the beam is heated continuously, the temperature of concrete distributed non-uniformly on the section causes the beam to deflect downwards but the deflection is restrained by the middle support, so the reaction there (R_B) is increased gradually while the reactions at the side supports ($R_A = R_C$) reduces correspondingly because the total load is a constant ($R_A + R_B + R_C = 2P_0$). In the meantime, the maximum bending moment at mid-span ($M_D = M_E = R_A l_1$) reduces while the bending moment at the section on the middle span (M_B , absolute value) increases, because the total bending moment $M_D + M_B (l_1/l) = M_0 = P_0 l_1 (l - l_1)/l$ should be a constant, i.e. the bending moment at the section under the concentrated load for a simply supported beam.

The internal forces including bending moment (M) and shear force (V) of the continuous beam redistribute continuously during testing (heating) and can be determined easily from the measured reactions. When the test temperature $T = 20^{\circ}\text{C}$ to 300°C , the internal forces redistribute obviously mainly because of thermal deformation caused by the non-uniform temperature field on section. As the mechanical behavior of concrete deteriorates and the cracks on the beam develop considerably when $T > 300^{\circ}\text{C}$, the sectional stiffness of the beam reduces greatly and the internal forces redistribute steadily with smaller amplitude. After the two plastic hinges form first at the sections under the concentrated loads of both spans, the ultimate bending

moments there ($M_D = M_E$) still reduce continuously as the test temperature increases, so the reactions at the side supports ($R_A = R_C$) reduce as well, while the reaction at the middle support (R_B) and corresponding bending moment (M_B) increases quickly. Finally, the continuous beam becomes a movable mechanism and then fails soon after another plastic hinge forms near the middle support.

If the continuous beam of two spans is loaded under normal temperature, the first plastic hinge usually forms at the section on the middle support and two other plastic hinges form later at the sections under the concentrated loads of both spans as the loads increase gradually, finally the beam becomes a movable mechanism and fails. It shows that the continuous beams tested respectively at elevated temperature and under normal temperature exhibit the same failure mechanism at the ultimate state, but the appearing orders of the plastic hinges are just opposite for them. Even though the bending moment in mid-span ($M_D = M_E$) of the beam reduces gradually during heating under constant load because of the redistribution of internal force, the ultimate bending moment of the section there reduces even more because of the tension zone exposed to high temperature, so the first plastic hinge should form there. On the other hand, the compression zone on the section near the middle support is exposed to high temperature and the ultimate bending moment there reduces less at elevated temperature (Fig. 19-22), so the plastic hinge there forms later at higher temperature.

The frame structure of more degrees of indeterminacy presents a more changeable and complicated process before failure at elevated temperature. The positions and appearing orders of the plastic hinges, final failure mechanism, and ultimate load (strength) and temperature of the tested frame, which are significantly different from that tested under normal temperature, can be obtained based on the observation and measured data during testing. Some simple examples are reported in detail in references [19-28] and [19-10].

Summarizing the experimental investigation on statically indeterminate structures at elevated temperature, several important characteristics can be concluded as below.

1. The mechanical behaviors, including deformation and ultimate strength, of the member and its section deteriorate seriously at elevated temperature.
2. The ultimate strengths and deformations are different significantly under the actions of positive and negative bending moments, respectively, for the member of symmetrical section but heated asymmetrically, e.g. with three, one, or two adjacent surfaces exposed to high temperature only.
3. The redistribution of internal force occurs severely in the structure as the temperature increases, and the bending moment will change sign from positive to negative or vice versa in some segment of its member.
4. The ultimate bending moment at the section of a plastic hinge is not a constant but reduces continuously if the temperature increases further, and the positive plastic hinge (under $+M$) is quite different from the negative one (under $-M$) for the same section.

5. The position and appearing order of the plastic hinge and the failure mechanism of a structure depend upon the load acted and the temperature sustained.
6. The thermal deformation of a structure is considerable at elevated temperature and has great influence on its internal force and ultimate strength.
7. Various load—temperature history experienced for a structure has influences on its internal force, deformation, failure process, and the ultimate strength (load) and temperature.
8. If only a part of the structure in a building is exposed to high temperature (or fire), this part should be constrained by other parts without being exposed to high temperature, then a constraint force should be caused and acted between them.

Therefore, more complications and difficulty are raised for the analysis of a structure at elevated temperature as these characteristics are introduced.

19.5.3 Analysis and approximate calculation

The thermal and mechanical analyses should be conducted for a structure under the situations, such as predicting the safety and possible damage for a structure existed or to be built if it is exposed to fire accident or other high temperature, estimating the damage level and residual strength (or safety) of a structure experiencing high temperature. The contents of the analyses mainly include:

1. Determining the actual or possible temperature—time curve and analyzing the corresponding temperature field of the structure and its members,
2. Determining the coupling constitutive relation of the material and analyzing the relevant characteristics between internal force-deformation-temperature-time for section of the structural member,
3. Analyzing the variable internal force and deformation and the failure mechanism and obtaining the ultimate strength or the fire endurance.

These analyses are related closely to one another, but they can be conducted successively and independently.

The general principle and method of mechanical analysis for the structure at elevated temperature are the same as those for the structure under normal temperature. However, the temperature field at time t should be determined first; then the constitutive relation of the material is established and substituted into the corresponding equations of geometric (deformation) compatibility and mechanical equilibrium, and the internal force and deformation of the structure or the stress and strain on the section are obtained after solving the equations. Finally, the ultimate strength (or load) and the fire endurance or ultimate temperature of the structure can be checked.

Usually, the temperature field is a dynamic or transient process as the surrounding temperature varies with time (e.g. standard temperature—time curve), the behaviors of concrete and reinforcement under stress and temperature acted together are non-linear and even coupled, and the geometric non-linearity has

to be considered for some structure, so the thermal and mechanical analyses of the structure at elevated temperature are very complicated and very seldom to be solved analytically. Frequently, the structure is divided geometrically into many elements and the period experienced at elevated temperature is divided into many time increments, then the finite element analysis or combined finite element and difference analyses are used and the digital calculation is conducted successively for every time step for the structure experienced a loading–heating history.

The computer program used for calculating accurately the structure of reinforced concrete experienced certain loading–heating history is rather difficult to be developed, because the material behaviors vary considerably and complicatedly and many characteristics listed above exist. Although some structural analysis programs, including the function of thermal analysis, are available on the market, the thermal parameters and constitutive relation used for the material are much simplified and the calculated results are not accurate enough. Some other computer programs suggested in the references, e.g. [19-10, 19-26, 19-42–19-44], are compiled specially for certain structures or their members, but the accuracy of the calculated results needs to be demonstrated.

Nevertheless, the most important index for fire resistance or thermal behavior of a structure is the ultimate strength or load at a certain temperature or after a maintained certain period under fire accident, or the ultimate temperature or fire endurance (ultimate time) under a certain load level. Therefore, several practical methods suggested in some design codes or instructions can be used for approximate calculation of the ultimate strength of structural section at elevated temperature, then the fire resistance safety of a statically indeterminate structure can be checked using the plastic method of structural analysis based on the failure mechanism at the ultimate state.

For example in reference [19-15], the strengths of various kinds of concrete and reinforcement (f_c^T , f_y^T) are given (Fig. 19-27(a)) and are about the lower bounds of the relevant experimental results, and the temperature distributions on the sections of slabs and T-shaped beams of several sizes are also given for different fire endurance (0.5–4 h). In addition, the stress distribution on critical section at ultimate state is simplified as shown in Fig. 19-27(b), the strengths of the reinforcements A_s and A'_s (f_y^T , $f'_y{}^T$) respectively depend upon the temperatures nearby (T_s , T'_s), and the action of concrete on tension zone is neglected and the strength of concrete is uniformly distributed on compression zone and is taken as $0.67f_c^T$, of which f_c^T is determined by the average temperature (\bar{T}_c) there. The ultimate strength (M_u^T or M_u^T and N_u^T) of the member at elevated temperature is easily calculated, similar to that shown in earlier chapters.

Another simplified calculation method is introduced in reference [19-12]. At first, the temperature contour of $T = 50^\circ\text{C}$ on the section after a certain period or fire endurance desired (0.5–4 h) is determined based on the given tables of temperature field, and the effective area ($T \leq 500^\circ\text{C}$) on the section is approximately taken as a rectangular one while other area ($T > 500^\circ\text{C}$) is neglected (Fig. 19-28(a)). The

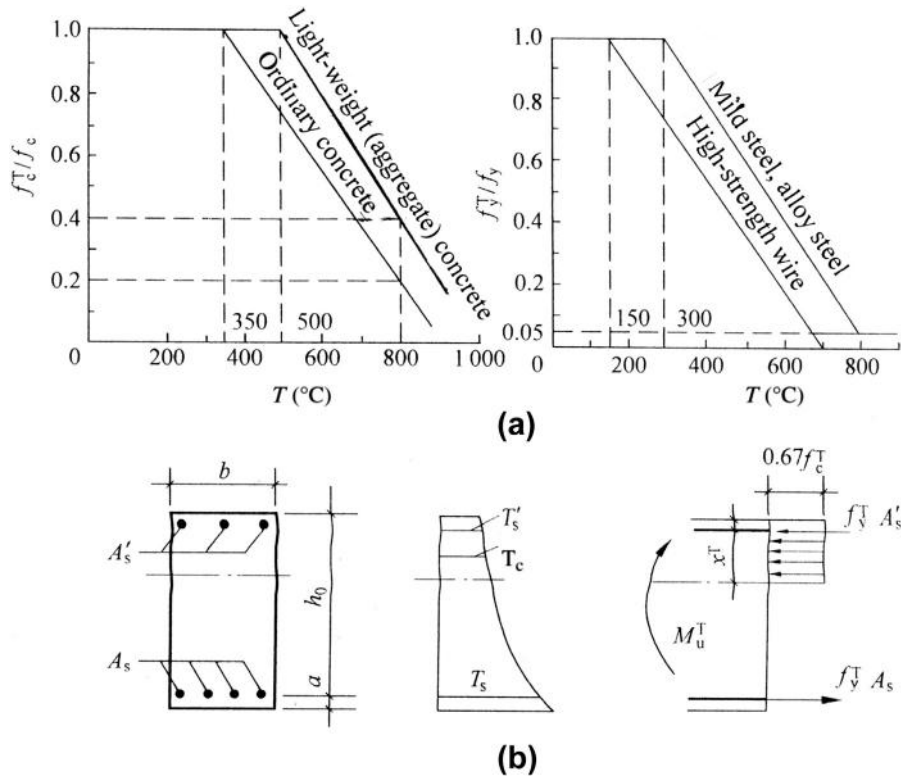


FIG. 19-27 Calculation for ultimate strength of member at elevated temperature [19-15]: (a) strengths of materials, (b) temperature and stress distributions on section

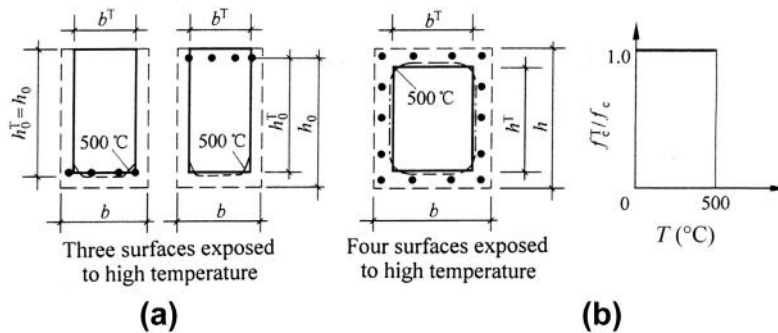


FIG. 19-28 Calculation of ultimate strength of member section at elevated temperature [19-12]: (a) calculation section, (b) strength for concrete

section used for calculation is then considered to be composed of the concrete on the rectangular area and all the existing reinforcements, and the compressive strength of the concrete is taken as the same as that under normal temperature ($f_c^T = f_c$, Fig. 19-28(b)) while the strengths of the reinforcements ($f_y^T, f_y^{T'}$) depend upon the temperatures nearby. The equilibrium equations at the ultimate state are then established for the forces acted on the section, and the ultimate strength of the member section is obtained after solving the equations.

The concept of equivalent section is suggested in references [19-10,19-34,19-37] for calculation of the ultimate strength of the member section at an elevated temperature. The strength-temperature curves of reinforcement and concrete are approximated first to a trapezoid or a few steps (Fig. 19-29(b), (c)). Determining the

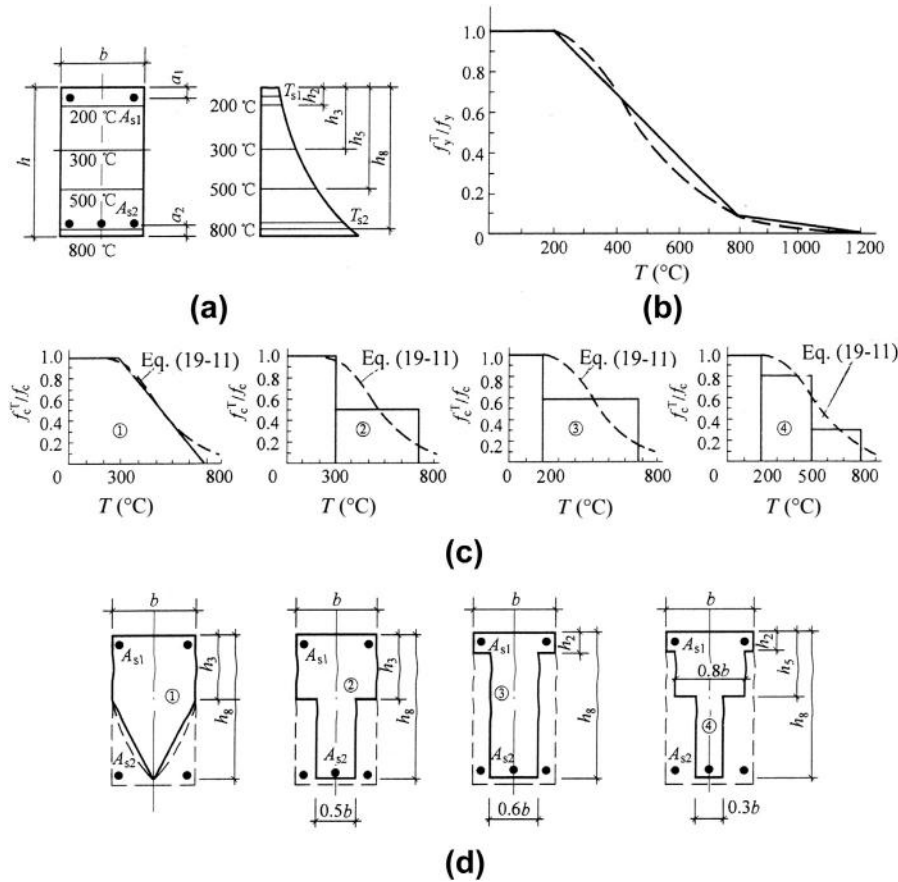


FIG. 19-29 Method of equivalent section for calculation of ultimate strength of member at elevated temperature [19-10]: (a) temperature distribution on section, (b) strength of reinforcement, (c) strength of concrete, (d) equivalent section

temperature field or certain temperature contours, e.g. $T = 500^{\circ}\text{C}$, 800°C , on the section, the width of each temperature area is multiplied by the corresponding ratio of concrete strengths (f_c^T/f_c) and the equivalent section of trapezoid or T-shape with one or two flanges (Fig. 19-29(d)) is then obtained correspondingly. Afterwards, the ultimate strength of the member section at elevated temperature can be calculated as if the equivalent section of homogeneous concrete works under normal temperature and the compressive strength of the concrete should be f_c , and the calculation methods and formulas introduced in Part 3 of this book can be used for various members.

Besides the calculation method and necessary parameters given, the importance of structural detailing is especially emphasized for fire-resistance structure in the relevant design codes or instructions, e.g. [19-4,19-5,19-9,19-12,19-15], of various countries. Some requirements are provided clearly for this, such as: reasonable selection of structural material, the minimum size of section, especially the thickness of thin-wall and hollow or box sections, the minimum thickness of concrete cover for reinforcement, adding extra reinforcement and stirrups to prevent spalling off of the outer-layer concrete, enhancing anchorage measure for the reinforcement, prolonging anchorage length for the longitudinal reinforcement especially the reinforcement on middle support, properly dealing with the joint between precast members to prevent fire and hot air passing through.

CHAPTER OUTLINE

20.1 Characteristics of durability of concrete structure	521
20.1.1 Relevant problems raised in engineering practice	521
20.1.2 Characteristics of durability failure.....	523
20.1.3 Porosity texture of concrete	524
20.1.3.1 Gelation hole.....	525
20.1.3.2 Capillary hole	525
20.1.3.3 Non-capillary holes.....	525
20.2 Several durability problems	527
20.2.1 Permeation	527
20.2.2 Freeze—thaw	530
20.2.3 Alkali—aggregate reaction.....	531
20.2.4 Carbonation	533
20.2.5 Chemical corrosion	536
20.2.6 Rust of reinforcement	538
20.3 Design and evaluation of structure durability	542
20.3.1 Design of durability	542
20.3.2 Examination and evaluation of durability for existing concrete structures	543

20.1 Characteristics of durability of concrete structure**20.1.1 Relevant problems raised in engineering practice**

The raw materials of structural concrete are mainly coarse and fine aggregates of various mineral compositions and cement used as the adhesive material, which is produced from limestone mine as well. Compared with the timber of organic material and the steel of metal, the physical and chemical behaviors of the natural mined materials are more stable in general environment, so the material has stronger resistance against the variations of temperature and humidity and various chemical action and biological corrosion. Therefore, concrete structure is more durable than timber and steel structures.

Since the first concrete structure was built more than one hundred years ago, so many concrete structures of various types have been completed at home and abroad. Most of them existing in the normal environment work well for long periods with little maintenance and are expected to be used for an even longer time.

However, it is also found in engineering practice, that local damage at different levels or even failure symptom appear apparently due to various reasons in some particular concrete structure or a group of structures located in the same place and under a certain environment, although they were built not long ago and the existing time is far earlier than the anticipated service life. Usually the concrete structure is a potential risk to safety and can not be used further when the concrete is severely cracked, loosened, and crushed, the reinforcement is bare and rusted significantly, and the member is bent down obviously and its bearing capacity reduced considerably, etc. For example, some workshops of chemical and metallurgical industries are damaged severely after only 2–10 years sustained chemical corrosion and then abandoned [20-1]; the concrete structure of offshore engineering or near coastal areas is corroded by chlorate; the outdoor bridge and pavement of highway are corroded due to spreading of salt for thawing snow or ice in winter; the concrete in extreme cold areas sustains repeatedly freeze–thaw cycles and the cracks form and expand gradually. All of these phenomena are described as durability deterioration or failure of structural concrete. According to the statistics of China [20-2], about half of the industrial workshops have need of durability evaluation and more than half among them have to be repaired or strengthened in advance before safely being used again, and about 19% of railway bridges are damaged already to different levels.

If the durability failure of a structure appears ahead of the predetermined service life, not only the normal function of daily life or production in it is influenced considerably, but also huge economic loss will be caused directly. Sometimes, the cost of repairing or strengthening for the structure damaged much earlier than expected may be several times greater than the initial investment, if the service life needs to be safely prolonged.

The durability of a concrete structure means that the structure and its components keep sufficient ability to resist deterioration of the material behavior and to satisfy safe use and service performance under long-term natural environment and service condition. When a structure works under normal condition and satisfies the safe and service functions without heavy repair, the period continued from the beginning is called the service life (years), which is used as the numerical index for durability of the structure.

The durability problems of concrete material and structure became aware of as early as the 1950s and the relevant research was started then. It has been paid great attention in the engineering and academic circles, and systematic investigations have been conducted and several international conferences have been convened on this topic since the 1960s. Similar investigations in multi-aspects were also conducted in China since the 1980s and many results are reported. Afterwards, the requirement and instruction of durability are provided clearly in the Code for Design of Concrete Structure [2-1].

Basing on the investigations of relevant accidents in engineering practice and the experimental and theoretical researches, the durability failure of concrete structure is mainly induced into several categories, such as permeance, freeze—thaw, alkali—aggregate reaction, carbonization, and chemical (chlorate) corrosion of concrete and rusting of reinforcement, besides fatigue (Chapter 17), wear (e.g. dam face, pavement of highway, runway of airport) and biological corrosion of concrete, and reinforcement corrosion under stress.

20.1.2 Characteristics of durability failure

The special behaviors of concrete structure introduced in earlier chapters, i.e. aseismic, fatigue, explosion, and fire resistance, have one characteristic in common. They mainly deal with the failure of bearing capacity which is closely related to the mechanical property of the structural materials (f , E) when they are acted on with various loads (forces) including inertia force and impact. However, the durability deterioration or failure of concrete structure and its materials is not directly resulted, in substance, due to the action of external load, but it has some important characteristics as below:

1. The durability failure is a result of the chemical and physical (except mechanical) actions between the external media and the structural materials or between the internal raw materials themselves under the existing environment. For example, CO_2 in the air, chlorion (Cl^-) in seawater or salt, or alkali in cement particles act chemically with concrete (aggregate) or reinforcement (steel), and the physical action of repeatedly expanding—contracting of concrete due to repeated temperature elevating—reducing or freeze—thaw cycles destroy gradually the microtexture in the interior of concrete and cause the deterioration of its mechanical behavior.
2. The durability failure of a structure is a slow and accumulative long-term process, while the failure of bearing capacity is a short-term phenomenon counted in hours or even minutes when the load is acted and increased to the ultimate value. As the concrete and reinforcement in a structure are acted continuously with the external environment and internal factors, the damage and deterioration of them are caused first and then developed gradually from small to greater area and from surface to interior. Usually this is an accumulative process counted in months or years, and even the exact criterion and period of durability failure is difficult to determine.
3. The factors causing the durability failure are related and have influences on one another. For example, the carbonization and chemical corrosion of concrete impel rusting of reinforcement: alkali—aggregate reaction and freeze—thaw cycles of concrete result in cracking, permeating of carbonization, and rusting of reinforcement: reinforcement rusting results in volume expansion of itself, longitudinal crack of concrete along it, and spalling off of concrete cover.
4. The durability failure usually first breaks the ultimate state of normal use (serviceability) rather than that of bearing capacity [20-3,20-4]. When the

exterior appearance of a concrete structure because of various reasons is unacceptable, e.g. wide crack and spalling off of concrete, reinforcement bared and rusted, member bent or inclined obviously, and the service function determined originally can not be satisfied any more, it means that the ultimate state of serviceability is reached. However, the bearing capacity of the structure usually loses less at this moment and the structure will not fail necessarily in this ultimate state. Of course, if the structure is used continuously for an even longer time and the deterioration of the material and the accumulation of damage develop severely, the structure should reach the ultimate state of bearing capacity sooner or later.

The material deterioration and durability reduction of concrete are a complicated and slow process under various chemical and physical reactions and are strongly under the influence of so many factors varying randomly, such as environmental conditions and their change, kinds and contents of relevant media, compositions of concrete raw materials, technique and quality of construction. Although the deterioration regularity, damage mechanism, and durability failure of concrete structure resulting from various factors are qualitatively verified, different academic points of view, mechanism analyses, and calculation models are provided and a unified method with clear concept and accurate quantization is not yet available. The main measures in engineering practice for guarantee and enhancement of the durability of concrete structure are controlling macroscopically composition and construction quality of concrete and optimization of structural detailing based on the engineering experiences. The main concepts, including the phenomenon, mechanism, influence factors, and measure for improvement, of durability failure of various categories are introduced briefly in this chapter, and the physical or chemical models and calculation methods of them may be consulted in detail from relevant references.

20.1.3 Porosity texture of concrete

Various factors may result in the material deterioration and durability failure of concrete as described above, and the seriousness caused depends to a great extent on the porosity and permeability of internal texture of concrete itself. Generally, if the compactness of a concrete structure is poor or its internal porosity is considerable, more possibly various liquids and gases penetrate into its interior with more quantity and larger depth, than the freeze–thaw damage, carbonation layer, and chemical corrosion of concrete and the rust of reinforcement are accelerated, even the liquid can pass easily through the structure. Therefore, the composition and characteristics of the porosity texture in the interior of concrete have to be understood before discussion on the durability problems of concrete structure.

Concrete is a mixed non-homogeneous and anisotropic material composed of the solid particles including coarse and fine aggregates and cement, the dissociated and crystal waters, and air in holes and cracks as introduced already in Chapter 2.

Various holes and cracks in the interior of concrete are the inevitable outcomes during mixing and hardening and have great influence on the permeability. The size, quantity, distribution, and shape (closed or opened) of them are different considerably and depend upon their causing reason and condition (Table 20-1). The internal porosity texture is divided into three categories [20-1] as below in accordance with the causing reason and size.

20.1.3.1 Gelation hole

When fresh concrete is mixed and then hardened, the cement meets water and the cement stone is formed after hydration. The clinker on surface layer of the cement particle is dissolved first, and the gelation and crystal textures are formed gradually and surround the un-hydrated cement core. As the cement hydration penetrates from the surface into the interior and the un-hydrated core reduces gradually, the surrounding gelation of a single cement particle thickens and connects together with that of adjacent particles.

The gelation holes are of tiny size and closed shape and spread in the cement gelation in the early stage of hydration, and the total volume of them is limited although the porosity increases gradually due to water evaporation in the later stage. Nevertheless, the permeability of these holes is poor, so the holes are harmless.

20.1.3.2 Capillary hole

The fine capillary hole is formed in the interior of cement-stone as water evaporates and gelation thickens and hardens during cement hydration. The capillary holes formed initially on the boundaries between cement-stone and coarse and fine aggregates are of slightly greater size as the water–cement ratio then is greater. When the hydration penetrates gradually into the interior of cement particle, its surface layer becomes the gelation with volume expansion (about 1.2 times) and the porosity of the capillary hole reduces.

The capillary holes in cement-stone are of various shapes and most of them are opened, and the volume of them is considerable. However, the capillary holes formed on the boundary between cement-stone and aggregate due to water evaporation are of greater size and quantity, so the volume is even greater. Therefore, the total volume of the capillary holes accounts for 10–15% of concrete volume and has the most influence on the permeability.

20.1.3.3 Non-capillary holes

Besides the two categories of holes generated inevitably during cement hydration, various non-capillary holes of different shapes and sizes form and distribute irregularly in concrete (structure) during construction. They include mainly: (1) the air holes occur naturally during mixing, casting, and compacting of fresh concrete; (2) the air holes are generated intentionally for enhancement of freeze–thaw resistance; (3) the cracks are induced as the mixture of concrete or the cement mortar dissociates underneath coarse aggregate and reinforcement and the water evaporates; (4) the surplus water after cement hydration evaporates later and causes a

Table 20-1 Type and Characteristics of Porosity Texture in Concrete [20-1]

Number	Type of Porosity	Main Causing Reason	Typical Size (μm)	Total Volume in Concrete (%)	Shape
1	Gelation hole	Chemical contraction of cement hydration	0.03–3	0.5–10	Closed (most parts)
2	Capillary hole	Remained after water evaporation	1–50	10–15	Opened (most parts)
3	Hole due to internal dissociation	Dissociation at boundaries of reinforcement and aggregate	10–100	0.1–1	Opened (most parts)
4	Horizontal crack	Dissociation by layers	100–1000	1–2	Opened (most parts)
5	Air hole	Introduced specially by air entraining agent	5–25	3–10	Closed (most parts)
		Introduced occasionally during mixing, casting, and compacting	$(0.1-5) \times 10^3$	1–3	Closed (most parts)
6	Micro crack	Shrinkage	$(1-5) \times 0^3$	0–0.1	Opened
		Changing temperature	$(1-20) \times 0^3$	0–1	Opened
7	Large hole and defect	Compacting inadequately or missed	$(1-500) \times 10^3$	0–5	Opened

void to remain; (5) the micro-cracks result under the internal stress state due to temperature or humidity difference between interior and outside of concrete; (6) the large holes and cracks remain in surface layer and interior of concrete by operation mistake during construction.

The main factors having influence on texture and porosity of concrete are as below.

Water—cement ratio (or water—binder ratio). The water layer surrounding a cement particle is thicker and other parts of the water mixed join together for the concrete for greater water—cement ratio, so an irregular but joining capillary system with greater diameter is formed after water evaporation and the total porosity of the concrete increases. Generally, the water (or W/C) mixed in fresh concrete is more than that actually needed for complete hydration of cement ($W/C \approx 0.20\text{--}0.25$). Therefore, the more the surplus water or the greater the water—cement ratio, the larger the porosity remains in concrete after water evaporation.

Kind and fineness of cement. When the concretes are mixed respectively with expanding-, alumina-, Portland-, volcanic ash-, and slag-cement under the same conditions, the porosities contained in them are increased successively. The larger sizes of gelation and capillary holes, and then the greater porosity result, if the cement used contains more coarse particles. The porosity of concrete reduces if fly ash or silicon powder of fine particles is mixed properly.

Kind of aggregate. When the coarse aggregate used in the concrete is a kind of natural dense rock, the internal porosity is usually small and most holes are closed. However, various rocks have different porosities of their own, e.g. granite is better than limestone. As far as various light-weight aggregates whether natural or artificial are concerned, considerable porosity exists certainly in itself and most holes are opened.

Producing quality. If the concrete is mixed, transported, cast, or compacted improperly during construction, considerable holes or other defects may result. The porosity reduces after careful construction.

Curing condition. When the concrete is cured in time and the cement is fully hydrated, the size and porosity of the capillary hole must be reduced. If the concrete is cured under heating, the temperature and humidity changes have great influence on the texture of the capillary hole, and sometimes the internal crack and even greater porosity may be formed under considerable gradients of temperature and humidity in concrete.

20.2 Several durability problems

20.2.1 Permeation

When a pressure difference exists between a concrete and its surrounding medium, the liquid or gas in the higher-pressure side should move towards the lower-pressure side. This physical phenomenon is called permeation. For example, the water under pressure permeates into the interior and even through the concrete dam, pool, pipe,

or pavement; the carbon dioxide (CO₂) and other corrosive gas in the air permeate into the interior of the concrete. Excessive permeation will cause the durability deterioration of concrete material and structure. For example, a hydraulic structure fails in water prevention as the water permeates through; the freeze–thaw failure is caused due to the water permeated; the corrosive gas entered causes gradual carbonization or corrosion of concrete.

The ability of concrete against permeations of liquid and gas is called permeability resistance. Water is the liquid medium most widely encountered in engineering practice. The quantitative index for the permeability resistance of concrete is usually taken as the permeability coefficient (k in cm/s) [20-5], of which the definition is the water quantity (Q in cm³/s) permeated through a thickness (L in cm) within per unit area (F in cm²) of concrete under per unit water head (h in cm) within per unit time (in s), i.e.

$$k = \frac{QL}{hF}, \quad (20-1)$$

$$\text{or } Q = k \frac{hF}{L}.$$

Alternatively, the dense concrete permeated with difficult is evaluated by the permeability grade which is measured following the standard test method [20-6]. The standard specimen is tested under water pressure which is increased slowly at the rate of 0.1 MPa/8 h. When wet or a water drop is found on the back surfaces the three specimens among a series of six, the corresponding water pressure (H in MPa) is recorded and the permeability grade is calculated as below:

$$S = 10 H - 1 \quad (20-2)$$

and then is rounded off to several whole numbers, e.g. S_2, S_4, \dots

The permeability coefficient and grade can be converted into each other as shown in Table 20-2. The required permeability grade (S_2 – S_{30}) or the limitation of permeated quantity (Q , cm³/s) should be determined for concretes of various structural engineering, depending upon the environment (water pressure) and service function.

Liquid and gas permeate into and through the concrete mainly via the capillary passage inside, so the intensity of permeability depends upon the hole texture and its porosity. All the factors causing greater porosity in concrete results in higher permeation, whereas reduction of porosity and improvement hole texture (closed) result in stronger resistance for permeability. The concrete of high resistance of permeability (e.g. $>S_{30}$) or, on the other hand, of well permeated can be produced in accordance with the service requirement for a particular structural engineering. For example, if the waterproof concrete is used for an underground room, water pool, and equipment foundation, the permeability grade $>S_6$ is usually required and can be achieved, when the mix is strictly controlled, the water–cement ratio is below the limitation (Table 20-2), and the concrete is compacted and cured properly during construction.

Table 20-2 Conversion between Permeability Coefficient and Grade [20-1]

Permeability Grade		S ₂	S ₄	S ₆	S ₈	S ₁₀	S ₁₂	S ₁₆	S ₃₀
Permeability coefficient <i>k</i> (10 ⁻⁹ cm/s)		19.6	7.83	4.19	2.61	1.77	1.29	0.767	0.236
Water-cement ratio controlled	Waterproof concrete			0.55–0.60	0.50–0.55			0.45–0.50	
	Hydraulic concrete	<0.75	0.60–0.65	0.55–0.60	0.50–0.55				

In addition, when a waterproof coating or mortar is covered on the outer surface or other external measures are used, the permeability resistance of the concrete structure can also be enhanced.

20.2.2 Freeze—thaw

Both the free water remaining after concrete has hardened and the water permeated into the interior of concrete via various passages exist in the internal voids (holes and cracks) of concrete. When the environmental temperature drops down below the freezing point, the water in the voids freezes with volume expansion, which causes damage to the internal texture of concrete material. If some gas also exists in a part of the voids and a part of the unfrozen water is compressed into the gelation or other hole, the expanding pressure resulting during water freezing is reduced and the freeze damage is then partly relaxed.

When the concrete is saturated with water, the water in the capillary holes freezes with expansion and great compression results and acts towards the outside. However, the water in the gelation holes will not freeze even under extreme low temperature, e.g. -78°C , because of the very tiny diameter of these holes. As the evaporating pressure of the water is greater than that of ice with the same temperature, the evaporated gas permeates towards the boundary of the ice in the capillary holes, and permeating pressure is then caused there [20-1]. Therefore, the capillary wall is acted together with the expanding and permeating pressures, and the wall texture is broken and internal cracks appear in the concrete when the fine-scopical strength of concrete is overcome.

The internal water is frozen into ice and the ice is thawed back to water cyclically in the concrete, as the environmental temperature descends and elevates repeatedly. Each freeze—thaw cycle impels damage accumulation in the interior of concrete, so the internal cracks expand and extend continuously and then link together. Therefore, cracks and crushes gradually develop inside the concrete from the surface layer, and the strength of the concrete reduces.

Resistance to freeze—thaw damage is called freeze resistance of concrete and its quantitative index is the antifreezing grade. According to the National Standard of China (GBJ 82-1985) [20-6], the standard specimens start to be tested at age 28 days following the slow freeze—thaw method, and the weight and compressive strength of the specimen are measured after every freeze—thaw cycle. When both the weight and compressive strength lose more than 5% and 25% respectively, the minimum number of freeze—thaw cycles tested is the antifreezing grade, e.g. D25, D300.

If concrete is frozen before hardening, two situations may occur. (1) When the concrete is frozen with expansion soon after mixing, the hardening process stops because hydration of the cement has not been carried out yet. When the ice thaws to water after the temperature is raised, the hydration of the cement starts as usual and the concrete is hardened gradually. However, a lot of holes are formed and remain in the concrete after the ice is thawed, so its strength should be reduced. (2) When the concrete is frozen after partly hardening, the expected strength is not reached yet as the cement does not fully hydrate. Because the gelation hole

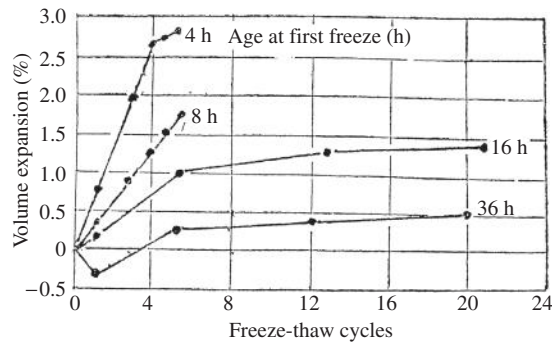


FIG. 20-1 Volume expansion and age at first freeze [20-1]

acting as a buffer has not formed then, the water in the capillary hole freezes with volume expansion which causes more damage to the internal texture, so the final strength of the concrete loses considerably after the ice has thawed. In addition, the earlier the concrete is frozen, the weaker the ability against expansion (Fig. 20-1), the poorer the ability against freeze failure, and the lower the strength of concrete reached finally.

Freeze resistance of concrete depends mainly upon the internal hole texture and porosity, water content or saturation, and age at first freeze. When the concrete is mixed properly with a smaller water–cement ratio, reasonable mixing, additional fly ash or silicon powder of good quality, and produced carefully and cured fully, the freeze resistance of the concrete should be enhanced after hardening as the compactness increases and the porosity reduces. In addition, there are other favorable measures. (1) The concrete can be mixed additionally with an air entraining agent and numerous fine gas bubbles are formed and distributed uniformly in the fresh concrete, and also numerous fine closed holes without links to one another exist after the concrete has hardened. These holes can suck up the expanding action during freezing of capillary water and then reduce the damage of internal texture. This is an easy and effective measure for enhancing the freeze resistance of concrete (Fig. 20-2). (2) When a concrete structure is constructed in winter, the concrete can be mixed with some additive for antifreeze or early strength or cured under heating, so the freeze is prevented and the hardening is impelled.

20.2.3 Alkali–aggregate reaction

As some active minerals in the aggregate react chemically with the alkaline solution, e.g. KOH, NaOH, within internal holes of the concrete and is then expanded, the expansion pressure resulted causes cracking and strength reducing of the concrete. This phenomenon is called the alkali–aggregate reaction, which usually happens several years after concrete has hardened. Because the alkali–aggregate reaction occurs widely over the whole concrete but not the surface layer only, it is difficult to be obstructed and repaired, and the concrete may even totally fail under some serious conditions.

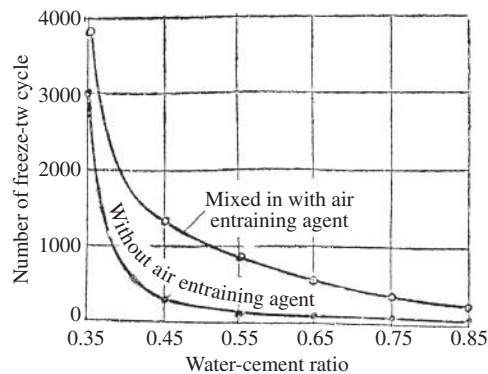


FIG. 20-2 Freeze resistance of concrete mixed in with air entraining agent [20-1]

According to different mineral composition of the aggregate in concrete, the alkali–aggregate reaction can be classified into three categories [20-7,20-8]:

1. Alkali–silicon reaction: when microcrystal silicon oxide in some mineral aggregates, such as flint rock, siliceous rock, sandstone, quartzite, reacts chemically with alkaline solution in the concrete, the relevant silicate is yielded and then expands when it meets water, so cracking of concrete is caused.
2. Alkali–silicate reaction: when the active silicate in some aggregates, such as phyllite, reacts chemically with alkali compound in the concrete, its volume expands gradually and light damage is caused in the concrete.
3. Alkali–carbonate reaction: some carbonate aggregates, such as dolomite, limestone, are active themselves and MgCO_3 among them reacts chemically with alkali substances in the concrete, then Mg(OH)_2 is yielded with volume expansion and internal cracks result in the concrete.

The necessary conditions for alkali–aggregate reaction in concrete are: alkali contained in concrete, aggregate being active, and water contained in internal holes, and their contents or index reaching certain levels.

The main sources of alkali in concrete are the dissolvable alkali contained in its raw materials, including cement, aggregate, water, and additional powder and agents, and the one entered from the surrounding environment. Usually, the maximum portion of alkali comes from the cement, and the composition and quantity of the alkali depend upon its raw material and manufacturing technology. The alkali content in cement can be expressed as the calculated value of equivalent sodium oxide ($\text{Na}_2\text{O} + 0.658 \text{K}_2\text{O}$). Generally, the cement is called a low-alkali one if the equivalent concentration of alkali is less than 0.6%, and the alkali–aggregate reaction can be avoided for the concrete mixed with the cement of this kind (Fig. 20-3).

Total alkali content in concrete mainly depends upon the cement content in concrete (kg/m^3) and the equivalent sodium oxide relating to the category of the cement used. The possibility and harmfulness for alkali–aggregate reaction can be macroscopically expressed as the quantity of alkali contained per unit of concrete volume

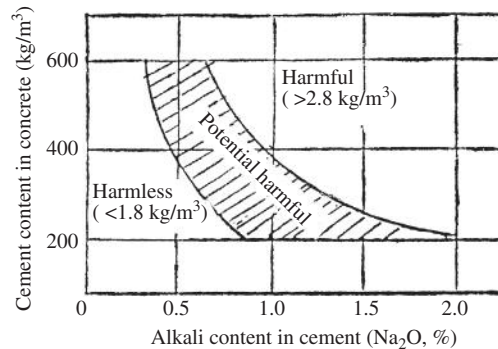


FIG. 20-3 Alkali content (kg/m³) in concrete and alkali–aggregate reaction [20-1]

(kg/m³) (Fig. 20-3). In order to prevent the damage caused by alkali–aggregate reaction, the maximum quantity of alkali (kg/m³) should be limited for the concrete located in different environments and is listed in the design codes of various countries (e.g. Table 20-4).

The most effective measure for prevention or reduction of the alkali–aggregate reaction in concrete is to control (reduce) the alkali content in the cementitious material used, e.g. using low-alkali cement or adding non-alkali fly ash, silicon or slag powder. In addition, the aggregate used is selected properly and the active mineral contained should be reduced; air entraining agent is added during concrete mixing and fine holes produced reduce the expansion pressure acted on the aggregate; manufacture technology is improved and compactness of concrete is enhanced to prevent or obstruct water entering from outside; the environment is kept dry or a waterproof layer is spread on the outer surface of the concrete, the penetrated water is reduced and the alkali–aggregate reaction is restrained.

20.2.4 Carbonation

As the acidic substances, e.g. CO₂, SO₂, HCl contained in the surrounding environment media, e.g. air, water, soil, of concrete contact directly its surface and permeate into its interior via various holes and gaps, the chemical reaction has to occur between them and the alkaline substances contained in the cement-stone. This is called neutralization of concrete [20-1], and the carbonation of concrete in the air occurs most widely in engineering practice. At first CO₂ in the air permeates into the capillary holes and gaps of concrete and is dissolved into the water in them, then it reacts with calcium hydroxide Ca(OH)₂ or calcium silicious yielded after cement hydration, so that calcium carbonate is eventually formed.

The gelation and capillary holes in concrete are partly blocked up after carbonation, so the compactness and compressive strength (f_c) are increased (Fig. 20-4). Although this is beneficial for concrete, the harmful results are dominant. As the alkalinity (pH value) of the concrete reduces after carbonation (neutralization), the inactive coating at the surface of reinforcement in the concrete will fail and

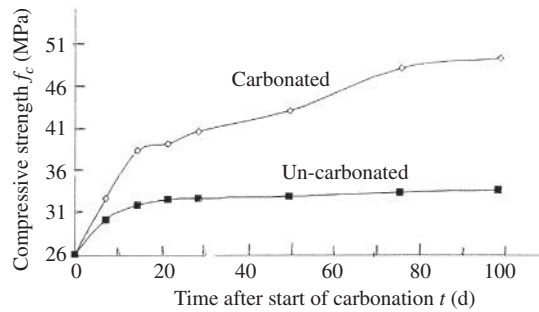


FIG. 20-4 Compressive strength of concrete after carbonization (accelerative test) [20-2]

rust is then developed gradually there, once the thickness of carbonated layer reaches there (see Section 20.2.6). In addition, shrinkage accelerates in carbonated concrete, and cracking, reducing of bond strength, and even spalling off of concrete cover then result successively.

Other gases in the air (e.g. SO_2 , HCl , Cl_2) are of higher acidity, but their concentrations are much lower than that of CO_2 (the usual ratio between them being one to several hundreds). When these gases directly contact concrete and enter into its internal holes, they react chemically with $\text{Ca}(\text{OH})_2$ there and the acid salt (e.g. CaSO_4 , CaCl_2) is yielded and sediments mostly in a thin layer near the surface (Fig. 20-5).

The carbonation of concrete develops gradually inside from its surface layer, but the content of calcium carbonate (CaCO_3) yielded tends to reduce (Fig. 20-5). The carbonated area of concrete can be divided into four zones, among them the carbonated zone contains the highest content of calcium carbonate and the transition and uncarbonated zones are succeeded inside. The acid salt in the surface layer destroys

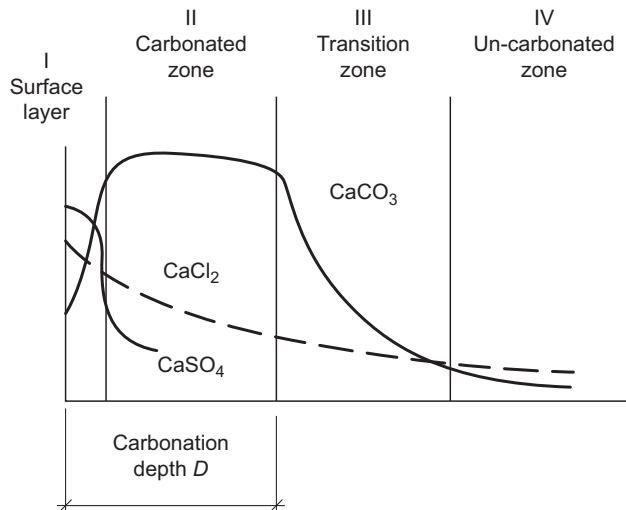


FIG. 20-5 Divisions of carbonated

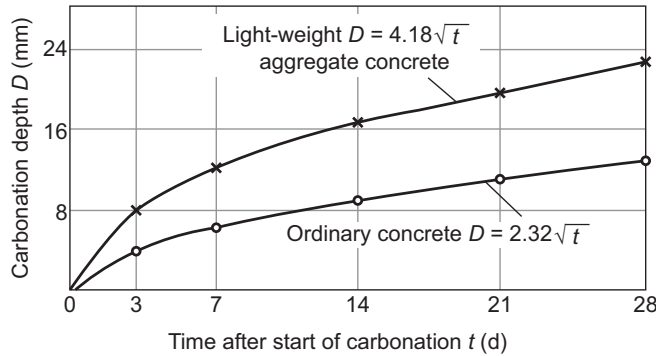


FIG. 20-6 Carbonation depth measured area in concrete from accelerative test [20-1]

partly the carbonate, so the content of CaCO_3 there is lower. The maximum thickness from the surface to the end of the carbonated zone of concrete is called the carbonation depth (D in mm).

Generally, the concentration of CO_2 in air is only about 0.03% and the carbonation of concrete develops very slowly. When the concrete cover, e.g. 20–40 mm, of a reinforced member is totally carbonated, it takes several years or decades depending upon the compactness. According to the national code GBJ 82—85 [20-6], the accelerative test, in which the specimen is surrounded with air of high concentration of CO_2 ($20 \pm 3\%$), can be used for measuring the carbonation depth of concrete (Fig. 20-6). Based on the experimental data in laboratory and the relevant survey in engineering practice, the relation between the carbonation depth (D in mm) and the concentration of CO_2 in the surrounding air (C in %) and the time after start of carbonization (t in days) is obtained and can be expressed as

$$D = \alpha\sqrt{Ct} \quad (20-3)$$

where α is the coefficient of carbonation rate.

If the concentration of CO_2 surrounded is C_k for the concrete specimen during accelerative test and the carbonation depth is D_k measured at the time after start of carbonation t_k , the carbonation depth of concrete under the natural environment can be predicted following the formula

$$D_n = \sqrt{\frac{C_n t_n}{C_k t_k}} D_k \quad (20-4)$$

where C_n is the concentration of CO_2 in environment, and t_n is the time counted from start of carbonization.

The coefficient of carbonation rate (α) is a physico-chemical index representing the resistance against carbonation for concrete, and its value mainly depends upon kinds of cement and aggregate, water–cement ratio, content of cement and admixture, curing condition, and environmental temperature, humidity, and concentration of CO_2 . Different empiric formulas [20-1] are suggested by researchers at home and

abroad and several complicated physical and chemical models are also provided in some references [20-2] for prediction of carbonation depth of concrete.

In order to enhance durability of structure, there are various measures as described below to reduce or delay the carbonation process of concrete in engineering practice. Ordinary Portland cement of better quality against carbonation is preferred; enough content of cement, lower water–cement ratio, additional fly ash or silicon powder are properly mixed on concrete to reduce the porosity; concrete is carefully mixed, cast, compacted, and cured during construction to enhance the compactness; paint or mortar is covered on the surface to obstruct penetration of CO_2 in the environmental air; concrete cover of reinforcement is properly thickened to delay the duration when the carbonation depth reaches the reinforcement.

20.2.5 Chemical corrosion

The environmental media directly surrounding a structure, including air, water, seawater, or soil, may contain corrosive substances, e.g. acid, salt, and alkali of different concentrations. When they permeate into the interior of concrete and react physically or chemically with the relevant composition, the concrete is gradually corroded and then expanded, cracked, and spalled off. Finally, the reinforcement rust is caused and even the structure fails.

The reason and mechanism of concrete corrosion vary with the corrosive medium and environmental condition and are divided into two categories:

1. Kind of dissolution. The substance like $\text{Ca}(\text{OH})_2$ yielded after hydration of cement particle is dissolved very easily in the water permeated in the concrete and promotes the hydrolysis of alkali compound, e.g. hydrated calcium silicate, then the hydrated substances (CaO , SiO_2) of low alkali are damaged and finally the texture of cement stone of the concrete is totally destroyed. In addition, when some acid solution containing SO_2 , H_2S , or CO_2 , permeates into the concrete, the spongy substance without coagulation yielded is dissolved easily. The dissolution level of cement stone increases with the flowing velocity of permeated water. The adhesion of cement stone is reduced after dissolution and the integrity of concrete is damaged.
2. Kind of crystalline expansion. When the water containing sulfate (SO_4) permeates into concrete and reacts chemically with the hydrated product $\text{Ca}(\text{OH})_2$ of cement, the gypsum solution $\text{CaSO}_4 \cdot 2\text{H}_2\text{O}$ is formed. As the gypsum acts again with hydrated aluminum sulfate, the hydrated aluminum calcium sulfate containing crystal water is formed with volume expansion, and crack and failure of the concrete finally results.

The concrete structure of offshore engineering usually experiences a long period of action in seawater or humid air, in which plenty of chlorate, magnesium, and sulfate (NaCl , MgCl_2 , MgSO_4 , CaSO_4 , etc) are contained. When they react with the hydrated substance of cement ($\text{Ca}(\text{OH})_2$) in concrete, the easily dissolvable products, e.g. CaCl_2 , CaSO_4 are yielded, so the porosity is increased and the internal

texture is weakened in the concrete, i.e. concrete is corroded. There are different features of corrosion for the concrete, depending upon the elevation and the position of the structure [20-1]. When a part of the structure is located above the highest tide and does not directly contact any seawater, still the concrete there is easily damaged due to freeze–thaw action and the reinforcement there rusts, as the humid air containing corrosive salt permeates into the concrete; when a part of the structure is located in the wave splash zone and the concrete there sustains cyclically dry-and-wet action, the concrete corrosion of expansion kind is caused and the reinforcement rust is accelerated; when a part of the structure is located in the variation zone of sea level during tides and the concrete there sustains cyclically the wave scour and dry–wet and freeze–thaw actions, the corrosion of dissolution kind is caused and the damage resulted there is most serious; when a part of the structure is located below the lowest tide and is always immersed in seawater, the concrete there sustains chemical dissolution and corrosion, but the freeze–thaw damage of concrete and the reinforcement rust are not serious.

As the underground structure always directly contacts soil and underground water surrounding it, the concrete will also be corroded if some chemical compositions contained in the environmental media are corrosive. When a dissolvable sulfate with concentration $>0.1\%$ is contained, the corrosion of crystalline expansion will occur in the concrete, even it is mixed with Portland cement and manufactured very carefully. If the concentration of salt contained in underground water is higher, e.g. 1% , the concrete may be totally corroded. It would be more harmful if C_3A is highly contained in the cement used for the concrete, so its concentration should be limited, e.g. $<3\%$ or 5% . If the acid, mainly carbonic acid H_2CO_3 , is contained in the underground water with a value of $pH < 6.5$, the cement stone in the concrete will be corroded; the value of pH ranges from 3 to 6, the corrosion develops quickly at the earlier period but slows down later. Generally, the massive concrete corroded due to acid is only limited in the surface layer. However, if the waterlevel in the underground is rather high and the concrete is not well compacted, the acid water will permeate into the deep layer and may cause serious corrosion.

As far as some workshops in the chemical, metallurgical, and papermaking industries are concerned, the products may be strong acid or alkali or many strong acids are used during the production process, so the environmental air with strong corrosion is caused and the underground soil and water also contain strong acid if it permeates. Therefore, the structures above and underground including foundation and pipe system sustain strong corrosion and may be seriously damaged within a short period, even if they are not worth repairing or strengthening but have to be totally discarded.

In order to mitigate or prevent the corrosion of concrete and to enhance the durability of a structure, its site should be selected carefully, and the environmental air, water, and soil should be examined in advance and the contents and values of pH of the corrosive media, e.g. sulfate, magnesia, and carbonate, should be controlled. Besides, the structural design, selection of concrete raw materials, and construction should be properly conducted. For example, the particular category of cement is selected for resistance to various corrosion (Table 20-3); the concrete is mixed

Table 20-3 Comparison of Chemical Corrosion Resistance between Various Categories of Cement [20-1]

Cause of Corrosion		Sulfate	Weak Acid	Seawater	Water
Portland cement	early hardened	Low	Low	Low	Low
	ordinary	Low	Low	Low	Low
	low hydration heat	Medium	Low	Low	Low
Anti-sulphate cement		High	Low	Medium	Low
Portland blast-furnace cement		Medium–High	Medium–High	Medium	Medium
Volcanic ash cement		High	Medium	High	Medium
Supper anti-sulphate cement		Very high	Very high	High	Low
Alumina cement		Very high	High	Very high	High

with low water–cement ratio, enough content of cement, and active admixture, and well compacted and cured, in order to enhance the compactness and permeation resistance; the concrete cover of reinforcement is properly thickened; the surface of structural concrete is coated or soak treated, in order to prevent the permeation of corrosive water and to reduce the corrosion and erosion of concrete.

20.2.6 Rust of reinforcement

Reinforcement is an essential part to carry tensile force in a concrete structure and is necessary for its load-carrying capacity. Although the durability of the structure is surely influenced after the concrete in the structure is deteriorated, damaged, and cracked due to various factors as above, the load-carrying capacity of the structure is not necessarily reduced much within a certain period. However, if the crack and corrosion and carbonation layers of concrete reach the reinforcement in it, the reinforcement is easily rusted. Because the diameter and area of the reinforcement is rather small, its strength will reduce significantly after rusting, so the load-carrying capacity of the structure is seriously reduced and the safety problem is then caused.

The rust of reinforcement in concrete is a process of electro-chemical corrosion [20-1,20-9]. When the concrete is mixed with Portland cement and well-compacted, the internal solution after hydration of cement is of high alkaline and the value of pH is about 13 before carbonization, and a thin layer (thickness 0.2–1 μm) of compact passive membrane composed of $\text{Fe}_3\text{O}_3 \cdot n\text{H}_2\text{O}$ or $\text{Fe}_3\text{O}_4 \cdot n\text{H}_2\text{O}$ is formed on the surface of the reinforcement, which can protect it from rust (Fig. 20-7).

When the carbonated layer of concrete is thickened and reaches the surface of reinforcement or the chlorine ion (Cl^-) contained in the environmental air, water or soil reaches the surface of reinforcement after concrete has cracked due to various reasons, the passive membrane on the surface of the reinforcement is locally failed due to reduction of concrete alkalinity (value of pH) and then the iron itself is

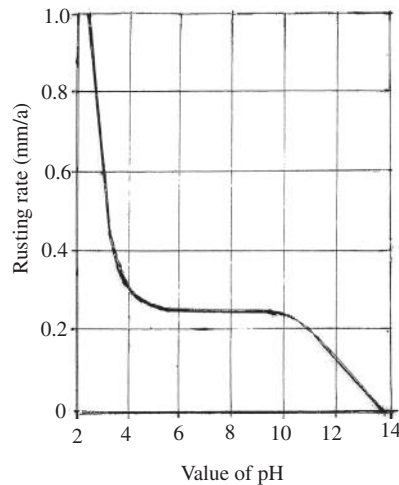


FIG. 20-7 Rusting rate of reinforcement and alkaline of concrete [20-1].

exposed. Consequently, a potential difference is resulted between the exposed iron and the undamaged passive membrane, and they are respectively a positive pole of small area and negative pole of larger area (Fig. 20-8). As the reaction progresses at the negative pole, OH^- is yielded there and the value of pH is increased, while the iron at the positive pole is dissolved and the solid corrodent $\text{Fe}(\text{OH})_2$ is generated there.

The spot rust appears first on the surface of reinforcement and develops gradually into a hole, and finally spreads out and over the whole surface and goes deep inside. Generally, the volume of rust corrodents is several times that of original iron (Fig. 20-9). Moreover, the rusted reinforcement also expands in the longitudinal direction and the concrete crack is also caused in the same direction, the extension and

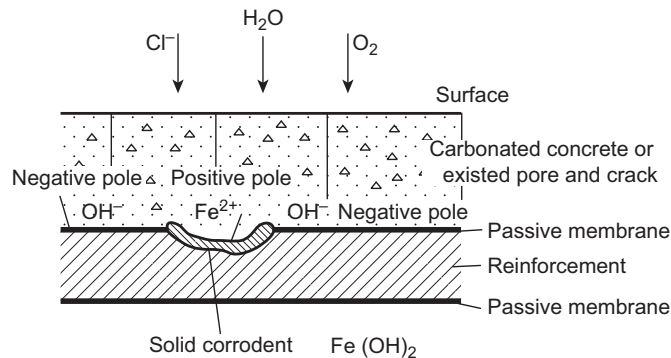


FIG. 20-8 Scheme of spot rust on reinforcement surface [20-2]

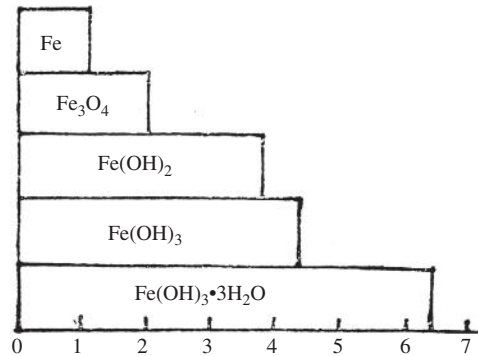


FIG. 20-9 Ratios of volume expansion for reinforcement corroducts [20-1]

expansion of the crack accelerate again rust of reinforcement and cause damage and spalling off of concrete cover and reduction of bond strength. Finally, the strength of the reinforcement is seriously reduced and the structure failure results.

The accelerative corrosion test is conducted for measuring the mechanical behavior of rusted reinforcement [20-10]. The specimens of reinforcement are immersed in the salt (NaCl) solution of concentration 4‰ with few hydrochloric acid (HCl) in, and they are respectively taken out and tested mechanically at pre-determined ages. It is demonstrated (Fig. 20-10) that not only the sectional area reduces but also the mechanical behavior degrades even more for the rusted specimen, compared with the original reinforcement, i.e. the strength loses more and the ultimate elongation reduces much more. In addition, the degradation level of rusted reinforcement varies with the category and strength grade.

Various measures can be taken in engineering practice in order to delay or prevent the rust of reinforcement and then to enhance the durability of concrete structure. From the environment aspect, the concentrations of various corrosive media should be controlled, and the carbonation layer of concrete and the chlorine

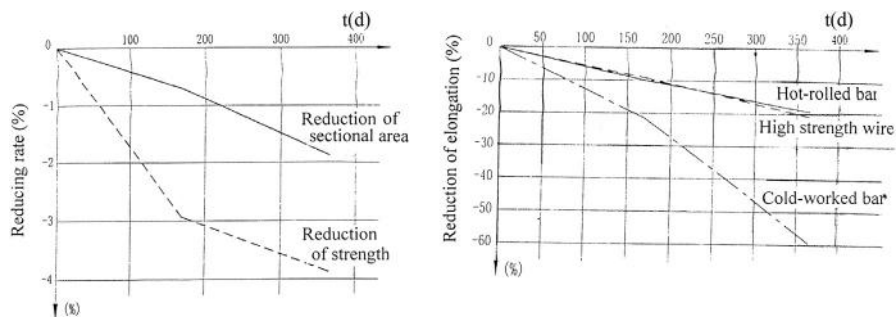


FIG. 20-10 Degradation of sectional area and mechanical behavior of rusted reinforcement [20-10]: (a) sectional area and yield strength, (b) ultimate elongation

ion should be limited and not reach the surface of reinforcement inside. From the material aspect, the anticorrosive cement and the admixture of good quality are preferable, the contents of chloride in the coarse and fine aggregates and admixture should be limited, the water–cement ratio should be lowered, the fresh concrete should be carefully compacted and cured to enhance its compactness, and the anti-rust agent is added during mixing; or the reinforcement of anti-rust category, e.g. epoxy-coated, galvanized, or stainless, is used. From the structural design and detailing aspect, the concrete cover of reinforcement should be properly thickened and kept without any damage, and anti-corrosive coating can be spread on the surface of concrete.

The various phenomena and main reasons, and also the mechanisms, influence factors, and improvement measures, of durability deterioration or failure of concrete structure are respectively introduced above. Because these deteriorations are related to one another and most of them closely depend upon the porosity and pore texture inside concrete, so many improvement measures are consistent and of mutual benefit:

1. The particular cement of good quality is reasonably selected, the content of cement is properly increased and the water–cement ratio is reduced, and the fine admixture, e.g. fly ash and silicon powder, of good quality is selected for concrete.
2. The special agents of various performances, such as super-plasticizer, early hardening, air entraining, anti-freezing, and anti-rusting of reinforcement, are added during mixing of concrete.
3. The coarse and fine aggregates of good quality are selected for concrete, i.e. the aggregates are of clean particles, reasonable shape and size, small and closed holes contained, low activity, low value of pH, and low content of chlorine ion. Otherwise, the light-weight aggregate of good quality is used.
4. The concrete is manufactured carefully for reducing internal porosity, i.e. mixed uniformly, preventing separation during transporting and casting, fully compacted and cured especially at early age.
5. The concrete cover of reinforcement is properly thickened during structural design to ensure its effectiveness.
6. The surface and outer layer of concrete are painted or immersed with various isolate materials to prevent permeating of harmful gas or liquid in the environmental media.
7. The environmental conditions, e.g. the temperature and humidity and their variable amplitudes, the concentration of corrosive substance in environmental media, are controlled and improved.

Nevertheless, it should also be known that some measures are favorable to enhance the durability of concrete in some aspects but are harmful to others aspects:

1. When the fly ash or silicon powder of good quality are added properly during mixing of concrete, the porosity inside is reduced and the compactness and

permeability resistance are increased, the alkaline and then the alkali—aggregate reaction are reduced and the carbonation is delayed as well for the hardened concrete. In addition, the corrosion resistance of the concrete and the anti-rust of the reinforcement in it are also enhanced. On the other hand, if the admixture is of bad quality or added excessively and more water is needed during mixing, so more porosity, and lower strength and freeze resistance are then the result for the hardened concrete and the reinforcement in it is easily rusted.

2. When the alkali content in the cement is within the right range, the value of pH is increased and it is favorable for anti-rust of the reinforcement in concrete. However, if the alkali content in cement is excessive, the unfavorable alkali—aggregate reaction is easily caused.
3. Although the concrete will gain higher strength at early age and stronger freeze resistance after hardening when it is cured under heating after cast and compacted, the carbonation will be accelerated and it is unfavorable for anti-rust of reinforcement in it.
4. When the air entraining agent is introduced in the concrete during mixing, numerous closed fine holes are formed and distribute uniformly in the interior of hardened concrete and it is favorable for the resistances against freezing, permeability, and corrosion. However, if these holes formed are of great diameter and do not distribute uniformly or their total volume is too much, the negative effect will be caused, e.g. the strength of concrete is reduced.
5. The concrete composed of porous light-weight aggregate is favorable for anti-freeze and can be used for making permeable concrete if needed. However, the concrete is obviously harmful for permeability resistance and the resistances against carbonation and chemical corrosion are weakened as well, so the reinforcement in it is easily rusted.

Therefore, the measure used for enhancement of concrete durability has to be analyzed and evaluated in all aspects and both favorable and harmful results should be considered comprehensively.

20.3 Design and evaluation of structure durability

20.3.1 Design of durability

Usually, the designed service life is 50 years for a general concrete structure or 100 years for the important one, while it may be shortened, e.g. 30 years, for a temporary one. The structure built and its members should work safely with all service functions under normal maintenance and not need to be essentially repaired and strengthened within the designed service life.

Because the durability of concrete structure was not fully understood and investigated in the past, some structures built were obviously deteriorated and damaged due to various reasons as above before the end of the service life. The examining, repairing, and strengthening of these structures would cost a lot in materials and

funds, and some of them are not worth being repaired and used again and have to be discarded totally.

As various phenomena of durability failure of concrete structure appeared gradually since the 1950s, they attract the structure engineer's and researcher's attention to conduct general investigation and many results have been reported since then. Consequently, some academic organizations of various countries, e.g. Japan and European, worked out relevant codes in the 1980s to guide the design and detailing of concrete structure. In China, the relevant provisions are also compiled for durability of concrete structure in the design code [2-1] and some standard [20-11].

Up to now, various physical and mathematical models [20-2,20-4] have been developed for quantitative analysis of the durability of concrete (structure) in many aspects, e.g. freezing depth, carbonation depth, permeation of chlorine ion, rust rate of reinforcement. However, these theoretical models are not unified and have different viewpoints and mechanism explanations and the universality and accuracy of their calculation methods do not satisfy the requirements of engineering practice, because the deterioration and failure of concrete durability depend upon the complicated physical and chemical reactions in a long period and are closely related to many random factors.

Therefore, in order to ensure the durability of a structure to be built, the measures can be taken as below within the design and construction periods: such as the position located and the environmental condition is reasonably selected, the structural detailing is improved, the construction is carefully managed, and the mixing and quality of concrete are strictly controlled. Based on the comprehensive results of the experience and lessons in engineering practice, the experimental investigation, and the theoretical analysis, the basic quantitative requirement can be provided for the concrete to ensure its durability. For example, the relevant provisions listed in the Design Code of China [2-1] are briefly shown in Table 20-4. Depending upon different environmental conditions of the structure, the limitations of the minimum strength grade, the maximum water—cement ratio, the minimum content of cement, the maximum contents of chlorine ion and alkali are respectively provided for structural concrete. In addition, the corresponding requirements, e.g. category of reinforcement and thickness of concrete cover, are also provided in the code for the reinforcement in the structure. When the permeability and freeze resistances of the concrete are also required, some other requirements listed in relevant standards should be satisfied.

20.3.2 Examination and evaluation of durability for existing concrete structures

After a concrete structure was built and put into service for years, the damage, deterioration, and durability reduction of various levels usually appear on its exterior and interior due to the unfavorable reactions of the environmental factors and the media surrounded or under a special load acted occasionally. The

Table 20-4 Basic Requirement for Durability of Structural Concrete [2-1]

Environment		The Minimum Strength Grade	The Maximum Water-Cement Ratio W/C	The Minimum Content of Cement (kg/m ³)	The Maximum Content of Chlorine ion in Cement (%)	The Maximum Content of Alkali (kg/m ³)
Category	Conditions					
I	Normal inside room	C20 (C30)	0.65	225	1.0 (0.06)	No limitation (3.0)
II	a	C25	0.60	250	0.3	3.0
	b	C30	0.55	275	0.2	3.0
III	Using ice remover, variation of water level during winter in cold area, outdoors nearby seaside	C30	0.50	300	0.1	3.0

The figures in the table and in the parentheses are respectively suitable for the structures with designed service lives of 50 and 100 years. The minimum strength grade should be two grades higher than that listed in the table, and the minimum content of cement is 300 kg/m³ and the maximum content of chlorine ion in the cement is 0.06% for the concrete used for prestressed structure. Other categories of environmental conditions are No. IV (seawater) and No. V (corrosive media), and the reinforcement for these categories are provided separately.

durability of the structure should be properly examined and evaluated, if the safety and service functions within the designed life are doubted when it is used continuously.

Inspection and examination in situ are the main measures to know correctly the current situation and deterioration level of the concrete structure and also form the important basis for the durability evaluation. The content and method of examination are as below and the non-destructive test is preferred.

1. Investigation on full views of the structure and its members, including structural system and size and position of its members, settlements of the structure and its foundation, macroscopic quality of construction, abnormal situation and harmful condition even occurred, e.g. fire accident, impact action, over-loaded locally, whether or not strengthened or rebuilt. In addition, loading test can be conducted to practically measure the actual mechanical behavior of the structure, if necessary.
2. Inspection on outward damage of the structure, including the details, including position, number, distribution, width, and depth, of the concrete cracks; the deformations, including deflection, lateral displacement, inclination, rotation, and vibration, of the members; the deformation and cracking of the supports and joints; the defects, including spalling off, losses of edge and corner, on surface layer of the member.
3. Examining and measuring of concrete behaviour, including the strength of concrete in the structure can be predicted after the non-destructive (e.g. counter-elastometry, ultrasonoscope) or locally destructive (e.g. pull-out) test; the actual strength, compactness and permeability resistance of the concrete can be directly measured after the cylinder specimen is drilled out from the structure; the internal holes or other defects of the concrete can be examined by the ultrasonoscope or soniscope; an inspection hole can be drilled in the structure and some samples of concrete are taken out for analyzing the carbonation depth, contents of chlorine ion and alkali, etc.
4. Inspection on reinforcement in structure, including the integrity of concrete cover is inspected carefully; the position, diameter, number, thickness of concrete cover, and rust level of the reinforcement can be measured by the special instruments without any destruction or after the concrete cover is locally cut off; the specimen can be cut off from the reinforcement in a structure if necessary, and then the actual area and strength (or strength loss) can be measured directly in the laboratory.
5. Investigation on environmental condition of the structure including the temperature, humidity and their variation regularities of the environment surrounded, and the categories and contents (concentrations) of various corrosion substances in the surrounding media, i.e. air, water, or soil.

Summarizing and statistically analyzing all the results obtained from the observation and investigation on the structure itself and the test and measurement of some specimen and sample at the laboratory, each part of the structure is

individually evaluated into a different grade [20-12] of the durability damage, if any, based on the levels of deterioration and damage. Afterwards, the structure is divided into several ranges of the same grade and treated correspondingly.

The carrying capacity of an existing structure, or a part of it, can be calculated based on the mechanical model, sectional size measured, and strength of the material. Alternatively, the load-carrying capacity can be directly measured based on the loading test on the structure itself. Both methods provide the results with sufficient accuracy which is helpful for making treatment decision, e.g. repairing, strengthening, or others.

However, the safe service life or residual life of an existing structure is difficult to be accurately determined, although many data of the structure can be collected and summarized from the inspection in situ and the test at laboratory and various theoretical methods [20-2] are provided already for evaluating the durability of concrete structures. Because the construction of a structure is random and the material and its behavior are not uniform but deviated, the durability is very complicated and depends upon many random factors, including environmental conditions, in a long period, so the durability failure and service life can only be predicted or estimated approximately based mainly on the experiences and statistic data in the engineering practice.

Exercises and discussion

- 2-1** Analyze and estimate the influences on the stress and strain distributions and possible damage in the interior of hardened concrete when it is loaded (compressed or tensed), shrinks, creeps, or experiences temperature and humidity variations respectively, based on the physical and mechanical indices of coarse aggregate and hardened cement mortar (Table 2-1).
- 2-2** A prism specimen of concrete has a size of 100 mm×100 mm×300 mm and the prism compressive strength and corresponding peak strain are $f_c = 26 \text{ N/mm}^2$ and $\varepsilon_p = 1.6 \times 10^{-3}$ respectively, which are calculated based on the cubic strength tested (f_{cu}). It is predicted that the complete stress-strain curve fits Eq. (2-6) with $\alpha_a = 1.7$ and $\alpha_d = 0.8$. Check whether the complete stress-strain curve, especially its descending branch, can be successfully obtained when an ordinary hydraulic test machine of total linear stiffness 150 kN/mm is used for loading.
- 2-3** Plot and compare the complete stress-strain curves (σ/f_c , $\varepsilon/\varepsilon_p$) of concrete under compression calculated by different models: Hognestad, Rüschi, Kent-Part, Sahlin, Young, Desayi, and Eq. (2-6) ($\alpha_a = 2.0$, $\alpha_d = 0.6$).
- 2-4** A concrete has a cubic compressive strength of $f_{cu} = 30 \text{ N/mm}^2$. Calculate and compare the prism compressive strength (f_c), tensile (f_t , $f_{t,s}$) and shear (τ_p) strengths; corresponding peak strains (ε_p , $\varepsilon_{t,p}$, γ_p), initial and peak moduli of elasticity (E_c , E_p , G_0 , G_p), and stress-strain curves ($\sigma/f_c - \varepsilon/\varepsilon_p$, $\sigma/f_t - \varepsilon/\varepsilon_{t,p}$, $\tau/\tau_p - \gamma/\gamma_p$).
- 3-1** Derive respectively Eqs. (3-3) and (3-4) for the load-bearing capacity and position of neutral axis for an eccentrically compressed member of rectangular section of elastic material.
- 3-2** A concrete has respectively compressive and tensile strengths of f_c and f_t . Calculate and plot the complete stress-strain curves of the concrete under compression and tension respectively with eccentricity $e_0/h = 0.3$. Calculate the areas under these curves ranging from $\varepsilon = 0$ to $\varepsilon = 2\varepsilon_p$, and compare them with the corresponding areas of that under central load.
- 3-3** A concrete experienced a compressive stress-time ($\sigma/f_c - t$) history as shown in the figure. Calculate and plot the modulus of elasticity-time ($E_c(t) / E_c - t$) curve and plot qualitatively the corresponding strain-time ($\varepsilon/\varepsilon_p - t$) curve.
- 4-1** The compressive strengths (f_c) and the parameters for corresponding complete stress-strain curves (α_a , α_d) are given in Table A4-1 for several structural concretes. Calculate the peak strains (ε_p) and plot the stress-strain curves ($\sigma/f_c - \varepsilon/\varepsilon_p$) for them, and calculate and compare the areas under these curves, including Ω_1 , $\Omega_2/2$, and $(\Omega_1 + \Omega_2)/3$ (Fig. A4-1, 2).

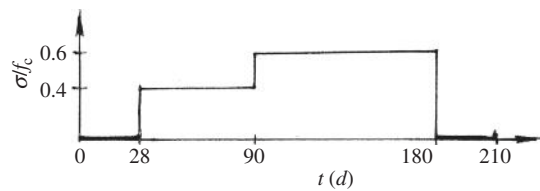


FIG. A3-3

Table A4-1		f_c (N/mm ²)	ε_p (10 ⁻³)	α_a	α_d	Ω_1	$\frac{\Omega_2}{2}$	$\frac{\Omega_1 + \Omega_2}{3}$
Category of Concrete								
Ordinary concrete	C20	20		2.0	0.6			
	C40	40		1.7	2.0			
High-strength concrete C60		60		1.5	3.0			
Light-weight concrete CL20		20		1.7	4.0			
Aerated concrete		3	2.0	1.1	6.0			
Steel-fiber concrete		25	3.0	2.5	0.2			

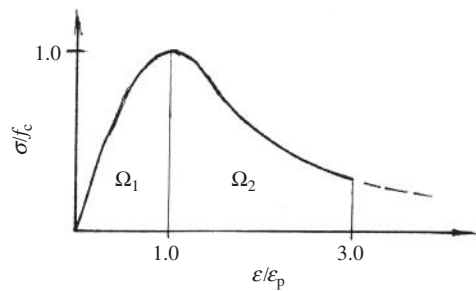


FIG. A4-1

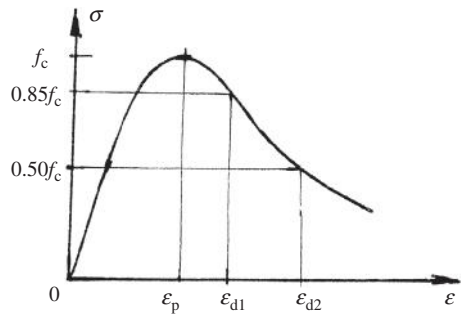


FIG. A4-2

4-2 Calculate and compare the strain values ε_{d1} and ε_{d2} respectively at the stresses $\sigma = 0.85f_c$ and $0.5f_c$ on the descending branch of stress–strain curve of the various structural concretes shown in Table A4-1.

5-1 Prove

(1) $\theta \equiv 0^\circ$ (tensile meridian) when $\sigma_1 > \sigma_2 = \sigma_3$,

(2) $\theta \equiv 60^\circ$ (compressive meridian) when $\sigma_1 = \sigma_2 > \sigma_3$

and (3) $\theta \equiv 30^\circ$ (shear meridian) when $\sigma_2 = (\sigma_1 + \sigma_3)/2$ or $\sigma_1 - \sigma_2 = \sigma_2 - \sigma_3$ for a three-dimensional stress state.

5-2 Three cubic specimens of concrete are tested under proportionally loading path ($\sigma_1:\sigma_2:\sigma_3 = \text{const.}$) and the triaxial strengths measured are listed in Table A5-2.

Specimen	Stress State	Triaxial Strength (N/mm ²)			Uniaxial Strength (N/mm ²)	
		f_1	f_2	f_3	f_c	f_t
A	C/C/C	-40.5	-40.5	-162	24.50	
B	C/C		-15.2	-30.4	21.66	
C	T/C/C	+1.26	-2.8	-6.9	19.00	1.89

Calculate separately the theoretical strengths of them following Ottosen and Guo-Wang criteria (Table 5-6) and compare these with the measured ones. The parameters in the criteria may be taken as below.

(1) Ottosen criterion: $a = 1.2759$, $b = 3.1962$,

$$\lambda = k_1 \cos \left[\frac{1}{3} \cos^{-1}(k_2 \cos 3\theta) \right] \quad \text{when } \cos 3\theta \geq 0,$$

$$\text{or } \lambda = k_1 \cos \left[\frac{\pi}{3} - \frac{1}{3} \cos^{-1}(-k_2 \cos 3\theta) \right] \quad \text{when } \cos 3\theta < 0,$$

where $k_1 = 11.7365$, $k_2 = 0.9801$.

(2) Guo-Wang criterion: $a = 6.9638$, $b = 0.09$, $d = 0.9297$, and $C_t = 12.2445$, $C_c = 7.3317$.

5-3 Determine the values of five parameters in Guo-Wang criterion (Table 5-6) if the five characteristic strengths of concrete are taken as below: $(0, 0, -f_c)$, $(f_t, 0, 0)$, $(0.95f_t, 0.95f_t, 0)$, $(0, -0.7f_c, -1.4f_c)$, and $(0, -1.2f_c, -1.2f_c)$. Then, calculate and plot the biaxial envelope (strength criterion) for the concrete.

6-1 A strand has an ultimate strength of $f_b = 1860 \text{ N/mm}^2$ and a modulus of elasticity of $E_s = 1.95 \times 10^5 \text{ N/mm}^2$. Calculate and plot the stress–strain curve for it, using Eq. (6-4).

- 6-2** Explain the differences of the mechanical behavior and stress—strain curve of the reinforcement, when it is loaded separately under repeated tension and cyclic tension and compression.
- 7-1** Compare the bond behaviors, including failure pattern during pull-out, between the plain and deformed reinforcements buried in concrete.
- 7-2** The yield strengths measured are $f_y = 420 \text{ N/mm}^2$ and 250 N/mm^2 respectively for the hot-rolled deformed and plain reinforcements and the average bond strengths are $\tau_u = 0.36f_{cu}$ and $0.08f_{cu}$ respectively for them buried in concrete. Calculate separately the minimum bond lengths needed for them, when the reinforcement has a diameter of 20 mm and is buried in the concrete of cubic strength $f_{cu} = 30 \text{ N/mm}^2$.
- 8-1** A short reinforced concrete column has a sectional area of A and is reinforced together with two categories of reinforcement (mild steel):
- (1) $\mu_1 = 1\%$, $f_{y1} = 300 \text{ N/mm}^2$, $E_s = 2 \times 10^5 \text{ N/mm}^2$,
 - (2) $\mu_2 = 1\%$, $f_{y2} = 600 \text{ N/mm}^2$, $E_s = 2 \times 10^5 \text{ N/mm}^2$.
- The stress-strain curve of the concrete used is shown in Fig. A8-1 and is composed of an ascending branch expressed as an equation

$$\frac{\sigma}{f_c} = 2 \left(\frac{\varepsilon}{\varepsilon_p} \right) - \left(\frac{\varepsilon}{\varepsilon_p} \right)^2$$

and a descending branch of an inclined line. Calculate the characteristic axial forces (compressions) for the column, including at initially yielding, ultimate state, and other turning points on the axial-deformation curve. And plot the axial force-strain ($N - \varepsilon$) and —stress ($N - \sigma_s$) curves for the column.

- 8-2** A reinforced concrete column has a square section of $300 \text{ mm} \times 300 \text{ mm}$ and is reinforced with the reinforcements $4\Phi 20$ ($f_y = 260 \text{ N/mm}^2$, $E_s = 2.1 \times 10^5 \text{ N/mm}^2$). The column is strengthened under a constant central compression $N_1 = 1500 \text{ kN}$ for some reason, and the section is enlarged to $400 \text{ mm} \times 400 \text{ mm}$ and the additional reinforcements are of $8\Phi 20$. The original and new concretes are of the same grade (C30) and their

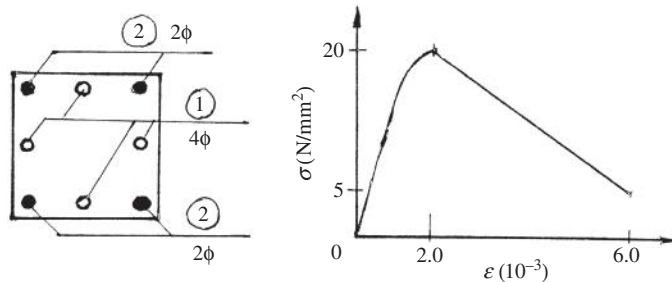


FIG. A8-1

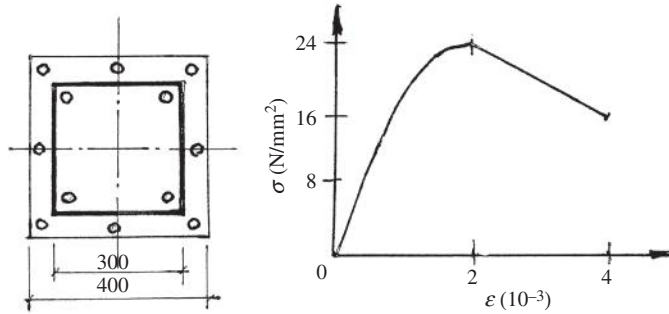


FIG. A8-2

stress—strain curves are assumed to be the same as well (Fig. A8-2), of which the equation for the ascending branch is

$$\frac{\sigma}{f_c} = 2\left(\frac{\varepsilon}{\varepsilon_p}\right) - \left(\frac{\varepsilon}{\varepsilon_p}\right)^2.$$

Calculate separately the central compressions acted on the strengthened column when the original and new concretes reach respectively the compressive strength ($f_c = 24 \text{ N/mm}^2$) and determine the ultimate strength of the column.

- 8-3** A prestressed concrete member has a rectangular section (area A) and is reinforced with four bars (total area A_s , yield strength f_y) near every corner, and a prestressing tendon (area A_p , tensile strength f_{py} , effective prestress σ_{p0}) without a bond is located on the sectional center. The stress—strain curve of concrete is the same as is shown in Fig. A8-2. Calculate separately the stresses of the concrete, bar, and tendon varying with the strains of the member (ε) during prestressing stage and after loaded with central tension (N), and plot the corresponding variation curves and the tension—strain ($N-\varepsilon$) curve of the member.
- 8-4** Analyze the regularity and influence factors of the tension stiffening of concrete varying with the axial force for a tensile member.
- 9-1** Compare the difference of confinement effect for a circle column of concrete confined separately by continuous spiral bar, separate ties, and steel tube.
- 9-2** A reinforced concrete column has a square section of $300 \text{ mm} \times 300 \text{ mm}$ and a concrete of compressive strength $f_c = 22 \text{ N/mm}^2$, and it is reinforced with eight bars $8\Phi 18$ of yield strength $f_y = 340 \text{ N/mm}^2$ with net cover 25 mm . The ties used are shown in Fig. A9-2 and have a yield strength of $f_y = 240 \text{ N/mm}^2$, and the diameter and space are respectively $\Phi 8 \text{ mm}$ and 50 mm . Calculate the confinement parameters ($f_{c,c}$, ε_{pc} , $\alpha_{a,c}$, and α_{dc} in Table 9-1) and ultimate strength (N) of the column, and discuss the influence of different thickness of concrete cover on them.

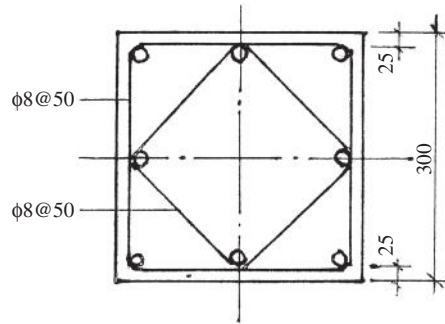


FIG. A9-2

- 9-3** Discuss the possible failure patterns and corresponding ways to control a concrete (structure) compressed locally.
- 10-1** A concrete slab is reinforced symmetrically but the shrinkage of the concrete is not uniform along the sectional depth as shown in Fig. A10-1. Derive the calculation formulas for the shrinkage stresses of the concrete and reinforcement in the slab and plot the diagram of stress distribution. (Note: the moduli of elasticity of concrete and reinforcement may be taken respectively as the constants E_c and E_s .)
- 10-2** A concrete girder of T section is reinforced as shown in Fig. A10-2. Calculate and plot the stress distribution on the section of the free shrinkage strain of the concrete occurred would be uniform and $\epsilon_{sh} = 500 \times 10^{-6}$. (Note: the moduli of elasticity may be taken as the constants $E_c = 3 \times 10^4 \text{ N/mm}^2$ and $E_s = 2.1 \times 10^5 \text{ N/mm}^2$ respectively for the concrete and reinforcement.)
- 10-3** A concrete column has a square section of $300 \text{ mm} \times 300 \text{ mm}$ and a concrete of grade C30 ($f_c = 24 \text{ N/mm}^2$, $E_c = 3 \times 10^4 \text{ N/mm}^2$), and it is reinforced with four bars $4\Phi 25$ of HRB 335 ($f_y = 335 \text{ N/mm}^2$, $E_s = 2.0 \times 10^5 \text{ N/mm}^2$). If the column is acted centrally with compression $N = 1800 \text{ kN}$ and maintained for three years, calculate the stresses of the concrete and reinforcement in the column separately at: (1) soon after loading, (2) after the load is maintained for three years, and (3) soon after unloading has been maintained for three years.

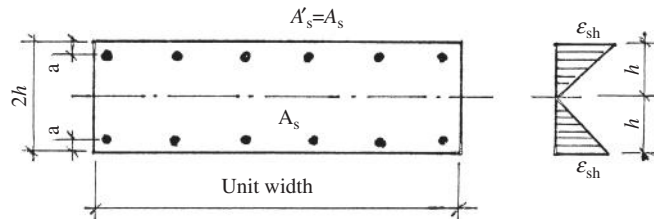


FIG A10-1

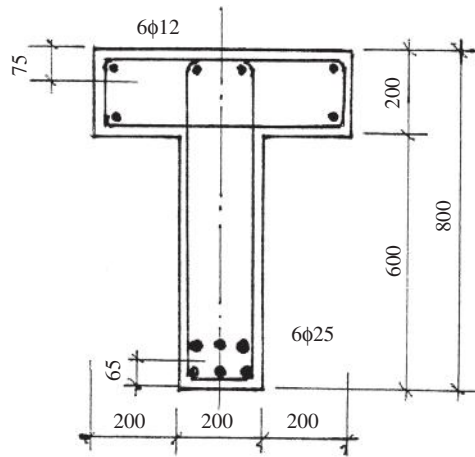


FIG. A10-2

- 11-1** Discuss the influences of stress that exist existed and its redistribution caused by shrinkage or creep of concrete, e.g. in exercises 10-1–10-3, on the ultimate strength of a reinforced concrete member.
- 11-2** A concrete member of rectangular section is reinforced asymmetrically ($A_{s2} = 2A_{s1}$). Plot qualitatively the ultimate envelope of axial force-bending, moment ($\pm N$, $\pm M$) for it, and determine the characteristic points on the envelope and explain separately their mechanical meanings.
- 11-3** Calculate the characteristic parameters α and β ($\gamma = 1$ is taken) of the equivalent rectangular stress diagram, if the concrete has different stress-strain relations under compression, as shown below (Fig. A11-1).
- 11-4** Calculate the characteristic parameters α and β ($\gamma = 1$ is taken) of the equivalent rectangular stress diagram for a beam of isosceles triangle section, if the stress-strain relation of the concrete is known as below (Fig. A11-2).
- 12-1** Different points of view are suggested for the mechanism analysis to tensile crack in concrete member under loading. Compare their main concepts and corresponding calculations.

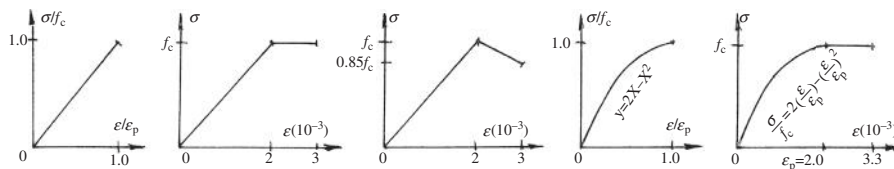


FIG. A11-1

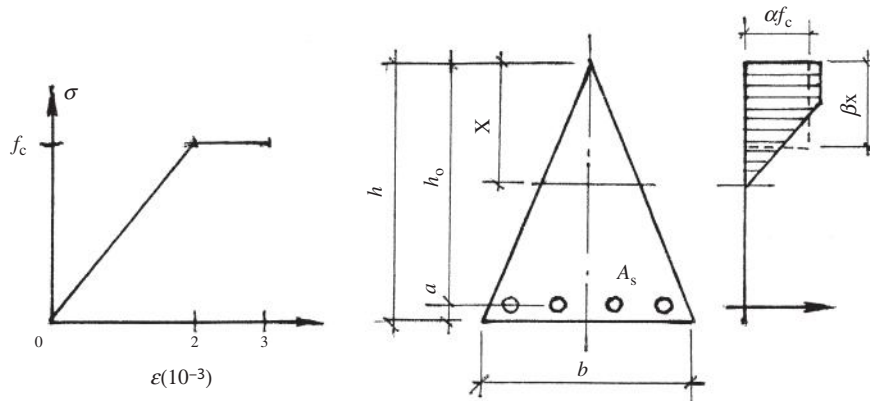


FIG. A11-2

- 12-2** A concrete beam has a rectangular section and a concrete of grade C30 ($f_c = 20 \text{ N/mm}^2$, $f_t = 2 \text{ N/mm}^2$, $E_c = 3 \times 10^4 \text{ N/mm}^2$), and it is reinforced with three bars $3\Phi 18$ ($f_y = 235 \text{ N/mm}^2$, $E_s = 2.1 \times 10^5 \text{ N/mm}^2$). Calculate: (1) cracking load P_{cr} and (2) the average space and the maximum width of the cracks under the loads shown in Fig. A12-1.
- 13-1** The section and reinforcements of a beam are shown in Fig. A13-1, and the concrete used is of grade C30 ($f_c = 25 \text{ N/mm}^2$, $f_t = 2.0 \text{ N/mm}^2$, $E_c = 3 \times 10^4 \text{ N/mm}^2$). Calculate:
- (1) the bending moment (M_{cr}) and curvature ($1/\rho_{cr}$) at cracking of the beam under loading,
 - (2) the bending moments (M_{y1} , M_{y2}) and curvatures ($1/\rho_{y1}$, $1/\rho_{y2}$) at yielding respectively of the reinforcements A_{s1} and A_{s2} ,
(Note: based on the converted section (Fig. 13-3) and $E_s = 2 \times 10^5 \text{ N/mm}^2$)
 - (3) the bending moment (M_u) and curvature ($1/\rho_u$) at ultimate state,
 - (4) plot the folded bending moment—curvature ($M-1/\rho$) diagram for the beam.

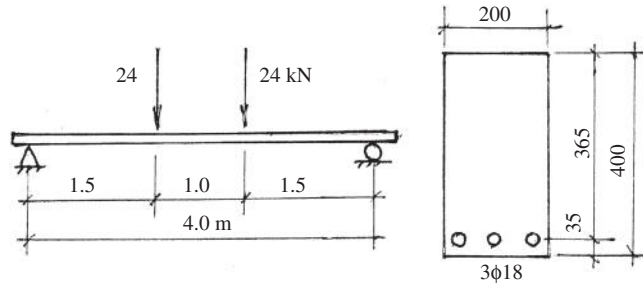


FIG. A12-1

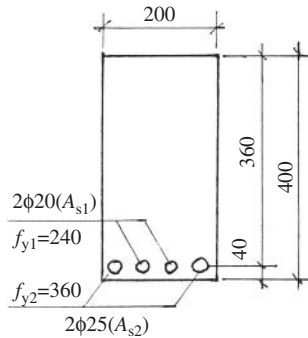


FIG. A13-1

- 13-2** A simply supported beam has a sectional bending moment—curvature relation and is loaded as shown in Fig. A13-2. Calculate:
- (1) the load (P_y) and deflection at midspan (ω_y) at first yield of the tensile reinforcement,
 - (2) the load (P_u) and deflection at midspan (ω_u) at ultimate state.
- 13-3** Calculate the sectional stiffness and deflection at midspan of the beam shown in Fig. A12-1, based separately on different methods: (1) neglecting totally the action of tension concrete (Fig. 13-3(c)), and (2) analytical method (Eq. 13-17). Compare both results and explain the tension stiffening of flexural member. (Note: the sectional stiffness may be taken as a constant along the whole span.)
- 14-1** List a table (similar to Table 2-8) and compare the three typical failure patterns under shear force of the beam without web reinforcement, and explain their main characteristics and influence factors.
- 14-2** A concrete beam of prismatic section has an ultimate bending moment of $M_u = \mu\eta bh_0^2 f_y$ and shear force of V_u (e.g. Eq. 14-5) under the symmetrical action of two concentrated loads. Determine the theoretical value of the boundary shear—span ratio (λ_b , Eq. (14-2)), at which the flexural and shear failure patterns occur simultaneously.

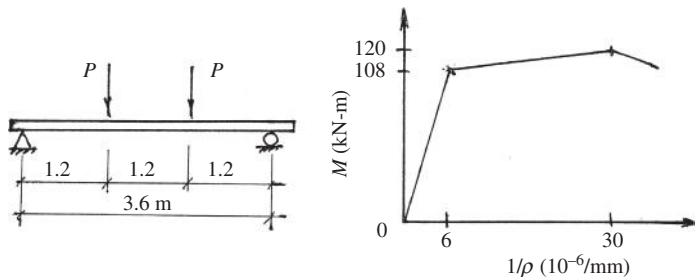


FIG. A13-2

- 15-1** Derive the plastic section modulus W_{tp} (Eq. (15-6b)) for a beam of rectangular section ($b \times h$) under torsion, based on the analog method of sand pile.
- 15-2** Explain the favorable or harmful effect of the additional internal force, including respectively axial force N , bending moment M , or shear V , on the ultimate torsion of a concrete member.
- 16-1** Calculate successively the ductility ratios of sectional curvature $\beta_{(1/\rho)}$ and deflection at midspan β_w for the beams shown separately in Exercises 13-1 and 13-2.
- 16-2** Calculate the angular rotation of plastic region of the beam shown in Exercise 13-2 at ultimate state.
- 16-3** Estimate and discuss the variation of ductility ratio of an eccentrically compressed member of reinforced concrete when the factors below change (increase or decrease) separately: strengths of the materials (f_y, f_c), contents of reinforcements (A_s, A'_s), axial force or compression—strength ratio ($N/f_c b h_0$), shear—span ratio, content of tie, etc. (Note: the member of rectangular section may be taken as an example.)
- 17-1** Discuss the concept and application method for Palmgren-Miner hypothesis used for determining the fatigue strength of a material under variable stress amplitude.
- 18-1** Explain the difference and similarity between the mechanical behaviors, including material strength, ultimate state and strength, and deformation, of the concrete members respectively under the actions of high-speed and normal loadings.
- 19-1** Explain the influence of different stress—temperature paths on the strength and deformation of concrete.
- 19-2** A concrete beam of rectangular section is reinforced with tensile bars only and is acted with elevated temperature as shown in Fig. A19-1. (Note: the temperature is uniformly distributed along the sectional width.) Calculate the ultimate bending moments ($\pm M_u^T$) for the beams respectively with tension and compression zones exposed to high temperature, and compare them with that under normal temperature.

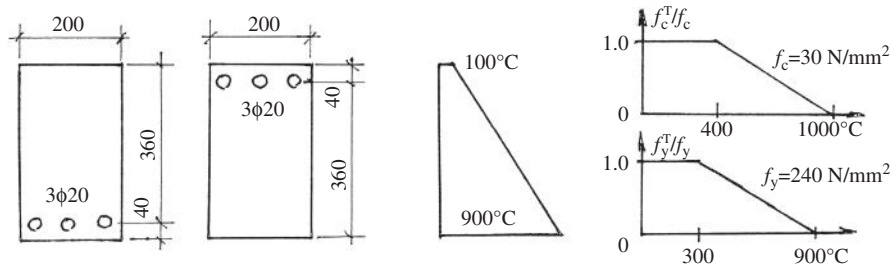


FIG. A19-1

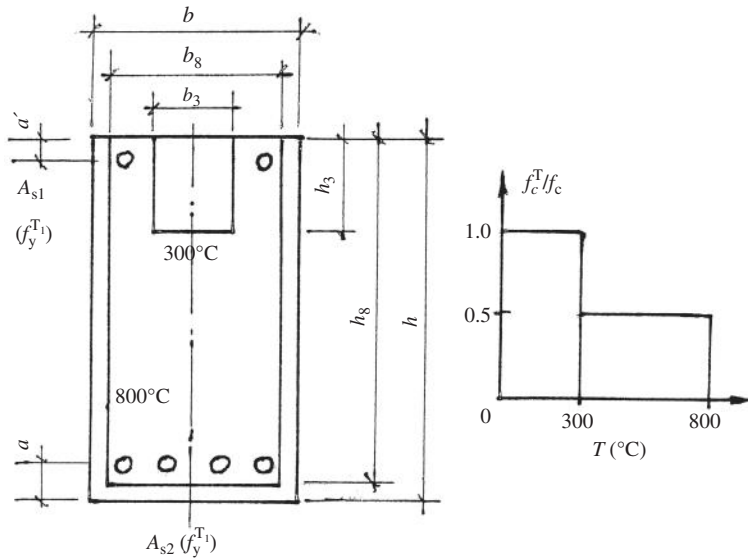


FIG. A19-2

19-3 A concrete beam of rectangular section is exposed to fire and the simplified temperature contours of 300°C and 800°C on the section are shown in Fig. A19-2. The yield strengths of the reinforcement are $f_y^{T_1}$ and $f_y^{T_2}$ respectively at T_1 and T_2 , and the compressive strength of concrete at elevated temperature (f_c^T/f_c) is assumed to be as shown in Fig. A19-2 as well. Determine the equivalent section for the beam and derive the calculation formulas of ultimate bending moments for the beams respectively with

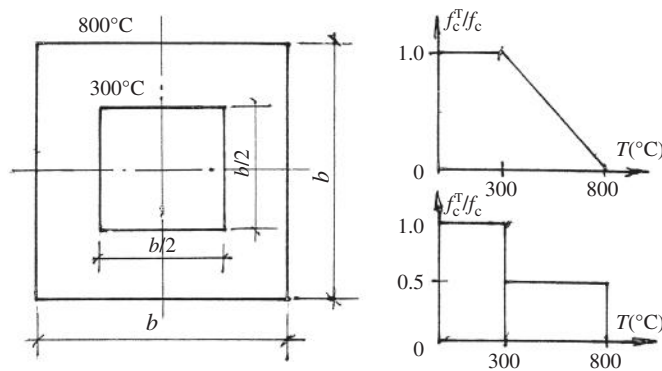


FIG. A19-3

tension and compression zones exposed to high temperature. (Note: the neutral axis may locate at different positions.)

- 19-4** A square column compressed centrally is exposed to fire and the simplified temperature contours of 300°C and 800°C on its section are shown in Fig. A19-3. Determine the ultimate strength of the column (N^T), if the compressive strength of concrete at elevated temperature is separately simplified into a trapezoid and two steps as shown in the figure.
- 20-1** List a table and explain the influences (favorable or harmful?, considerable or slight?, mutually beneficial or harmful?) of various factors of concrete material, such as category and content of cement, water—cement ratio, additional admixture, curing condition, and thickness of cover, on the durability damage or failure in several aspects, including permeation, freeze—thaw, alkali—aggregate reaction, carbonation, chemical corrosion, and rust of reinforcement.

References

- [1-1] Chuanzhi Wang, Zhiming Teng, Theory of Reinforced Concrete Structure, Construction Industry Press of China, Beijing, 1985.
- [1-2] Zhenhai Guo, Strength and Deformation of Concrete (Experimental Basis and Constitutive Relationship), Tsinghua University Press, Beijing, 1997.
- [1-3] Zhenhai Guo, The Principle of Reinforced Concrete, Tsinghua University Press, Beijing, 1999.
- [1-4] Zhenhai Guo, Xudong Shi, Reinforced Concrete Theory and Analysis, Tsinghua University Press, Beijing, 2003.
- [1-5] Zhiming Teng, et al., Basic Member of Reinforced Concrete, Tsinghua University Press, Beijing, 1987.
- [1-6] Jumin Shen, Chuangzhi Wang, Jianjing Jiang, Finite Element of Reinforced Concrete and Limit Analyses of Plates and Shells, Tsinghua University Press, Beijing, 1993.
- [2-1] National Standard of People's Republic of China, Code for Design of Concrete Structures GB 50010-2002, Construction Industry Press of China, Beijing, 2002.
- [2-2] K. Newman, J.B. Newman, Failure theories and design criteria for plain concrete. Structure, Solid Mechanics and Engineering Design, The Proceedings London, Wiley-Interscience, 1971.
- [2-3] National Standard of People's Republic of China, Standard for test method of mechanical properties on ordinary concrete GB/T 50081-2002, Construction Industry Press of China, Beijing, 2003.
- [2-4] F.O. Slate, et al., Volume Changes on Setting and Curing of Cement Paste and Concrete from Zero to Seven Days, ACI, Jan 1967.
- [2-5] F.O. Slate, et al., X-ray for Study of Internal Structures of Microcracking of Concrete, ACI, May 1963.
- [2-6] T.T.C. Hsu, et al., Microcracking of Plain Concrete and the Shape of the Stress-Strain Curve, ACI, Feb. 1963, 209-224.
- [2-7] T.C. Liu, et al., Stress-Strain Response and Fracture of Concrete in Uniaxial and Biaxial Compression, ACI, May 1972, 291-295.
- [2-8] A.M. Neville, Properties of Concrete, Pitman, London, 1963.
- [2-9] R. L'Hermite, Hong Translated by Mong Yu, Problems of Concrete Technology, Construction Industry Press of China, Beijing, 1964.
- [2-10] M.D. Kotsovos, et al., Generalized Stress-Strain Relation for Concrete, ASCE 104 (EM4) (1978).
- [2-11] ACI Committee 318, Building Code Requirement for Structural Concrete (ACI 318-95) and Comment (ACI 318R-95), American Concrete Institute, 1995.
- [2-12] Comité Euro-International du Béton, Bulletin D'information No. 213/214 CEB-FIP Model Code 1990 (Concrete Structures), Lausanne, May 1993.
- [2-13] Zhenhai Guo, Xiuqin Zhang, Experimental investigation on complete stress-strain curve of concrete under monotonically loading, Symposium No. 3 Aseismic Behaviors of Reinforced Concrete Structures, Tsinghua University Press, Beijing, 1981, pp. 1-18.
- [2-14] Research group, Several indices for basic mechanical behavior of concrete. Symposium of Experimental Investigation of Reinforced Concrete Structure, Construction Industry Press of China, Beijing, 1977, 21-36.

- [2-15] Dayan Lin, Chuanzhi Wang, Experimental investigation of complete stress-strain curve of concrete confined by rectangular stirrups, Symposium No. 3, Aseismic Behaviors of Reinforced Concrete Structures, Tsinghua University Press, Beijing, 1981, pp. 19–37.
- [2-16] C.S. Whitney, Discussion on VP Jensen's paper, ACI, Nov. 1943.
- [2-17] H. Rüschi, Research Toward a General Flexural Theory for Structural Concrete, ACI, July 1960, 1–28.
- [2-18] M. Sargin, Stress-Strain Relationships for Concrete and the Analysis of Structural Concrete Section. Canada, 1971.
- [2-19] P.T. Wang, et al., Stress-strain Curves of Normal and Lightweight Concrete in Compression, ACI, Nov. 1978.
- [2-20] Zhenhai Guo, Xiuqin Zhang, Experimental investigation on complete stress-strain curve of concrete, Journal of Building Structures 3 (1) (1982) 1–12.
- [2-21] E. Hognestad, Concrete Stress Distribution in Ultimate Strength Design, ACI, Dec. 1955, 455~479.
- [2-22] D.C. Kent, R. Park, Flexural Members with Confined Concrete, ASCE 97 (ST7) (1971) 1969–1990.
- [2-23] R. Park, T. Paulay, Reinforced Concrete Structures, John Wiley & Sons, New York, 1975.
- [2-24] S. Popovics, A Review of Stress-Strain Relationships of Concrete, ACI, March 1970.
- [2-25] B.P. Hughes, G.P. Chapman, The Complete Stress-Strain Curve for Concrete in Direct Tension, RILEM Bulletin, Paris, March 1966. New Series No. 30, 95–97.
- [2-26] R.H. Evans, M.S. Marathe, Microcracking and Stress-Strain Curves for Concrete in Tension. Materials and Structures, Research and Testing 1 (1) (1968) 61–64.
- [2-27] P.E. Petersson, Crack Growth and Development of Fracture Zone in Plain Concrete and Similar Materials, Doctoral dissertation, Lund Institute of Technology, Sweden, 1981, 174.
- [2-28] V.S. Gopalaratnam, S.P. Shah, Softening Response of Plain Concrete in Direct Tension, ACI 82 (3) (1985) 310–323.
- [2-29] Guo, Z H, X.Q. Zhang, Investigation of Complete Stress-Deformation Curves for Concrete in Tension, ACI Materials Journal 84 (4) (1987) 278–285.
- [2-30] Yonglu Li, Zhenhai Guo, Experimental investigation on complete stress-strain curve of concrete under eccentric tension, Symposium No. 6, Research on Mechanical Behavior of Concrete, Tsinghua University Press, Beijing, 1996, pp. 131–157.
- [2-31] Qi Zhang, Zhenhai Guo, Experimental research on shear strength and deformation of concrete, Journal of Building Structures (5) (1992) 17–24.
- [2-32] H. Mattock, Shear Transfer in Reinforced Concrete, ACI 52 (Feb. 1969).
- [2-33] N. Iosipescu, A. Negoita, A New Method for Determining the Pure Shearing Strength of Concrete, Journal of Concrete Society 3 (1) (1969) 63.
- [2-34] B. Bresler, K.S. Pister, Strength of Concrete under Combined stresses, ACI, Sept (1958) 321–346.
- [3-1] Zhenhai Guo, Xiuqin Zhang, Experimental investigation on complete stress-strain curve of concrete under repeated loading, Symposium No. 3, Aseismic Behavior of Reinforced Concrete Structures, Tsinghua University Press, Beijing, 1981, pp. 38–53.

- [3-2] B.P. Sinha, K.H. Gerstle, L.G. Tulin, Stress-Strain Relations for Concrete under cyclic Loading, ACI, Feb. 1964, 195–211.
- [3-3] I.D. Karsan, J.O. Jirsa, Behavior of Concrete under Compression Loading, ASCE 45 (ST12) (1969).
- [3-4] Yuke Du, Chuanzhi Wang, Experimental investigation of complete stress-strain curve of concrete under eccentric compression, Symposium No. 6, Research on Mechanical Behavior of Concrete, Tsinghua University Press, Beijing, 1996, pp. 111–130.
- [3-5] G.M. Sturman, S.P. Shah, G. Winter, Effect of Flexural Strain Gradients on Microcracking and Stress-Strain Behavior of Concrete, ACI (July 1965) 805–821.
- [3-6] L.E. Clark, K.H. Gerstle, L.G. Tulin, Effect of Strain-Gradient on the Stress-strain Curves of Mortar and Concrete, ACI, Sept (1967) 580–586.
- [3-7] J.Y. Uppal, K.Q. Kemp, The effect of longitudinal gradient of compressive stress upon the failure of concrete, Magazine of Concrete Research 23 (74) (1971) 11–22.
- [3-8] H.G. Heilmann, Zugspannung und Dehnung im Unbewehrten Betonquer Schnitten bei Exzentrischer Belastung, Deutscher Ausschuss für Stahlbeton, Heft 269, Berlin, 1976.
- [3-9] Tongchun Li, Influence of Stress Gradient on Ultimate Tensile Strain of Concrete: [Master Dissertation], Hehai University, Nanjing, 1986.
- [3-10] Guofan Zhao, et al., Experiments and calculation method for cracking resistance and the maximum crack width of reinforced concrete structural member, Journal of Building Structures (4) (1980).
- [3-11] Shaohuai Cai, Improvement of calculation for plastic coefficient γ_s of cracking resistance of concrete. Symposium of Experimental Investigation of Reinforced Concrete Structure, Construction Industry Press of China, Beijing, 1977, 298–315.
- [3-12] Comité Euro-International du Béton. Bulletin D'information No. 217, Selected Justification Notes, CEB FIP Model Code 1990, Lausanne, 1993.
- [3-13] G. Pickett, Effect of Aggregate on Shrinkage of Concrete and a Hypothesis Concerning Shrinkage, ACI (Feb. 1956).
- [3-14] ACI Committee 209, Prediction of Creep. Shrinkage and Temperature Effect in Concrete Structures, ACI SP-27 (1971) 51–93.
- [3-15] B.L. Meyers, E.W. Thomas, Elasticity, shrinkage, creep, and thermal movement of concrete, in: F.K. Kong, et al. (Eds.), Handbook of Structural Concrete, Pitman, London, 1983, 11-1–11-33.
- [3-16] A.M. Neville, W.H. Dilger, J.J. Brooks, Creep of plain and structural concrete, Construction Press, London and New York, 1983.
- [3-17] Rongyan Hui, Guoxing Huang, Bingyan Yi, Creep of Concrete, Railway Press of China, Beijing, 1988.
- [3-18] Guoxing Huang, Gaixin Chen, Research on Creep of Concrete, Research Institute of Irrigation and Hydraulic Power of China, Beijing, 1996.
- [3-19] Professional Standard of Electric Industry of People's Republic of China. Design Code for Hydraulic Concrete Structures DL/T 5057-1996, Electric Power Press of China, Beijing, 1997.
- [3-20] Bofang Zhu, Elastic modulus, specific creep, and relaxation coefficient of concrete, Journal of Hydraulic Engineering 9 (1985).

- [4-1] Zhaoyuan Chen, Jinqian Zhu, Peigang Wu, High Strength Concrete and its Application, Tsinghua University Press, Beijing, 1992.
- [4-2] Committee of High Strength Concrete, Chinese Society of Civil Engineering, Guidance for Design and Construction of High Strength Concrete Structure, Construction Industry Press of China, Beijing, 1994.
- [4-3] D.W. Fowler, Polymers in Concrete, in: F.K. Kong, et al. (Eds.), Handbook of Structural Concrete, Pitman, London, 1983, 8-1–8-32.
- [4-4] Naiqian Feng, High Performance Concrete, Construction Industry Press of China, Beijing, 1996.
- [4-5] E.G. Nawy, P.N. Balaguru, High-Strength Concrete, in: F.K. Kong, et al. (Eds.), Handbook of Structural Concrete, Pitman, London, 1983, 5-1–5-33.
- [4-6] Jinfeng Xu, Experimental Investigation on Complete Stress-Strain Curve of High Strength Concrete: [Master Dissertation], Tsinghua University, Beijing, 1986.
- [4-7] Haitao Hu, Stress-Strain Relation of High Strength Concrete Confined by Compound Stirrups: [Master Dissertation], Tsinghua University, Beijing, 1990.
- [4-8] Peigang Wu, et al., Physical and mechanical behaviors of high strength concrete, Symposium No. 3, Experimental Investigation of Reinforced Concrete Structure, Construction Industry Press of China, Beijing, 1994, pp. 399–406.
- [4-9] ACI Committee 363, State-of-the-Art Report on High-Strength Concrete, ACI 81 (4) (1984).
- [4-10] Zhenhai Guo, Xiuqin Zhang, Calculation of Aerated Concrete Members and its Experimental Basis. Symposium No. 2, Tsinghua University Press, Beijing, 1981.
- [4-11] Ministry of Construction, People's Republic of China, Technical Specification for Application of Autoclaved Aerated Concrete JGJ 17-84, Construction Industry Press of China, Beijing, 1984.
- [4-12] Ministry of Construction, People's Republic of China, Technical Specification for Concrete of Light Weight Aggregate JGJ 51-90, Construction Industry Press of China, Beijing, 1990.
- [4-13] Ministry of Construction, People's Republic of China, Technical Specification for Design of Reinforced Concrete Structure of Light Weight Aggregate JGJ 12-82, Construction Industry Press of China, Beijing, 1982.
- [4-14] T.A. Holm, Structural Light weight Concrete, in: F.K. Kong, et al. (Eds.), Handbook of Structural Concrete, Pitman, London, 1983, 7-1–7-34.
- [4-15] Wanli Gu, et al., Experimental investigation of complete stress-strain curve of concrete of light weight aggregate, Symposium No. 3, Experimental Investigation of Reinforced Concrete structures, Construction Industry Press of China, Beijing, 1994, pp. 303–315.
- [4-16] ACI Committee 544, State-of-the-Art Report on Fiber Reinforced Concrete (ACI 544. IR-82), ACI, Detroit, 1982.
- [4-17] American Concrete Institute, Fiber-Reinforced Concrete. SP-44, Detroit, 1974.
- [4-18] S.P. Shah, Fiber Reinforced Concrete, in: F.K. Kong, et al. (Eds.), Handbook of Structural Concrete, Pitman, London, 1983, 6-1–6-14.
- [4-19] S.P. Shah, B.V. Rangan, Fiber Reinforced Concrete Properties, ACI 68 (2) (1971) 126–135.
- [4-20] Zhonggang Zhang, Basic Properties of Steel Fiber Concrete and Flexural Behavior of Composite Member: [Master Dissertation], Technical University of Dalian, Dalian, 1987.

- [4-21] Danying Gao, Research on Mechanical Behaviors of Material and Structural Members of Steel Fiber Concrete: [Doctor Thesis], Technical University of Dalian, Dalian, 1989.
- [4-22] ACI Committee 544, Design Consideration for Steel Fiber Reinforced Concrete, ACI Structural Journal (Sept.-Oct. 1988).
- [5-1] Raozhong Yu, et al., Strength and deformation of concrete under biaxial stresses, Rock Concrete Fracture and Strength 1 (1982).
- [5-2] Jishan Xu, Strength Theory of Concrete and Its Application, Irrigation Press, Beijing, 1981.
- [5-3] Chuazhi Wang, Zhenhai Guo, Xiuqin Zhang, Strength experiments of concrete under bi- and tri-axial compressions, China Civil Engineering Journal 20 (1) (1987) 15–26.
- [5-4] Zhenhai Guo, Chuazhi Wang, Xiuqin Zhang, Researches on strength and failure criterion of concrete under multiaxial stress states, China Civil Engineering Journal 24 (3) (1991) 1–14.
- [5-5] Yupu Song, Researches on Mechanical Models for Finite-Element Analysis of Reinforced Concrete: [Doctor Thesis], Technical University of Dalian, Dalian, 1988.
- [5-6] Linhua Xue, Experimental Investigation of Characteristics of Concrete under Biaxial Tension-Compression: [Master Dissertation], Hehai University, Nanjing, 1989.
- [5-7] G. Shickert, Design of an Apparatus for Short-Time Testing of Concrete under Triaxial Load, Concrete for Nuclear Reactors, ACI SP (1972) 34–63. III: 1355–1376.
- [5-8] K.H. Gerstle, et al., Behavior of Concrete under Multi-axial Stress States, ASCE 106 (EM6) (1980) 1383–1403.
- [5-9] J.B. Newman, Apparatus for testing concrete under multi-axial states of stress, Magazine of Concrete Research 26 (81) (1974) 221–238.
- [5-10] H. Kupfer, H.K. Hilsdorf, H. Rüschi, Behavior of Concrete under Biaxial Stresses, ACI 66 (8) (1969) 656–666.
- [5-11] P. Launay, H. Gachon, Strain and Ultimate Strength of Concrete under Triaxial Stress, Concrete for Nuclear Reactors, ACI SP (1972) 34–63. I: 269–282.
- [5-12] G.S. Robinson, Behavior of Concrete in Biaxial Compression, ASCE 93 (ST2) (1967) 71–86.
- [5-13] Zhenhai Guo, Yunlong Zhou, Dirk Nechvatal, Auswertung von Versuchen zur mehrachsigen Betonfestigkeit, die an der Technischen Universität München durchgeführt wurden. Deutscher Ausschuss für Stahlbeton, Heft 447, Berlin, 1995.
- [5-14] H. Reimann, Kritische Spannungszustände des Betons bei mehrachsiger ruhender Kurzzeitbelastung, Deutscher Ausschuss für Stahlbeton, Heft 175, Berlin, 1965.
- [5-15] L.L. Mills, R.M. Zimmerman, Compressive Strength of Plain Concrete under Multiaxial Loading Conditions, ACI 67 (10) (1970) 802–807.
- [5-16] H. Kupfer, Das Verhalten des Betons unter mehrachsigter Kurzzeitbelastung unter besonderer Berücksichtigung der zweiachsiggen Beanspruchung, Deutscher Ausschuss für Stahlbeton, Heft 229, Berlin, 1973.
- [5-17] G. Schickert, H. Winkler, Versuchsergebnisse zur Festigkeit und Verformung von Beton bei mehraxialer Druckbeanspruchung, Deutscher Ausschuss für Stahlbeton, Heft 277, Berlin, 1977.

- [5-18] J.G.M. Van Mier, Strain-Softening of Concrete under Multiaxial Loading Conditions, Doctoral Thesis, Eindhoven University of Technology, The Netherlands, Nov. 1984.
- [5-19] A.A. Gvozdzhev, P.M. Beech, Strength of concrete under bi-axial stress states, *Concrete and Reinforced Concrete* (7) (1974) 10–11 (in Russian).
- [5-20] A.A. Cheche, Strength of concrete under tri-axial tensile stresses of same value, *Concrete and Reinforced Concrete* (6) (1979) 33–34 (in Russian).
- [5-21] C.Z. Wang, Z.H. Guo, X.Q. Zhang, Experimental Investigation of Biaxial and Triaxial Compressive Concrete Strength, *ACI Materials, Journal* 84 (2) (1987) 92–100.
- [5-22] C.Z. Wang, Z.H. Guo, et al., An experimental investigation of biaxial and triaxial compressive concrete strength and deformation, 9th International Conference on SMiRT, Lausanne, Aug. 1987, A, 193–198.
- [5-23] Yutao Guo, Experimental Investigation of Strength and Deformation of High-Strength Concrete under Biaxial Stress States: [Master Dissertation], Tsinghua University, Beijing, 1995.
- [5-24] Xiuqin Zhang, Ying Liu, Zhenhai Guo, Strength and deformation of aerated concrete under biaxial compression, *Aerated Concrete Industry* (3) (1988) 19–23.
- [5-25] Fang Peng, Investigation on Failure Criterion and Constitutive Model of Various Concrete Material under Complicated Stress: [Doctor Thesis], Technical University of Dalian, Dalian, 1990.
- [5-26] L.A. Traina, S.A. Manson, Biaxial Strength and Deformational Behavior of Plain and Steel Fiber Concrete, *ACI Materials Journal* 88 (4) (1991).
- [5-27] O. Buykozturk, T.M. Tseng, Concrete in Biaxial Cyclic Compression, *ASCE* 113 (ST3) (1984).
- [5-28] M.R. Salami, C.S. Desai, Constitutive Modeling Including Multiaxial Testing for Plain Concrete under Low-Confining Pressure, *ACI Materials Journal* 87 (3) (1990).
- [5-29] Shengrui Lan, Zhenhai Guo, Experimental investigation of deformation property of concrete under biaxial compression with constant compression in one direction, *China Civil Engineering Journal* 29 (2) (1996) 28–36.
- [5-30] Shengrui Lan, Zhenhai Guo, Experimental Investigation of Multiaxial Compressive Strength of Concrete under Different Stress Paths, *ACI Material Journal* 94 (5) (1997) 427–434.
- [5-31] Shengrui Lan, Zhenhai Guo, Biaxial Compressive Behavior of Concrete under Repeated Loading, *Journal of Materials in Civil Engineering ASCE* 11 (No. 2) (May 1999) 105–115.
- [5-32] W.F. Chen, *Plasticity in Reinforced Concrete*, McGraw-Hill Book Company, New York, 1982.
- [5-33] K.J. Willam, E.P. Warnke, Constitutive Models for the Triaxial Behavior of Concrete, *IABSE Proceeding* 19 (1975) 1–30.
- [3-34] N.S. Ottosen, A Failure Criterion for Concrete, *ASCE* 103 (EM4) (1977) 527–535.
- [3-35] S.S. Hsieh, E.C. Ting, W.F. Chen, An Elastic-Fracture Model for Concrete. *Proceeding of 3rd Engineering Mechanics Division, Special Conference ASCE, Austin, 1979*, 437–440.
- [3-36] M.D. Kotsovos, A mathematical description of the strength properties of concrete under generalized stress, *Magazine of Concrete Research* 31 (108) (1979) 151–158.

- [5-37] J. Podgorski, General Failure Criterion for Isotropic Media, ASCE 111 (EM2) (1985) 188–201.
- [5-38] Maohong Yu, New System of Strength Theory, Xian Jiaotong University Press, Xian, 1992.
- [5-39] Fédération Internationale de la Précontrainte. The design and construction of prestressed concrete reactor vessels, FIP/3/3, 1978.3
- [5-40] H. Kupfer, K.H. Gerstle, Behavior of Concrete under Biaxial Stresses, ASCE 99 (EM4) (1973).
- [5-41] M.E. Tasuji, F.O. Slate, A.H. Nilson, Stress-Strain Response and fracture of Concrete in Biaxial loading, ACI 75 (7) (1978) 306–312.
- [5-42] K.M. Romstad, M.A. Taylor, L.R. Herrmann, Numerical Biaxial Characterization for Concrete, ASCE 100 (EM5) (1974) 935–948.
- [5-43] R. Palaniswamy, S.P. Shah, Fracture and Stress-Strain Relationship of Concrete under triaxial Compression, ASCE 100 (ST5) (1974) 901–915.
- [5-44] L. Cedolin, Y.R.J. Crutzen, S. Dei Poli, Triaxial Stress-Strain Relationship for Concrete, ASCE 103 (EM3) (1977) 423–439.
- [5-45] N.S. Ottosen, Constitutive Model for Short-Time Loading of Concrete, ASCE 105 (EM1) (1979) 127–141.
- [5-46] Comité Euro-International du Béton. Bulletin D'information No. 156, Concrete under Multiaxial States of Stress Constitutive Equations for Practical Design, Paris, 1983.
- [5-47] T.C.Y. Liu, A.H. Nilson, F.O. Slate, Biaxial Stress-Strain Relations for Concrete, ASCE 98 (ST5) (1972) 1025–1034.
- [5-48] M.E. Tasuji, A.H. Nilson, F.O. Slate, Biaxial Stress-Strain Relationship for Concrete, Magazine of Concrete research 31 (109) (1979) 217–224.
- [5-49] D. Darwin, D.A. Pecknold, Nonlinear Biaxial Stress-Strain Law for Concrete, ASCE 103 (EM2) (1977) 229–241.
- [5-50] A.A. Elwi, D.W. Murray, A 3D Hypoelastic Concrete Constitutive Relationship, ASCE 105 (EM4) (1979) 623–641.
- [5-51] M.D. Kotsovos, J.B. Newman, Generalized Stress-Strain Relationship for Concrete, ASCE 104 (EM4) (1978) 845–855.
- [5-52] M.D. Kotsovos, A mathematical model of the deformational behavior of concrete under generalized stress based on fundamental materials properties, Materials and Structures 13 (76) (1980) 289–298.
- [5-53] K.H. Gerstle, Simple Formulation of Biaxial Concrete Behavior, ACI 78 (1) (1981) 62–68.
- [5-54] K.H. Gerstle, Simple Formulation of Triaxial Concrete Behavior, ACI 78 (5) (1981) 382–387.
- [5-55] T. Stankowski, K.H. Gerstle, Simple Formulation of Concrete Behavior under Multiaxial Load, ACI 82 (2) (1985) 213–221.
- [5-56] Zhenhai Guo, Gutao Guo, Yan Xu, Nonlinear elastic orthogonal anisotropic constitutive model for concrete, Journal of Tsinghua University, (Science and Technology) 37 (6) (1997) 78–81.
- [5-57] Zongda Yan, Theory of Plasticity, Tianjin University Press, Tianjin, 1988.
- [5-58] D.J. Han, W.F. Chen, A Nonuniform Hardening Plasticity Model for Concrete Materials, Mechanics of Materials (4) (1985).
- [5-59] P.J. Yoder, W.D. Iwan, On the Formulation of Strain-Space Plasticity with Multiple Loading Surfaces. ASME, Journal of Applied Mechanics 48 (12) (1981) 773–778.

- [5-60] J.W. Dougill, Some Remarks on Path Independence in the Small in Plasticity, *Quarterly of Applied Mathematics* 32 (1975) 233–243.
- [5-61] Z.P. Bazant, S.S. Kim, Plastic-Fracturing Theory for Concrete, *ASCE* 105 (EM3) (1979) 407–428.
- [5-62] W. Flügge, *Visco-elasticity*, Springer-Verlag, 1975.
- [5-63] N. Cristescu, I. Suliciu, *Visco-plasticity*, Bucharest Martinus Nijhoff Publishers, 1982.
- [5-64] Z.P. Bazant, P.D. Bhat, Endochronic Theory of Inelasticity and Failure of Concrete, *ASCE* 102 (EM4) (1976) 701–722.
- [5-65] Dajian Han, Plasticity, fracture, and damage mechanics used for establishing constitutive model of concrete, *Mechanics and Practice* 10 (1) (1988).
- [5-66] S. Yazdani, H.L. Schreyer, An Anisotropic Damage Model with Dilatation for Concrete, *Mechanics of Materials* 7 (1988) 231–244.
- [5-67] S. Yazdani, H.L. Schreyer, Combined Plasticity and Damage Mechanics Model for Plain Concrete, *ASCE* 116 (EM7) (1990).
- [5-68] Yupu Song, Guofan Zhao, Endochronic-damage constitutive model for concrete, *Journal of Dalian Technical University* 30 (5) (1990).
- [5-69] M. Klisinski, Plasticity Theory based on Fuzzy Sets, *ASCE* 114 (EM4) (1988).
- [5-70] J. Ghaboussi, J.H. Garrett, X. Wu, Knowledge Based Modeling of Material Behavior with Neural Networks, *ASCE* 117 (EM1) (1991).
- [6-1] National Standard of People's Republic of China. Hot-rolled Plain Bar Used for Reinforced Concrete GB1303–1991, Standard Press of China, Beijing, 1999, 322.
- [6-2] National Standard of People's Republic of China. Hot-rolled Ribbed Bar Used for Reinforced Concrete GB 1499–1998, Standard Press of China, Beijing, 1999, 312.
- [6-3] National Standard of People's Republic of China. Residual Heat Treated Bar Used for Reinforced Concrete GB 13014-1991, Standard Press of China, Beijing, 1999, 327.
- [6-4] National Standard of People's Republic of China. Wire Used for Prestressed Concrete GB/T 5223–1995, Standard Press of China, Beijing, 1999, 79.
- [6-5] National Standard of People's Republic of China. Strand Used for Prestressed Concrete GB/T 5224–1995, Standard Press of China, Beijing, 1999, 88.
- [6-6] National Standard of People's Republic of China. Heat-treated Bar Used for Prestressed Concrete GB 4463–1984, Standard Press of China, Beijing, 1999, 13.
- [6-7] Chengruo Huang, Yinqing Li, Strength calculation of flexural member of pre-stressed concrete reinforced with the steel without yield plateau, *Symposium of Design and Detailing of Reinforced Concrete Structure*. Beijing, 1985, pp. 105–111.
- [6-8] R. Park, T. Paulay, *Reinforced Concrete Structures*, John Wiley & Son Inc, New York, 1975.
- [6-9] B. Kato, H. Aoki, H. Yamanonchi, Experimental Study of Structural Steel Subjected to Tensile and Compressive Cycle Loads, *Proceeding 14th Japan Congress on Materials Research* (March 1971).
- [6-10] A. Singh, K.H. Gerstle, L.G. Tulin, The Behavior of Reinforcing Steel under Reversed Loading, *Journal of ASTM, Materials Research & Standards* 5 (1) (1965).
- [6-11] Research group, Some problems on cold-stretched bar and cold-drawn wire of low carbon, *Symposium of Experimental Investigation of Reinforced Concrete Structures*, Construction Industry Press of China, Beijing, 1977, pp. 37–54.

- [6-12] Wenshan Cheng, Analyses of bending moment and curvature of flexural member of concrete reinforced with the bar without obvious yield point, *China Civil Engineering Journal* 15 (4) (1982) 1–10.
- [6-13] Chinese Academy of Building Science, Experimental investigation of relaxation behavior of reinforcement under room temperature, *Symposium of Experimental Investigation of Reinforced Concrete Structure*, Construction Industry Press of China, Beijing, 1977, pp. 55–65.
- [7-1] ACI Committee 408, Bond Stress – The States of the Art, *ACI* 63 (11) (1966) 1161–1190.
- [7-2] Youlin Xu, Experimental Study of Bond Properties for Deformed Bar in Concrete: [Doctor Thesis], Tsinghua University, Beijing, 1990.
- [7-3] E.L. Kemp, F.S. Brenzy, J.A. Unterspan, Effect of Rust and Scale on the Bond Characteristics of Deformed Reinforcing Bars, *ACI* 65 (9) (1968).
- [7-4] RILEM–FIP–CEB, Tentative Recommendation Bond Test for Reinforcing Steel, *Materials and Structures* (32) (1973).
- [7-5] ACI Committee 408, A Guide of the Determination of Bond Strength in Beam Specimens, *ACI* (1964).
- [7-6] S. Soretz, A comparison of beam tests and pull out tests, *Materials and Structures* (28) (1972).
- [7-7] R.M. Mains, Measurement of the Distribution of Tensile and Bond Stresses along Reinforcing Bars, *ACI* (Nov. 1951).
- [7-8] B.B. Broms, Technique for Investigation of Internal Cracks in Reinforced Concrete Members, *ACI* 62 (1) (1965) 35–44.
- [7-9] Y. Goto, Cracks Formed in Concrete around Deformed Tension Bars, *ACI* 68 (4) (1971) 244–251.
- [7-10] G. Rehm, Über die Grundlagen des Verbundes zwischen Stahl und Beton, *Deutscher Ausschuss für Stahlbeton*, Heft 138, Berlin, 1961.
- [7-11] L.A. Lutz, P. Gergely, Mechanics of Bond and Slip of Deformed Bars in Concrete, *ACI* 64 (11) (1967) 711–721.
- [7-12] L.A. Lutz, Analysis of Stresses in Concrete near a Reinforcing Bar due to Bond and Transverse Cracking, *ACI* 67 (10) (1970) 778–787.
- [7-13] S.M. Mirza, J. Honde, Study of Bond Stress–Slip Relationship in Reinforced Concrete, *ACI* 76 (1) (1979) 19–46.
- [7-14] R. Tepfers, Cracking of concrete cover along anchored deformed reinforcing bars, *Magazine of Concrete Research* (March 1979) 3–12.
- [7-15] A. Losberg, P.A. Olssen, Bond Failure of Deformed Reinforcing Bars Based on the Longitudinal Splitting Effect of the Bars, *ACI* 76 (1) (1979) 5–18.
- [7-16] E.L. Kemp, W.J. Wilhelm, Investigation of the Parameters Influencing Bond Cracking, *ACI* 76 (1) (1979) 47–72.
- [7-17] S. Soretz, H. Hölzenbein, Influence of Rib Dimensions of Reinforcing Bars on Bond and Bondability, *ACI* 76 (1) (1979) 111–125.
- [7-18] T.R. Robinson, Influence of Transverse Reinforcement on Shear and Bond Strength, *ACI* 62 (3) (1965) 343–362.
- [7-19] R.E. Untrauer, R.L. Henry, Influence of Normal Pressure on Bond Strength, *ACI* 62 (5) (1965) 577–586.
- [7-20] C.O. Orangun, J.O. Jirsa, J.E. Breen, A Reevaluation of Test Data on Development Length and Splices, *ACI* 74 (3) (1977).

- [7-21] N.M. Hawkins, I.J. Liu, F.L. Jeang, Local bond strength of concrete for cyclic reversed loadings, *Proceeding of the International Conference on Bond in Concrete* (1982) 151–161.
- [7-22] T.P. Tassios, Properties of bond between concrete and steel under load cycles idealizing seismic action, National Technical University Athens, Greece, 1982.
- [7-23] A.H. Nilson, Internal Measurement of Bond–Slip, *ACI 69* (7) (1972) 439–441.
- [9-1] J.W.H. King, Some investigation of the effect of core size and steel and concrete quality in short reinforced concrete columns, *Magazine of Concrete Research* (2) (1949).
- [9-2] M.T.M. Soliman, C.W. Tu, The flexural stress-strain relationship of concrete confined by rectangular transverse reinforcement, *Magazine of Concrete Research* 19 (61) (1967) 223–238.
- [9-3] R.K.T.S. Iyengar, P. Desayi, K.N. Reddy, Stress-strain characteristic of concrete confined in steel binders, *Magazine of Concrete Research* 22 (72) (1970) 173–184.
- [9-4] M. Sargin, *Stress-Strain Relationships for Concrete and the Analysis of Structural Concrete Sections*, University of Waterloo, Canada, 1971.
- [9-5] S.A. Sheikh, S.M. Uzumeri, Strength and Ductility of Tied Concrete Columns, *ASCE* (ST5) (1980) 106.
- [9-6] Dayan Lin, Chuanzhi Wang, Investigation on complete stress-strain curve of concrete confined by rectangular tie, *Symposium No. 3, Aseismic Behaviors of Reinforced Concrete Structures*, Tsinghua University Press, Beijing, 1981, pp. 19–37.
- [9-7] Zhenhai Guo, Xiuqin Zhang, Yijun Weng, Strength and deformation of concrete confined by rectangular tie, *Symposium on Earthquake Resistance and Disaster Prevention*, Beijing, 1986, 143–150.
- [9-8] Linglong Luo, *Analytical Method for Complete Stress-Strain Curve of Confined Concrete with Stirrups*: [Master Dissertation], Tsinghua University, Beijing, 1988.
- [9-9] J.P. Mochle, T. Cavanagh, Confinement Effectiveness of Cross Ties in Reinforced Concrete, *ASCE* 111 (ST10) (1985).
- [9-10] Baomin Ma, *Experimental Investigation on Aseismic Behavior of Reinforced Concrete Column with Different Forms of Tie*: [Master Dissertation], Tsinghua University, Beijing, 1983.
- [9-11] S.A. Sheikh, S.M. Uzumeri, Analytical Model for Concrete Confinement in Tied Columns, *ASCE* 108 (ST12) (1982).
- [9-12] D.C. Kent, R. Park, Flexural Members with Confined Concrete, *ASCE* 97 (ST7) (1971) 1969–1990.
- [9-13] Xiuqin Zhang, Zhenhai Guo, Chuanzhi Wang, Equations for complete stress-strain curve of rectangular tie confined concrete under repeated loading, *Industrial Construction* (12) (1985) 16–20.
- [9-14] N.J. Gardner, E.R. Jacobson, Structural Behavior of Concrete Filled Steel Tubes, *ACI* 64 (7) (1967) 402–412.
- [9-15] K.B. Park, Axial Load Design for Concrete Filled Steel Tubes, *ASCE* 96 (ST10) (1970).
- [9-16] Shantong Zhong, Yongchun Wang, Research on calculation theory of concrete filled steel tube under central compression, *Journal of Building Structures* (1) (1980) 61–71.

- [9-17] Guanzuo Tang, et al., Research on basic mechanical behavior of concrete filled steel tube, *Journal of Building Structures* (1) (1982) 13–31.
- [9-18] Shaohuai Cai, Zhanshuan Jiao, Basic behavior and strength calculation of short column of steel tube confined concrete, *Journal of Building Structures* (6) (1984) 13–29.
- [9-19] Shaohuai Cai, Calculation and Application of Steel Tube Confined Concrete Structures, Construction Industry Press of China, Beijing, 1989.
- [9-20] Shaohuai Cai, Modern Steel Tube Confined Concrete Structures, China Communications Press, Beijing, 2003.
- [9-21] Shantong Zhong, Concrete Filled Steel Tube Structures, Haerbin: Science and Technology Press of Helongjiang (1994).
- [9-22] Linhai Hang, Shantong Zhong, Mechanics of Concrete Filled Steel Tube, Dalian Technical University Press, Dalin, 1996.
- [9-23] G.G. Meyerhof, The Bearing capacity of concrete and rock, *Magazine of Concrete Research* 4 (12) (1953) 107–116.
- [9-24] W. Shelon, Bearing Capacity of Concrete, *ACI* 29 (5) (1957) 405–414.
- [9-25] T. An, D.L. Baird, Bearing Capacity of Concrete Blocks, *ACI* 31 (9) (1960) 869–879.
- [9-26] Shaohui Cai, Local compressive strength of plain and reinforced concretes, *China Civil Engineering Journal* 9 (6) (1963) 1–10.
- [9-27] N.M. Hawkins, The bearing strength of concrete loaded through rigid plates, *Magazine of Concrete Research* 20 (62) (1968) 31–40.
- [9-28] N.M. Hawkins, The bearing strength of concrete loaded through flexible plates, *Magazine of Concrete Research* 20 (63) (1968) 95–102.
- [9-29] S.K. Niyogi, Bearing Strength of Concrete Geometric Variations, *ASCE* 99 (ST7) (1973) 1471–1490.
- [9-30] N.M. Hawkins, The bearing strength of concrete for strip loadings, *Magazine of Concrete Research* 22 (71) (1970) 87–98.
- [9-31] Yongyi Liu, et al., Calculation of local compression acted on plain and reinforced concrete, *Symposium of Design and Detailing of Reinforced Concrete Structures*, Beijing (1985) 156–161.
- [9-32] S.K. Niyogi, Concrete Bearing Strength Support, Mix, Size Effect, *ASCE* 100 (ST8) (1974) 1685–1702.
- [9-33] Shaohuai Cai, Lihong Xue, Local compressive strength of high strength concrete, *China Civil Engineering Journal* 27 (5) (1994) 52–61.
- [9-34] Shaohuai Cai, Shangmin Wei, Zhanshuan Jiao, Local compressive strength of concrete confined by square wire mesh, *China Civil Engineering Journal* 19 (4) (1986) 17–25.
- [9-35] Chinese Academy of Building Science, Code for Design of Concrete Structures TJ 10-74, Construction Industry Press of China, Beijing, 1974.
- [11-1] J.G. MacGregor, J.E. Breen, E.O. Pfrang, Design of Slender Concrete Columns, *ACI* 67 (1) (1970) 6–28.
- [11-2] Chinese Academy of Building Science. Longitudinal bending of eccentrically compressed member of reinforced concrete, *Symposium of Experimental Investigation of Reinforced Concrete Structures*, Construction Industry Press of China, Beijing, 1977, 182–200.

- [11-3] Jiakui Chen, et al., Calculation of increasing coefficient η of eccentricity for reinforced concrete member, Symposium of Design and Detailing of Reinforced Concrete Structures, Beijing (1985) 69–87.
- [11-4] Jumin Shen, Yijun Weng, Stiffness and ductility of reinforced concrete member, Symposium No. 3, Aseismic Behaviors of Reinforced Concrete Structures, Tsinghua University Press, Beijing, 1981, pp. 54–71.
- [11-5] Bolong Zhu, Zhenxiang Dong, Non-Linear Analysis of Reinforced Concrete, Tongji University Press, Shanghai, 1985.
- [11-6] Zhiming Teng, Chen Jiakui, et al., Strength calculation on normal section of reinforced concrete member, Symposium of Design and Detailing of Reinforced Concrete Structures. Beijing (1985) 53–60.
- [11-7] Research group, Experimental investigation on ultimate strength of normal section of eccentrically compressed member of reinforced concrete, Symposium No. 2, Experimental Investigation of Reinforced Concrete Structures, Construction Industry Press of China, Beijing, 1981, pp. 19–61.
- [11-8] B. Bresler, Design Criteria for Reinforced Columns under Axial Load and Biaxial Bending, ACI (11) (1960) 481–490.
- [11-9] A.L. Parme, J.M. Nieves, A. Gonwens, Capacity of Reinforced Rectangular Columns Subject to Biaxial Bending, ACI 63 (9) (1966) 911–920.
- [11-10] R.W. Furlong, Concrete Columns under Biaxially Eccentric Thrust, ACI 76 (10) (1979) 1093–1118.
- [11-11] Zhisun Bao, Calculation on strength of reinforced concrete compressed member with biaxial eccentricities, Symposium of Experimental Investigation of Reinforced Concrete Structures, Construction Industry Press of China, Beijing, 1977, pp. 201–215.
- [11-12] Zongjian Lan, Zhiming Teng, Strength of normal section of reinforced concrete compressed member with biaxial bending, Symposium of Design and Detailing of Reinforced Concrete Structures. Beijing (1985) 88–96.
- [11-13] Zhisun Bao, Zhitao Lu, Strength of normal section of reinforced concrete tensed member with biaxial bending, Symposium of Design and Detailing of Reinforced Concrete Structures. Beijing (1985) 97–104.
- [11-14] Yaping Zhuang, et al., Ultimate strength of eccentrically compressed member of high-strength concrete, Symposium No. 3, Experimental Investigation of Reinforced Concrete Structures, Construction Industry Press of China, Beijing, 1994, pp. 407–414.
- [11-15] Chengruo Huang, Wenda Sun, Chengxi Zheng, Probability analyses on strength calculation and reliability design of reinforced concrete flexural member with reinforcement without yielding plateau, Journal of Building Structures 3 (4) (1982) 1–11.
- [11-16] Zhiming Teng, Jiahui Chen, Calculation of ultimate strength of normal section of concrete member reinforced uniformly, Symposium of Design and Detailing of Reinforced concrete Structures, Beijing (1985) 61–68.
- [12-1] Wenjiang Xu, Dexin Hu, Requirement and grades of crack control of reinforced concrete members, Symposium of Design and Detailing of Reinforced Concrete Structures, Beijing (1985) 38–44.
- [12-2] Shuyao Li, et al., Calculation of crack resistance of reinforced concrete member, Symposium of Design and Detailing of Reinforced Concrete Structures, Beijing (1985) 174–178.

- [12-3] Shaohuai Cai, Improvement on determination method for plasticity coefficient γ_s of cracking resistance, Symposium of Experimental Investigation of Reinforced Concrete Structures, Construction Industry Press of China, Beijing, 1977, pp. 298–315.
- [12-4] Weijian Yi, Pusheng Shen, Crack and deformation of reinforced concrete slabs. Symposium No. 3, Experimental Investigation of Reinforced Concrete Structures, Construction Industry Press of China, Beijing, 1994, 102–112.
- [12-5] R. Saliger, High grade steel in reinforced concrete, Preliminary publication, 2nd Congress of IABSE, Berlin-Munich, 1936.
- [12-6] V.E. Molasher, crack resistance, stiffness, and strength of reinforced concrete, Moscow, 1950.
- [12-7] H. Rüsch, G. Rehm, Notes on crack spacing in members subjected to bending, RILEM, Symposium on Bond and Crack Formation in Reinforced Concrete, Stockholm, 1957.
- [12-8] K. Chi, A. Kirstein, Flexural Cracks in Reinforced Concrete Beams, ACI (April 1958).
- [12-9] P. Desayi, Determination of the w_{\max} in Reinforced Members, ACI 73 (8) (1976).
- [12-10] Technical University of Nanjing, Calculation of deformation and crack of flexural reinforced concrete members, Symposium of Experimental Investigation of Reinforced Concrete Structures, Construction Industry Press of China, Beijing, 1977, pp. 237–290.
- [12-11] Research Institute of Building Science of Sichuan Province. Calculation of crack width of reinforced concrete member under central tension, Symposium of Experimental Investigation of Reinforced Concrete Structures, Construction Industry Press of China, Beijing, 1977, pp. 291–297.
- [12-12] G.D. Base, J.B. Read, A.W. Beeby, H.P.J. Taylor, An investigation of the crack control, characteristics of various types of bar in reinforced concrete beams. Research Report No. 18 Part I, Cement and Concrete Association, London, 1966.
- [12-13] G.D. Base, Crack control in reinforced concrete – present position, Symposium on Serviceability of Concrete, Melbourne, 1975.
- [12-14] B.B. Broms, L.A. Lutz, Effects of Arrangement of Reinforcement on Crack Width and Spacing of Reinforced Concrete Members, ACI 62 (11) (1965).
- [12-15] B.B. Broms, Stress Distribution in Reinforced Concrete Members with Tension Cracks, ACI 62 (9) (1965) 1095–1108.
- [12-16] B.B. Broms, Crack Width and Spacing in Reinforced Concrete Members, ACI 62 (10) (1965).
- [12-17] B.B. Broms, Technique for Investigation of Internal Cracks in Reinforced Concrete Members, ACI 62 (1) (1965) 39–44.
- [12-18] Yukimasa Kofuji, Koshi Otsuka, Research on Experiment about Fracture Happened to the Concrete Around the Deformed Steel Bearing the Tension, Japan Civil Engineering Society Essay Collection (2) (1982).
- [12-19] D. Watstein, R.G. Mathey, Width of Cracks in Concrete at the Surface of Reinforcing Steel Evaluated by Means of Tensile Bond Specimens, ACI (July 1959).
- [12-20] G.M. Mills, F.A. Albamder, The prediction of crack width in reinforced concrete beams, Magazine of Concrete Research 9 (1974).
- [12-21] A.W. Beeby, The Prediction and Control of Flexural Cracking in Reinforced Concrete Members, ACI SP 30, Detroit, 1971.

- [12-22] J.F. Borges, J.A. Lima, Formation of cracks in beams with low percentage of reinforcement, RILEM Symposium, Stockholm, 1957.
- [12-23] Qingrong Yu, et al., Research on unified calculation model of crack and stiffness of reinforced concrete members, Symposium No. 3, Experimental Investigation of Reinforced Concrete Structures, Construction Industry Press of China, Beijing, 1994, pp. 136–141.
- [12-24] G.C. Frantz, J.E. Breen, Cracking on the Side Faces of Large Reinforced Concrete Beams, ACI 77 (5) (1980).
- [12-25] Zongjian Lan, Shuyao Li, Calculation of crack width of reinforced concrete members, Symposium of Design and Detailing of Reinforced Concrete Structures, Beijing (1985) 183–195.
- [12-26] Zongjian Lan, Qingxiang Wang, Experimental investigation on influence of concrete cover thickness on crack width of reinforced concrete member, Symposium No. 3, Experimental Investigation of Reinforced Concrete Structures, Construction Industry Press of China, Beijing, 1994, pp. 90–101.
- [12-27] P. Gergely, L.A. Lutz, Maximum Crack width in Reinforced Concrete Members, ACI SP-20, Detroit, 1968, 87–117.
- [13-1] R.S. Fling, et al., Allowable Deflection, ACI 65 (6) (1968) 433–444.
- [13-2] ACI Committee 435, Proposed Revisions by Committee 435 to ACI Building Code and Commentary Provisions on Deflections, ACI 75 (6) (1978) 229–238.
- [13-3] Zongjian Lan, et al., Improvement and simplicity of formula for stiffness calculation of flexural reinforced concrete member, Symposium of Design and Detailing of Reinforced Concrete Structures, Beijing (1985) 196–200.
- [13-4] D.E. Branson, Discussion of “Proposed Revision of ACI 318-63: Building Code Requirement for Reinforced Concrete”, by ACI Committee 318, ACI 67 (9) (1970) 692–695.
- [13-5] G.W. Washa, P.G. Fluck, The Effect of Compressive Reinforcement on the Plastic Flow of Reinforced Concrete Beams, ACI 48 (8) (1952) 89–108.
- [13-6] W.W. Yu, G. Winter, Instantaneous and Long Time Deflections of Reinforced Concrete Beams under Working Loads, ACI 57 (1) (1960) 29–50.
- [13-7] K. Hajnal-Konyi, Tests on beams with sustained loading, Magazine of Concrete Research (1963).
- [13-8] D.E. Branson, Compressive Steel Effect on Long-Time Deflections, ACI 68 (8) (1971) 555–559.
- [14-1] Report of ACI–ASCE Committee 326, Shear and Diagonal Tension, ACI 59 (1) (1962) 1–30 (2): 277–333, (3): 353–395.
- [14-2] Joint ASCE-ACI Task Committee 426, The Shear Strength of Reinforced Concrete Members, ASCE (ST6) (1973) 1091–1187.
- [14-3] J.G. MacGregor, J.M. Hanson, Proposed Changes in Shear Provisions for Reinforced and Prestressed Concrete Beams, ACI 66 (4) (1969) 276–288.
- [14-4] Research Group, Calculation of ultimate shear strength of reinforced concrete, Symposium of Experimental Investigation of Reinforced Concrete Structures, Construction Industry Press of China, Beijing, 1977, pp. 125–152.
- [14-5] Langqing Shi, Yongyan Yu, et al., Calculation of shear strength along inclined section of reinforced concrete members, Symposium of Design and Detailing of Reinforced Concrete Structures. Beijing (1985) 112–139.
- [14-6] P. Watsein, R.G. Mathy, Strains in Beams Having Diagonal Cracks, ACI (Dec. 1958).

- [14-7] G.N.J. Kani, Basic Facts Concerning Shear Failure, *ACI* 63 (5) (1966) 675–692.
- [14-8] T. Baumann, H. Rüschi, Schubversuche mit indirekter Krafteinleitung. Deutscher Ausschuss für Stahlbeton, Heft 210, Berlin, 1970.
- [14-9] O. Moretto, An Investigation of the Strength of Welding Stirrups in Reinforced Concrete beams, *ACI* 42 (2) (1945) 141–162.
- [14-10] D. Ngo, A.C. Scordelis, Finite Element Analysis of Reinforced Concrete Beams, *ACI* 63 (3) (1967) 152–164.
- [14-11] R. Taylor, Some shear tests on reinforced concrete beams without web reinforcement, *Magazine of Concrete Research* (1960).
- [14-12] Technical Institute of Building Engineering, Chongqing, Ultimate shear strength of reinforced concrete beam loaded indirectly, Symposium No. 2. Experimental Investigation of Reinforced Concrete Structure, Construction Industry Press of China, Beijing, 1981, pp. 129–151.
- [14-13] A. Placas, P.E. Regan, Shear Failure of Reinforced Concrete Beams, *ACI* 68 (10) (1971) 763–773.
- [14-14] F. Leonhard, R. Walther, Beiträge zur Behandlung der Schubprobleme in Stahlbetonbau, *Beton und Stahlbetonbau* (1962) (2), (3), (5), (6), (7).
- [14-15] Chinese Academy of Building Science, Experimental investigation of ultimate shear strength of concrete beam with inclined tension surface, Symposium of Experimental Investigation of Reinforced Concrete Structures, Construction Industry Press of China, Beijing, 1977, pp. 153–181.
- [14-16] K.G. Moody, I.M. Viest, et al., Strength of Reinforced Concrete Beams, Part II. *ACI* (1955).
- [14-17] L.B. Kriz, C.H. Rath, Connection in Precast Concrete Structures—Strength of Carbels, *Journal of Prestressed Concrete Institute* (1) (1965) 10.
- [14-18] Building Research Institute of Metallurgy Ministry, Experimental investigation of reinforced concrete bracket, Symposium of Experimental Investigation of Reinforced Concrete Structures, Construction Industry Press of China, Beijing, 1977, pp. 397–419.
- [14-19] Jihua Shu, et al., Design method for reinforced concrete bracket, Symposium of Design and Detailing of Reinforced Concrete Structures. Beijing (1985) 280–284.
- [14-20] F.E. Richart, Reinforced Concrete Wall and Column Footings, *ACI* 45 (2) (1948), 97 ~ 127, (3): 237–260.
- [14-21] R.C. Elstner, E. Hognestad, Shearing Strength of Reinforced concrete Slabs, *ACI* 1 (1956) 29–58.
- [14-22] Research Group, Experimental investigation on punching strength of reinforced concrete slab and foundation, *Journal of Building Structures* 8 (4) (1987) 12–22.
- [14-23] Jiaji Fan, et al., Punching strength of reinforced concrete arbitrary foundation under column, Symposium No. 3, Experimental Investigation of Reinforced Concrete Structures, Construction Industry Press of China, Beijing, 1994, pp. 36–50.
- [15-1] T.T.C. Hsu, Torsion of Structural Concrete – A Summary on Pure Torsion, *ACI SP-18*, Detroit, 1968, 165–178.
- [15-2] E.L. Kemp, Behavior of Concrete Members Subject to Torsion and to Combined Torsion, Bending and Shear, *ACI SP-18*, Detroit, 1968, 179–201.
- [15-3] H.J. Cowan, Design of Beams Subjected to Torsion Related to the New Australian Code, *ACI* (1960) 591–618.

- [15-4] T.T.C. Hsu, Ultimate Torque of Reinforced Rectangular Beams, ASCE 94 (ST2) (1968) 485–510.
- [15-5] D.L. Osburn, B. Mayoglon, A.H. Mattock, Strength of Reinforced Concrete Beams with Web Reinforcement in Combined Torsion, Shear and Bending, ACI 66 (1) (1969) 31–41.
- [15-6] Zhendong Wang, et al., Design method for reinforced and prestressed concrete members under torsion, Symposium of Design and Detailing of Reinforced Concrete Structures. Beijing (1985) 140–147.
- [15-7] Songlin Hu, Yuliang Xie, Discussion on mechanism of reinforced concrete member under torsion, Journal of Nanjing Institute of Building Engineering (1) (1985).
- [15-8] Zuoqian Zheng, Yanhai Wu, et al., Experimental investigation of high-strength concrete member under torsion alone, Symposium No. 3, Experimental Investigation of Reinforced Concrete Structures, Construction Industry Press of China, Beijing, 1994, pp. 433–439.
- [15-9] S.P. Timoshenko, J.N. Goodier, Theory of Elasticity, third ed., McGraw Hill Book Co., Inc, New York, 1970.
- [15-10] Bingye Xu, Sencan Chen, Theory of Plasticity (Simple Textbook), Tsinghua University Press, Beijing, 1981.
- [15-11] T.T.C. Hsu, E.L. Kemp, Background and Practical Application of Tentative Design Criterion for Torsion, ACI 66 (1) (1969) 12–23.
- [15-12] P. Lampert, M.P. Collins, Torsion, Bending and Confusion — An Attempt to Establish the Facts, ACI 69 (8) (1972) 500–504.
- [15-13] L. Elfren, I. Karlsson, A. Losberg, Torsion-Bending Shear Interaction for Concrete Beams, ASCE 100 (ST8) (1974) 1657–1676.
- [15-14] Zhendong Wang, Lanqing Shi, et al., Application of truss model to analyses of reinforced concrete members under bending moment, shear force, and torsion, Symposium No. 3, Experimental Investigation of Reinforced Concrete Structures, Construction Industry Press of China, Beijing, 1994, pp. 1–13.
- [15-15] Zhendong Wang, Lanqing Shi, et al., Application of truss model to analysis of reinforced concrete member acted together with bending moment, shear force, and torsion, Symposium No. 3, Experimental Investigation of Reinforced Concrete Structures, Construction Industry Press of China, Beijing, 1994, pp. 14–26.
- [15-16] Zhendong Wang, Guyi Kang, et al., Experimental investigation and model analysis of reinforced concrete members under bending moment, shear force, torsion, and their combination, Collection of Research Reports on Design Code for Concrete Structures, Beijing, 1996, 11, III-1–III-28.
- [15-17] A.A. Gvozdev, N.N. Lessig, L.K. Rulle, Research on Reinforced Concrete Beams under Combined Bending and Torsion in Soviet Union, ACI SP-18, Detroit, 1968, 307~336.
- [15-18] A.E. McMullen, J. Warwaruk, Concrete Beams in Bending, Torsion and Shear, ASCE 96 (ST5) (1970) 885–903.
- [16-1] National Standard of People's Republic of China. Code for Aseismic Design of Building GB50011–2001, Construction Industry Press of China, Beijing, 2001.
- [16-2] Edited by Chinese Academy of Building Science. Structural Design of Tall Buildings. Beijing: Science Press of China, 1984.

- [16-3] Zhuqing Lu, et al., General rules for aseismic design of reinforced concrete structural members, Symposium of Design and Detailing of Reinforced Concrete Structures. Beijing (1985) 285–289.
- [16-4] Jumin Shen, Yijun Weng, Stiffness and ductility of reinforced concrete structural members, Symposium No. 3, Aseismic Behaviors of Reinforced Concrete Structures, Tsinghua University Press, Beijing, 1981, pp. 54–71.
- [16-5] Bolong Zhu, Mingshun Wu, Research on ductility coefficient of flexural member of reinforced concrete, Journal of Tongji University (1) (1978).
- [16-6] Ehua Fang, et al., Influences of compression-strength ratio and content of reinforcement on ductility of frame column, Reports on Construction Technique (Building Structures) (3) (1983).
- [16-7] Huizhong Sun, et al., Aseismic design of beams in reinforced concrete multi-storeys frame, Symposium of Design and Detailing of Reinforced Concrete Structures. Beijing (1985) 294–298.
- [16-8] Yinsheng Zou, et al., Aseismic design of column in reinforced concrete multi-storey frame, Symposium of Design and Detailing of Reinforced Concrete Structures. Beijing (1985) 299–308.
- [16-9] W.G. Corley, Rotational Capacity of Reinforced Concrete Beams, ASCE 92 (ST5) (1966) 121–146.
- [16-10] A.H. Mattok, Discussion of [16-9], ASCE 93 (ST2) (1967) 519–522.
- [16-11] Jumin Shen, Yijun Weng, Shiping Feng, Behavior of compressed-flexural member of reinforced concrete under reversed load of low cycles, Symposium No. 3, Aseismic Behaviors of Reinforced Concrete Structures, Tsinghua University Press, Beijing, 1981, pp. 72–95.
- [16-12] Bolong Zhu, Research on recovering characteristic of reinforced concrete in China, Symposium on Earthquake Resistance and Disaster Prevention, Beijing, 1987.
- [16-13] Ehua Fang, Guowei Li, Experimental investigation of shear wall with openings, Symposium No. 3, Aseismic Behaviors of Reinforced Concrete Structures, Tsinghua University Press, Beijing, 1981, pp. 96–117.
- [16-14] Youlin Xu, Degradation of bond behavior between reinforcement and concrete under reversed load, Chinese Academy of Building Science, 1996.
- [16-15] Research Group, Experimental investigation of shear strength of beam–column joint of reinforced concrete frame under reversed load of low cycles, Journal of Building Structures (6) (1983).
- [16-16] Shaoliang Bai, et al., Experimental investigation of static and aseismic behaviors of side joint on top floor of reinforced concrete frame, Symposium No. 3, Experimental Investigation of Reinforced Concrete Structures, Construction Industry Press of China, Beijing, 1994, pp. 184–216.
- [16-17] Xinliang Jiao, Liande Zhang, Yunting Wei, Research on aseismic behavior of middle joint on top floor of reinforced concrete frame, Building Structures (11) (1995).
- [16-18] Weishan Jiang, et al., Aseismic design of joints in reinforced concrete multi-storey frame, Symposium of Design and Detailing of Reinforced Concrete Structures, Beijing, 1985, pp. 314–321.
- [16-19] Research Group, Symposium of Investigation and Application of Joints and Aseismic Detailing of Reinforced Concrete Structure, Construction Industry Press of China, Beijing, 1996.

- [17-1] J.M. Hanson, Design for Fatigue, F.K. Kong, et al., Handbook of Structural Concrete, Pitman, London, 1983, 16-1–16-35.
- [17-2] G.M. Nordby, A Review of Research Fatigue of Concrete, ACI 55 (2) (1958) 191–220.
- [17-3] ACI Committee 215, Consideration for Design of Concrete Structure Subjected to Fatigue Loading, ACI 71 (3) (1974) 97–121.
- [17-4] Mingchu Yao, Yupu Song, Huimin Li, et al., Study on calculation method for checking reliability of fatigue of flexural concrete member. Symposium No. 3, Experimental Investigation of Reinforced Concrete Structures, Construction Industry Press of China, Beijing, 1994, 583–592.
- [17-5] Yupu Song, Peigong Wu, et al., Research on design method for ultimate fatigue, Collection of Research Reports on Design Code for Concrete Structures, Beijing, (11) 1996. XI-1–XI-21.
- [17-6] F.S. Ople, C.L. Hulskos, Probable Fatigue Life of Plain Concrete with Stress Gradient, ACI 63 (1) (1966) 59–81.
- [17-7] Liming Bai, Peigang Wu, Guangyi Zhao, Investigation of fatigue behavior of high-strength concrete under compression, Symposium No. 6 Research on Mechanical Behavior of Concrete, Tsinghua University Press, Beijing, 1996, pp. 158–171.
- [17-8] R. Tepfers, T. Kutti, Fatigue Strength of Plain, Ordinary, and Lightweight Concrete, ACI 76 (5) (1979) 635–652.
- [17-9] Weiwei Zhan, Guangyi Zhao, Peigang Wu, Investigation of fatigue behavior of high-strength concrete under tension, Symposium No. 6 Research on Mechanical Behavior of Concrete, Tsinghua University Press, Beijing, 1996, pp. 172–180.
- [17-10] Huiling Chen, Faren Zhou, Investigation on fatigue strength of high-strength prestressing wire, Collection of Research Reports on Prestressed Concrete Crane Beam (1978).
- [17-11] R. Taylor, Some fatigue test on reinforced concrete beams, Magazine of Concrete Research 16 (46) (1964).
- [17-12] B. Bresler, V. Bertero, Behavior of Reinforced Concrete under Repeated Load, ASCE 94 (ST6) (1968) 1576–1590.
- [17-13] H.A.F. Ismail, J.O. Jirsa, Bond Deterioration in Reinforced Concrete Subject to Low Cycle Load, ACI 69 (6) (1972) 334–343.
- [17-14] T.S. Chang, C.E. Kesler, Fatigue Behavior of Reinforced Concrete Beams, ACI 55 (2) (1958) 245–254.
- [17-15] T.S. Chang, C.E. Kesler, Static and Fatigue Strength in Shear of Beams with Tensile Reinforcement, ACI 54 (12) (1958) 1033–1057.
- [17-16] Zhishen Lin, Xiuzhen Li, Fengzhen Zhou, Experimental investigation on cracking fatigue of prestressed concrete crane beam under bending, Metallurgical Building (6) (1981).
- [17-17] Zhongde Tian, Huimin Li, et al., Research on checking method for fatigue strength of reinforced concrete flexural member, Symposium No. 2, Experimental Investigation of Reinforced Concrete Structures, Construction Industry Press of China, Beijing, 1981, pp. 235–254.
- [17-18] Zaikang Shen, Huizhong Sun, Fatigue behavior of partially prestressed concrete beam existing crack, Symposium No. 2, Experimental Investigation of Reinforced Concrete Structures, Construction Industry Press of China, Beijing, 1981, pp. 184–234.

- [17-19] Qingxiang Wang, et al., Calculation of crack width of reinforced concrete slab under repeated load, Symposium No. 3, Experimental Investigation of Reinforced Concrete Structures, Construction Industry Press of China, Beijing, 1994, pp. 113–122.
- [18-1] Tsinghua University, et al., Protective Structure Underground, Construction Industry Press of China, Beijing, 1982.
- [18-2] Comité Euro-International Du Béton, Bulletin D'information No. 187, Concrete Structures under Impact and Impulsive Loading, Lausanne, 1988.
- [18-3] Zhaoyuan Chen, Behavior of high-strength reinforcement under high speed straining and its application in anti-explosion structure, Symposium No. 4, Behaviors of Reinforced Concrete Structural Members under Explosion Load, Tsinghua University Press, Beijing, 1986, pp. 63–72.
- [18-4] D. Watstein, Effect of Straining Rate on the Compressive Strength and Elastic Properties of Concrete, ACI 49 (6) (1953) 729–744.
- [18-5] B.P. Hughes, R. Gregory, Concrete subject to high rates of loading in compression, Magazine of Concrete Research (24) (1972) 25–36.
- [18-6] Zhaoyuan Chen, Yongkui Kan, Some problems of high strength concrete used for anti-explosion structure, Symposium No. 4, Behaviors of Reinforced Concrete Structural Members under Explosion Load, Tsinghua University Press, Beijing, 1986, pp. 73–83.
- [18-7] Renjie Shang, Research on Dynamic Constitutive Behavior of Concrete: [Doctor Thesis], Technical University of Dalian, Dalian, 1994.
- [18-8] Yongkui Kan, Tensile strength of concrete under high speed straining, Symposium No. 4, Behaviors of Reinforced Concrete Structural Members under Explosion Load, Tsinghua University Press, Beijing, 1986, pp. 84–89.
- [18-9] A.J. Zielinski, H.A. Körmeling, H.W. Reinhardt, Experiment on concrete under uniaxial impact tensile loading, RILEM Materials and Structures 14 (80) (1981) 102–112.
- [18-10] E. Vos, H.W. Reinhardt, Influence of loading rate on bond behavior of reinforcing steel and prestressing strands, RILEM Materials and Structures 15 (85) (1982) 3–10.
- [18-11] Zhaoyuan Chen, Lanqing Shi, Flexural behaviors of reinforced concrete beams under static and high speed deforming, Symposium No. 4, Behaviors of Reinforced Concrete Structural Members under Explosion Load, Tsinghua University Press, Beijing, 1986, pp. 1–32.
- [18-12] Zhaoyuan Chen, Jiaqian Luo, Behaviors of centrally and eccentrically compressed members of reinforced concrete under high speed deforming, Symposium No. 4, Behaviors of Reinforced Concrete Structural Members under Explosion Load, Tsinghua University Press, Beijing, 1986, pp. 33–44.
- [19-1] Bofang Zhu, Tongsheng Wang, Baoying Din, Zhizhang Guo, Thermal Stress and Temperature Control of Hydraulic Concrete Structures, Hydraulic and Electric Power Press, Beijing, 1976.
- [19-2] Professional Standard of Metallurgical Industry of People's Republic of China. Code for Heat-Resistance Design of Reinforced Concrete Structure of Metallurgical Workshop, Metallurgical Industry Press, Beijing, 1979.
- [19-3] Fédération Internationale de la Précontrainte, The design and construction of prestressed concrete reactor vessels. FIP/3/3, March 1978.

- [19-4] ASME. Boiler and Pressure Vessels Code, An American National Standard (ACI Standard 359–74). Section III, Division 2. Jan. 1975.
- [19-5] Fédération Internationale de la Précontrainte. FIP/CEB Recommendations for the Design of Reinforced and Prestressed Concrete Structural Members for Fire Resistance FIP/1/1. First Edition, June 1975.
- [19-6] Fédération Internationale de la Précontrainte. FIP/CEB Report on Methods of Assessment of the Fire Resistance of Concrete Structural Members. FIP, 1978.
- [19-7] National Standard of People's Republic of China. Code for Architectural Design of Fire Prevention GBJ 16-87, Construction Industry Press of China, Beijing, 1988.
- [19-8] B.K. Bardhan-Roy, Fire Resistance-Design and Detailing, in: F.K. Kong, et al. (Eds.), Handbook of Structural Concrete, Pitman, London, 1983 (14) :14-1–14-46.
- [19-9] Yinqing Li, Daozhen Ma, Jian Xu, Calculation and Detailing for Fire Prevention Design of Building Structure, Construction Industry Press of China, Beijing, 1991.
- [19-10] Zhenhai Guo, Xudong Shi, Behavior and Calculation of Reinforced Concrete at Elevated Temperature, Tainghua University Press of China, Beijing, 2003.
- [19-11] Jianlin Nan, Zhenhai Guo, Xudong Shi, Experimental investigation on deformation behavior of concrete under heating-cooling cycles, Building Science (2) (1997) (Total 52): 16–21.
- [19-12] Commission of the European Communities, Euro-code No. 2, Design of Concrete Structures, Part 10, Structural Fire Design (April, 1990).
- [19-13] Tongguang Lu, Experimental Investigation of Strength and Deformation of Reinforcing Bars under High Temperature. [Master Dissertation], Tsinghua University, Beijing, 1996.
- [19-14] Honggang Wang, An Introduction to Thermal Elasticity, Tsinghua University Press, Beijing, 1989.
- [19-15] Joint Committee of the Institution of Structural Engineers and the Concrete Society, Design and Detailing of Concrete Structures for Fire Resistance. London, 1978.
- [19-16] Hong Niu, Zhoudao Lu, Lei Chen, Experimental investigation of constitutive relations of reinforcement and concrete under high temperature, Journal of Tongji University 18 (3) (1990).
- [19-17] Harada T, et al. Strength, Elasticity and Thermal Properties of Concrete Subjected to Elevated Temperature. Concrete for Nuclear Reactors, Vol. I, II, III. ACI SP 34–21, Detroit, 1972: 377–406.
- [19-18] Wei Li, Zhenhai Guo, Experimental investigation on strength and deformation behaviors of concrete at elevated temperature, Journal of Building Structures 14 (1) (1993) 8–16.
- [19-19] R. Baldwin, M.A. North, A stress-strain relationship for concrete at high temperature, Magazine of Concrete Research (12) (1973) 208–211.
- [19-20] J.C. Marechal, Variations in the modulus of Elasticity and Poisson's Ratio with Temperature. Concrete for Nuclear Reactors, Vol. I, II, III. ACI SP 34–27. 495–503
- [19-21] U. Diederichs, U. Schneider, Bond strength at high temperature, Magazine of Concrete Research (6) (1981) 75–84.
- [19-22] Zhenhai Guo, Wei Li, Deformation and constitutive relation of concrete under different stress-temperature paths, China Civil Engineering Journal 26 (5) (1993) 58–69.

- [19-23] Jianlin Nan, Zhenhai Guo, Xudong Shi, Temperature—stress coupling constitutive relationship of concrete, *Journal of Tsinghua University (Science and Technology)* 37 (6) (1997) 87–90.
- [19-24] G.A. Khoury, B.N. Grainger, P.J.E. Sullivan, Strain of concrete during first heating to 600°C under load, *Magazine of Concrete Research* 37 (133) (1985) 195–215.
- [19-25] G.A. Khoury, B.N. Grainger, P.J.E. Sullivan, Strain of concrete during first cooling from 600°C under load, *Magazine of Concrete Research* 38 (134) (1986) 3–12.
- [19-26] Y. Anderberg, Predicted fire behavior of steel and concrete structures, *International Seminar on Three Decades of Structural Fire Safety*, London, 1983, pp. 115–137.
- [19-27] B. Ellingwood, T.D. Lin, Flexure and Shear Behavior of Concrete Beams During Fires, *ASCE* 117 (ST2) (1991) 440–457.
- [19-28] Xudong Shi, Experimental Investigation and Non-Linear Finite Element Analysis of Reinforced Concrete Beam-Column Structures under Loading and Heating: [Doctor Thesis], Tsinghua University, Beijing, 1992.
- [19-29] Jieying Zhang, Experimental Study of Reinforced Concrete Columns and Beams under Loading and Heating: [Master Dissertation], Tsinghua University, Beijing, 1997.
- [19-30] A.H.B. Ng, N.S. Mirza, T.T. Lie, Response of Direct Models of Reinforced Concrete Columns Subjected to Fire, *ACI Structural Journal* 87 (5–6) (1990) 313–323.
- [19-31] Nan Su, Tongzhu Lin, T.T. Lie, Fire-resistant behavior of reinforced concrete column, *China Civil Engineering Journal* 25 (6) (1992) 25–36.
- [19-32] Huadong Li, Experimental Investigation of Reinforced Concrete Columns and Beams at Elevated Temperature: [Master Dissertation], Tsinghua University, Beijing, 1994.
- [19-33] Xudong Shi, Huadong Li, Zhenhai Guo, Experimental investigation on mechanical behavior of reinforced concrete central compression column with three surfaces exposed to fire, *Journal of Building Structures* 18 (4) (1997) 13–22.
- [19-34] Jianping Yang, Experimental Research, Theoretical Analysis and Practical Calculation of Eccentrically Compressed Reinforced Concrete Members under Loading and Heating: [Doctor Thesis], Tsinghua University, Beijing, 2000.
- [19-35] Jianping Yang, Xudong Shi, Zhenhai Guo, Experimental research on reinforced concrete members with flexural and axial load and two surfaces exposed to high temperature, *Building Structure* 30 (2) (2000) 23–27.
- [19-36] Jianping Yang, Xudong Shi, Zhenhai Guo, Comparison of mechanical behaviors between reinforced concrete eccentric compression members heated separately on two adjacent and three surfaces, *Industrial Construction* 30 (6) (2000) 34–37 (Total 314).
- [19-37] Jinfeng Sun, Comparative Research on Behaviors of Reinforced Concrete Members under Several Temperature Situations: [Master Dissertation], Tsinghua University, Beijing, 2001.
- [19-38] Jinfeng Sun, Yan Li, Xudong Shi, Zhenhai Guo, Experimental investigation on behaviors of eccentrically compressed reinforced concrete members heated on three surfaces under different temperature conditions, *Journal of Building Structures* 22 (4) (2001) 84–89.

- [19-39] Jinfeng Sun, Xudong Shi, Zhenhai Guo, Behaviors of reinforced concrete beams (heated on three surfaces) at elevated temperature and after cooling, *Building Structure* 32 (1) (2002) 34–36.
- [19-40] Xudong Shi, Zhenhai Guo, Investigation on redistribution of internal force and failure mechanism of reinforced concrete continuous beams at elevated temperature, *Building Structure* (7) (1996) 34–37.
- [19-41] Xudong Shi, Zhenhai Guo, Experimental investigation on behavior of reinforced concrete frames at elevated temperature, *China Civil Engineering Journal* 33 (1) (2000) 36–45.
- [19-42] T.T. Lie, A Procedure to Calculate Fire Resistance of Structural Members, *International Seminar on Three Decades of Structural Fire Safety*, London, 1983, pp. 139–153.
- [19-43] Xueqian Wang, Calculation of ultimate bending moment of reinforced concrete beam under high temperature of fire, *Building Structure* (7) (1996) 38–42.
- [19-44] M. Becker, B. Bresler, Reinforced Concrete Frames in Fire Environment, *ASCE* 103 (ST1) (1977) 211–223.
- [20-1] Luoshu Gong, Chunpu Liu, *Durability, Protection and Reparation of Concrete*, Construction Industry Press of China, Beijing, 1990.
- [20-2] Weiliang Jin, Yuxi Zhao, *Durability of Concrete Structure*, Science Press, Beijing, 2002.
- [20-3] Xiaotan Di, Xiaowang Gao, Youlin Xu, Problems of durability and safety of concrete structures in China, *Proceeding of Safety and Durability of Building Structure Engineering*, Beijing, 2001, pp. 191–196.
- [20-4] Zhaoyuan Chen, Durability design of concrete structure, *Symposium of Durability and its Design of Concrete Structures*, Tsinghua University, Beijing, 2002, pp. 59–79.
- [20-5] Weizhong Xu, et al., *Building Materials*, Industry Press of China, Beijing, 1962.
- [20-6] National Standard of People's Republic of China. Test Methods for Long-term Behavior and Durability of Ordinary Concrete GBJ 82 1985, *Construction Industry Press of China*, Beijing, 1985.
- [20-7] Tingyu Hao, Alkali-aggregate reaction of concrete and its prevention. *Symposium of Durability and its Design of Concrete Structures*, Tsinghua University, Beijing, 2002, 273–282.
- [20-8] Zengzhong Wang, Jianxin Liu, Discussion on alkali-aggregate reaction and durability of concrete, *Proceeding of Safety and Durability of Building Structure Engineering*, Beijing, 2001, 213–219.
- [20-9] Naifeng Hong, Considerations of reinforcement rusting resulted by chlorate and durability during design, *Symposium of Durability and its Design of Concrete Structures*, Tsinghua University, Beijing, 2002, pp. 20–35.
- [20-10] Youlin Xu, Xiaofeng Wang, et al., Experimental investigation of mechanical behavior of rusted reinforcement, *Symposium of Durability and its Design of Concrete Structures*, Tsinghua University, Beijing, 2002, pp. 291–297.
- [20-11] Standard of China Civil Engineering Society. Guide to Design and Construction for Durability of Concrete Structure (CCES 01–2004), *Construction Industry Press of China*, Beijing, 2004.
- [20-12] Qinglin Wang, Huotao Niu, Compilation of evaluation criterion for durability of concrete structures, *Proceeding of Safety and Durability of Building Structure Engineering*, Beijing, 2001, 178–180.

Index

Note: Page numbers with “f” denote figures; “t” tables.

A

Aerated concrete slab, 259–261, 260f
Age, 71–74
 compressive strength, 72–73
 hardening, 173–175
 at loading, 83
 modulus of elasticity, 74
Alkali–aggregate reaction, 531–533
Analogue explosion load, 462–463
Analytical method, for stiffness, 337–340
Anchorage bond, of reinforcement end, 183, 183f
Angular rotation
 of plastic region, 418–421
 ultimate, 422f
Anisotropic constitutive model, 150
 orthogonal, 150
Average value of linear expansion coefficient, 483
Axial compression, 205–206
Axial force
 influence on web reinforcement, 377–378
 mechanical behavior under, *see* Axial force,
 mechanical behavior under
 members with, 395
Axial force, mechanical behavior under, 205–220
 compressive member, 206–212
 basic equations, 206–208
 stress–strain analysis, 209–212
 general regularity, 218–219
 tensile member, 212–218
 basic equations, 212–213
 minimum reinforcement rate, 215–216
 stress–strain analysis, 213–215
 tension stiffening, 216–218
Axial tension, 205–206
Axial torsion, 395

B

Bauschinger effect, 169–170, 169f, 251
Beam
 composite beam, shrinkage difference of, 258–259,
 258f
 deflection, of high-strength concrete, 298f
 failure pattern in
 less-reinforced, 272–274
 over-reinforced, 274–275
 rectangular beam with tensile reinforcement,
 269–272
 suitably reinforced, 275
 model, 369–370, 370f
 of T section, 374–376
 test, for reinforcement–concrete bonding, 187–188

 web, load acted on, 373–374
 with variable section, 376
Beam–column joint, hysteretic curve of, 432–434
Bending, member strength under, 269–304
Bending moment
 at cracking, 306f
 curvature, constitutive model for, 341f
 of eccentrically compressed long column, 284t
 fatigue under, 450–454
 members with, 397–400
 positive and negative, within shear span, 378–380
 sectional stiffness varying with, 340f
Bending moment–shear force–torsion, 400–401
Biaxial bending, 295–298, 296f–297f
Biaxial compressions, 119–121
Biaxial stress states, 119–122
Biaxial tensions, 121–122
 and compression, 121
Blast wave of nuclear explosion, 458–461, 458f
Bond stress–slip relation, constitutive model for,
 199–203
 characteristic values, calculation of, 200–201
 splitting stress, 200–201
 ultimate bond strength, 201
 τ – s curve, equation for, 201–203
 model of continuous curve, 202–203
 segmental model, 201–202
Bond-and-slip method, 312–314
Bracket, 380–382
Breaking in tension, 132–133
Bridge and communication engineering,
 reinforced concrete structure in, 1
Building engineering, reinforced concrete
 structure in, 1

C

Calculation model
 for ductility under monotonic load, 416–418
 for reversed load of low cycles, 434–436
Capillary hole, in concrete, 525
Carbonation, 533–536
Cato model, 170–171, 170f
CEB-FIP Model Code
 for confined concrete, 237–238, 250–251
 for fatigue strength of tensile reinforcement, 445f
 for tensile cracking, 324
Cement gelation, viscous flow of, 14, 15f
Central compressive member at elevated
 temperature, behavior and calculation of,
 507–508
Central tensile strength, 34–36
Chemical corrosion, 536–538

- Chinese Code, 147, 167, 330, 347, 367–368, 378, 390, 395, 402, 412, 418
 tensile reinforcement, fatigue strength of, 443f, 445f
 Clough's M - $1/\rho$ model, 435–436, 435f
 Coefficient of heat conduction, 483
 Cold-drawn, 175–176
 Cold-stretching, 173–175
 Column
 eccentrically compressed column, failure pattern in, 275–280
 long column, flexure of, 280–283
 with spiral bar, 222–226
 mechanical mechanism and failure process, 222–223
 ultimate strength, 224–226
 Columnar crushing, 133
 Complete stress–strain curve, equations for, 33t, 94t
 eccentric/flexural tension, 70–71
 Composite beam, shrinkage difference of, 258–259, 258f
 Composite internal forces, members with, 395–401
 axial force and torsion, 395
 bending moment and torsion, 397–400
 bending moment–shear force–torsion, 400–401
 shear force and torsion, 395–397
 Composite materials, non-uniform distribution of, 11f
 Composition
 of reinforced concrete, 10–15
 of reinforcement–concrete bonding, 184–185
 Comprehensive analysis, of tensile cracking, 318–321
 Compression
 axial, 205–206
 eccentric, *see* Eccentric compression
 inclined, failure pattern of, 354
 local (bearing strength), 244–252
 mechanical characteristic and mechanism, 244–249
 strength calculation, 249–252
 member strength under, 269–304
 triaxial, 122–125
 Compression–strength ratio, hysteretic curve of, 427
 Compressive depth, boundary of, 292–293, 292f
 Compressive member
 behavior of, 472–474
 mechanical behavior of, 206–212
 basic equations, 206–208
 stress–strain analysis, 209–212
 Compressive peak strain, of concrete, 25–27, 26f, 26t
 Compressive strength, 19–27
 age and, 72–73
 cubic, 19–21, 20f
 prism specimen, failure process of, 21–24, 22f, 22t, 23f
 upper and lower bounds of, 500–501
 Compressive–flexural member at elevated temperature, 508–511
 Concrete
 behavior under high-speed loading, 465–468
 confined, 221–252
 coupling constitutive relation of, 499–520
 cover thickness, 195
 creep of, 263–266
 existing structures, durability evaluation and examination for, 543–546
 fatigue of, 438–442
 experimental results and expression, 438–441
 influence factors and calculation formula, 441–442
 high-strength, 298–299
 low-weight, 299, 300f
 mechanical behaviors of, at elevated temperature, 491–499
 porosity texture of, 524–527, 526t
 shrinkage of, 254–259
 strength, 194, 358, 358f
 Concrete and reinforcement, bond between, 181–204
 bond stress–slip relation, constitutive model for, 199–203
 characteristic values, calculation of, 200–201
 τ - s curve, equation for, 201–203
 composition, 184–185
 deformed reinforcement, 190–193
 fatigue of, 446–449
 function and classification, 182–184
 anchorage bond, of reinforcement end, 183, 183f
 cracks, bond between, 183–184, 183f
 hysteretic curve of, 430–432
 influence factors, 193–199
 concrete cover thickness, 195
 concrete strength, 194
 other factors, 198–199
 reinforcement, bond length of, 195
 reinforcement, diameter and shape of, 196–197
 transverse compressive stress, 198
 transverse stirrup, 197–198
 plain reinforcement, 189–190
 test method, 186–188
 beam test, 187–188
 tension test, 186–187
 Confined concrete, 221–252
 column with spiral bar, 222–226
 mechanical mechanism and failure process, 222–223
 ultimate strength, 224–226
 local compression, 244–252
 mechanical characteristic and mechanism, 244–249
 strength calculation, 249–252
 rectangular tied column, 226–238
 complete stress–strain curve, equation for, 234–238
 failure process, 226–229
 rectangular tie, working mechanism of, 229–232
 steel-tube-confined concrete, 238–244
 mechanical characteristic and mechanism, 238–241
 ultimate strength calculation, 241–244
 Confinement index, 231–232
 Constitutive relation, 147–155
 linear elasticity models, 149–150

models of other categories, 151–155, 152t
 non-linear elasticity models, 150–151
 Content of reinforcement, hysteretic curve of, 427
 Continuous beam, 507, 513–515, 514f
 Control stress, sustaining time of, 178
 Coupling constitutive relation, of concrete, 499–505
 Crack(s/ing), 10, 13–14
 bending moment at, 306f
 bond between, 183–184, 183f
 of concrete
 inertia moment of converted section, 336
 inertia moment of converted section before, 335–336, 335f
 developing stage of, 18–19
 stable, 18–19
 unstable, 19
 formation and expansion of, 14–15, 15f
 microcrack, 11, 13–14, 16–19, 23–24, 40–41, 49–50
 repeated load and, 55
 space between, 313–314, 319
 tensile, 305–328
 tension at, 306f
 width, 322–327
 Creep, 78–87, 176–179
 age at loading, 83
 basic concept, 78–81
 of concrete, 263–266
 stress distribution on section under sustained load, 263–265
 stress state after unloading, 265–266
 control stress, sustaining time of, 178
 manufacturing and curing conditions, 83
 raw materials and mixture, 83
 relationship with relaxation, 79–80, 80f
 service stage, environmental condition during, 83–84
 short-term, at elevated temperature, 504
 steel, 178
 stress level, 82–83, 178–179
 structural member size, 84
 temperature, 179
 Cyclic loads, deformation under action of, 167–172

D

Deformation, 33–44
 under action of cyclic loads, 167–172
 under biaxial compression, 120f, 122f
 under biaxial tension, 122f–123f
 calculation, 342–348
 general method, 342–344
 practical methods, 344–348
 difference, *see* Deformation difference,
 mechanical response of
 elastic, 14, 15f
 flexural stiffness and, 329–348
 member, and sectional stiffness, 331–334
 plural compositions of, 14–15, 15f
 shrinkage, 75, 75t

structural behavior under earthquake, 413
 under triaxial compression, 124f, 126f
 Deformation difference, mechanical response of,
 253–266
 creep of concrete, 263–266
 stress distribution on section under sustained load,
 263–265
 stress state after unloading, 265–266
 shrinkage of concrete, 254–259
 general analysis method, 254–256
 practical calculation method, 256–259
 thermal deformation, 259–263
 Deformed reinforcement, 190–193
 Ductility
 under monotonic load, 413–421
 calculation method, 416–418
 concept and expression, 413–416
 plastic region, angular rotation of, 418–421
 ratio, 416, 417f
 Durability, 521–546
 of concrete structure, characteristics of, 521–527
 durability failure, characteristics of, 523–524
 porosity texture, 524–527, 526t
 problems raised in engineering practice, 521–523
 problems
 alkali–aggregate reaction, 531–533
 carbonation, 533–536
 chemical corrosion, 536–538
 freeze–thaw cycle, 530–531
 permeation, 527–530
 rust of reinforcement, 538–542
 structure durability, design and evaluation of,
 542–546
 durability design, 542–543
 existing concrete structures, examination and
 evaluation of, 543–546
 Dynamic response of structure, 460, 460f

E

Earthquakes, 412–413, 434
 structural behavior under, characteristics of,
 411–413
 Eccentric compression, 59–66
 experimental results, 60–64
 failure pattern, 61–63
 neutral axis variation, 64
 sectional strain, 63
 ultimate bearing capacity, maximum strain and,
 60–61
 testing method, 59–60
 loaded with constant eccentricity, 59–60
 loaded with constant gradient, 60
 loaded with zero strain at one side, 60
 Eccentric load, 59–60
 Eccentric tension, 66–71
 complete stress–strain curve, equations for, 70–71
 failure process, 66–67
 maximum tensile strain at ultimate load, 69

- Eccentric tension (*Continued*)
 - neutral axis variation, 69–70
 - strain variation, 69–70
 - ultimate tensile strength and plasticity-dependent coefficient, 67–69
- Eccentrically compressed column, failure pattern in, 275–280
- Eccentrically tensed member, 294–295
- Elasticity solutions, 386–390
- Empirical formulas, for ultimate strength
 - calculation, 401–403
- Empirical regression, 365–369
- Envelope, 55
- Environmental conditions, influence on reinforced concrete, 16–17
- Equivalent rectangular stress diagram, 289–292, 289f, 291f
- Explosion resistance, 457–474
 - materials behavior under high-speed loading, 461–468
 - concrete, 465–468
 - reinforcement, 463–465
 - testing equipment and method, 461–463
 - structural members behavior, 468–474
 - compressive member, 472–474
 - flexural member, 468–472
 - of structures, characteristics of, 457–461
- Extruding, 135
- F**
- Failure criterion, 137–147, 138f
 - failure envelope, shape and expression of, 137–141, 143t
 - multiaxial strength, calculation charts for, 146–147
- Failure pattern, 269–280
 - in biaxial/triaxial tension, 132–135, 133f, 136t
 - breaking in tension, 132–133
 - columnar crushing, 133
 - extruding and shifting, 135
 - inclined shearing, 134
 - splitting into pieces, 134
 - of eccentric compression, 61–63
 - of eccentric/flexural tension, 66–67
 - eccentrically compressed column, 275–280
 - of inclined compression, 354
 - of inclined tension of, 355–356
 - less-reinforced beam, 272–274
 - of member without web reinforcement, 396–397, 396f
 - over-reinforced beam, 274–275
 - rectangular beam with tensile reinforcement, 269–272
 - of reinforced concrete member under torsion, 403
 - in shear compression, 350–354
 - suitably reinforced beam, 275
- Failure process
 - characteristic, shear strength and, 44–48
 - of confined concrete column with spiral bar, 222–223
 - general mechanism of, 17–19
 - of prism specimen, 21–24, 22f, 22t, 23f
 - of rectangular tied column, 226–229
 - repeated load and, 55
 - tensile, 39–42
- Fatigue resistance, 437–456
 - concrete, 438–442
 - experimental results and expression, 438–441
 - influence factors and calculation formula, 441–442
 - reinforcement, 443–446
 - reinforcement and concrete, bond between, 446–449
 - structural member and checking calculation, 449–456
 - fatigue under bending moment, 450–454
 - fatigue under shear force, 454–456
- Fatigue strength under tension, 442
- Ferrocement, 162, 162f
- Fiber concrete, 106–112
 - classification of, 106–108
 - mechanical behavior of, 108–112
- Finite element method, 364–365
- Fire resistance, 475–520
 - concrete, coupling constitutive relation of, 499–505
 - compressive strength, upper and lower bounds of, 500–501
 - short-term creep at elevated temperature, 504
 - thermal strain under stress, 501–504
 - transient thermal strain, 501–504
 - materials at elevated temperature, mechanical behaviors of, 487–499
 - concrete, 491–499
 - reinforcement, 487–491
 - structural members at elevated temperature, behavior and calculation of, 505–520
 - analysis and approximate calculation, 516–520
 - central compressive member, 507–508
 - compressive–flexural member, 508–511
 - flexural member, 505–507
 - load-temperature paths, influences of, 511–513
 - statistically indeterminate structure, 513–516
 - of structures, characteristics of, 475–479
 - temperature field on section, 479–486
 - heat conduction, basic equation for, 485–486
 - materials, thermal behaviors of, 481–485
 - temperature field, determination of, 485–486
 - temperature–time curve, 479–481
- Flexural member
 - behavior of, 468–472
 - at elevated temperature, behavior and calculation of, 505–507
 - of reinforced concrete, fatigue resistance of, 453
- Flexural stiffness and deformation, 329–348
 - deformation calculation, 342–348
 - general method, 342–344
 - practical methods, 344–348
 - section stiffness calculation, 334–342
 - analytical method, 337–340
 - effective moment of inertia, 334–337
 - tension stiffening, modification of, 340–342

sectional stiffness and member deformation, 331–334
 structural deformation, influences of, 329–331
 Flexural tension, 66–71
 complete stress–strain curve, equations for, 70–71
 failure process, 66–67
 maximum tensile strain at ultimate load, 69
 neutral axis variation, 69–70
 strain variation, 69–70
 ultimate tensile strength and plasticity-dependent coefficient, 67–69
 Freeze–thaw cycle, 530–531
 Friction on specimen surface, reducing, 117

G

Gelation hole, in concrete, 525
 Geometrical (deformation) condition
 compressive member, 206–207
 for flexural stiffness, 338
 sectional analysis, 285–286
 shrinkage of concrete, 254–255
 Goodman diagram, 440, 442–443
 Guo-Wang criterion, 549

H

Hard steel, stress–strain relation in, 166–167
 Hardened cement mortar, 10, 12t
 Hawkins model, 251
 Heat conduction, basic equation for, 485–486
 Heat diffusivity, 483–484
 High temperature, 476
 High-speed loading, materials behavior under, 461–468
 concrete, 465–468
 reinforcement, 463–465
 testing equipment and method, 461–463
 High-strength concrete, 90–99, 298–299, 298f
 application and preparation of, 90–92
 accelerating hydration, 90–91
 cement strength, 90–91
 compacting, 90–91
 polymers, as adhesive material, 91–92
 water–cement ratio, reducing, 91
 mechanical behavior of, 92–99
 High-strength wire, 161
 Holes, 10
 capillary, 525
 gelation, 525
 non-capillary, 525–527
 Homogenous porous light-weight concrete, 99
 Hydraulic and harbor engineering, reinforced concrete structure in, 1
 Hysteretic curve
 characteristics of, 421–426
 under reversed load of low cycles
 beam–column joint, 432–434
 compression–strength ratio, 427

content of reinforcement, 427
 reinforcement and concrete, bond-slip between, 430–432
 shear wall, 428–429
 short column, shearing of, 427–428

I

Inclined twisted surface, ultimate equilibrium of, 405–408
 Internal force at cracking, 309–311
 Internal structure, of reinforced concrete, 10–13
 Isotropic constitutive model, 150

K

Kent-Park model
 for confined concrete, 236–237
 deformation under action of cyclic loads, 171–172, 171f

L

Larger torsion–shear force ratio, 396–397
 Less-reinforced beam, failure pattern in, 272–274
 Light-weight concrete, 99–106
 concrete of light-weight aggregate, 101
 homogenous porous, 99
 mechanical behavior of, 101–106
 Linear elasticity models, 149–150
 Linear elasticity stress–strain relation, 149f
 Load(s/ing)
 acted on beam web, 373–374
 action of, 305–306
 cyclic loads, deformation under action of, 167–172
 frequency, influence on fatigue resistance, 442, 446
 high-speed, materials behavior under, 461–468
 concrete, 465–468
 reinforcement, 463–465
 testing equipment and method, 461–463
 repeated, 54–59
 paths, 129–132
 stress distribution on section under sustained, 263–265
 sustained load, deformation under, 346–348
 -temperature paths, influences on structural members, 511–513
 Local compression (bearing strength), 244–252
 mechanical characteristic and mechanism, 244–249
 strength calculation, 249–252
 Loci of principle stresses, 353–354
 Locus of common point, 238
 repeated loading, 57–58
 Locus of stability point, 238
 repeated loading, 58–59
 Long column
 eccentrically compressed, bending moment of, 284t
 flexure of, 280–283
 Longitudinal reinforcement, content of, 358–360
 Low-weight concrete, 299, 300f

M

Mass density, 483
 Mass heat capacity, 483
 Material composition, influence on fatigue resistance, 442
 Materials, thermal behaviors of, 481–485
 Mechanical (equilibrium) equations
 compressive member, 208
 for flexural stiffness, 339
 sectional analysis, 286–287
 shrinkage of concrete, 255–256
 Mechanical behavior, *see also* Mechanical behavior,
 of reinforced concrete
 of fiber concrete, 108–112
 of high-strength concrete, 92–99
 of light-weight concrete, 101–106
 of material, 460, 464
 concrete, 491–499
 reinforcement, 159–180, 487–491
 Mechanical behavior, of reinforced concrete, 9–52
 basic characteristics, 13–17
 composition and internal structure, 10–13
 compressive strength, 19–27
 cubic, 19–21
 prism specimen, failure process of, 21–24
 failure process, 17–19
 indices of, 24–27
 shear strength and deformation, 44–52
 failure characteristic, 44–48
 rational testing method, 44–48
 shear strain and modulus, 49–52
 stress–strain curve, complete compressive, 28–33
 complete curve, equation for, 29–33
 testing method, 28–29
 tensile strength and deformation, 33–44
 complete stress–strain curve, equation for,
 42–44
 failure process and characteristic, 39–42
 tensile behavior, testing method and index of,
 33–38
 Medium torsion–shear force ratio, 397
 Mild steel, stress–strain relation in, 163–166
 Minimum reinforcement rate, 215–216
 Modulus of elasticity, 27, 27f, 28t, 37–38
 age and, 74
 of bamboo, 162
 of cold-drawn wire, 176
 flexural stiffness and, 332
 of mild steel, 164
 Modulus of rupture, 34
 Moment of inertia
 of converted crack section, 336
 of converted section before concrete cracking,
 335–336, 335f
 effective, 334–337
 Multiaxial strength, calculation charts for, 146–147
 Multiaxial strength and deformation, general
 regularities of, 118–132

biaxial stress states, 119–122
 biaxial compressions, 119–121
 biaxial tension–compression, 121
 biaxial tensions, 121–122
 materials and loading paths, 129–132
 triaxial stress states, 122–129
 conventional triaxial compressions, 122–124
 real triaxial compressions, 124–125
 triaxial tension–compression, 126–128
 triaxial tensions, 128–129

N

Neutral axis variation
 in eccentric compression, 64
 in eccentric/flexural tension, 69–70
 Non-capillary holes, in concrete, 525–527
 Non-linear elasticity stress–strain relation, 151f
 Non-loading factors, of tensile crack, 306–309
 Non-rectangular sections, 303–304, 304f
 Non-slip method, 314–318

O

Orthogonal anisotropic constitutive model, 150
 Ottosen criterion, 549
 Over-reinforced beam, failure pattern in, 274–275

P

Palmgren-Miner hypothesis, 440–441, 445
 Permeation, 527–530
 Physical (constitutive) relation
 compressive member, 207–208
 for flexural stiffness, 338–339
 sectional analysis, 286
 shrinkage of concrete, 255
 Plain reinforcement, 189–190
 Plastic region, angular rotation of, 418–421
 Plasticity solutions, 386–390
 Plasticity-dependent coefficient, 67–69
 Poisson's ratio of concrete, 38
 Polymers, as adhesive material, 91–92
 Porosity texture of concrete, 524–527, 526t
 Prism compressive strength, of concrete, 24, 25f, 25t
 Prism specimen
 compression test of, 22f
 failure process of, 21–24, 22f, 22t, 23f
 Pull-out test of reinforcement, 189–190, 189f, 191f,
 193, 199

R

Rectangular beam with tensile reinforcement, failure
 pattern in, 269–272
 Rectangular tied column, 226–238
 complete stress–strain curve, equation for,
 234–238
 failure process, 226–229
 rectangular tie, working mechanism of, 229–232

- Reinforced concrete
 - mechanical behavior of, 9–52
 - member, mechanical behavior of, *see* Reinforced concrete member, mechanical behavior of
 - concrete member, mechanical behavior of structure
 - advantages of, 2
 - applications of, 1–2
 - development and features of, 1–4
 - disadvantages of, 2
 - historical development of, 1
 - Reinforced concrete member, mechanical behavior of, 205–220
 - compressive member, 206–212
 - basic equations, 206–208
 - stress–strain analysis, 209–212
 - general regularity, 218–219
 - tensile member, 212–218
 - basic equations, 212–213
 - minimum reinforcement rate, 215–216
 - stress–strain analysis, 213–215
 - tension stiffening, 216–218
 - Reinforcement, *see also* Reinforcement and concrete, bond between
 - appearance of, 160f
 - behavior under high-speed loading, 463–465
 - bond length of, 195
 - deformed, 190–193
 - diameter and shape of, 196–197
 - with different strengths, 300–301, 300f
 - distributed along sectional depth, 301–303, 302f
 - fatigue of, 443–446
 - forms of, 4
 - less-, 394
 - longitudinal, 358–360, 393–395
 - mechanical behaviors of, at elevated temperature, 487–491
 - plain, 189–190
 - over-, 394
 - partly over-, 394
 - rectangular beam with tensile reinforcement, failure pattern in, 269–272
 - rust of, 538–542
 - web, *see* Web reinforcement
 - working after yielding of, 412
 - without yielding plateau, 301
 - Reinforcement, mechanical behavior of, 159–180
 - behavior after cold-worked, 172–176
 - cold-drawn, 175–176
 - cold-stretching and age hardening, 173–175
 - concrete structure, 159–163
 - ferrocement, 162, 162f
 - high-strength wire, 161
 - reinforcement, 160
 - shape steel, 161–162
 - substitutive materials, 162–163
 - creep and relaxation, 176–179
 - control stress, sustaining time of, 178
 - steel, 178
 - stress level, 178–179
 - temperature, 179
 - deformation under action of cyclic loads, 167–172
 - stress–strain relation, 163–167
 - hard steel, 166–167
 - mild steel, 163–166
 - Reinforcement and concrete, bond between, 181–204
 - bond stress–slip relation, constitutive model for, 199–203
 - characteristic values, calculation of, 200–201
 - τ – s curve, equation for, 201–203
 - deformed reinforcement, 190–193
 - fatigue of, 446–449
 - function and classification, 182–184
 - anchorage bond, of reinforcement end, 183, 183f
 - cracks, bond between, 183–184, 183f
 - composition, 184–185
 - hysteretic curve of, 430–432
 - influence factors, 193–199
 - concrete cover thickness, 195
 - concrete strength, 194
 - other factors, 198–199
 - reinforcement, bond length of, 195
 - reinforcement, diameter and shape of, 196–197
 - transverse compressive stress, 198
 - transverse stirrup, 197–198
 - plain reinforcement, 189–190
 - test method, 186–188
 - beam test, 187–188
 - tension test, 186–187
 - Relative stability, of reinforced concrete, 18
 - Relaxation, 79–80, 176–179
 - control stress, sustaining time of, 178
 - steel, 178
 - stress level, 178–179
 - temperature, 179
 - Repeated load, 54–59
 - τ – s curve under, 448f
 - Rust of reinforcement, 538–542
- ## S
- San Venient Principle, 245
 - Sargin model, for confined concrete, 233f, 234–235
 - Section modulus
 - elastic, 387
 - plastic, 387–390, 402–403
 - Section stiffness
 - calculation, 334–342
 - analytical method, 337–340
 - effective inertia moment, 334–337
 - tension stiffening, modification of, 340–342
 - distribution of, 345–346
 - member deformation, 331–334
 - Sectional analysis
 - flow chart for, 288f
 - general method for, 283–288
 - for temperature deformation, 261–263, 262f–263f

- Sectional strain, and eccentric compression, 63
- Segmental model, 201–202
- Seismic load, reverse, 413
- Seismic resistance, 411–436
 - ductility under monotonic load, 413–421
 - calculation method, 416–418
 - concept and expression, 413–416
 - plastic region, angular rotation of, 418–421
 - reversed load of low cycles, hysteretic
 - characteristic under, 421–436
 - beam–column joint, 432–434
 - calculation model, 434–436
 - compression–strength ratio, 427
 - content of reinforcement, 427
 - hysteretic curves, characteristics of, 421–426
 - reinforcement and concrete, bond-slip between, 430–432
 - shear wall, 428–429
 - short column, shearing of, 427–428
 - structural behavior under earthquake,
 - characteristics of, 411–413
- Seismic response, 411–412
- Shape steel, 161–162, 161f
- Shape of ties, 232, 232f
- Shear force, fatigue under, 454–456
- Shear force, member strength under, 349–384
 - members and mechanical conditions, 373–384
 - axial force, influence of, 377–378
 - beam of T section, 374–376
 - beam with variable section, 376
 - bracket, 380–382
 - load acted on beam web, 373–374
 - shear span, positive and negative bending moments within, 378–380
 - slab punching, 382–384
 - ultimate shear strength, calculation of, 364–372
 - beam model, 369–370, 370f
 - empirical regression, 365–369
 - finite element method, 364–365
 - truss model, 370–372, 371f
 - ultimate shear strength, composition of, 363–364
 - web reinforcement, effect of, 360–363
 - web reinforcement, failure pattern and beam strength without, 350–360
 - inclined compression, failure pattern of, 354
 - inclined tension, failure pattern of, 355–356
 - typical failure pattern (shear compression), 350–354
 - ultimate shear strength, 356–360
- Shear force, members with, 395–397
- Shear modulus, 49–52
- Shear resistance, components of, 360–364
- Shear span, positive and negative bending moments within, 378–380
- Shear torsion, members with, 395–397
- Shear wall, hysteretic curve of, 428–429
- Shear-bending segment
 - near support, mechanical characteristics of, 354f
 - stress distribution on, 351f–352f
- Shearing, inclined, 134
- Shear-span ratio, 356–357, 357f
- Shear-stress flow, 389–390, 390f, 404–405
- Sheikh model, for confined concrete, 233f, 235
- Shifting, 135
- Short column, shearing of
 - hysteretic curve, 427–428
- Shrinkage, 75–78
 - cement, kind and quantity of, 76
 - of concrete, 254–259
 - cracks caused by, 307f
 - general analysis method, 254–256
 - practical calculation method, 256–259
 - curing condition, 76
 - other factors, 76–78
 - property, size, and aggregate quantity, 76
 - service stage, environmental condition of, 76
 - structural member, shape and size of, 76
- Slab punching, 382–384
- Slender column, 281–282
- Smaller torsion–shear force ratio, 397
- Solid granule, 10
- Space between cracks, 313–314, 319
- Space of ties, 232
- Special engineering, reinforced concrete structure in, 1–2
- Specific heat capacity, 483
- Spiral bar, confined concrete column with, 222–226
 - mechanical mechanism and failure process, 222–223
 - ultimate strength, 224–226
- Splitting
 - into pieces, 134
 - stress, in reinforcement–concrete bonding, 200–201
 - tensile strength, 36–37
- Statistically indeterminate structure, 513–516
- Steel, creep and relaxation, 178
- Steel-tube-confined concrete, 238–244
 - mechanical characteristic and mechanism, 238–241
 - ultimate strength calculation, 241–244
- Stirrups
 - influence on ultimate strength, 393–395
 - transverse, 197–198
- Strain
 - gradient, 59
 - internal micro strain states, 13–14
 - measuring, 118
 - path, controlling, 118
 - sectional, 63
 - tensile peak, 37
 - transient thermal, 501–504
 - transverse, 57, 58f
 - variation, in eccentric/flexural tension, 69–70
- Straining rate, structural materials, 461t
- Stress
 - distribution on section under sustained load, 263–265
 - gradient, influence on fatigue resistance, 441–442

- level, in creep and relaxation, 178–179
 - measuring, 118
 - path, controlling, 118
 - relaxation, 79
 - states
 - after unloaded, 265–266
 - biaxial, 119–122
 - influences of, 16
 - internal micro stress states, 13–14
 - triaxial, 122–129
 - of symmetrically reinforced concrete member during
 - uniformly shrinking, 257–258, 257f
 - thermal strain under, 501–504
 - transverse compressive, 198
 - Stress–strain analysis
 - compressive member, 209–212
 - tensile member, 213–215
 - Stress–strain curve
 - of concrete, repeated loading, 55
 - of rectangular tied column, 234–238
 - of reinforce concrete
 - complete compressive, 28–33, 29f–30f, 31t, 32f, 33t, 35f
 - under unloading and loading test, 40f
 - Stress–strain relation, 64–66
 - of cold-drawn, 176
 - after cold-stretching and age-hardening, 173f
 - ideal elasto-plastic, 154f
 - linear elasticity, 149f
 - non-linear elasticity, 151f
 - of reinforcement, 163–167
 - at elevated temperature, 491f
 - hard steel, 166–167
 - mild steel, 163–166
 - Stress–temperature (loading–heating) path, 499–501, 499f, 503–505, 503f
 - Structural members at elevated temperature, behavior
 - and calculation of, 505–520
 - analysis and approximate calculation, 516–520
 - central compressive member, 507–508
 - compressive–flexural member, 508–511
 - flexural member, 505–507
 - load–temperature paths, influences of, 511–513
 - statistically indeterminate structure, 513–516
 - Structures, explosion resistance of, 457–461
 - Substitutive materials, for reinforcement, 162–163
 - Suitably reinforced beam, failure pattern in, 275
 - Sustained load, 72–73, 81
 - deformation under, 346–348
- T**
- T section, beam of, 374–376
 - τ – s curve, equation for, 201–203
 - model of continuous curve, 202–203
 - segmental model, 201–202
 - Temperature, creep/relaxation and, 179
 - Temperature field
 - determination of, 485–486
 - on section, 479–486
 - heat conduction, basic equation for, 485–486
 - materials, thermal behaviors of, 481–485
 - temperature field, determination of, 485–486
 - temperature–time curve, 479–481
 - Tensile behavior, testing method and index of, 33–38
 - Tensile crack, 305–328
 - cause and limitation of, 305–309
 - action of load, 305–306
 - non-loading factors, 306–309
 - internal force at, 309–311
 - mechanism of, 311–321
 - bond-and-slip method, 312–314
 - comprehensive analysis, 318–321
 - non-slip method, 314–318
 - width calculation, 322–327
 - Tensile member, mechanical behavior of, 212–218
 - basic equations, 212–213
 - minimum reinforcement rate, 215–216
 - stress–strain analysis, 213–215
 - tension stiffening, 216–218
 - Tensile peak strain, 37
 - Tensile strength, 33–44
 - central, 34–36
 - complete stress–strain curve, equation for, 42–44
 - failure process and characteristic, 39–42, 42t
 - splitting, 36–37
 - tensile behavior, testing method and index of, 33–38
 - Tension
 - axial, 205–206
 - biaxial, 121–122
 - breaking in, 132–133
 - at cracking, 306f
 - exerting, 117–118
 - inclined, failure pattern of, 355–356
 - test, for reinforcement–concrete bonding, 186–187
 - triaxial, 128–129
 - stiffening, 216–218, 340–342
 - Tension–compression
 - biaxial, 121
 - triaxial, 126–128
 - Thermal behavior of material, 481–485
 - Thermal conductivity, 483
 - Thermal deformation difference, 259–263
 - Thermal strain under stress, 501–504
 - Time factors, influence on reinforced concrete, 16–17
 - Torsion, member strength under, 385–408
 - composite internal forces, members with, 395–401
 - axial force and torsion, members with, 395
 - bending moment and torsion, members with, 397–400
 - bending moment–shear force–torsion, members with, 400–401
 - shear force and torsion, members with, 395–397

- Torsion, member strength under (*Continued*)
 - elasticity and plasticity solutions, 386–390
 - ultimate strength, 390–395
 - reinforcement content and stirrup, influence of, 393–395
 - web reinforcement, member with, 392–393
 - web reinforcement, member without, 390–392
 - ultimate strength, calculation of, 401–408
 - empirical formulas, 401–403
 - inclined twisted surface, ultimate equilibrium of, 405–408
 - truss model, 403–405
 - Torsion, members with, 397–400
 - axial, 395
 - shear, 395–397
 - Transient thermal strain, 501–504
 - Transverse compressive stress, 198
 - Transverse reinforcement, 221–222, 224, 249, 251
 - Transverse stirrup, 197–198
 - Transverse strain, in repeated loading, 57, 58f
 - Triaxial compressions
 - conventional, 122–124
 - real, 124–125
 - Triaxial stress states, 122–129
 - Triaxial tension–compression, 126–128
 - Triaxial tensions, 128–129
 - Triaxial test equipment
 - conventional, 115–116
 - real, 116–117, 117f
 - Truss model
 - for member under torsion, 403–405
 - for member under shear force, 370–372, 371f
- U**
- Ultimate bond strength, of reinforcement–concrete bonding, 201
 - Ultimate load, maximum tensile strain at, 69
 - Ultimate shear strength, *see also* Ultimate strength
 - of beam without web reinforcement, 356–360
 - calculation of, for member under shear force, 364–372
 - beam model, 369–370, 370f
 - empirical regression, 365–369
 - finite element method, 364–365
 - truss model, 370–372, 371f
 - composition of, 363–364, 363f
 - Ultimate strength, *see also* Ultimate shear strength, Ultimate tensile strength
 - calculation of, for member under torsion, 401–408
 - empirical formulas, 401–403
 - inclined twisted surface, ultimate equilibrium of, 405–408
 - truss model, 403–405
 - of cold-drawn wire, 175–176
 - of column under central compression, 209, 211
 - of confined concrete column with spiral bar, 224–226
 - of hard steel, 166
 - local compression (bearing length), 249–252
 - of member under torsion, 390–395
 - reinforcement content and stirrup, influence of, 393–395
 - web reinforcement, member with, 392–393
 - web reinforcement, member without, 390–392
 - of mild steel, 164–165, 172
 - reinforced concrete, eccentrically compressed member of, 289–298
 - calculation formulas, 289–295
 - of reinforcement after cold-stretching, 173–175
 - steel-tube-confined concrete, 241–244
 - Ultimate tensile strength, eccentric/flexural tension, 67–69
 - Underground engineering, reinforced concrete structure in, 1
 - Unloading curve, 55–57, 56f
 - USA AASHTO, for fatigue strength of tensile reinforcement, 445f
- V**
- Variable section, beam with, 376
 - Volume density, *see* Mass density
- W**
- Water–binder ratio, 527
 - Water–cement ratio, 91, 527
 - Web reinforcement
 - failure pattern and beam strength without, 350–360
 - inclined compression, failure pattern of, 354
 - inclined tension, failure pattern of, 355–356
 - typical failure pattern (shear compression), 350–354
 - ultimate shear strength, 356–360
 - member with, 392–393
 - member without, 390–392
 - Wohler diagram, 440
- Y**
- Yield strength
 - of cold-drawn wire, 175–176
 - of hard steel, 166–167
 - of mild steel, 164–165, 172
 - of reinforcement after cold-stretching, 173–175